

**Ongoing Face Recognition
Vendor Test (FRVT)**
Part 1: Verification

Patrick Grother
Mei Ngan
Kayee Hanaoka
*Information Access Division
Information Technology Laboratory*

This publication is available free of charge from:
<https://www.nist.gov/programs-projects/face-recognition-vendor-test-frvt-ongoing>

2021/11/22

ACKNOWLEDGMENTS

The authors are grateful for the long-standing support and collaboration of the the Department of Homeland Security's Science & Technology Directorate (S&T) and the Office of Biometric Identity Management (OBIM).

Additionally, the authors are grateful to staff in the NIST Biometrics Research Laboratory for infrastructure supporting rapid evaluation of algorithms.

DISCLAIMER

Specific hardware and software products identified in this report were used in order to perform the evaluations described in this document. In no case does identification of any commercial product, trade name, or vendor, imply recommendation or endorsement by the National Institute of Standards and Technology, nor does it imply that the products and equipment identified are necessarily the best available for the purpose.

INSTITUTIONAL REVIEW BOARD

The National Institute of Standards and Technology's Research Protections Office reviewed the protocol for this project and determined it is not human subjects research as defined in Department of Commerce Regulations, 15 CFR 27, also known as the Common Rule for the Protection of Human Subjects (45 CFR 46, Subpart A).

FRVT STATUS

This report is a draft NIST Interagency Report, and is open for comment. It is the thirty fifth edition of the report since the first was published in June 2017. Prior editions of this report are maintained on the FRVT [website](#), and may contain useful information about older algorithms and datasets no longer used in FRVT.

FRVT remains open: All [four tracks](#) of the FRVT are open to new algorithm submissions.

2021-11-22 changes since 2021-10-28:

- ▷ We have added results to the [website](#) for kiosk-collected images where the design and geometry configuration mean that many images have considerable downward pitch angle. In some images, the face is partially cropped. Some images have other background faces.
- ▷ We have stopped using child exploitation images in FRVT, as we lost access to the imagery. All results for that set have been removed from the [website](#), and will be removed from future PDF reports.
- ▷ We have added results for first algorithms from seven new developers: CUDO Communication, Daon, KuKe3D Technology, Mantra Softech India, Maxvision Technology, Multi-Modality Intelligence, and Samsung-SDS.
- ▷ We have added results for new algorithms from seven returning developers: Acer Incorporated, Cloudwalk-Moontime Smart Technology, Gorilla Technology, ID3 Technology, Incode Technologies, NSENSE Corp., and SQISoft.
- ▷ We have retired results for six algorithms per our policy to only list results for two algorithms per developer. Results for retired algorithms appear in prior versions of this report in the [archive](#).

2021-10-28 changes since 2021-09-08:

- ▷ We have substantially revised the algorithm-specific report cards that are linked from the [FRVT results page](#). (Example: [HTML](#)).
- ▷ We have added results for first algorithms from eight new developers: Beijing Mendaxia Technology, Beijing Hisign Technology, Biocube Matrics, Clearview AI, Reveal Media, Toppan ID Gate, Verigram, and Viettel High Technology.
- ▷ We have added results for new algorithms from thirty returning developers: 20Face, 3divi, Canon Inc Chunghwa Telecom, Corsight, Decatur Industries, Deepglint, Dermalog, FaceTag, Fiberhome Telecommunication Technologies, GeoVision, ICM Airport Technics, Imagus Technology, InsightFace AI, Kakao Enterprise, Kookmin University, Line Corporation, N-Tech Lab, NotionTag Technologies, Realnetworks, Suprema ID, Taiwan-Certificate Authority, Toshiba, Tripleize, Trueface.ai, Veridas Digital Authentication, Visidon, VisionLabs, YooniK, and Yuan High-Tech Development.
- ▷ We have retired results for twenty algorithms per our policy to only list results for two algorithms per developer. Results for retired algorithms appear in prior versions of this report in the [archive](#).

2021-09-08 changes since 2021-08-02:

- ▷ We have added results for first algorithms from seven new developers: Griaule, SQISoft, Qnap Security, Techsign, Smart Engines, Verihubs, and Wuhan Tianyu Information Industry.
- ▷ We have added results for new algorithms from sixteen returning developers: ADVANCE.AI, AuthenMetric, CloudSmart Consulting, Code Everest Pvt, Cognitec Systems, Thales Gemalto Cogent, Intel Research Group, Omnidarde, Oz Forensics, Rank One Computing, Samsung S1 Corp, Securif AI, Tevian, TigerIT Americas, Universidade de Coimbra, and Vigilant Solutions

- ▷ We have retired results for eleven algorithms per our policy to only list results for two algorithms per developer. Results for retired algorithms appear in prior versions of this report in the [archive](#).

2021-08-02 changes since 2021-06-25:

- ▷ We have added results for first algorithms from eight new developers: Bee the Data, Closeli Inc, Coretech Knowledge Inc, Deepsense (France), ioNetworks Inc, Kakao Pay Corp, Seventh Sense Artificial Intelligence, and SK Telecom.
- ▷ We have added results for new algorithms from fifteen returning developers: Alchera Inc, Adera Global PTE, Aware, Bresee Technology, Cyberlink Corp, Expasoft LLC, Fujitsu Research and Development Center, Gorilla Technology, Idemia, Neurotechnology, NEO Systems, NHN Corp, Paravision, Panasonic R+D Center Singapore, and Shenzhen University-Macau University of Science and Technology.
- ▷ We have retired results for twelve algorithms per our policy to only list results for two algorithms per developer. Results for retired algorithms appear in prior versions of this report in the [archive](#).

2021-06-25 changes since 2021-05-21:

- ▷ We have added results for first algorithms from six new developers: Alice Biometrics, BOE Technology Group, Fincore, Neosecu, Sodec App, and Yuntu Data and Technology.
- ▷ We have added results for new algorithms from seven returning developers: Incode Technologies, HyperVerge, Mobbeel Solutions, Guangzhou Pixel Solutions, Remark Holdings, Sensetime, and Vietnam Posts and Telecommunications Group.
- ▷ We have retired results for four algorithms per our policy to only list results for two algorithms per developer. Results for retired algorithms appear in prior versions of this report in the [archive](#).

2021-05-21 changes since 2021-04-26:

- ▷ We have added results for first algorithms from five new developers: Ekin Smart City Technologies, Suprema ID, Tripleize, Taiwan-Certificate Authority, and Vision Intelligence Center of Meituan.
- ▷ We have added results for new algorithms from eight returning developers: ID3 Technology, Imagus Technology, Momentum Digital, N-Tech Lab, NSENSE, Shanghai Jiao Tong University, Vision-Box, and Yuan High-Tech Development
- ▷ We have retired results for seven algorithms per our policy to only list results for two algorithms per developer. Results for retired algorithms appear in prior versions of this report in the [archive](#).

2021-04-26 changes since 2021-04-16:

- ▷ We have added results for first algorithms from three new developers: Quantasoft, Rendip, and NEO Systems.
- ▷ We have added results for new algorithms from four returning developers: 3Divi, Realnetworks, Veridas Digital Authentication Solutions, and Universidade de Coimbra.
- ▷ We have retired results for three algorithms per our policy to only list results for two algorithms per developer. Results for retired algorithms appear in prior versions of this report in the [archive](#).

2021-04-16 changes since 2021-03-19:

- ▷ We have added results for first algorithms from six new developers: 20Face, Beijing DeepSense Technologies, BitCenter UK, Enface, FaceTag, InsightFace AI, Line Corporation, Lema Labs, Nanjing Kiwi Network Technology, Omnidarde, Regula Forensics, and Suprema.
- ▷ We have added results for new algorithms from ten returning developers: CloudSmart Consulting, Dermalog, GeoVision, Neurotechnology, Panasonic R+D Center Singapore, Samsung S1, Securif AI, Trueface.ai, Vigilant Solutions, and Visidon.
- ▷ We have retired results for ten algorithms per our policy to only list results for two algorithms per developer. Results for retired algorithms appear in prior versions of this report in the [archive](#).

2021-03-19 changes since 2021-03-05:

- ▷ We have added results for first algorithms from six new developers: Ajou University, AuthenMetric, Code Everest, Corsight, Papilon Savunma, and NHN Corp
- ▷ We have added results for new algorithms from seven returning developers: Alchera, Deepglint, Fiber-home Telecommunication Technologies, Kakao Enterprise, Kookmin University, Megvii/Face++, and NotionTag Technologies.
- ▷ We have updated many of the hyperlinked HTML report-cards to include seven figures on demographic dependence. Figures of this kind first appeared, and are documented in, the December 2019 document, [NIST Interagency Report 8280](#) on demographic differentials in face recognition. The figures quantify false negative dependence on demographics using “visa-border” comparisons, and false positive dependence using comparisons of “application” photos that uniformly of quality and similar to visa photos.

2021-03-05 changes since 2021-01-19:

- ▷ We have added results for first algorithms from three new developers: IVA Cognitive, Mobbeel, and MoreDian Technology.
- ▷ We have added results for new algorithms from returning developers: Ability Enterprise - Andro Video, ACI Software, Adera Global, AnyVision, BioID Technologies, China Electronics Import-Export, Cognitec Systems, Fujitsu Research and Development Center, Glory, Guangzhou Pixel Solutions, Hengrui AI Technology, Incode Technologies, Intel Research, iQIYI, Mobai, Oz Forensics, Paravision, VisionLabs, and Xforward AI Technology.
- ▷ We have added a new “resources” tab to the main [webpage](#). It includes sortable columns for data related to speed, model size, storage, and memory consumption.
- ▷ We have retired results for 13 algorithms per our policy to only list results for two algorithms per developer. Results for retired algorithms appear in prior versions of this report in the [archive](#).

2021-01-19 changes since 2020-12-18:

- ▷ This report adds results for first algorithms from four developers: Herta Security, Irex AI, Shenzhen University-Macau University of Science and Technology, and Vietnam Posts and Telecommunications Group. See Table 6 for more information.

- ▷ The report also includes results for thirteen developers who have previously submitted algorithms: Bresee Technology, Canon (previously Canon Information Technology (Beijing)), Cyberlink, CSA IntelliCloud Technology, Dahua Technology, ID3 Technology, Imagus Technology (Vixvizon), Moontime Smart Technology, N-Tech Lab, Thales Cogent, Veridas Digital Authentication Solutions, Vocord, and Yuan High-Tech Development.
- ▷ We have retired results for ten algorithms per our policy to only list results for two algorithms per developer. Results for retired algorithms appear in prior versions of this report in the [archive](#).

2020-12-18 changes since 2020-10-09:

- ▷ This report adds results for first algorithms from ten developers: BitCenter UK, CloudSmart Consulting, Cubox, Institute of Computing Technology, Naver Corp, Minivision, NSENSE Corp, Viettel Group, Visage Technologies, and Xiamen University. See Table 6 for more information.
- ▷ The report also includes results for eighteen developers who have previously submitted algorithms: ADVANCE.AI, Awidit Systems, Chosun University, Dermalog, GeoVision, ICM Airport Technics, Idemia, Institute of Information Technologies, Kakao Enterprise, Neurotechnology, Panasonic R+D Center Singapore, Rank One Computing, Sensetime Group, Shanghai Jiao Tong University, TigerIT Americas LLC, Vigilant Solutions, Winsense, and YooniK
- ▷ We have retired results for twelve algorithms per our policy to only list results for two algorithms per developer. Results for retired algorithms appear in prior versions of this report in the [archive](#).

Changes since September 18, 2020:

- ▷ This report adds results for first algorithms from five developers: Aigen, Cortica, Kookmin University, Securif AI and Vinai.
- ▷ The report also includes results for three developers who have previously submitted algorithms: Fujitsu Laboratories, Hengrui AI, and X-Forward AI.
- ▷ In the per-algorithm report-cards linked from tables and the main webpage, we have added a chart to showing reduction in error rates over the course of FRVT i.e. from 2017 onwards for all algorithms supplied by that developer. Similarly we have added a chart showing error rate reductions for our test of protective face mask verification.
- ▷ We plan to continue evaluating algorithms on various mask datasets. We hold that algorithms should be capable of detecting masks and verifying identity of all combinations of masked and unmasked faces. We have accordingly increased the amount of time allowed to extract those features from 1.0 to 1.5 seconds.

Changes since August 25, 2020:

- ▷ This report adds results for first algorithms from eight new developers: Akurat Satu Indonesia, Cybercore, Decatur Industries, Innef Labs, Satellite Innovation/Eocortex, Expasoft, and Mobai.
- ▷ The report includes results for seven developers who have previously submitted algorithms: 3Divi, BioID Technologies, Incode Technologies, Innovatrics, iSAP Solution, Synology, and Tevian.
- ▷ We have retired results for five algorithms per our policy to only list results for two algorithms per developer. Results for retired algorithms appear in prior versions of this report in the [archive](#).

Changes since July 27, 2020:

- ▷ We have introduced per-algorithm report sheets. These are HTML documents linked from the accuracy tables in this report (i.e. Table 24) and on the FRVT 1:1 [homepage](#). The sheets contain interactive graphics allowing, for example, mouseover exploration of FNMR(T) and FMR(T). Some of their content had previously appeared in this document.
- ▷ This report adds results for algorithms from six new developers. ACI Software, Bresee Technology, Fiberhome Telecommunication Technologies, Imageware Systems, Oz Forensics, and Pensees.
- ▷ The report includes results for thirteen developers who have previously submitted algorithms: Canon Information Technology (Beijing), Cyberlink, Dahua Technology, Gorilla Technology, ID3 Technology, Intel Research Group, iQIYI Inc, Momentum Digital, Netbridge Technology, Tech5 SA, Shenzhen AiMall Tech, Vigilant Solutions, and VisionLabs.
- ▷ We have retired results for nine algorithms per our policy to only list results for two algorithms per developer. Results for retired algorithms appear in prior versions of this report in the [archive](#).

Changes since May 18, 2020:

- ▷ The report is the first FRVT update since the pandemic closed it from March to June 2020.
- ▷ This report includes results for algorithms from nine new developers: GeoVision Inc, Su Zhou NaZhi-TianDi Intelligent Technology, YooniK, AYF Technology, PXL Vision AG, Yuan High-Tech Development, Beihang University-ERCACAT, ICM Airport Technics, and Staqu Technologies
- ▷ This report includes results for algorithms from 15 returning developers Acer Incorporated, Antheus Technologia, Chosun University, Chunghwa Telecom, Idemia, Moontime Smart Technology, Neurotechnology, Guangzhou Pixel Solutions, Panasonic R+D Center Singapore, Rank One Computing, Scanovate, Shanghai Universiy - Shanghai Film Academy, Synesis, Trueface.ai, and Veridas Digital Authentication Solutions
- ▷ We have retired results for ten algorithms per our policy to only list results for two algorithms per developer. Results for retired algorithms appear in prior versions of this report in the [archive](#).
- ▷ We separated timing and other resource consumption from the main participation table. The new Table 15 includes template generation durations for four kinds of images, not just mugshots.
- ▷ We have published a separate report, [NIST Interagency Report 8311](#) on accuracy of pre-pandemic algorithms on subjects wearing face masks. We plan to track improvements in accuracy on masked images going forward. In particular, we invite submission of algorithms that can detect whether a person is wearing a mask, extract features from the full face or the exposed periocular region, and do appropriate comparison. We do not intend to evaluate algorithms that assume 100% of images will be of masked individuals.

Changes since March 25, 2020:

- ▷ The report is a maintenance release - it does not add any new algorithms, and FRVT has been closed to new algorithms since mid March 2020.
- ▷ We modified the primary accuracy summary, Table 24, as follows:

- ▷▷ For visa images, the column for FNMR at FMR = 0.0001 has been removed. The visa images are so highly controlled that the error rates for the most accurate algorithms are dominated by false rejection of very young children and by the presence of a few noisy greyscale images. For now, two visa columns remain: FNMR at $FMR = 10^{-6}$ and, for matched covariates, FNMR at $FMR = 10^{-4}$.
- ▷▷ We have inserted a new column labelled “BORDER” giving accuracy for comparison of moderately poor webcam border-crossing photos that exhibit pose variations, poor compression, and low contrast due to strong background illumination. The accuracies are the worst from all cooperative image datasets used in FRVT.
- ▷ Accordingly, we updated the failure-to-template rates in Table 31.
- ▷ We withdrew a figure showing how false matches are concentrated in certain visa images used in cross-comparison, because it didn’t attempt to include demographic information.

Changes since February 27, 2020:

- ▷ The report adds results algorithms from two new developers: Beijing Alleyes Technology, and the Chinese University of Hong Kong. Results for newly submitted algorithms from two other developers will appear in the next report.
- ▷ The report adds results for algorithms from thirteen returning developers: ASUSTek Computer, Aware, Cyberlink Corp, Gorilla Technology, Innovative Technology, Kakao Enterprise, Lomonosov Moscow State University, Panasonic R+D Center Singapore, Shenzhen AiMall Technology, Shenzhen Intellifusion Technologies, Synology, Tech5 SA, and Via Technologies.
- ▷ Per policy to only list results for two algorithms per developer, we have dropped results for algorithms from Aware, Cyberlink, Gorilla Technology, Kakao Enterprise, Lomonosov Moscow State University, Panasonic R+D Center Singapore, and Tech5 SA.

Changes since January 20, 2020:

- ▷ The report adds results for five new developers: Ability Enterprise (Andro Video), Chosun University, Fujitsu Research and Development Center, University of Coimbra, and Xforward AI Technology.
- ▷ The report adds results for algorithms from six returning developers: AlphaSSTG, Incode Technologies, Kneron, Shanghai Jiao Tong University, Vocord, and X-Laboratory.
- ▷ We have corrected template comparison timing numbers for algorithms submitted September 2019 to January 2020. The values reported previously were slower due to a software bug.
- ▷ We have dropped results for algorithms from Vocord and Incode per policy to only list results for two algorithms per developer.
- ▷ The [FRVT 1:1 homepage](#) has been updated with latest accuracy results.
- ▷ The [FRVT 1:N homepage](#) now includes an update to the September 2019 NIST Interagency Report 8271. The new report adds results for one-to-many search algorithms submitted to NIST from June 2019 to January 2020.

Changes since January 6, 2020:

- ▷ Section 2 has been updated to better describe the Visa and Border images. The caption for Table 24 has been updated to better relate the accuracy values to particular image comparisons.

- ▷ The report adds results for five new developers: Acer, Advance.AI, Expasoft, Netbridge Technology, and Videmo Intelligent Videoanalyse.
- ▷ The report adds results for algorithms from 7 returning developers: China Electronics Import-Export Corp, Intel Research Group, ITMO University, Neurotechnology, N-Tech Lab, Rokid, and VisionLabs.
- ▷ We have dropped results from this edition of the report per policy to only list results for two algorithms per developer: N-Tech Lab, Neurotechnology, ITMO, Visionlabs, and CEIEC.
- ▷ The [FRVT homepage](#) has been updated with latest accuracy results.

Changes since November 11, 2019:

- ▷ Table 15 has been updated to include runtime memory usage. This is the first time such a quantity has been reported. The value is the peak size of the resident set size logged during enrollment of single images.
- ▷ We have migrated summary results table to a new platform that supports sortable tables:
<https://pages.nist.gov/frvt/html/frvt11.html>
- ▷ The report adds results for four new developers: Antheus Technologia, BioID Technologies SA, Canon Information Tech. (Beijing), Samsung S1 (listed in the tables as S1), and Taiwan AI Labs.
- ▷ The report adds results for algorithms from 13 returning developers: Anke Investments, Chunghwa Telecom, Deepglint, Institute of Information Technologies, iQIYI, Kneron, Ping An Technology, Paravision, KanKan Ai, Rokid Corporation, Shanghai Universiy - Shanghai Film Academy, Veridas Digital Authentication Solutions, and Videonetics Technology.
- ▷ We have dropped results from this edition of the report per policy to only list results for two algorithms per developer: remarkai-000, veridas-001, sensetime-001, iit-000, anke-003, and everai-002. Results for these are available in prior editions of this report linked from the FRVT page.
- ▷ We issued [NIST Interagency Report 8280: FRVT Part 3: Demographics](#) on 2019-12-19. It includes results for many of the algorithms covered by this report.

Changes since October 16, 2019:

- ▷ The report adds results for ten new developers: Ai-Union Technology, ASUSTek Computer, DiDi ChuXing Technology, Innovative Technology, Luxand, MVision, Pyramid Cyber Security + Forensic, Scanovate, Shenzhen AiMall Tech, and TUPU Technology.
- ▷ The report adds results for 12 returning developers: CTBC Bank Glory Gorilla Technology Guangzhou Pixel Solutions Imagus Technology Incode Technologies Lomonosov Moscow State University Rank One Computing Samtech InfoNet Shanghai Ulucu Electronics Technology Synesis, and Winsense.
- ▷ We have dropped results from this edition of the report per policy to only list results for two algorithms per developer: glory-000, gorilla-002, incode-003, rankone-006, and synesis-004.
- ▷ Results for five recently submitted algorithms will appear in the next report.

Changes since September 11, 2019:

- ▷ The report adds results for five new participants: Awidit Systems (Awiros), Momentum Digital (Sertis), Trueface AI, Shanghai Jiao Tong University, and X-Laboratory.

- ▷ The report adds results for five new algorithms from returning developers: Cyberlink, Hengrui AI Technology, Idemia, Panasonic R+D Singapore, and Tevian. This causes three algorithm, to be de-listed from the report per policy to list results for two algorithms per developer.

Changes since July 31 2019:

- ▷ The HTML table on the [FRVT 1:1 homepage](#) has been updated to include a column for cross-domain Visa-Border verification. Results for this new dataset appeared in the July 29 report under the name "CrossEV" - these are now renamed "Visa-Border".
- ▷ The [FRVT 1:1 homepage](#) lists algorithms according to lowest mean rank accuracy:

$$\begin{aligned} &\text{Rank(FNMR}_{\text{VISA}} \text{ at FMR = 0.000001}) + \\ &\text{Rank(FNMR}_{\text{VISA-BORDER}} \text{ at FMR = 0.000001}) + \\ &\text{Rank(FNMR}_{\text{MUGSHOT}} \text{ at FMR = 0.00001 after 14 years}) + \\ &\text{Rank(FNMR}_{\text{WILD}} \text{ at FMR = 0.00001}) \end{aligned}$$

This ordering rewards high accuracy across all datasets.
- ▷ The main results in Table 24 is now in landscape format to accomodate extra columns for the Visa-Border set, and mugshot comparisons after at least 12 years.
- ▷ The report adds results for nine new participants: Alpha SSTG, Intel Research, ULSee, Chungwa Telecon, iSAP Solution, Rokid, Shenzhen EI Networks, CSA Intellicloud, Shenzhen Intellifusion Technologies.
- ▷ The reports adds results for six new algorithms from returning developers: Innovatrics, Dahua Technology, Tech5 SA, Intellivision, Nodeflux and Imperial College, London. One algorithm, from Imperial has been retired, per policy to list results for two algorithms per developer.
- ▷ The cross-country false match rate heatmaps have been replotted to reveal more structure by listing countries by region instead of alphabetically.
- ▷ The next version of this report will be posted around October 18, 2019.

Changes since July 3 2019:

- ▷ The HTML table on the [FRVT 1:1 homepage](#) has been updated to list the 20 most accurate developers rather than algorithms, choosing the most accurate algorithm from each developer based on visa and mugshot results. Also, the algorithms are ordered in terms of lowest mean rank across mugshot, visa and wild datasets, rewarding broad accuracy over a good result on one particular dataset.
- ▷ This report includes results for a new dataset - see the column labelled "visa-border" in Table 5. It compares a new set of high quality visa-like portraits with a set webcam border-crossing photos that exhibit moderately poor pose variations and background illumination. The two new sets are described in sections 2.2 and 2.3. The comparisons are "cross-domain" in that the algorithm must compare "visa" and "wild" images. Results for other algorithms will be added in future reports as they become available.
- ▷ This report adds results for algorithms from 9 developers submitted in early July 2019. These are from 3DiVi, Camvi, EverAI-Paravision, Facesoft, Farbar (F8), Institute of Information Technologies, Shanghai U. Film Academy, Via Technologies, and Ulucu Electronics Tech. Six of these are new participants.
- ▷ Several other algorithms have been submitted and are being evaluated. Results will be released in the next report, scheduled for September 5. That report will include results for new datasets.
- ▷ Older algorithms from Everai, Camvi and 3DiVi, have been retired, per the policy to list only two algorithms per developer.

Changes since June 20 2019:

- ▷ This report adds results for algorithms from 18 developers submitted in early June 2019. These are from CTBC Bank, Deep Glint, Thales Cogent, Ever AI Paravision, Gorilla Technology, Imagus, Incode, Kneron, N-Tech Lab, Neurotechnology, Notiontag Technologies, Star Hybrid, Videonetics, Vigilant Solutions, Winsense, Anke Investments, CEIEC, and DSK. Nine of these are new participants.

- ▷ Several other algorithms have been submitted and are being evaluated. Results will be released in the next report, scheduled for August 1.
- ▷ Older algorithms from Everai, Thales Cogent, Gorilla Technology, Incode, Neurotechnology, N-Tech Lab and Vigilant Solutions have been retired, per the policy to list only two algorithms per developer.

Changes since April 2019:

- ▷ This report adds results for nine algorithms from nine developers submitted in early June 2019. These are from Tencent Deepsea, Hengrui, Kedacom, Moontime, Guangzhou Pixel, Rank One Computing, Synesis, Sensetime and Vocord.
- ▷ Another 23 algorithms have been submitted and are being evaluated. Results will be released in the next report, scheduled for July 3.
- ▷ Older algorithms for Rank One, Synesis, and Vocord have been retired, per the policy to list only two algorithms per developer.

Changes since February 2019:

- ▷ This report adds results for 49 algorithms from 42 developers submitted in early March 2019.
- ▷ This report omits results for algorithms that we retired. We retired for three reasons: 1. The developer submitted a new algorithm, and we only list two. 2. The algorithm needs a GPU, and we no longer allow GPU-based algorithms. 3. Inoperable algorithms.
- ▷ Previous results for retired algorithms are available in older editions of this report linked [here](#).
- ▷ The mugshot database used from February 2017 to January 2019 has been replaced with an extract of the mugshot database documented in NIST Interagency Report 8238, November 2018. The new mugshot set is described in section [2.4](#) and is adopted because:
 - ▷▷ It has much better identity label integrity, so that false non-match rates are substantially lower than those reported in FRVT 1:1 reports to date - see Figure [75](#).
 - ▷▷ It includes images collected over a 17 year period such that ageing can be much better characterized - - see Figure [270](#).
- ▷ Using the new mugshot database, Figure [270](#) shows accuracy for four demographic groups identified in the biographic metadata that accompanies the data: black females, black males, white females and white males.
- ▷ The report adds Figure [19](#) with results for the twenty human-difficult pairs used in the May 2018 paper *Face recognition accuracy of forensic examiners, superrecognizers, and face recognition algorithms* by Phillips et al. [[1](#)].
- ▷ The report uses an update to the wild image database that corrects some ground truth labels.
- ▷ Some results for the child exploitation database are not complete. They are typically updated less frequently than for other image sets.

Contents

ACKNOWLEDGMENTS	1
DISCLAIMER	1
INSTITUTIONAL REVIEW BOARD	1
1 METRICS	44
1.1 CORE ACCURACY	44
2 DATASETS	45
2.1 VISA IMAGES	45
2.2 APPLICATION IMAGES	45
2.3 BORDER CROSSING IMAGES	45
2.4 MUGSHOT IMAGES	46
2.5 WILD IMAGES	46
3 RESULTS	46
3.1 TEST GOALS	46
3.2 TEST DESIGN	47
3.3 FAILURE TO ENROLL	50
3.4 RECOGNITION ACCURACY	57
3.5 GENUINE DISTRIBUTION STABILITY	271
3.5.1 EFFECT OF BIRTH PLACE ON THE GENUINE DISTRIBUTION	271
3.5.2 EFFECT OF AGEING	303
3.5.3 EFFECT OF AGE ON GENUINE SUBJECTS	327
3.6 IMPOSTOR DISTRIBUTION STABILITY	360
3.6.1 EFFECT OF BIRTH PLACE ON THE IMPOSTOR DISTRIBUTION	360
3.6.2 EFFECT OF AGE ON IMPOSTORS	364

List of Tables

1 PARTICIPANT INFORMATION	18
2 PARTICIPANT INFORMATION	19
3 PARTICIPANT INFORMATION	20
4 PARTICIPANT INFORMATION	21
5 PARTICIPANT INFORMATION	22
6 PARTICIPANT INFORMATION	23
7 ALGORITHM SUMMARY	24
8 ALGORITHM SUMMARY	25
9 ALGORITHM SUMMARY	26
10 ALGORITHM SUMMARY	27
11 ALGORITHM SUMMARY	28
12 ALGORITHM SUMMARY	29
13 ALGORITHM SUMMARY	30
14 ALGORITHM SUMMARY	31
15 ALGORITHM SUMMARY	32
16 FALSE NON-MATCH RATE	33
17 FALSE NON-MATCH RATE	34
18 FALSE NON-MATCH RATE	35
19 FALSE NON-MATCH RATE	36
20 FALSE NON-MATCH RATE	37
21 FALSE NON-MATCH RATE	38

22	FALSE NON-MATCH RATE	39
23	FALSE NON-MATCH RATE	40
24	FALSE NON-MATCH RATE	41
25	FAILURE TO ENROL RATES	50
26	FAILURE TO ENROL RATES	51
27	FAILURE TO ENROL RATES	52
28	FAILURE TO ENROL RATES	53
29	FAILURE TO ENROL RATES	54
30	FAILURE TO ENROL RATES	55
31	FAILURE TO ENROL RATES	56

List of Figures

1	PERFORMANCE SUMMARY: FNMR VS. TEMPLATE SIZE TRADEOFF	42
2	PERFORMANCE SUMMARY: FNMR VS. TEMPLATE TIME TRADEOFF	43
3	EXAMPLE IMAGES	47
(A)	VISA	47
(B)	MUGSHOT	47
(C)	WILD	47
(D)	BORDER	47
4	PERFORMANCE ON 20 HUMAN-DIFFICULT PAIRS	58
5	PERFORMANCE ON 20 HUMAN-DIFFICULT PAIRS	59
6	PERFORMANCE ON 20 HUMAN-DIFFICULT PAIRS	60
7	PERFORMANCE ON 20 HUMAN-DIFFICULT PAIRS	61
8	PERFORMANCE ON 20 HUMAN-DIFFICULT PAIRS	62
9	PERFORMANCE ON 20 HUMAN-DIFFICULT PAIRS	63
10	PERFORMANCE ON 20 HUMAN-DIFFICULT PAIRS	64
11	PERFORMANCE ON 20 HUMAN-DIFFICULT PAIRS	65
12	PERFORMANCE ON 20 HUMAN-DIFFICULT PAIRS	66
13	PERFORMANCE ON 20 HUMAN-DIFFICULT PAIRS	67
14	PERFORMANCE ON 20 HUMAN-DIFFICULT PAIRS	68
15	PERFORMANCE ON 20 HUMAN-DIFFICULT PAIRS	69
16	PERFORMANCE ON 20 HUMAN-DIFFICULT PAIRS	70
17	PERFORMANCE ON 20 HUMAN-DIFFICULT PAIRS	71
18	PERFORMANCE ON 20 HUMAN-DIFFICULT PAIRS	72
19	PERFORMANCE ON 20 HUMAN-DIFFICULT PAIRS	73
20	ERROR TRADEOFF CHARACTERISTIC: VISA IMAGES	74
21	ERROR TRADEOFF CHARACTERISTIC: VISA IMAGES	75
22	ERROR TRADEOFF CHARACTERISTIC: VISA IMAGES	76
23	ERROR TRADEOFF CHARACTERISTIC: VISA IMAGES	77
24	ERROR TRADEOFF CHARACTERISTIC: VISA IMAGES	78
25	ERROR TRADEOFF CHARACTERISTIC: VISA IMAGES	79
26	ERROR TRADEOFF CHARACTERISTIC: VISA IMAGES	80
27	ERROR TRADEOFF CHARACTERISTIC: VISA IMAGES	81
28	ERROR TRADEOFF CHARACTERISTIC: VISA IMAGES	82
29	ERROR TRADEOFF CHARACTERISTIC: VISA IMAGES	83
30	ERROR TRADEOFF CHARACTERISTIC: VISA IMAGES	84
31	ERROR TRADEOFF CHARACTERISTIC: VISA IMAGES	85
32	ERROR TRADEOFF CHARACTERISTIC: VISA IMAGES	86
33	ERROR TRADEOFF CHARACTERISTIC: VISA IMAGES	87
34	ERROR TRADEOFF CHARACTERISTIC: VISA IMAGES	88
35	ERROR TRADEOFF CHARACTERISTIC: VISA IMAGES	89
36	ERROR TRADEOFF CHARACTERISTIC: VISA IMAGES	90
37	ERROR TRADEOFF CHARACTERISTIC: VISA IMAGES	91
38	ERROR TRADEOFF CHARACTERISTIC: VISA IMAGES	92

39	ERROR TRADEOFF CHARACTERISTIC: VISA IMAGES	93
40	ERROR TRADEOFF CHARACTERISTIC: VISA IMAGES	94
41	ERROR TRADEOFF CHARACTERISTIC: VISA IMAGES	95
42	ERROR TRADEOFF CHARACTERISTIC: VISA IMAGES	96
43	ERROR TRADEOFF CHARACTERISTIC: VISA IMAGES	97
44	ERROR TRADEOFF CHARACTERISTIC: VISA IMAGES	98
45	ERROR TRADEOFF CHARACTERISTIC: VISA IMAGES	99
46	ERROR TRADEOFF CHARACTERISTIC: VISA IMAGES	100
47	ERROR TRADEOFF CHARACTERISTIC: VISA IMAGES	101
48	ERROR TRADEOFF CHARACTERISTIC: VISA IMAGES	102
49	ERROR TRADEOFF CHARACTERISTIC: VISA IMAGES	103
50	ERROR TRADEOFF CHARACTERISTIC: VISA IMAGES	104
51	ERROR TRADEOFF CHARACTERISTIC: VISA IMAGES	105
52	ERROR TRADEOFF CHARACTERISTIC: VISA IMAGES	106
53	ERROR TRADEOFF CHARACTERISTIC: VISA IMAGES	107
54	ERROR TRADEOFF CHARACTERISTIC: VISA IMAGES	108
55	ERROR TRADEOFF CHARACTERISTIC: VISA IMAGES	109
56	ERROR TRADEOFF CHARACTERISTIC: VISA IMAGES	110
57	ERROR TRADEOFF CHARACTERISTIC: MUGSHOT IMAGES	111
58	ERROR TRADEOFF CHARACTERISTIC: MUGSHOT IMAGES	112
59	ERROR TRADEOFF CHARACTERISTIC: MUGSHOT IMAGES	113
60	ERROR TRADEOFF CHARACTERISTIC: MUGSHOT IMAGES	114
61	ERROR TRADEOFF CHARACTERISTIC: MUGSHOT IMAGES	115
62	ERROR TRADEOFF CHARACTERISTIC: MUGSHOT IMAGES	116
63	ERROR TRADEOFF CHARACTERISTIC: MUGSHOT IMAGES	117
64	ERROR TRADEOFF CHARACTERISTIC: MUGSHOT IMAGES	118
65	ERROR TRADEOFF CHARACTERISTIC: MUGSHOT IMAGES	119
66	ERROR TRADEOFF CHARACTERISTIC: MUGSHOT IMAGES	120
67	ERROR TRADEOFF CHARACTERISTIC: MUGSHOT IMAGES	121
68	ERROR TRADEOFF CHARACTERISTIC: MUGSHOT IMAGES	122
69	ERROR TRADEOFF CHARACTERISTIC: MUGSHOT IMAGES	123
70	ERROR TRADEOFF CHARACTERISTIC: MUGSHOT IMAGES	124
71	ERROR TRADEOFF CHARACTERISTIC: MUGSHOT IMAGES	125
72	ERROR TRADEOFF CHARACTERISTIC: MUGSHOT IMAGES	126
73	ERROR TRADEOFF CHARACTERISTIC: MUGSHOT IMAGES	127
74	ERROR TRADEOFF CHARACTERISTIC: MUGSHOT IMAGES	128
75	ERROR TRADEOFF CHARACTERISTIC: MUGSHOT IMAGES	129
76	ERROR TRADEOFF CHARACTERISTIC: WILD IMAGES	130
77	ERROR TRADEOFF CHARACTERISTIC: WILD IMAGES	131
78	ERROR TRADEOFF CHARACTERISTIC: WILD IMAGES	132
79	ERROR TRADEOFF CHARACTERISTIC: WILD IMAGES	133
80	ERROR TRADEOFF CHARACTERISTIC: WILD IMAGES	134
81	ERROR TRADEOFF CHARACTERISTIC: WILD IMAGES	135
82	ERROR TRADEOFF CHARACTERISTIC: WILD IMAGES	136
83	ERROR TRADEOFF CHARACTERISTIC: WILD IMAGES	137
84	ERROR TRADEOFF CHARACTERISTIC: WILD IMAGES	138
85	ERROR TRADEOFF CHARACTERISTIC: WILD IMAGES	139
86	ERROR TRADEOFF CHARACTERISTIC: WILD IMAGES	140
87	ERROR TRADEOFF CHARACTERISTIC: WILD IMAGES	141
88	ERROR TRADEOFF CHARACTERISTIC: WILD IMAGES	142
89	ERROR TRADEOFF CHARACTERISTIC: WILD IMAGES	143
90	ERROR TRADEOFF CHARACTERISTIC: WILD IMAGES	144
91	ERROR TRADEOFF CHARACTERISTIC: WILD IMAGES	145
92	FALSE MATCH RATES WITHIN AND ACROSS DEMOGRAPHIC GROUPS	146
93	FALSE MATCH RATES WITHIN AND ACROSS DEMOGRAPHIC GROUPS	147
94	FALSE MATCH RATES WITHIN AND ACROSS DEMOGRAPHIC GROUPS	148
95	FALSE MATCH RATES WITHIN AND ACROSS DEMOGRAPHIC GROUPS	149

96	FALSE MATCH RATES WITHIN AND ACROSS DEMOGRAPHIC GROUPS	150
97	FALSE MATCH RATES WITHIN AND ACROSS DEMOGRAPHIC GROUPS	151
98	FALSE MATCH RATES WITHIN AND ACROSS DEMOGRAPHIC GROUPS	152
99	FALSE MATCH RATES WITHIN AND ACROSS DEMOGRAPHIC GROUPS	153
100	FALSE MATCH RATES WITHIN AND ACROSS DEMOGRAPHIC GROUPS	154
101	FALSE MATCH RATES WITHIN AND ACROSS DEMOGRAPHIC GROUPS	155
102	FALSE MATCH RATES WITHIN AND ACROSS DEMOGRAPHIC GROUPS	156
103	FALSE MATCH RATES WITHIN AND ACROSS DEMOGRAPHIC GROUPS	157
104	FALSE MATCH RATES WITHIN AND ACROSS DEMOGRAPHIC GROUPS	158
105	FALSE MATCH RATES WITHIN AND ACROSS DEMOGRAPHIC GROUPS	159
106	FALSE MATCH RATES WITHIN AND ACROSS DEMOGRAPHIC GROUPS	160
107	FALSE MATCH RATES WITHIN AND ACROSS DEMOGRAPHIC GROUPS	161
108	FALSE MATCH RATES WITHIN AND ACROSS DEMOGRAPHIC GROUPS	162
109	FALSE MATCH RATES WITHIN AND ACROSS DEMOGRAPHIC GROUPS	163
110	FALSE MATCH RATES WITHIN AND ACROSS DEMOGRAPHIC GROUPS	164
111	SEX AND RACE EFFECTS: MUGSHOT IMAGES	165
112	SEX AND RACE EFFECTS: MUGSHOT IMAGES	166
113	SEX AND RACE EFFECTS: MUGSHOT IMAGES	167
114	SEX AND RACE EFFECTS: MUGSHOT IMAGES	168
115	SEX AND RACE EFFECTS: MUGSHOT IMAGES	169
116	SEX AND RACE EFFECTS: MUGSHOT IMAGES	170
117	SEX AND RACE EFFECTS: MUGSHOT IMAGES	171
118	SEX AND RACE EFFECTS: MUGSHOT IMAGES	172
119	SEX AND RACE EFFECTS: MUGSHOT IMAGES	173
120	SEX AND RACE EFFECTS: MUGSHOT IMAGES	174
121	SEX AND RACE EFFECTS: MUGSHOT IMAGES	175
122	SEX AND RACE EFFECTS: MUGSHOT IMAGES	176
123	SEX AND RACE EFFECTS: MUGSHOT IMAGES	177
124	SEX AND RACE EFFECTS: MUGSHOT IMAGES	178
125	SEX AND RACE EFFECTS: MUGSHOT IMAGES	179
126	SEX AND RACE EFFECTS: MUGSHOT IMAGES	180
127	SEX AND RACE EFFECTS: MUGSHOT IMAGES	181
128	SEX AND RACE EFFECTS: MUGSHOT IMAGES	182
129	SEX AND RACE EFFECTS: MUGSHOT IMAGES	183
130	SEX EFFECTS: VISA IMAGES	184
131	SEX EFFECTS: VISA IMAGES	185
132	SEX EFFECTS: VISA IMAGES	186
133	SEX EFFECTS: VISA IMAGES	187
134	SEX EFFECTS: VISA IMAGES	188
135	SEX EFFECTS: VISA IMAGES	189
136	SEX EFFECTS: VISA IMAGES	190
137	SEX EFFECTS: VISA IMAGES	191
138	SEX EFFECTS: VISA IMAGES	192
139	SEX EFFECTS: VISA IMAGES	193
140	SEX EFFECTS: VISA IMAGES	194
141	SEX EFFECTS: VISA IMAGES	195
142	SEX EFFECTS: VISA IMAGES	196
143	SEX EFFECTS: VISA IMAGES	197
144	SEX EFFECTS: VISA IMAGES	198
145	SEX EFFECTS: VISA IMAGES	199
146	SEX EFFECTS: VISA IMAGES	200
147	SEX EFFECTS: VISA IMAGES	201
148	SEX EFFECTS: VISA IMAGES	202
149	SEX EFFECTS: VISA IMAGES	203
150	SEX EFFECTS: VISA IMAGES	204
151	SEX EFFECTS: VISA IMAGES	205
152	SEX EFFECTS: VISA IMAGES	206

153	SEX EFFECTS: VISA IMAGES	207
154	SEX EFFECTS: VISA IMAGES	208
155	SEX EFFECTS: VISA IMAGES	209
156	SEX EFFECTS: VISA IMAGES	210
157	SEX EFFECTS: VISA IMAGES	211
158	SEX EFFECTS: VISA IMAGES	212
159	SEX EFFECTS: VISA IMAGES	213
160	SEX EFFECTS: VISA IMAGES	214
161	FALSE MATCH RATE CALIBRATION: MUGSHOT IMAGES	215
162	FALSE MATCH RATE CALIBRATION: MUGSHOT IMAGES	216
163	FALSE MATCH RATE CALIBRATION: MUGSHOT IMAGES	217
164	FALSE MATCH RATE CALIBRATION: MUGSHOT IMAGES	218
165	FALSE MATCH RATE CALIBRATION: MUGSHOT IMAGES	219
166	FALSE MATCH RATE CALIBRATION: MUGSHOT IMAGES	220
167	FALSE MATCH RATE CALIBRATION: MUGSHOT IMAGES	221
168	FALSE MATCH RATE CALIBRATION: MUGSHOT IMAGES	222
169	FALSE MATCH RATE CALIBRATION: MUGSHOT IMAGES	223
170	FALSE MATCH RATE CALIBRATION: MUGSHOT IMAGES	224
171	FALSE MATCH RATE CALIBRATION: MUGSHOT IMAGES	225
172	FALSE MATCH RATE CALIBRATION: MUGSHOT IMAGES	226
173	FALSE MATCH RATE CALIBRATION: MUGSHOT IMAGES	227
174	FALSE MATCH RATE CALIBRATION: MUGSHOT IMAGES	228
175	FALSE MATCH RATE CALIBRATION: MUGSHOT IMAGES	229
176	FALSE MATCH RATE CALIBRATION: MUGSHOT IMAGES	230
177	FALSE MATCH RATE CALIBRATION: MUGSHOT IMAGES	231
178	FALSE MATCH RATE CALIBRATION: MUGSHOT IMAGES	232
179	FALSE MATCH RATE CALIBRATION: MUGSHOT IMAGES	233
180	FALSE MATCH RATE CALIBRATION: VISA IMAGES	234
181	FALSE MATCH RATE CALIBRATION: VISA IMAGES	235
182	FALSE MATCH RATE CALIBRATION: VISA IMAGES	236
183	FALSE MATCH RATE CALIBRATION: VISA IMAGES	237
184	FALSE MATCH RATE CALIBRATION: VISA IMAGES	238
185	FALSE MATCH RATE CALIBRATION: VISA IMAGES	239
186	FALSE MATCH RATE CALIBRATION: VISA IMAGES	240
187	FALSE MATCH RATE CALIBRATION: VISA IMAGES	241
188	FALSE MATCH RATE CALIBRATION: VISA IMAGES	242
189	FALSE MATCH RATE CALIBRATION: VISA IMAGES	243
190	FALSE MATCH RATE CALIBRATION: VISA IMAGES	244
191	FALSE MATCH RATE CALIBRATION: VISA IMAGES	245
192	FALSE MATCH RATE CALIBRATION: VISA IMAGES	246
193	FALSE MATCH RATE CALIBRATION: VISA IMAGES	247
194	FALSE MATCH RATE CALIBRATION: VISA IMAGES	248
195	FALSE MATCH RATE CALIBRATION: VISA IMAGES	249
196	FALSE MATCH RATE CALIBRATION: VISA IMAGES	250
197	FALSE MATCH RATE CALIBRATION: VISA IMAGES	251
198	FALSE MATCH RATE CALIBRATION: VISA IMAGES	252
199	FALSE MATCH RATE CALIBRATION: VISA IMAGES	253
200	FALSE MATCH RATE CALIBRATION: VISA IMAGES	254
201	FALSE MATCH RATE CALIBRATION: VISA IMAGES	255
202	FALSE MATCH RATE CALIBRATION: VISA IMAGES	256
203	FALSE MATCH RATE CALIBRATION: VISA IMAGES	257
204	FALSE MATCH RATE CALIBRATION: VISA IMAGES	258
205	FALSE MATCH RATE CALIBRATION: VISA IMAGES	259
206	FALSE MATCH RATE CALIBRATION: VISA IMAGES	260
207	FALSE MATCH RATE CALIBRATION: VISA IMAGES	261
208	FALSE MATCH RATE CALIBRATION: VISA IMAGES	262
209	FALSE MATCH RATE CALIBRATION: VISA IMAGES	263

210	FALSE MATCH RATE CALIBRATION: VISA IMAGES	264
211	FALSE MATCH RATE CALIBRATION: VISA IMAGES	265
212	FALSE MATCH RATE CALIBRATION: VISA IMAGES	266
213	FALSE MATCH RATE CALIBRATION: VISA IMAGES	267
214	FALSE MATCH RATE CALIBRATION: VISA IMAGES	268
215	FALSE MATCH RATE CALIBRATION: VISA IMAGES	269
216	FALSE MATCH RATE CALIBRATION: VISA IMAGES	270
217	EFFECT OF COUNTRY OF BIRTH ON FNMR	272
218	EFFECT OF COUNTRY OF BIRTH ON FNMR	273
219	EFFECT OF COUNTRY OF BIRTH ON FNMR	274
220	EFFECT OF COUNTRY OF BIRTH ON FNMR	275
221	EFFECT OF COUNTRY OF BIRTH ON FNMR	276
222	EFFECT OF COUNTRY OF BIRTH ON FNMR	277
223	EFFECT OF COUNTRY OF BIRTH ON FNMR	278
224	EFFECT OF COUNTRY OF BIRTH ON FNMR	279
225	EFFECT OF COUNTRY OF BIRTH ON FNMR	280
226	EFFECT OF COUNTRY OF BIRTH ON FNMR	281
227	EFFECT OF COUNTRY OF BIRTH ON FNMR	282
228	EFFECT OF COUNTRY OF BIRTH ON FNMR	283
229	EFFECT OF COUNTRY OF BIRTH ON FNMR	284
230	EFFECT OF COUNTRY OF BIRTH ON FNMR	285
231	EFFECT OF COUNTRY OF BIRTH ON FNMR	286
232	EFFECT OF COUNTRY OF BIRTH ON FNMR	287
233	EFFECT OF COUNTRY OF BIRTH ON FNMR	288
234	EFFECT OF COUNTRY OF BIRTH ON FNMR	289
235	EFFECT OF COUNTRY OF BIRTH ON FNMR	290
236	EFFECT OF COUNTRY OF BIRTH ON FNMR	291
237	EFFECT OF COUNTRY OF BIRTH ON FNMR	292
238	EFFECT OF COUNTRY OF BIRTH ON FNMR	293
239	EFFECT OF COUNTRY OF BIRTH ON FNMR	294
240	EFFECT OF COUNTRY OF BIRTH ON FNMR	295
241	EFFECT OF COUNTRY OF BIRTH ON FNMR	296
242	EFFECT OF COUNTRY OF BIRTH ON FNMR	297
243	EFFECT OF COUNTRY OF BIRTH ON FNMR	298
244	EFFECT OF COUNTRY OF BIRTH ON FNMR	299
245	EFFECT OF COUNTRY OF BIRTH ON FNMR	300
246	EFFECT OF COUNTRY OF BIRTH ON FNMR	301
247	EFFECT OF COUNTRY OF BIRTH ON FNMR	302
248	ERROR TRADEOFF CHARACTERISTIC: MUGSHOT IMAGES	304
249	ERROR TRADEOFF CHARACTERISTIC: MUGSHOT IMAGES	305
250	ERROR TRADEOFF CHARACTERISTIC: MUGSHOT IMAGES	306
251	ERROR TRADEOFF CHARACTERISTIC: MUGSHOT IMAGES	307
252	ERROR TRADEOFF CHARACTERISTIC: MUGSHOT IMAGES	308
253	ERROR TRADEOFF CHARACTERISTIC: MUGSHOT IMAGES	309
254	ERROR TRADEOFF CHARACTERISTIC: MUGSHOT IMAGES	310
255	ERROR TRADEOFF CHARACTERISTIC: MUGSHOT IMAGES	311
256	ERROR TRADEOFF CHARACTERISTIC: MUGSHOT IMAGES	312
257	ERROR TRADEOFF CHARACTERISTIC: MUGSHOT IMAGES	313
258	ERROR TRADEOFF CHARACTERISTIC: MUGSHOT IMAGES	314
259	ERROR TRADEOFF CHARACTERISTIC: MUGSHOT IMAGES	315
260	ERROR TRADEOFF CHARACTERISTIC: MUGSHOT IMAGES	316
261	ERROR TRADEOFF CHARACTERISTIC: MUGSHOT IMAGES	317
262	ERROR TRADEOFF CHARACTERISTIC: MUGSHOT IMAGES	318
263	ERROR TRADEOFF CHARACTERISTIC: MUGSHOT IMAGES	319
264	ERROR TRADEOFF CHARACTERISTIC: MUGSHOT IMAGES	320
265	ERROR TRADEOFF CHARACTERISTIC: MUGSHOT IMAGES	321
266	ERROR TRADEOFF CHARACTERISTIC: MUGSHOT IMAGES	322

267	ERROR TRADEOFF CHARACTERISTIC: MUGSHOT IMAGES	323
268	ERROR TRADEOFF CHARACTERISTIC: MUGSHOT IMAGES	324
269	ERROR TRADEOFF CHARACTERISTIC: MUGSHOT IMAGES	325
270	ERROR TRADEOFF CHARACTERISTIC: MUGSHOT IMAGES	326
271	EFFECT OF SUBJECT AGE ON FNMR	328
272	EFFECT OF SUBJECT AGE ON FNMR	329
273	EFFECT OF SUBJECT AGE ON FNMR	330
274	EFFECT OF SUBJECT AGE ON FNMR	331
275	EFFECT OF SUBJECT AGE ON FNMR	332
276	EFFECT OF SUBJECT AGE ON FNMR	333
277	EFFECT OF SUBJECT AGE ON FNMR	334
278	EFFECT OF SUBJECT AGE ON FNMR	335
279	EFFECT OF SUBJECT AGE ON FNMR	336
280	EFFECT OF SUBJECT AGE ON FNMR	337
281	EFFECT OF SUBJECT AGE ON FNMR	338
282	EFFECT OF SUBJECT AGE ON FNMR	339
283	EFFECT OF SUBJECT AGE ON FNMR	340
284	EFFECT OF SUBJECT AGE ON FNMR	341
285	EFFECT OF SUBJECT AGE ON FNMR	342
286	EFFECT OF SUBJECT AGE ON FNMR	343
287	EFFECT OF SUBJECT AGE ON FNMR	344
288	EFFECT OF SUBJECT AGE ON FNMR	345
289	EFFECT OF SUBJECT AGE ON FNMR	346
290	EFFECT OF SUBJECT AGE ON FNMR	347
291	EFFECT OF SUBJECT AGE ON FNMR	348
292	EFFECT OF SUBJECT AGE ON FNMR	349
293	EFFECT OF SUBJECT AGE ON FNMR	350
294	EFFECT OF SUBJECT AGE ON FNMR	351
295	EFFECT OF SUBJECT AGE ON FNMR	352
296	EFFECT OF SUBJECT AGE ON FNMR	353
297	EFFECT OF SUBJECT AGE ON FNMR	354
298	EFFECT OF SUBJECT AGE ON FNMR	355
299	EFFECT OF SUBJECT AGE ON FNMR	356
300	EFFECT OF SUBJECT AGE ON FNMR	357
301	EFFECT OF SUBJECT AGE ON FNMR	358
302	WORST CASE REGIONAL EFFECT FNMR	361
303	IMPOSTOR DISTRIBUTION SHIFTS FOR SELECT COUNTRY PAIRS	363

	Location	Developer Name	Short Name	Seq. Num.	Validation Date
1	NL	20Face	20face-000	000	2021-04-12
2	NL	20Face	20face-001	001	2021-09-29
3	US	3Divi	3divi-006	006	2021-04-14
4	US	3Divi	3divi-007	007	2021-09-27
5	TH	ACI Software	acisw-003	003	2020-08-03
6	TH	ACI Software	acisw-006	006	2021-02-25
7	SG	ADVANCE.AI	advance-002	002	2019-12-19
8	SG	ADVANCE.AI	advance-003	003	2021-08-05
9	TW	ASUSTek Computer Inc	asusaics-000	000	2019-10-24
10	TW	ASUSTek Computer Inc	asusaics-001	001	2020-02-25
11	CN	AYF Technology	ayftech-001	001	2020-07-06
12	TW	Ability Enterprise - Andro Video	androvideo-000	000	2021-01-25
13	TW	Acer Incorporated	acer-001	001	2020-06-30
14	TW	Acer Incorporated	acer-002	002	2021-11-10
15	SG	Adera Global PTE	adera-002	002	2021-02-16
16	SG	Adera Global PTE	adera-003	003	2021-07-12
17	TH	Ai First	aifirst-001	001	2019-11-21
18	TW	AiUnion Technology	aiunionface-000	000	2019-10-22
19	TH	Aigen	aigen-001	001	2020-10-06
20	TH	Aigen	aigen-002	002	2021-03-15
21	KR	Ajou University	ajou-001	001	2021-03-08
22	ID	Akurat Satu Indonesia	ptakuratsatu-000	000	2020-09-11
23	KR	Alchera Inc	alchera-002	002	2021-03-05
24	KR	Alchera Inc	alchera-003	003	2021-07-13
25	ES	Alice Biometrics	alice-000	000	2021-06-15
26	RU	Alivia / Innovation Sys	isystems-001	001	2018-06-12
27	RU	Alivia / Innovation Sys	isystems-002	002	2018-10-18
28	IN	AllGoVision	allgovision-000	000	2019-03-01
29	CN	AlphaSSTG	alphaface-001	001	2019-09-03
30	CN	AlphaSSTG	alphaface-002	002	2020-02-20
31	GB	Amplified Group	amplifiedgroup-001	001	2019-03-01
32	CN	Anke Investments	anke-004	004	2019-06-27
33	CN	Anke Investments	anke-005	005	2019-11-21
34	BR	Antheus Technologia	antheus-000	000	2019-12-05
35	BR	Antheus Technologia	antheus-001	001	2020-06-25
36	GB	AnyVision	anyvision-004	004	2018-06-15
37	GB	AnyVision	anyvision-005	005	2021-02-03
38	CN	AuthenMetric	authenmetric-002	002	2021-03-10
39	CN	AuthenMetric	authenmetric-003	003	2021-08-09
40	US	Aware	aware-005	005	2020-02-27
41	US	Aware	aware-006	006	2021-07-03
42	IN	Awidit Systems	awiros-001	001	2019-09-23
43	IN	Awidit Systems	awiros-002	002	2020-10-28
44	JP	Ayonix	ayonix-000	000	2017-06-22
45	CN	BOE Technology Group	boetech-001	001	2021-06-22
46	ES	Bee the Data	beethedata-000	000	2021-07-26
47	CN	Beihang University-ERCACAT	ercacat-001	001	2020-07-06
48	CN	Beijing Alleyes Technology	alleyes-000	000	2020-03-09
49	CN	Beijing DeepSense Technologies	deepsense-000	000	2021-03-19
50	CN	Beijing Hisign Technology	hisign-001	001	2021-09-24
51	CN	Beijing Mendaxia Technology	mendaxiatech-000	000	2021-09-15
52	CN	Beijing Vion Technology Inc	vion-000	000	2018-10-19
53	CH	BioID Technologies SA	boidtechswiss-001	001	2020-08-28
54	CH	BioID Technologies SA	boidtechswiss-002	002	2021-02-17
55	IN	Biocube Matrics	biocube-001	001	2021-09-08
56	UK	BitCenter UK	farfaces-001	001	2021-04-09
57	CN	Bitmain	bm-001	001	2018-10-17
58	CN	Bresee Technology	bresee-001	001	2020-12-30
59	CN	Bresee Technology	bresee-002	002	2021-06-30
60	CN	CSA IntelliCloud Technology	intellicloudai-001	001	2019-08-13
61	CN	CSA IntelliCloud Technology	intellicloudai-002	002	2020-12-17
62	TW	CTBC Bank	ctbcbank-000	000	2019-06-28
63	TW	CTBC Bank	ctbcbank-001	001	2019-10-28
64	KR	CUDO Communication	cudocommunication-001	001	2021-10-20
65	US	Camvi Technologies	camvi-002	002	2018-10-19
66	US	Camvi Technologies	camvi-004	004	2019-07-12
67	CN	Canon Inc	canon-002	002	2020-12-29
68	JP	Canon Inc	canon-003	003	2021-09-15
69	CN	China Electronics Import-Export Corp	ceiec-003	003	2020-01-06
70	CN	China Electronics Import-Export Corp	ceiec-004	004	2021-01-18

Table 1: Summary of participant information included in this report.

	Location	Developer Name	Short Name	Seq. Num.	Validation Date
71	CN	China University of Petroleum	upc-001	001	2019-06-05
72	CN	Chinese University of Hong Kong	cuhkee-001	001	2020-03-18
73	KR	Chosun University	chosun-001	001	2020-07-01
74	KR	Chosun University	chosun-002	002	2020-11-25
75	TW	Chunghwa Telecom	chtface-003	003	2020-06-24
76	TW	Chunghwa Telecom	chtface-004	004	2021-10-08
77	US	Clearview AI Inc	clearviewai-000	000	2021-09-22
78	CN	Closeli Inc	closeli-001	001	2021-07-15
79	US	CloudSmart Consulting LLC	csc-002	002	2021-03-24
80	US	CloudSmart Consulting LLC	csc-003	003	2021-08-26
81	CN	Cloudwalk - Hengrui AI Technology	cloudwalk-hr-003	003	2020-09-25
82	CN	Cloudwalk - Hengrui AI Technology	cloudwalk-hr-004	004	2021-02-10
83	CN	Cloudwalk - Hengrui AI Technology	cloudwalk-mt-004	004	2021-11-09
84	CN	Cloudwalk - Moontime Smart Technology	cloudwalk-mt-003	003	2020-12-22
85	IN	Code Everest Pvt	facex-001	001	2021-03-08
86	IN	Code Everest Pvt	facex-002	002	2021-08-24
87	DE	Cognitec Systems GmbH	cognitec-002	002	2021-02-24
88	DE	Cognitec Systems GmbH	cognitec-003	003	2021-07-30
89	TW	Coretech Knowledge Inc	coretech-000	000	2021-07-12
90	IL	Corsight	corsight-001	001	2021-03-11
91	IL	Corsight	corsight-002	002	2021-09-01
92	IL	Cortica	cor-001	001	2020-09-24
93	KR	Cubox	cubox-001	001	2020-12-07
94	KR	Cubox	cubox-002	002	2021-08-24
95	JP	Cybercore	cybercore-000	000	2020-08-26
96	US	Cyberextruder	cyberextruder-001	001	2017-08-02
97	US	Cyberextruder	cyberextruder-002	002	2018-01-30
98	TW	Cyberlink Corp	cyberlink-006	006	2021-01-08
99	TW	Cyberlink Corp	cyberlink-007	007	2021-07-16
100	CN	DSK	dsk-000	000	2019-06-28
101	CN	Dahua Technology	dahua-005	005	2020-08-13
102	CN	Dahua Technology	dahua-006	006	2020-12-30
103	IE	Daon	daon-000	000	2021-11-03
104	US	Decatur Industries Inc	decatur-000	000	2020-08-18
105	US	Decatur Industries Inc	decatur-001	001	2021-09-27
106	CN	Deepglint	deepglint-003	003	2021-03-03
107	CN	Deepglint	deepglint-004	004	2021-09-17
108	FR	Deepsense	dps-000	000	2021-07-16
109	DE	Dermalog	dermalog-008	008	2021-03-25
110	DE	Dermalog	dermalog-009	009	2021-10-06
111	CN	DiDi ChuXing Technology	didiglobalface-001	001	2019-10-23
112	GB	Digital Barriers	digitalbarriers-002	002	2019-03-01
113	TR	Ekin Smart City Technologies	ekin-002	002	2021-05-04
114	RU	Enface	enface-000	000	2021-04-09
115	RU	Expasoft LLC	expasoft-001	001	2020-09-03
116	RU	Expasoft LLC	expasoft-002	002	2021-07-26
117	GB	FaceSoft	facesoft-000	000	2019-07-10
118	KR	FaceTag Co	facetag-000	000	2021-03-22
119	KR	FaceTag Co	facetag-001	001	2021-08-17
120	TW	FarBar Inc	f8-001	001	2019-07-11
121	UK	Fincore Ltd	fincore-000	000	2021-06-07
122	CN	Fujitsu Research and Development Center	fujitsulab-002	002	2021-02-24
123	CN	Fujitsu Research and Development Center	fujitsulab-003	003	2021-07-12
124	US	Gemalto Cogent	cogent-005	005	2020-12-29
125	US	Gemalto Cogent	cogent-006	006	2021-07-28
126	TW	GeoVision Inc	geo-002	002	2021-04-01
127	TW	GeoVision Inc	geo-003	003	2021-09-15
128	JP	Glory	glory-002	002	2019-11-12
129	JP	Glory	glory-003	003	2021-01-15
130	TW	Gorilla Technology	gorilla-007	007	2021-06-28
131	TW	Gorilla Technology	gorilla-008	008	2021-11-08
132	US	Griaule	griaule-000	000	2021-08-20
133	CN	Guangzhou Pixel Solutions	pixelall-005	005	2021-02-05
134	CN	Guangzhou Pixel Solutions	pixelall-006	006	2021-06-17
135	ES	Herta Security	hertasecurity-000	000	2021-01-05
136	CN	Hikvision Research Institute	hik-001	001	2019-03-01
137	IN	HyperVerge Inc	hyperverge-001	001	2020-12-13
138	IN	HyperVerge Inc	hyperverge-002	002	2021-05-27
139	AU	ICM Airport Technics	icm-002	002	2020-11-13
140	AU	ICM Airport Technics	icm-003	003	2021-09-06

Table 2: Summary of participant information included in this report.

	Location	Developer Name	Short Name	Seq. Num.	Validation Date
141	FR	ID3 Technology	id3-006	006	2020-12-17
142	FR	ID3 Technology	id3-008	008	2021-11-10
143	RU	ITMO University	itmo-006	006	2019-03-01
144	RU	ITMO University	itmo-007	007	2020-01-06
145	RU	IVA Cognitive	ivacognitive-001	001	2021-01-29
146	FR	Idemia	idemia-007	007	2020-12-04
147	FR	Idemia	idemia-008	008	2021-07-07
148	US	Imageware Systems	iws-000	000	2020-08-12
149	AU	Imagus Technology Pty	imagus-002	002	2020-12-31
150	AU	Imagus Technology Pty	imagus-004	004	2021-09-20
151	GB	Imperial College London	imperial-000	000	2019-03-01
152	GB	Imperial College London	imperial-002	002	2019-08-28
153	US	Incode Technologies Inc	incode-009	009	2021-06-22
154	US	Incode Technologies Inc	incode-010	010	2021-10-22
155	IN	Innef Labs	innefulabs-000	000	2020-09-04
156	GB	Innovative Technology	innovativetechnologyltd-001	001	2019-10-22
157	GB	Innovative Technology	innovativetechnologyltd-002	002	2020-02-26
158	SK	Innovatrics	innovatrics-006	006	2019-08-13
159	SK	Innovatrics	innovatrics-007	007	2020-08-19
160	CN	InsightFace AI	insightface-000	000	2021-03-17
161	CN	InsightFace AI	insightface-001	001	2021-09-27
162	CN	Institute of Computing Technology	ichttc-000	000	2020-11-29
163	RU	Institute of Information Technologies	iit-002	002	2019-12-04
164	RU	Institute of Information Technologies	iit-003	003	2020-12-01
165	IS	Intel Research Group	intelresearch-003	003	2021-01-18
166	IS	Intel Research Group	intelresearch-004	004	2021-08-24
167	US	Intellivision	intellivision-001	001	2017-10-10
168	US	Intellivision	intellivision-002	002	2019-08-23
169	US	IrexAI	irex-000	000	2020-12-17
170	IL	Is It You	isityou-000	000	2017-06-26
171	KR	Kakao Enterprise	kakao-005	005	2021-03-09
172	KR	Kakao Enterprise	kakao-006	006	2021-10-13
173	KR	Kakao Pay Corp	kakaopay-001	001	2021-07-06
174	SG	Kedacom International Pte	kedacom-000	000	2019-06-03
175	US	Kneron Inc	kneron-003	003	2019-07-01
176	US	Kneron Inc	kneron-005	005	2020-02-21
177	KR	Kookmin University	kookmin-002	002	2021-03-05
178	KR	Kookmin University	kookmin-003	003	2021-10-07
179	CN	KuKe3D Technology	kuke3d-001	001	2021-10-28
180	IN	Lema Labs	lemalabs-001	001	2021-04-13
181	JP	Line Corporation	line-000	000	2021-03-31
182	JP	Line Corporation	line-001	001	2021-09-26
183	RU	Lomonosov Moscow State University	intsysmsu-001	001	2019-10-22
184	RU	Lomonosov Moscow State University	intsysmsu-002	002	2020-03-12
185	IN	Lookman Electroplast Industries	lookman-002	002	2018-06-13
186	IN	Lookman Electroplast Industries	lookman-004	004	2019-06-03
187	US	Luxand Inc	luxand-000	000	2019-11-07
188	RU	MVision	mvision-001	001	2019-11-12
189	IN	Mantra Softech India	mantra-000	000	2021-10-28
190	CN	Maxvision Technology	maxvision-000	000	2021-10-27
191	CN	Megvii/Face++	megvii-002	002	2018-10-19
192	CN	Megvii/Face++	megvii-003	003	2021-03-08
193	GB	MicroFocus	microfocus-001	001	2018-06-13
194	GB	MicroFocus	microfocus-002	002	2018-10-17
195	CN	Minivision	minivision-000	000	2020-10-28
196	NO	Mobai	mobai-000	000	2020-08-26
197	NO	Mobai	mobai-001	001	2021-02-17
198	ES	Mobbel Solutions	mobbl-000	000	2021-01-28
199	ES	Mobbel Solutions	mobbl-001	001	2021-06-16
200	TH	Momentum Digital	sertis-000	000	2019-10-07
201	TH	Momentum Digital	sertis-002	002	2021-05-13
202	CN	MoreDian Technology	moredian-000	000	2021-02-24
203	CN	Multi-Modality Intelligence	multimodality-000	000	2021-10-19
204	RU	N-Tech Lab	ntechlab-010	010	2021-04-30
205	RU	N-Tech Lab	ntechlab-011	011	2021-09-13
206	CA	NEO Systems	neosystems-001	001	2021-03-02
207	CA	NEO Systems	neosystems-002	002	2021-07-03
208	KR	NHN Corp	nhn-001	001	2021-03-15
209	KR	NHN Corp	nhn-002	002	2021-07-15
210	KR	NSENSE Corp	nsensecorp-002	002	2021-05-06

Table 3: Summary of participant information included in this report.

	Location	Developer Name	Short Name	Seq. Num.	Validation Date
211	KR	NSENSE Corp	nsensecorp-003	003	2021-10-29
212	CN	Nanjing Kiwi Network Technology	kiwitech-000	000	2021-03-19
213	KR	Naver Corp	clova-000	000	2020-10-21
214	KR	Neosecu Co	openface-001	001	2021-06-15
215	TW	Netbridge Technology Incoporation	netbridgetech-001	001	2020-01-08
216	TW	Netbridge Technology Incoporation	netbridgetech-002	002	2020-08-11
217	LT	Neurotechnology	neurotechnology-011	011	2021-03-26
218	LT	Neurotechnology	neurotechnology-012	012	2021-07-26
219	ID	Nodeflux	nodeflux-002	002	2019-08-13
220	IN	NotionTag Technologies Private Limited	notiontag-001	001	2021-03-04
221	IN	NotionTag Technologies Private Limited	notiontag-002	002	2021-09-17
222	US	Omnigarde Ltd	omnigarde-000	000	2021-04-05
223	US	Omnigarde Ltd	omnigarde-001	001	2021-08-23
224	RU	Oz Forensics LLC	oz-002	002	2021-01-18
225	RU	Oz Forensics LLC	oz-003	003	2021-08-09
226	CH	PXL Vision AG	pxl-001	001	2020-06-30
227	SG	Panasonic R+D Center Singapore	psl-007	007	2021-03-19
228	SG	Panasonic R+D Center Singapore	psl-008	008	2021-07-21
229	TR	Papilon Savunma	papsav1923-001	001	2021-03-10
230	US	Paravision (EverAI)	paravision-004	004	2019-12-11
231	US	Paravision (EverAI)	paravision-008	008	2021-06-30
232	SG	Pensees Pte	pensees-001	001	2020-08-17
233	IN	Pyramid Cyber Security + Forensic (P)	pyramid-000	000	2019-11-04
234	TW	Qnap Security	qnap-000	000	2021-08-09
235	CZ	Quantasoft	quantasoft-003	003	2021-04-19
236	US	Rank One Computing	rankone-010	010	2020-11-05
237	US	Rank One Computing	rankone-011	011	2021-08-27
238	US	Realnetworks Inc	realnetworks-004	004	2021-04-15
239	US	Realnetworks Inc	realnetworks-005	005	2021-09-27
240	US	Regula Forensics	regula-000	000	2021-04-13
241	CN	Remark Holdings	remarkai-001	001	2019-03-01
242	CN	Remark Holdings	remarkai-003	003	2021-06-22
243	SG	Rendip	rendip-000	000	2021-04-19
244	UK	Reveal Media Ltd	revealmedia-005	005	2021-09-24
245	CN	Rokid Corporation	rokid-000	000	2019-08-01
246	CN	Rokid Corporation	rokid-001	001	2019-12-13
247	KR	SK Telecom	sktelecom-000	000	2021-07-09
248	KR	SQIsoft	sqisoft-001	001	2021-07-27
249	KR	SQIsoft	sqisoft-002	002	2021-11-03
250	DE	Saffe	saffe-001	001	2018-10-19
251	DE	Saffe	saffe-002	002	2019-03-01
252	KR	Samsung S1 Corp	s1-002	002	2021-03-24
253	KR	Samsung S1 Corp	s1-003	003	2021-08-24
254	KR	Samsung-SDS	samsungsds-000	000	2021-10-28
255	IN	Samtech InfoNet Limited	samtech-001	001	2019-10-15
256	RU	Satellite Innovation/Eocortex	eocortex-000	000	2020-08-26
257	IL	Scanovate	scanovate-001	001	2019-11-12
258	IL	Scanovate	scanovate-002	002	2020-06-26
259	RO	Securif AI	securifai-001	001	2020-10-06
260	RO	Securif AI	securifai-003	003	2021-08-03
261	CN	Sensetime Group	sensetime-004	004	2020-11-20
262	CN	Sensetime Group	sensetime-005	005	2021-05-24
263	SG	Seventh Sense Artificial Intelligence	seventhsense-000	000	2021-06-29
264	US	Shaman Software	shaman-000	000	2017-12-05
265	US	Shaman Software	shaman-001	001	2018-01-13
266	CN	Shanghai Jiao Tong University	sjtu-003	003	2020-11-02
267	CN	Shanghai Jiao Tong University	sjtu-004	004	2021-05-13
268	CN	Shanghai Ulucu Electronics Technology	uluface-002	002	2019-07-10
269	CN	Shanghai Ulucu Electronics Technology	uluface-003	003	2019-11-12
270	CN	Shanghai University - Shanghai Film Academy	shu-002	002	2019-12-10
271	CN	Shanghai University - Shanghai Film Academy	shu-003	003	2020-06-24
272	CN	Shanghai Yitu Technology	yitu-003	003	2019-03-01
273	CN	Shenzhen AiMall Tech	aimall-002	002	2020-03-12
274	CN	Shenzhen AiMall Tech	aimall-003	003	2020-08-12
275	CN	Shenzhen EI Networks	einetworks-000	000	2019-08-13
276	CN	Shenzhen Inst Adv Integrated Tech CAS	siat-002	002	2018-06-13
277	CN	Shenzhen Inst Adv Integrated Tech CAS	siat-004	004	2019-03-01
278	CN	Shenzhen Intellifusion Technologies	intellifusion-001	001	2019-08-22
279	CN	Shenzhen Intellifusion Technologies	intellifusion-002	002	2020-03-18
280	CN	Shenzhen University-Macau University of Science and Technology	sztu-000	000	2020-12-17

Table 4: Summary of participant information included in this report.

	Location	Developer Name	Short Name	Seq. Num.	Validation Date
281	CN	Shenzhen University-Macau University of Science and Technology	sztu-001	001	2021-07-13
282	RU	Smart Engines	smartengines-000	000	2021-08-25
283	DE	Smilart	smilart-002	002	2018-02-06
284	DE	Smilart	smilart-003	003	2018-06-18
285	TR	Sodec App Inc	sodec-000	000	2021-06-02
286	IN	Staqu Technologies	staqu-000	000	2020-07-15
287	CN	Star Hybrid Limited	starhybrid-001	001	2019-06-19
288	CN	Su Zhou NaZhiTianDi intelligent technology	nazhiai-000	000	2020-06-25
289	KR	Suprema	suprema-000	000	2021-03-31
290	KR	Suprema ID Inc	suprema-001	001	2021-09-23
291	KR	Suprema ID Inc	supremaid-001	001	2021-05-04
292	RU	Synesis	synesis-006	006	2019-10-10
293	RU	Synesis	synesis-007	007	2020-06-24
294	TW	Synology Inc	synology-000	000	2019-10-23
295	TW	Synology Inc	synology-002	002	2020-08-20
296	CN	TUPU Technology	tuputech-000	000	2019-10-11
297	TW	Taiwan AI Labs	ailabs-001	001	2019-12-18
298	TW	Taiwan-Certificate Authority Incorporation	twface-000	000	2021-05-14
299	TW	Taiwan-Certificate Authority Incorporation	twface-001	001	2021-09-14
300	CH	Tech5 SA	tech5-004	004	2020-03-09
301	CH	Tech5 SA	tech5-005	005	2020-07-24
302	TR	Techsign	techsign-000	000	2021-08-25
303	CN	Tencent Deepsea Lab	deepsea-001	001	2019-06-03
304	RU	Tevian	tevian-006	006	2020-09-11
305	RU	Tevian	tevian-007	007	2021-08-06
306	US	TigerIT Americas LLC	tiger-003	003	2018-10-16
307	US	TigerIT Americas LLC	tiger-005	005	2021-07-29
308	RU	Tinkoff Bank	tinkoff-001	001	2021-05-13
309	CN	TongYi Transportation Technology	tongyi-005	005	2019-06-12
310	TW	Toppan ID Gate	toppanidgate-000	000	2021-09-28
311	JP	Toshiba	toshiba-003	003	2019-03-01
312	JP	Toshiba	toshiba-004	004	2021-09-27
313	JP	Tripleize	aize-001	001	2021-04-23
314	JP	Tripleize	aize-002	002	2021-10-08
315	US	Trueface.ai	trueface-002	002	2021-03-29
316	US	Trueface.ai	trueface-003	003	2021-09-30
317	CN	ULSee Inc	ulsee-001	001	2019-07-31
318	PT	Universidade de Coimbra	visteam-001	001	2021-03-16
319	PT	Universidade de Coimbra	visteam-002	002	2021-08-20
320	US	VCognition	vcog-002	002	2017-06-12
321	ES	Veridas Digital Authentication Solutions S.L.	veridas-006	006	2021-04-15
322	ES	Veridas Digital Authentication Solutions S.L.	veridas-007	007	2021-09-02
323	KZ	Verigram	verigram-000	000	2021-09-06
324	TW	Via Technologies Inc	via-000	000	2019-07-08
325	TW	Via Technologies Inc	via-001	001	2020-01-08
326	DE	Videmo Intelligent Videoanalyse	videmo-000	000	2019-12-19
327	IN	Videonetics Technology Pvt	videonetics-001	001	2019-06-19
328	IN	Videonetics Technology Pvt	videonetics-002	002	2019-11-21
329	VN	Vietnam Posts and Telecommunications Group	vnpt-001	001	2021-01-08
330	VN	Vietnam Posts and Telecommunications Group	vnpt-002	002	2021-06-08
331	VN	Viettel Group	vts-000	000	2020-11-04
332	VN	Viettel High Technology	viettelhightech-000	000	2021-08-04
333	US	Vigilant Solutions	vigilantsolutions-010	010	2021-04-07
334	US	Vigilant Solutions	vigilantsolutions-011	011	2021-08-07
335	VN	VinAI Research VietNam	vinai-000	000	2020-09-24
336	SE	Visage Technologies	visage-000	000	2020-12-09
337	FI	Visidon	vd-002	002	2021-04-12
338	FI	Visidon	vd-003	003	2021-10-12
339	CN	Vision Intelligence Center of Meituan	meituan-000	000	2021-05-14
340	PT	Vision-Box	visionbox-001	001	2019-03-01
341	PT	Vision-Box	visionbox-002	002	2021-04-29
342	RU	VisionLabs	visionlabs-010	010	2021-01-25
343	RU	VisionLabs	visionlabs-011	011	2021-10-13
344	RU	Vocord	vocord-008	008	2020-01-31
345	RU	Vocord	vocord-009	009	2020-12-28
346	CN	Winsense	winsense-001	001	2019-10-16
347	CN	Winsense	winsense-002	002	2020-11-20
348	CN	Wuhan Tianyu Information Industry	wuhantianyu-001	001	2021-08-05
349	CN	Xforward AI Technology	xforwardai-001	001	2020-09-25
350	CN	Xforward AI Technology	xforwardai-002	002	2021-02-10

Table 5: Summary of participant information included in this report.

	Location	Developer Name	Short Name	Seq. Num.	Validation Date
351	CN	Xiamen Meiya Pico Information	meiya-001	001	2019-03-01
352	CN	Xiamen University	xm-000	000	2020-10-19
353	PT	Yoonik	yoonik-001	001	2020-10-26
354	PT	Yoonik	yoonik-002	002	2021-09-06
355	TW	Yuan High-Tech Development	yuan-002	002	2021-05-17
356	TW	Yuan High-Tech Development	yuan-003	003	2021-09-17
357	CN	Yuntu Data and Technology	ytu-000	000	2021-06-16
358	CN	Zhuhai Yisheng Electronics Technology	yisheng-004	004	2018-06-12
359	CN	iQIYI Inc	iqface-000	000	2019-06-04
360	CN	iQIYI Inc	iqface-003	003	2021-02-23
361	TW	iSAP Solution Corporation	isap-001	001	2019-08-07
362	TW	iSAP Solution Corporation	isap-002	002	2020-09-01
363	TW	ioNetworks Inc	ionetworks-000	000	2021-07-20

Table 6: Summary of participant information included in this report.

ALGORITHM		CONFIG	LIBRARY	TEMPLATE								COMPARISON ⁴		
NAME		DATA	DATA	MEMORY	SIZE	GENERATION TIME (ms) ⁴				TIME (ns) ⁵				
		(KB) ¹	(KB) ²	(MB) ³	(B)	MUGSHOT	480x720	960x1440	1600x2400	3000x4500	GENUINE	IMPOSTOR		
1	20face-000	119967175	324083	173 ⁹⁰⁵	129 ^{2048 ± 0}	33 ^{232 ± 1}	19 ^{223 ± 1}	14 ^{226 ± 4}	12 ^{222 ± 1}	10 ^{224 ± 1}	344 ^{44880 ± 134}	343 ^{44462 ± 163}		
2	20face-001	232267835	324119	294 ¹⁹⁴⁰	324 ^{4096 ± 0}	42 ^{279 ± 2}	24 ^{266 ± 1}	17 ^{266 ± 1}	16 ^{267 ± 1}	13 ^{267 ± 0}	271 ^{5553 ± 54}	270 ^{5541 ± 65}		
3	3divi-006	280439478	52656	70 ⁴⁷²	157 ^{2048 ± 0}	175 ^{654 ± 1}	134 ^{651 ± 0}	119 ^{660 ± 1}	103 ^{678 ± 2}	104 ^{759 ± 13}	88 ^{775 ± 19}	88 ^{770 ± 22}		
4	3divi-007	494710400	24723	231 ¹²⁸⁵	124 ^{2048 ± 0}	159 ^{615 ± 1}	126 ^{616 ± 1}	106 ^{623 ± 1}	91 ^{644 ± 1}	94 ^{727 ± 5}	74 ^{707 ± 31}	77 ^{712 ± 25}		
5	acer-001	37530576	66086	56 ⁴¹⁷	27 ^{512 ± 0}	27 ^{199 ± 0}	21 ^{237 ± 28}	15 ^{229 ± 26}	15 ^{242 ± 37}	12 ^{259 ± 21}	206 ^{2453 ± 44}	208 ^{2461 ± 62}		
6	acer-002	44976775	624858	27 ¹⁸⁷	133 ^{2048 ± 0}	24 ^{184 ± 0}	13 ^{184 ± 0}	9 ^{185 ± 0}	7 ^{185 ± 0}	7 ^{186 ± 0}	240 ^{3370 ± 47}	240 ^{3350 ± 54}		
7	acisw-003	288798384	35664	40 ²⁸²	366 ^{18467 ± 8}	32 ^{232 ± 1}	26 ^{267 ± 22}	65 ^{488 ± 28}	194 ^{990 ± 24}	291 ^{2977 ± 129}	307 ^{847908 ± 16757}	367 ^{851850 ± 17018}		
8	acisw-006	288798384	36107	44 ³⁰³	363 ^{18465 ± 8}	31 ^{219 ± 0}	20 ^{227 ± 0}	37 ^{410 ± 1}	149 ^{838 ± 1}	282 ^{2532 ± 10}	364 ^{548137 ± 16513}	364 ^{549586 ± 9238}		
9	adera-002	0	749797	178 ⁹²¹	353 ^{5120 ± 0}	353 ^{1394 ± 11}	308 ^{1381 ± 1}	302 ^{1393 ± 1}	278 ^{1403 ± 1}	239 ^{1464 ± 2}	196 ^{2163 ± 32}	197 ^{2158 ± 28}		
10	adera-003	0	749778	176 ⁹¹⁷	355 ^{5120 ± 0}	352 ^{1381 ± 12}	309 ^{1385 ± 1}	303 ^{1394 ± 1}	276 ^{1401 ± 1}	240 ^{1469 ± 1}	195 ^{2148 ± 34}	194 ^{2130 ± 32}		
11	advance-002	263345868	20434	42 ²⁹⁵	128 ^{2048 ± 0}	226 ^{811 ± 2}	181 ^{803 ± 2}	133 ^{696 ± 2}	109 ^{699 ± 4}	89 ^{718 ± 1}	106 ^{987 ± 10}	106 ^{988 ± 45}		
12	advance-003	265080773	78699	87 ⁵¹⁸	188 ^{2048 ± 0}	140 ^{586 ± 0}	113 ^{584 ± 0}	93 ^{583 ± 0}	75 ^{588 ± 0}	59 ^{591 ± 1}	175 ^{1813 ± 17}	173 ^{1788 ± 26}		
13	aifirst-001	229537224	808777	73 ⁴⁸⁵	212 ^{2048 ± 0}	143 ^{587 ± 2}	107 ^{568 ± 2}	94 ^{584 ± 3}	80 ^{601 ± 6}	103 ^{755 ± 5}	121 ^{1099 ± 14}	124 ^{1087 ± 45}		
14	aigen-001	263125848	595227	214 ¹¹³⁶	217 ^{2048 ± 0}	363 ^{1448 ± 9}	318 ^{1451 ± 8}	319 ^{1759 ± 6}	319 ^{2594 ± 4}	307 ^{5691 ± 44}	251 ^{3772 ± 57}	250 ^{3736 ± 56}		
15	aigen-002	210228007	1316138	168 ⁸⁷⁴	160 ^{2048 ± 0}	141 ^{586 ± 24}	112 ^{582 ± 4}	194 ^{920 ± 4}	300 ^{1758 ± 5}	305 ^{5427 ± 17}	249 ^{3678 ± 44}	247 ^{3646 ± 48}		
16	ailabs-001	1079975494	338989	226 ¹²⁵²	179 ^{2048 ± 0}	180 ^{664 ± 4}	173 ^{774 ± 50}	257 ^{1145 ± 12}	307 ^{1972 ± 74}	303 ^{5205 ± 272}	356 ^{104034 ± 661}	356 ^{103415 ± 7722}		
17	aimall-002	379040058	25210	267 ¹⁵⁷⁶	107 ^{2048 ± 0}	216 ^{776 ± 4}	225 ^{927 ± 27}	203 ^{940 ± 21}	187 ^{955 ± 34}	155 ^{1003 ± 75}	354 ^{72811 ± 7399}	353 ^{71216 ± 6286}		
18	aimall-003	516428479	171935	60 ¹⁹¹³	60 ^{1024 ± 0}	179 ^{662 ± 1}	164 ^{740 ± 51}	150 ^{752 ± 62}	124 ^{741 ± 46}	112 ^{807 ± 47}	339 ^{34565 ± 93}	340 ^{34598 ± 118}		
19	aiunionface-000	247442204	840295	51 ⁴⁰²	146 ^{2048 ± 0}	167 ^{637 ± 13}	168 ^{754 ± 41}	228 ^{1025 ± 28}	234 ^{1179 ± 29}	251 ^{1639 ± 47}	115 ^{1072 ± 19}	122 ^{1080 ± 47}		
20	aize-001	274899563	168970	251 ¹⁴³⁶	83 ^{2048 ± 0}	87 ^{437 ± 10}	64 ^{440 ± 8}	83 ^{542 ± 17}	129 ^{756 ± 27}	248 ^{1583 ± 53}	183 ^{1937 ± 22}	181 ^{1919 ± 23}		
21	aize-002	263276668	182517	105 ⁵⁸⁶	99 ^{2048 ± 0}	97 ^{467 ± 1}	76 ^{479 ± 1}	151 ^{756 ± 1}	289 ^{1477 ± 1}	302 ^{4617 ± 41}	43 ^{597 ± 16}	49 ^{598 ± 14}		
22	ajou-001	371975940	31734	62 ⁴⁴²	159 ^{2048 ± 0}	118 ^{530 ± 0}	96 ^{536 ± 0}	80 ^{535 ± 0}	67 ^{549 ± 0}	56 ^{577 ± 0}	42 ^{597 ± 19}	47 ^{596 ± 13}		
23	alchera-002	415139706	22275	224 ¹²³³	119 ^{2048 ± 0}	285 ^{968 ± 1}	236 ^{976 ± 2}	216 ^{979 ± 1}	193 ^{988 ± 1}	159 ^{1025 ± 2}	246 ^{3488 ± 63}	244 ^{3430 ± 63}		
24	alchera-003	499423744	24613	241 ¹³⁷⁶	132 ^{2048 ± 0}	247 ^{854 ± 3}	201 ^{862 ± 2}	177 ^{870 ± 1}	163 ^{882 ± 2}	136 ^{918 ± 1}	243 ^{3426 ± 57}	241 ^{3383 ± 53}		
25	alice-000	1783085023	19355	278 ¹⁷³²	325 ^{4096 ± 0}	278 ^{950 ± 2}	227 ^{933 ± 1}	208 ^{949 ± 1}	200 ^{1011 ± 3}	203 ^{1264 ± 8}	312 ^{14975 ± 201}	311 ^{14890 ± 229}		
26	alleyes-000	519819601	997090	165 ⁸⁵⁷	110 ^{2048 ± 0}	218 ^{784 ± 1}	234 ^{970 ± 61}	214 ^{974 ± 62}	183 ^{943 ± 69}	168 ^{1057 ± 23}	139 ^{1298 ± 34}	141 ^{1303 ± 51}		
27	allgovision-000	176649434	155862	100 ⁵⁶¹	237 ^{2048 ± 0}	69 ^{384 ± 8}	50 ^{395 ± 17}	39 ^{413 ± 14}	46 ^{471 ± 14}	86 ^{710 ± 21}	337 ^{29903 ± 406}	338 ^{29735 ± 194}		
28	alphaface-001	266086261	81636	90 ⁵²⁷	162 ^{2048 ± 0}	156 ^{612 ± 1}	123 ^{613 ± 3}	103 ^{612 ± 1}	84 ^{619 ± 1}	71 ^{640 ± 2}	111 ^{1008 ± 10}	112 ^{1002 ± 19}		
29	alphaface-002	787451788	70692	250 ¹⁴³⁴	230 ^{2048 ± 0}	164 ^{628 ± 2}	166 ^{746 ± 19}	149 ^{751 ± 18}	135 ^{779 ± 22}	117 ^{828 ± 40}	99 ^{945 ± 25}	101 ^{935 ± 17}		
30	amplifiedgroup-001	0	47053	9 ⁸¹	51 ^{866 ± 2}	8 ^{93 ± 0}	-	-	-	-	351 ^{57803 ± 4210}	348 ^{56365 ± 1196}		
31	androvideo-000	179043623	585063	52 ⁴⁰³	101 ^{2048 ± 0}	40 ^{277 ± 0}	32 ^{285 ± 0}	21 ^{314 ± 0}	24 ^{372 ± 1}	65 ^{620 ± 0}	223 ^{2860 ± 28}	222 ^{2847 ± 22}		
32	anke-004	357773976	410776	134 ⁷⁰⁶	272 ^{2056 ± 0}	162 ^{625 ± 1}	127 ^{627 ± 2}	114 ^{635 ± 3}	96 ^{653 ± 2}	151 ^{982 ± 8}	59 ^{633 ± 22}	62 ^{632 ± 34}		
33	anke-005	336438306	429160	213 ¹¹³⁴	275 ^{2056 ± 0}	144 ^{590 ± 2}	118 ^{594 ± 5}	99 ^{601 ± 3}	90 ^{638 ± 4}	116 ^{821 ± 24}	69 ^{685 ± 19}	73 ^{687 ± 26}		
34	antheus-000	122319905	41994	16 ¹¹⁶	40 ^{520 ± 0}	12 ^{109 ± 1}	15 ^{187 ± 1}	11 ^{189 ± 1}	8 ^{195 ± 1}	11 ^{236 ± 2}	287 ^{6901 ± 268}	287 ^{6936 ± 103}		
35	antheus-001	122319905	41962	17 ¹¹⁸	41 ^{520 ± 0}	14 ^{120 ± 1}	23 ^{265 ± 13}	59 ^{468 ± 22}	244 ^{1223 ± 27}	283 ^{2660 ± 87}	284 ^{6218 ± 47}	283 ^{6216 ± 45}		
36	anyvision-004	410625029	630797	210 ¹¹⁰²	53 ^{1024 ± 0}	61 ^{355 ± 1}	-	-	-	-	181 ^{1891 ± 51}	176 ^{1829 ± 85}		
37	anyvision-005	195563434	116595	187 ⁹⁶³	58 ^{1024 ± 0}	288 ^{985 ± 1}	239 ^{997 ± 1}	225 ^{1004 ± 1}	195 ^{995 ± 1}	153 ^{995 ± 1}	79 ^{733 ± 14}	82 ^{733 ± 16}		
38	asusaics-000	263596044	245320	113 ⁶⁰⁵	220 ^{2048 ± 0}	105 ^{484 ± 13}	90 ^{506 ± 21}	173 ^{850 ± 26}	302 ^{1789 ± 61}	309 ^{6305 ± 188}	269 ^{5455 ± 78}	269 ^{5422 ± 112}		
39	asusaics-001	263596114	245330	109 ⁵⁹⁵	320 ^{4096 ± 0}	244 ^{842 ± 17}	241 ^{1008 ± 20}	301 ^{1377 ± 28}	318 ^{2423 ± 90}	314 ^{7284 ± 277}	297 ^{8618 ± 42}	297 ^{8638 ± 136}		
40	authenmetric-002	460742912	91489	212 ¹¹¹²	241 ^{2048 ± 0}	274 ^{942 ± 1}	231 ^{950 ± 1}	212 ^{960 ± 1}	189 ^{960 ± 1}	152 ^{991 ± 2}	160 ^{1712 ± 20}	162 ^{1719 ± 19}		
41	authenmetric-003	300645864	39492	191 ⁹⁸²	174 ^{2048 ± 0}	291 ^{992 ± 1}	240 ^{1006 ± 1}	224 ^{1003 ± 2}	199 ^{1002 ± 1}	162 ^{1036 ± 1}	165 ^{1757 ± 19}	165 ^{1755 ± 19}		
42	aware-005	307217546	26320	228 ¹²⁶⁵	79 ^{1572 ± 0}	260 ^{886 ± 23}	252 ^{1038 ± 21}	250 ^{1121 ± 22}	267 ^{1337 ± 58}	268 ^{2195 ± 144}	149 ^{1475 ± 63}	147 ^{1427 ± 115}		
43	aware-006	305708324	14124	184 ⁹⁴³	14 ^{352 ± 0}	317 ^{1148 ± 3}	274 ^{1146 ± 2}	267 ^{1190 ± 2}	259 ^{1306 ± 20}	258 ^{1754 ± 84}	213 ^{2598 ± 42}	215 ^{2559 ± 60}		
44	awiros-001	15871971	87480	12 ⁸⁸	17 ⁵									

ALGORITHM		CONFIG	LIBRARY	TEMPLATE							COMPARISON ⁴		
NAME		DATA	DATA	MEMORY	SIZE	GENERATION TIME (ms) ⁴				TIME (ns) ⁵			
		(KB) ¹	(KB) ²	(MB) ³	(B)	MUGSHOT	480x720	960x1440	1600x2400	3000x4500	GENUINE	IMPOSTOR	
45	awiros-002	295953108	203723	¹⁰¹ 562	⁸⁴ 2048 ± 0	¹⁰² 479 ± 0	⁸⁷ 500 ± 0	⁷⁹ 534 ± 0	⁸³ 618 ± 0	¹⁴³ 946 ± 1	¹⁸⁴ 1966 ± 31	¹⁸⁵ 1957 ± 25	
46	ayftech-001	200113346	43580	¹⁴⁰ 731	¹⁹ 512 ± 0	⁷⁶ 408 ± 23	⁷⁵ 476 ± 52	¹⁶⁰ 814 ± 108	³⁰³ 1827 ± 384	³⁰⁴ 5412 ± 1029	⁵³ 615 ± 16	⁹⁹ 885 ± 44	
47	ayonix-000	59909936	5252	⁵ 69	⁶⁵ 1036 ± 0	² 18 ± 2	-	-	-	-	⁵⁵ 621 ± 23	⁵⁸ 620 ± 26	
48	beethedata-000	233318297	1087592	⁹⁹ 555	¹⁸⁵ 2048 ± 0	⁹⁵ 465 ± 0	⁷⁴ 467 ± 0	⁵⁸ 468 ± 0	⁴⁴ 467 ± 0	²⁹ 467 ± 0	¹⁹³ 2121 ± 34	¹⁹³ 2110 ± 38	
49	biocube-001	25631585	6192987	⁶⁶ 458	³¹⁸ 4096 ± 0	⁴⁵ 282 ± 22	³³ 292 ± 24	⁷⁷ 521 ± 57	¹⁰⁴ 684 ± 59	²⁰⁷ 1282 ± 68	³²⁵ 21787 ± 96	³²⁵ 21812 ± 109	
50	bioidtechswiss-001	1207059515	120811	²⁵⁵ 1455	³⁰ 512 ± 0	²⁸⁴ 966 ± 4	²⁹⁶ 1270 ± 270	²⁸⁶ 1294 ± 96	²⁷⁹ 1409 ± 157	²⁶¹ 1793 ± 79	²¹⁶ 2610 ± 25	²¹⁷ 2624 ± 32	
51	bioidtechswiss-002	762660868	114842	¹⁹⁴ 993	²³ 512 ± 0	²⁶⁵ 917 ± 2	²²⁶ 930 ± 2	²⁰⁹ 952 ± 2	¹⁸⁵ 947 ± 3	¹⁶⁹ 1058 ± 11	¹⁹⁷ 2177 ± 29	¹⁹⁸ 2170 ± 31	
52	bm-001	294640228	38076	²¹ 148	¹ 64 ± 0	⁸⁸ 444 ± 88	-	-	-	-	¹⁸⁰ 1887 ± 31	¹⁸⁰ 1877 ± 26	
53	boetech-001	267649084	88710	²⁴³ 1384	²²⁷ 2048 ± 0	³⁹ 271 ± 1	²⁷ 268 ± 1	¹⁸ 273 ± 0	¹⁷ 286 ± 1	¹⁶ 318 ± 1	³⁵² 68519 ± 1921	³⁵² 67648 ± 822	
54	breesee-001	294790077	23227	²²⁰ 1214	¹³⁷ 2048 ± 0	³³¹ 1223 ± 3	²⁸⁵ 1216 ± 1	²⁹⁹ 1331 ± 1	²⁴⁶ 1227 ± 1	²²² 1360 ± 1	³⁴⁰ 37240 ± 655	³⁴¹ 37167 ± 584	
55	breesee-002	321154814	30902	²⁹⁶ 1956	¹⁸¹ 2048 ± 0	²⁰⁶ 743 ± 4	²⁷² 1143 ± 2	²⁵⁸ 1146 ± 2	²²⁹ 1148 ± 2	¹⁹² 1176 ± 2	¹⁶⁷ 1778 ± 22	¹⁶⁸ 1775 ± 23	
56	camvi-002	241949538	225285	¹⁴¹ 737	⁶¹ 1024 ± 0	¹⁸⁵ 677 ± 7	¹⁶⁰ 726 ± 36	¹⁷⁶ 869 ± 28	²²³ 1129 ± 43	²⁸⁸ 2785 ± 113	⁵² 612 ± 26	⁵² 603 ± 20	
57	camvi-004	287471548	615819	¹⁷⁷ 919	²³¹ 2048 ± 0	²⁰⁹ 759 ± 10	²⁰⁰ 861 ± 17	²¹⁹ 986 ± 34	²⁵⁵ 1279 ± 51	²⁹⁰ 2891 ± 158	¹⁰⁰ 948 ± 40	¹⁰³ 963 ± 31	
58	canon-002	457207046	130232	¹⁷¹ 891	³³² 4096 ± 0	³⁴⁶ 1308 ± 2	³⁰³ 1315 ± 1	²⁹³ 1326 ± 2	²⁷⁰ 1345 ± 1	²³⁸ 1452 ± 1	²⁸³ 6211 ± 25	²⁸² 6194 ± 25	
59	canon-003	2612070631	101378	³⁵⁶ 5472	³⁵⁹ 6180 ± 0	³³⁹ 1263 ± 3	²⁹⁴ 1263 ± 1	²⁸⁰ 1283 ± 1	²⁶⁵ 1320 ± 1	²⁴³ 1482 ± 2	²⁶³ 4783 ± 17	²⁶⁰ 4780 ± 19	
60	ceiec-003	266620201	88707	⁶⁰ 430	¹³⁰ 2048 ± 0	²³⁰ 817 ± 4	²¹⁰ 883 ± 57	¹⁸⁶ 897 ± 60	¹⁶⁹ 899 ± 72	¹⁴² 944 ± 72	²⁰¹ 2256 ± 38	²⁰¹ 2241 ± 54	
61	ceiec-004	269799940	67011	⁵³ 408	¹⁹³ 2048 ± 0	²⁹⁴ 1024 ± 1	²⁴⁶ 1027 ± 1	²³⁰ 1027 ± 1	²⁰³ 1030 ± 1	¹⁶⁶ 1055 ± 1	¹⁷⁷ 1844 ± 26	¹⁷⁷ 1836 ± 20	
62	chosun-001	783990750	707	⁷⁷ 491	¹¹⁴ 2048 ± 0	²¹⁷ 783 ± 2	¹⁸⁸ 826 ± 4	³¹⁸ 1662 ± 13	³²³ 3679 ± 67	³²⁰ 11694 ± 243	¹⁰⁸ 998 ± 25	¹¹⁰ 1035 ± 11	
63	chosun-002	239617968	31875	⁶³ 450	¹⁴⁰ 2048 ± 0	³⁴ 248 ± 3	²⁸ 273 ± 3	³¹³ 1495 ± 14	³²⁵ 9720 ± 90	³²² 80302 ± 1349	⁵⁷ 623 ± 17	⁶⁵ 634 ± 13	
64	chtface-003	371869498	369529	²¹⁶ 1178	¹⁶³ 2048 ± 0	¹⁴⁸ 594 ± 16	¹⁵⁸ 720 ± 33	²³⁸ 1050 ± 41	³⁰⁶ 1884 ± 90	³⁰⁶ 5606 ± 334	¹⁹² 2110 ± 37	²⁰⁰ 2219 ± 65	
65	chtface-004	419487869	311027	²⁵⁸ 1487	¹¹³ 2048 ± 0	⁵⁵ 332 ± 0	³⁶ 323 ± 1	²⁴ 329 ± 1	¹⁹ 335 ± 1	²⁰ 377 ± 1	¹⁶³ 1727 ± 17	¹⁶³ 1720 ± 16	
66	clearviewai-000	350711038	211852	³²⁴ 2750	²²² 2048 ± 0	³⁵⁵ 1402 ± 1	³¹² 1403 ± 1	³⁰⁵ 1412 ± 1	²⁸² 1420 ± 1	²³⁴ 1418 ± 1	¹⁵³ 1592 ± 37	¹⁵³ 1561 ± 37	
67	closeli-001	430430427	9851	¹⁴⁵ 773	³³⁴ 4096 ± 0	²⁴³ 839 ± 1	¹⁹⁵ 843 ± 1	¹⁷¹ 841 ± 1	¹⁵³ 845 ± 1	¹²⁶ 865 ± 1	²⁶⁸ 5404 ± 17	²⁶⁸ 5400 ± 25	
68	cloudwalk-hr-003	392949139	144263	¹⁹³ 984	²⁸¹ 2057 ± 0	¹⁵² 606 ± 0	¹¹⁵ 588 ± 0	⁹⁵ 594 ± 0	⁸² 612 ± 1	-	²⁹⁰ 6982 ± 80	²⁸⁹ 6972 ± 84	
69	cloudwalk-hr-004	514986414	520169	²⁴⁵ 1394	²⁴⁴ 2049 ± 0	²⁵ 873 ± 1	²⁰⁸ 877 ± 1	¹⁸¹ 876 ± 1	¹⁶² 879 ± 1	¹³³ 902 ± 3	³⁰³ 11652 ± 127	³⁰² 11608 ± 123	
70	cloudwalk-mt-003	502133796	494959	²³⁷ 1342	²⁴⁶ 2049 ± 0	²⁶⁷ 923 ± 1	²²⁰ 918 ± 1	¹⁹⁹ 926 ± 1	¹⁷⁵ 925 ± 1	¹⁴⁰ 936 ± 1	³⁰² 11620 ± 179	³⁰⁴ 11661 ± 128	
71	cloudwalk-mt-004	1417833104	512628	³⁵⁵ 5426	⁹⁵ 2048 ± 0	²⁶⁹ 923 ± 2	²²¹ 919 ± 1	¹⁹³ 918 ± 0	¹⁷⁴ 919 ± 0	¹³⁷ 927 ± 1	³⁰⁴ 11744 ± 170	³⁰³ 11631 ± 126	
72	clova-000	203182777	6824	⁶⁸ 464	¹⁹¹ 2048 ± 0	⁸⁶ 437 ± 0	⁶⁰ 431 ± 0	⁴⁶ 435 ± 0	³⁸ 452 ± 2	³⁶ 508 ± 7	¹⁶⁹ 1794 ± 16	¹⁷⁴ 1795 ± 19	
73	cogent-005	1921839276	75276	³²⁶ 2806	²⁹⁵ 2523 ± 0	³³⁰ 1221 ± 2	²⁸⁸ 1236 ± 1	²⁸² 1289 ± 2	²⁸³ 1420 ± 4	²⁴⁹ 1602 ± 5	³³¹ 24854 ± 69	³³¹ 24858 ± 71	
74	cogent-006	1104043825	58108	²⁶³ 1547	⁶⁸ 1062 ± 0	²¹³ 768 ± 0	¹⁷⁶ 789 ± 1	¹⁶⁶ 831 ± 2	¹⁷⁷ 930 ± 1	¹⁴⁹ 971 ± 1	¹⁷² 1802 ± 17	¹⁷⁵ 1797 ± 23	
75	cognitec-002	403546749	62354	¹¹⁶ 624	²⁴⁸ 2052 ± 0	²⁵ 192 ± 6	¹⁸ 219 ± 6	¹⁶ 233 ± 8	¹⁴ 241 ± 6	¹⁵ 314 ± 10	²³⁷ 3250 ± 41	²³⁷ 3241 ± 48	
76	cognitec-003	482773320	62502	¹⁵⁵ 817	²⁵⁴ 2052 ± 0	⁶⁷ 366 ± 9	⁵² 403 ± 9	³⁶ 408 ± 9	³¹ 424 ± 9	³⁷ 509 ± 13	²⁴² 3417 ± 51	²⁴⁵ 3433 ± 53	
77	cor-001	1223627342	11240	²²⁵ 1249	²⁸³ 2060 ± 0	¹⁹⁷ 699 ± 3	²⁰² 863 ± 76	¹⁷⁵ 865 ± 80	¹⁵⁸ 872 ± 89	¹⁴⁵ 952 ± 39	³⁶² 270145 ± 2259	³⁶² 282686 ± 11788	
78	coretech-000	190897979	43964	⁵⁰ 393	²⁴ 512 ± 0	¹⁵¹ 602 ± 15	¹³⁵ 659 ± 12	²⁵⁵ 1139 ± 24	²³⁰ 1149 ± 25	¹⁸⁹ 1165 ± 23	²⁰ 333 ± 14	²⁰ 321 ± 13	
79	corsight-001	1472269967	31525	³⁰² 2040	²⁸⁵ 2064 ± 0	³⁴³ 1291 ± 3	²⁹⁷ 1285 ± 1	²⁸⁹ 1293 ± 1	²⁵⁸ 1303 ± 2	²²³ 1379 ± 3	³⁶¹ 249340 ± 1713	³⁶¹ 248929 ± 1909	
80	corsight-002	1510319809	32093	³⁰³ 2061	²⁸⁹ 2080 ± 0	³⁴² 1290 ± 1	²⁹⁸ 1287 ± 1	²⁸³ 1290 ± 1	²⁶⁰ 1307 ± 2	²²⁶ 1388 ± 4	³³² 24953 ± 637	³³⁰ 24263 ± 578	
81	csc-002		0	519768	²⁴² 1376	⁴⁶ 544 ± 0	⁹⁹ 473 ± 0	⁸⁴ 494 ± 0	⁶¹ 481 ± 1	⁵⁰ 490 ± 1	⁴¹ 514 ± 5	²⁴ 367 ± 11	²⁶ 371 ± 10
82	csc-003		0	400435	²⁷¹ 1609	⁴⁵ 544 ± 0	¹⁰⁹ 499 ± 0	⁸⁸ 500 ± 1	⁷⁰ 502 ± 0	⁵⁶ 508 ± 1	⁴⁶ 535 ± 4	²⁶ 393 ± 8	²⁹ 397 ± 7
83	ctcbank-000	263381717	599238	¹⁰³ 570	¹⁷⁰ 2048 ± 0	¹³³ 568 ± 43	¹²¹ 606 ± 38	¹³⁰ 690 ± 53	¹¹⁴ 711 ± 50	¹¹⁸ 831 ± 51	²⁴⁷ 3551 ± 87	²⁶² 4805 ± 209	
84	ctcbank-001	282123885	599238	¹¹¹ 603	²¹¹ 2048 ± 0	¹⁷² 652 ± 35	¹⁷⁵ 781 ± 30	¹⁸⁰ 875 ± 43	¹⁶⁸ 898 ± 51	¹⁶⁰ 1030 ± 47	²⁵² 3926 ± 45	²⁵² 3924 ± 56	
85	cubox-001	378498689	75427	¹¹⁸ 649	¹⁶¹ 2048 ± 0	²⁶² 907 ± 1	²¹⁸ 902 ± 1	¹⁸⁸ 903 ± 0	¹⁷² 917 ± 0	¹³⁸ 931 ± 0	¹⁴⁰ 1379 ± 37	¹⁴⁶ 1417 ± 38	
86	cubox-002	555268218	90975	²⁹⁷ 1964	¹⁷⁶ 2048 ± 0	²⁶⁶ 921 ± 1	²²² 921 ± 1	¹⁹⁷ 922 ± 1	¹⁷⁹ 933 ± 1	¹⁵⁶ 1003 ± 1	¹⁸⁶ 2008 ± 72	¹⁸⁷ 1969 ± 57	
87	cudocommunication-001	394504775	341277	²⁰⁵ 1077	¹¹⁷ 2048 ± 0	²⁷⁰ 925 ± 1	²²³ 923 ± 1	²⁰¹ 928 ± 1	¹⁷⁸ 932 ± 0	¹⁴⁷ 964 ± 1	²¹⁰ 2534 ± 20	²¹² 2537 ± 20	
88	cuhkee-001	806762318	74917	³¹⁶ 2515	²⁵⁵ 2052 ± 0	²⁸⁶ 977 ± 31	-	-	-	-	²¹⁹ 2719 ± 60	²²⁰ 2783 ± 56	

Notes

1 The configuration size does not capture static data included in libraries.

2 The library size is the combined total of all files provided in the submission lib folder. These libraries e.g. OpenCV may or may not be installed on any end user's platform natively and would not need to be installed with the algorithm. Some developers put neural network models in their libraries.

3 The memory usage is the peak resident set size reported by the ps system call during template generation.

4 The median template creation times are measured on Intel®Xeon®CPU E5-2630 v4 @ 2.20GHz processors.

5 The comparison durations, in nanoseconds, are estimated using std::chrono::high_resolution_clock which on the machine in (2) counts 1ns clock ticks. Precision is somewhat worse than that however. The ± value is the median absolute deviation times 1.48 for Normal consistency.

ALGORITHM		CONFIG	LIBRARY	TEMPLATE								COMPARISON ⁴		
NAME		DATA	DATA	MEMORY	SIZE	GENERATION TIME (ms) ⁴				TIME (ns) ⁵				
		(KB) ¹	(KB) ²	(MB) ³	(B)	MUGSHOT	480x720	960x1440	1600x2400	3000x4500	GENUINE	IMPOSTOR		
89	cybercore-000	88073082	55441	³² 200	²¹ 512 ± 0	¹⁷⁶ 655 ± 3	¹⁴⁶ 689 ± 71	¹¹⁸ 649 ± 6	⁹² 648 ± 8	⁷⁹ 680 ± 6	³¹¹ 14800 ± 75	³¹³ 15757 ± 782		
90	cyberextruder-001	124120800	13629	²⁶ 178	⁵ 256 ± 0	²⁶¹ 893 ± 25	-	-	-	-	¹¹⁸ 1083 ± 16	¹²¹ 1079 ± 19		
91	cyberextruder-002	172963574	13924	³¹ 194	¹³¹ 2048 ± 0	¹²¹ 532 ± 6	-	-	-	-	¹⁷⁴ 1803 ± 14	¹⁷¹ 1779 ± 22		
92	cyberlink-006	349866738	102456	²⁴⁶ 1400	³⁶¹ 6212 ± 0	¹⁹¹ 690 ± 1	¹⁵² 702 ± 0	¹³⁷ 703 ± 0	¹¹⁵ 712 ± 0	¹⁰⁰ 741 ± 0	¹⁴ 270 ± 13	¹⁷ 271 ± 13		
93	cyberlink-007	389168020	102446	²⁷⁹ 1743	³⁶⁰ 6212 ± 0	²⁰⁰ 725 ± 1	¹⁶² 732 ± 1	¹⁴⁵ 734 ± 1	¹²² 736 ± 1	¹⁰⁸ 767 ± 1	¹⁸ 304 ± 19	¹⁸ 304 ± 16		
94	dahua-005	1624985571	169478	³⁶¹ 7360	³⁵⁵ 4096 ± 0	³⁵⁹ 1418 ± 34	-	-	-	-	¹⁰¹ 957 ± 23	¹⁰⁴ 969 ± 19		
95	dahua-006	851600617	119261	³⁵⁴ 5068	²²⁴ 2048 ± 0	³⁵⁴ 1398 ± 2	³¹¹ 1397 ± 1	³⁰⁴ 1404 ± 1	²⁷⁷ 1402 ± 1	²³⁰ 1402 ± 1	¹⁷ 249 ± 13	¹⁴ 250 ± 11		
96	daon-000	287464249	2307	³⁰¹ 2013	²⁸⁷ 2065 ± 0	¹³⁰ 562 ± 3	¹¹¹ 581 ± 5	¹⁵⁴ 791 ± 9	¹⁴⁸ 838 ± 15	¹⁶⁷ 1055 ± 32	³¹⁴ 16052 ± 88	³¹⁴ 16041 ± 85		
97	decatur-000	358907752	171271	¹⁷⁴ 907	³³⁸ 4100 ± 0	²⁹⁵ 1024 ± 2	-	-	-	-	³⁰¹ 11439 ± 80	³⁰¹ 11418 ± 112		
98	decatur-001	351095179	253734	²⁶⁰ 1507	²⁶² 2052 ± 0	³⁰⁷ 1103 ± 2	²⁵⁵ 1064 ± 2	²⁴¹ 1063 ± 2	²¹³ 1067 ± 2	¹⁷⁴ 1084 ± 2	⁵⁰ 610 ± 19	⁵¹ 602 ± 8		
99	deepglint-003	858178673	262081	³¹⁰ 2374	³⁵⁶ 6144 ± 0	³¹⁹ 1159 ± 1	²⁷³ 1145 ± 1	²⁵⁹ 1148 ± 1	²²⁸ 1148 ± 1	¹⁸⁸ 1163 ± 1	³¹⁶ 17227 ± 41	³¹⁶ 17210 ± 51		
100	deepglint-004	1099143717	261571	³³⁵ 3084	¹⁸³ 2048 ± 0	³⁶⁴ 1470 ± 1	³²¹ 1474 ± 1	³¹² 1485 ± 1	²⁸⁸ 1474 ± 1	²⁴⁴ 1492 ± 2	²⁷⁷ 5961 ± 34	²⁷⁸ 5955 ± 29		
101	deepsea-001	151037339	336250	⁴⁷ 358	⁵⁹ 1024 ± 0	¹⁶⁵ 630 ± 7	¹⁶⁷ 752 ± 37	¹⁴⁸ 746 ± 30	¹¹⁹ 727 ± 32	¹¹⁵ 820 ± 32	¹⁴⁴ 1401 ± 37	¹⁴⁸ 1467 ± 50		
102	deebsense-000	365684327	936618	³⁶² 7618	¹⁴⁸ 2048 ± 0	¹⁸¹ 664 ± 3	¹³³ 645 ± 1	¹²⁰ 660 ± 2	¹⁰⁶ 687 ± 2	¹¹³ 808 ± 3	³⁰ 480 ± 22	³³ 459 ± 34		
103	dermalog-008	0	937895	³⁵³ 4989	²⁹ 512 ± 0	⁷³ 404 ± 2	⁵³ 410 ± 3	⁴³ 424 ± 5	³³ 430 ± 5	³² 477 ± 5	²⁹ 468 ± 31	²² 328 ± 13		
104	dermalog-009	0	319363	¹²² 664	²² 512 ± 0	⁵⁹ 349 ± 0	⁴² 351 ± 0	²⁶ 352 ± 0	²² 357 ± 0	²¹ 389 ± 0	³¹ 487 ± 34	²⁸ 385 ± 29		
105	didiglobalface-001	266086235	70680	⁸⁹ 527	¹⁹⁵ 2048 ± 0	¹⁵⁵ 612 ± 1	¹³⁰ 633 ± 3	¹¹³ 634 ± 3	⁹⁴ 650 ± 15	⁷⁷ 666 ± 4	¹⁰³ 973 ± 20	¹⁰⁵ 988 ± 20		
106	digitalbarriers-002	84994577	598577	²⁹² 1930	²⁸⁰ 2056 ± 0	²⁸ 209 ± 11	²² 250 ± 19	³⁸ 411 ± 37	¹³⁹ 808 ± 72	²⁷⁰ 2236 ± 123	³⁰⁹ 13409 ± 228	³⁰⁹ 13267 ± 206		
107	dps-000	607	2211812	²⁰⁰ 1058	³¹¹ 4096 ± 0	²⁴⁹ 886 ± 2	²¹⁵ 893 ± 6	³⁰⁹ 1445 ± 9	³²¹ 2910 ± 38	³¹⁷ 9345 ± 17	¹⁴⁸ 1473 ± 37	¹⁴⁹ 1479 ± 37		
108	dsk-000	12254510	782905	³⁵ 252	²⁰ 512 ± 0	⁵⁰ 304 ± 47	³⁵ 317 ± 33	²²³ 1001 ± 96	³²⁰ 2660 ± 170	³¹⁸ 10451 ± 832	²⁹⁴ 7152 ± 115	²⁹² 7134 ± 111		
109	einetworks-000	381551539	219883	¹⁶⁹ 880	²⁷³ 2056 ± 0	¹⁷⁰ 645 ± 3	-	-	-	-	²⁶⁴ 4876 ± 66	²⁶⁴ 5156 ± 77		
110	ekin-002	52668576	278	¹⁸ 139	²⁹⁹ 3072 ± 0	³²⁶ 1186 ± 13	²⁸⁰ 1180 ± 12	²⁶⁴ 1181 ± 11	²⁴⁰ 1191 ± 11	¹⁹⁶ 1207 ± 8	²⁵⁶ 4294 ± 80	²⁷² 5569 ± 112		
111	enface-000	378468370	153781	¹²¹ 662	⁵⁶ 1024 ± 0	¹²⁹ 555 ± 4	¹⁰⁵ 558 ± 4	¹²³ 669 ± 6	¹⁹² 987 ± 15	²⁷⁵ 2349 ± 54	²⁹² 7059 ± 62	²⁹⁰ 6980 ± 65		
112	eocortex-000	262080175	59432	³⁴ 224	¹³⁶ 2048 ± 0	⁵¹ 305 ± 22	⁴¹ 341 ± 25	⁵⁰ 440 ± 47	⁴² 464 ± 45	³⁹ 513 ± 44	⁹⁸ 923 ± 11	¹⁰⁰ 918 ± 11		
113	ercacat-001	831102356	58012	³²⁷ 2816	²⁴⁹ 2052 ± 0	³⁰² 1052 ± 3	-	-	-	-	²¹¹ 2551 ± 62	²⁰⁹ 2501 ± 81		
114	expasoft-001	39994987	983064	¹⁹ 142	²⁴⁰ 2048 ± 0	⁶ 70 ± 0	³ 74 ± 0	³ 77 ± 0	³ 73 ± 0	³ 74 ± 0	¹⁵⁶ 1660 ± 35	¹⁵⁷ 1676 ± 48		
115	expasoft-002	39691196	59825	²³ 168	¹⁵² 2048 ± 0	⁴ 34 ± 0	² 34 ± 0	² 34 ± 0	¹ 34 ± 0	¹ 34 ± 0	²⁹⁸ 8870 ± 78	²⁹⁸ 8838 ± 77		
116	f8-001	279529297	19668	²²⁹ 1276	¹³⁹ 2048 ± 0	²³⁷ 822 ± 39	-	-	-	-	³¹³ 15262 ± 139	³¹² 15277 ± 212		
117	facesoft-000	379002927	10612	¹⁴⁹ 796	¹²⁶ 2048 ± 0	¹⁸⁴ 675 ± 18	¹³⁹ 669 ± 3	¹²⁸ 686 ± 3	¹⁰¹ 675 ± 5	⁸¹ 687 ± 2	²⁰⁰ 2239 ± 28	²⁰² 2277 ± 96		
118	facetag-000	1261907727	4022	¹⁸⁹ 965	⁵⁰ 684 ± 0	⁶⁰ 355 ± 17	⁴⁷ 369 ± 8	²²¹ 989 ± 33	³¹⁷ 2408 ± 91	³¹⁵ 7930 ± 316	³⁵³ 72003 ± 625	³⁵⁴ 71912 ± 612		
119	facetag-001	1288445598	4022	²³⁶ 1329	³⁴³ 4100 ± 0	²⁹⁰ 991 ± 3	²³⁸ 995 ± 3	²²⁷ 1018 ± 3	²¹⁴ 1069 ± 5	²⁰⁸ 1284 ± 8	²³⁸ 3323 ± 28	²³⁸ 3287 ± 34		
120	facex-001	312396751	930372	³³³ 2931	²⁰⁰ 2048 ± 0	⁸⁰ 422 ± 4	⁶² 434 ± 4	⁷⁶ 520 ± 7	¹²³ 737 ± 13	²⁵³ 1670 ± 27	¹⁷⁸ 1871 ± 23	¹⁷⁸ 1846 ± 29		
121	facex-002	312396751	928334	³³⁶ 3095	¹⁵⁸ 2048 ± 0	⁸¹ 426 ± 5	⁵⁹ 429 ± 4	⁷⁴ 516 ± 8	¹²⁰ 730 ± 12	²⁵⁷ 1738 ± 36	⁵⁸ 631 ± 25	⁵⁶ 614 ± 19		
122	farfaces-001	354810878	44581	³⁶ 261	²⁵ 512 ± 0	³²² 1179 ± 1	²⁷⁹ 1180 ± 1	²⁶³ 1180 ± 0	²³⁶ 1185 ± 1	¹⁹⁷ 1209 ± 2	⁹⁶ 855 ± 25	⁹⁶ 860 ± 31		
123	fiberhome-nanjing-003	361365058	1482309	¹⁶² 845	²⁰⁹ 2048 ± 0	³¹³ 1136 ± 7	²⁶⁹ 1134 ± 4	²⁵⁴ 1132 ± 3	²²⁶ 1139 ± 3	¹⁸⁴ 1154 ± 5	¹²⁰ 1097 ± 38	¹²³ 1083 ± 42		
124	fiberhome-nanjing-004	454429945	1482313	¹⁹⁷ 1048	³⁰⁷ 4096 ± 0	³⁴⁸ 1321 ± 5	³⁰¹ 1304 ± 3	²⁹⁰ 1307 ± 2	²⁶¹ 1308 ± 3	²¹⁸ 1326 ± 5	¹³⁸ 1276 ± 40	¹³⁹ 1265 ± 38		
125	fincore-000	262774045	19409	⁹³ 535	⁹² 2048 ± 0	¹¹⁴ 508 ± 3	⁸⁹ 505 ± 0	⁷¹ 508 ± 1	⁴⁵ 535 ± 1	¹⁶⁶ 1765 ± 31	¹⁶⁶ 1763 ± 22			
126	fujitsulab-002	0	1088887	²⁷² 1613	³⁴⁶ 4104 ± 0	³³⁵ 1237 ± 2	²⁸⁰ 1222 ± 2	²⁷³ 1236 ± 1	²⁴⁹ 1251 ± 2	²²⁰ 1327 ± 2	²²¹ 2836 ± 25	²²¹ 2809 ± 44		
127	fujitsulab-003	678158225	318209	³⁶⁰ 6907	³⁴⁷ 4104 ± 0	²⁸⁰ 951 ± 20	²²⁹ 941 ± 19	²¹¹ 952 ± 19	¹⁹⁰ 971 ± 20	¹⁶⁴ 1045 ± 21	²²² 2855 ± 16	²²³ 2849 ± 19		
128	geo-002	378781240	98667	¹⁹³ 1018	¹¹² 2048 ± 0	²²¹ 791 ± 1	¹⁷⁷ 793 ± 0	¹⁵⁵ 794 ± 0	¹³⁶ 795 ± 1	¹¹⁰ 803 ± 1	²⁴¹ 3407 ± 45	²⁴³ 3422 ± 65		
129	geo-003	380634047	102175	²²³ 1224	¹⁷⁵ 2048 ± 0	³⁴¹ 1283 ± 1	³⁰⁰ 1290 ± 1	²⁸¹ 1285 ± 1	²⁵⁷ 1292 ± 1	²¹¹ 1302 ± 1	¹⁰⁷ 997 ± 13	¹¹⁰ 1001 ± 20		
130	glory-002	0	385177	¹⁹⁰ 982	²⁹² 2106 ± 0	¹⁴⁹ 594 ± 3	¹⁶⁵ 740 ± 3	²⁰⁷ 948 ± 3	³¹⁰ 2168 ± 6	⁸ 191 ± 15	²⁸⁶ 6787 ± 85	²⁸⁶ 6551 ± 249		
131	glory-003	0	536910	²⁴⁷ 1400	³⁴⁹ 4234 ± 0	¹⁰⁷ 489 ± 0	¹⁰⁶ 565 ± 0	¹⁴⁴ 732 ± 0	³⁰⁵ 1876 ± 2	³¹⁶ 8941 ± 20	²⁷⁹ 6020 ± 90	²⁸¹ 6003 ± 72		
132	gorilla-007	451643974	708166	²⁷³ 1691	³⁶² 6288 ± 0	¹⁴⁶ 592 ± 1	¹¹⁷ 592 ± 1	¹⁰¹ 603 ± 1	⁸⁷ 625 ± 2	⁹² 722 ± 9	²⁵⁰ 3686 ± 37	²⁴⁹ 3709 ± 36		

Notes
 1 The configuration size does not capture static data included in libraries.
 2 The library size is the combined total of all files provided in the submission lib folder. These libraries e.g. OpenCV may or may not be installed on any end user's platform natively and would

	ALGORITHM	CONFIG	LIBRARY	TEMPLATE								COMPARISON ⁴			
				NAME		DATA		MEMORY		SIZE		GENERATION TIME (ms) ⁴			
				(KB) ¹	(KB) ²	(MB) ³	(B)	MUGSHOT	480x720	960x1440	1600x2400	3000x4500	GENUINE	IMPOSTOR	
133	gorilla-008	460979429	707000	²⁸² 1789	³⁶⁴ 8338 ± 0	¹⁵⁰ 595 ± 1	¹¹⁶ 590 ± 0	⁹⁸ 600 ± 1	⁸⁶ 621 ± 2	⁹⁰ 720 ± 9	²⁶⁰ 4530 ± 44	²⁵⁸ 4524 ± 38			
134	griaule-000	0	598214	¹⁹⁹ 1054	²⁶⁰ 2052 ± 0	⁷⁹ 416 ± 6	⁵⁷ 425 ± 7	¹⁵³ 770 ± 14	²⁹⁹ 1749 ± 43	³¹¹ 6406 ± 189	²⁵³ 3987 ± 42	²⁵³ 3938 ± 38			
135	hertasecurity-000	5	780014	⁸⁶ 516	⁶ 256 ± 0	¹⁰ 99 ± 0	⁶ 98 ± 0	⁵ 100 ± 0	⁵ 107 ± 0	⁵ 139 ± 0	⁷⁵ 710 ± 31	⁷⁰ 667 ± 28			
136	hik-001	683894884	9290	³⁵⁸ 6597	⁷⁴ 1408 ± 0	¹⁷¹ 651 ± 0	¹³⁸ 667 ± 8	¹²⁵ 677 ± 16	¹⁰⁵ 686 ± 13	⁹⁷ 737 ± 12	³² 488 ± 19	³⁴ 477 ± 22			
137	hisign-001	749990524	167488	²⁶⁴ 1553	²⁸⁸ 2080 ± 0	³⁴³ 1306 ± 1	³⁰⁴ 1320 ± 1	²⁹¹ 1315 ± 1	²⁶⁴ 1312 ± 1	²¹⁷ 1325 ± 1	⁹ 201 ± 10	⁶ 185 ± 13			
138	hyperverge-001	267079500	88624	⁸¹ 507	⁹² 2048 ± 0	¹⁸⁷ 682 ± 20	¹⁴⁸ 695 ± 17	²⁷⁰ 1196 ± 37	³¹⁶ 2400 ± 68	³¹³ 7178 ± 204	²⁸¹ 6026 ± 40	²⁸⁰ 5984 ± 38			
139	hyperverge-002	3022745705	198832	²⁹⁸ 1975	⁵⁷ 1024 ± 0	²⁷² 938 ± 1	²²⁸ 939 ± 1	²⁰⁴ 941 ± 1	¹⁸⁴ 945 ± 1	¹⁵⁰ 975 ± 1	²⁸⁰ 6023 ± 37	²⁷⁹ 5966 ± 40			
140	icm-002	636504686	903	⁷² 484	¹⁶⁶ 2048 ± 0	²⁹⁸ 1031 ± 7	-	-	-	-	³²⁹ 24052 ± 118	³²⁸ 24049 ± 124			
141	icm-003	1550323712	940	⁷⁹ 500	¹⁷² 2048 ± 0	¹⁸⁶ 681 ± 6	¹⁴¹ 672 ± 4	¹⁴⁰ 714 ± 11	¹⁴⁷ 837 ± 41	²²⁴ 1381 ± 131	³³⁰ 24351 ± 161	³²⁹ 24227 ± 146			
142	icthtc-000	176598609	1471004	²⁸⁴ 1805	²³⁸ 2048 ± 0	⁵⁸ 338 ± 11	⁴⁰ 338 ± 9	⁴⁷ 437 ± 16	¹¹² 705 ± 24	²⁵⁶ 1719 ± 44	²⁶⁷ 5284 ± 63	²⁶⁷ 5290 ± 54			
143	id3-006	215159624	7706	¹⁹² 982	⁴² 520 ± 0	¹⁸⁸ 683 ± 0	²⁵⁸ 1088 ± 1	²⁶⁸ 1192 ± 1	²⁴³ 1209 ± 1	²⁰⁴ 1270 ± 1	²⁷⁰ 5547 ± 34	²⁷¹ 5563 ± 34			
144	id3-008	248234648	8151	²⁰³ 1068	⁹ 264 ± 0	²³² 819 ± 0	²⁸³ 1209 ± 2	²⁶⁶ 1329 ± 1	²³⁷ 1433 ± 1	²⁷³ 5658 ± 44	²⁷⁴ 5624 ± 40				
145	idemia-007	361720312	67485	¹⁹⁸ 1051	¹⁵ 468 ± 0	⁷⁰ 384 ± 0	⁴⁹ 389 ± 0	³³ 393 ± 1	²⁶ 405 ± 2	²⁴ 441 ± 8	²³⁶ 3243 ± 63	²³⁵ 3202 ± 63			
146	idemia-008	382993834	69922	²¹⁷ 1194	¹³ 348 ± 0	⁹¹ 457 ± 1	⁷¹ 461 ± 0	⁵⁶ 466 ± 1	⁴⁷ 476 ± 2	⁴⁰ 513 ± 10	²³¹ 3080 ± 41	²²⁸ 3046 ± 56			
147	iit-002	265809599	52070	¹³⁹ 731	¹⁶⁷ 2048 ± 0	¹¹⁵ 514 ± 1	⁹² 531 ± 2	⁸⁶ 547 ± 1	⁷⁰ 583 ± 1	⁹⁵ 733 ± 2	¹¹³ 1023 ± 7	¹¹³ 1011 ± 66			
148	iit-003	267559145	53791	¹⁵⁷ 817	¹⁹⁴ 2048 ± 0	¹⁰³ 482 ± 0	⁸² 493 ± 0	⁷² 509 ± 0	⁶⁴ 541 ± 0	⁷⁵ 661 ± 0	¹⁹ 324 ± 17	²¹ 326 ± 8			
149	imagus-002	233233236	318409	⁵⁵ 411	¹⁷¹ 2048 ± 0	²¹⁹ 786 ± 1	¹⁷⁰ 766 ± 2	¹⁸³ 885 ± 3	²⁸⁴ 1430 ± 3	²⁹⁹ 4080 ± 10	⁶⁶ 676 ± 16	⁶⁰ 630 ± 20			
150	imagus-004	260510770	380049	¹³² 697	¹⁰⁸ 2048 ± 0	¹⁶¹ 624 ± 1	¹¹⁴ 587 ± 10	¹⁰⁸ 626 ± 3	⁷⁸ 592 ± 3	⁸⁸ 717 ± 6	⁸⁴ 760 ± 22	⁷⁶ 703 ± 28			
151	imperial-000	379002927	10623	¹⁵⁰ 796	²⁰² 2048 ± 0	¹⁸² 669 ± 1	¹⁴² 675 ± 3	¹²⁷ 683 ± 17	¹⁰² 676 ± 2	⁸² 689 ± 2	¹⁹⁴ 2130 ± 32	¹⁹¹ 2052 ± 100			
152	imperial-002	483663560	16134	²⁸⁵ 1826	²¹⁴ 2048 ± 0	¹³⁴ 569 ± 1	¹¹⁰ 581 ± 15	⁹¹ 575 ± 5	⁶⁹ 576 ± 2	⁵⁸ 588 ± 3	²⁰² 2278 ± 90	¹⁹⁵ 2131 ± 44			
153	incode-009	272489716	21014	¹⁸² 939	¹⁰⁵ 2048 ± 0	¹¹¹ 503 ± 0	⁸¹ 490 ± 1	⁶⁹ 498 ± 0	⁵⁵ 505 ± 0	⁴⁷ 537 ± 0	¹²² 1102 ± 28	¹²⁶ 1113 ± 29			
154	incode-010	642876348	21014	³¹⁹ 2628	¹⁵⁶ 2048 ± 0	³²³ 1180 ± 2	²⁷⁶ 1178 ± 1	²⁶⁵ 1182 ± 1	²³⁵ 1184 ± 1	¹⁹⁹ 1221 ± 1	¹²⁸ 1164 ± 32	¹²⁹ 1144 ± 32			
155	innefulabs-000	379482783	162172	⁶¹ 439	¹⁰⁹ 2048 ± 0	²⁹² 1006 ± 3	²⁴⁴ 1025 ± 3	²³² 1030 ± 4	²⁰⁷ 1041 ± 2	¹⁸¹ 1135 ± 3	²⁷⁴ 5782 ± 41	²⁷⁷ 5741 ± 45			
156	innovativetechnologyltd-001	181485901	335757	⁴² 341	¹²² 2048 ± 0	⁸⁴ 433 ± 7	⁶⁶ 446 ± 8	⁴⁸ 439 ± 4	³⁷ 452 ± 4	³⁴ 485 ± 7	¹⁷⁹ 1877 ± 42	¹⁸² 1924 ± 97			
157	innovativetechnologyltd-002	178114027	372324	¹⁷⁵ 912	²³⁹ 2048 ± 0	¹⁷⁷ 661 ± 2	¹⁵⁹ 726 ± 4	²¹⁷ 981 ± 27	¹⁹⁶ 997 ± 40	¹⁰⁷ 766 ± 3	¹⁷⁶ 1841 ± 50	¹⁷⁹ 1857 ± 59			
158	innovatrics-006	74	466269	²¹¹ 1107	⁴³ 538 ± 0	²³⁴ 820 ± 5	¹⁷⁹ 799 ± 4	¹⁵⁷ 805 ± 3	¹³⁷ 796 ± 9	¹²⁸ 890 ± 15	²⁷⁵ 5855 ± 204	²⁶⁵ 5266 ± 118			
159	innovatrics-007	74	493269	²⁹³ 1937	⁶⁹ 1064 ± 0	³⁶⁶ 1485 ± 7	³²⁴ 1785 ± 184	³²² 2078 ± 24	³⁰⁹ 2123 ± 15	²⁶⁹ 2210 ± 42	²⁷⁸ 5978 ± 88	²⁷⁶ 5690 ± 102			
160	insightface-000	826320727	16606	³⁴⁷ 3912	³²³ 4096 ± 0	²⁹³ 1009 ± 1	²⁴³ 1019 ± 2	²²⁶ 1017 ± 2	²⁰¹ 1020 ± 2	¹⁶¹ 1032 ± 2	¹⁶⁸ 1778 ± 31	¹⁶⁷ 1773 ± 35			
161	insightface-001	795419807	16606	³⁴⁴ 3852	²³⁶ 2048 ± 0	³⁵⁰ 1366 ± 2	³⁰⁷ 1368 ± 3	²⁹⁹ 1372 ± 3	²⁷³ 1375 ± 5	²²⁵ 1386 ± 4	¹²⁴ 1119 ± 29	¹²⁵ 1108 ± 34			
162	intelliloudai-001	226131619	868246	¹¹⁹ 655	¹¹¹ 2048 ± 0	⁹⁸ 468 ± 2	⁶⁸ 456 ± 1	⁵⁵ 466 ± 3	⁵³ 492 ± 1	⁶⁶ 632 ± 2	¹¹⁴ 1056 ± 4	¹¹⁸ 1051 ± 72			
163	intelliloudai-002	265264200	58559	³⁴⁰ 3584	³³⁷ 4100 ± 0	²⁴⁵ 847 ± 1	¹⁹⁶ 847 ± 2	¹⁷² 849 ± 1	¹⁵⁵ 853 ± 1	¹²⁷ 878 ± 4	⁹³ 822 ± 28	⁹⁴ 818 ± 23			
164	intellifusion-001	278397082	289387	¹⁴³ 762	⁹⁶ 2048 ± 0	²¹⁰ 764 ± 38	¹⁷² 774 ± 39	¹⁵⁶ 797 ± 42	¹³⁸ 803 ± 34	¹¹¹ 805 ± 33	¹²³ 1112 ± 28	¹²⁷ 1128 ± 41			
165	intellifusion-002	781037413	385841	¹⁸³ 941	³¹⁰ 4096 ± 0	²⁷⁹ 950 ± 2	²⁶² 1096 ± 42	²⁴⁹ 1088 ± 33	²³² 1168 ± 31	¹⁹⁰ 1171 ± 10	¹⁶¹ 1713 ± 57	¹⁵⁶ 1665 ± 87			
166	intellivision-001	44741184	11649	⁷⁴ 271	²⁰⁵⁶ 2048 ± 0	⁵ 62 ± 2	-	-	-	-	²¹³ 2573 ± 91	²¹³ 2544 ± 38			
167	intellivision-002	44741184	14505	¹⁰ 81	²⁶⁵ 2056 ± 0	⁵³ 322 ± 1	⁴⁴ 355 ± 2	³⁰ 372 ± 1	²⁹ 422 ± 2	⁶¹ 600 ± 1	³¹⁰ 13525 ± 134	³⁰⁸ 12782 ± 278			
168	intelresearch-003	410975551	85085	²¹⁵ 1177	¹⁵⁴ 2048 ± 0	³³³ 1232 ± 3	²⁸⁹ 1237 ± 2	²⁷⁵ 1242 ± 2	²⁵³ 1263 ± 2	²¹⁶ 1324 ± 3	²⁵⁸ 4443 ± 75	²⁵⁶ 4374 ± 77			
169	intelresearch-004	662444267	85290	²⁸⁸ 1856	¹⁰⁰ 2048 ± 0	³⁴⁷ 1319 ± 2	³⁰⁵ 1322 ± 3	²⁹⁴ 1330 ± 3	²⁶⁹ 1345 ± 3	²³² 1411 ± 5	²⁶¹ 4696 ± 63	²⁵⁹ 4692 ± 66			
170	intsyssmu-001	393635676	172480	¹⁴⁸ 789	²¹⁹ 2048 ± 0	¹⁵⁷ 614 ± 2	¹²⁵ 615 ± 2	¹¹⁶ 642 ± 2	¹²⁷ 750 ± 3	¹⁸⁷ 1159 ± 4	⁵⁶ 621 ± 8	⁵⁴ 611 ± 31			
171	intsyssmu-002	784303912	172298	¹⁴⁷ 786	⁵⁵ 1024 ± 0	¹⁴⁷ 593 ± 1	¹⁷⁸ 793 ± 2	¹⁶² 827 ± 1	¹⁶⁰ 875 ± 104	²¹⁰ 1293 ± 3	³⁶ 549 ± 25	³⁹ 548 ± 29			
172	ionetworks-000	294511946	51236	⁴⁶ 351	¹⁹⁹ 2048 ± 0	⁸³ 430 ± 0	⁶³ 435 ± 0	⁴⁵ 433 ± 0	³⁴ 432 ± 0	²⁶ 444 ± 0	²⁸⁸ 6913 ± 102	²⁹³ 7150 ± 160			
173	iqiface-000	275271315	596337	¹³³ 704	³⁵¹ 4750 ± 32	¹²³ 538 ± 26	⁸³ 494 ± 2	⁸⁴ 543 ± 3	¹²¹ 734 ± 4	²²⁷ 1393 ± 4	³⁶⁶ 636433 ± 38446	³⁶⁶ 632654 ± 85615			
174	iqiface-003	379702979	963398	¹⁵⁴ 817	³⁵² 4763 ± 37	¹¹⁷ 529 ± 1	⁹⁴ 532 ± 2	⁹⁷ 599 ± 8	¹⁵⁴ 850 ± 2	²⁵⁴ 1694 ± 2	³⁶⁵ 575924 ± 2601	³⁶⁵ 576653 ± 2051			
175	irex-000	759705187	47419	³⁰⁴ 2086	³⁰¹ 3080 ± 0	²⁴⁶ 852 ± 2	¹⁹⁸ 850 ± 1	¹⁷⁹ 874 ± 2	¹⁸¹ 939 ± 1	²⁰² 1249 ± 5	⁷ 201 ± 11	⁹ 208 ± 8			
176	isap-001	101427082	204201	¹ 18	³⁰⁶ 4096 ± 0	¹⁰ ± 0	-	-	-	-	²⁸ 459 ± 17	³² 456 ± 11			

Notes

- 1 The configuration size does not capture static data included in libraries.
- 2 The library size is the combined total of all files provided in the submission lib folder. These libraries e.g. OpenCV may or may not be installed on any end user's platform natively and would not need to be installed with the algorithm. Some developers put neural network models in their libraries.
- 3 The memory usage is the peak resident set size reported by the ps system call during template generation.
- 4 The median template creation times are measured on Intel®Xeon®CPU E5-2630 v4 @ 2.20GHz processors.
- 5 The comparison durations, in nanoseconds, are estimated using std::chrono::high_resolution_clock which on the machine in (2) counts 1ns clock ticks. Precision is somewhat worse than that however. The ± value is the median absolute deviation times 1.48 for Normal consistency.

Table 10: Summary of algorithms and properties included in this report. The red superscripts give ranking for the quantity in that column.

	ALGORITHM	CONFIG	LIBRARY	TEMPLATE								COMPARISON ⁴			
				NAME	DATA	DATA	MEMORY	SIZE	GENERATION TIME (ms) ⁴				TIME (ns) ⁵		
									(KB) ¹	(KB) ²	(MB) ³	(B)	MUGSHOT	480x720	960x1440
177	isap-002	262928187	49931	⁴¹ isap-002	288	²²⁸ 2048 ± 0	²¹⁴ 769 ± 3	²⁴⁵ 1027 ± 2	¹⁸² 877 ± 2	¹³² 761 ± 1	¹³⁴ 912 ± 2	²²⁹ 3045 ± 94	²²⁴ 2973 ± 66		
178	isityou-000	49163234	36621	¹⁴ isityou-000	110	³⁶⁷ 19200 ± 0	¹³ 113 ± 5	-	-	-	-	³⁶⁰ 237517 ± 1318	³⁶⁰ 237374 ± 1279		
179	isystems-001	281212446	639268	²⁰⁹ isystems-001	1091	¹⁴² 2048 ± 0	⁴⁷ 291 ± 9	-	-	-	-	³⁸ 557 ± 16	⁴¹ 564 ± 22		
180	isystems-002	367599646	803389	²⁶⁹ isystems-002	1595	¹⁹² 2048 ± 0	²³⁶ 822 ± 8	-	-	-	-	⁸¹ 749 ± 31	⁶³ 632 ± 28		
181	itmo-006	613567913	96762	²⁵⁹ itmo-006	1489	²⁹⁴ 2121 ± 0	²²⁹ 814 ± 1	¹⁹¹ 831 ± 26	¹⁶⁵ 830 ± 17	¹⁴⁵ 830 ± 3	¹⁴⁴ 952 ± 38	³³⁵ 26154 ± 148	³³⁴ 26217 ± 260		
182	itmo-007	425962652	245376	³⁰⁸ itmo-007	2199	⁸⁵ 2048 ± 0	²⁰⁵ 741 ± 2	-	-	-	-	²¹² 2551 ± 50	²¹¹ 2529 ± 80		
183	ivacognitive-001	263125888	62791	¹⁸⁵ ivacognitive-001	947	⁹⁰ 2048 ± 0	³⁴⁴ 1292 ± 3	²⁹⁹ 1289 ± 4	²⁸⁴ 1292 ± 4	²⁵⁶ 1292 ± 3	²¹⁵ 1321 ± 4	²⁵⁵ 4228 ± 41	²⁵⁴ 4226 ± 41		
184	iws-000	31616555	3063	⁸⁷⁷ iws-000	77	¹⁸ 512 ± 0	⁴¹ 277 ± 5	³¹ 283 ± 1	⁶⁷ 494 ± 3	¹⁹¹ 984 ± 3	²⁹² 2987 ± 39	¹⁰⁹ 999 ± 40	¹⁰⁸ 992 ± 22		
185	kakao-005	424259623	152216	²⁶⁸ kakao-005	1581	²⁵⁹ 2052 ± 0	³⁰⁴ 1068 ± 1	²⁵⁷ 1073 ± 1	²⁴³ 1079 ± 0	²¹⁵ 1077 ± 1	¹⁷⁶ 1089 ± 1	¹⁹¹ 2067 ± 26	¹⁹⁰ 2043 ± 34		
186	kakao-006	603822288	127879	³¹⁴ kakao-006	2470	¹¹⁸ 2048 ± 0	³⁶⁷ 1652 ± 3	³²³ 1655 ± 2	³¹⁷ 1662 ± 3	²⁹⁵ 1660 ± 3	²⁵² 1664 ± 3	¹⁰⁵ 985 ± 28	¹⁰² 948 ± 25		
187	kakaopay-001	407413757	179869	¹²⁶ kakaopay-001	684	³¹⁵ 4096 ± 0	⁸⁹ 448 ± 0	⁹⁹ 542 ± 0	⁸² 542 ± 0	⁶⁵ 542 ± 0	⁵⁰ 553 ± 0	⁶⁰ 633 ± 22	⁶¹ 630 ± 22		
188	kedacom-000	251179996	37401	³⁶⁷ kedacom-000	23574	¹¹ 292 ± 0	¹¹² 506 ± 3	¹⁰² 547 ± 10	¹⁰⁵ 614 ± 9	⁷³ 588 ± 10	⁷⁶ 665 ± 24	⁶⁷ 684 ± 14	⁷¹ 682 ± 16		
189	kiwitech-000	378584700	21375	¹⁵² kiwitech-000	808	¹⁸⁰ 2048 ± 0	¹⁴⁵ 591 ± 0	¹¹⁹ 594 ± 0	⁹⁶ 595 ± 1	⁷⁹ 596 ± 0	⁶² 609 ± 0	¹⁶⁴ 1755 ± 20	¹⁶⁴ 1734 ± 16		
190	kneron-003	59767577	1747	²⁸ kneron-003	188	¹⁶⁴ 2048 ± 0	⁴³ 281 ± 3	³⁰ 280 ± 1	²² 315 ± 13	²³ 365 ± 7	²⁰⁰ 1224 ± 30	²⁶⁶ 5237 ± 63	²⁶⁶ 5274 ± 99		
191	kneron-005	384383985	13633	⁶⁵ kneron-005	457	⁸⁸ 2048 ± 0	¹¹⁶ 518 ± 2	⁹¹ 522 ± 4	⁸⁹ 556 ± 5	¹³⁰ 757 ± 19	²⁵⁵ 1760 ± 25	¹⁸² 1922 ± 11	¹⁸² 1926 ± 20		
192	kookmin-002	380693533	30734	¹⁵⁹ kookmin-002	827	⁸⁹ 2048 ± 0	³⁰⁰ 1038 ± 2	²⁵³ 1047 ± 1	²³⁶ 1045 ± 1	²¹¹ 1061 ± 1	¹⁷⁸ 1116 ± 1	⁶³ 638 ± 19	⁶⁶ 636 ± 20		
193	kookmin-003	597396019	30734	²⁵⁴ kookmin-003	1448	¹⁸² 2048 ± 0	³⁶⁸ 2221 ± 6	³²⁶ 2220 ± 4	³²³ 2233 ± 2	³¹² 2237 ± 2	²⁷² 2275 ± 2	⁴⁸ 605 ± 16	⁵⁰ 600 ± 14		
194	kuke3d-001	413145303	68786	⁹¹ kuke3d-001	530	³²⁸ 4096 ± 0	²²⁸ 814 ± 2	¹⁸³ 811 ± 2	¹⁶¹ 814 ± 2	¹⁴⁰ 814 ± 1	¹²² 834 ± 1	²⁸⁵ 6412 ± 57	²⁸⁵ 6413 ± 51		
195	lemalabs-001	766361714	198794	³²³ lemalabs-001	2738	¹⁸⁷ 2048 ± 0	²²⁵ 810 ± 0	¹⁸⁴ 812 ± 0	¹⁵⁹ 813 ± 0	¹⁴² 819 ± 0	¹²³ 844 ± 1	³⁰⁶ 11930 ± 35	³⁰⁶ 11913 ± 37		
196	line-000	270789845	407003	¹⁰⁶ line-000	590	²³⁵ 2048 ± 0	¹³⁹ 586 ± 0	¹²² 612 ± 0	¹⁰² 609 ± 1	⁸¹ 611 ± 0	⁶⁴ 618 ± 1	²²⁰ 2753 ± 19	²¹⁹ 2745 ± 23		
197	line-001	967019668	407058	³⁰⁹ line-001	2373	¹⁷⁸ 2048 ± 0	²⁴¹ 833 ± 10	¹⁹⁰ 830 ± 3	¹⁶⁴ 828 ± 4	¹⁵⁰ 838 ± 8	¹²⁰ 833 ± 4	²¹⁸ 2696 ± 23	²¹⁸ 2677 ± 35		
198	lookman-002	141516916	25410	³⁶⁵ lookman-002	16518	⁴⁸ 548 ± 0	²⁰ 173 ± 1	-	-	-	-	⁵¹ 610 ± 19	⁵⁵ 612 ± 22		
199	lookman-004	250650528	37401	³⁶⁶ lookman-004	23548	⁴⁷ 548 ± 0	¹¹³ 507 ± 5	¹⁰⁰ 545 ± 12	¹⁰⁴ 613 ± 12	⁷⁷ 590 ± 11	⁷² 656 ± 16	⁹⁷ 871 ± 29	⁹⁸ 878 ± 29		
200	luxand-000	0	57908	²³⁹ luxand-000	1366	⁶⁶ 1040 ± 0	⁷⁴ 407 ± 23	⁶¹ 433 ± 11	⁵¹ 444 ± 14	⁴³ 464 ± 14	⁵⁴ 562 ± 25	⁹⁴ 828 ± 28	⁹⁵ 828 ± 32		
201	mantra-000	482773318	62566	¹⁴² mantra-000	749	²⁴⁷ 2052 ± 0	⁷⁷ 413 ± 18	⁸⁰ 487 ± 19	⁶⁶ 494 ± 18	⁵⁷ 511 ± 18	⁶⁰ 598 ± 19	²³⁴ 3151 ± 51	²³² 3127 ± 63		
202	maxvision-000	136309395	56426	²⁸³ maxvision-000	1791	³⁵ 512 ± 0	⁶⁴ 359 ± 0	⁴⁵ 356 ± 0	²⁸ 359 ± 0	²¹ 356 ± 0	¹⁹ 370 ± 1	²⁰⁷ 2461 ± 20	²⁰⁶ 2452 ± 17		
203	megvii-002	185299399	16491	²⁸⁹ megvii-002	1879	³⁴¹ 4100 ± 0	¹⁶⁹ 644 ± 0	-	-	-	-	³⁴⁷ 50630 ± 183	³⁴⁷ 47591 ± 716		
204	megvii-003	4536617822	42790	³⁵² megvii-003	4878	³⁰⁹ 4096 ± 0	³²⁸ 1210 ± 1	²⁸⁷ 1223 ± 0	²⁹⁷ 1356 ± 4	²⁹³ 1582 ± 7	²⁸⁵ 2727 ± 23	³⁵⁹ 225342 ± 3574	³⁵⁹ 225413 ± 644		
205	meituan-000	265743335	333178	⁹⁷ meituan-000	554	¹⁰⁶ 2048 ± 0	⁸⁵ 436 ± 4	⁶⁸ 441 ± 1	¹⁰⁷ 626 ± 5	²¹⁶ 1098 ± 15	²⁹ 3126 ± 53	⁶² 638 ± 17	⁶⁴ 633 ± 16		
206	meiya-001	286777340	264913	⁸² meiya-001	507	²⁴⁵ 2049 ± 0	¹⁶⁰ 622 ± 12	-	-	-	-	²⁹⁶ 8356 ± 615	²⁹⁶ 8134 ± 97		
207	mendaxiatech-000	1988071377	45484	³³⁸ mendaxiatech-000	3195	³³⁶ 4097 ± 0	³³⁶ 1243 ± 2	²⁹¹ 1255 ± 1	³⁰⁰ 1373 ± 2	²⁹⁴ 1598 ± 3	²⁸⁴ 2689 ± 8	³⁴⁶ 46906 ± 275	³⁴⁶ 46872 ± 217		
208	microfocus-001	107032902	27242	²⁹ microfocus-001	190	³²⁵ 256 ± 0	³⁸ 264 ± 18	-	-	-	-	¹⁰ 215 ± 8	¹⁰ 217 ± 10		
209	microfocus-002	98599914	27362	²⁸ microfocus-002	176	⁴ 256 ± 0	³³ 259 ± 18	-	-	-	-	²¹ 337 ± 34	¹² 230 ± 25		
210	minivision-000	856777875	16597	³⁴⁹ minivision-000	4013	³¹⁴ 4096 ± 0	²⁹⁹ 1035 ± 1	²⁵⁰ 1033 ± 2	²³⁵ 1035 ± 1	²⁰⁵ 1037 ± 1	¹⁷⁰ 1059 ± 2	²⁰⁸ 2466 ± 26	²⁰⁷ 2460 ± 25		
211	mobai-000	374222377	80573	¹⁴⁶ mobai-000	786	³⁵⁸ 6144 ± 0	²¹¹ 766 ± 8	²⁰⁴ 869 ± 6	²⁷² 1205 ± 31	³⁰⁴ 1867 ± 45	²⁹⁸ 3549 ± 190	³¹⁵ 16458 ± 333	³¹⁵ 16423 ± 1473		
212	mobai-001	271664763	60164	⁹² mobai-001	534	¹⁸⁶ 2048 ± 0	¹⁵⁴ 612 ± 3	¹²⁴ 614 ± 3	¹²⁹ 687 ± 9	¹⁶⁵ 886 ± 31	¹⁵⁷ 1707 ± 103	¹⁴¹ 1386 ± 25	¹⁴² 1377 ± 26		
213	mobbl-000	186421478	58727	³⁷ mobbl-000	262	¹⁹⁰ 2048 ± 0	³⁶ 261 ± 16	²⁵ 267 ± 22	³¹ 375 ± 92	⁹⁷ 655 ± 273	²⁶⁵ 2059 ± 1129	³⁰⁸ 12061 ± 142	³⁰⁷ 12050 ± 133		
214	mobbl-001	236708614	58706	³³ mobbl-001	223	¹⁰² 2048 ± 0	²³ 183 ± 32	¹⁴ 184 ± 25	²⁷ 354 ± 76	¹⁴² 823 ± 396	²⁸⁷ 2781 ± 1166	³⁰⁵ 11832 ± 109	³⁰⁵ 11851 ± 88		
215	moreedian-000	537865562	21374	¹⁸⁰ moreedian-000	932	²¹³ 2048 ± 0	¹⁹⁴ 694 ± 0	¹⁴⁹ 698 ± 0	¹³⁵ 699 ± 0	¹¹⁰ 700 ± 0	⁸⁷ 713 ± 1	¹⁷³ 1803 ± 11	¹⁷⁰ 1779 ± 23		
216	multimodality-000	0	503924	²⁴⁸ multimodality-000	1417	²¹⁶ 2048 ± 0	⁷⁸ 416 ± 0	⁵⁶ 420 ± 0	⁴² 423 ± 0	³² 427 ± 0	²⁸ 463 ± 0	⁹⁵ 848 ± 25	⁹² 800 ± 28		
217	mvision-001	232962922	149531	¹³⁷ mvision-001	723	²⁸ 512 ± 0	¹⁹² 691 ± 21	¹⁵¹ 702 ± 19	¹³⁴ 697 ± 24	¹¹³ 708 ± 29	⁸⁵ 710 ± 27	¹²⁵ 1123 ± 40	¹³¹ 1154 ± 38		
218	nazhiai-000	560624381	16141	³²⁰ nazhiai-000	2716	¹²⁰ 2048 ± 0	¹⁸⁹ 683 ± 3	¹⁴⁵ 687 ± 2	¹⁶⁸ 835 ± 27	¹⁵² 840 ± 31	¹²¹ 834 ± 34	¹⁹⁹ 2230 ± 34	¹⁹⁶ 2133 ± 81		
219	neosystems-001	589102173	349959	²¹⁹ neosystems-001	1214	²¹⁰ 2048 ± 0	³¹⁴ 1137 ± 4	²⁶³ 1098 ± 1	³²⁰ 1767 ± 4	³⁰¹ 1769 ± 3	²⁶⁰ 1765 ± 4	³¹⁸ 18557 ± 189	³²⁰ 18640 ± 192		
220	neosystems-002	613827997	349942	²²² neosystems-002	1222	⁸⁷ 2048 ± 0	<sup								

ALGORITHM			CONFIG	LIBRARY	TEMPLATE						COMPARISON ⁴	
NAME		DATA	DATA	MEMORY	SIZE	GENERATION TIME (ms) ⁴				TIME (ns) ⁵		
		(KB) ¹	(KB) ²	(MB) ³	(B)	MUGSHOT	480x720	960x1440	1600x2400	3000x4500	GENUINE	IMPOSTOR
221	netbridge-tech-001	136302786	205875	83 ⁵⁰⁸	333 ^{4096 ± 0}	785 ± 1	483 ± 0	484 ± 0	492 ± 0	4113 ± 4	299 ^{9280 ± 74}	299 ^{9446 ± 512}
222	netbridge-tech-002	263871604	49931	43 ²⁹⁹	144 ^{2048 ± 0}	242 ^{838 ± 6}	194 ^{838 ± 2}	169 ^{839 ± 1}	151 ^{839 ± 3}	124 ^{859 ± 3}	224 ^{2893 ± 65}	229 ^{3050 ± 123}
223	neurotechnology-011	372877031	51141	256 ¹⁴⁶²	38 ^{514 ± 0}	222 ^{798 ± 1}	180 ^{802 ± 1}	163 ^{827 ± 3}	159 ^{873 ± 2}	171 ^{1059 ± 15}	2 ^{114 ± 11}	2 ^{114 ± 8}
224	neurotechnology-012	151378192	51395	153 ⁸¹⁴	2 ^{256 ± 0}	71 ^{384 ± 0}	48 ^{387 ± 0}	36 ^{404 ± 1}	435 ± 1	57 ^{583 ± 7}	3 ^{119 ± 7}	3 ^{116 ± 7}
225	nhn-001	34464916	817674	120 ⁶⁶²	319 ^{4096 ± 0}	297 ^{1027 ± 3}	248 ^{1029 ± 1}	231 ^{1029 ± 1}	208 ^{1044 ± 1}	177 ^{1090 ± 1}	349 ^{56650 ± 260}	350 ^{56639 ± 210}
226	nhn-002	372194536	817674	124 ⁶⁶⁷	308 ^{4096 ± 0}	315 ^{1141 ± 3}	270 ^{1138 ± 2}	256 ^{1141 ± 2}	231 ^{1151 ± 6}	193 ^{1203 ± 2}	348 ^{56608 ± 579}	349 ^{56549 ± 606}
227	nodeflux-002	793260136	690213	69 ⁴⁶⁶	223 ^{2048 ± 0}	199 ^{708 ± 4}	154 ^{709 ± 4}	141 ^{716 ± 5}	118 ^{716 ± 7}	96 ^{736 ± 3}	245 ^{3475 ± 62}	242 ^{3408 ± 143}
228	notiontag-001	94979467	427967	102 ⁵⁶⁶	49 ^{584 ± 0}	271 ^{929 ± 35}	259 ^{1092 ± 39}	326 ^{3709 ± 81}	326 ^{10233 ± 180}	-	342 ^{43636 ± 286}	342 ^{43724 ± 330}
229	notiontag-002	278515288	967207	329 ²⁸⁴⁰	293 ^{2120 ± 0}	90 ^{453 ± 2}	67 ^{453 ± 3}	52 ^{453 ± 3}	39 ^{458 ± 2}	30 ^{471 ± 3}	324 ^{20278 ± 194}	324 ^{20195 ± 186}
230	nsensecorp-002	191919991	122407	98 ⁵⁵⁴	201 ^{2048 ± 0}	56 ^{333 ± 0}	39 ^{333 ± 0}	25 ^{337 ± 0}	20 ^{338 ± 0}	18 ^{351 ± 0}	345 ^{45965 ± 213}	345 ^{45988 ± 158}
231	nsensecorp-003	204692907	117041	136 ⁷¹⁰	127 ^{2048 ± 0}	178 ^{661 ± 0}	136 ^{664 ± 0}	122 ^{662 ± 1}	98 ^{659 ± 1}	73 ^{659 ± 0}	343 ^{44658 ± 51}	344 ^{44654 ± 72}
232	ntechlab-010	715357382	217167	334 ²⁹⁹¹	73 ^{1280 ± 0}	321 ^{1177 ± 2}	281 ^{1180 ± 2}	271 ^{1197 ± 2}	245 ^{1224 ± 1}	219 ^{1326 ± 3}	27 ^{405 ± 13}	30 ^{416 ± 31}
233	ntechlab-011	805820346	209458	359 ⁶⁸⁶⁷	71 ^{1280 ± 0}	318 ^{1148 ± 2}	271 ^{1142 ± 1}	260 ^{1159 ± 1}	237 ^{1185 ± 1}	209 ^{1290 ± 3}	4 ^{179 ± 11}	5 ^{173 ± 11}
234	omnigarde-000	270395030	32882	88 ⁵²³	54 ^{1024 ± 0}	270 ^{944 ± 0}	213 ^{887 ± 0}	188 ^{888 ± 1}	167 ^{892 ± 0}	132 ^{902 ± 0}	217 ^{2671 ± 35}	216 ^{2620 ± 29}
235	omnigarde-001	205336408	32882	67 ⁴⁶⁴	33 ^{512 ± 0}	273 ^{941 ± 0}	211 ^{883 ± 1}	184 ^{886 ± 1}	166 ^{891 ± 1}	130 ^{898 ± 0}	145 ^{1405 ± 31}	143 ^{1379 ± 26}
236	openface-001	0	40111	13 ¹⁰⁰	149 ^{2048 ± 0}	17 ^{148 ± 1}	10 ^{154 ± 0}	29 ^{365 ± 3}	28 ^{409 ± 9}	63 ^{616 ± 31}	49 ^{608 ± 14}	53 ^{604 ± 13}
237	oz-002	733207161	170261	339 ³⁵⁶¹	286 ^{2065 ± 0}	303 ^{1064 ± 3}	275 ^{1171 ± 3}	325 ^{2953 ± 6}	324 ^{7352 ± 13}	321 ^{26658 ± 29}	358 ^{131108 ± 1408}	358 ^{126758 ± 913}
238	oz-003	495766974	519652	364 ¹¹⁹⁴⁹	263 ^{2053 ± 0}	351 ^{1375 ± 12}	310 ^{1388 ± 3}	321 ^{1773 ± 16}	308 ^{2039 ± 6}	296 ^{3209 ± 5}	356 ^{73905 ± 456}	356 ^{73892 ± 444}
239	papsav1923-001	285911345	52652	71 ⁴⁷³	104 ^{2048 ± 0}	162 ^{626 ± 1}	128 ^{628 ± 1}	109 ^{630 ± 1}	93 ^{648 ± 2}	101 ^{744 ± 3}	78 ^{725 ± 25}	81 ^{731 ± 28}
240	paravision-004	570030501	145440	266 ¹⁵⁷²	312 ^{4096 ± 0}	238 ^{829 ± 2}	193 ^{834 ± 6}	167 ^{832 ± 2}	146 ^{833 ± 4}	119 ^{833 ± 2}	80 ^{737 ± 31}	79 ^{718 ± 38}
241	paravision-008	555203492	204400	253 ¹⁴⁴⁸	322 ^{4096 ± 0}	196 ^{699 ± 0}	150 ^{700 ± 0}	136 ^{701 ± 0}	111 ^{702 ± 1}	84 ^{702 ± 0}	22 ^{337 ± 17}	23 ^{330 ± 13}
242	pensees-001	1658297650	408932	291 ¹⁹²²	363 ^{8200 ± 0}	309 ^{1108 ± 3}	317 ^{1448 ± 17}	308 ^{1439 ± 10}	287 ^{1464 ± 5}	247 ^{1546 ± 9}	233 ^{3151 ± 34}	233 ^{3143 ± 25}
243	pixelall-005	0	1001355	232 ¹²⁹²	354 ^{5120 ± 0}	311 ^{1112 ± 3}	265 ^{1115 ± 1}	249 ^{1120 ± 1}	221 ^{1124 ± 2}	183 ^{1143 ± 2}	136 ^{1259 ± 29}	137 ^{1243 ± 23}
244	pixelall-006	0	746305	181 ⁹³⁴	296 ^{2560 ± 0}	296 ^{1024 ± 3}	247 ^{1028 ± 2}	233 ^{1033 ± 1}	204 ^{1032 ± 1}	165 ^{1054 ± 2}	82 ^{754 ± 14}	80 ^{722 ± 10}
245	psl-007	977255992	524521	350 ⁴⁰⁴²	302 ^{3144 ± 0}	357 ^{1408 ± 5}	315 ^{1417 ± 3}	307 ^{1418 ± 3}	281 ^{1419 ± 2}	235 ^{1422 ± 3}	13 ^{265 ± 22}	16 ^{258 ± 17}
246	psl-008	977255943	524525	343 ³⁸⁰⁷	303 ^{3144 ± 0}	358 ^{1412 ± 4}	314 ^{1415 ± 3}	306 ^{1416 ± 2}	280 ^{1418 ± 2}	233 ^{1418 ± 2}	12 ^{259 ± 22}	15 ^{252 ± 22}
247	ptakuratsatu-000	29	585434	238 ¹³⁴⁷	44 ^{538 ± 0}	256 ^{875 ± 3}	203 ^{863 ± 48}	202 ^{928 ± 9}	188 ^{958 ± 17}	173 ^{1066 ± 26}	276 ^{5900 ± 103}	275 ^{5687 ± 167}
248	pxl-001	112759507	78231	22 ¹⁶⁸	32 ^{512 ± 0}	11 ^{101 ± 5}	7 ^{104 ± 5}	12 ^{189 ± 12}	27 ^{408 ± 27}	241 ^{1470 ± 144}	272 ^{5598 ± 45}	273 ^{5590 ± 68}
249	pyramid-000	381551539	219883	151 ⁸⁰⁴	267 ^{2056 ± 0}	138 ^{583 ± 2}	-	-	-	-	293 ^{7147 ± 59}	294 ^{7586 ± 425}
250	qnap-000	191213193	15598	39 ²⁷²	150 ^{2048 ± 0}	201 ^{726 ± 9}	69 ^{457 ± 1}	53 ^{458 ± 0}	41 ^{464 ± 1}	33 ^{482 ± 2}	65 ^{660 ± 25}	68 ^{654 ± 29}
251	quantasoft-003	379410922	211354	201 ¹⁰⁵⁸	232 ^{2048 ± 0}	166 ^{632 ± 2}	131 ^{634 ± 0}	110 ^{632 ± 0}	88 ^{631 ± 1}	68 ^{634 ± 0}	8 ^{201 ± 7}	8 ^{203 ± 8}
252	rankone-010	441	138435	11 ⁸³	7 ^{261 ± 0}	26 ^{193 ± 1}	-	-	-	-	15 ^{282 ± 13}	13 ^{234 ± 16}
253	rankone-011	437	179209	20 ¹⁴⁶	8 ^{261 ± 0}	132 ^{567 ± 1}	104 ^{557 ± 1}	90 ^{567 ± 1}	72 ^{586 ± 1}	80 ^{682 ± 3}	16 ^{283 ± 14}	11 ^{220 ± 19}
254	realnetworks-004	176471448	913988	313 ²⁴⁶⁷	264 ^{2056 ± 0}	54 ^{330 ± 4}	38 ^{333 ± 3}	34 ^{402 ± 7}	71 ^{585 ± 15}	229 ^{1402 ± 51}	129 ^{1210 ± 29}	134 ^{1202 ± 17}
255	realnetworks-005	176387363	56755	131 ⁶⁹⁷	274 ^{2056 ± 0}	29 ^{211 ± 4}	16 ^{205 ± 3}	19 ^{290 ± 6}	59 ^{515 ± 17}	212 ^{1312 ± 78}	130 ^{1213 ± 17}	135 ^{1207 ± 16}
256	regula-000	268743079	29384	114 ⁶¹⁰	207 ^{2048 ± 0}	327 ^{1187 ± 1}	268 ^{1126 ± 1}	253 ^{1129 ± 0}	224 ^{1132 ± 1}	186 ^{1159 ± 1}	34 ^{491 ± 16}	36 ^{500 ± 22}
257	remarkai-001	247662347	868314	138 ⁷³⁰	257 ^{2052 ± 0}	240 ^{831 ± 6}	197 ^{849 ± 18}	239 ^{1055 ± 25}	241 ^{1198 ± 34}	246 ^{1519 ± 38}	134 ^{1229 ± 20}	93 ^{805 ± 56}
258	remarkai-003	287249016	58559	346 ³⁸⁹⁶	340 ^{4100 ± 0}	289 ^{986 ± 1}	237 ^{993 ± 1}	222 ^{992 ± 1}	197 ^{999 ± 3}	158 ^{1019 ± 2}	90 ^{787 ± 20}	90 ^{793 ± 22}
259	rendip-000	0	437653	125 ⁶⁸²	196 ^{2048 ± 0}	94 ^{464 ± 2}	70 ^{458 ± 0}	60 ^{473 ± 0}	48 ^{483 ± 1}	53 ^{556 ± 4}	39 ^{576 ± 13}	42 ^{573 ± 11}
260	revealmedia-005	300987562	202465	144 ⁷⁶³	339 ^{4100 ± 0}	82 ^{428 ± 0}	58 ^{428 ± 0}	44 ^{430 ± 0}	35 ^{433 ± 0}	25 ^{442 ± 0}	187 ^{2023 ± 38}	188 ^{2009 ± 26}
261	rokid-000	264818990	396624	221 ¹²¹⁸	270 ^{2056 ± 0}	125 ^{546 ± 3}	98 ^{542 ± 2}	85 ^{545 ± 1}	60 ^{522 ± 3}	55 ^{563 ± 4}	244 ^{3457 ± 62}	246 ^{3463 ± 77}
262	rokid-001	656613085	413733	204 ¹⁰⁷¹	284 ^{2060 ± 0}	263 ^{911 ± 2}	217 ^{901 ± 5}	187 ^{899 ± 2}	170 ^{900 ± 3}	131 ^{901 ± 3}	239 ^{3345 ± 50}	239 ^{3346 ± 149}
263	s1-002	532647605	95479	240 ¹³⁷⁴	357 ^{6144 ± 0}	338 ^{1257 ± 1}	293 ^{1260 ± 1}	278 ^{1261 ± 1}	252 ^{1262 ± 1}	206 ^{1273 ± 1}	259 ^{4513 ± 25}	257 ^{4479 ± 25}
264	s1-003	149001906	95446	156 ⁸¹⁷	305 ^{4096 ± 0}	277 ^{947 ± 0}	232 ^{959 ± 0}	210 ^{952 ± 0}	186 ^{952 ± 1}	146 ^{955 ± 1}	248 ^{3657 ± 19}	248 ^{3652 ± 16}

Notes

- 1 The configuration size does not capture static data included in libraries.
- 2 The library size is the combined total of all files provided in the submission lib folder. These libraries e.g. OpenCV may or may not be installed on any end user's platform natively and would not need to be installed with the algorithm. Some developers put neural network models in their libraries.
- 3 The memory usage is the peak resident set size reported by the ps system call during template generation.
- 4 The median template creation times are measured on Intel®Xeon®CPU E5-2630 v4 @ 2.20GHz processors.
- 5 The comparison durations, in nanoseconds, are estimated using std::chrono::high_resolution_clock which on the machine in (2) counts 1ns clock ticks. Precision is somewhat worse than that however. The ± value is the median absolute deviation times 1.48 for Normal consistency.

Table 12: Summary of algorithms and properties included in this report. The red superscripts give ranking for the quantity in that column.

	ALGORITHM	CONFIG	LIBRARY	TEMPLATE								COMPARISON ⁴	
				NAME				GENERATION TIME (ms) ⁴				TIME (ns) ⁵	
				DATA (KB) ¹	DATA (KB) ²	MEMORY (MB) ³	SIZE (B)	MUGSHOT	480x720	960x1440	1600x2400	3000x4500	GENUINE
265	saffe-001	88036907	62488	²⁴ 168	⁷⁰ 1280 ± 0	⁴⁴ 281 ± 1	-	-	-	-	-	¹³⁷ 1274 ± 19	¹⁴⁰ 1277 ± 26
266	saffe-002	266877685	28285	¹⁶⁴ 855	⁹⁸ 2048 ± 0	²³¹ 817 ± 11	¹⁸² 805 ± 15	¹⁵⁸ 809 ± 19	¹⁴¹ 815 ± 29	¹¹⁴ 813 ± 23	⁷⁶ 717 ± 7	⁷⁸ 714 ± 29	
267	samsungsds-000	0	307431	²⁰⁷ 1083	²⁰⁴ 2048 ± 0	⁵² 316 ± 0	³⁷ 326 ± 5	²³ 328 ± 4	¹⁸ 327 ± 1	¹⁷ 343 ± 0	³²⁷ 23722 ± 295	³²⁷ 23874 ± 305	
268	samtech-001	294996593	219883	¹¹² 605	²⁷⁷ 2056 ± 0	⁴⁸ 294 ± 3	-	-	-	-	²⁹⁵ 7694 ± 59	²⁹⁵ 7678 ± 91	
269	scanovate-001	263253470	328532	¹¹⁰ 601	¹⁹⁵ 2048 ± 0	¹³⁵ 577 ± 24	¹⁰⁸ 577 ± 21	¹¹² 632 ± 27	¹³³ 770 ± 28	²³¹ 1404 ± 32	³⁰⁷ 12054 ± 699	³¹⁰ 13795 ± 705	
270	scanovate-002	263153867	457227	¹⁶³ 850	⁹⁷ 2048 ± 0	¹⁹⁵ 696 ± 32	¹⁵⁵ 713 ± 33	¹⁴⁶ 738 ± 28	¹³⁴ 779 ± 32	¹⁹¹ 1172 ± 53	²²⁸ 3021 ± 38	²³¹ 3120 ± 163	
271	securifai-001	123178989	12456	²⁵² 1445	³⁴⁵ 4104 ± 0	³⁰ 211 ± 1	¹⁷ 211 ± 1	¹³ 211 ± 1	¹⁰ 211 ± 1	⁹ 211 ± 1	¹⁵⁷ 1681 ± 29	¹⁶⁰ 1701 ± 25	
272	securifai-003	311085322	13512	³³¹ 2868	³⁴⁸ 4104 ± 0	¹²⁶ 549 ± 7	¹⁰³ 550 ± 7	⁸⁷ 549 ± 7	⁶⁶ 546 ± 6	⁴⁸ 546 ± 6	¹⁶² 1714 ± 26	¹⁶¹ 1713 ± 37	
273	sensetime-004	977575461	30733	³⁶³ 7843	⁶² 1028 ± 0	³⁶¹ 1437 ± 15	-	-	-	-	¹³⁵ 1239 ± 31	¹³² 1171 ± 22	
274	sensetime-005	783721534	37673	³⁵⁷ 6133	⁶³ 1028 ± 0	³⁴⁹ 1361 ± 27	³⁰² 1304 ± 1	²⁹² 1319 ± 1	²⁷² 1360 ± 1	²⁴⁵ 1514 ± 1	¹³³ 1223 ± 28	¹³³ 1184 ± 29	
275	sertis-000	271945833	68770	⁵⁸ 427	¹¹⁶ 2048 ± 0	²⁰⁸ 754 ± 0	¹⁶⁹ 759 ± 0	¹⁵² 764 ± 0	¹³¹ 760 ± 0	¹⁰⁵ 763 ± 0	¹⁵⁰ 1497 ± 29	¹⁵⁴ 1582 ± 38	
276	sertis-002	471849050	68929	²⁴⁴ 1391	¹⁰³ 2048 ± 0	³²⁵ 1181 ± 1	²⁷⁷ 1178 ± 0	²⁶⁶ 1183 ± 0	²³⁹ 1187 ± 0	¹⁹⁸ 1221 ± 0	¹¹⁹ 1086 ± 32	¹¹⁹ 1076 ± 31	
277	seventhsense-000	378726405	1561668	¹⁵⁸ 824	²⁶¹ 2052 ± 0	³³⁷ 1250 ± 3	²⁹² 1257 ± 1	²⁷⁷ 1261 ± 1	²⁵¹ 1259 ± 1	²⁰⁵ 1272 ± 2	¹⁷¹ 1800 ± 35	¹⁷² 1787 ± 32	
278	shaman-000	0	120033	⁸⁰ 507	³²⁹ 4096 ± 0	¹⁷³ 653 ± 16	-	-	-	-	²⁵ 380 ± 25	²⁷ 379 ± 31	
279	shaman-001	0	174446	⁸⁵ 511	³¹ 4096 ± 0	⁴⁹ 294 ± 2	-	-	-	-	⁶¹ 635 ± 19	³¹ 441 ± 25	
280	shu-002	748800469	148309	¹⁷⁰ 890	³²⁶ 4096 ± 0	²⁰⁷ 751 ± 2	¹⁷¹ 769 ± 4	¹⁹⁶ 922 ± 4	²⁸⁵ 1431 ± 9	²⁹⁷ 3489 ± 47	³⁶⁸ 2930763 ± 47355	³⁶⁸ 2929759 ± 39149	
281	shu-003	439065557	146940	⁸⁴ 511	²¹⁵ 2048 ± 0	²³³ 820 ± 6	¹⁸⁹ 828 ± 3	²⁰⁵ 941 ± 9	²⁶² 1308 ± 15	²⁹³ 3045 ± 44	²⁰⁹ 2506 ± 26	²¹⁰ 2512 ± 38	
282	siat-002	498527179	7738	³¹¹ 2434	²⁵⁶ 2052 ± 0	¹³⁶ 579 ± 0	-	-	-	-	⁸⁷ 769 ± 13	⁸⁵ 750 ± 13	
283	siat-004	962642717	6984	³⁴⁵ 3860	³⁴² 4100 ± 0	¹⁸³ 670 ± 0	¹⁴⁰ 671 ± 7	¹³¹ 693 ± 10	¹²⁶ 742 ± 10	¹³⁹ 935 ± 17	²⁵⁴ 4013 ± 45	²⁵¹ 3782 ± 173	
284	sjtu-003	492334366	148243	⁹⁴ 538	¹⁵³ 2048 ± 0	²³⁵ 821 ± 2	¹⁸⁵ 820 ± 2	¹⁹⁸ 923 ± 3	²⁴² 1201 ± 3	²⁷⁶ 2373 ± 9	¹⁵² 1560 ± 20	¹⁵² 1560 ± 14	
285	sjtu-004	2000146156	241108	³²¹ 2727	³⁵⁰ 4608 ± 0	³³⁴ 1236 ± 2	²⁸⁴ 1209 ± 2	²⁸⁷ 1294 ± 4	²⁹¹ 1554 ± 5	²⁸⁶ 2738 ± 8	²³⁰ 3057 ± 14	²³⁰ 3070 ± 20	
286	sktelecom-000	539783520	298496	²³⁵ 1311	⁷⁵ 1536 ± 0	³¹⁰ 1110 ± 1	²⁶⁴ 1113 ± 1	²⁴⁷ 1114 ± 1	²¹⁹ 1120 ± 1	¹⁸⁵ 1155 ± 1	³³⁶ 26583 ± 128	³³⁵ 26508 ± 126	
287	smartengines-000	1752429	3025	³⁵⁰	¹⁰ 288 ± 0	¹⁹ 168 ± 7	¹¹ 180 ± 1	¹⁰ 188 ± 3	¹¹ 217 ± 3	¹⁴ 275 ± 1	⁶ 197 ± 5	⁴ 167 ± 11	
288	smilart-002	114509977	87805	³⁸ 263	⁵² 1024 ± 0	²¹ 176 ± 16	-	-	-	-	³²⁰ 18784 ± 136	³²¹ 18795 ± 151	
289	smilart-003	68956056	91670	³⁰ 192	³⁴ 512 ± 0	²² 180 ± 12	¹² 181 ± 10	²⁰ 313 ± 22	⁹⁹ 665 ± 49	²⁷³ 2299 ± 196	¹⁴² 1395 ± 74	¹¹⁵ 1027 ± 66	
290	sodec-000	856670801	13142	³³⁷ 3186	³¹³ 4096 ± 0	³⁰¹ 1041 ± 2	²⁴⁹ 1032 ± 1	²³⁴ 1035 ± 1	²⁰⁶ 1037 ± 2	¹⁷² 1061 ± 2	¹⁷⁰ 1794 ± 37	¹⁶⁹ 1775 ± 23	
291	sqisoft-001	285664127	386291	¹²⁸ 688	²⁷⁶ 2056 ± 0	¹⁰⁰ 477 ± 5	³⁰⁶ 1348 ± 18	²⁹⁶ 1353 ± 26	²⁶⁸ 1340 ± 14	²²⁸ 1393 ± 28	⁹¹ 797 ± 22	⁸⁹ 788 ± 22	
292	sqisoft-002	284712154	386291	¹²³ 666	²⁷⁸ 2056 ± 0	⁹⁶ 466 ± 8	⁷³ 466 ± 2	⁵⁷ 468 ± 11	⁴⁰ 461 ± 6	³¹ 472 ± 4	⁸³ 758 ± 11	⁸⁶ 760 ± 23	
293	stauq-000	900773557	624676	²⁰² 1064	³³⁰ 4096 ± 0	²²⁷ 813 ± 25	-	-	-	-	²²⁵ 2979 ± 31	²²⁷ 3007 ± 75	
294	starhybrid-001	102921306	289356	¹⁶¹ 845	¹⁴¹ 2048 ± 0	⁶³ 358 ± 82	⁴³ 355 ± 49	³² 379 ± 58	²⁵ 401 ± 79	²² 393 ± 67	¹¹⁶ 1075 ± 51	¹²⁰ 1078 ± 53	
295	suprema-000	252683488	38507	¹¹⁷ 625	²¹⁸ 2048 ± 0	²¹⁵ 771 ± 2	¹⁷⁴ 778 ± 1	¹⁷⁴ 864 ± 2	²¹⁸ 1109 ± 2	²⁶⁷ 2150 ± 4	¹⁵⁹ 1690 ± 17	¹⁵⁹ 1688 ± 13	
296	suprema-001	382385268	41460	²⁷⁷ 1731	¹²¹ 2048 ± 0	²²⁰ 788 ± 1	¹⁸⁷ 826 ± 2	¹⁹¹ 914 ± 2	²²⁷ 1146 ± 7	²⁸⁰ 2443 ± 4	²³⁵ 3212 ± 16	²³⁶ 3220 ± 22	
297	supremaid-001	264389887	23479	⁹⁵ 541	¹⁷⁷ 2048 ± 0	¹⁰¹ 479 ± 1	⁷⁸ 481 ± 0	⁶² 481 ± 0	⁵¹ 490 ± 0	⁴⁴ 522 ± 0	⁷² 704 ± 19	⁶⁷ 652 ± 19	
298	synesis-006	749508090	21817	²⁵⁷ 1472	³⁴⁴ 4104 ± 0	¹²⁷ 549 ± 1	¹⁰¹ 546 ± 1	⁸⁸ 552 ± 1	⁶⁸ 558 ± 2	⁷⁰ 639 ± 28	⁷¹ 697 ± 32	⁷⁴ 688 ± 31	
299	synesis-007	1477592536	24145	³¹² 2443	³⁰³ 3080 ± 0	³²⁹ 1215 ± 5	²⁹⁵ 1268 ± 30	²⁸⁹ 1306 ± 67	²⁶³ 1311 ± 58	²³⁶ 1423 ± 52	⁶⁸ 684 ± 32	⁷² 686 ± 25	
300	synology-000	226326270	25809	⁶⁴ 453	⁸⁶ 2048 ± 0	⁷⁵ 407 ± 14	⁵⁴ 415 ± 14	¹³² 694 ± 31	²⁷⁵ 1396 ± 58	³⁰¹ 4568 ± 211	³²³ 19720 ± 203	³²² 19767 ± 379	
301	synology-002	262874215	25943	⁷⁵ 488	¹⁶⁹ 2048 ± 0	²⁵⁹ 886 ± 4	²¹⁴ 892 ± 3	¹⁹⁵ 920 ± 2	¹⁹⁸ 1000 ± 5	²¹³ 1317 ± 12	¹⁴⁷ 1466 ± 32	¹⁵⁰ 1496 ± 45	
302	sztu-000	346765308	15871	²³³ 1298	¹⁵⁵ 2048 ± 0	¹²⁰ 531 ± 0	⁹³ 532 ± 0	⁷⁸ 533 ± 0	⁶¹ 537 ± 0	⁴⁹ 548 ± 0	⁴⁰ 585 ± 11	⁴⁵ 592 ± 13	
303	sztu-001	346778532	15871	²³⁴ 1298	¹⁴³ 2048 ± 0	¹²² 535 ± 0	⁹⁷ 537 ± 0	⁸¹ 538 ± 0	⁶³ 540 ± 0	⁵¹ 553 ± 0	⁴⁶ 599 ± 10	⁴⁸ 598 ± 10	
304	tech5-004	2468118640	118858	³²² 2733	¹² 321 ± 0	²⁵³ 872 ± 2	²⁶⁶ 1117 ± 164	²⁴⁸ 1114 ± 182	²²⁵ 1134 ± 179	¹⁵⁴ 999 ± 44	⁴⁴ 597 ± 13	⁴⁶ 592 ± 16	
305	tech5-005	1207059515	120517	²⁴⁹ 1426	²⁶ 512 ± 0	³⁴⁰ 1272 ± 109	²⁵¹ 1038 ± 63	²³⁷ 1046 ± 39	²²⁰ 1124 ± 38	²²¹ 1351 ± 44	²¹⁴ 2573 ± 37	²¹⁴ 2545 ± 32	
306	techsign-000	0	1101622	²⁹⁵ 1955	²²⁶ 2048 ± 0	⁶⁶ 366 ± 1	⁵¹ 398 ± 1	²⁶¹ 1172 ± 3	³²² 3065 ± 18	³¹⁹ 10460 ± 65	²⁶² 4758 ± 112	²⁶¹ 4789 ± 93	
307	tevian-006	709112566	19339	¹⁸⁶ 954	¹⁴⁵ 2048 ± 0	¹⁵³ 611 ± 1	¹³⁷ 666 ± 41	¹²¹ 661 ± 32	¹⁰⁰ 672 ± 37	⁹³ 723 ± 31	⁴¹ 591 ± 19	⁴³ 573 ± 28	
308	tevian-007	798653251	19523	²⁷⁶ 1714	⁶⁴ 1032 ± 0	¹³⁷ 583 ± 1	¹⁰⁹ 579 ± 0	⁹² 580 ± 0	⁷⁴ 588 ± 1	⁶⁹ 636 ± 0	²⁶⁵ 4894 ± 65	²⁶³ 4841 ± 83	

Notes

- 1 The configuration size does not capture static data included in libraries.
- 2 The library size is the combined total of all files provided in the submission lib folder. These libraries e.g. OpenCV may or may not be installed on any end user's platform natively and would not need to be installed with the algorithm. Some developers put neural network models in their libraries.
- 3 The memory usage is the peak resident set size reported by the ps system call during template generation.
- 4 The median template creation times are measured on Intel®Xeon®CPU E5-2630 v4 @ 2.20GHz processors.
- 5 The comparison durations, in nanoseconds, are estimated using std::chrono::high_resolution_clock which on the machine in (2) counts 1ns clock ticks. Precision is somewhat worse than that however. The ± value is the median absolute deviation times 1.48 for Normal consistency.

NAME	ALGORITHM	CONFIG	LIBRARY	TEMPLATE								COMPARISON ⁴		
				DATA		MEMORY		SIZE (B)	GENERATION TIME (ms) ⁴				TIME (ns) ⁵	
				(KB) ¹	(KB) ²	(MB) ³	(B)		MUGSHOT	480x720	960x1440	1600x2400	3000x4500	GENUINE
309	tiger-003	436392290	560292	¹³⁵ 708	²⁶⁶ 2056 ± 0	⁹² 458 ± 21	-	-	-	-	-	-	¹⁸⁸ 2031 ± 35	¹⁸⁹ 2029 ± 38
310	tiger-005	351095179	253734	²⁶² 1531	²⁵³ 2052 ± 0	³⁰⁵ 1097 ± 2	²⁵⁶ 1065 ± 2	²⁴² 1066 ± 2	²¹² 1067 ± 3	¹⁷⁵ 1088 ± 3	⁵⁴ 620 ± 19	⁵⁷ 615 ± 16		
311	tinkoff-001	281251860	389272	¹⁰⁸ 592	¹⁶⁵ 2048 ± 0	³²⁰ 1176 ± 3	²⁷⁸ 1179 ± 3	²⁶² 1178 ± 3	²³³ 1169 ± 2	¹⁹⁵ 1203 ± 3	²⁵⁷ 4361 ± 74	²⁵⁵ 4364 ± 75		
312	tongyi-005	1168078115	138919	³⁰⁵ 2121	²⁹¹ 2089 ± 0	¹⁸ 165 ± 1	-	-	-	-	³²¹ 18924 ± 65	³²³ 20158 ± 103		
313	toppanidgate-000	687290174	711850	²⁸¹ 1786	³²⁷ 4096 ± 0	²⁶⁴ 915 ± 1	²¹⁹ 916 ± 1	¹⁹² 916 ± 1	¹⁷³ 917 ± 1	¹³⁵ 917 ± 1	³³³ 25262 ± 84	³³² 25264 ± 97		
314	toshiba-003	1007744192	114264	²¹⁸ 1197	⁷⁸ 1560 ± 0	¹²⁴ 540 ± 0	-	-	-	-	²⁰⁵ 2390 ± 41	²⁰⁵ 2407 ± 81		
315	toshiba-004	613681072	27880	²⁷⁰ 1595	²⁶⁹ 2056 ± 0	³⁶² 1447 ± 3	³¹⁹ 1453 ± 2	³¹¹ 1457 ± 9	²⁸⁶ 1457 ± 3	²⁴² 1479 ± 4	¹¹² 1020 ± 25	¹⁰⁹ 998 ± 32		
316	trueface-002	260042323	123116	⁷⁴ 486	⁸¹ 2000 ± 0	⁶⁵ 360 ± 0	⁴⁶ 361 ± 0	⁴¹ 423 ± 0	⁷⁶ 590 ± 1	-	⁵ 192 ± 14	⁷ 186 ± 19		
317	trueface-003	354847574	24308	³⁴⁸ 3915	¹³³ 2048 ± 0	³⁰⁸ 1107 ± 22	¹⁴³ 677 ± 3	¹⁴³ 732 ± 7	¹⁷¹ 905 ± 5	-	¹ 103 ± 11	¹ 112 ± 29		
318	tuputech-000	11752256	17185	² 33	¹²³ 2048 ± 0	¹⁵ 122 ± 4	⁸ 120 ± 1	⁷ 142 ± 2	⁹ 196 ± 5	²³ 411 ± 14	³²⁸ 23893 ± 406	³³³ 25279 ± 406		
319	twface-000	677617540	11782	³¹⁸ 2610	²²⁹ 2048 ± 0	²⁵¹ 871 ± 1	²⁰⁶ 873 ± 1	¹⁷⁸ 873 ± 2	¹⁶¹ 876 ± 2	¹²⁹ 898 ± 1	¹⁵¹ 1504 ± 29	¹⁵¹ 1510 ± 34		
320	twface-001	687627801	11782	³³⁰ 2855	¹⁸⁹ 2048 ± 0	²⁶⁸ 923 ± 1	²²⁴ 925 ± 2	²⁰⁰ 926 ± 1	¹⁷⁶ 929 ± 2	¹⁴¹ 940 ± 2	¹⁴³ 1400 ± 32	¹⁴⁴ 1402 ± 37		
321	ulsee-001	379412284	57261	-	²⁰³ 2048 ± 0	¹⁷⁴ 654 ± 2	-	-	-	-	²⁸² 6065 ± 94	²⁸⁴ 6228 ± 77		
322	uluface-002	72	480761	²⁰⁸ 1088	²⁰⁵ 2048 ± 0	²⁵⁴ 873 ± 42	¹⁹⁹ 855 ± 9	²¹⁸ 978 ± 24	²⁵⁴ 1271 ± 40	²⁷⁴ 2333 ± 68	³²² 19207 ± 1114	³¹⁸ 18501 ± 274		
323	uluface-003	99694042	529422	²²⁷ 1264	²⁹⁸ 3072 ± 0	²⁸² 965 ± 11	²³³ 968 ± 10	²⁴⁴ 1087 ± 20	²⁷⁴ 1387 ± 36	²⁸¹ 2469 ± 86	³³⁴ 26057 ± 195	³³⁷ 26865 ± 566		
324	upc-001	0	89914	²⁰⁶ 1077	⁶⁷ 1052 ± 0	¹²⁸ 551 ± 15	¹⁵³ 703 ± 56	¹⁴² 724 ± 51	¹²⁸ 751 ± 49	¹²⁵ 863 ± 33	²³² 3114 ± 44	²³⁴ 3165 ± 97		
325	vcog-002	3306941103	118946	³⁴¹ 3666	³⁶⁸ 61504 ± 5	⁶² 357 ± 25	-	-	-	-	³⁶³ 296436 ± 3077	³⁶³ 296436 ± 4183		
326	vd-002	260606257	34389	¹²⁹ 688	³⁹ 516 ± 0	¹⁹⁰ 684 ± 5	¹⁴⁴ 679 ± 4	¹²⁴ 676 ± 5	¹⁰⁸ 693 ± 5	¹⁰² 754 ± 5	¹⁷ 300 ± 14	¹⁹ 319 ± 32		
327	vd-003	260613205	44051	¹³⁰ 696	²⁵² 2052 ± 0	¹⁹³ 691 ± 5	¹⁴⁷ 690 ± 5	¹²⁶ 683 ± 4	¹⁰⁷ 691 ± 5	⁹¹ 722 ± 5	¹¹⁰ 1003 ± 11	¹¹¹ 1001 ± 7		
328	veridas-006	364205776	896424	³⁰⁰ 1990	¹⁹⁷ 2048 ± 0	²⁵⁸ 880 ± 8	²¹² 885 ± 8	²⁷⁹ 1271 ± 18	³¹⁵ 2242 ± 38	³¹² 6414 ± 156	³⁵⁰ 56940 ± 149	³⁵¹ 66077 ± 194		
329	veridas-007	363627878	891492	³¹⁷ 2527	¹⁴⁷ 2048 ± 0	²⁵² 872 ± 9	²⁰⁷ 875 ± 8	²⁷⁶ 1261 ± 18	³¹³ 2238 ± 38	³¹⁰ 6374 ± 147	⁶⁴ 655 ± 16	⁶⁹ 660 ± 19		
330	verigram-000	262358850	7798	²⁸⁶ 1842	²⁰⁶ 2048 ± 0	²²³ 807 ± 1	¹⁸⁶ 821 ± 1	²¹³ 972 ± 2	²⁷¹ 1358 ± 3	²⁸⁹ 2848 ± 13	¹³² 1222 ± 17	¹³⁶ 1219 ± 17		
331	verihubs-inteligensia-000	214591858	51877	⁵⁹ 427	²⁴³ 2048 ± 0	¹³¹ 567 ± 0	³²² 1558 ± 8	³¹⁶ 1560 ± 8	²⁹² 1568 ± 8	²⁵⁰ 1621 ± 8	³²⁶ 22351 ± 91	³²⁶ 22371 ± 81		
332	via-000	127408592	11151	¹⁸⁸ 964	¹³⁸ 2048 ± 0	¹⁹⁸ 707 ± 8	¹⁶³ 740 ± 5	¹⁸⁹ 906 ± 41	¹⁸² 941 ± 40	¹⁶³ 1040 ± 5	¹⁰² 966 ± 28	¹¹⁴ 1021 ± 44		
333	via-001	379141776	11151	²⁷⁴ 1697	²²¹ 2048 ± 0	²⁸² 964 ± 3	²⁴² 1011 ± 3	²²⁹ 1026 ± 4	²⁰⁹ 1045 ± 3	¹⁸² 1137 ± 28	¹⁰⁴ 983 ± 31	¹⁰⁷ 989 ± 40		
334	videmo-000	142994889	39470	⁴⁹ 390	²²⁵ 2048 ± 0	¹⁶ 142 ± 5	⁹ 150 ± 4	⁸ 150 ± 6	⁶ 151 ± 4	³⁵ 513 ± 16	³⁷ 523 ± 38			
335	videonetics-001	31616555	5963	⁴ 61	¹⁶ 512 ± 0	³⁷ 262 ± 3	²⁹ 273 ± 1	⁴⁹ 439 ± 3	¹⁴³ 820 ± 3	²⁷⁷ 2393 ± 43	¹²⁶ 1153 ± 38	¹²⁸ 1142 ± 65		
336	videonetics-002	124908941	6289	¹⁵ 115	²⁵¹ 2052 ± 0	⁴⁸ 282 ± 5	³⁴ 295 ± 1	⁷³ 513 ± 4	²⁰² 1029 ± 3	²⁹⁵ 3151 ± 46	¹³¹ 1219 ± 57	¹³⁸ 1262 ± 56		
337	viettelhightech-000	265698769	215557	⁵⁷ 419	¹⁸⁴ 2048 ± 0	⁹³ 461 ± 1	⁷² 461 ± 2	⁵⁴ 461 ± 1	⁴⁵ 467 ± 2	³⁵ 494 ± 0	⁴⁵ 599 ± 11	⁴⁴ 591 ± 13		
338	vigilantsolutions-010	357169886	49973	¹⁶⁰ 840	⁷⁷ 1548 ± 0	¹⁵⁸ 615 ± 0	¹²⁹ 631 ± 0	¹¹¹ 632 ± 0	⁸⁹ 636 ± 0	⁷⁴ 659 ± 50	³³ 490 ± 13	³⁵ 488 ± 11		
339	vigilantsolutions-011	261797614	49973	¹⁰⁷ 591	⁷⁶ 1548 ± 0	⁷² 402 ± 0	⁵⁵ 418 ± 0	⁴⁰ 418 ± 0	³⁰ 422 ± 0	²⁷ 445 ± 0	²³ 339 ± 20	²⁵ 366 ± 37		
340	vinai-000	412049069	866522	¹⁹⁶ 1032	⁹¹ 2048 ± 0	³⁰⁶ 1099 ± 1	²⁶¹ 1095 ± 1	²⁴⁶ 1093 ± 1	²¹⁷ 1099 ± 1	¹⁷⁹ 1126 ± 1	²²⁶ 2996 ± 20	²²⁶ 2993 ± 26		
341	vion-000	233696726	7533	⁷⁸ 498	²⁵⁸ 2052 ± 0	⁵⁷ 333 ± 1	-	-	-	-	³⁴¹ 39839 ± 3561	³³⁶ 26830 ± 2241		
342	visage-000	50400173	70150	⁶ 73	³¹ 512 ± 0	³ 27 ± 0	¹ 27 ± 0	¹ 31 ± 0	² 38 ± 0	² 63 ± 0	¹⁹⁸ 2220 ± 14	¹⁹⁹ 2218 ± 14		
343	visionbox-001	263034670	190645	¹⁰⁴ 579	¹³⁴ 2048 ± 0	²⁸⁷ 983 ± 7	²⁶⁰ 1093 ± 46	²⁹⁸ 1360 ± 68	³¹¹ 2181 ± 105	³⁰⁸ 5955 ± 281	¹²⁷ 1161 ± 22	¹³⁰ 1154 ± 20		
344	visionbox-002	265280900	135281	¹¹⁵ 612	²⁸² 2059 ± 0	¹⁰⁴ 482 ± 1	⁷⁹ 482 ± 0	⁶³ 484 ± 1	⁵² 492 ± 1	⁴² 517 ± 3	¹⁸⁵ 1969 ± 44	¹⁸⁴ 1931 ± 42		
345	visionlabs-010	1092895531	19357	¹⁷² 902	³⁶ 513 ± 0	²⁰² 730 ± 0	¹⁵⁶ 717 ± 1	¹³⁸ 709 ± 0	¹¹⁶ 713 ± 1	⁹⁸ 739 ± 0	⁴⁷ 600 ± 41	⁵⁹ 626 ± 35		
346	visionlabs-011	1092895620	19353	¹⁶⁶ 862	³⁷ 513 ± 0	²⁰³ 731 ± 1	¹⁵⁷ 717 ± 1	¹³⁹ 710 ± 1	¹¹⁷ 714 ± 1	⁹⁹ 741 ± 1	³⁷ 556 ± 26	⁴⁰ 559 ± 25		
347	visteam-001	190915457	30878	⁵⁴ 410	³³¹ 4096 ± 0	²⁵⁰ 869 ± 7	²⁰⁵ 872 ± 6	²⁵¹ 1121 ± 15	²⁹⁸ 1719 ± 38	³⁰⁰ 4375 ± 157	²⁹¹ 7054 ± 108	²⁹¹ 7025 ± 109		
348	visteam-002	190915457	30888	⁹⁶ 547	³¹⁶ 4096 ± 0	²³⁹ 829 ± 5	¹⁹² 832 ± 6	¹⁷⁰ 839 ± 7	¹⁵⁰ 853 ± 6	¹⁵⁷ 1013 ± 14	²⁸⁹ 6952 ± 118	²⁸⁸ 6970 ± 120		
349	vnpt-001	272895047	535529	⁴⁸ 384	⁸² 2048 ± 0	¹¹⁰ 499 ± 2	⁸⁶ 499 ± 2	⁶⁸ 494 ± 3	⁵⁴ 502 ± 3	³⁸ 512 ± 2	¹⁸⁹ 2049 ± 29	²⁴ 337 ± 121		
350	vnpt-002	278169517	3203296	⁷⁶ 489	¹⁷³ 2048 ± 0	²⁰⁴ 739 ± 2	¹⁶¹ 731 ± 2	¹⁴⁷ 740 ± 1	¹²⁵ 742 ± 2	¹⁰⁶ 763 ± 2	⁸⁶ 766 ± 13	⁸⁷ 762 ± 13		
351	vocard-008	618359916	345047	²⁶⁵ 1559	²⁹⁷ 2688 ± 0	²⁸¹ 962 ± 2	²³⁵ 976 ± 2	²⁴⁰ 1061 ± 3	²⁴⁷ 1236 ± 23	²⁶² 1851 ± 9	²²⁷ 3015 ± 50	²²⁵ 2988 ± 62		
352	vocard-009	1413255249	201560	³⁵¹ 4162	⁸⁰ 1920 ± 0	³⁶⁵ 1472 ± 2	³²⁰ 1472 ± 1	³¹⁸ 1549 ± 1	²⁹⁶ 1667 ± 2	²⁶⁶ 2064 ± 2	¹⁹⁰ 2052 ± 50	¹⁹² 2056 ± 39		

Notes

- 1 The configuration size does not capture static data included in libraries.
- 2 The library size is the combined total of all files provided in the submission lib folder. These libraries e.g. OpenCV may or may not be installed on any end user's platform natively and would not need to be installed with the algorithm. Some developers put neural network models in their libraries.
- 3 The memory usage is the peak resident set size reported by the ps system call during template generation.
- 4 The median template creation times are measured on Intel®Xeon®CPU E5-2630 v4 @ 2.20GHz processors.
- 5 The comparison durations, in nanoseconds, are estimated using std::chrono::high_resolution_clock which on the machine in (2) counts 1ns clock ticks. Precision is somewhat worse than that however. The ± value is the median absolute deviation times 1.48 for Normal consistency.

Table 14: Summary of algorithms and properties included in this report. The red superscripts give ranking for the quantity in that column.

	ALGORITHM	CONFIG	LIBRARY	TEMPLATE								COMPARISON ⁴		
				NAME	DATA	DATA	MEMORY	SIZE	GENERATION TIME (ms) ⁴				TIME (ns) ⁵	
									(KB) ¹	(KB) ²	(MB) ³	(B)	MUGSHOT	480x720
353	vts-000	262747358	169760	²⁷⁵ vts-000	1704	²³⁴ 2048 ± 0	¹⁰⁶ 486 ± 1	⁷⁷ 481 ± 0	⁶⁴ 484 ± 0	⁴⁹ 485 ± 1	⁴³ 517 ± 0	³⁵⁷ 124209 ± 352	³⁵⁷ 123652 ± 358	
354	winsense-001	270774312	32035	¹⁷⁹ winsense-001	922	⁷² 1280 ± 0	²¹² 766 ± 7	²⁵⁴ 1058 ± 47	²¹⁸ 983 ± 97	²¹⁰ 1053 ± 119	²¹⁴ 1320 ± 84	¹⁵⁴ 1631 ± 28	¹⁸⁶ 1964 ± 171	
355	winsense-002	288132712	25780	²⁸⁰ winsense-002	1781	⁹⁴ 2048 ± 0	¹⁰⁸ 494 ± 2	⁸⁵ 498 ± 1	⁷⁵ 519 ± 1	⁶² 537 ± 1	⁶⁷ 634 ± 1	¹⁵⁸ 1683 ± 8	¹⁵⁸ 1685 ± 7	
356	wuhantianyu-001	476280956	66457	¹⁶⁷ wuhantianyu-001	866	¹⁶⁸ 2048 ± 0	¹⁶⁸ 642 ± 1	¹³² 642 ± 1	¹¹⁷ 644 ± 0	⁹⁵ 652 ± 0	⁸³ 697 ± 0	³⁰⁰ 9502 ± 151	³⁰⁰ 9920 ± 253	
357	x-laboratory-000	532501437	197310	²⁶¹ x-laboratory-000	1524	²⁷⁹ 2056 ± 0	²²⁴ 808 ± 7	²¹⁶ 897 ± 113	¹⁹⁰ 907 ± 103	¹⁶⁴ 886 ± 103	⁷⁸ 673 ± 39	⁷⁷ 725 ± 19	⁸⁴ 749 ± 34	
358	x-laboratory-001	640144084	398792	²⁸⁷ x-laboratory-001	1844	²⁶⁸ 2056 ± 0	¹⁴² 586 ± 2	¹²⁰ 596 ± 5	¹⁰⁰ 603 ± 6	⁸⁵ 620 ± 7	¹⁰⁹ 793 ± 14	⁹² 813 ± 28	⁹⁷ 872 ± 32	
359	xfowardai-001	348262545	51163	³⁰⁶ xfowardai-001	2173	¹²⁵ 2048 ± 0	³²⁴ 1180 ± 2	²⁸² 1182 ± 1	²⁶⁹ 1194 ± 1	²³⁸ 1186 ± 2	¹⁹⁴ 1203 ± 1	⁸⁹ 779 ± 17	⁹¹ 797 ± 13	
360	xfowardai-002	724700382	51163	²⁹⁹ xfowardai-002	1989	³²¹ 4096 ± 0	²⁷⁵ 944 ± 1	²³⁰ 942 ± 1	²⁰⁶ 943 ± 4	¹⁸⁰ 935 ± 1	¹⁴⁸ 967 ± 1	¹⁴⁶ 1406 ± 8	¹⁴⁵ 1405 ± 13	
361	xm-000	591914905	148920	¹²⁷ xm-000	688	²⁵⁰ 2052 ± 0	²⁵⁷ 878 ± 2	²⁰⁹ 882 ± 1	²²⁰ 988 ± 2	²⁵⁰ 1258 ± 3	²⁷⁹ 2434 ± 7	¹⁵⁵ 1634 ± 17	¹⁵⁵ 1632 ± 20	
362	yisheng-004	498023846	38653	²³⁰ yisheng-004	1279	³⁰⁴ 3704 ± 0	⁶⁸ 378 ± 12	-	-	-	-	⁷⁰ 693 ± 137	³⁸ 526 ± 34	
363	yitu-003	1562336990	138919	³⁴² yitu-003	3737	²⁹⁰ 2082 ± 0	²⁴⁸ 860 ± 0	-	-	-	-	³¹⁷ 18305 ± 71	³¹⁷ 18286 ± 62	
364	yoonik-001	354948637	265353	³⁰⁷ yoonik-001	2192	¹⁵¹ 2048 ± 0	³³² 1223 ± 3	²⁹⁰ 1238 ± 1	²⁷⁴ 1238 ± 1	²⁴⁸ 1240 ± 1	²⁰¹ 1240 ± 1	⁷³ 706 ± 29	⁷⁵ 690 ± 26	
365	yoonik-002	464609963	265415	³²⁸ yoonik-002	2755	²³³ 2048 ± 0	³¹⁶ 1145 ± 4	²⁶⁷ 1123 ± 2	²⁵² 1124 ± 2	²²² 1125 ± 2	¹⁸⁰ 1126 ± 3	⁸⁵ 761 ± 32	⁸³ 736 ± 32	
366	ytu-000	1512817409	44032	³¹⁵ ytu-000	2484	¹¹⁵ 2048 ± 0	¹¹⁹ 530 ± 0	⁹⁵ 533 ± 0	¹¹⁵ 640 ± 0	¹⁵⁷ 861 ± 2	²⁶⁴ 1949 ± 8	³³⁸ 31797 ± 131	³³⁹ 31794 ± 133	
367	yuan-002	379363758	165662	³²⁸ yuan-002	2838	²⁰⁸ 2048 ± 0	³⁶⁹ 1420 ± 3	³¹⁶ 1429 ± 4	³¹⁴ 1511 ± 4	²⁹⁷ 1695 ± 4	²⁷⁸ 2408 ± 5	²⁰³ 2297 ± 23	²⁰⁴ 2310 ± 31	
368	yuan-003	379309572	147783	³³² yuan-003	2885	²⁴² 2048 ± 0	³⁵⁶ 1405 ± 2	³¹³ 1413 ± 3	³¹⁰ 1446 ± 3	²⁹⁰ 1547 ± 5	²⁶³ 1878 ± 5	²⁰⁴ 2320 ± 32	²⁰³ 2287 ± 34	

Notes

- 1 The configuration size does not capture static data included in libraries.
- 2 The library size is the combined total of all files provided in the submission lib folder. These libraries e.g. OpenCV may or may not be installed on any end user's platform natively and would not need to be installed with the algorithm. Some developers put neural network models in their libraries.
- 3 The memory usage is the peak resident set size reported by the ps system call during template generation.
- 4 The median template creation times are measured on Intel® Xeon® CPU E5-2630 v4 @ 2.20GHz processors.
- 5 The comparison durations, in nanoseconds, are estimated using std::chrono::high_resolution_clock which on the machine in (2) counts 1ns clock ticks. Precision is somewhat worse than that however. The ± value is the median absolute deviation times 1.48 for Normal consistency.

Table 15: Summary of algorithms and properties included in this report. The red superscripts give ranking for the quantity in that column.

	Algorithm	FALSE NON-MATCH RATE (FNMR)																	
		CONSTRAINED, COOPERATIVE												LESS CONSTRAINED, NON-COOP.					
		Name	VISAMC	VISA	MUGSHOT	MUGSHOT12+YRS	VISABORDER	BORDER	BORDER	WILD	CHILDEXP								
	FMR	0.0001	1E-06	1E-05	1E-05	1E-05	1E-06	1E-06	1E-05	0.0001	0.01								
1	20face-000	0.1268	313	0.1828	310	0.1748	318	0.2768	318	0.1765	306	0.1864	256	0.0927	282	0.0405	223	-	
2	20face-001	0.0521	296	0.0732	295	0.1414	313	0.2549	315	0.0769	290	0.1354	252	0.0419	252	0.0295	128	-	
3	3divi-006	0.0064	129	0.0094	127	0.0047	104	0.0066	106	0.0091	111	0.0191	131	0.0113	116	0.0289	110	-	
4	3divi-007	0.0024	26	0.0038	29	0.0028	26	0.0034	27	0.0046	36	0.0101	53	0.0082	64	0.0300	139	-	
5	acer-001	0.0294	278	0.0504	283	0.0240	277	0.0463	277	0.0436	272	0.0622	223	0.0360	245	0.0307	151	-	
6	acer-002	0.0169	250	0.0262	253	0.0103	207	0.0167	215	0.0182	212	0.0281	173	0.0159	170	0.0297	133	-	
7	acisw-003	0.9682	366	0.9971	365	0.7892	356	0.8738	354	0.8752	348	0.8275	317	0.6698	337	0.4470	337	-	
8	acisw-006	0.2945	331	0.9788	363	0.6044	342	-	-	0.9900	352	1.0000	347	0.9999	355	1.0000	366	-	
9	adera-002	0.0052	96	0.0071	91	0.0047	102	0.0064	101	0.0087	104	0.0159	103	0.0136	142	0.0990	280	-	
10	adera-003	0.0043	74	0.0059	70	0.0036	64	0.0043	50	0.0076	85	0.0151	92	0.0128	134	0.0989	279	-	
11	advance-002	0.0089	175	0.0137	178	0.0073	164	0.0115	169	0.0400	266	0.0722	229	0.0593	267	0.0498	245	-	
12	advance-003	0.0060	123	0.0087	116	0.0052	117	0.0067	107	0.0389	265	0.4914	286	0.1291	291	0.0508	247	-	
13	aifirst-001	0.0119	214	0.0170	207	0.0084	185	0.0127	181	0.0131	170	0.0212	140	0.0138	146	0.0432	231	0.4301	10
14	aigen-001	0.0124	218	0.0219	228	0.0143	242	0.0217	238	0.0236	237	0.8960	320	0.3255	312	0.0681	264	-	
15	aigen-002	0.0192	263	0.0343	267	0.0256	278	0.0402	272	0.0389	264	0.9196	323	0.3876	318	0.1096	287	-	
16	ailabs-001	0.0158	245	0.0276	258	0.0192	263	0.0317	263	0.0352	259	0.0608	220	0.0434	256	0.0338	191	-	
17	aimall-002	0.0119	213	0.0167	205	0.0224	271	0.0411	273	0.0233	233	0.0373	199	0.0235	220	0.0327	179	-	
18	aimall-003	0.0033	47	0.0041	38	0.0033	54	0.0035	32	0.0056	59	0.0109	60	0.0087	75	0.0312	162	-	
19	aiunionface-000	0.0104	198	0.0154	196	0.0082	182	0.0122	172	0.0141	180	0.0243	156	0.0169	178	0.0306	148	-	
20	aize-001	0.0223	270	0.0344	268	0.0199	264	0.0313	261	0.0367	260	0.0522	215	0.0359	244	0.0446	236	-	
21	aize-002	0.0210	268	0.0327	263	0.0280	281	0.0489	280	0.0504	277	0.0692	226	0.0434	255	0.0854	275	-	
22	ajou-001	0.0093	183	0.0147	190	0.0071	161	0.0126	176	0.0173	209	0.0274	168	0.0186	193	0.0348	197	-	
23	alchera-002	0.0107	202	0.0157	198	0.0104	210	0.0229	240	0.0144	185	0.0246	157	0.0198	204	0.0328	181	-	
24	alchera-003	0.0044	75	0.0055	66	0.0031	41	0.0039	41	0.0042	25	0.0077	23	0.0065	25	0.0339	193	-	
25	alice-000	0.0119	215	0.0192	217	0.0106	212	0.0170	216	0.0167	202	0.0265	165	0.0150	162	0.0288	103	-	
26	alleyes-000	0.0058	113	0.0090	122	0.0055	126	0.0087	144	0.0068	80	0.0105	58	0.0076	48	0.0282	69	-	
27	allgovision-000	0.0346	285	0.0527	286	0.0232	273	0.0339	264	0.0372	263	0.0620	222	0.0443	257	0.0607	260	-	
28	alphaface-001	0.0065	133	0.0097	136	0.0039	76	0.0063	100	0.0083	99	-	-	-	-	0.0280	55	-	
29	alphaface-002	0.0052	98	0.0075	101	0.0030	32	0.0044	52	1.0000	357	0.0115	68	0.0084	70	0.0279	47	-	
30	amplifiedgroup-001	0.5034	353	0.5848	347	0.6973	349	0.8316	348	0.7807	340	0.7724	311	0.6354	334	0.4250	335	-	
31	androvideo-000	0.0243	273	0.0438	279	0.0239	275	0.0365	270	0.0483	276	0.1870	257	0.0635	269	0.1163	290	-	
32	anke-004	0.0080	165	0.0154	195	0.0073	163	0.0112	167	0.0102	140	0.0178	121	0.0118	123	0.0288	105	0.3577	5
33	anke-005	0.0070	143	0.0109	156	0.0059	136	0.0094	150	0.0105	143	0.0142	81	0.0102	96	0.0289	109	0.3337	4
34	antheus-000	0.2564	326	0.3776	329	0.7240	351	0.8699	351	0.8899	349	0.9872	329	0.9483	345	0.7668	349	0.9233	48
35	antheus-001	0.1311	314	0.2306	316	0.5113	335	0.6797	335	0.8748	347	0.9908	331	0.9649	349	0.7586	348	-	
36	anyvision-004	0.0267	277	0.0385	274	0.0258	279	0.0487	279	0.0234	236	0.0301	178	0.0191	197	0.0470	240	0.4633	11
37	anyvision-005	0.0023	23	0.0037	27	0.0027	25	0.0035	31	0.0049	42	0.0084	31	0.0069	34	0.0285	83	-	
38	asusaics-000	0.0125	223	0.0209	223	0.0085	186	0.0134	189	0.0143	183	0.7189	305	0.0285	236	0.0295	127	-	
39	asusaics-001	0.0125	224	0.0210	224	0.0085	188	0.0134	190	0.0143	184	0.7437	308	0.0289	237	0.0295	126	-	
40	authenmetric-002	0.0092	181	0.0134	177	0.0095	204	0.0177	219	0.0192	219	0.0463	208	0.0236	221	0.0306	150	-	
41	authenmetric-003	0.0036	56	0.0053	62	0.0039	79	0.0051	71	0.0095	127	0.9930	332	0.5932	332	0.0290	113	-	
42	aware-005	0.0457	293	0.0643	290	0.0603	300	0.1094	301	0.0613	283	0.1075	247	0.0491	259	0.0314	164	-	
43	aware-006	0.0487	294	0.0819	299	0.0529	296	0.1090	300	0.1011	299	0.1058	243	0.0502	261	0.0317	167	-	
44	awiros-001	0.4044	340	0.4622	337	0.5530	337	0.6518	334	0.2008	310	0.1994	261	0.1386	294	0.5584	346	-	

Table 16: FNMR is the proportion of mated comparisons below a threshold set to achieve the FMR given in the header on the fourth row. FMR is the proportion of impostor comparisons at or above that threshold. The light grey values give rank over all algorithms in that column. The pink columns use only same-sex impostors; others are selected regardless of demographics. The exception, in the green column, uses “matched-covariates” i.e. impostors of the same sex, age group, and country of birth. The second pink column includes effects of extended ageing. Missing entries for border, visa, mugshot and wild images generally mean the algorithm did not run to completion. For child exploitation, missing entries arise because NIST executes those runs only infrequently. The VISA columns compare images described in section 2.1. The MUGSHOT columns compare images described in section 2.4. The VISA-BORDER column compare images described in section 2.2 with those of section 2.3. The BORDER column compares images described in section 2.3. The WILD columns compare images described in section 2.5. The CHILD-EXPLOITATION columns compare images described in section ??.

	Algorithm	FALSE NON-MATCH RATE (FNMR)																	
		CONSTRAINED, COOPERATIVE								LESS CONSTRAINED, NON-COOP.									
		VISAMC	VISA	MUGSHOT	MUGSHOT12+YRS	VISABORDER	BORDER	BORDER	WILD	CHILDEXP									
FMR	0.0001	1E-06	1E-05	1E-05	1E-06	1E-06	1E-06	1E-05	0.0001	0.01									
45	awiros-002	0.1990	321	0.2561	319	0.3319	327	0.4411	327	0.3821	325	0.9938	333	0.2634	306	0.0997	281	-	
46	ayftech-001	0.0946	309	0.1941	311	0.2438	322	0.3625	321	0.1558	304	0.1589	253	0.0936	283	0.0785	271	-	
47	ayonix-000	0.4351	345	0.4872	338	0.6150	344	0.7510	342	0.6557	333	0.6361	297	0.4981	326	0.3635	331	0.8434	42
48	beethedata-000	0.0127	225	0.0195	218	0.0092	198	0.0157	208	0.0171	206	0.0306	180	0.0204	206	0.0285	84	-	
49	bicubice-001	0.5596	356	0.6834	353	0.7700	355	0.8712	352	0.8446	344	0.9661	326	0.7922	340	0.2377	317	-	
50	bioditechswiss-001	0.0054	103	0.0072	93	0.0069	156	0.0124	175	0.0060	65	0.0094	42	0.0065	28	0.0313	163	-	
51	bioditechswiss-002	0.0049	86	0.0067	86	0.0064	146	0.0116	170	0.0067	79	0.0117	69	0.0086	73	0.0279	40	-	
52	bm-001	0.7431	361	0.9494	361	0.9586	358	0.9843	356	0.9049	350	0.9021	322	0.8395	343	0.9935	356	0.8845	45
53	boetech-001	0.0662	303	0.0802	298	0.0493	293	0.0791	293	0.0682	287	0.1074	246	0.0758	277	0.1719	302	-	
54	bresee-001	0.0085	172	0.0143	184	0.0086	192	0.0153	206	0.0108	148	0.0168	111	0.0115	120	0.0355	208	-	
55	bresee-002	0.0079	164	0.0101	147	0.0065	149	0.0079	127	0.0129	166	0.0263	163	0.0224	216	0.0327	180	-	
56	camvi-002	0.0125	222	0.0221	230	0.0089	196	0.0145	199	0.0142	181	0.2650	271	0.0166	177	0.0288	101	0.5760	21
57	camvi-004	0.0171	254	0.0316	262	0.0042	86	0.0049	67	0.0097	133	0.6636	300	0.0141	150	0.0284	77	0.5788	22
58	canon-002	0.0034	52	0.0050	54	0.0026	18	0.0033	26	0.0043	27	0.0182	124	0.0065	27	0.0279	44	-	
59	canon-003	0.0041	70	0.0059	71	0.0030	31	0.0040	43	0.0040	20	0.0073	16	0.0059	16	0.0274	16	-	
60	ceiec-003	0.0071	149	0.0107	154	0.0061	140	0.0079	129	0.0160	194	0.0316	183	0.0260	230	0.0308	156	-	
61	ceiec-004	0.0038	62	0.0051	55	0.0045	101	0.0053	75	0.0062	72	0.3939	280	0.0104	103	0.0325	176	-	
62	chosun-001	0.0525	297	0.0936	301	0.0742	304	0.1263	304	0.0978	298	1.0000	352	0.9354	344	0.4446	336	-	
63	chosun-002	0.0390	288	0.0646	291	0.0339	288	0.0576	288	0.0455	274	0.6904	302	0.1746	300	0.0696	267	-	
64	chtface-003	0.0091	177	0.0146	189	0.0083	184	0.0128	183	0.0132	171	0.0220	147	0.0149	160	0.0301	140	-	
65	chtface-004	0.0046	80	0.0062	80	0.0052	116	0.0080	131	0.0088	109	0.0152	93	0.0106	106	0.0306	149	-	
66	clearviewai-000	0.0010	4	0.0019	6	0.0024	5	0.0028	12	0.0030	5	0.0058	6	0.0050	4	0.0271	4	-	
67	closeli-001	0.0136	228	0.0163	200	0.0039	77	0.0054	78	0.0072	82	1.0000	348	0.0094	87	0.0318	168	-	
68	cloudwalk-hr-003	0.0026	30	0.0041	37	0.0040	82	0.0058	86	0.0060	70	0.9992	339	0.0094	85	0.7206	347	-	
69	cloudwalk-hr-004	0.0009	1	0.0018	4	0.0034	56	0.0028	16	0.0052	49	0.9992	340	0.0093	84	0.1625	301	-	
70	cloudwalk-mt-003	0.0013	7	0.0022	7	0.0026	15	0.0027	9	0.0039	16	0.0076	18	0.0067	30	0.0347	195	-	
71	cloudwalk-mt-004	0.0009	3	0.0013	1	0.0024	7	0.0021	1	0.0028	3	0.0054	3	0.0050	5	0.0285	87	-	
72	clova-000	0.0099	192	0.0150	191	0.0094	202	0.0147	202	0.0136	173	0.0213	142	0.0152	166	0.0307	152	-	
73	cogent-005	0.0060	122	0.0112	160	0.0064	148	0.0070	111	0.0095	126	0.0184	127	0.0135	139	0.0423	229	-	
74	cogent-006	0.0046	82	0.0059	73	0.0036	61	0.0047	58	0.0058	63	0.0113	65	0.0091	80	0.0343	194	-	
75	cognitec-002	0.0066	134	0.0101	148	0.0079	173	0.0108	164	0.0181	211	0.0317	184	0.0237	222	0.0372	212	-	
76	cognitec-003	0.0038	61	0.0052	57	0.0054	125	0.0057	84	0.0225	230	0.0416	206	0.0388	248	0.0348	198	-	
77	cor-001	0.0075	156	0.0113	163	0.0055	129	0.0084	138	0.0091	113	0.0148	87	0.0092	83	0.0277	33	-	
78	coretech-000	0.7699	363	1.0000	370	1.0000	365	-	1.0000	358	1.0000	362	1.0000	369	1.0000	363	-		
79	corsight-001	0.0040	66	0.0057	69	0.0033	53	0.0047	57	0.0045	30	0.0095	45	0.0063	23	0.0276	23	-	
80	corsight-002	0.0053	100	0.0068	88	0.0030	36	0.0041	45	0.0039	18	0.0079	25	0.0054	10	0.0276	28	-	
81	csc-002	0.0099	194	0.0132	175	0.0077	168	0.0142	196	0.0126	164	0.0195	133	0.0146	156	0.1779	305	-	
82	csc-003	0.0053	99	0.0065	83	0.0037	69	0.0047	60	0.0074	83	0.0124	75	0.0112	115	0.1773	304	-	
83	ctbcbank-000	0.0168	249	0.0250	246	0.0146	245	0.0224	239	0.0211	227	0.8964	321	0.3779	317	1.0000	362	0.8803	44
84	ctbcbank-001	0.0155	243	0.0235	239	0.0148	250	0.0243	245	0.0207	224	0.9279	324	0.3469	314	1.0000	365	-	
85	cubox-001	0.0064	130	0.0080	109	0.0037	68	0.0055	80	0.0060	66	0.0111	62	0.0077	49	0.0300	137	-	
86	cubox-002	0.0034	51	0.0041	39	0.0025	12	0.0025	7	0.0033	8	0.0064	10	0.0058	15	0.0480	243	-	
87	cudocommunication-001	0.4777	350	1.0000	367	0.4373	332	0.5360	329	1.0000	368	1.0000	366	1.0000	360	1.0000	368	-	
88	cuhkee-001	0.0036	57	0.0045	47	0.0031	45	0.0046	55	0.0051	48	0.0095	46	0.0079	54	0.1492	298	-	

Table 17: FNMR is the proportion of mated comparisons below a threshold set to achieve the FMR given in the header on the fourth row. FMR is the proportion of impostor comparisons at or above that threshold. The light grey values give rank over all algorithms in that column. The pink columns use only same-sex impostors; others are selected regardless of demographics. The exception, in the green column, uses “matched-covariates” i.e. impostors of the same sex, age group, and country of birth. The second pink column includes effects of extended ageing. Missing entries for border, visa, mugshot and wild images generally mean the algorithm did not run to completion. For child exploitation, missing entries arise because NIST executes those runs only infrequently. The VISA columns compare images described in section 2.1. The MUGSHOT columns compare images described in section 2.4. The VISA-BORDER column compare images described in section 2.2 with those of section 2.3. The BORDER column compares images described in section 2.3. The WILD columns compare images described in section 2.5. The CHILD-EXPLOITATION columns compare images described in section ??.

Algorithm	FALSE NON-MATCH RATE (FNMR)																		
	CONSTRAINED, COOPERATIVE																		
	Name	VisAMC	VISA	MUGSHOT	MUGSHOT12+YRS	VISABORDER	BORDER	BORDER	LESS CONSTRAINED, NON-COOP.										
	FMR	0.0001	1E-06	1E-05	1E-05	1E-06	1E-06	1E-06	0.0001	0.01									
89	cybercore-000	0.0728	305	0.1110	304	0.1521	315	0.2375	312	0.1874	309	0.1907	258	0.1178	289	0.1191	293	-	
90	cyberextruder-001	0.1972	319	0.2547	318	0.4686	334	0.6387	333	0.3807	324	0.3806	279	0.2582	303	0.1747	303	0.7804	41
91	cyberextruder-002	0.0811	307	0.1336	306	0.1465	314	0.2266	311	0.2086	313	1.0000	354	1.0000	368	0.1000	282	0.6105	23
92	cyberlink-006	0.0042	72	0.0054	65	0.0043	88	0.0049	65	0.0052	53	0.0097	49	0.0077	50	0.0278	34	-	
93	cyberlink-007	0.0032	45	0.0053	61	0.0041	84	0.0043	48	0.0052	52	0.0243	155	0.0084	71	0.0280	53	-	
94	dahua-005	0.0031	43	0.0046	49	0.0035	60	0.0049	68	0.0046	33	0.0076	19	0.0062	22	0.0277	32	-	
95	dahua-006	0.0027	34	0.0039	32	0.0031	43	0.0039	42	0.0039	17	0.0067	13	0.0058	14	0.0280	49	-	
96	daon-000	0.0095	188	0.0117	165	0.0068	153	0.0077	124	0.0092	118	0.0174	117	0.0137	145	0.0331	184	-	
97	decatur-000	0.0714	304	0.1115	305	0.0608	301	0.1106	302	0.0866	293	1.0000	350	0.0714	274	0.0658	263	-	
98	decatur-001	0.0424	290	0.0711	293	0.0237	274	0.0458	276	0.0447	273	1.0000	345	0.9969	352	0.0280	54	-	
99	deepglint-003	0.0027	35	0.0038	28	0.0030	35	0.0032	25	0.0043	26	0.0082	29	0.0076	47	0.0279	41	-	
100	deepglint-004	0.0025	29	0.0034	24	0.0039	78	0.0061	97	0.0050	46	0.0091	38	0.0082	63	0.0285	89	-	
101	deepsea-001	0.0136	229	0.0215	226	0.0142	241	0.0214	237	0.0163	198	0.0250	159	0.0192	198	0.0347	196	0.5606	19
102	deeplsense-000	0.0145	235	0.0265	254	0.0113	226	0.0196	230	0.0151	187	0.0215	144	0.0129	135	0.0290	114	-	
103	dermalog-008	0.0096	190	0.0166	204	0.0086	190	0.0133	188	0.0165	200	0.0586	219	0.0226	217	0.0277	31	-	
104	dermalog-009	0.0067	137	0.0094	128	0.0051	115	0.0069	109	0.0116	157	0.0312	181	0.0177	185	0.0270	3	-	
105	didiglobalface-001	0.0055	107	0.0092	124	0.0030	33	0.0045	53	0.0088	106	0.0119	72	0.0085	72	0.0282	67	0.4270	8
106	digitalbarriers-002	0.3360	336	0.3690	327	0.0877	306	0.1557	305	0.0971	297	0.0951	239	0.0497	260	0.0436	233	-	
107	dps-000	0.0115	208	0.0176	210	0.0149	253	0.0185	225	0.0173	208	0.0275	170	0.0180	188	0.1067	285	-	
108	dsk-000	0.1526	316	0.2169	314	0.3787	329	0.5426	331	0.3115	317	0.3089	274	0.1994	301	0.2201	313	0.7313	34
109	einetworks-000	0.0099	193	0.0180	213	0.0088	195	0.0140	194	0.0130	168	0.0225	150	0.0147	158	0.0293	121	-	
110	ekin-002	0.1168	311	0.2042	312	0.1530	316	0.2524	314	0.1777	308	0.2773	272	0.1347	293	0.4801	340	-	
111	enface-000	0.0028	38	0.0049	52	0.0043	92	0.0072	113	0.0058	64	0.0150	90	0.0090	79	0.0290	117	-	
112	eocortex-000	0.3485	337	0.6943	354	0.1122	309	0.1574	306	0.2155	315	0.2257	267	0.1606	299	0.2546	323	-	
113	ercacat-001	0.0036	54	0.0044	45	0.0033	51	0.0047	61	0.0106	145	0.0202	137	0.0184	190	0.0258	1	-	
114	expasoft-001	0.0328	284	0.0488	281	0.0211	268	0.0342	266	0.0629	286	0.6483	298	0.2816	308	0.0552	255	-	
115	expasoft-002	0.0170	251	0.0274	256	0.0787	305	0.0768	292	0.1629	305	0.9996	341	0.9631	348	0.0337	189	-	
116	f8-001	0.0249	274	0.0336	265	0.0178	260	0.0232	241	0.0303	253	0.0615	221	0.0408	251	0.0475	242	0.5272	16
117	facesoft-000	0.0085	173	0.0112	162	0.0064	147	0.0107	163	0.0091	112	0.0171	114	0.0107	107	0.0275	18	0.4992	13
118	facetag-000	0.2836	327	0.4081	333	0.2933	324	0.4303	324	0.3448	320	0.6312	296	0.3530	315	0.2087	312	-	
119	facetag-001	0.2920	329	0.4538	335	0.3220	326	0.4371	325	1.0000	361	1.0000	360	0.3254	311	0.3072	329	-	
120	facex-001	1.0000	367	1.0000	368	1.0000	362	-	1.0000	369	1.0000	367	1.0000	358	1.0000	359	-		
121	facex-002	0.0803	306	0.1404	307	0.1283	311	0.1979	309	0.1440	303	0.1952	260	0.1299	292	0.2377	316	-	
122	farfaces-001	0.4890	352	0.5860	348	0.5650	338	0.7268	339	0.8015	342	0.7511	309	0.5892	331	0.1976	310	-	
123	fiberhome-nanjing-003	0.0090	176	0.0139	181	0.0082	181	0.0144	197	0.0110	152	0.0174	115	0.0107	108	0.0272	8	-	
124	fiberhome-nanjing-004	0.0037	59	0.0056	68	0.0031	40	0.0043	49	0.0043	28	0.0083	30	0.0061	20	0.0272	7	-	
125	fincore-000	0.0309	281	0.0502	282	0.0281	282	0.0510	282	0.0521	279	0.0815	232	0.0522	262	0.0681	265	-	
126	fujitsulab-002	0.0091	178	0.0124	169	0.0105	211	0.0156	207	0.0169	205	0.0345	192	0.0146	157	0.0282	64	-	
127	fujitsulab-003	0.0045	78	0.0065	84	0.0057	134	0.0083	136	0.0080	93	0.0154	98	0.0101	93	0.0280	48	-	
128	geo-002	0.0171	253	0.0187	216	0.0035	59	0.0051	74	0.0064	74	0.0117	70	0.0083	68	0.0302	143	-	
129	geo-003	0.0180	258	0.0313	261	0.0239	276	0.0552	283	0.0319	257	0.0487	211	0.0222	214	0.0308	159	-	
130	glory-002	0.0241	272	0.0311	260	0.0116	230	0.0151	205	0.0157	191	0.0264	164	0.0188	195	0.1265	294	-	
131	glory-003	0.0076	159	0.0125	171	0.0077	170	0.0103	160	0.0130	167	0.0205	138	0.0143	153	0.0763	269	-	
132	gorilla-007	0.0074	155	0.0111	159	0.0065	150	0.0126	177	0.0100	138	0.0151	91	0.0102	95	0.0278	35	-	

Table 18: FNMR is the proportion of mated comparisons below a threshold set to achieve the FMR given in the header on the fourth row. FMR is the proportion of impostor comparisons at or above that threshold. The light grey values give rank over all algorithms in that column. The pink columns use only same-sex impostors; others are selected regardless of demographics. The exception, in the green column, uses “matched-covariates” i.e. impostors of the same sex, age group, and country of birth. The second pink column includes effects of extended ageing. Missing entries for border, visa, mugshot and wild images generally mean the algorithm did not run to completion. For child exploitation, missing entries arise because NIST executes those runs only infrequently. The VISA columns compare images described in section 2.1. The MUGSHOT columns compare images described in section 2.4. The VISA-BORDER column compare images described in section 2.2 with those of section 2.3. The BORDER column compares images described in section 2.3. The WILD columns compare images described in section 2.5. The CHILD-EXPLOITATION columns compare images described in section ??.

Algorithm	FALSE NON-MATCH RATE (FNMR)									
	CONSTRAINED, COOPERATIVE								LESS CONSTRAINED, NON-COOP.	
	Name	VISAMC	VISA	MUGSHOT	MUGSHOT12+YRS	VISABORDER	BORDER	BORDER	WILD	CHILDEXP
FMR	0.0001	1E-06	1E-05	1E-05	1E-06	1E-06	1E-06	1E-05	0.0001	0.01
133 gorilla-008	0.0058	112	0.0091	123	0.0049	108	0.0079	128	0.0079	92
134 griaule-000	0.0071	147	0.0099	140	0.0050	111	0.0072	112	0.0160	192
135 hertasecurity-000	0.0630	301	0.0780	297	0.0503	295	0.0898	295	0.0738	288
136 hik-001	0.0096	189	0.0125	172	0.0093	201	0.0164	213	0.0108	149
137 hisign-001	0.0036	55	0.0050	53	0.0034	55	0.0046	54	0.0079	91
138 hyperverge-001	1.0000	369	1.0000	369	1.0000	368	-	1.0000	370	1.0000
139 hyperverge-002	0.0050	87	0.0066	85	0.0035	58	0.0051	70	0.0062	71
140 icm-002	0.0143	233	0.0249	245	0.0144	243	0.0256	247	0.0236	239
141 icm-003	0.0138	230	0.0222	231	0.0149	251	0.0282	256	0.0227	231
142 icthtc-000	0.0260	276	0.0396	275	0.0207	267	0.0339	265	0.0291	250
143 id3-006	0.0072	152	0.0103	149	0.0049	109	0.0074	118	0.0095	125
144 id3-008	0.0039	64	0.0055	67	0.0032	48	0.0042	46	0.0081	97
145 idemia-007	0.0024	25	0.0039	33	0.0032	50	0.0038	39	0.0046	35
146 idemia-008	0.0023	24	0.0032	20	0.0023	3	0.0028	11	0.0034	11
147 iit-002	0.0111	206	0.0177	212	0.0085	187	0.0140	193	0.0193	220
148 iit-003	0.0082	171	0.0151	193	0.0053	119	0.0084	139	0.0122	162
149 imagus-002	0.0062	125	0.0086	114	0.0053	121	0.0075	119	0.0121	160
150 imagus-004	0.0063	127	0.0094	131	0.0055	128	0.0081	133	0.0098	134
151 imperial-000	0.0067	139	0.0108	155	0.0080	177	0.0134	191	0.0087	105
152 imperial-002	0.0058	115	0.0081	110	0.0055	127	0.0085	141	0.0083	100
153 incode-009	0.0044	76	0.0067	87	0.0034	57	0.0051	69	0.0049	43
154 incode-010	0.0041	69	0.0063	81	0.0028	27	0.0043	47	0.0047	40
155 innefulabs-000	0.0122	216	0.0199	219	0.0112	224	0.0197	231	0.0222	229
156 innovativetechnologyltd-001	0.0578	299	0.0938	302	0.0501	294	0.0981	296	0.0592	282
157 innovativetechnologyltd-002	0.0451	292	0.0716	294	0.0541	297	0.1009	298	0.0506	278
158 innovatrics-006	0.0058	114	0.0089	121	0.0061	141	0.0096	154	0.0096	130
159 innovatrics-007	0.0040	67	0.0054	64	0.0057	133	0.0078	125	0.0079	90
160 insightface-000	0.0018	17	0.0027	16	0.0029	28	0.0030	24	0.0038	15
161 insightface-001	0.0009	2	0.0014	2	0.0027	21	0.0024	4	0.0035	13
162 intellicloudai-001	0.0142	232	0.0234	237	0.0092	200	0.0145	198	0.0162	196
163 intellicloudai-002	0.0059	119	0.0085	113	0.0060	138	0.0069	110	0.0108	147
164 intellifusion-001	0.0072	151	0.0094	132	0.0056	132	0.0085	142	0.0111	154
165 intellifusion-002	0.0059	118	0.0077	102	0.0040	81	0.0074	117	0.0085	103
166 intellivision-001	0.1335	315	0.2205	315	0.1090	307	0.1670	307	0.1385	301
167 intellivision-002	0.1000	310	0.1775	309	0.0610	302	0.1009	297	0.0805	292
168 intelresearch-003	0.0046	81	0.0062	78	0.0038	73	0.0060	91	0.0088	108
169 intelresearch-004	0.0025	27	0.0035	25	0.0032	47	0.0038	37	0.0049	44
170 intsysmsu-001	0.9543	365	0.9888	364	0.9923	359	-	0.9977	353	0.9955
171 intsysmsu-002	0.0130	226	0.0254	248	0.0137	239	0.0267	254	0.0160	193
172 ionetworks-000	0.0060	124	0.0087	117	0.0044	93	0.0058	88	0.0080	96
173 iqface-000	0.0091	180	0.0143	183	0.0075	167	0.0110	165	0.0171	207
174 iqface-003	0.0058	116	0.0079	108	0.0051	114	0.0058	89	0.0104	142
175 irex-000	0.0052	95	0.0099	139	0.0056	131	0.0083	137	0.0137	176
176 isap-001	0.5092	354	0.6588	351	0.6899	348	0.7978	345	0.7200	336

Table 19: FNMR is the proportion of mated comparisons below a threshold set to achieve the FMR given in the header on the fourth row. FMR is the proportion of impostor comparisons at or above that threshold. The light grey values give rank over all algorithms in that column. The pink columns use only same-sex impostors; others are selected regardless of demographics. The exception, in the green column, uses “matched-covariates” i.e. impostors of the same sex, age group, and country of birth. The second pink column includes effects of extended ageing. Missing entries for border, visa, mugshot and wild images generally mean the algorithm did not run to completion. For child exploitation, missing entries arise because NIST executes those runs only infrequently. The VISA columns compare images described in section 2.1. The MUGSHOT columns compare images described in section 2.4. The VISA-BORDER column compare images described in section 2.2 with those of section 2.3. The BORDER column compares images described in section 2.3. The WILD columns compare images described in section 2.5. The CHILD-EXPLOITATION columns compare images described in section ??.

		FALSE NON-MATCH RATE (FNMR)																	
		CONSTRAINED, COOPERATIVE								LESS CONSTRAINED, NON-COOP.									
Algorithm	Name	VISAMC	VISA	MUGSHOT	MUGSHOT12+YRS	VISABORDER	BORDER	BORDER	WILD	CHILDEXP									
		FMR		0.0001		1E-06		1E-05		1E-05		1E-06							
177	isap-002	0.0114	207	0.0186	215	0.0087	193	0.0151	204	0.0156	190	0.5134	289	0.0333	239	0.0354	207	-	
178	isityou-000	0.5682	357	0.7033	355	1.0000	363	-		1.0000	363	1.0000	356	1.0000	367	1.0000	361	1.0000	343
179	isystems-001	0.0149	240	0.0245	243	0.0138	240	0.0210	235	0.0209	226	0.0332	188	0.0223	215	0.0524	251	0.5152	15
180	isystems-002	0.0118	210	0.0182	214	0.0111	221	0.0162	211	0.0166	201	0.0284	174	0.0195	201	0.0516	248	0.4876	12
181	itmo-006	0.0125	220	0.0220	229	0.0149	252	0.0266	252	0.0233	234	0.0383	200	0.0285	235	0.0329	182	-	
182	itmo-007	0.0080	166	0.0125	170	0.0107	213	0.0185	223	0.0167	203	0.0222	149	0.0144	154	0.0300	138	-	
183	ivacognitive-001	0.0189	261	0.0351	269	0.0123	233	0.0235	242	0.0198	222	0.0274	169	0.0155	167	0.0296	130	-	
184	iws-000	0.4824	351	0.5801	346	0.6859	347	0.8155	347	0.8251	343	0.7756	312	0.6400	336	0.3251	330	-	
185	kakao-005	0.0040	65	0.0059	72	0.0036	67	0.0057	83	0.0085	102	0.0239	153	0.0125	131	0.0280	52	-	
186	kakao-006	0.0016	13	0.0029	17	0.0024	4	0.0028	17	0.0035	12	0.0065	11	0.0057	13	0.0335	187	-	
187	kakaopay-001	0.0152	242	0.0252	247	0.0145	244	0.0270	255	0.0232	232	0.0344	191	0.0194	200	0.0416	228	-	
188	kedacom-000	0.0055	105	0.0081	111	0.0111	223	0.0120	171	0.0415	268	0.0966	241	0.0686	271	0.2511	321	0.7650	38
189	kiwitech-000	0.0076	158	0.0105	151	0.0081	179	0.0128	184	0.0096	128	0.0163	107	0.0101	94	0.0279	46	-	
190	kneron-003	0.0542	298	0.0902	300	0.0346	289	0.0562	286	0.0919	295	0.1251	250	0.0973	284	0.3053	328	0.6962	30
191	kneron-005	0.0157	244	0.0259	250	0.0126	236	0.0212	236	0.0406	267	0.0693	227	0.0542	264	0.0471	241	-	
192	kookmin-002	0.0054	102	0.0077	104	0.0043	89	0.0065	102	0.0123	163	0.7591	310	0.0198	203	0.0285	86	-	
193	kookmin-003	0.0043	73	0.0060	75	0.0036	66	0.0053	77	0.0111	155	0.9831	328	0.0185	192	0.0286	92	-	
194	kuke3d-001	0.0058	111	0.0104	150	0.0083	183	0.0093	149	0.0270	247	0.9901	330	0.8341	342	0.0404	222	-	
195	lemalabs-001	0.0111	205	0.0175	209	0.0088	194	0.0142	195	0.0143	182	0.0228	151	0.0140	148	0.0281	56	-	
196	line-000	0.0172	255	0.0236	240	0.0109	217	0.0194	228	0.0183	213	0.0291	176	0.0204	207	0.0298	134	-	
197	line-001	0.0025	28	0.0040	34	0.0026	20	0.0034	30	0.0045	32	0.4127	282	0.0080	58	0.0283	74	-	
198	lookman-002	0.0297	279	0.0547	287	0.0339	287	0.0562	285	0.0614	284	0.0960	240	0.0790	278	0.2640	325	-	
199	lookman-004	0.0074	154	0.0099	142	0.0124	235	0.0149	203	0.0430	271	0.0866	235	0.0694	272	0.2516	322	0.7664	39
200	luxand-000	0.2056	322	0.2814	321	0.4053	331	0.5365	330	0.3497	321	0.3743	277	0.2605	304	0.2222	315	-	
201	mantra-000	0.0037	58	0.0052	59	0.0054	123	0.0056	82	0.0097	132	0.0181	123	0.0151	163	0.0350	203	-	
202	maxvision-000	0.0078	162	0.0106	153	0.0110	219	0.0147	201	0.0368	262	1.0000	355	0.1545	297	0.0445	235	-	
203	megvii-002	0.0104	200	0.0145	187	0.0225	272	0.0345	267	0.0099	137	0.0286	175	0.0240	224	0.0692	266	0.3013	2
204	megvii-003	0.0064	132	0.0094	129	0.0136	238	0.0260	249	0.0050	45	0.0080	26	0.0059	18	0.0288	98	-	
205	meituan-000	0.0197	264	0.0424	278	0.0078	171	0.0074	116	0.0103	141	0.0193	132	0.0164	174	0.1063	284	-	
206	meiya-001	0.0171	252	0.0275	257	0.0159	257	0.0261	251	0.0311	255	0.2250	266	0.0245	226	0.0363	211	-	
207	mendaxiatech-000	0.0027	36	0.0036	26	0.0029	29	0.0036	34	0.0031	6	0.0057	5	0.0051	7	0.0275	19	-	
208	microfocus-001	0.4482	347	0.5524	345	0.7256	352	0.8416	349	0.7301	337	0.6926	303	0.5180	327	0.2567	324	0.6890	29
209	microfocus-002	0.3605	338	0.5057	340	0.5783	340	0.7223	338	0.5909	329	0.5963	295	0.4160	322	0.1582	300	0.6517	26
210	minivision-000	0.0033	48	0.0048	51	0.0038	74	0.0049	64	0.0055	58	0.0094	44	0.0079	56	0.0273	9	-	
211	mobai-000	0.0360	287	0.0439	280	0.0372	290	0.0700	290	0.0367	261	0.0939	238	0.0795	279	0.2640	326	-	
212	mobai-001	0.0199	266	0.0219	227	0.0047	103	0.0061	94	0.0093	123	0.0174	116	0.0138	147	0.1045	283	-	
213	mobbl-000	0.2938	330	0.3861	330	0.5391	336	0.6888	336	0.6545	332	0.8027	313	0.6207	333	0.5471	344	-	
214	mobbl-001	0.3208	333	0.4375	334	0.5680	339	0.7193	337	0.6282	330	0.5783	293	0.3984	319	0.1866	306	-	
215	moreedian-000	0.3874	339	0.4912	339	0.9988	360	-		0.9990	354	0.9999	343	0.9998	354	0.4788	339	-	
216	multimodality-000	0.0034	50	0.0047	50	0.0036	65	0.0044	51	0.0077	87	0.9976	337	0.4456	323	0.0287	96	-	
217	mvision-001	0.0191	262	0.0233	235	0.0204	266	0.0356	268	0.0198	223	0.0337	190	0.0242	225	0.0431	230	-	
218	nazhiai-000	0.0040	68	0.0059	74	0.0036	62	0.0048	63	0.0057	60	0.0125	76	0.0083	67	0.0275	20	-	
219	neosystems-001	1.0000	370	1.0000	366	0.2987	325	0.4382	326	0.5173	328	0.6570	299	0.4043	321	0.5091	342	-	
220	neosystems-002	0.2905	328	0.4077	332	0.2028	320	0.3252	319	0.4088	326	0.5519	291	0.3331	313	0.4500	338	-	

Table 20: FNMR is the proportion of mated comparisons below a threshold set to achieve the FMR given in the header on the fourth row. FMR is the proportion of impostor comparisons at or above that threshold. The light grey values give rank over all algorithms in that column. The pink columns use only same-sex impostors; others are selected regardless of demographics. The exception, in the green column, uses “matched-covariates” i.e. impostors of the same sex, age group, and country of birth. The second pink column includes effects of extended ageing. Missing entries for border, visa, mugshot and wild images generally mean the algorithm did not run to completion. For child exploitation, missing entries arise because NIST executes those runs only infrequently. The VISA columns compare images described in section 2.1. The MUGSHOT columns compare images described in section 2.4. The VISA-BORDER column compare images described in section 2.2 with those of section 2.3. The BORDER column compares images described in section 2.3. The WILD columns compare images described in section 2.5. The CHILD-EXPLOITATION columns compare images described in section ??.

Algorithm	FALSE NON-MATCH RATE (FNMR)																	
	CONSTRAINED, COOPERATIVE																	
	Name	VisAMC	VISA	MUGSHOT	MUGSHOT12+YRS	VisABORDER	BORDER	BORDER	WILD	CHILDEXP								
FMR	0.0001	1E-06	1E-05	1E-05	1E-06	1E-06	1E-05	0.0001	0.01									
221	netbridge-tech-001	0.4749	349	0.6599	352	0.4438	333	0.5676	332	0.4491	327	1.0000	346	0.9541	346	0.1098	288	-
222	netbridge-tech-002	0.0101	196	0.0166	203	0.0077	169	0.0127	180	0.0133	172	0.8215	315	0.0523	263	0.0351	205	-
223	neurotechnology-011	0.0050	91	0.0087	115	0.0061	142	0.0097	156	0.0077	89	0.0404	205	0.0092	82	0.0293	124	-
224	neurotechnology-012	0.0051	94	0.0070	90	0.0038	71	0.0056	81	0.0066	78	0.0112	64	0.0075	44	0.0279	45	-
225	rhn-001	0.0066	136	0.0098	137	0.0053	120	0.0079	130	0.0093	119	0.0156	100	0.0109	110	0.0308	158	-
226	rhn-002	0.0068	141	0.0096	133	0.0057	135	0.0087	145	0.0136	175	0.0253	161	0.0186	194	0.0302	142	-
227	nodeflux-002	0.0186	260	0.0340	266	0.0261	280	0.0451	275	0.0548	280	1.0000	351	1.0000	357	0.0299	136	-
228	notiontag-001	0.6846	359	0.8006	358	0.3955	330	0.5247	328	0.8669	346	0.8313	318	0.6362	335	0.2221	314	-
229	notiontag-002	0.0066	135	0.0089	119	0.0045	99	0.0061	95	0.0077	88	0.0137	80	0.0104	101	0.0299	135	-
230	nsensecorp-002	0.4277	343	0.5375	343	0.6734	346	0.7924	344	0.7194	335	0.6937	304	0.5617	329	0.5530	345	-
231	nsensecorp-003	0.0251	275	0.0295	259	0.0212	269	0.0305	259	0.0131	169	0.2139	264	0.0141	151	0.0872	277	-
232	ntechlab-010	0.0013	8	0.0017	3	0.0024	11	0.0029	21	0.0031	7	0.0058	7	0.0050	6	0.0292	119	-
233	ntechlab-011	0.0012	5	0.0019	5	0.0024	9	0.0028	19	0.0029	4	0.0055	4	0.0047	3	0.0288	104	-
234	omnigarde-000	0.0633	302	0.1002	303	0.1109	308	0.2042	310	0.1288	300	0.5113	288	0.1227	290	0.0357	209	-
235	omnigarde-001	0.0168	248	0.0260	251	0.0203	265	0.0402	271	0.0243	242	0.0327	186	0.0177	183	0.0288	100	-
236	openface-001	0.1804	318	0.2921	322	0.2878	323	0.3906	323	0.2054	312	0.2338	269	0.1549	298	0.2445	319	-
237	oz-002	0.0071	148	0.0099	143	0.0099	205	0.0100	158	0.0139	178	0.0502	212	0.0202	205	0.5084	341	-
238	oz-003	0.0095	186	0.0143	182	0.0054	124	0.0077	123	0.0096	129	0.0175	119	0.0118	124	0.0288	106	-
239	papsav1923-001	0.0078	161	0.0130	174	0.0068	154	0.0105	162	0.0119	158	0.0221	148	0.0136	141	0.0293	122	-
240	paravision-004	0.0030	41	0.0046	48	0.0030	34	0.0036	33	0.0091	115	0.0188	130	0.0173	181	0.0288	102	0.2467
241	paravision-008	0.0018	16	0.0025	12	0.0024	6	0.0025	6	0.0036	14	0.0070	15	0.0063	24	0.0279	42	-
242	pensees-001	0.0087	174	0.0133	176	0.0071	159	0.0122	174	0.0145	186	0.0252	160	0.0195	202	0.0283	72	-
243	pixelall-005	0.0038	60	0.0052	58	0.0043	90	0.0051	72	0.0077	86	0.0839	234	0.0136	143	0.0279	39	-
244	pixelall-006	0.0032	46	0.0042	41	0.0032	46	0.0039	40	0.0063	73	0.9960	335	0.0723	275	0.0283	71	-
245	psl-007	0.0026	33	0.0040	35	0.0027	23	0.0030	22	0.0054	54	0.0101	54	0.0081	61	0.0282	65	-
246	psl-008	0.0026	31	0.0040	36	0.0024	8	0.0028	18	0.0041	22	0.0077	20	0.0055	11	0.0280	50	-
247	ptakuratsatu-000	0.0060	120	0.0089	120	0.0070	157	0.0104	161	0.0096	131	0.0152	95	0.0100	91	0.0284	78	-
248	pxl-001	0.0488	295	0.0752	296	0.0586	299	0.1087	299	0.0946	296	0.1065	244	0.0625	268	0.1088	286	-
249	pyramid-000	0.0136	227	0.0233	236	0.0117	231	0.0192	227	0.0185	215	0.0322	185	0.0206	209	0.0304	145	-
250	qnap-000	0.0149	238	0.0228	233	0.0155	255	0.0267	253	0.0238	241	0.8329	319	0.0396	250	0.0324	174	-
251	quantasoft-003	0.0081	169	0.0113	164	0.0056	130	0.0076	121	0.0091	114	0.0161	105	0.0107	109	0.0414	227	-
252	rankone-010	0.0079	163	0.0112	161	0.0061	139	0.0081	134	0.0088	107	0.0149	88	0.0117	122	0.0320	172	-
253	rankone-011	0.0049	84	0.0075	100	0.0038	70	0.0048	62	0.0060	69	0.0143	84	0.0080	59	0.0359	210	-
254	realnetworks-004	0.0075	157	0.0101	146	0.0066	151	0.0097	157	0.0108	151	0.0187	129	0.0131	136	0.0285	90	-
255	realnetworks-005	0.0070	142	0.0093	126	0.0063	145	0.0089	147	0.0092	117	0.0161	106	0.0104	102	0.0289	112	-
256	regula-000	0.0184	259	0.0376	273	0.0103	208	0.0185	222	0.0120	159	0.9983	338	0.0231	218	0.0273	12	-
257	remarkai-001	0.0144	234	0.0256	249	0.0102	206	0.0159	209	0.0162	197	0.0582	218	0.0185	191	0.0308	155	-
258	remarkai-003	0.0047	83	0.0063	82	0.0033	52	0.0049	66	0.0054	55	0.0100	52	0.0072	39	0.0275	22	-
259	rendip-000	0.0055	106	0.0077	103	0.0048	106	0.0060	92	0.0080	94	0.0142	83	0.0110	111	0.0433	232	-
260	revealmedia-005	0.0050	89	0.0074	99	0.0050	112	0.0068	108	0.0075	84	0.0124	74	0.0104	105	0.3960	333	-
261	rokid-000	0.0093	184	0.0145	186	0.0073	165	0.0102	159	0.0164	199	0.0280	172	0.0214	211	0.0857	276	-
262	rokid-001	0.0105	201	0.0162	199	0.0094	203	0.0163	212	0.0181	210	0.0276	171	0.0165	176	0.0325	177	-
263	s1-002	0.0095	187	0.0144	185	0.0112	225	0.0196	229	0.0234	235	0.0371	196	0.0282	234	0.1167	291	-
264	s1-003	0.0051	93	0.0073	95	0.0044	94	0.0063	99	0.0052	51	0.0096	48	0.0070	35	0.1321	295	-

Table 21: FNMR is the proportion of mated comparisons below a threshold set to achieve the FMR given in the header on the fourth row. FMR is the proportion of impostor comparisons at or above that threshold. The light grey values give rank over all algorithms in that column. The pink columns use only same-sex impostors; others are selected regardless of demographics. The exception, in the green column, uses “matched-covariates” i.e. impostors of the same sex, age group, and country of birth. The second pink column includes effects of extended ageing. Missing entries for border, visa, mugshot and wild images generally mean the algorithm did not run to completion. For child exploitation, missing entries arise because NIST executes those runs only infrequently. The VISA columns compare images described in section 2.1. The MUGSHOT columns compare images described in section 2.4. The VISA-BORDER column compare images described in section 2.2 with those of section 2.3. The BORDER column compares images described in section 2.3. The WILD columns compare images described in section 2.5. The CHILD-EXPLOITATION columns compare images described in section ??.

Algorithm	FALSE NON-MATCH RATE (FNMR)																	
	CONSTRAINED, COOPERATIVE								LESS CONSTRAINED, NON-COOP.									
	Name	VISAMC	VISA	MUGSHOT	MUGSHOT12+YRS	VISABORDER	BORDER	BORDER	WILD	CHILDEXP								
FMR	0.0001	1E-06	1E-05	1E-05	1E-05	1E-06	1E-06	1E-05	0.0001	0.01								
265 saffe-001	0.4339	344	0.5261	341	0.7539	354	0.8736	353	0.7977	341	0.9810	327	0.7435	339	0.3887	332	0.8973	46
266 saffe-002	0.0119	212	0.0206	220	0.0107	216	0.0177	218	0.0244	243	0.9998	342	0.2785	307	0.0308	154	-	
267 samsungsds-000	0.0046	79	0.0069	89	0.0132	237	0.0081	132	0.0099	135	0.0179	122	0.0162	173	0.1874	307	-	
268 samtech-001	0.0197	265	0.0365	271	0.0146	248	0.0241	244	0.0238	240	0.0394	203	0.0251	227	0.0337	188	-	
269 scanovate-001	0.0175	257	0.0331	264	0.0163	258	0.0248	246	0.2476	316	0.3801	278	0.3740	316	0.4060	334	-	
270 scanovate-002	0.0175	256	0.0355	270	0.0146	246	0.0286	257	0.0269	246	0.0301	177	0.0178	186	0.0301	141	-	
271 securifai-001	0.4538	348	0.6142	349	0.5844	341	0.7428	340	0.7051	334	0.9961	336	0.9558	347	0.1963	309	-	
272 securifai-003	0.4086	341	0.7577	357	0.7233	350	0.8070	346	0.7787	339	1.0000	353	0.9988	353	0.8326	352	-	
273 sensetime-004	0.0026	32	0.0038	30	0.0022	2	0.0023	3	0.0042	24	0.0082	28	0.0078	51	0.0293	120	-	
274 sensetime-005	0.0019	18	0.0029	18	0.0022	1	0.0021	2	0.0023	1	0.0044	1	0.0039	1	0.0273	10	-	
275 sertis-000	0.0118	211	0.0208	222	0.0080	175	0.0127	179	0.0110	153	0.0176	120	0.0114	118	0.0285	88	-	
276 sertis-002	0.0049	85	0.0061	76	0.0039	80	0.0061	98	0.0055	57	0.0099	51	0.0070	36	0.0281	57	-	
277 seventhsense-000	0.0067	140	0.0099	144	0.0045	97	0.0065	103	0.0093	120	0.0169	113	0.0124	130	0.0275	21	-	
278 shaman-000	0.9297	364	0.9774	362	0.9990	361	-		0.9999	355	1.0000	349	0.9999	356	0.9575	355	0.9618	50
279 shaman-001	0.3346	335	0.4616	336	0.2368	321	0.3723	322	0.3574	322	0.3527	276	0.2304	302	0.1498	299	0.8990	47
280 shu-002	-		0.0079	107	0.0146	247	0.0308	260	1.0000	356	0.0183	125	0.0115	119	0.0284	79	-	
281 shu-003	0.0028	37	0.0041	40	0.0050	110	0.0088	146	0.0081	98	0.0133	79	0.0094	86	0.0283	76	-	
282 siat-002	0.0091	179	0.0126	173	0.0109	218	0.0190	226	0.0276	249	0.0516	214	0.0464	258	0.0520	250	0.4277	9
283 siat-004	0.0067	138	0.0099	141	0.0152	254	-		0.0275	248	0.4823	285	0.4823	324	1.0000	358	-	
284 sjtu-003	0.0017	15	0.0033	21	0.0030	37	0.0037	35	0.0058	61	0.0104	55	0.0081	62	0.0284	82	-	
285 sjtu-004	0.0014	9	0.0025	11	0.0027	22	0.0028	20	0.0046	34	0.0086	33	0.0073	40	0.0272	6	-	
286 sktelecom-000	0.0038	63	0.0054	63	0.0031	38	0.0051	73	0.0042	23	0.3418	275	0.0061	21	0.0293	123	-	
287 smartengines-000	0.6240	358	0.7562	356	0.9552	357	0.9784	355	0.9515	351	0.9288	325	0.8200	341	0.8037	351	-	
288 smilart-002	0.2440	324	0.3532	326	-		-		0.3785	323	0.4145	283	0.2611	305	-		0.6999	31
289 smilart-003	0.6944	360	0.8836	359	0.0695	303	0.1193	303	0.0894	294	0.1221	249	0.0737	276	0.1190	292	-	
290 sodec-000	0.0033	49	0.0044	46	0.0040	83	0.0053	76	0.0054	56	0.0096	47	0.0080	57	0.0274	14	-	
291 sqisoft-001	0.1220	312	0.2088	313	0.1978	319	0.3386	320	0.2111	314	0.2798	273	0.1474	296	0.0519	249	-	
292 sqisoft-002	0.0082	170	0.0124	167	0.0051	113	0.0086	143	0.0102	139	0.0183	126	0.0122	128	0.0287	97	-	
293 stagu-000	0.0139	231	0.0208	221	0.0104	209	0.0145	200	0.0156	189	0.8063	314	0.1408	295	0.0332	185	-	
294 starhybrid-001	0.0108	203	0.0138	179	0.0081	178	0.0113	168	0.0152	188	0.0265	166	0.0189	196	0.0350	204	0.5584	18
295 suprema-000	0.0064	131	0.0092	125	0.0081	180	0.0096	155	0.0139	179	0.0254	162	0.0220	212	0.1131	289	-	
296 suprema-001	0.0041	71	0.0053	60	0.0038	75	0.0047	59	0.0060	68	0.0111	61	0.0095	88	0.0382	216	-	
297 supremaid-001	0.0053	101	0.0073	97	0.0045	98	0.0066	105	0.0099	136	0.0186	128	0.0148	159	0.0352	206	-	
298 synesis-006	0.0070	146	0.0096	134	0.0107	214	0.0166	214	-		0.0128	78	0.0089	77	0.0292	118	-	
299 synesis-007	0.0050	90	0.0073	98	0.0062	144	0.0076	120	-		0.0105	56	0.0080	60	0.0288	99	-	
300 synology-000	0.0149	239	0.0238	241	0.0148	249	0.0261	250	0.0221	228	0.0331	187	0.0209	210	0.0330	183	-	
301 synology-002	0.0104	199	0.0153	194	0.0107	215	0.0184	221	0.0189	217	0.2032	262	0.0180	187	0.0312	161	-	
302 sztu-000	0.0092	182	0.0139	180	0.0091	197	0.0201	233	0.0136	174	0.0685	225	0.0118	125	0.0270	2	-	
303 sztu-001	0.0031	42	0.0043	44	0.0025	14	0.0028	15	0.0051	47	0.0113	66	0.0089	78	0.0275	17	-	
304 tech5-004	0.0123	217	0.0234	238	0.0086	191	0.0162	210	0.0065	77	0.0112	63	0.0082	65	0.0281	61	-	
305 tech5-005	0.0054	104	0.0072	92	0.0069	155	0.0122	173	0.0060	67	0.0094	43	0.0066	29	0.0349	201	-	
306 techsign-000	0.0325	283	0.0511	284	0.0435	292	0.0710	291	0.0746	289	0.1104	248	0.0841	280	0.0639	262	-	
307 tevian-006	0.0045	77	0.0061	77	0.0045	100	0.0066	104	0.0046	38	0.0091	36	0.0075	46	0.0308	157	-	
308 tevian-007	0.0019	19	0.0027	15	0.0032	49	0.0041	44	0.0045	29	0.0086	32	0.0078	53	0.0310	160	-	

Table 22: FNMR is the proportion of mated comparisons below a threshold set to achieve the FMR given in the header on the fourth row. FMR is the proportion of impostor comparisons at or above that threshold. The light grey values give rank over all algorithms in that column. The pink columns use only same-sex impostors; others are selected regardless of demographics. The exception, in the green column, uses “matched-covariates” i.e. impostors of the same sex, age group, and country of birth. The second pink column includes effects of extended ageing. Missing entries for border, visa, mugshot and wild images generally mean the algorithm did not run to completion. For child exploitation, missing entries arise because NIST executes those runs only infrequently. The VISA columns compare images described in section 2.1. The MUGSHOT columns compare images described in section 2.4. The VISA-BORDER column compare images described in section 2.2 with those of section 2.3. The BORDER column compares images described in section 2.3. The WILD columns compare images described in section 2.5. The CHILD-EXPLOITATION columns compare images described in section ??.

Algorithm	Name	FALSE NON-MATCH RATE (FNMR)												LESS CONSTRAINED, NON-COOP.					
		CONSTRAINED, COOPERATIVE																	
		VISAMC	VISA	MUGSHOT	MUGSHOT12+YRS	VISABORDER	BORDER	BORDER	WILD	CHILDEXP									
FMR		0.0001	1E-06	1E-05	1E-05	1E-06	1E-06	1E-05	0.0001	0.01									
309	tiger-003	0.0313	282	0.0602	289	0.0188	262	0.0359	269	0.0344	258	-	-	0.0482	244	0.5610	20		
310	tiger-005	0.0624	300	0.2450	317	0.0292	285	0.0556	284	0.0430	270	1.0000	344	0.9964	351	0.0278	37	-	
311	tinkoff-001	0.0145	236	0.0244	242	0.0318	286	0.0636	289	0.0236	238	1.0000	359	0.0339	240	0.0563	257	-	
312	tongyi-005	0.0073	153	0.0146	188	0.0187	261	0.0421	274	0.0161	195	0.0215	143	0.0149	161	0.0399	219	0.6195	24
313	toppanidgate-000	0.0021	20	0.0033	22	0.0026	16	0.0028	13	0.0039	19	0.0075	17	0.0068	32	0.0376	214	-	
314	toshiba-003	0.0125	221	0.0214	225	0.0085	189	0.0131	187	-	-	0.0241	154	0.0151	165	0.0282	62	-	
315	toshiba-004	0.0030	40	0.0042	42	0.0025	13	0.0027	10	0.0034	10	0.0063	9	0.0053	9	0.0278	36	-	
316	trueface-002	0.0060	121	0.0096	135	0.0048	105	0.0061	96	0.0112	156	0.0198	134	0.0155	168	0.0793	273	-	
317	trueface-003	0.0070	145	0.0094	130	0.0053	118	0.0081	135	0.0122	161	0.0217	146	0.0159	171	0.0785	272	-	
318	tuputech-000	0.3218	334	0.3696	328	-	-	-	0.3237	318	0.4304	284	0.2973	310	0.9415	354	-		
319	twface-000	0.0051	92	0.0072	94	0.0041	85	0.0058	85	0.0071	81	0.0153	96	0.0100	90	0.0276	26	-	
320	twface-001	0.0036	53	0.0051	56	0.0031	44	0.0038	36	0.0049	41	0.0091	39	0.0075	45	0.0277	29	-	
321	ulsee-001	0.0151	241	0.0246	244	0.0113	227	0.0185	224	0.0187	216	0.6766	301	0.0181	189	0.0316	166	-	
322	ultinous-000	0.2343	323	0.3484	324	-	-	-	-	-	-	-	-	-	-	0.9447	49		
323	ultinous-001	0.2485	325	0.4003	331	-	-	-	-	-	-	-	-	-	-	0.6847	28		
324	uluface-002	0.0081	168	0.0123	166	0.0071	158	0.0095	153	0.0107	146	1.0000	363	0.0140	149	0.0444	234	0.6729	27
325	uluface-003	0.0100	195	0.0150	192	0.0079	172	0.0128	182	-	-	-	-	-	-	0.0635	261	-	
326	upc-001	0.0234	271	0.0519	285	0.0291	284	0.0490	281	0.0294	251	0.2316	268	0.0389	249	0.0314	165	0.4224	7
327	vcog-002	0.7522	362	0.9033	360	-	-	-	-	-	-	-	-	-	-	0.7523	36		
328	vd-002	0.0429	291	0.0704	292	0.0569	298	0.0844	294	0.0801	291	0.0937	236	0.0577	266	0.0556	256	-	
329	vd-003	0.0199	267	0.0222	232	0.0115	229	0.0130	186	0.0138	177	0.0239	152	0.0177	184	0.0389	217	-	
330	veridas-006	0.0098	191	0.0167	206	0.0079	174	0.0127	178	0.0127	165	0.0217	145	0.0151	164	0.0286	94	-	
331	veridas-007	0.0063	128	0.0083	112	0.0044	95	0.0058	87	0.0080	95	0.0152	94	0.0120	127	0.0284	80	-	
332	verigram-000	0.0032	44	0.0043	43	0.0031	39	0.0034	28	0.0093	122	0.0175	118	0.0164	175	0.0276	24	-	
333	verihubs-inteligensia-000	0.0070	144	0.0098	138	0.0048	107	0.0076	122	0.0092	116	0.0160	104	0.0117	121	0.0283	73	-	
334	via-000	0.0216	269	0.0365	272	0.0177	259	0.0287	258	0.0296	252	0.0572	216	0.0290	238	0.0349	200	0.7638	37
335	via-001	0.0149	237	0.0229	234	0.0114	228	0.0177	220	0.0183	214	0.4056	281	0.0176	182	0.0373	213	-	
336	videoemo-000	0.0298	280	0.0423	276	0.0155	256	0.0260	248	0.0246	244	0.0397	204	0.0239	223	0.0541	253	-	
337	videonetics-001	0.5483	355	0.6446	350	0.7517	353	0.8607	350	0.8664	345	0.8255	316	0.6956	338	0.2986	327	0.7297	33
338	videonetics-002	0.4274	342	0.5329	342	0.6081	343	0.7438	341	0.7775	338	0.7297	307	0.5756	330	0.1976	311	0.7435	35
339	viettelhightech-000	0.0117	209	0.0166	202	0.0110	220	0.0198	232	0.0167	204	0.0249	158	0.0158	169	0.0409	226	-	
340	vigilantsolutions-010	0.0109	204	0.0164	201	0.0074	166	0.0095	152	0.0209	225	0.0365	195	0.0233	219	0.0277	30	-	
341	vigilantsolutions-011	0.0124	219	0.0176	211	0.0073	162	0.0095	151	0.0196	221	0.0360	194	0.0221	213	0.0274	13	-	
342	vinai-000	0.0081	167	0.0124	168	0.0045	96	0.0072	114	0.0089	110	0.1814	255	0.0112	114	0.0274	15	-	
343	vion-000	0.0419	289	0.0590	288	0.0422	291	0.0478	278	0.0581	281	0.0968	242	0.0847	281	0.2479	320	0.8765	43
344	visage-000	0.0933	308	0.1441	308	0.1316	312	0.2416	313	0.1395	302	0.1920	259	0.1001	285	0.0500	246	-	
345	visionbox-001	0.0159	246	0.0270	255	0.0111	222	0.0173	217	0.0190	218	0.0315	182	0.0205	208	0.0389	218	-	
346	visionbox-002	0.0058	110	0.0079	106	0.0060	137	0.0074	115	0.0084	101	0.0149	89	0.0113	117	0.0447	237	-	
347	visionlabs-010	0.0017	14	0.0024	10	0.0026	17	0.0030	23	0.0033	9	0.0061	8	0.0052	8	0.0282	68	-	
348	visionlabs-011	0.0012	6	0.0022	8	0.0024	10	0.0026	8	0.0028	2	0.0053	2	0.0046	2	0.0280	51	-	
349	visteam-001	0.4417	346	0.5385	344	0.6410	345	0.7788	343	0.6386	331	0.5904	294	0.4023	320	0.1413	297	-	
350	visteam-002	0.1564	317	0.2789	320	0.1581	317	0.2567	316	0.1776	307	0.2090	263	0.1021	286	0.0349	202	-	
351	vnpt-001	0.3117	332	0.3523	325	0.3474	328	0.2747	317	0.3405	319	0.5015	287	0.4827	325	0.5337	343	-	
352	vnpt-002	0.0351	286	0.0424	277	0.0220	270	0.0316	262	0.0471	275	0.0817	233	0.0698	273	0.0400	220	-	

Table 23: FNMR is the proportion of mated comparisons below a threshold set to achieve the FMR given in the header on the fourth row. FMR is the proportion of impostor comparisons at or above that threshold. The light grey values give rank over all algorithms in that column. The pink columns use only same-sex impostors; others are selected regardless of demographics. The exception, in the green column, uses “matched-covariates” i.e. impostors of the same sex, age group, and country of birth. The second pink column includes effects of extended ageing. Missing entries for border, visa, mugshot and wild images generally mean the algorithm did not run to completion. For child exploitation, missing entries arise because NIST executes those runs only infrequently. The VISA columns compare images described in section 2.1. The MUGSHOT columns compare images described in section 2.4. The VISA-BORDER column compare images described in section 2.2 with those of section 2.3. The BORDER column compares images described in section 2.3. The WILD columns compare images described in section 2.5. The CHILD-EXPLOITATION columns compare images described in section ??.

	Algorithm	FALSE NON-MATCH RATE (FNMR)												LESS CONSTRAINED, NON-COOP.					
		CONSTRAINED, COOPERATIVE																	
		Name	VISAMC	VISA	MUGSHOT	MUGSHOT12+YRS	VISABORDER	BORDER	BORDER	WILD	CHILDEXP								
FMR		0.0001	1E-06	1E-05	1E-05	1E-05	1E-06	1E-06	1E-05	0.0001	0.01								
353	vocord-008	0.0029	39	0.0038	31	0.0042	87	0.0055	79	0.0045	31	0.0086	34	0.0073	41	0.0286	91	-	
354	vocord-009	0.0022	22	0.0029	19	0.0036	63	0.0046	56	0.0052	50	0.0098	50	0.0086	74	0.0284	81	-	
355	vts-000	0.0103	197	0.0174	208	0.0080	176	0.0129	185	0.0250	245	0.0450	207	0.0372	247	0.0596	259	-	
356	winsense-001	0.0062	126	0.0099	145	0.0092	199	0.0210	234	0.0093	121	0.0144	86	0.0098	89	0.0320	171	0.4155	6
357	winsense-002	0.0050	88	0.0073	96	0.0038	72	0.0059	90	0.0064	75	0.0118	71	0.0084	69	0.0307	153	-	
358	wuhantianyu-001	0.0163	247	0.0262	252	0.0281	283	0.0569	287	0.0316	256	0.0486	210	0.0344	241	0.0324	175	-	
359	x-laboratory-000	0.0071	150	0.0106	152	0.0123	234	0.0138	192	0.0419	269	0.5629	292	0.2852	309	0.0295	129	0.9686	51
360	x-laboratory-001	0.0059	117	0.0110	157	0.0054	122	0.0078	126	0.0094	124	0.0142	82	0.0100	92	0.0294	125	-	
361	xforwardai-001	0.0021	21	0.0034	23	0.0027	24	0.0028	14	0.0046	37	0.0088	35	0.0079	55	0.0281	60	-	
362	xforwardai-002	0.0016	12	0.0023	9	0.0026	19	0.0025	5	0.0040	21	0.0081	27	0.0074	42	0.0282	63	-	
363	xm-000	0.0015	10	0.0026	14	0.0031	42	0.0038	38	0.0058	62	0.0105	57	0.0082	66	0.0282	66	-	
364	yisheng-004	0.1988	320	0.3329	323	0.1147	310	0.1849	308	0.2044	311	-	-	-	-	0.0908	278	0.7152	32
365	yitu-003	0.0015	11	0.0026	13	0.0066	152	0.0085	140	0.0064	76	0.0114	67	0.0103	100	0.0325	178	-	
366	yoonik-001	0.0057	108	0.0079	105	0.0043	91	0.0061	93	0.0307	254	0.0762	230	0.0556	265	0.0526	252	-	
367	yoonik-002	0.0052	97	0.0062	79	0.0029	30	0.0034	29	0.0615	285	0.1279	251	0.1166	287	0.0549	254	-	
368	ytu-000	0.0057	109	0.0087	118	0.0121	232	0.0238	243	0.0047	39	0.0078	24	0.0059	17	0.0286	93	-	
369	yuan-002	0.0094	185	0.0154	197	0.0071	160	0.0110	166	0.0108	150	0.0348	193	0.0127	133	0.0319	170	-	
370	yuan-003	0.0078	160	0.0111	158	0.0062	143	0.0091	148	0.0106	144	0.0511	213	0.0123	129	0.0320	173	-	

Table 24: FNMR is the proportion of mated comparisons below a threshold set to achieve the FMR given in the header on the fourth row. FMR is the proportion of impostor comparisons at or above that threshold. The light grey values give rank over all algorithms in that column. The pink columns use only same-sex impostors; others are selected regardless of demographics. The exception, in the green column, uses “matched-covariates” i.e. impostors of the same sex, age group, and country of birth. The second pink column includes effects of extended ageing. Missing entries for border, visa, mugshot and wild images generally mean the algorithm did not run to completion. For child exploitation, missing entries arise because NIST executes those runs only infrequently. The VISA columns compare images described in section 2.1. The MUGSHOT columns compare images described in section 2.4. The VISA-BORDER column compare images described in section 2.2 with those of section 2.3. The BORDER column compares images described in section 2.3. The WILD columns compare images described in section 2.5. The CHILD-EXPLOITATION columns compare images described in section ??.

FNMR(T)
FMR(T)“False non-match rate”
“False match rate”

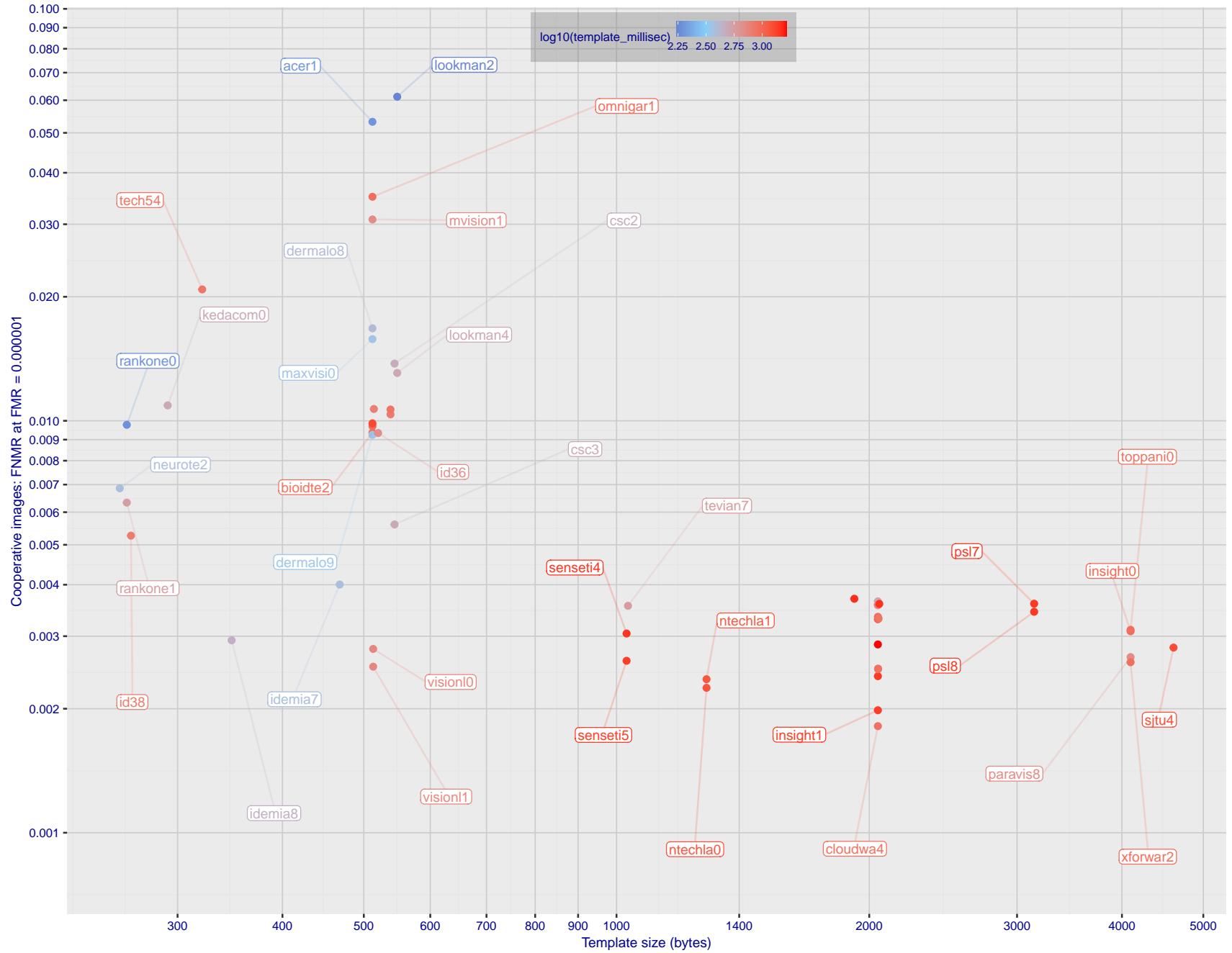


Figure 1: The points show false non-match rates (FNMR) versus the size of the encoded template. FNMR is the geometric mean of FNMR values for visa and mugshot images (from Figs. 56 and 75) at the false match rate (FMR) given in the y-axis label. The color of the points encodes template generation time - which spans at least one order of magnitude. Durations are measured on a single core of a c. 2016 Intel Xeon CPU E5-2630 v4 running at 2.20GHz. Algorithms with poor FNMR are omitted.

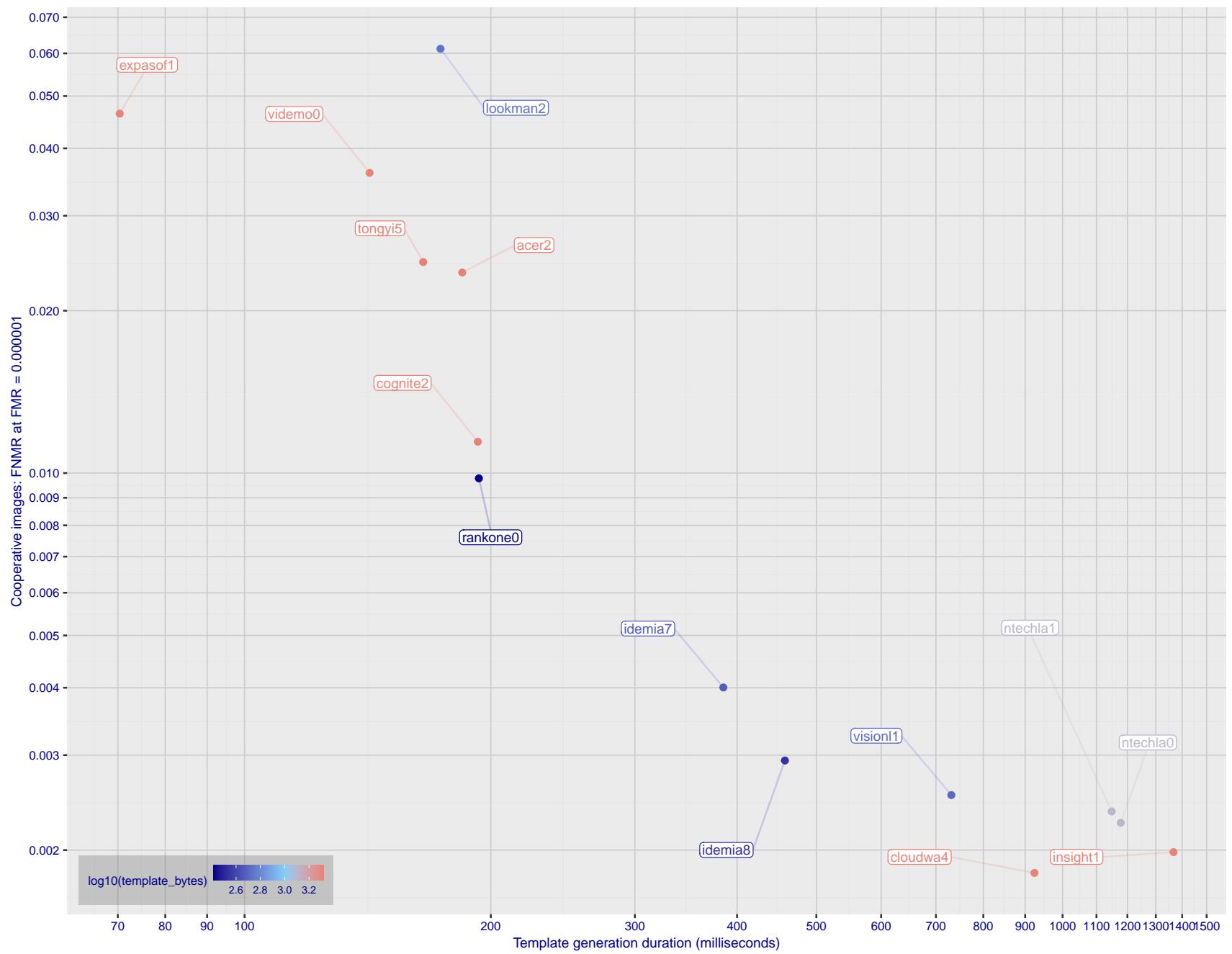


Figure 2: The points show false non-match rates (FNMR) versus the duration of the template generation operation. FNMR is the geometric mean of FNMR values for visa and mugshot images (from Figs. 56 and 75) at a false match rate (FMR) given in the y-axis label. Template generation time is a median estimated over 640 x 480 pixel portraits. It is measured on a single core of a c. 2016 Intel Xeon CPU E5-2630 v4 running at 2.20GHz. The color of the points encodes template size - which span two orders of magnitude. Algorithms with poor FNMR are omitted.

1 Metrics

1.1 Core accuracy

Given a vector of N genuine scores, u , the false non-match rate (FNMR) is computed as the proportion below some threshold, T:

$$\text{FNMR}(T) = 1 - \frac{1}{N} \sum_{i=1}^N H(u_i - T) \quad (1)$$

where $H(x)$ is the unit step function, and $H(0)$ taken to be 1.

Similarly, given a vector of N impostor scores, v , the false match rate (FMR) is computed as the proportion above T:

$$\text{FMR}(T) = \frac{1}{N} \sum_{i=1}^N H(v_i - T) \quad (2)$$

The threshold, T, can take on any value. We typically generate a set of thresholds from quantiles of the observed impostor scores, v , as follows. Given some interesting false match rate range, $[\text{FMR}_L, \text{FMR}_U]$, we form a vector of K thresholds corresponding to FMR measurements evenly spaced on a logarithmic scale

$$T_k = Q_v(1 - \text{FMR}_k) \quad (3)$$

where Q is the quantile function, and FMR_k comes from

$$\log_{10} \text{FMR}_k = \log_{10} \text{FMR}_L + \frac{k}{K} [\log_{10} \text{FMR}_U - \log_{10} \text{FMR}_L] \quad (4)$$

Error tradeoff characteristics are plots of FNMR(T) vs. FMR(T). These are plotted with $\text{FMR}_U \rightarrow 1$ and FMR_L as low as is sustained by the number of impostor comparisons, N. This is somewhat higher than the “rule of three” limit $3/N$ because samples are not independent, due to re-use of images.

2 Datasets

2.1 Visa images

- ▷ The number of images is on the order of 10^5 .
- ▷ The number of subjects is on the order of 10^5 .
- ▷ The number of subjects with two images is on the order of 10^4 .
- ▷ The images have geometry in reasonable conformance with the ISO/IEC 19794-5 Full Frontal image type. Pose is generally excellent.
- ▷ The images are of size 252x300 pixels. The mean interocular distance (IOD) is 69 pixels.
- ▷ The images are of subjects from greater than 100 countries, with significant imbalance due to visa issuance patterns.
- ▷ The images are of subjects of all ages, including children, again with imbalance due to visa issuance demand.
- ▷ Many of the images are live capture. A substantial number of the images are photographs of paper photographs.
- ▷ When these images are input to the algorithm, they are labelled as being of type "ISO" - see Table 4 of the FRVT API.

2.2 Application images

- ▷ The number of images is on the order of 10^6 .
- ▷ The number of subjects is on the order of 10^6 .
- ▷ The number of subjects with two images is on the order of 10^6 .
- ▷ The images have geometry in good conformance with the ISO/IEC 19794-5 Full Frontal image type. Pose is generally excellent.
- ▷ The images are of size 300x300 pixels. The mean interocular distance (IOD) is 61 pixels.
- ▷ The images are of subjects from greater than 100 countries, with significant imbalance due to population and immigration patterns.
- ▷ The images are of subjects of adults with imbalance due to population and immigration patterns and demand.
- ▷ All of the images are live capture.
- ▷ When these images are input to the algorithm, they are labelled as being of type "ISO" - see Table 4 of the FRVT API.

2.3 Border crossing images

- ▷ The number of images is on the order of 10^6 .
- ▷ The number of subjects is on the order of 10^6 .
- ▷ The number of subjects with two images is on the order of 10^6 .
- ▷ The images are taken with a camera oriented by an attendant toward a cooperating subject. This is done under time constraints so there are roll, pitch and yaw angle variations. Also background illumination is sometimes strong, so the face is under-exposed. There is some perspective distortion due to close range images. Some faces are partially cropped.
- ▷ The images are of subjects from greater than 100 countries, with significant imbalance due to population and immigration patterns.
- ▷ The images are of subjects of adults with imbalance due to population and immigration patterns and demand.

- ▷ The images have mean IOD of 38 pixels.
- ▷ The images are all live capture.
- ▷ When these images are input to the algorithm, they are labelled as being of type "WILD" - see Table 4 of the FRVT API.

2.4 Mugshot images

- ▷ The number of images is on the order of 10^6 .
- ▷ The number of subjects is on the order of 10^6 .
- ▷ The number of subjects with two images is on the order of 10^6 .
- ▷ The images have geometry in reasonable conformance with the ISO/IEC 19794-5 Full Frontal image type.
- ▷ The images are of variable sizes. The median IOD is 105 pixels. The mean IOD is 113 pixels. The 1-st, 5-th, 10-th, 25-th, 75-th, 90-th and 99-th percentiles are 34, 58, 70, 87, 121, 161 and 297 pixels.
- ▷ The images are of subjects from the United States.
- ▷ The images are of adults.
- ▷ The images are all live capture.
- ▷ When these images are input to the algorithm, they are labelled as being of type "mugshot" - see Table 4 of the FRVT API.

2.5 Wild images

- ▷ The number of images is on the order of 10^5 .
- ▷ The number of subjects is on the order of 10^3 .
- ▷ The number of subjects with two images on the order of 10^3 .
- ▷ The images include many photojournalism-style images. Images are given to the algorithm using a variable but generally tight crop of the head. Resolution varies very widely. The images are very unconstrained, with wide yaw and pitch pose variation. Faces can be occluded, including hair and hands.
- ▷ The images are of adults.
- ▷ All of the images are live capture, none are scanned.
- ▷ When these images are input to the algorithm, they are labelled as being of type "WILD" - see Table 4 of the FRVT API.

3 Results

3.1 Test goals

- ▷ To state absolute accuracy for different kinds of images, including those with and without subject cooperation.
- ▷ To state comparative accuracy, across algorithms.



Figure 3: The figure gives simulated samples of image types used in this report.

3.2 Test design

Method: For visa images:

- ▷ The comparisons are of visa photos against visa photos.
 - ▷ The number of genuine comparisons is on the order of 10^4 .
 - ▷ The number of impostor comparisons is on the order of 10^{10} .
 - ▷ The comparisons are fully zero-effort, meaning impostors are paired without attention to sex, age or other covariates. However, later analysis is conducted on subsets.
 - ▷ The number of persons is on the order of 10^5 .
 - ▷ The number of images used to make 1 template is 1.
 - ▷ The number of templates used to make each comparison score is two corresponding to simple one-to-one verification.

Method: For mugshot images:

- ▷ The comparisons are of mugshot photos against mugshot photos.
 - ▷ The number of genuine comparisons is on the order of 10^6 .
 - ▷ The number of impostor comparisons is on the order of 10^8 .
 - ▷ The impostors are paired by sex, but not by age or other covariates.
 - ▷ The number of persons is on the order of 10^6 .
 - ▷ The number of images used to make 1 template is 1.
 - ▷ The number of templates used to make each comparison score is two corresponding to simple one-to-one verification.

Method: For visa-border comparisons:

- ▷ The comparisons are of visa-like frontals against border crossing webcam photos.
 - ▷ The number of genuine comparisons is on the order of 10^6 .
 - ▷ The number of impostor comparisons is on the order of 10^8 .

- ▷ The impostors are paired by sex, but not by age or other covariates.
- ▷ The number of persons is on the order of 10^6 .
- ▷ The number of images used to make 1 template is 1.
- ▷ The number of templates used to make each comparison score is two corresponding to simple one-to-one verification.

Method: For border-border comparisons:

- ▷ The comparisons are of border crossing webcam photos.
- ▷ The number of genuine comparisons is on the order of 10^6 .
- ▷ The number of impostor comparisons is on the order of 10^8 .
- ▷ The impostors are paired by sex, but not by age or other covariates.
- ▷ The number of persons is on the order of 10^6 .
- ▷ The number of images used to make 1 template is 1.
- ▷ The number of templates used to make each comparison score is two corresponding to simple one-to-one verification.

Method: For wild images:

- ▷ The comparisons are of wild photos against wild photos.
- ▷ The number of genuine comparisons is on the order of 10^6 .
- ▷ The number of impostor comparisons is on the order of 10^7 .
- ▷ The comparisons are fully zero-effort, meaning impostors are paired without attention to sex, age or other covariates.
- ▷ The number of persons is on the order of 10^4 .
- ▷ The number of images used to make 1 template is 1.
- ▷ The number of templates used to make each comparison score is two corresponding to simple one-to-one verification.

Method: For child exploitation images:

- ▷ The comparisons are of unconstrained child exploitation photos against others of the same type.
- ▷ The number of genuine comparisons is on the order of 10^4 .
- ▷ The number of impostor comparisons is on the order of 10^7 .
- ▷ The comparisons are fully zero-effort, meaning impostors are paired without attention to sex, age or other covariates.
- ▷ The number of persons is on the order of 10^3 .
- ▷ The number of images used to make 1 template is 1.
- ▷ The number of templates used to make each comparison score is two corresponding to simple one-to-one verification.
- ▷ We produce two performance statements. First, is a DET as used for visa and mugshot images. The second is a cumulative match characteristic (CMC) summarizing a simulated one-to-many search process. This is done as follows.
 - We regard M enrollment templates as items in a gallery.

- These M templates come from $M > N$ individuals, because multiple images of a subject are present in the gallery under separate identifiers.
- We regard the verification templates as search templates.
- For each search we compute the rank of the highest scoring mate.
- This process should properly be conducted with a 1:N algorithm, such as those tested in NIST IR 8009. We use the 1:1 algorithms in a simulated 1:N mode here to a) better reflect what a child exploitation analyst does, and b) to show algorithm efficacy is better than that revealed in the verification DETs.

3.3 Failure to enroll

	Algorithm Name	Failure to Enrol Rate ¹											
		APPLICATION	BORDER	CHILD-EXPLOIT	MUGSHOT	VISA	WILD	SEC. 2.2	SEC. 2.3	SEC. ??	SEC. 2.4	SEC. 2.1	SEC. 2.5
1	20face-000	0.0000	215	0.0008	186	-	118	0.0000	110	0.0004	199	0.0004	153
2	20face-001	0.0000	159	0.0008	185	-	234	0.0000	111	0.0004	197	0.0004	156
3	3divi-006	0.0000	209	0.0007	163	-	54	0.0001	193	0.0002	112	0.0005	192
4	3divi-007	0.0000	236	0.0007	161	-	196	0.0001	192	0.0002	111	0.0005	193
5	acer-001	0.0000	218	0.0011	226	-	95	0.0001	172	0.0004	221	0.0004	164
6	acer-002	0.0000	301	0.0008	180	-	287	0.0003	255	0.0004	218	0.0011	240
7	acisw-003	0.0000	135	0.0000	66	-	143	0.0000	9	0.0000	54	0.0001	101
8	acisw-006	0.0000	41	0.0000	23	-	269	0.0000	95	0.0000	44	0.0001	97
9	adera-002	0.0000	286	0.0034	296	-	341	0.0003	263	0.0005	301	0.0505	336
10	adera-003	0.0000	287	0.0034	297	-	60	0.0003	262	0.0005	302	0.0505	335
11	advance-002	0.0000	202	0.0013	247	-	351	0.0000	157	0.0004	215	0.0009	231
12	advance-003	0.0000	279	0.0012	237	-	167	0.0001	209	0.0004	254	0.0011	236
13	aifirst-001	0.0000	95	0.0000	85	0.0000	2	0.0000	39	0.0000	85	0.0000	81
14	aigen-001	0.0000	131	0.0000	62	-	133	0.0000	11	0.0000	58	0.0000	35
15	aigen-002	0.0000	74	0.0000	1	-	335	0.0000	71	0.0000	20	0.0000	67
16	ailabs-001	0.0000	208	0.0090	336	-	78	0.0007	311	0.0005	273	0.0016	253
17	aimall-002	0.0000	293	0.0043	309	-	181	0.0012	325	0.0005	294	0.0005	203
18	aimall-003	0.0000	270	0.0012	240	-	159	0.0004	278	0.0005	267	0.0004	176
19	aiunionface-000	0.0000	42	0.0000	13	-	321	0.0000	60	0.0000	7	0.0000	86
20	aize-001	0.0001	325	0.0040	304	-	124	0.0026	343	0.0022	346	0.0058	283
21	aize-002	0.0000	17	0.0014	251	-	228	0.0005	299	0.0004	198	0.0071	290
22	ajou-001	0.0000	192	0.0020	273	-	310	0.0001	194	0.0004	257	0.0045	277
23	alchera-002	0.0000	241	0.0008	190	-	179	0.0001	216	0.0004	171	0.0003	143
24	alchera-003	0.0001	336	0.0013	245	-	104	0.0002	241	0.0004	225	0.0036	270
25	alice-000	0.0000	138	0.0006	139	-	194	0.0000	122	0.0004	170	0.0004	175
26	alleyes-000	0.0000	170	0.0010	211	-	232	0.0002	223	0.0004	234	0.0004	181
27	allgovision-000	0.0007	348	0.0062	327	-	116	0.0026	342	0.0052	359	0.0131	306
28	alphaface-001	0.0000	238	0.0012	232	-	175	0.0000	159	0.0004	236	0.0004	160
29	alphaface-002	0.0000	183	0.0012	231	-	322	0.0000	161	0.0004	232	0.0004	163
30	amplifiedgroup-001	0.0114	361	0.1023	363	-	304	0.0189	363	0.0279	367	0.1390	360
31	androvideo-000	0.0000	50	0.0000	15	-	328	0.0000	54	0.0000	6	0.0002	105
32	anke-004	0.0000	164	0.0011	223	0.0944	32	0.0001	200	0.0004	240	0.0006	215
33	anke-005	0.0000	224	0.0012	234	0.1228	34	0.0001	213	0.0004	250	0.0007	218
34	antheus-000	0.0000	31	0.0000	28	0.0000	15	0.0000	90	0.0000	40	0.0242	319
35	antheus-001	0.0000	12	0.0000	34	-	208	0.0000	84	0.0000	33	0.0242	320
36	anyvision-004	0.0000	275	0.0017	264	0.1660	37	0.0001	214	0.0004	209	0.0080	293
37	anyvision-005	0.0000	228	0.0013	242	-	139	0.0000	137	0.0004	168	0.0004	177
38	asusaics-000	0.0000	111	0.0000	80	-	126	0.0000	42	0.0000	91	0.0000	5
39	asusaics-001	0.0000	154	0.0000	50	-	185	0.0000	24	0.0000	70	0.0000	21
40	authenmetric-002	0.0000	46	0.0000	18	-	332	0.0000	56	0.0000	1	0.0000	78
41	authenmetric-003	0.0000	100	0.0000	78	-	117	0.0000	48	0.0000	92	0.0000	11
42	aware-005	0.0000	251	0.0020	272	-	63	0.0001	222	0.0004	242	0.0011	234
43	aware-006	0.0000	171	0.0009	198	-	233	0.0000	141	0.0004	208	0.0006	210
44	awirots-001	0.0039	353	0.0369	355	-	278	0.0386	364	0.0872	368	0.3415	364
45	awirots-002	0.0000	304	0.0038	302	-	70	0.0007	310	0.0012	334	0.0208	315
46	ayftech-001	0.0002	338	0.0046	315	-	94	0.0043	352	0.0011	325	0.0091	298
47	ayonix-000	0.0053	356	0.0341	352	0.0000	7	0.0113	360	0.0137	364	0.1194	355
48	beethedata-000	0.0005	344	0.0042	308	-	178	0.0002	227	0.0010	320	0.0006	207
49	bilocube-001	0.0006	346	0.0391	356	-	315	0.0015	330	0.0020	345	0.0253	324
50	biodtechswiss-001	0.0000	174	0.0007	157	-	280	0.0000	128	0.0004	227	0.0025	266
51	biodtechswiss-002	0.0000	227	0.0007	160	-	147	0.0000	130	0.0004	223	0.0005	204
52	bm-001	0.0000	132	0.0000	61	0.0000	8	0.0000	101	0.0000	57	0.0000	36
53	bootech-001	0.0087	359	0.0272	345	-	368	0.0032	349	0.0160	365	0.0946	349
54	bresee-001	0.0000	165	0.0010	216	-	244	0.0002	228	0.0003	141	0.0003	115
55	bresee-002	0.0000	283	0.0020	275	-	87	0.0008	312	0.0004	187	0.0031	269
56	camvi-002	0.0000	10	0.0000	35	0.0000	12	0.0000	88	0.0000	32	0.0000	56
57	camvi-004	0.0000	98	0.0000	102	0.0000	4	0.0000	36	0.0000	82	0.0000	12
58	canon-002	0.0000	4	0.0000	41	-	237	0.0000	79	0.0000	28	0.0000	60

Table 25: FTE is the proportion of failed template generation attempts. Failures can occur because the software throws an exception, or because the software electively refuses to process the input image. This would typically occur if a face is not detected. FTE is measured as the number of function calls that give EITHER a non-zero error code OR that give a “small” template. This is defined as one whose size is less than 0.3 times the median template size for that algorithm. This second rule is needed because some algorithms incorrectly fail to return a non-zero error code when template generation fails.

¹The effects of FTE are included in the accuracy results of this report by regarding any template comparison involving a failed template to produce a low similarity score. Thus higher FTE results in higher FNMR and lower FMR.

	Algorithm	Failure to Enrol Rate ¹						
		APPLICATION	BORDER	CHILD-EXPLOIT	MUGSHOT	VISA	WILD	
Name	SEC. 2.2	SEC. 2.3	SEC. ??	SEC. 2.4	SEC. 2.1	SEC. 2.5		
59 canon-003	0.0000	213	0.0008	175	-	65	0.0000	156
60 cieiec-003	0.0000	102	0.0013	248	-	108	0.0001	175
61 cieiec-004	0.0000	23	0.0008	184	-	223	0.0000	136
62 chosun-001	0.0000	86	0.0000	93	-	81	0.0000	30
63 chosun-002	0.0000	144	0.0000	57	-	198	0.0000	12
64 chtface-003	0.0000	282	0.0018	267	-	86	0.0001	182
65 chtface-004	0.0000	60	0.0017	261	-	311	0.0000	147
66 clearviewai-000	0.0000	187	0.0003	120	-	325	0.0000	149
67 closeli-001	0.0000	139	0.0000	53	-	193	0.0000	21
68 cloudwalk-hr-003	0.0000	235	0.0008	187	-	197	0.0001	181
69 cloudwalk-hr-004	0.0000	239	0.0011	230	-	173	0.0004	280
70 cloudwalk-mt-003	0.0000	217	0.0007	152	-	113	0.0002	235
71 cloudwalk-mt-004	0.0000	195	0.0009	191	-	356	0.0002	242
72 clova-000	0.0000	295	0.0022	277	-	83	0.0006	305
73 cogent-005	0.0000	109	0.0000	79	-	127	0.0000	41
74 cogent-006	0.0000	127	0.0000	69	-	162	0.0000	4
75 cognitec-002	0.0001	320	0.0069	329	-	84	0.0003	273
76 cognitec-003	0.0001	321	0.0194	342	-	56	0.0003	270
77 cor-001	0.0000	185	0.0006	143	-	330	0.0002	249
78 coretech-000	0.0000	89	0.0000	92	-	79	0.0000	28
79 corsight-001	0.0000	157	0.0006	148	-	242	0.0001	219
80 corsight-002	0.0000	205	0.0005	137	-	73	0.0001	201
81 csc-002	0.0015	350	0.0033	292	-	283	0.0006	307
82 csc-003	0.0015	351	0.0033	293	-	174	0.0006	306
83 ctcbank-000	0.0001	323	0.0051	320	0.3285	44	0.0011	323
84 ctcbank-001	0.0000	305	0.0036	301	-	92	0.0005	295
85 cubox-001	0.0000	15	0.0000	32	-	212	0.0000	87
86 cubox-002	0.0000	245	0.0006	146	-	271	0.0002	250
87 cudocommunication-001	0.0000	68	0.0000	4	-	370	0.0000	67
88 cuhkee-001	0.0000	178	0.0011	229	-	256	0.0000	112
89 cybercore-000	0.0000	167	0.0073	332	-	215	0.0001	189
90 cyberextruder-001	0.0029	352	0.0293	346	0.5338	50	0.0024	338
91 cyberextruder-002	0.0013	349	0.0840	362	0.2672	43	0.0027	344
92 cyberlink-006	0.0000	72	0.0005	131	-	337	0.0000	107
93 cyberlink-007	0.0000	63	0.0003	114	-	364	0.0000	106
94 dahua-005	0.0000	90	0.0000	99	-	62	0.0000	138
95 dahua-006	0.0000	55	0.0000	96	-	308	0.0000	151
96 daon-000	0.0000	309	0.0028	286	-	125	0.0014	329
97 decatur-000	0.0000	244	0.0020	271	-	273	0.0004	286
98 decatur-001	0.0000	186	0.0009	202	-	333	0.0001	185
99 deepglint-003	0.0000	160	0.0004	127	-	239	0.0002	243
100 deepglint-004	0.0000	232	0.0005	132	-	186	0.0002	246
101 deepsea-001	0.0000	53	0.0000	10	0.0000	16	0.0000	64
102 deepsense-000	0.0000	123	0.0006	149	-	154	0.0000	120
103 dermalog-008	0.0000	299	0.0031	289	-	359	0.0006	302
104 dermalog-009	0.0000	298	0.0031	290	-	270	0.0006	303
105 didiglobalface-001	0.0000	207	0.0012	233	0.2175	39	0.0000	160
106 digitalbarriers-002	0.0001	328	0.0045	312	-	205	0.0028	346
107 dps-000	0.0000	113	0.0000	72	-	96	0.0000	51
108 dsk-000	0.0000	44	0.0000	12	0.0000	18	0.0000	59
109 einetworks-000	0.0000	303	0.0017	263	-	319	0.0002	239
110 ekin-002	0.0000	155	0.0000	100	-	177	0.0000	105
111 enface-000	0.0000	64	0.0012	239	-	362	0.0000	145
112 eocortex-000	0.0095	360	0.0602	359	-	164	0.0094	359
113 ercacat-001	0.0000	116	0.0005	133	-	106	0.0000	143
114 expasoft-001	0.0000	140	0.0000	52	-	187	0.0000	19
115 expasoft-002	0.0000	145	0.0000	58	-	195	0.0000	13
116 f8-001	0.0003	341	0.0059	326	0.2026	38	0.0035	350
						0.0030	357	0.0087
								296

Table 26: FTE is the proportion of failed template generation attempts. Failures can occur because the software throws an exception, or because the software electively refuses to process the input image. This would typically occur if a face is not detected. FTE is measured as the number of function calls that give EITHER a non-zero error code OR that give a “small” template. This is defined as one whose size is less than 0.3 times the median template size for that algorithm. This second rule is needed because some algorithms incorrectly fail to return a non-zero error code when template generation fails.

¹ The effects of FTE are included in the accuracy results of this report by regarding any template comparison involving a failed template to produce a low similarity score. Thus higher FTE results in higher FNMR and lower FMR.

	Algorithm	Failure to Enrol Rate ¹											
		APPLICATION	BORDER	CHILD-EXPLOIT	MUGSHOT	VISA	WILD	SEC. 2.2	SEC. 2.3	SEC. ??	SEC. 2.4	SEC. 2.1	SEC. 2.5
117	facesoft-000	0.0000	84	0.0000	89	0.0000	5	0.0000	31	0.0000	80	0.0000	18
118	facetag-000	0.0000	35	0.0000	22	-	257	0.0000	97	0.0000	45	0.0000	44
119	facetag-001	0.0000	20	0.0000	37	-	224	0.0000	81	0.0000	31	0.0000	51
120	facex-001	0.0001	335	0.0360	353	-	345	0.0047	355	0.0027	352	0.1109	353
121	facex-002	0.0001	334	0.0360	354	-	317	0.0047	354	0.0027	351	0.1109	352
122	farfaces-001	0.0000	302	0.0007	159	-	67	0.0003	266	0.0003	133	0.0006	216
123	fiberhome-nanjing-003	0.0000	73	0.0004	125	-	336	0.0000	72	0.0003	122	0.0001	90
124	fiberhome-nanjing-004	0.0000	120	0.0004	126	-	153	0.0000	5	0.0003	123	0.0001	89
125	fincore-000	0.0000	231	0.0008	189	-	189	0.0001	167	0.0004	228	0.0006	209
126	fujitsulab-002	0.0000	69	0.0009	196	-	365	0.0001	210	0.0003	121	0.0003	123
127	fujitsulab-003	0.0000	71	0.0008	178	-	338	0.0001	199	0.0001	105	0.0003	119
128	geo-002	0.0000	233	0.0015	253	-	204	0.0001	164	0.0004	251	0.0017	254
129	geo-003	0.0000	222	0.0010	212	-	157	0.0000	113	0.0004	247	0.0013	249
130	glory-002	0.0003	339	0.0045	311	-	128	0.0015	331	0.0011	329	0.0557	339
131	glory-003	0.0000	262	0.0027	283	-	265	0.0004	279	0.0005	272	0.0244	321
132	gorilla-007	0.0000	204	0.0009	207	-	346	0.0001	187	0.0004	222	0.0004	168
133	gorilla-008	0.0000	240	0.0009	208	-	182	0.0001	183	0.0004	229	0.0004	167
134	griaule-000	0.0000	310	0.0026	281	-	274	0.0004	289	0.0010	319	0.0023	263
135	hertasecurity-000	0.0133	363	0.0077	334	-	209	0.0025	341	0.0243	366	0.0171	312
136	hik-001	0.0000	1	0.0000	103	-	243	0.0000	80	0.0000	24	0.0000	63
137	hisign-001	0.0000	28	0.0000	30	-	295	0.0000	92	0.0000	38	0.0000	48
138	hyperverge-001	0.0000	317	0.0072	330	-	316	0.0015	333	0.0014	338	0.0042	274
139	hyperverge-002	0.0000	99	0.0008	177	-	69	0.0002	251	0.0004	184	0.0004	184
140	icm-002	0.0000	81	0.0001	106	-	71	0.0000	32	0.0000	99	0.0000	85
141	icm-003	0.0000	82	0.0001	105	-	76	0.0000	34	0.0000	100	0.0000	84
142	icthtc-000	0.0001	333	0.0047	318	-	100	0.0028	347	0.0029	354	0.0086	295
143	id3-006	0.0000	268	0.0009	206	-	103	0.0004	282	0.0005	290	0.0008	227
144	id3-008	0.0000	97	0.0006	147	-	68	0.0001	217	0.0004	158	0.0003	117
145	idemia-007	0.0000	34	0.0004	128	-	263	0.0000	117	0.0003	145	0.0003	128
146	idemia-008	0.0000	143	0.0004	129	-	207	0.0000	115	0.0003	147	0.0003	127
147	iit-002	0.0000	308	0.0021	276	-	342	0.0009	320	0.0005	300	0.0443	334
148	iit-003	0.0000	198	0.0008	188	-	334	0.0000	135	0.0004	161	0.0069	288
149	imagus-002	0.0000	266	0.0018	265	-	354	0.0000	144	0.0004	213	0.0296	325
150	imagus-004	0.0000	130	0.0000	60	-	134	0.0000	10	0.0000	56	0.0000	37
151	imperial-000	0.0000	83	0.0000	90	-	75	0.0000	33	0.0000	79	0.0000	19
152	imperial-002	0.0000	142	0.0000	59	0.0000	11	0.0000	18	0.0000	59	0.0000	31
153	incode-009	0.0000	252	0.0009	200	-	64	0.0002	231	0.0004	180	0.0007	223
154	incode-010	0.0000	243	0.0009	199	-	261	0.0002	234	0.0004	178	0.0007	224
155	innefublabs-000	0.0000	197	0.0024	278	-	339	0.0003	267	0.0005	285	0.0004	172
156	innovativetechnologyltd-001	0.0001	332	0.0050	319	-	66	0.0024	340	0.0025	349	0.0055	282
157	innovativetechnologyltd-002	0.0000	271	0.0046	314	-	140	0.0057	358	0.0005	289	0.0247	323
158	innovatrics-006	0.0000	194	0.0009	205	0.0350	25	0.0000	140	0.0004	159	0.0003	147
159	innovatrics-007	0.0000	203	0.0007	168	-	353	0.0001	166	0.0003	132	0.0003	132
160	insightface-000	0.0000	58	0.0000	8	-	299	0.0000	62	0.0000	14	0.0000	69
161	insightface-001	0.0000	36	0.0000	21	-	262	0.0000	98	0.0000	46	0.0000	43
162	intellilcloudai-001	0.0000	136	0.0000	63	-	142	0.0000	7	0.0000	55	0.0001	96
163	intellilcloudai-002	0.0000	80	0.0008	181	-	344	0.0000	134	0.0004	156	0.0012	243
164	intellifusion-001	0.0000	188	0.0005	135	0.0949	33	0.0001	179	0.0003	148	0.0005	200
165	intellifusion-002	0.0000	115	0.0000	101	-	91	0.0000	103	0.0000	98	0.0001	95
166	intellivision-001	0.0042	354	0.0296	347	0.5495	51	0.0048	356	0.0042	358	0.1358	358
167	intellivision-002	0.0000	318	0.0046	313	-	169	0.0012	324	0.0005	304	0.0146	308
168	intelresearch-003	0.0000	190	0.0006	140	-	301	0.0000	124	0.0004	173	0.0003	151
169	intelresearch-004	0.0000	184	0.0006	141	-	318	0.0000	123	0.0004	172	0.0003	138
170	intsysmsu-001	0.0000	61	0.0010	213	-	361	0.0001	196	0.0004	202	0.0004	178
171	intsysmsu-002	0.0000	59	0.0010	214	-	300	0.0001	195	0.0004	201	0.0004	179
172	ionetworks-000	0.0000	112	0.0016	259	-	93	0.0004	276	0.0005	274	0.0004	182
173	iqface-000	0.0000	5	0.0000	42	0.0000	14	0.0000	78	0.0000	27	0.0000	61
174	iqface-003	0.0000	306	0.0076	333	-	158	0.0006	301	0.0005	303	0.0069	287

Table 27: FTE is the proportion of failed template generation attempts. Failures can occur because the software throws an exception, or because the software electively refuses to process the input image. This would typically occur if a face is not detected. FTE is measured as the number of function calls that give EITHER a non-zero error code OR that give a “small” template. This is defined as one whose size is less than 0.3 times the median template size for that algorithm. This second rule is needed because some algorithms incorrectly fail to return a non-zero error code when template generation fails.

¹The effects of FTE are included in the accuracy results of this report by regarding any template comparison involving a failed template to produce a low similarity score. Thus higher FTE results in higher FNMR and lower FMR.

	Algorithm	Failure to Enrol Rate ¹											
		APPLICATION	BORDER	CHILD-EXPLOIT	MUGSHOT	VISA	WILD	SEC. 2.2	SEC. 2.3	SEC. ??	SEC. 2.4	SEC. 2.1	SEC. 2.5
175	irex-000	0.0000	278	0.0009	204	-	89	0.0000	148	0.0005	268	0.0003	144
176	isap-001	0.0000	29	0.0000	29	-	296	0.0000	93	0.0000	37	0.0000	47
177	isap-002	0.0000	14	0.0000	33	-	210	0.0000	86	0.0000	36	0.0000	54
178	isityou-000	0.0068	358	0.0316	350	0.4714	47	0.0023	336	0.0010	322	0.0663	342
179	isystems-001	0.0000	313	0.0035	299	0.1421	35	0.0010	321	0.0007	314	0.0128	303
180	isystems-002	0.0000	312	0.0035	298	0.1421	36	0.0010	322	0.0007	313	0.0128	304
181	itmo-006	0.0000	9	0.0015	254	-	245	0.0004	287	0.0004	205	0.0006	213
182	itmo-007	0.0000	56	0.0009	194	-	302	0.0003	274	0.0000	12	0.0004	166
183	ivacognitive-001	0.0000	247	0.0011	225	-	312	0.0001	173	0.0004	249	0.0011	235
184	iws-000	0.0005	345	0.0650	360	-	120	0.0024	339	0.0012	330	0.0936	348
185	kakao-005	0.0000	76	0.0000	95	-	352	0.0000	70	0.0000	102	0.0000	65
186	kakao-006	0.0000	257	0.0009	201	-	138	0.0000	118	0.0004	194	0.0037	272
187	kakaoPay-001	0.0000	253	0.0013	246	-	115	0.0001	176	0.0004	255	0.0078	292
188	kedacom-000	0.0000	75	0.0000	3	0.0000	21	0.0000	69	0.0000	18	0.0000	66
189	kiwitech-000	0.0000	226	0.0009	193	-	148	0.0004	283	0.0005	271	0.0004	188
190	kneron-003	0.0239	365	0.0306	348	0.4883	49	0.0044	353	0.0016	342	0.1823	362
191	kneron-005	0.0000	314	0.0226	343	-	293	0.0006	300	0.0005	280	0.0097	299
192	kookmin-002	0.0000	8	0.0000	45	-	250	0.0000	75	0.0000	23	0.0000	57
193	kookmin-003	0.0000	48	0.0000	19	-	331	0.0000	58	0.0000	4	0.0000	75
194	kuke3d-001	0.0000	151	0.0000	47	-	170	0.0000	26	0.0000	74	0.0000	24
195	lemalabs-001	0.0000	65	0.0005	136	-	357	0.0002	237	0.0004	160	0.0004	162
196	line-000	0.0000	94	0.0000	84	-	59	0.0000	38	0.0000	86	0.0000	87
197	line-001	0.0000	85	0.0000	94	-	82	0.0000	29	0.0000	76	0.0001	98
198	lookman-002	0.0000	124	0.0000	71	-	160	0.0000	1	0.0000	47	0.0000	40
199	lookman-004	0.0000	45	0.0000	17	0.0000	20	0.0000	55	0.0000	2	0.0000	77
200	luxand-000	0.0000	57	0.0000	7	-	303	0.0000	61	0.0000	13	0.0000	70
201	mantra-000	0.0001	322	0.0041	307	-	190	0.0003	265	0.0004	263	0.0037	271
202	maxvision-000	0.0000	153	0.0000	98	-	184	0.0000	23	0.0000	69	0.0000	22
203	megvii-002	0.0000	79	0.0006	142	0.0274	24	0.0054	357	0.0004	165	0.0126	302
204	megvii-003	0.0000	162	0.0010	221	-	249	0.0002	247	0.0004	239	0.0011	242
205	meituian-000	0.0000	122	0.0001	108	-	155	0.0000	114	0.0002	108	0.0001	99
206	meiya-001	0.0000	311	0.0028	287	-	90	0.0004	288	0.0010	323	0.0025	265
207	mendaxiatech-000	0.0000	234	0.0010	209	-	206	0.0002	245	0.0004	235	0.0011	237
208	microfocus-001	0.0001	331	0.0053	322	0.0791	31	0.0008	315	0.0016	341	0.0220	317
209	microfocus-002	0.0001	330	0.0053	323	0.0791	30	0.0008	314	0.0016	340	0.0220	316
210	minivision-000	0.0000	149	0.0000	55	-	201	0.0000	16	0.0000	63	0.0000	26
211	mobai-000	0.0000	284	0.0114	339	-	112	0.0003	269	0.0012	332	0.1242	356
212	mobai-001	0.0000	246	0.0040	303	-	313	0.0001	202	0.0012	331	0.0523	337
213	mobbl-000	0.0116	362	0.0720	361	-	161	0.0119	361	0.0063	361	0.1136	354
214	mobbl-001	0.0000	307	0.0052	321	-	105	0.0002	225	0.0005	293	0.0181	314
215	moreedian-000	0.0000	161	0.0009	192	-	236	0.0004	284	0.0005	270	0.0004	189
216	multimodality-000	0.0000	52	0.0000	11	-	306	0.0000	63	0.0000	10	0.0000	73
217	mvision-001	0.0000	106	0.0000	81	-	132	0.0000	45	0.0000	89	0.0000	7
218	nazhiai-000	0.0000	146	0.0000	54	-	203	0.0000	14	0.0000	62	0.0000	28
219	neosystems-001	0.0000	30	0.0000	97	-	298	0.0013	327	0.9994	370	0.0002	114
220	neosystems-002	0.0000	150	0.0000	48	-	168	0.0000	25	0.0000	72	0.0000	25
221	netbridgeTech-001	0.0000	104	0.0000	83	-	130	0.0000	43	0.0000	88	0.0000	9
222	netbridgeTech-002	0.0000	101	0.0000	76	-	111	0.0000	46	0.0000	93	0.0000	10
223	neurotechnology-011	0.0000	258	0.0013	241	-	199	0.0002	226	0.0003	150	0.0020	260
224	neurotechnology-012	0.0000	297	0.0010	222	-	254	0.0001	212	0.0004	212	0.0005	199
225	nhn-001	0.0000	191	0.0019	268	-	314	0.0001	186	0.0004	256	0.0020	261
226	nhn-002	0.0000	37	0.0004	130	-	260	0.0000	133	0.0003	127	0.0003	121
227	nodeflux-002	0.0000	180	0.0261	344	-	277	0.0008	313	0.0005	288	0.0008	230
228	notiontag-001	0.0000	134	0.0000	65	-	145	0.0027	345	0.0000	52	0.0132	307
229	notiontag-002	0.0000	19	0.0000	38	-	230	0.0000	83	0.0000	29	0.0000	52
230	nsensecorp-002	0.0000	172	0.0009	195	-	222	0.0003	256	0.0011	324	0.0178	313
231	nsensecorp-003	0.0000	77	0.0000	104	-	348	0.0000	125	0.0007	316	0.0150	309
232	ntechlab-010	0.0000	211	0.0005	134	-	58	0.0001	198	0.0004	163	0.0006	206

Table 28: FTE is the proportion of failed template generation attempts. Failures can occur because the software throws an exception, or because the software electively refuses to process the input image. This would typically occur if a face is not detected. FTE is measured as the number of function calls that give EITHER a non-zero error code OR that give a “small” template. This is defined as one whose size is less than 0.3 times the median template size for that algorithm. This second rule is needed because some algorithms incorrectly fail to return a non-zero error code when template generation fails.

¹ The effects of FTE are included in the accuracy results of this report by regarding any template comparison involving a failed template to produce a low similarity score. Thus higher FTE results in higher FNMR and lower FMR.

	Algorithm Name	Failure to Enrol Rate ¹											
		APPLICATION	BORDER	CHILD-EXPLOIT	MUGSHOT	VISA	WILD						
	Name	SEC. 2.2	SEC. 2.3	SEC. ??	SEC. 2.4	SEC. 2.1	SEC. 2.5						
233	ntechlab-011	0.0000	16	0.0003	116	-	227	0.0000	153	0.0004	154	0.0003	142
234	omnigarde-000	0.0000	158	0.0008	174	-	241	0.0000	127	0.0004	206	0.0003	150
235	omnigarde-001	0.0000	179	0.0008	173	-	279	0.0000	129	0.0004	210	0.0003	148
236	openface-001	0.0000	291	0.0104	338	-	146	0.0004	281	0.0006	310	0.0856	345
237	oz-002	0.0000	129	0.0003	117	-	136	0.0000	121	0.0003	136	0.0002	111
238	oz-003	0.0000	40	0.0002	110	-	268	0.0000	108	0.0003	115	0.0002	106
239	papsav1923-001	0.0000	225	0.0007	162	-	137	0.0001	191	0.0002	110	0.0005	194
240	paravision-004	0.0000	276	0.0007	171	0.0570	27	0.0002	236	0.0004	189	0.0008	226
241	paravision-008	0.0000	22	0.0010	210	-	225	0.0001	188	0.0004	157	0.0003	149
242	pensees-001	0.0000	175	0.0000	27	-	291	0.0000	89	0.0000	39	0.0000	46
243	pixelall-005	0.0000	49	0.0000	16	-	326	0.0000	53	0.0000	5	0.0000	74
244	pixelall-006	0.0000	133	0.0000	64	-	144	0.0000	8	0.0000	53	0.0000	34
245	psl-007	0.0000	176	0.0007	151	-	266	0.0000	155	0.0003	142	0.0003	134
246	psl-008	0.0000	216	0.0003	118	-	109	0.0000	109	0.0003	137	0.0002	113
247	ptakuratsatu-000	0.0000	220	0.0007	169	-	99	0.0001	165	0.0003	134	0.0003	130
248	pxl-001	0.0000	319	0.0044	310	-	107	0.0005	293	0.0022	347	0.0323	327
249	pyramid-000	0.0001	327	0.0041	306	-	267	0.0005	292	0.0007	315	0.0015	251
250	qnap-000	0.0000	43	0.0007	170	-	323	0.0002	232	0.0002	106	0.0003	120
251	quantasoft-003	0.0000	280	0.0015	256	-	231	0.0005	291	0.0006	308	0.0088	297
252	rankone-010	0.0000	78	0.0000	2	-	343	0.0000	68	0.0000	19	0.0000	64
253	rankone-011	0.0000	47	0.0000	20	-	329	0.0000	57	0.0000	3	0.0000	76
254	realnetworks-004	0.0000	163	0.0003	115	-	251	0.0000	104	0.0002	113	0.0003	129
255	realnetworks-005	0.0000	229	0.0002	113	-	141	0.0000	100	0.0002	114	0.0003	126
256	regula-000	0.0000	148	0.0000	56	-	202	0.0000	17	0.0000	64	0.0000	27
257	remarkai-001	0.0000	103	0.0000	77	-	110	0.0000	47	0.0000	94	0.0000	88
258	remarkai-003	0.0000	223	0.0007	158	-	165	0.0000	146	0.0004	167	0.0004	173
259	rendip-000	0.0000	267	0.0016	258	-	77	0.0002	230	0.0004	264	0.0013	248
260	revealmedia-005	0.0000	277	0.0007	165	-	114	0.0009	319	0.0004	265	0.0076	291
261	rokid-000	0.0000	26	0.0072	331	-	281	0.0001	190	0.0005	281	0.0354	331
262	rokid-001	0.0000	147	0.0013	244	-	200	0.0000	15	0.0000	65	0.0007	222
263	s1-002	0.0000	260	0.0089	335	-	171	0.0001	207	0.0005	286	0.0571	340
264	s1-003	0.0000	27	0.0002	112	-	282	0.0007	308	0.0003	124	0.0415	333
265	saffe-001	0.0000	114	0.0000	73	0.0000	6	0.0000	52	0.0000	97	0.0000	3
266	saffe-002	0.0000	25	0.0000	25	-	284	0.0000	94	0.0000	42	0.0000	49
267	samsungsds-000	0.0000	269	0.0055	325	-	149	0.0038	351	0.0005	282	0.0925	347
268	samtech-001	0.0001	326	0.0032	291	-	211	0.0004	285	0.0008	317	0.0013	246
269	scanovate-001	0.0208	364	0.2388	364	-	288	0.0024	337	0.0014	337	0.2751	363
270	scanovate-002	0.0000	242	0.0018	266	-	297	0.0000	162	0.0004	259	0.0008	228
271	securifai-001	0.0000	88	0.0000	91	-	80	0.0000	102	0.0000	77	0.0017	255
272	securifai-003	0.0000	2	0.0000	40	-	238	0.0000	76	0.0000	26	0.0005	198
273	sensetime-004	0.0000	221	0.0011	228	-	151	0.0000	99	0.0004	193	0.0003	140
274	sensetime-005	0.0000	51	0.0004	124	-	305	0.0000	132	0.0003	131	0.0002	112
275	sertis-000	0.0000	87	0.0007	164	-	85	0.0000	163	0.0004	179	0.0004	165
276	sertis-002	0.0000	33	0.0007	155	-	264	0.0000	158	0.0004	177	0.0004	161
277	seventhsense-000	0.0000	177	0.0006	150	-	255	0.0001	169	0.0004	211	0.0003	141
278	shaman-000	0.0000	96	0.0000	88	0.0000	3	0.0000	35	0.0000	81	0.0000	13
279	shaman-001	0.0000	92	0.0000	86	0.0000	1	0.0000	37	0.0000	84	0.0000	82
280	shu-002	0.0000	255	0.0010	217	-	156	0.0005	290	0.0004	248	0.0007	220
281	shu-003	0.0000	107	0.0007	154	-	123	0.0001	171	0.0003	130	0.0004	186
282	siat-002	0.0000	189	0.0012	238	0.0616	28	0.0000	142	0.0004	191	0.0048	279
283	siat-004	0.0000	210	0.0011	227	-	55	0.0000	131	0.0004	188	0.0003	136
284	sjtu-003	0.0000	110	0.0005	138	-	129	0.0000	150	0.0003	128	0.0003	139
285	sjtu-004	0.0000	117	0.0000	75	-	101	0.0000	49	0.0003	125	0.0000	2
286	sktelecom-000	0.0000	200	0.0008	183	-	350	0.0000	152	0.0004	214	0.0013	247
287	smartengines-000	0.0066	357	0.0150	341	-	248	0.0022	335	0.0013	335	0.0826	343
288	smilart-002	0.0000	315	0.0036	300	0.2422	42	-	366	0.0011	327	-	368
289	smilart-003	0.0003	340	0.0100	337	-	217	0.0014	328	0.0013	336	0.0555	338
290	sodec-000	0.0000	125	0.0000	68	-	166	0.0000	2	0.0000	48	0.0000	39

Table 29: FTE is the proportion of failed template generation attempts. Failures can occur because the software throws an exception, or because the software electively refuses to process the input image. This would typically occur if a face is not detected. FTE is measured as the number of function calls that give EITHER a non-zero error code OR that give a “small” template. This is defined as one whose size is less than 0.3 times the median template size for that algorithm. This second rule is needed because some algorithms incorrectly fail to return a non-zero error code when template generation fails.

¹ The effects of FTE are included in the accuracy results of this report by regarding any template comparison involving a failed template to produce a low similarity score. Thus higher FTE results in higher FNMR and lower FMR.

	Algorithm	Failure to Enrol Rate ¹						
		APPLICATION	BORDER	CHILD-EXPLOIT	MUGSHOT	VISA	WILD	
Name	SEC. 2.2	SEC. 2.3	SEC. ??	SEC. 2.4	SEC. 2.1	SEC. 2.5		
291	sqisoft-001	0.0000	11	0.0003	122	-	218	0.0000
292	sqisoft-002	0.0000	108	0.0003	121	-	122	0.0000
293	staqu-000	0.0000	156	0.0000	49	-	176	0.0000
294	starhybrid-001	0.0001	329	0.0033	295	0.2340	41	0.0009
295	suprema-000	0.0000	259	0.0017	262	-	172	0.0002
296	suprema-001	0.0000	261	0.0027	282	-	214	0.0003
297	supremaid-001	0.0000	173	0.0020	274	-	289	0.0001
298	synesis-006	0.0000	38	0.0003	123	-	272	0.0000
299	synesis-007	0.0000	182	0.0013	243	-	324	0.0002
300	synology-000	0.0000	7	0.0000	43	-	253	0.0000
301	synology-002	0.0000	13	0.0000	31	-	213	0.0000
302	sztu-000	0.0000	118	0.0000	74	-	102	0.0000
303	sztu-001	0.0000	32	0.0000	26	-	292	0.0000
304	tech5-004	0.0000	230	0.0008	176	-	191	0.0003
305	tech5-005	0.0000	219	0.0007	172	-	88	0.0000
306	techsign-000	0.0007	347	0.0334	351	-	290	0.0020
307	tevian-006	0.0000	119	0.0012	235	-	98	0.0003
308	tevian-007	0.0000	206	0.0015	257	-	74	0.0002
309	tiger-003	0.0000	237	-	368	0.0619	29	0.0001
310	tiger-005	0.0000	214	0.0009	203	-	119	0.0001
311	tinkoff-001	0.0000	249	0.0008	182	-	355	0.0001
312	tongyi-005	0.0000	152	0.0000	46	0.0000	9	0.0000
313	toppanidgate-000	0.0000	199	0.0008	179	-	347	0.0004
314	toshiba-003	0.0000	70	0.0001	107	-	340	0.0001
315	toshiba-004	0.0000	6	0.0000	44	-	252	0.0000
316	trueface-002	0.0000	248	0.0046	316	-	363	0.0003
317	trueface-003	0.0000	250	0.0046	317	-	72	0.0003
318	tuputech-000	0.0003	342	0.0116	340	-	247	-
319	twface-000	0.0000	3	0.0000	39	-	240	0.0000
320	twface-001	0.0000	91	0.0000	87	-	61	0.0000
321	ulsee-001	0.0000	66	0.0000	5	-	369	0.0000
322	ultinous-000	-	369	-	366	0.0007	23	-
323	ultinous-001	-	370	-	369	0.0007	22	-
324	uluface-002	0.0000	141	0.0000	51	0.0000	10	0.0000
325	uluface-003	0.0000	24	0.0001	109	-	285	0.0002
326	upc-001	0.0000	294	0.0003	119	0.0450	26	0.0003
327	vcog-002	-	368	-	367	0.2209	40	-
328	vd-002	0.0000	39	0.0000	24	-	276	0.0000
329	vd-003	0.0001	324	0.0041	305	-	183	0.0030
330	veridas-006	0.0000	290	0.0026	279	-	309	0.0001
331	veridas-007	0.0000	289	0.0026	280	-	307	0.0001
332	verigram-000	0.0000	264	0.0068	328	-	327	0.0003
333	verihubs-inteligensia-000	0.0000	166	0.0029	288	-	246	0.0001
334	via-000	0.0000	54	0.0000	9	0.0000	17	0.0000
335	via-001	0.0000	126	0.0000	70	-	163	0.0000
336	videomo-000	0.0000	254	0.0019	269	-	121	0.0003
337	videonetics-001	0.0004	343	0.0309	349	0.4799	48	0.0015
338	videonetics-002	0.0000	265	0.0459	358	0.4598	46	0.0006
339	viettelhightech-000	0.0000	296	0.0019	270	-	226	0.0007
340	vigilantsolutions-010	0.0000	285	0.0028	285	-	97	0.0001
341	vigilantsolutions-011	0.0000	281	0.0028	284	-	258	0.0001
342	vinai-000	0.0000	105	0.0000	82	-	131	0.0000
343	vion-000	0.0050	355	0.0392	357	0.6388	52	0.0130
344	visage-000	0.0000	300	0.0054	324	-	180	0.0009
345	visionbox-001	0.0000	316	0.0033	294	-	221	0.0005
346	visionbox-002	0.0000	128	0.0017	260	-	135	0.0000
347	visionlabs-010	0.0000	272	0.0009	197	-	235	0.0001
348	visionlabs-011	0.0000	18	0.0006	145	-	229	0.0001

Table 30: FTE is the proportion of failed template generation attempts. Failures can occur because the software throws an exception, or because the software electively refuses to process the input image. This would typically occur if a face is not detected. FTE is measured as the number of function calls that give EITHER a non-zero error code OR that give a “small” template. This is defined as one whose size is less than 0.3 times the median template size for that algorithm. This second rule is needed because some algorithms incorrectly fail to return a non-zero error code when template generation fails.

¹The effects of FTE are included in the accuracy results of this report by regarding any template comparison involving a failed template to produce a low similarity score. Thus higher FTE results in higher FNMR and lower FMR.

	Algorithm	Failure to Enrol Rate ¹											
		Name	APPLICATION	BORDER	CHILD-EXPLOIT	MUGSHOT	VISA	WILD	SEC. 2.2	SEC. 2.3	SEC. ??	SEC. 2.4	SEC. 2.1
349	visteam-001	0.0000	274	0.0014	249	-	294	0.0002	233	0.0004	217	0.0011	239
350	visteam-002	0.0000	273	0.0014	250	-	220	0.0002	229	0.0004	216	0.0011	238
351	vnpt-001	0.0652	367	0.2829	365	-	286	0.2116	365	0.1598	369	0.3544	365
352	vnpt-002	0.0000	193	0.0002	111	-	358	0.0003	271	0.0003	117	0.0001	100
353	vocord-008	0.0000	201	0.0015	255	-	349	0.0003	272	0.0001	103	0.0007	221
354	vocord-009	0.0000	169	0.0006	144	-	219	0.0001	220	0.0003	118	0.0003	122
355	vts-000	0.0000	263	0.0011	224	-	259	0.0001	221	0.0004	261	0.0013	244
356	winsense-001	0.0000	21	0.0000	36	0.0000	13	0.0000	82	0.0000	30	0.0000	50
357	winsense-002	0.0000	121	0.0000	67	-	152	0.0000	6	0.0000	51	0.0000	41
358	wuhantianyu-001	0.0000	62	0.0007	156	-	360	0.0001	168	0.0004	203	0.0002	110
359	x-laboratory-000	0.0247	366	0.0000	14	0.0000	19	0.0005	297	0.0002	109	0.0000	80
360	x-laboratory-001	0.0000	196	0.0012	236	-	366	0.0001	208	0.0004	246	0.0007	217
361	xforwardai-001	0.0000	212	0.0007	167	-	57	0.0003	260	0.0004	244	0.0004	154
362	xforwardai-002	0.0000	181	0.0007	166	-	320	0.0003	261	0.0004	238	0.0004	157
363	xm-000	0.0000	137	0.0007	153	-	192	0.0001	170	0.0003	129	0.0004	187
364	yisheng-004	0.0002	337	-	370	0.4279	45	0.0013	326	0.0006	309	0.0321	326
365	yitu-003	0.0000	67	0.0000	6	-	367	0.0009	317	0.0000	16	0.0000	68
366	yoonik-001	0.0000	93	0.0014	252	-	53	0.0001	218	0.0004	243	0.0017	256
367	yoonik-002	0.0000	256	0.0010	215	-	150	0.0003	252	0.0006	305	0.0005	197
368	ytu-000	0.0000	168	0.0010	220	-	216	0.0002	248	0.0004	241	0.0011	241
369	yuan-002	0.0000	292	0.0010	219	-	188	0.0005	294	0.0005	284	0.0005	201
370	yuan-003	0.0000	288	0.0010	218	-	275	0.0005	296	0.0005	283	0.0005	202

Table 31: FTE is the proportion of failed template generation attempts. Failures can occur because the software throws an exception, or because the software electively refuses to process the input image. This would typically occur if a face is not detected. FTE is measured as the number of function calls that give EITHER a non-zero error code OR that give a “small” template. This is defined as one whose size is less than 0.3 times the median template size for that algorithm. This second rule is needed because some algorithms incorrectly fail to return a non-zero error code when template generation fails.

¹ The effects of FTE are included in the accuracy results of this report by regarding any template comparison involving a failed template to produce a low similarity score. Thus higher FTE results in higher FNMR and lower FMR.

3.4 Recognition accuracy

Core algorithm accuracy is stated via:

▷ **Cooperative subjects**

- The summary table of Figure 24;
- The visa image DETs of Figure 56;
- The mugshot DETs of Figure 75;
- The mugshot ageing profiles of Figure 270;
- The human-difficult pairs of Figure 19

▷ **Non-cooperative subjects**

- The photojournalism DET of Figure 91

Figure 216 shows dependence of false match rate on algorithm score threshold. This allows a deployer to set a threshold to target a particular false match rate appropriate to the security objectives of the application.

Figure 179 likewise shows FMR(T) but for mugshots, and specially four subsets of the population.

Note that in both the mugshot and visa sets false match rates vary with the ethnicity, age, and sex, of the enrollee and impostor. For example figure 110 summarizes FMR for impostors paired from four groups black females, black males, white females, white males.

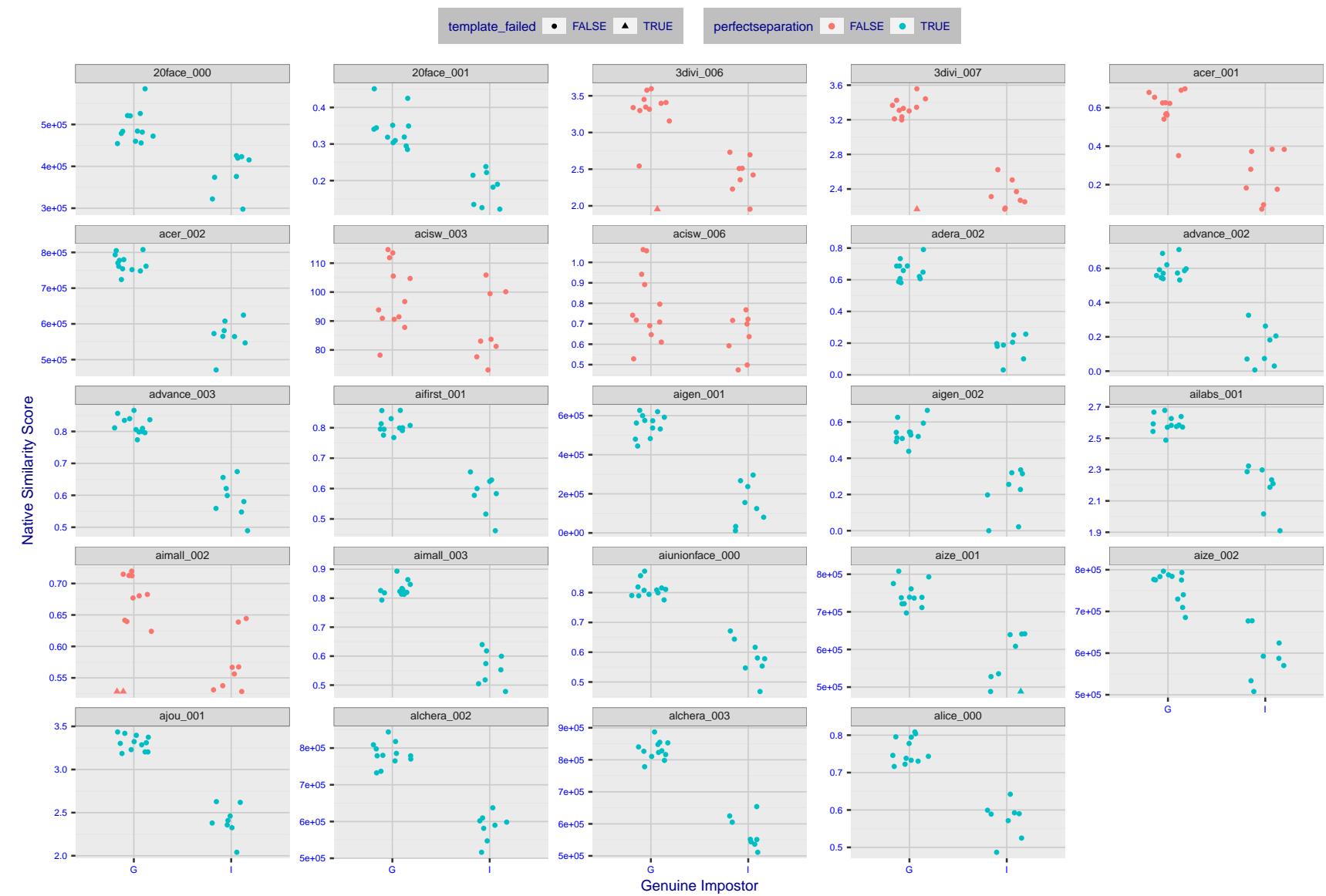


Figure 4: The Figure shows, in blue, algorithms that correctly separate the 12 genuine and 8 impostor pairs used in the May 2018 paper [Face recognition accuracy of forensic examiners, superrecognizers, and face recognition algorithms](#) (Phillips et al. [1]). In red are algorithms that are imperfect. Some algorithms fail only because they failed to make a template e.g. due to face detection failure (shown as a triangle). Others fail because the pairs were selected for that study because they had been difficult for three leading algorithms used in FRVT 2006. Caution: Given the small sample size ($n=20$) the figure may change substantially if larger or different sets were used. The images can be downloaded from the [Supplemental Information](#) page provided with that publication.



Figure 5: The Figure shows, in blue, algorithms that correctly separate the 12 genuine and 8 impostor pairs used in the May 2018 paper Face recognition accuracy of forensic examiners, superrecognizers, and face recognition algorithms (Phillips et al. [1]). In red are algorithms that are imperfect. Some algorithms fail only because they failed to make a template e.g. due to face detection failure (shown as a triangle). Others fail because the pairs were selected for that study because they had been difficult for three leading algorithms used in FRVT 2006. Caution: Given the small sample size ($n=20$) the figure may change substantially if larger or different sets were used. The images can be downloaded from the [Supplemental Information](#) page provided with that publication.

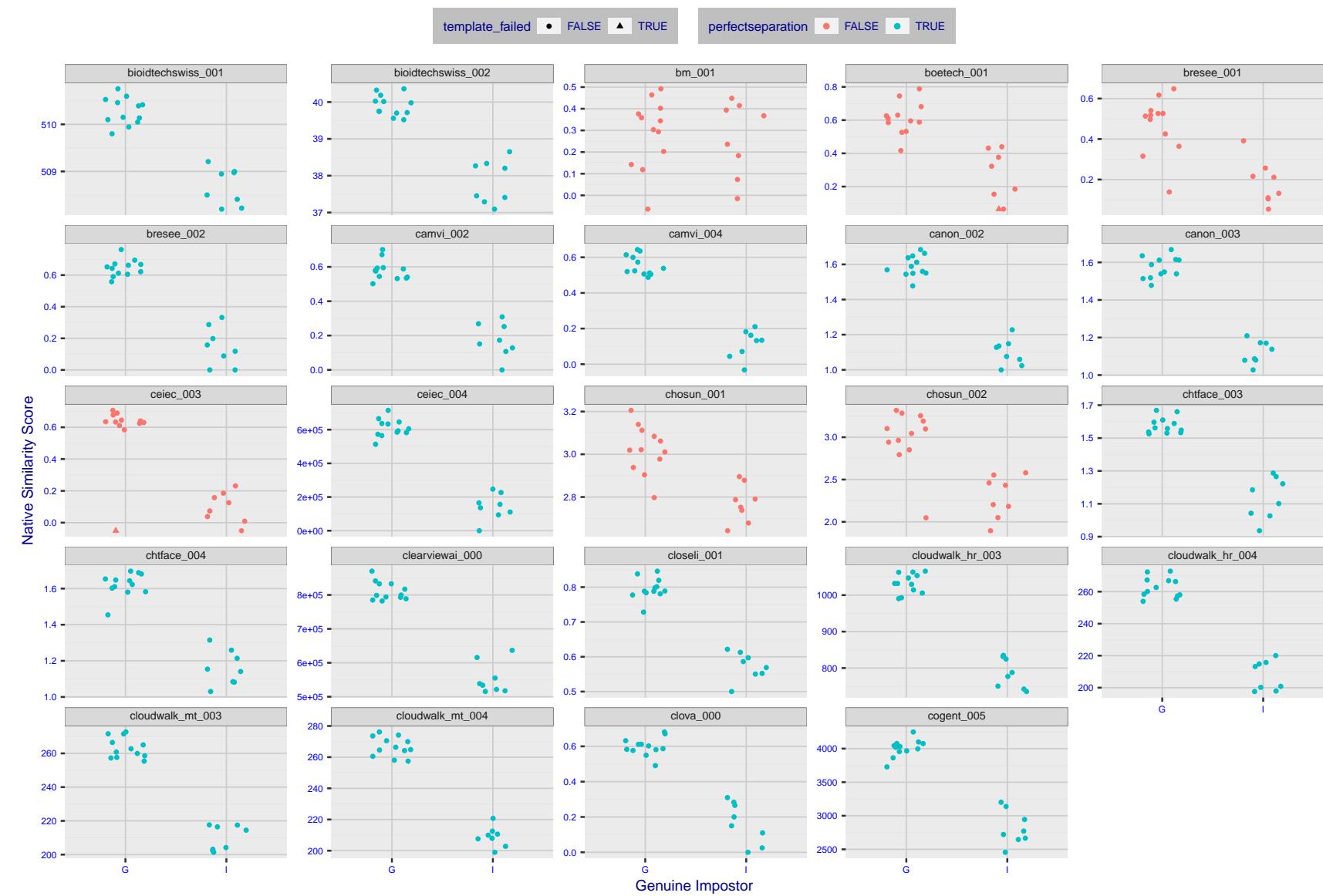


Figure 6: The Figure shows, in blue, algorithms that correctly separate the 12 genuine and 8 impostor pairs used in the May 2018 paper [Face recognition accuracy of forensic examiners, superrecognizers, and face recognition algorithms](#) (Phillips et al. [1]). In red are algorithms that imperfect. Some algorithms fail only because they failed to make a template e.g. due to face detection failure (shown as a triangle). Others fail because the pairs were selected for that study because they had been difficult for three leading algorithms used in FRVT 2006. Caution: Given the small sample size ($n=20$) the figure may change substantially if larger or different sets were used. The images can be downloaded from the [Supplemental Information](#) page provided with that publication.

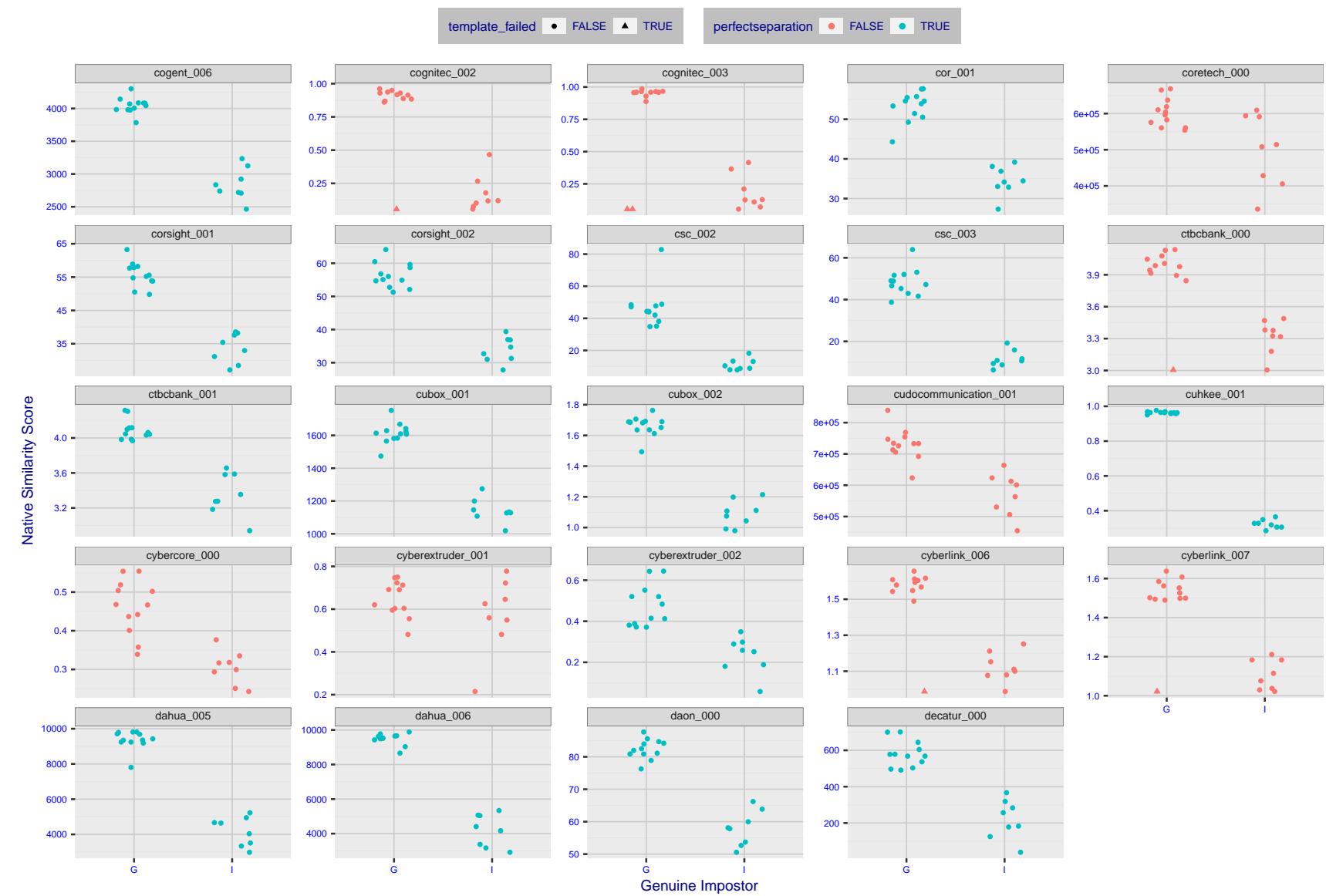


Figure 7: The Figure shows, in blue, algorithms that correctly separate the 12 genuine and 8 impostor pairs used in the May 2018 paper [Face recognition accuracy of forensic examiners, superrecognizers, and face recognition algorithms](#) (Phillips et al. [1]). In red are algorithms that are imperfect. Some algorithms fail only because they failed to make a template e.g. due to face detection failure (shown as a triangle). Others fail because the pairs were selected for that study because they had been difficult for three leading algorithms used in FRVT 2006. Caution: Given the small sample size ($n=20$) the figure may change substantially if larger or different sets were used. The images can be downloaded from the [Supplemental Information](#) page provided with that publication.

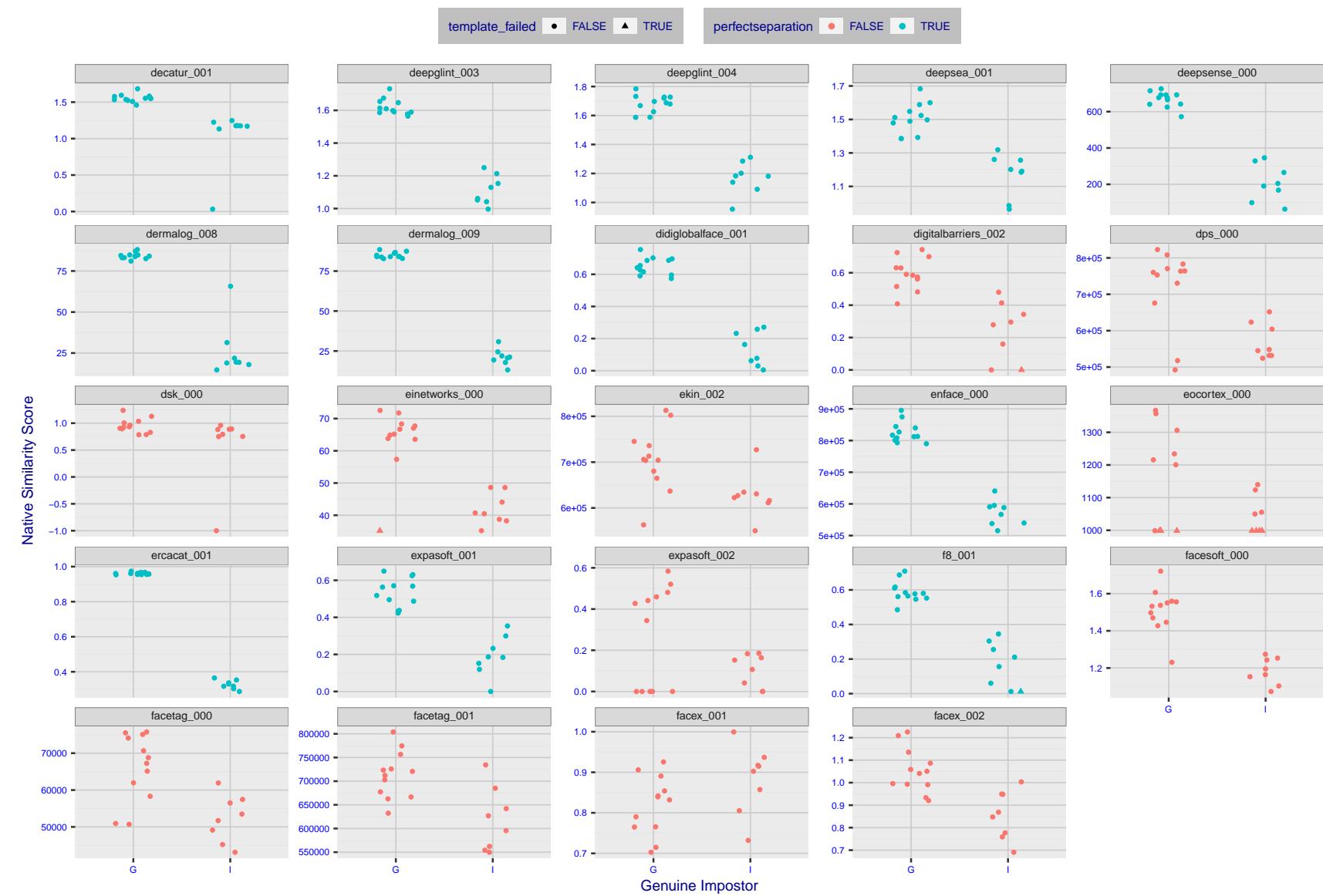


Figure 8: The Figure shows, in blue, algorithms that correctly separate the 12 genuine and 8 impostor pairs used in the May 2018 paper [Face recognition accuracy of forensic examiners, superrecognizers, and face recognition algorithms](#) (Phillips et al. [1]). In red are algorithms that are imperfect. Some algorithms fail only because they failed to make a template e.g. due to face detection failure (shown as a triangle). Others fail because the pairs were selected for that study because they had been difficult for three leading algorithms used in FRVT 2006. Caution: Given the small sample size ($n=20$) the figure may change substantially if larger or different sets were used. The images can be downloaded from the [Supplemental Information](#) page provided with that publication.



Figure 9: The Figure shows, in blue, algorithms that correctly separate the 12 genuine and 8 impostor pairs used in the May 2018 paper Face recognition accuracy of forensic examiners, superrecognizers, and face recognition algorithms (Phillips et al. [1]). In red are algorithms that are imperfect. Some algorithms fail only because they failed to make a template e.g. due to face detection failure (shown as a triangle). Others fail because the pairs were selected for that study because they had been difficult for three leading algorithms used in FRVT 2006. Caution: Given the small sample size ($n=20$) the figure may change substantially if larger or different sets were used. The images can be downloaded from the [Supplemental Information](#) page provided with that publication.

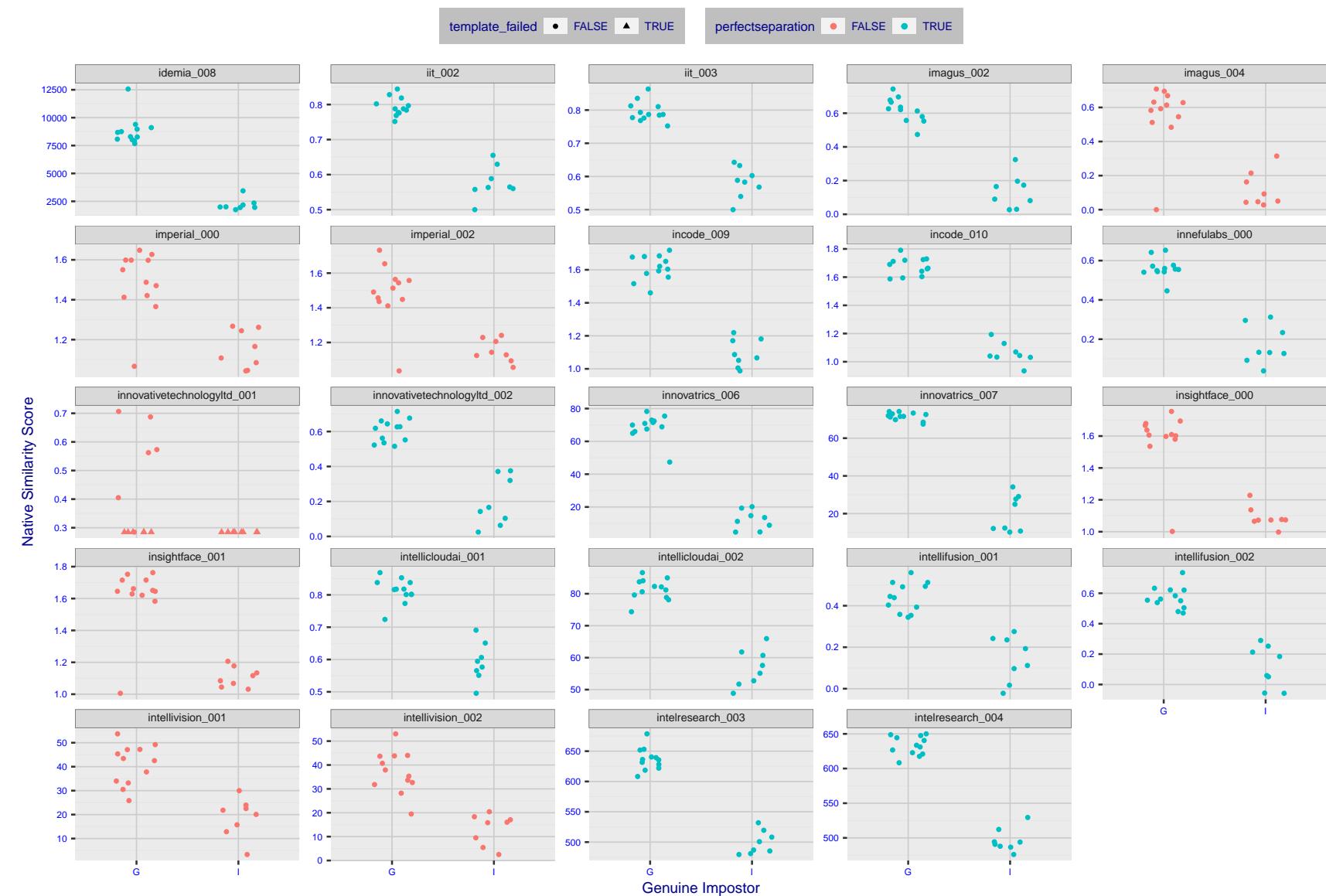


Figure 10: The Figure shows, in blue, algorithms that correctly separate the 12 genuine and 8 impostor pairs used in the May 2018 paper [Face recognition accuracy of forensic examiners, superrecognizers, and face recognition algorithms](#) (Phillips et al. [1]). In red are algorithms that are imperfect. Some algorithms fail only because they failed to make a template e.g. due to face detection failure (shown as a triangle). Others fail because the pairs were selected for that study because they had been difficult for three leading algorithms used in FRVT 2006. Caution: Given the small sample size ($n=20$) the figure may change substantially if larger or different sets were used. The images can be downloaded from the [Supplemental Information](#) page provided with that publication.

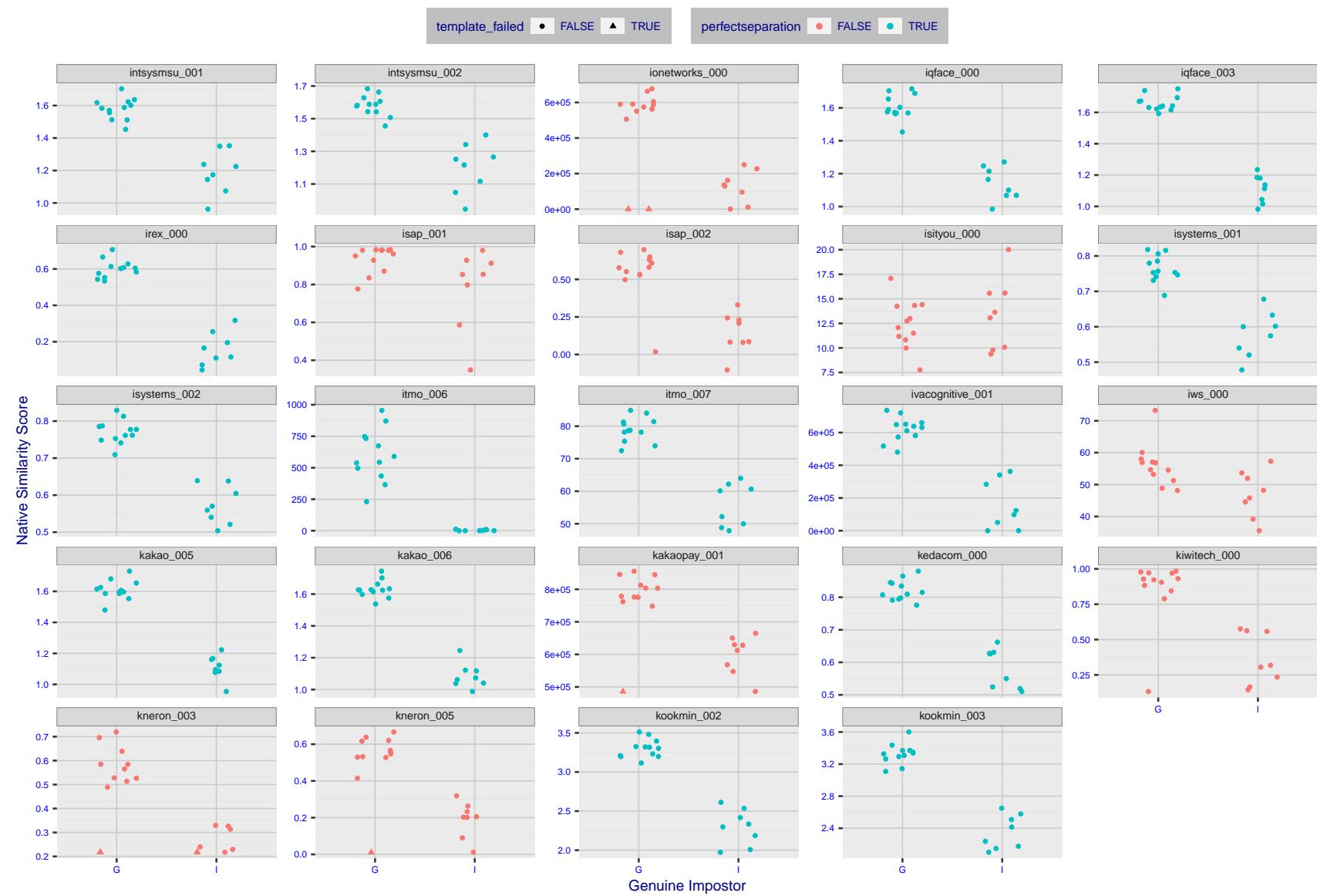


Figure 11: The Figure shows, in blue, algorithms that correctly separate the 12 genuine and 8 impostor pairs used in the May 2018 paper Face recognition accuracy of forensic examiners, superrecognizers, and face recognition algorithms (Phillips et al. [1]). In red are algorithms that are imperfect. Some algorithms fail only because they failed to make a template e.g. due to face detection failure (shown as a triangle). Others fail because the pairs were selected for that study because they had been difficult for three leading algorithms used in FRVT 2006. Caution: Given the small sample size ($n=20$) the figure may change substantially if larger or different sets were used. The images can be downloaded from the [Supplemental Information](#) page provided with that publication.

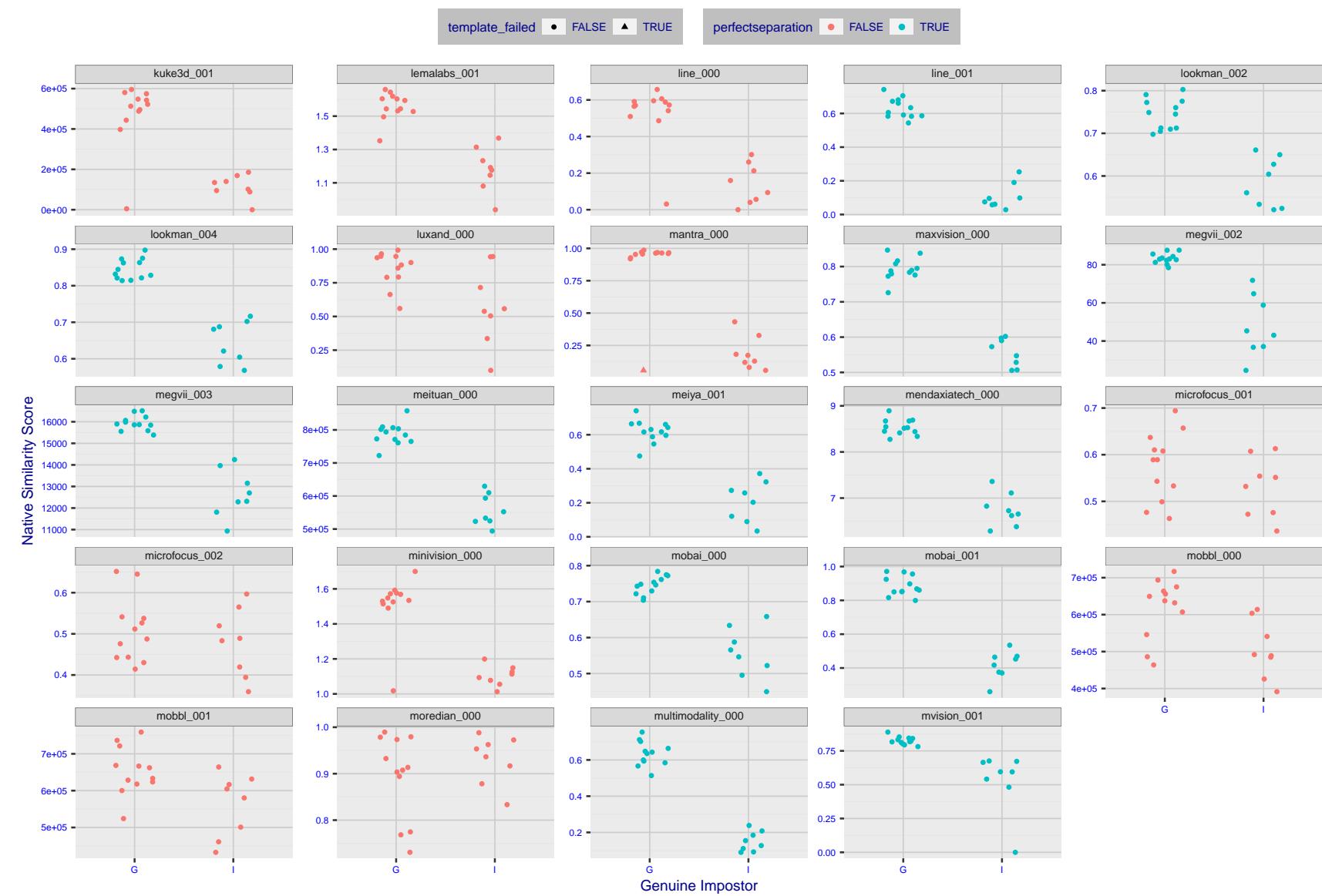


Figure 12: The Figure shows, in blue, algorithms that correctly separate the 12 genuine and 8 impostor pairs used in the May 2018 paper [Face recognition accuracy of forensic examiners, superrecognizers, and face recognition algorithms](#) (Phillips et al. [1]). In red are algorithms that are imperfect. Some algorithms fail only because they failed to make a template e.g. due to face detection failure (shown as a triangle). Others fail because the pairs were selected for that study because they had been difficult for three leading algorithms used in FRVT 2006. Caution: Given the small sample size ($n=20$) the figure may change substantially if larger or different sets were used. The images can be downloaded from the [Supplemental Information](#) page provided with that publication.

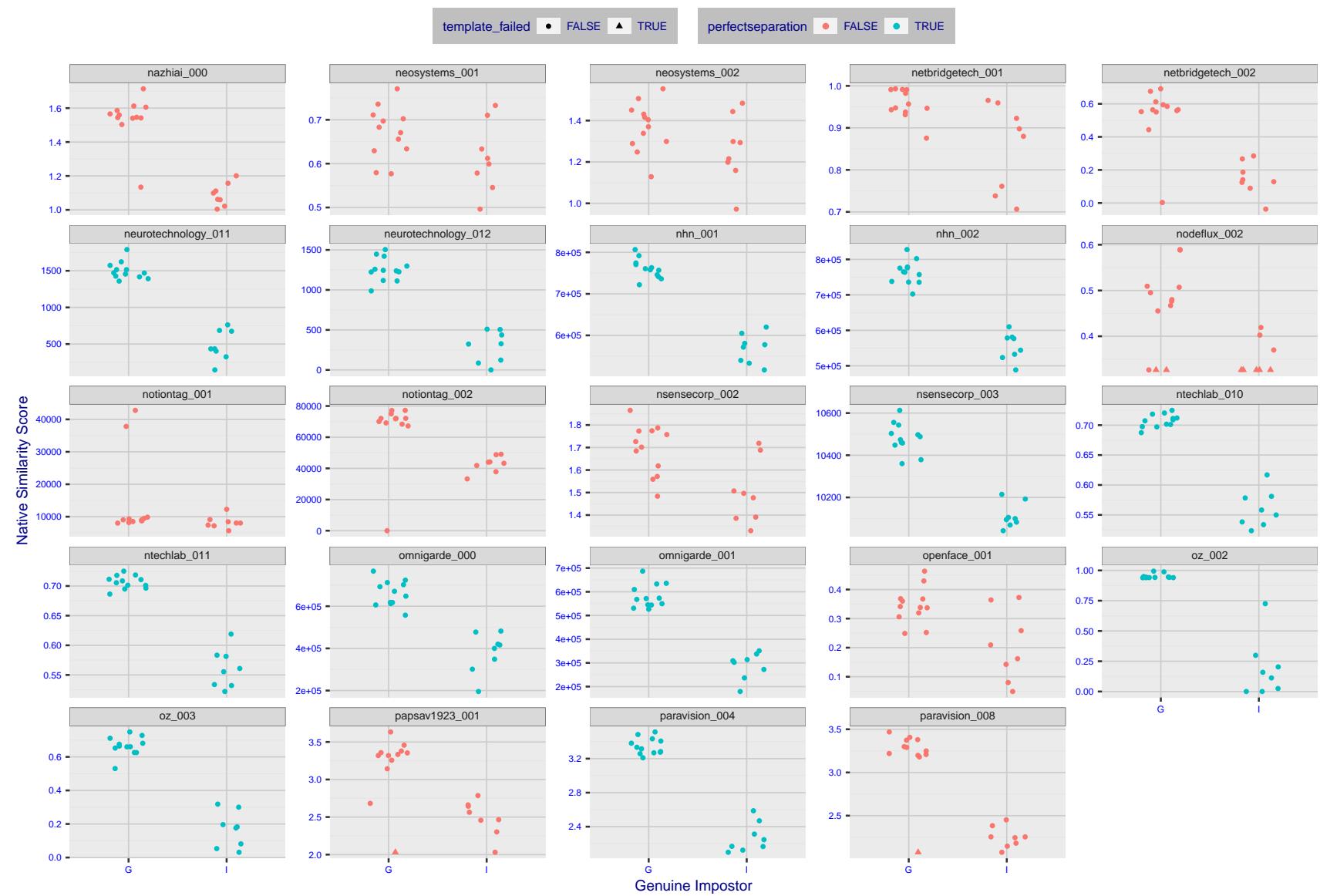


Figure 13: The Figure shows, in blue, algorithms that correctly separate the 12 genuine and 8 impostor pairs used in the May 2018 paper [Face recognition accuracy of forensic examiners, superrecognizers, and face recognition algorithms](#) (Phillips et al. [1]). In red are algorithms that are imperfect. Some algorithms fail only because they failed to make a template e.g. due to face detection failure (shown as a triangle). Others fail because the pairs were selected for that study because they had been difficult for three leading algorithms used in FRVT 2006. Caution: Given the small sample size ($n=20$) the figure may change substantially if larger or different sets were used. The images can be downloaded from the [Supplemental Information](#) page provided with that publication.

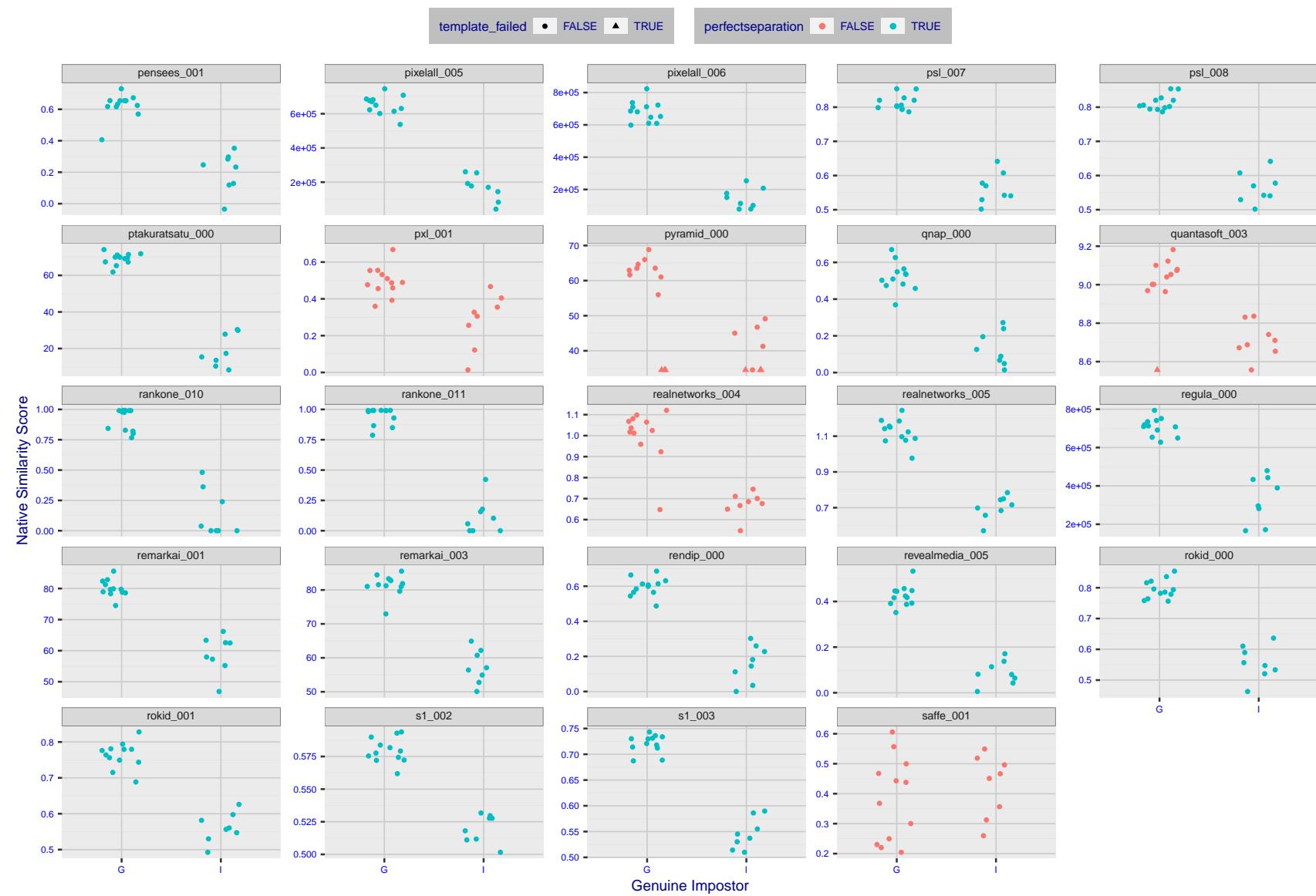


Figure 14: The Figure shows, in blue, algorithms that correctly separate the 12 genuine and 8 impostor pairs used in the May 2018 paper Face recognition accuracy of forensic examiners, superrecognizers, and face recognition algorithms (Phillips et al. [1]). In red are algorithms that are imperfect. Some algorithms fail only because they failed to make a template e.g. due to face detection failure (shown as a triangle). Others fail because the pairs were selected for that study because they had been difficult for three leading algorithms used in FRVT 2006. Caution: Given the small sample size ($n=20$) the figure may change substantially if larger or different sets were used. The images can be downloaded from the [Supplemental Information](#) page provided with that publication.

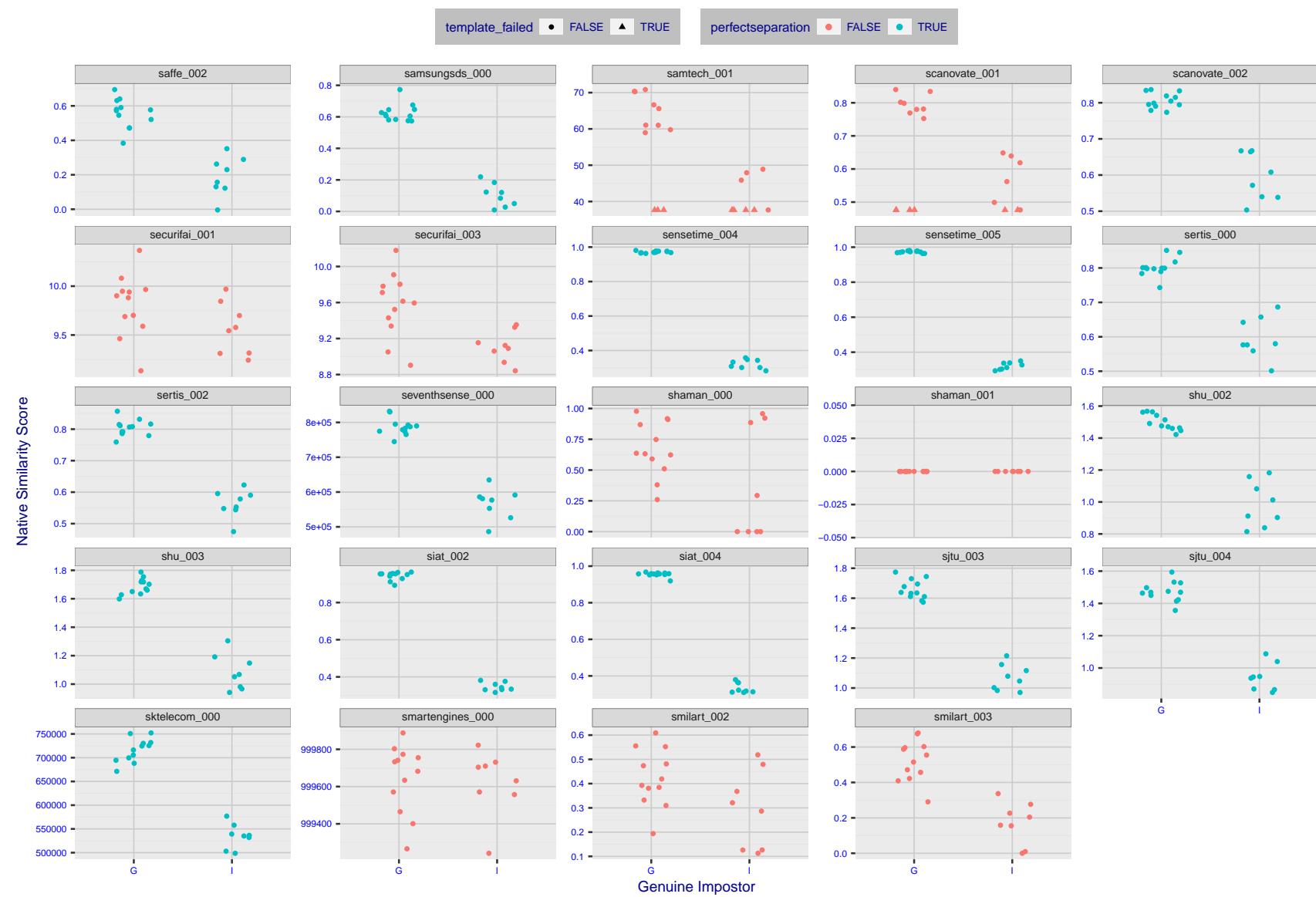


Figure 15: The Figure shows, in blue, algorithms that correctly separate the 12 genuine and 8 impostor pairs used in the May 2018 paper Face recognition accuracy of forensic examiners, superrecognizers, and face recognition algorithms (Phillips et al. [1]). In red are algorithms that are imperfect. Some algorithms fail only because they failed to make a template e.g. due to face detection failure (shown as a triangle). Others fail because the pairs were selected for that study because they had been difficult for three leading algorithms used in FRVT 2006. Caution: Given the small sample size ($n=20$) the figure may change substantially if larger or different sets were used. The images can be downloaded from the [Supplemental Information](#) page provided with that publication.

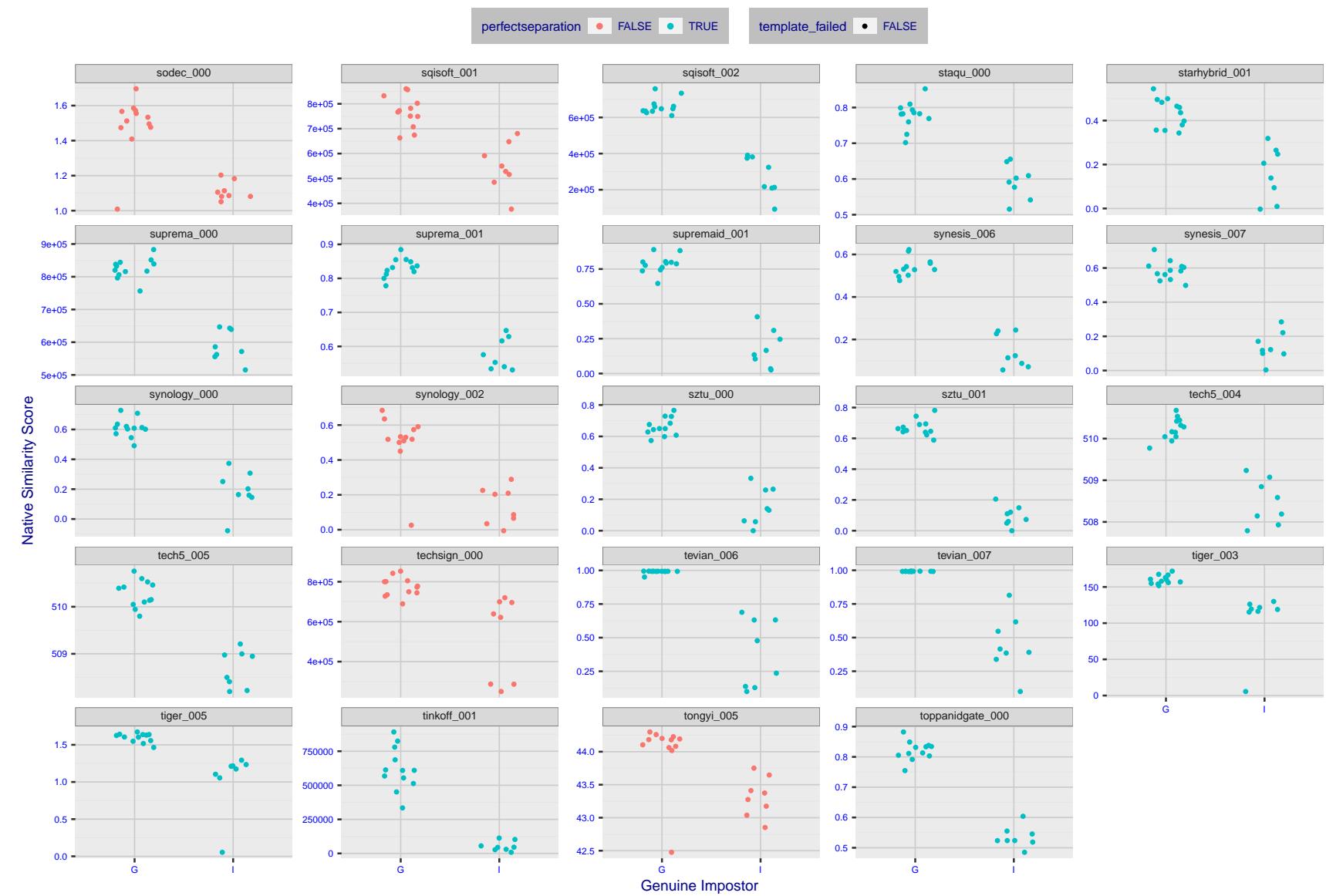


Figure 16: The Figure shows, in blue, algorithms that correctly separate the 12 genuine and 8 impostor pairs used in the May 2018 paper Face recognition accuracy of forensic examiners, superrecognizers, and face recognition algorithms (Phillips et al. [1]). In red are algorithms that are imperfect. Some algorithms fail only because they failed to make a template e.g. due to face detection failure (shown as a triangle). Others fail because the pairs were selected for that study because they had been difficult for three leading algorithms used in FRVT 2006. Caution: Given the small sample size ($n=20$) the figure may change substantially if larger or different sets were used. The images can be downloaded from the [Supplemental Information](#) page provided with that publication.

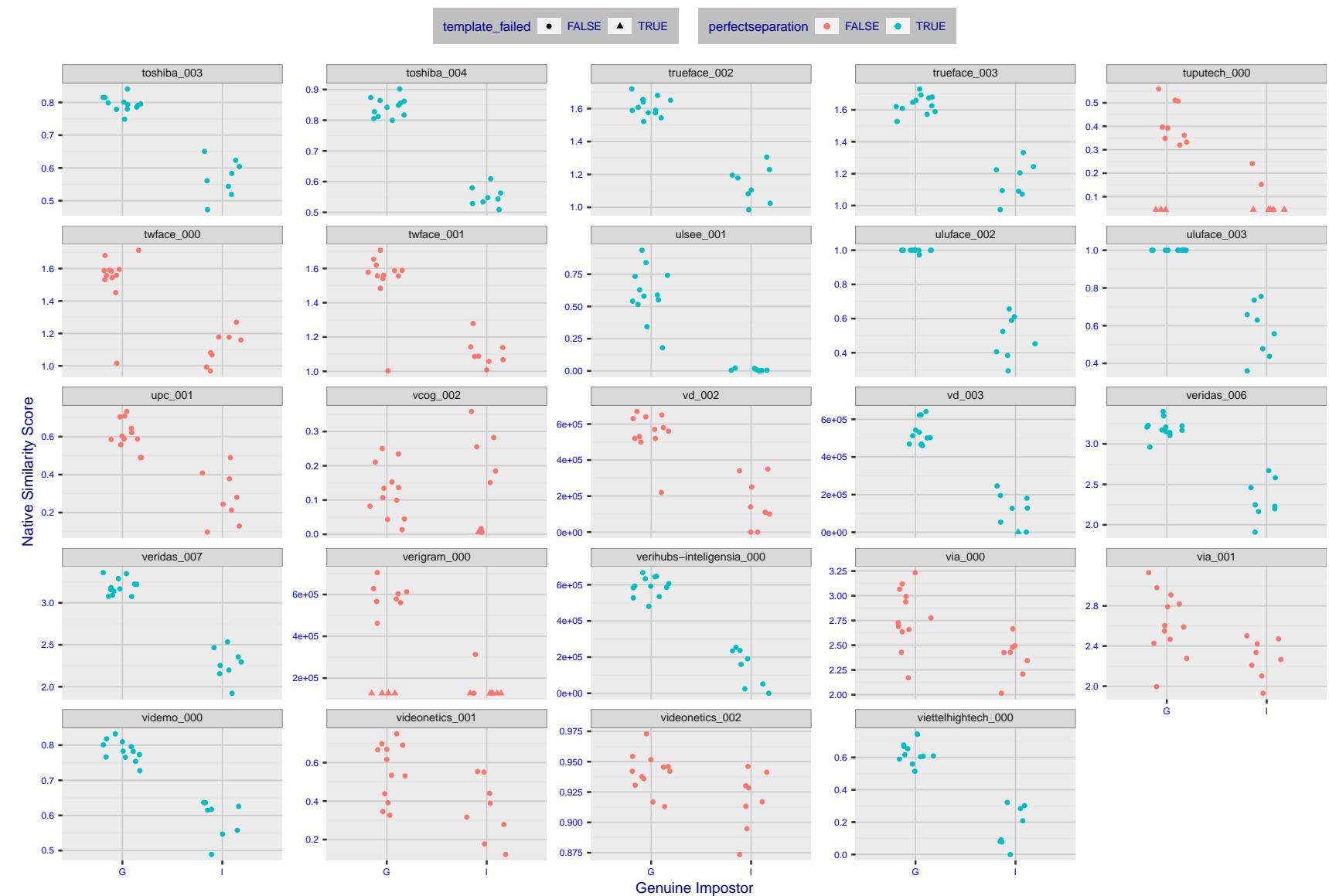


Figure 17: The Figure shows, in blue, algorithms that correctly separate the 12 genuine and 8 impostor pairs used in the May 2018 paper [Face recognition accuracy of forensic examiners, superrecognizers, and face recognition algorithms](#) (Phillips et al. [1]). In red are algorithms that are imperfect. Some algorithms fail only because they failed to make a template e.g. due to face detection failure (shown as a triangle). Others fail because the pairs were selected for that study because they had been difficult for three leading algorithms used in FRVT 2006. Caution: Given the small sample size ($n=20$) the figure may change substantially if larger or different sets were used. The images can be downloaded from the [Supplemental Information](#) page provided with that publication.

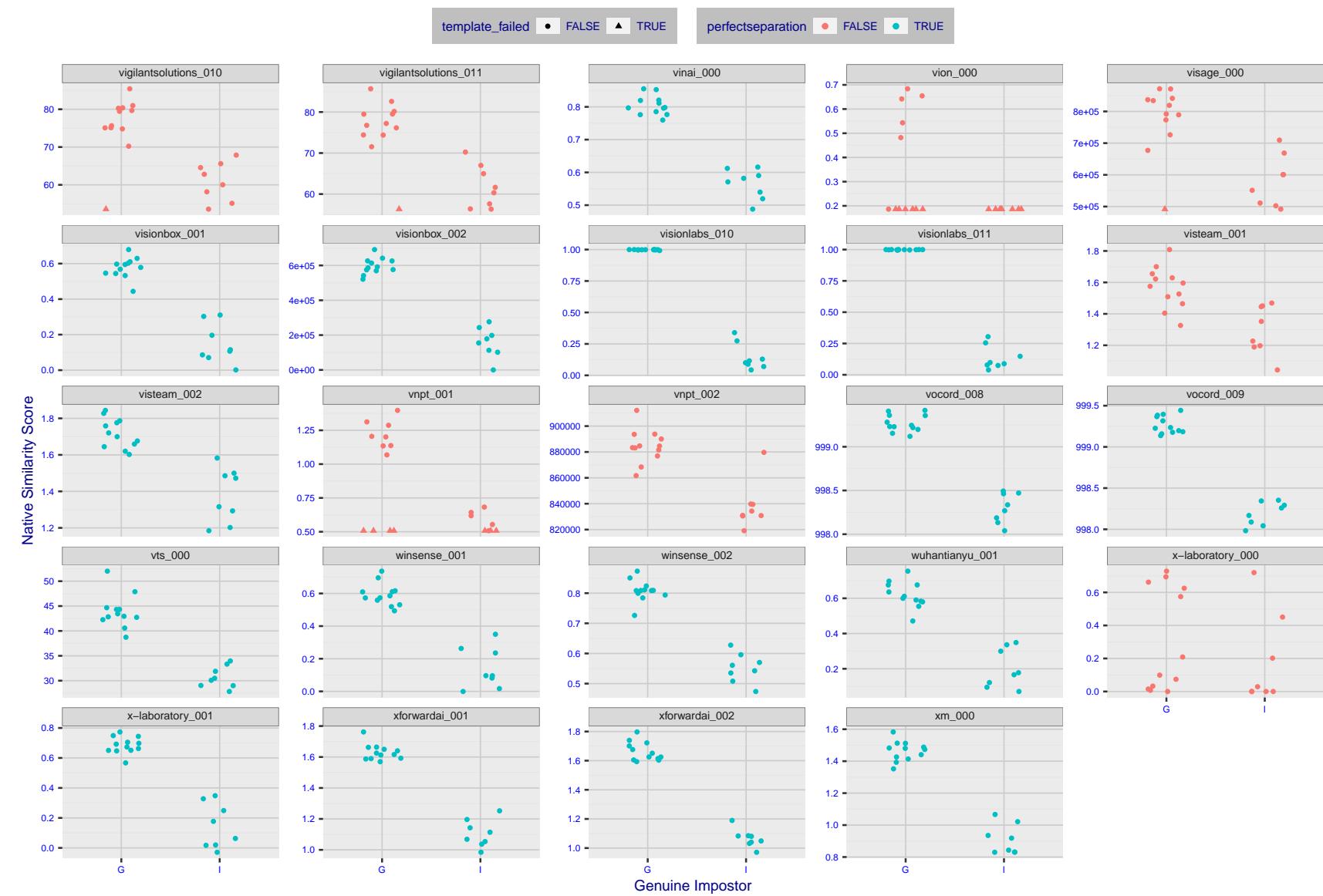


Figure 18: The Figure shows, in blue, algorithms that correctly separate the 12 genuine and 8 impostor pairs used in the May 2018 paper Face recognition accuracy of forensic examiners, superrecognizers, and face recognition algorithms (Phillips et al. [1]). In red are algorithms that are imperfect. Some algorithms fail only because they failed to make a template e.g. due to face detection failure (shown as a triangle). Others fail because the pairs were selected for that study because they had been difficult for three leading algorithms used in FRVT 2006. Caution: Given the small sample size ($n=20$) the figure may change substantially if larger or different sets were used. The images can be downloaded from the [Supplemental Information](#) page provided with that publication.

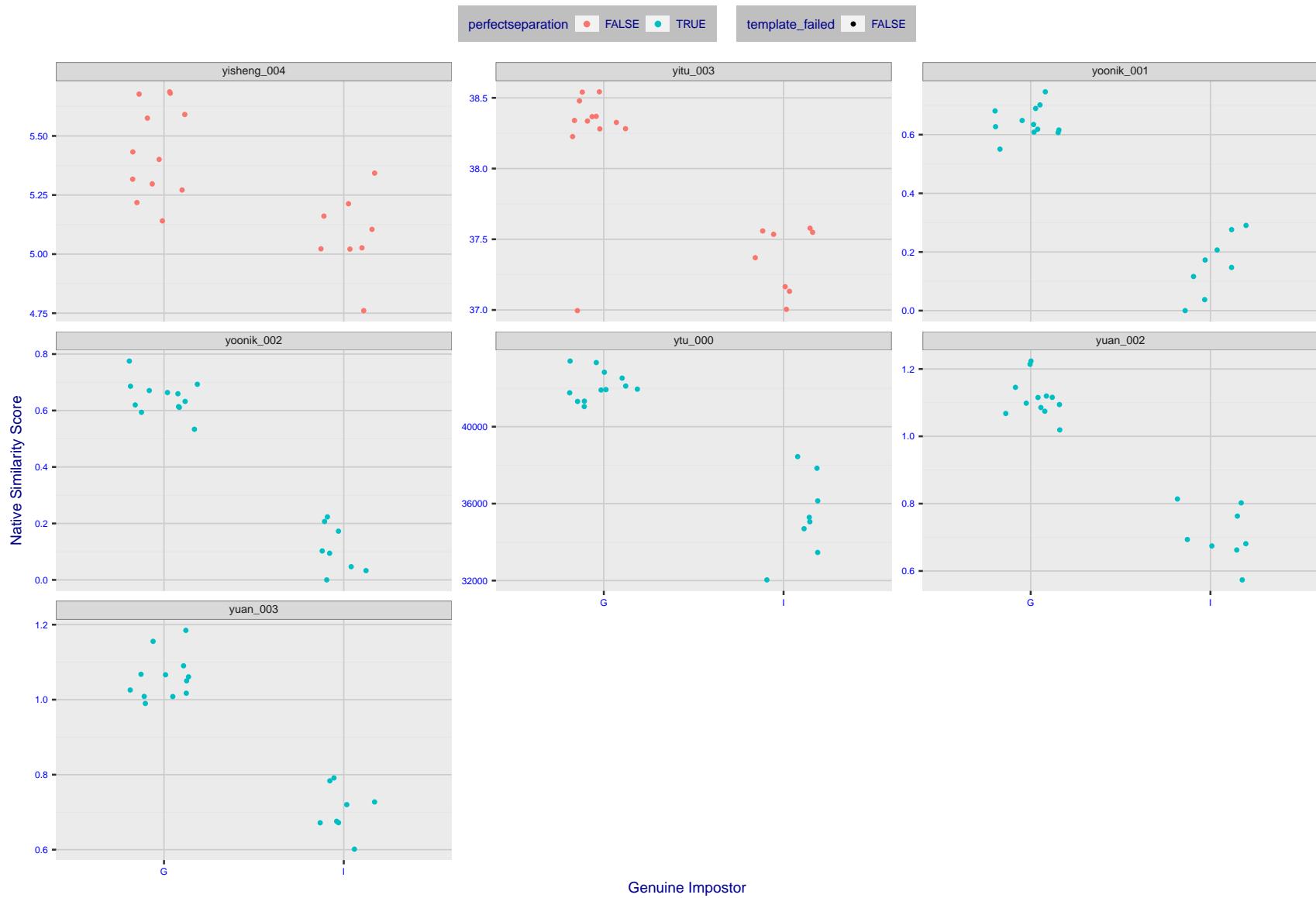


Figure 19: The Figure shows, in blue, algorithms that correctly separate the 12 genuine and 8 impostor pairs used in the May 2018 paper [Face recognition accuracy of forensic examiners, superrecognizers, and face recognition algorithms](#) (Phillips et al. [1]). In red are algorithms that are imperfect. Some algorithms fail only because they failed to make a template e.g. due to face detection failure (shown as a triangle). Others fail because the pairs were selected for that study because they had been difficult for three leading algorithms used in FRVT 2006. Caution: Given the small sample size ($n=20$) the figure may change substantially if larger or different sets were used. The images can be downloaded from the [Supplemental Information](#) page provided with that publication.

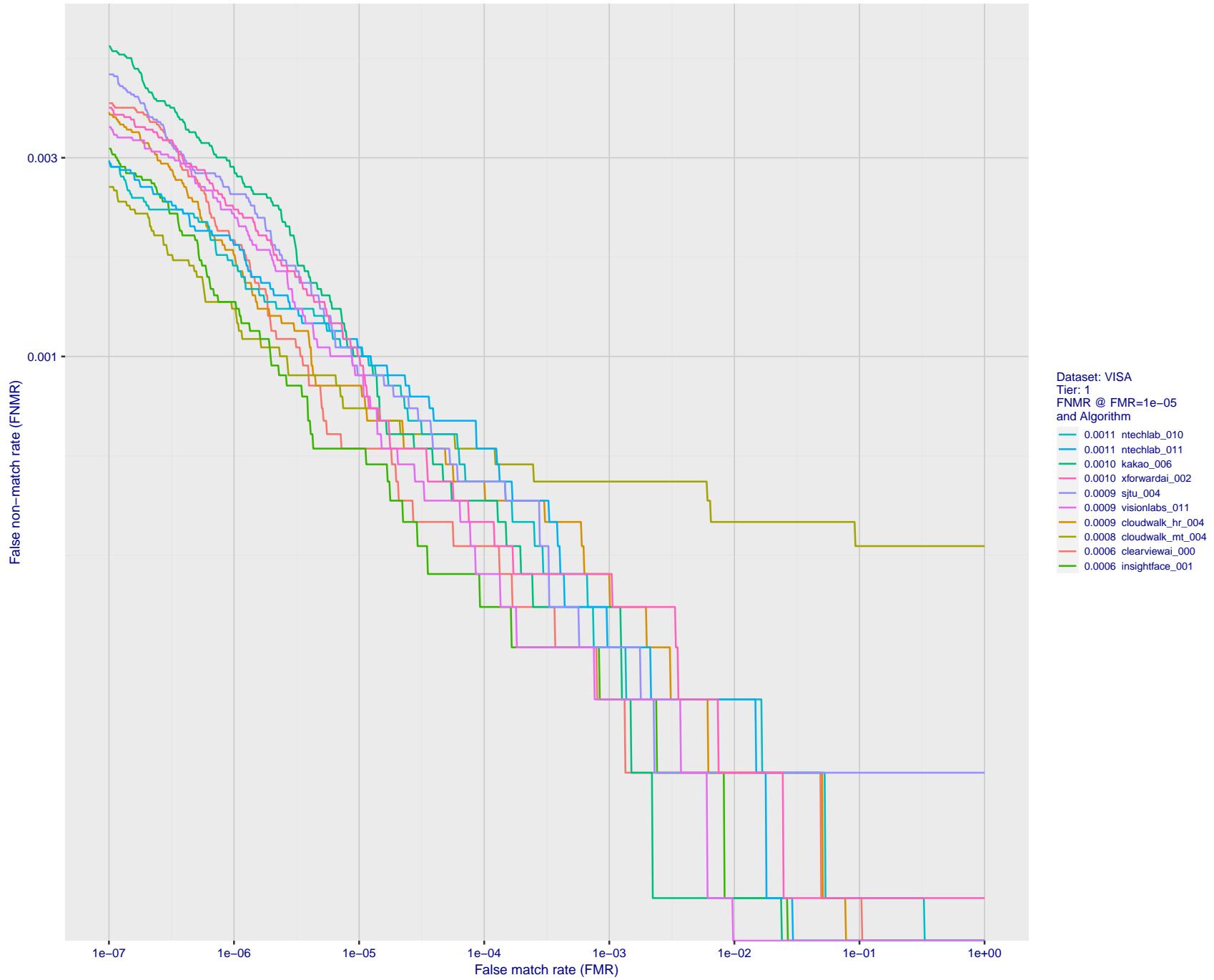


Figure 20: For the visa images, detection error tradeoff (DET) characteristics showing false non-match rate vs. false match rate plotted parametrically on threshold, T . The scales are logarithmic in order to show many decades of FMR.

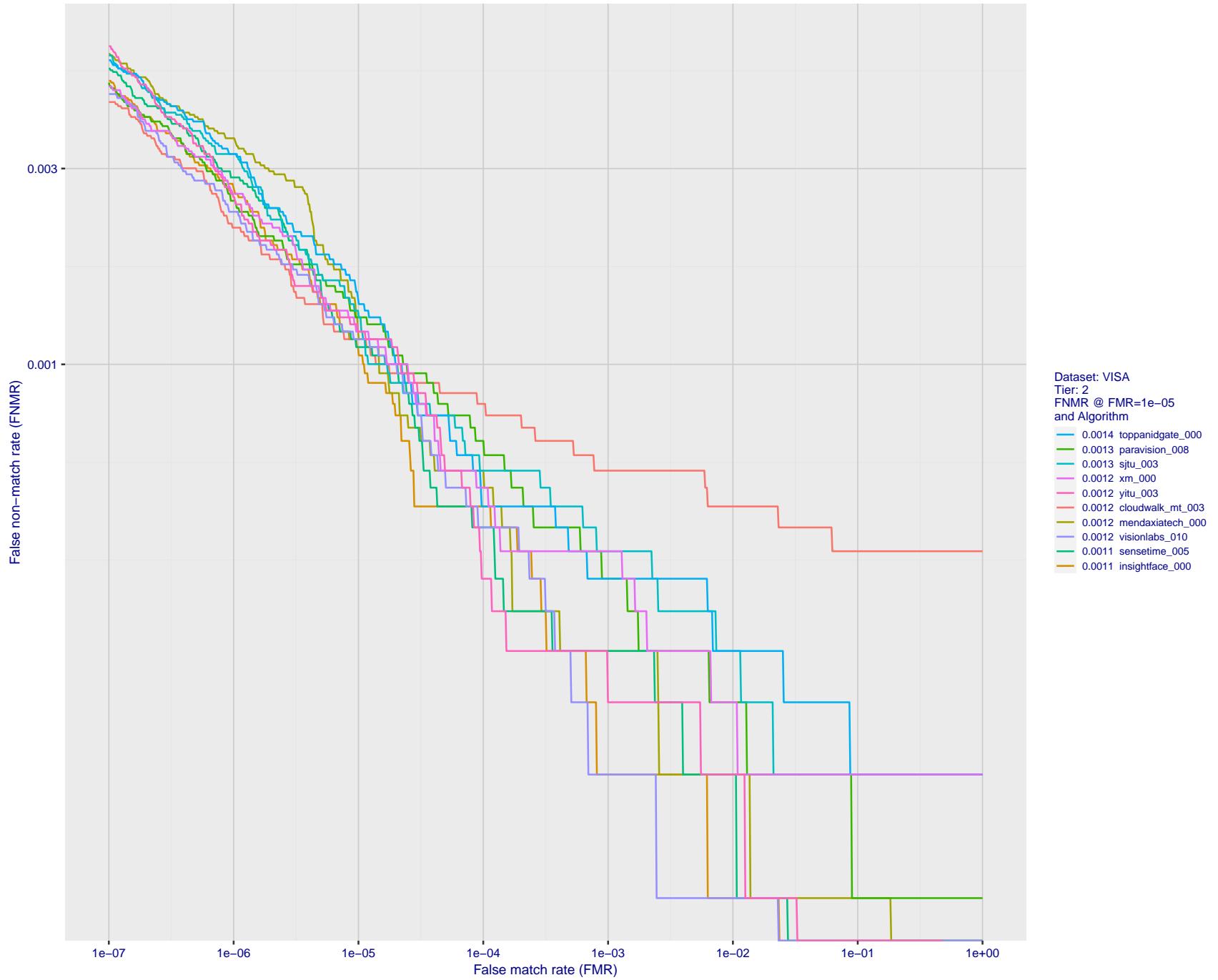


Figure 21: For the visa images, detection error tradeoff (DET) characteristics showing false non-match rate vs. false match rate plotted parametrically on threshold, T . The scales are logarithmic in order to show many decades of FMR.

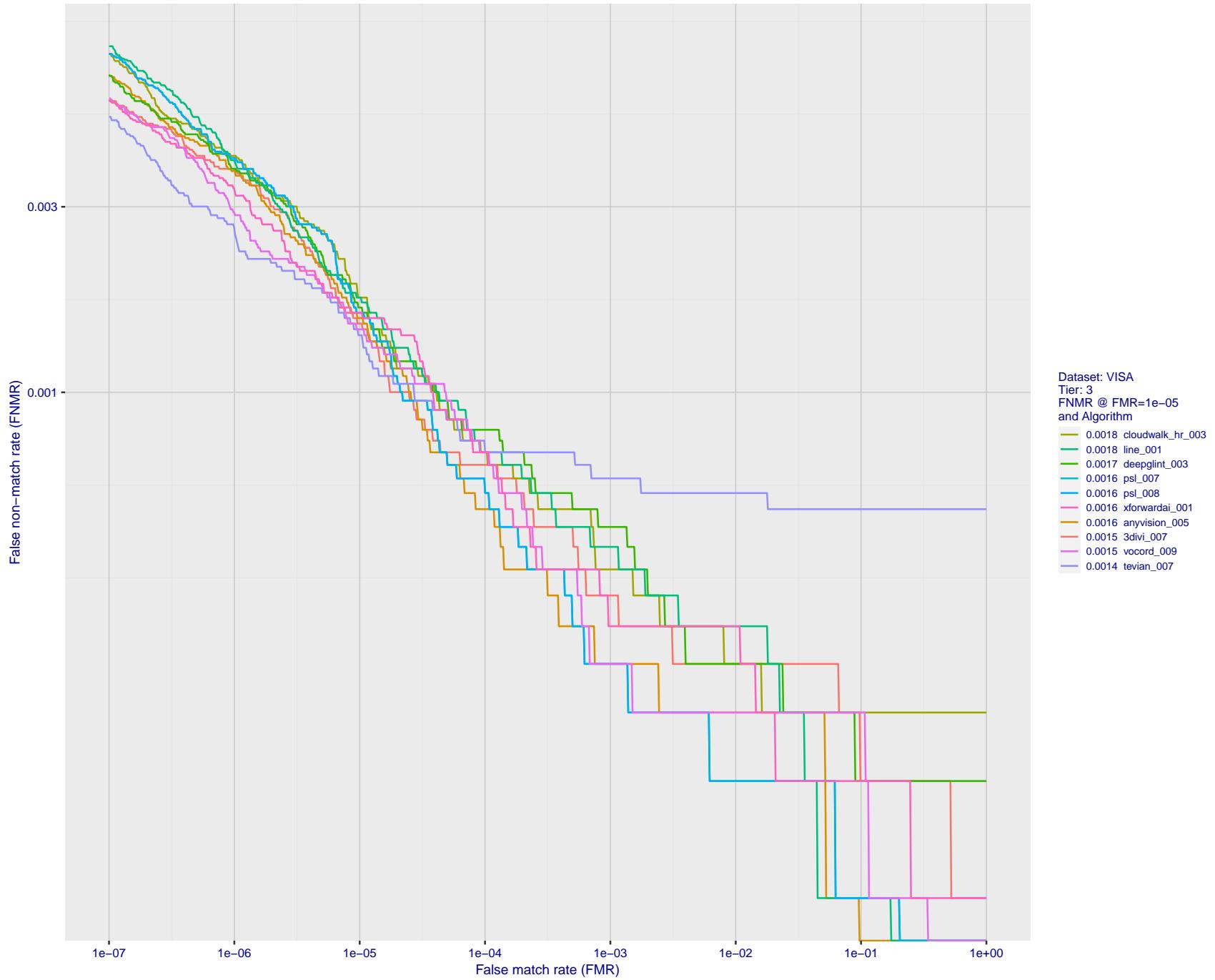


Figure 22: For the visa images, detection error tradeoff (DET) characteristics showing false non-match rate vs. false match rate plotted parametrically on threshold, T . The scales are logarithmic in order to show many decades of FMR.

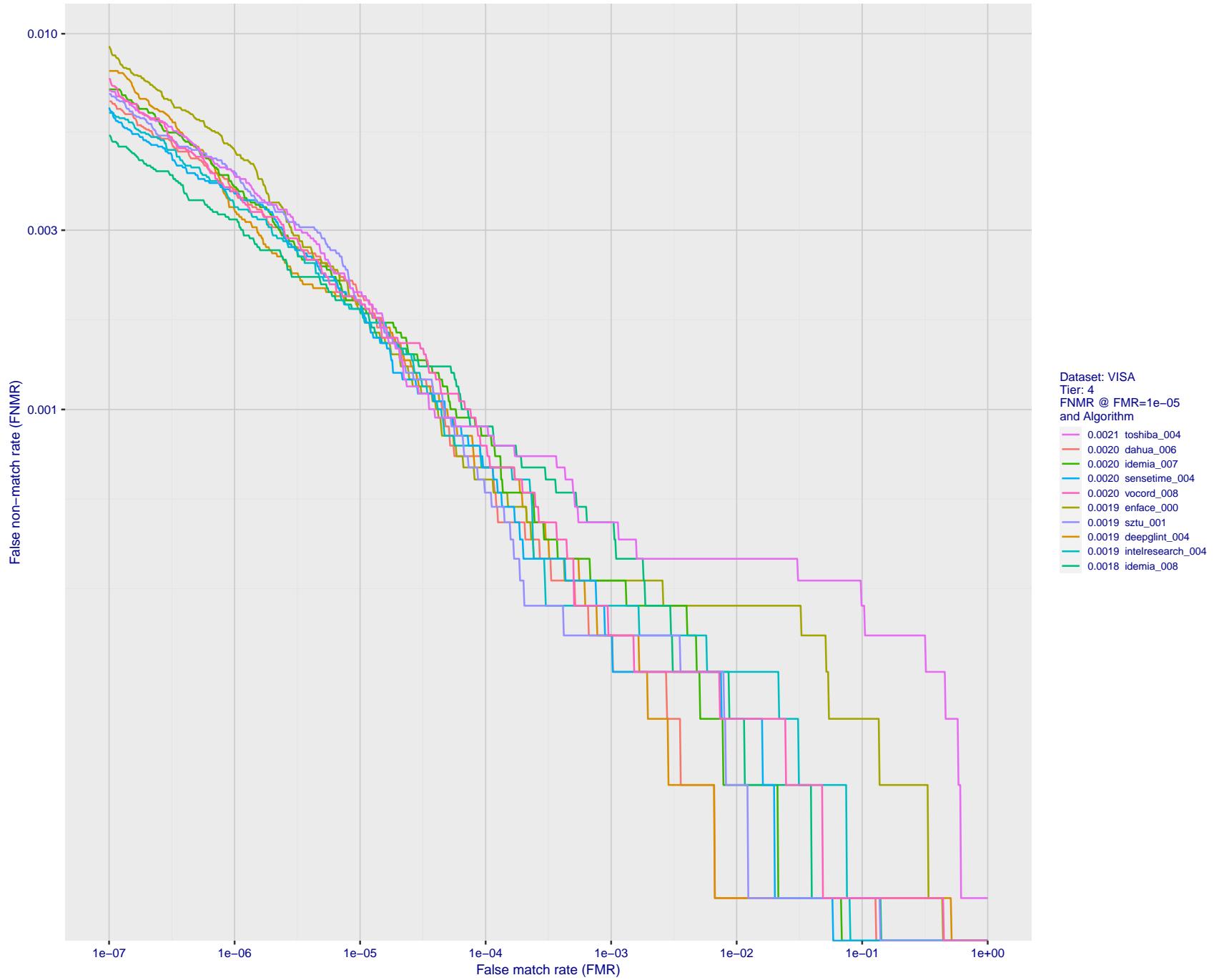


Figure 23: For the visa images, detection error tradeoff (DET) characteristics showing false non-match rate vs. false match rate plotted parametrically on threshold, T . The scales are logarithmic in order to show many decades of FMR.

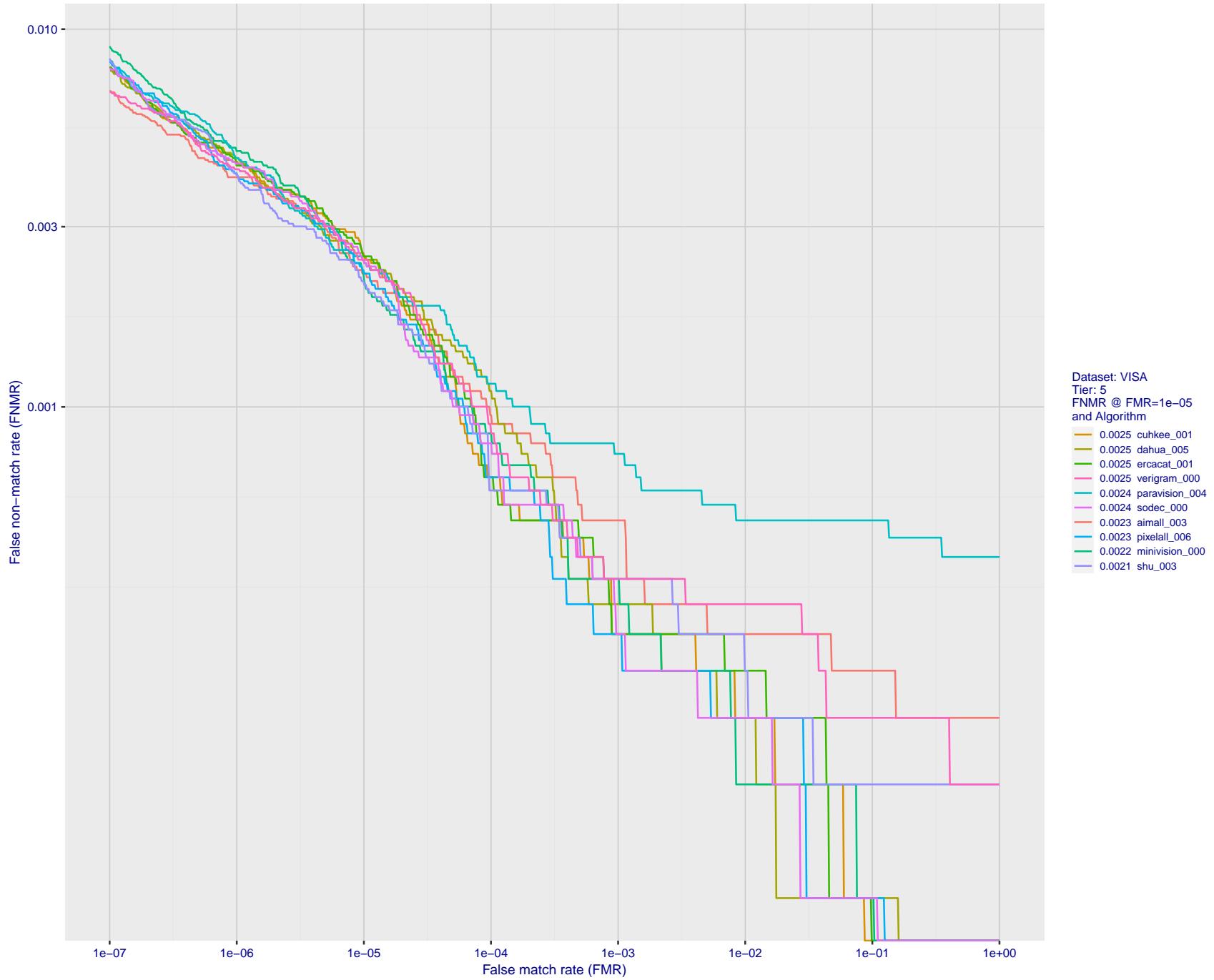


Figure 24: For the visa images, detection error tradeoff (DET) characteristics showing false non-match rate vs. false match rate plotted parametrically on threshold, T . The scales are logarithmic in order to show many decades of FMR.

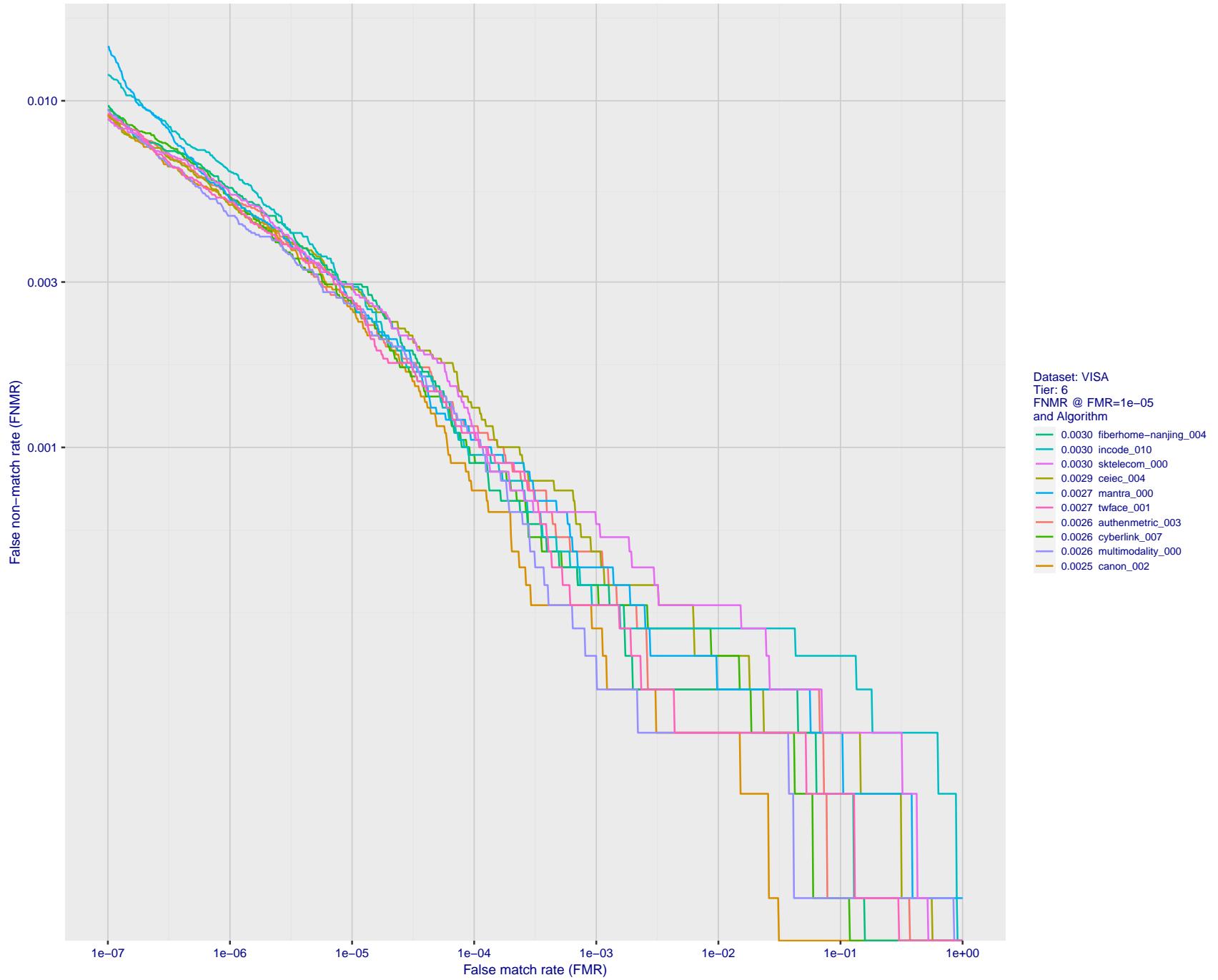


Figure 25: For the visa images, detection error tradeoff (DET) characteristics showing false non-match rate vs. false match rate plotted parametrically on threshold, T . The scales are logarithmic in order to show many decades of FMR.

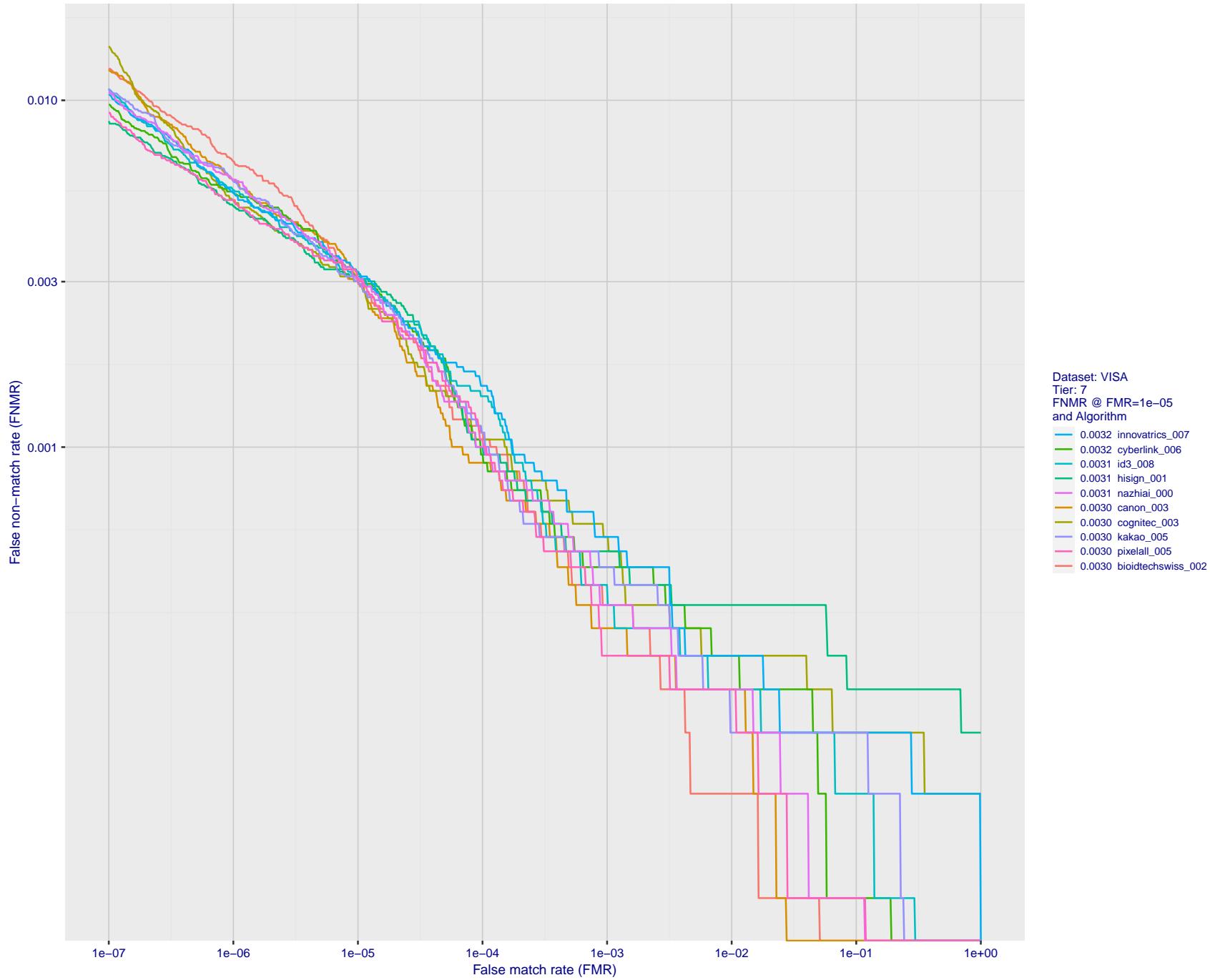


Figure 26: For the visa images, detection error tradeoff (DET) characteristics showing false non-match rate vs. false match rate plotted parametrically on threshold, T . The scales are logarithmic in order to show many decades of FMR.

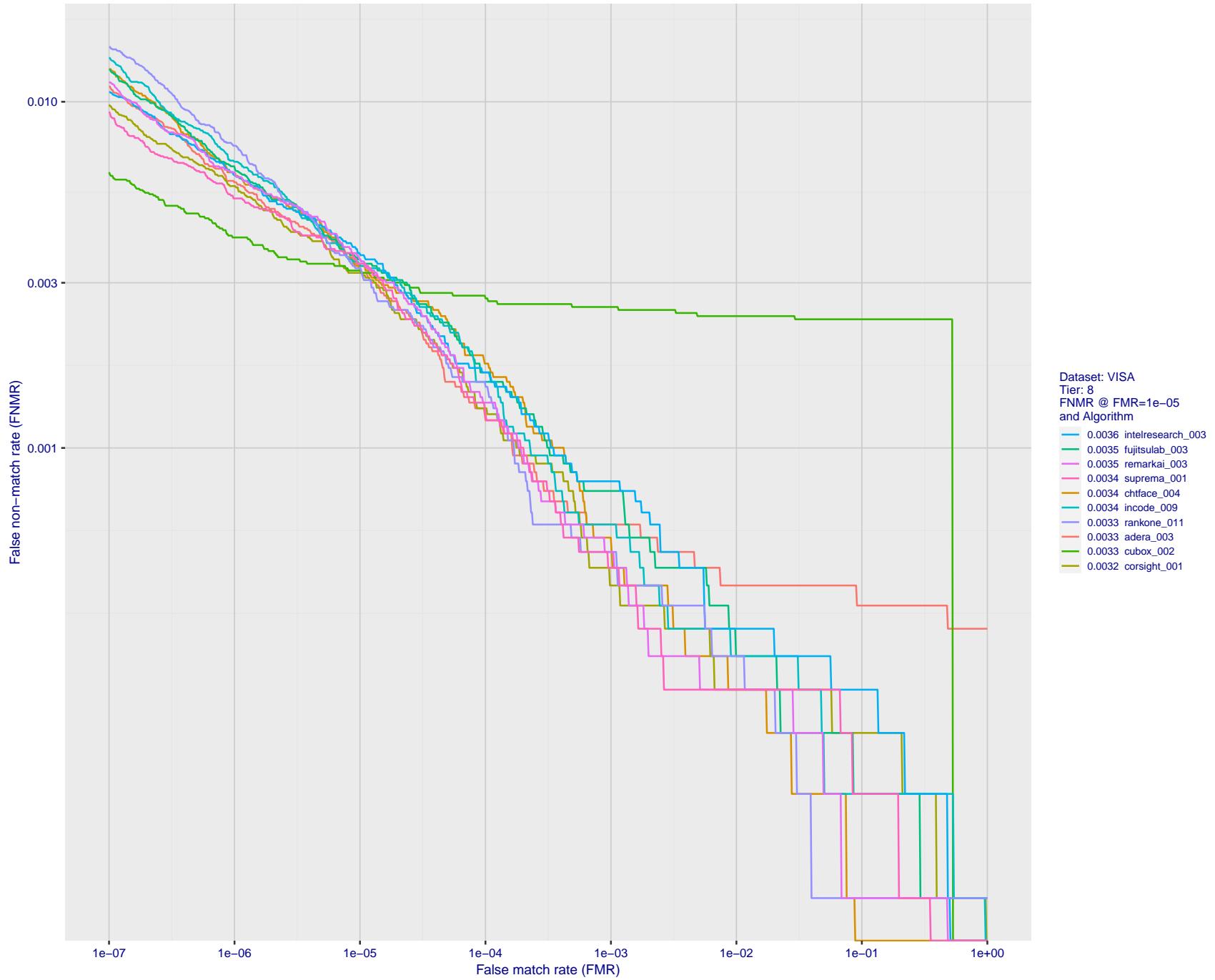


Figure 27: For the visa images, detection error tradeoff (DET) characteristics showing false non-match rate vs. false match rate plotted parametrically on threshold, T . The scales are logarithmic in order to show many decades of FMR.

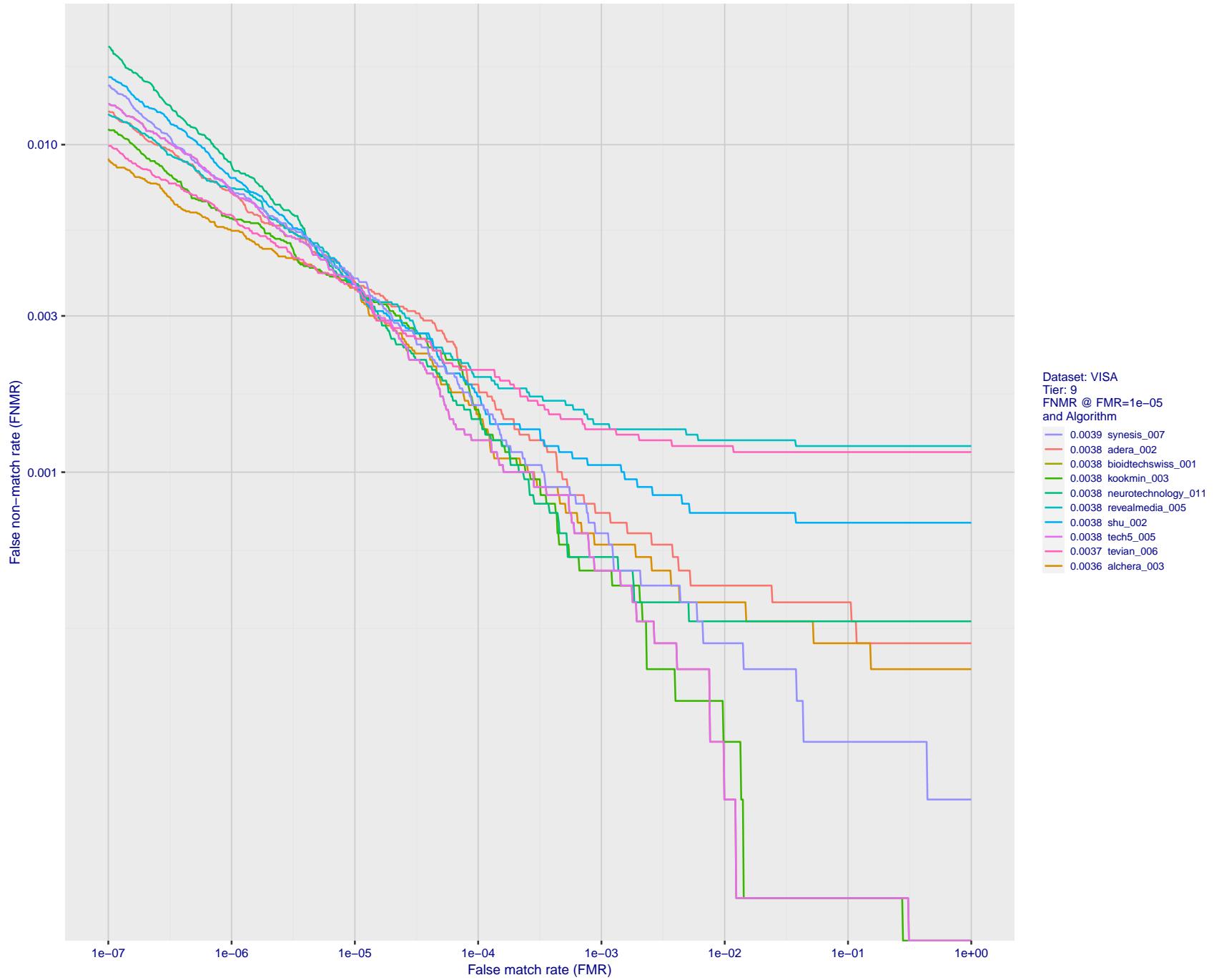


Figure 28: For the visa images, detection error tradeoff (DET) characteristics showing false non-match rate vs. false match rate plotted parametrically on threshold, T . The scales are logarithmic in order to show many decades of FMR.

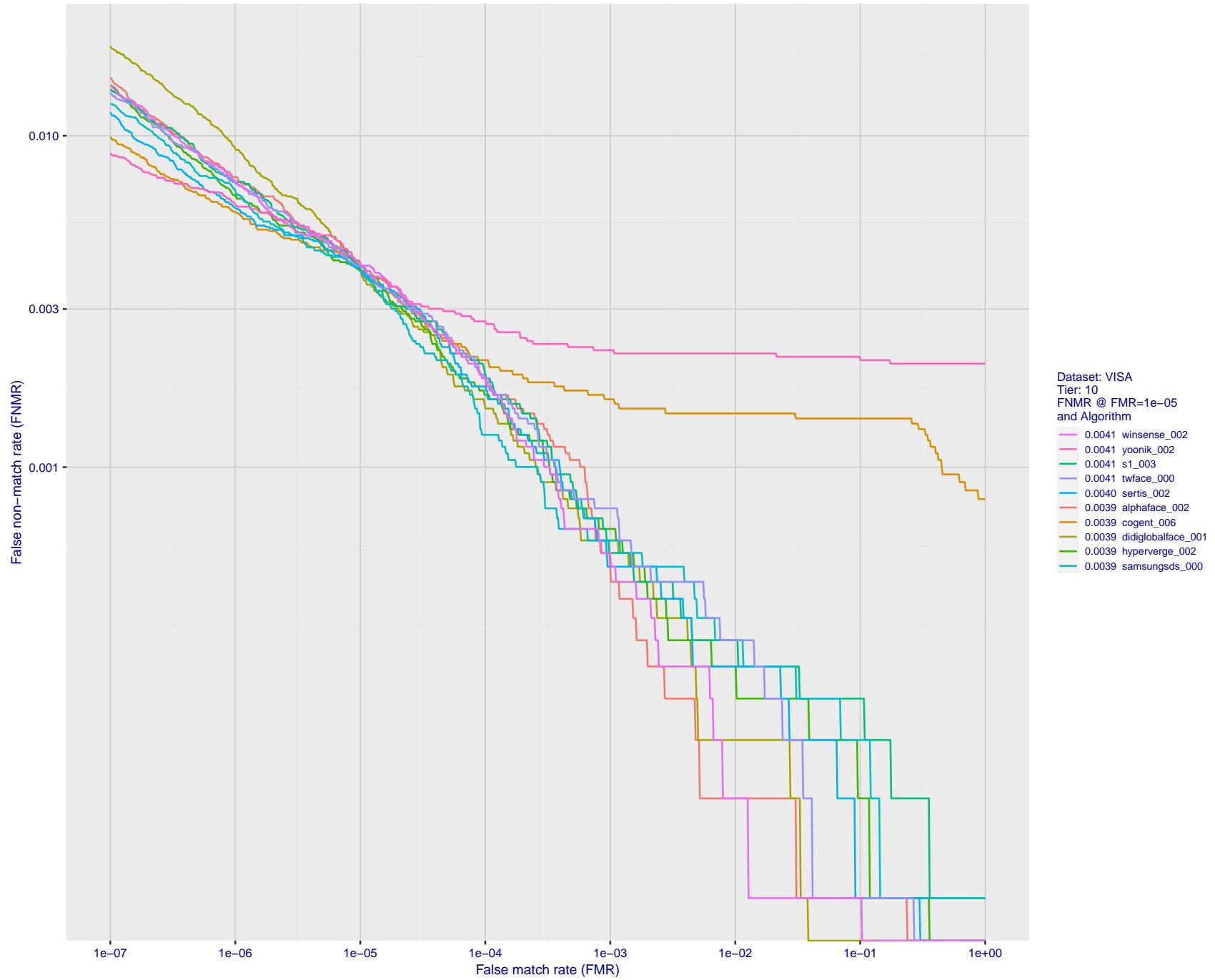


Figure 29: For the visa images, detection error tradeoff (DET) characteristics showing false non-match rate vs. false match rate plotted parametrically on threshold, T . The scales are logarithmic in order to show many decades of FMR.

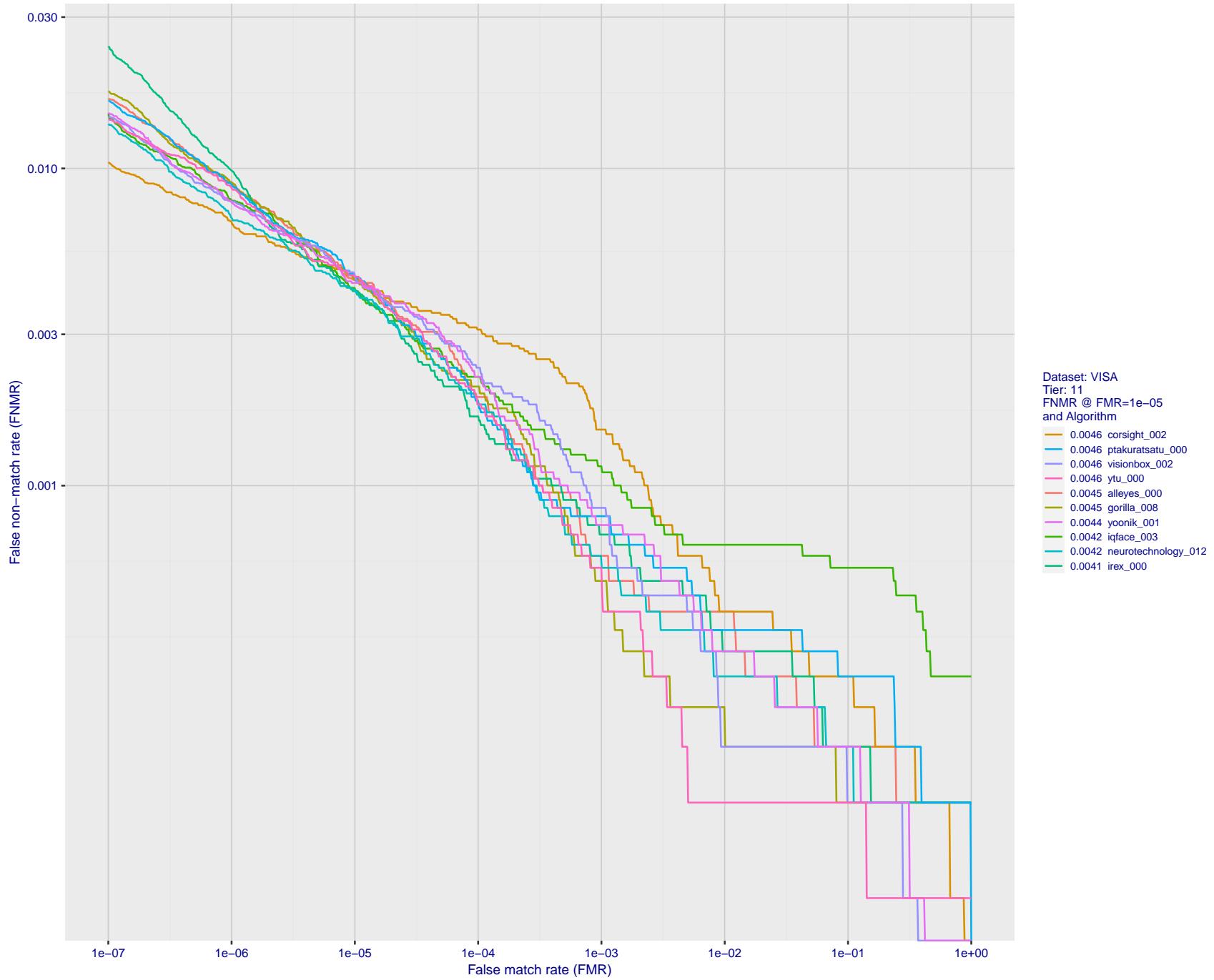


Figure 30: For the visa images, detection error tradeoff (DET) characteristics showing false non-match rate vs. false match rate plotted parametrically on threshold, T . The scales are logarithmic in order to show many decades of FMR.

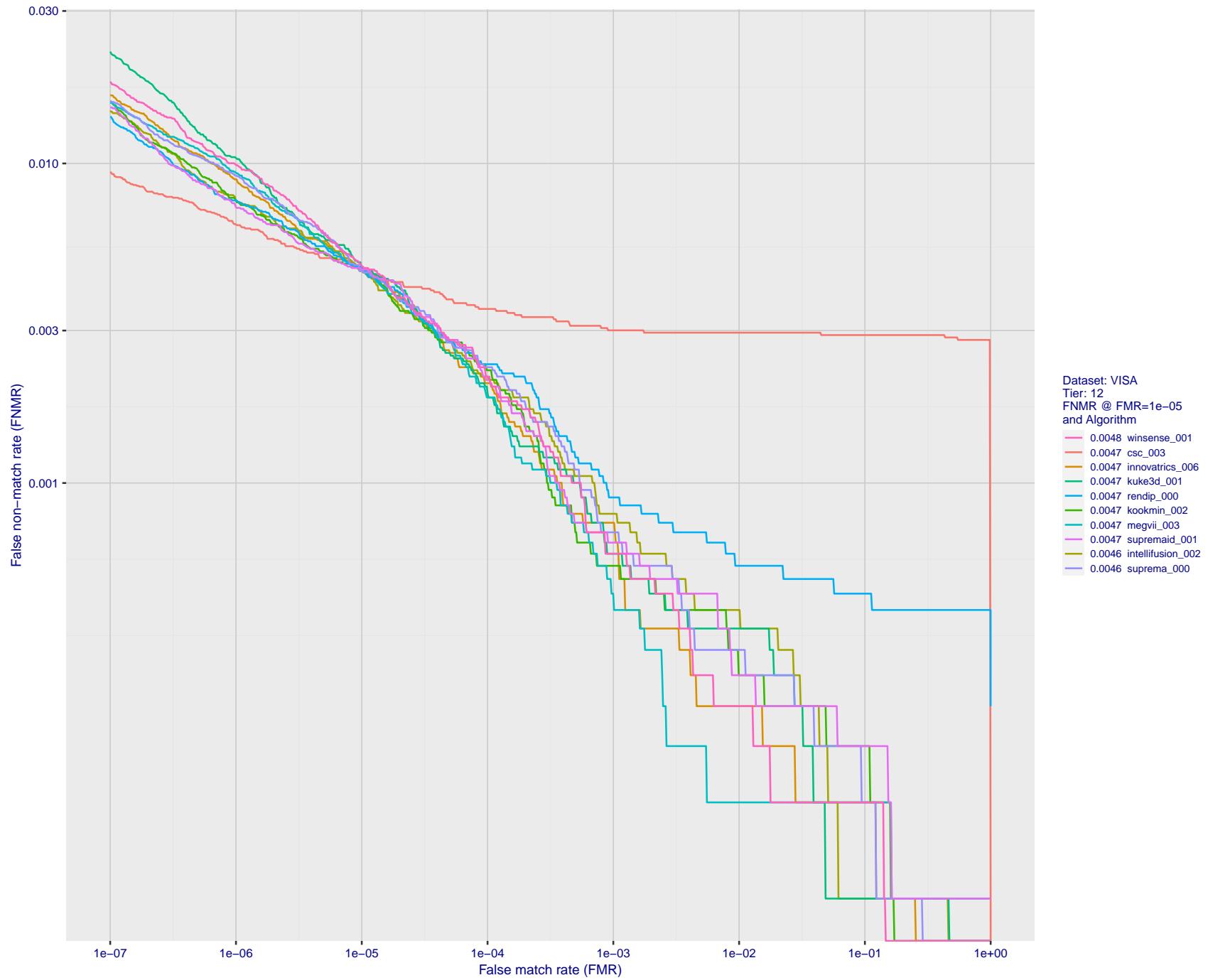


Figure 31: For the visa images, detection error tradeoff (DET) characteristics showing false non-match rate vs. false match rate plotted parametrically on threshold, T . The scales are logarithmic in order to show many decades of FMR.

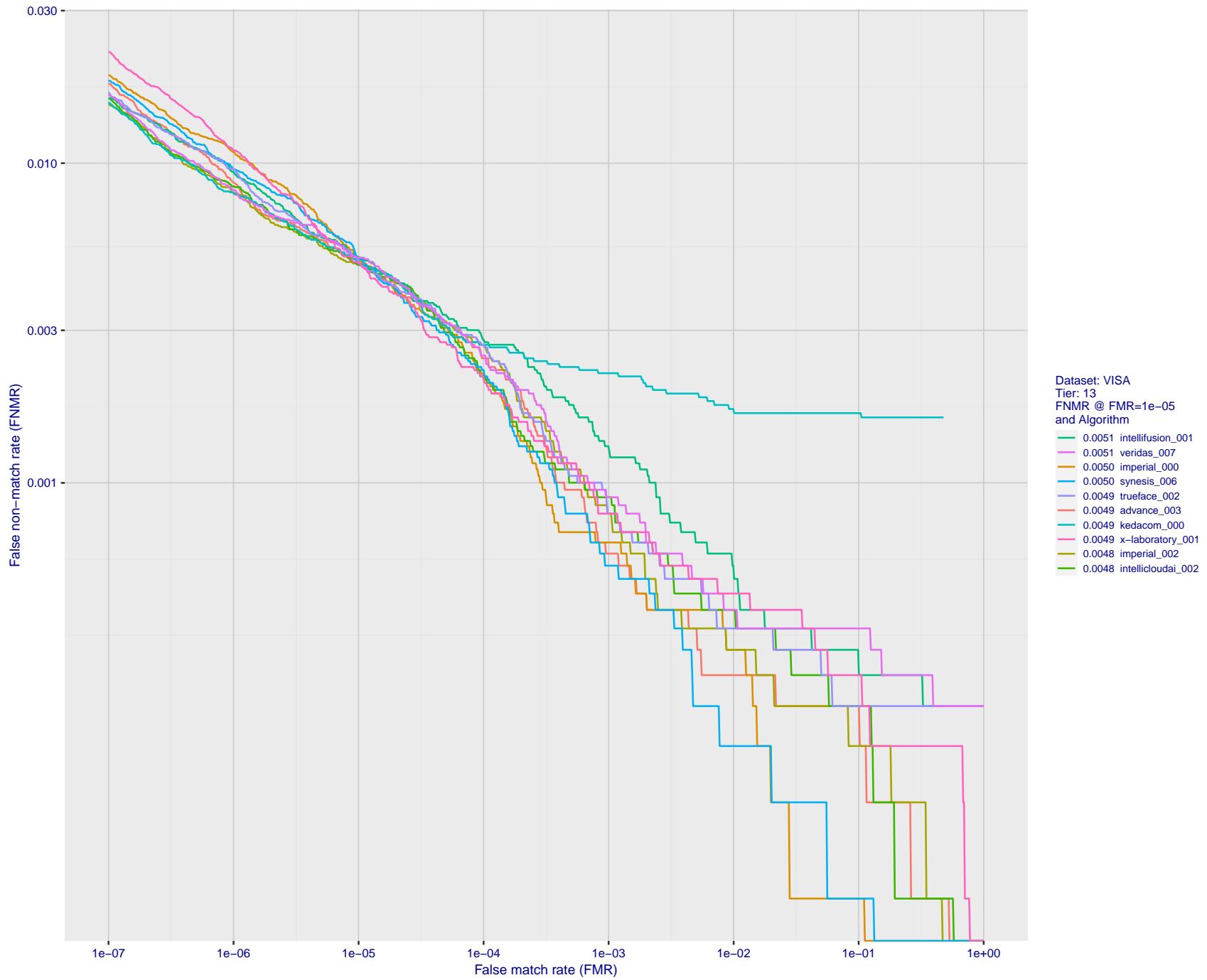


Figure 32: For the visa images, detection error tradeoff (DET) characteristics showing false non-match rate vs. false match rate plotted parametrically on threshold, T . The scales are logarithmic in order to show many decades of FMR.

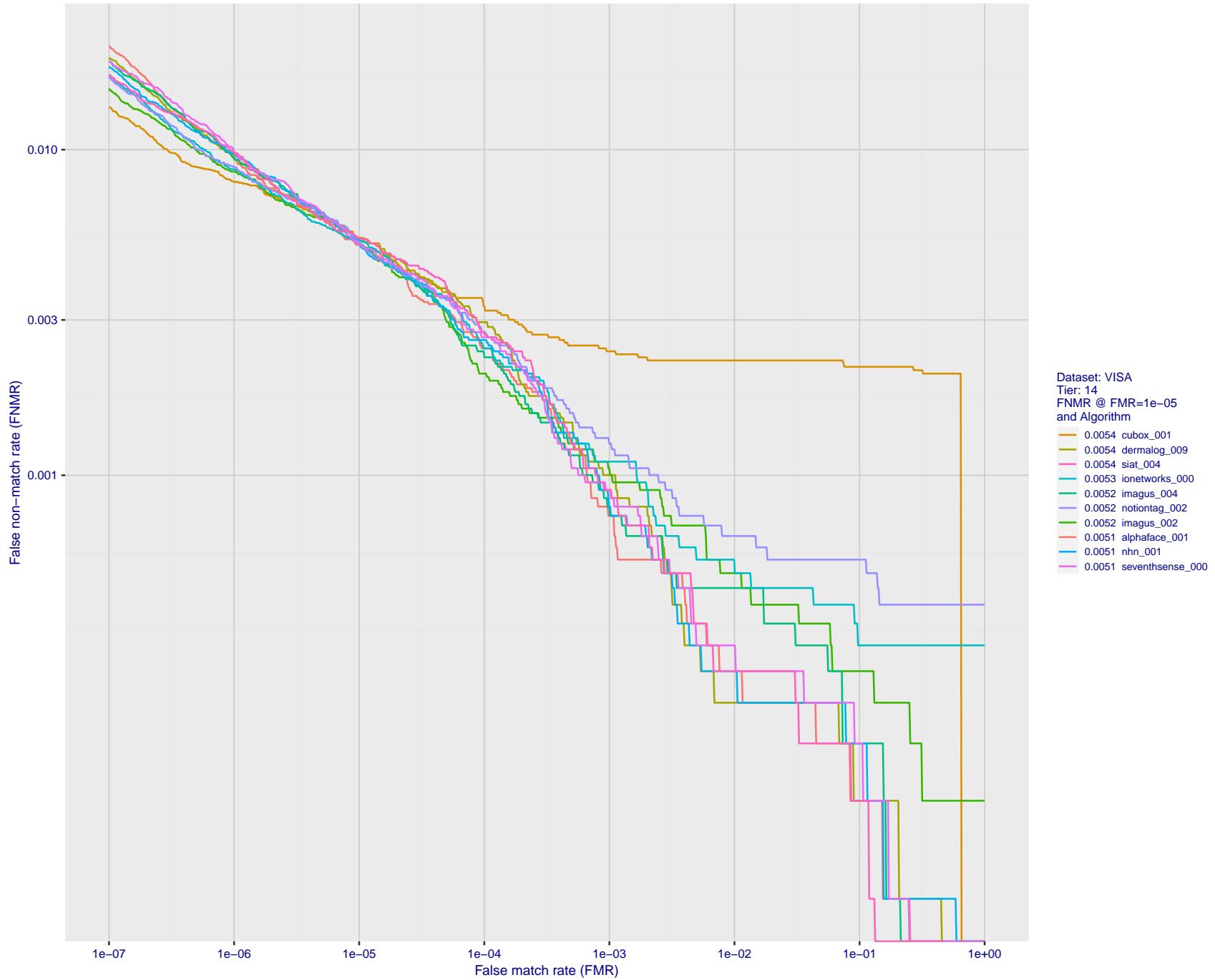


Figure 33: For the visa images, detection error tradeoff (DET) characteristics showing false non-match rate vs. false match rate plotted parametrically on threshold, T . The scales are logarithmic in order to show many decades of FMR.

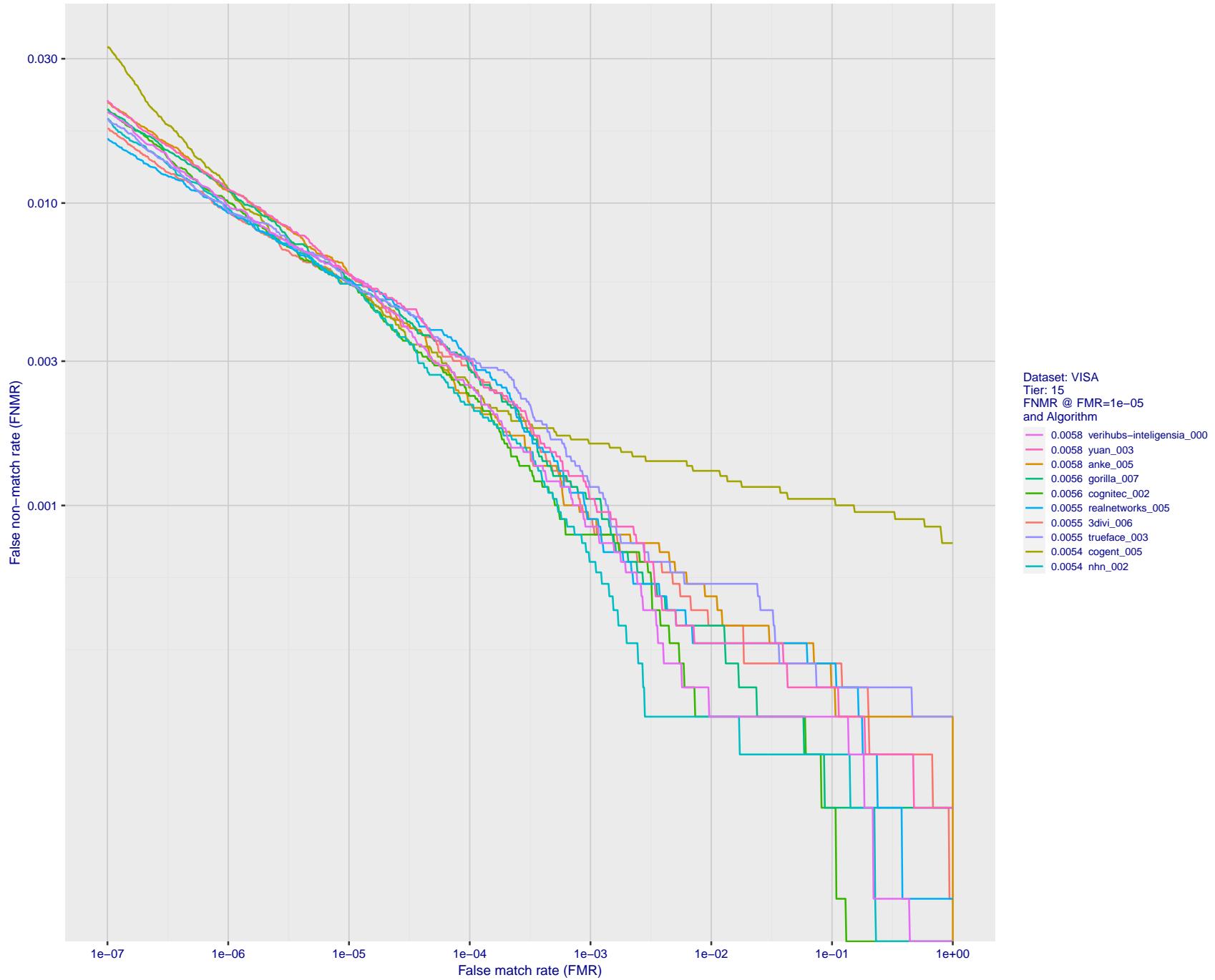


Figure 34: For the visa images, detection error tradeoff (DET) characteristics showing false non-match rate vs. false match rate plotted parametrically on threshold, T . The scales are logarithmic in order to show many decades of FMR.

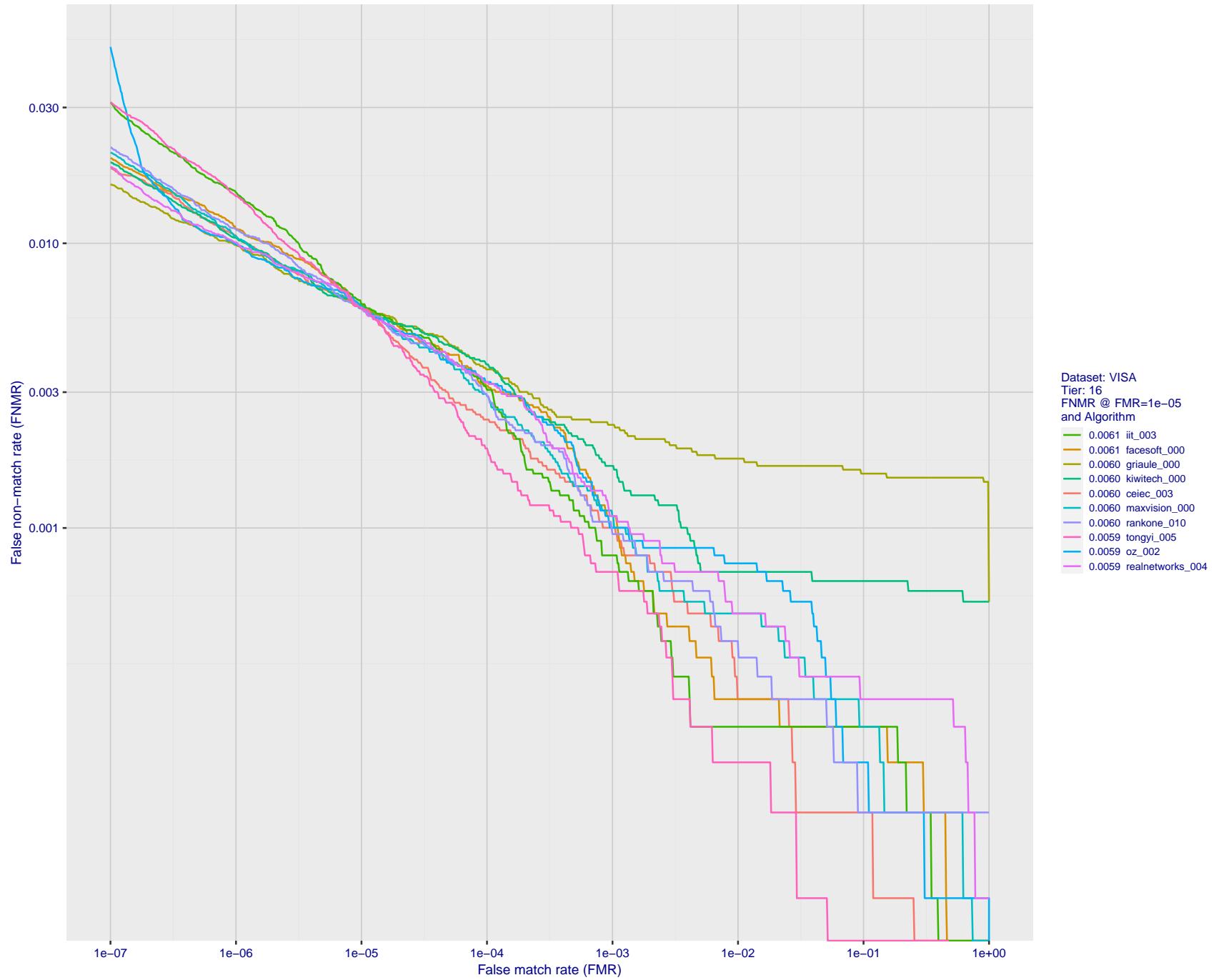


Figure 35: For the visa images, detection error tradeoff (DET) characteristics showing false non-match rate vs. false match rate plotted parametrically on threshold, T . The scales are logarithmic in order to show many decades of FMR.

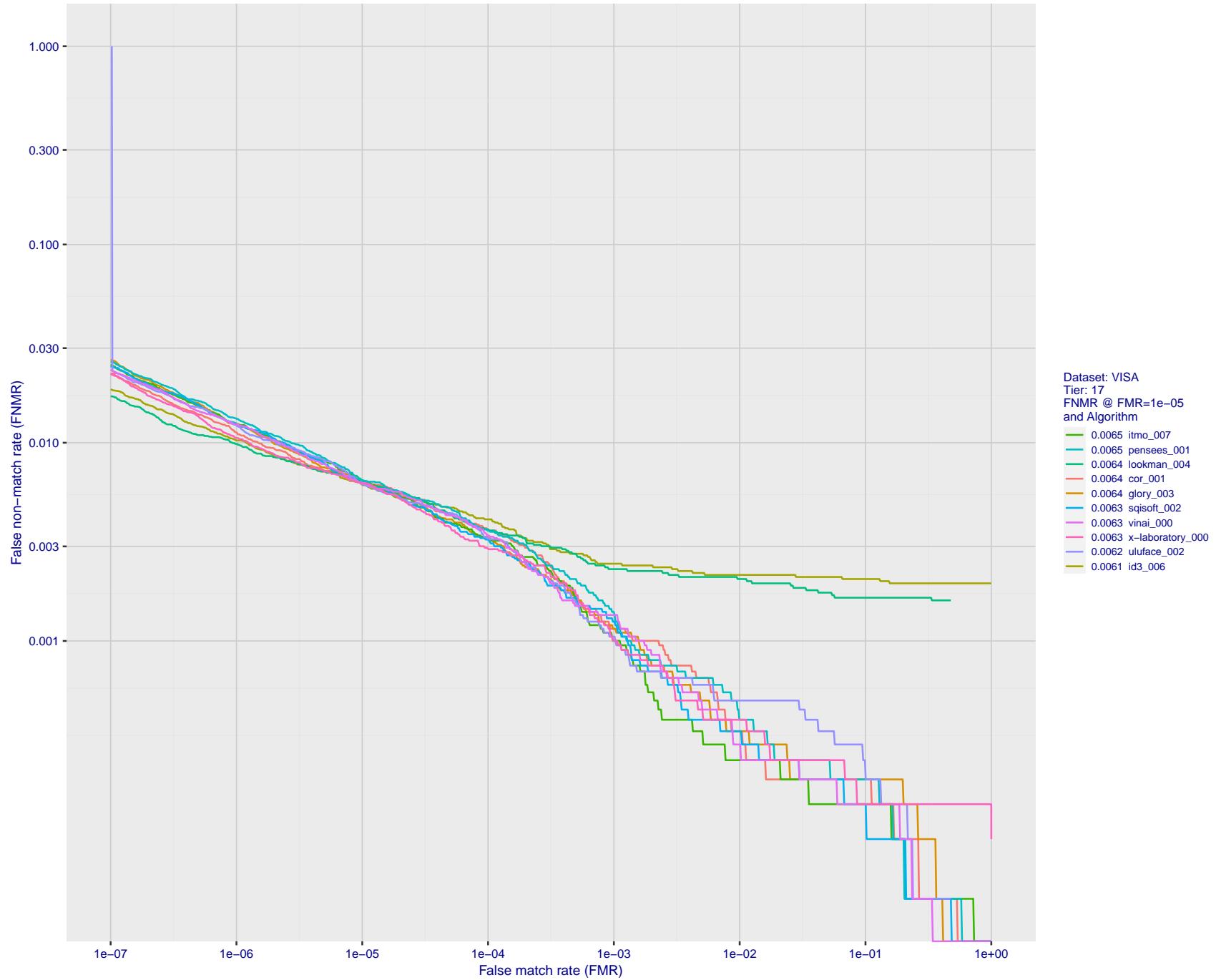


Figure 36: For the visa images, detection error tradeoff (DET) characteristics showing false non-match rate vs. false match rate plotted parametrically on threshold, T . The scales are logarithmic in order to show many decades of FMR.

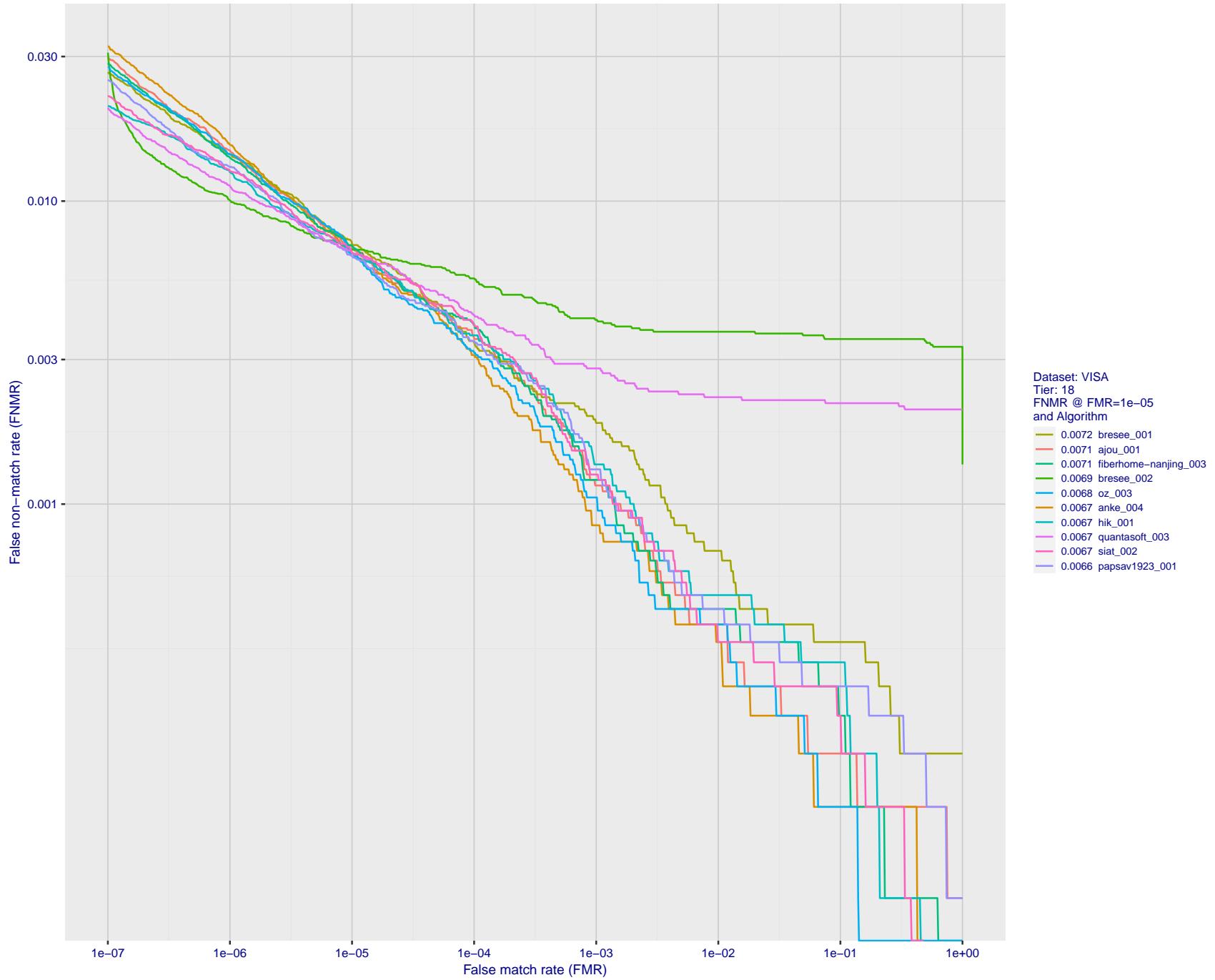


Figure 37: For the visa images, detection error tradeoff (DET) characteristics showing false non-match rate vs. false match rate plotted parametrically on threshold, T . The scales are logarithmic in order to show many decades of FMR.

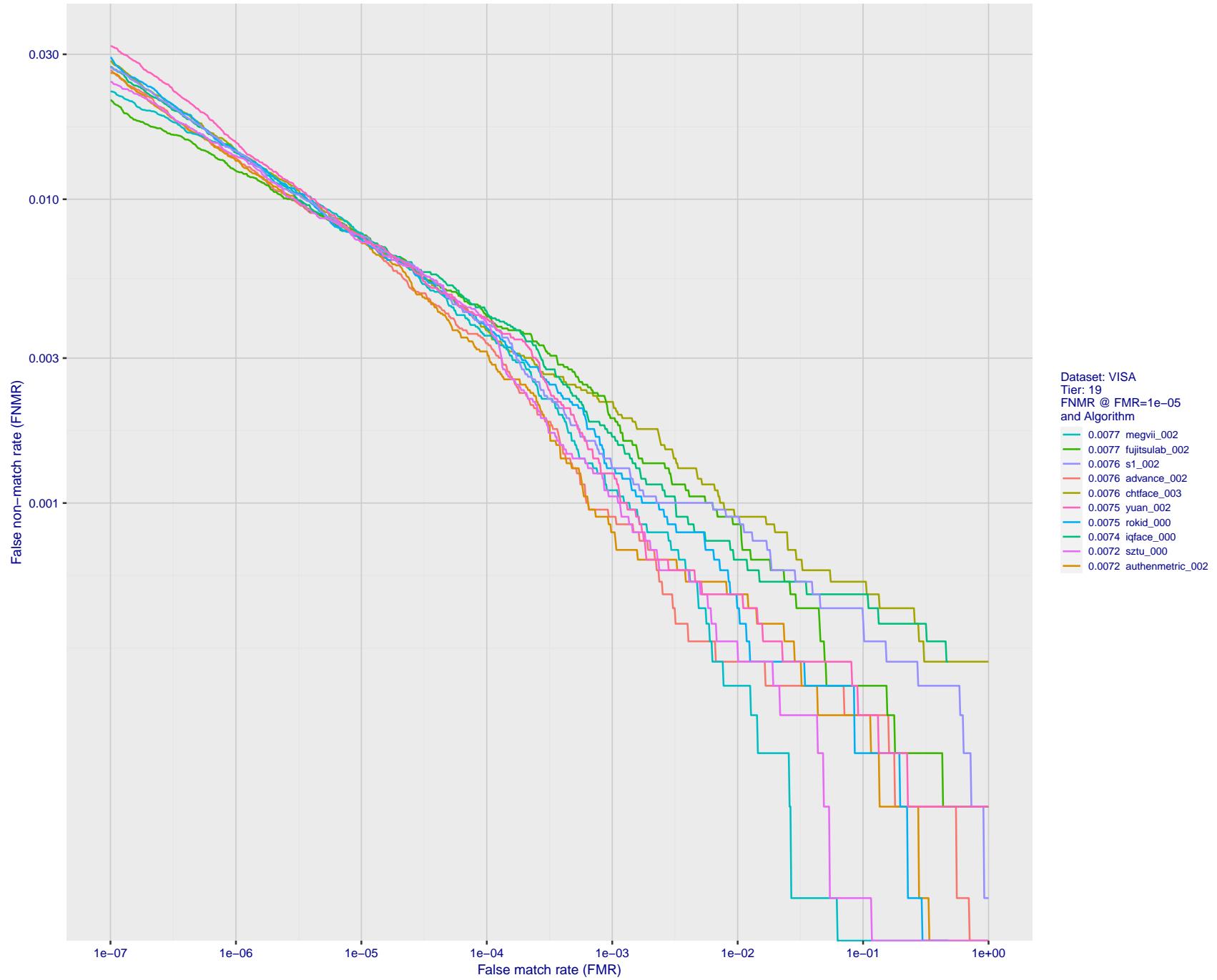


Figure 38: For the visa images, detection error tradeoff (DET) characteristics showing false non-match rate vs. false match rate plotted parametrically on threshold, T . The scales are logarithmic in order to show many decades of FMR.

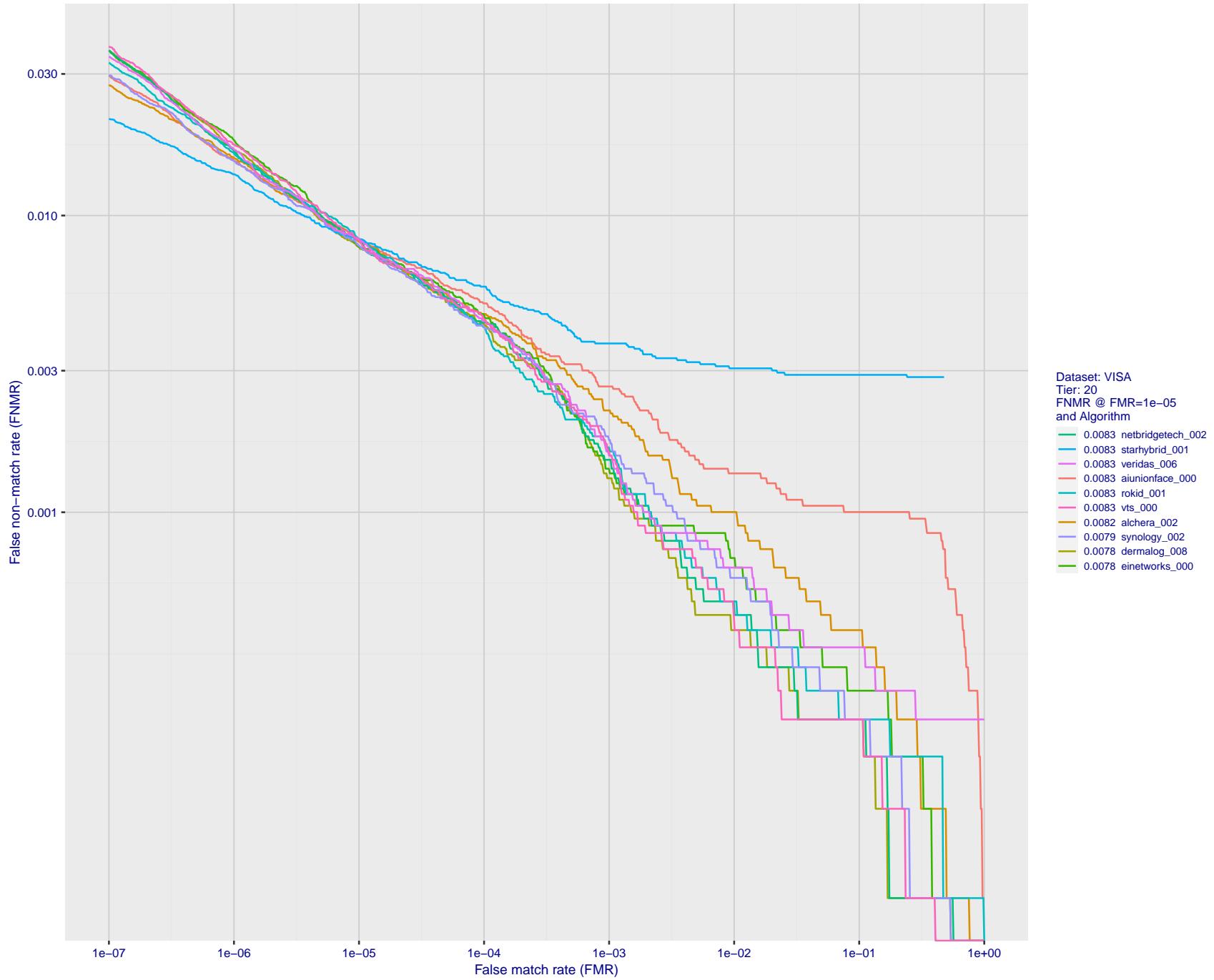


Figure 39: For the visa images, detection error tradeoff (DET) characteristics showing false non-match rate vs. false match rate plotted parametrically on threshold, T . The scales are logarithmic in order to show many decades of FMR.

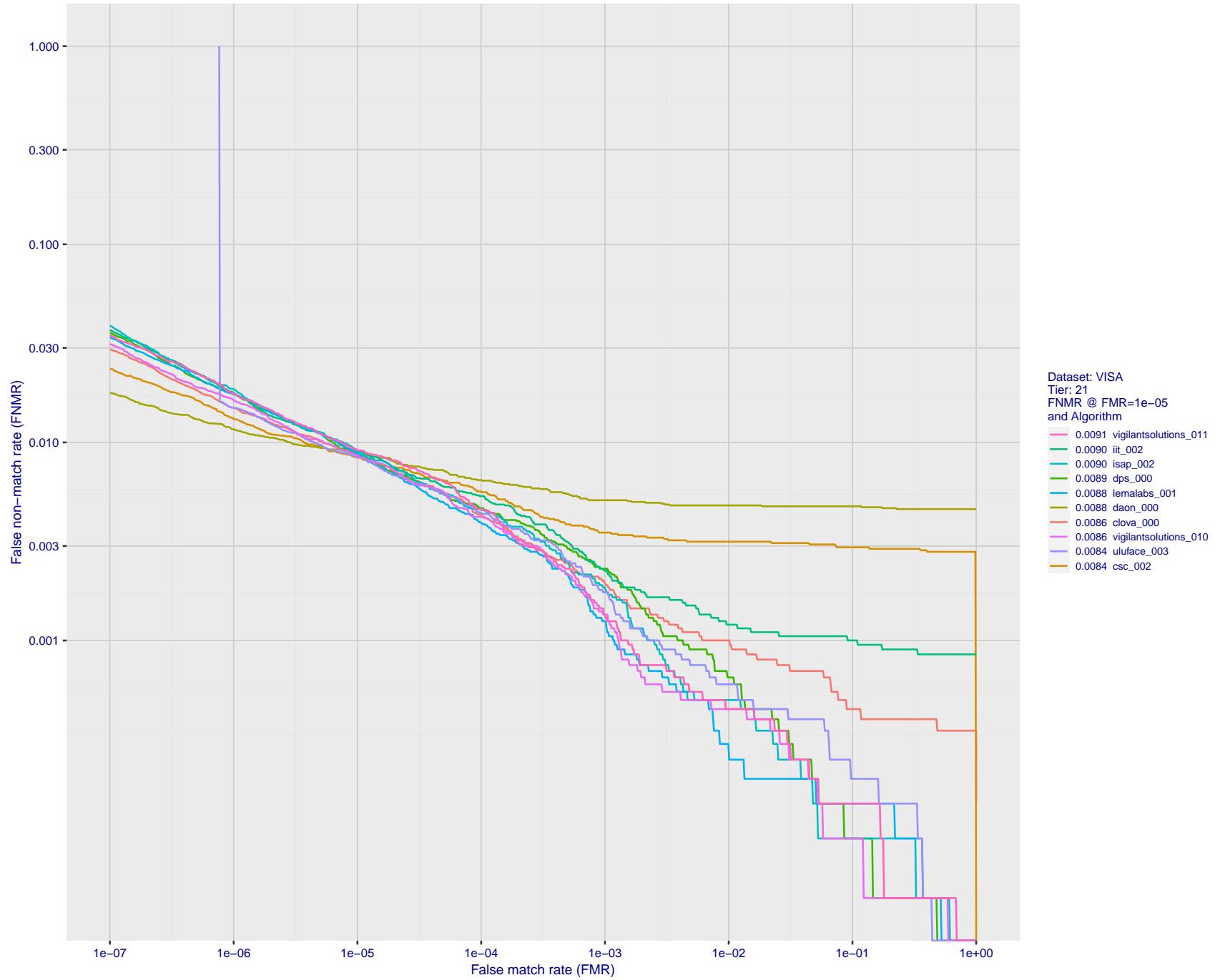


Figure 40: For the visa images, detection error tradeoff (DET) characteristics showing false non-match rate vs. false match rate plotted parametrically on threshold, T . The scales are logarithmic in order to show many decades of FMR.

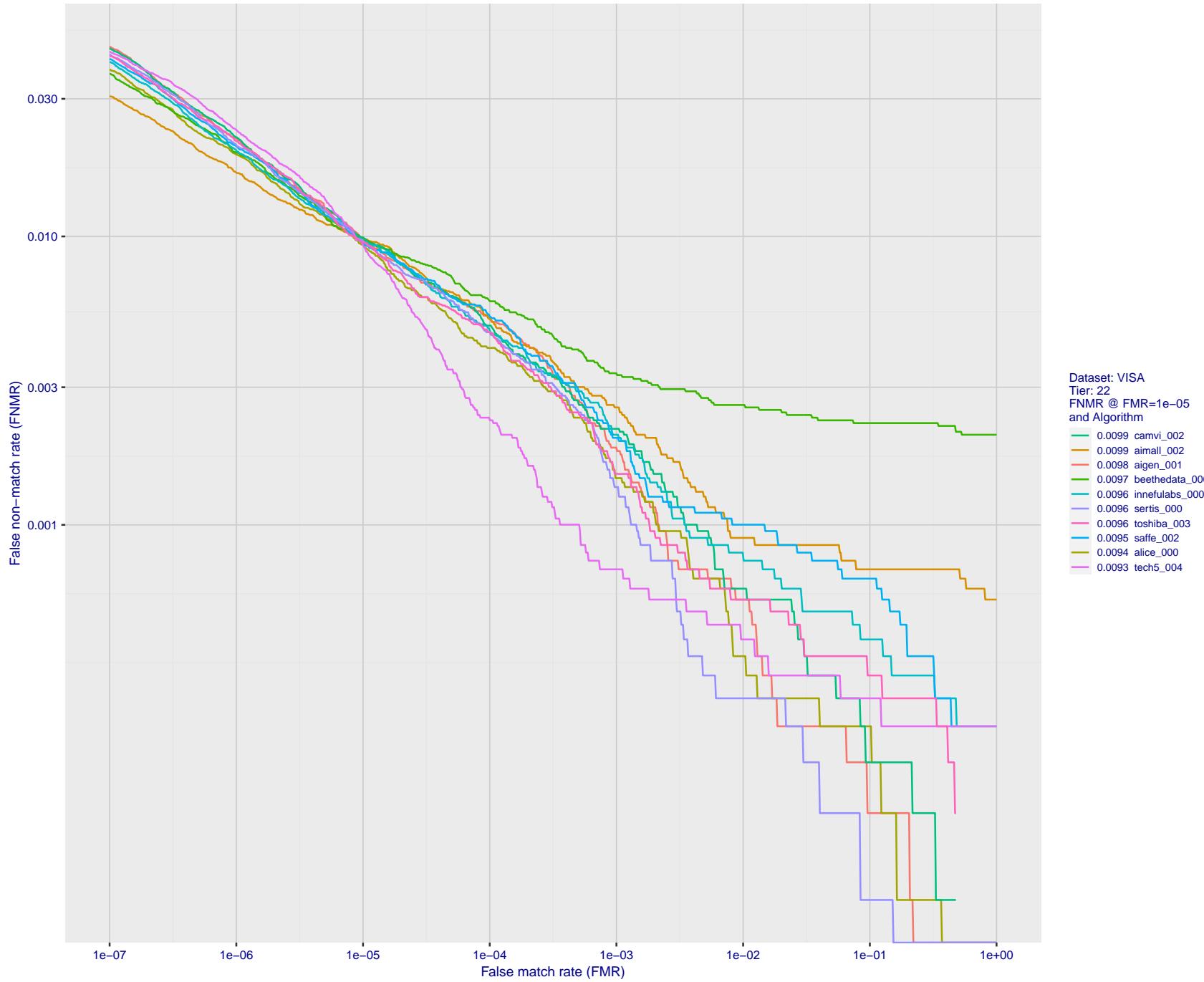


Figure 41: For the visa images, detection error tradeoff (DET) characteristics showing false non-match rate vs. false match rate plotted parametrically on threshold, T . The scales are logarithmic in order to show many decades of FMR.

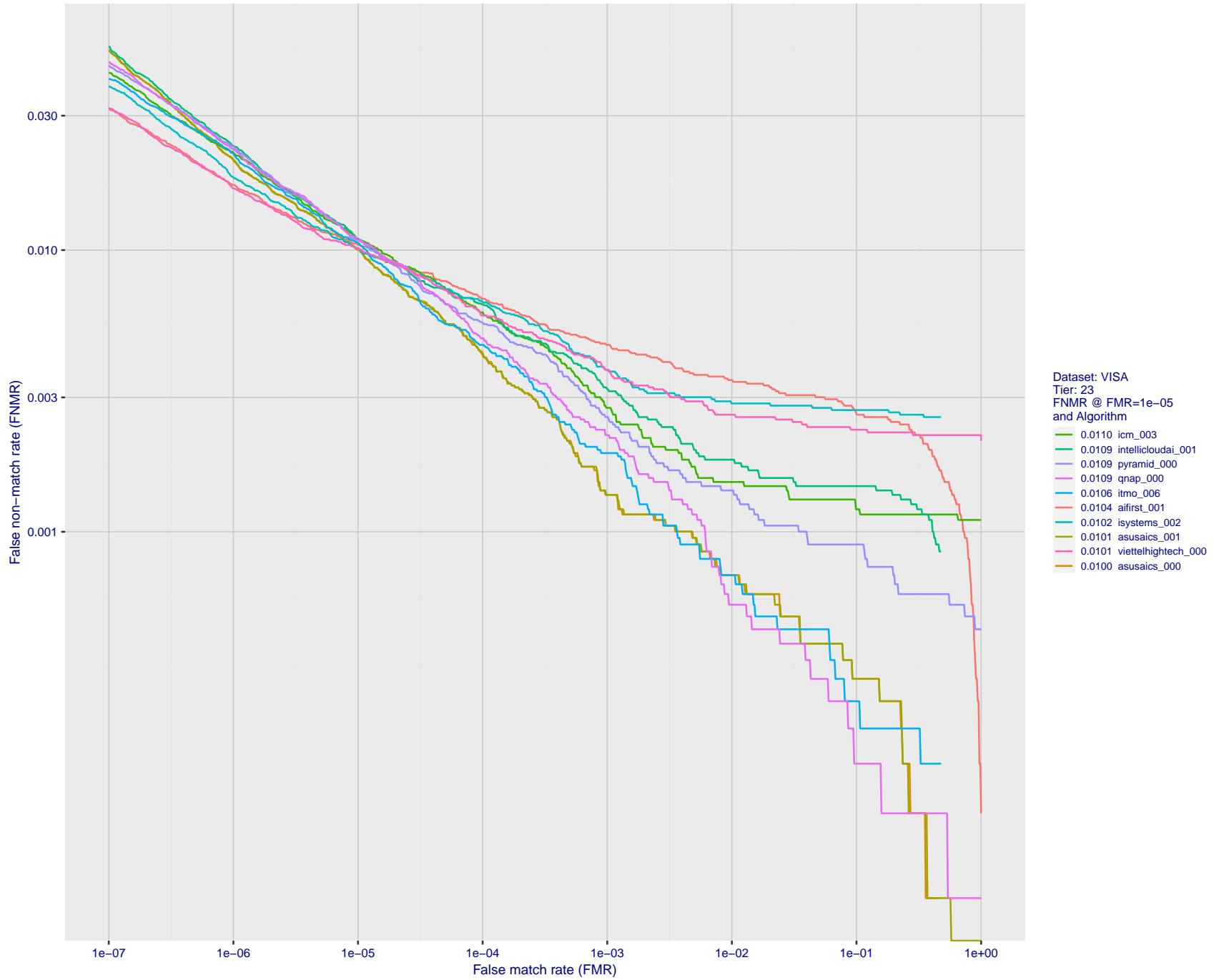


Figure 42: For the visa images, detection error tradeoff (DET) characteristics showing false non-match rate vs. false match rate plotted parametrically on threshold, T . The scales are logarithmic in order to show many decades of FMR.

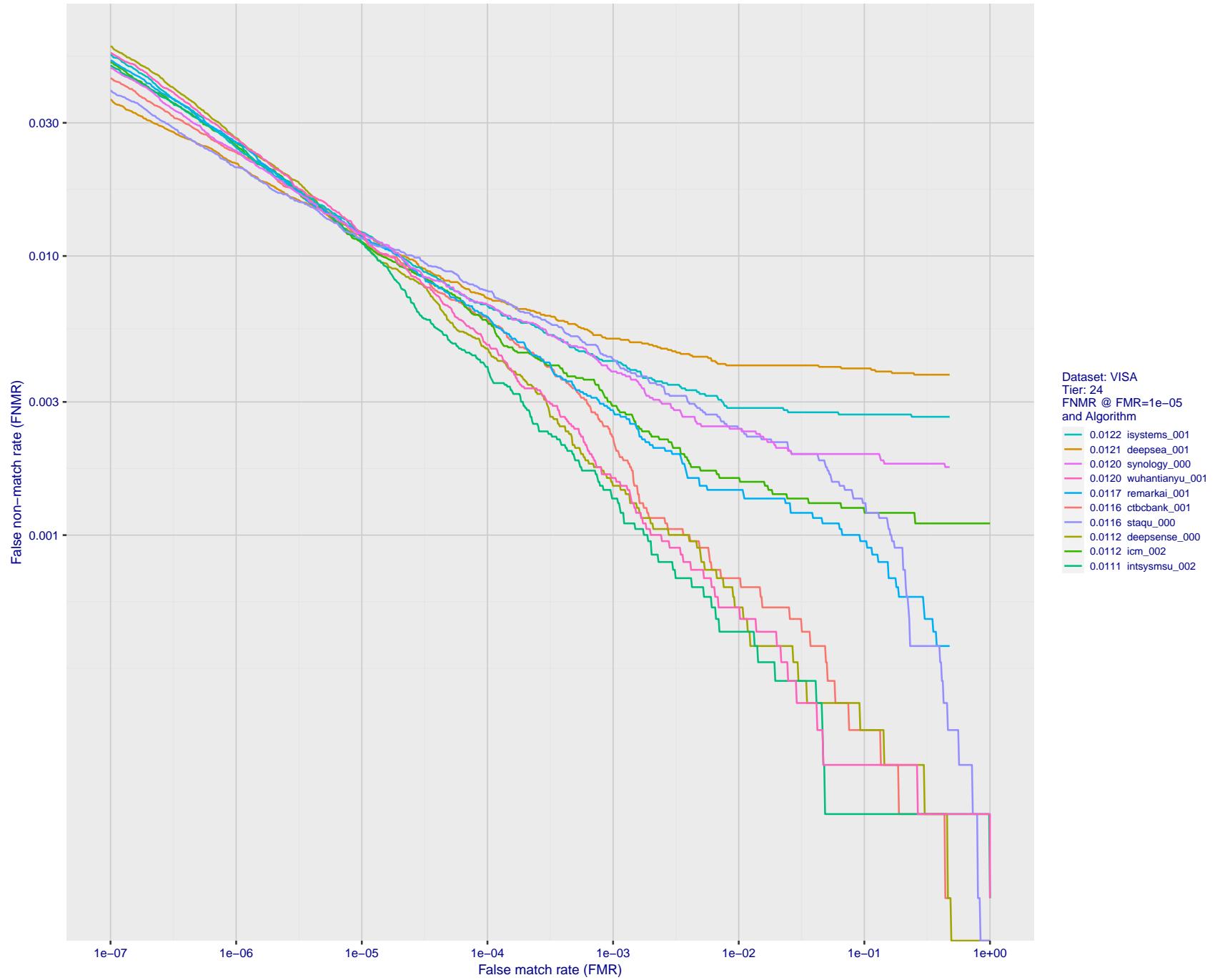


Figure 43: For the visa images, detection error tradeoff (DET) characteristics showing false non-match rate vs. false match rate plotted parametrically on threshold, T . The scales are logarithmic in order to show many decades of FMR.

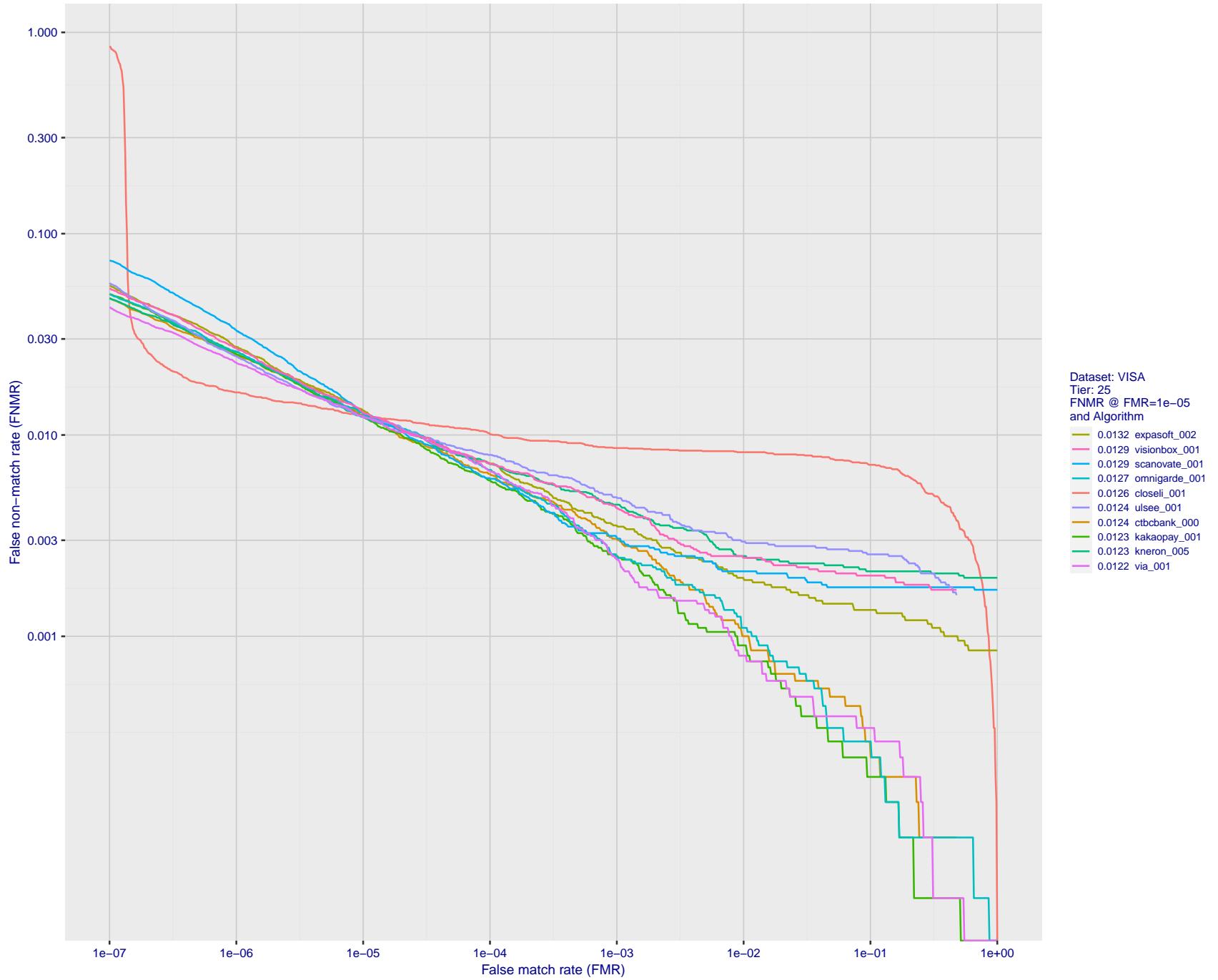


Figure 44: For the visa images, detection error tradeoff (DET) characteristics showing false non-match rate vs. false match rate plotted parametrically on threshold, T . The scales are logarithmic in order to show many decades of FMR.

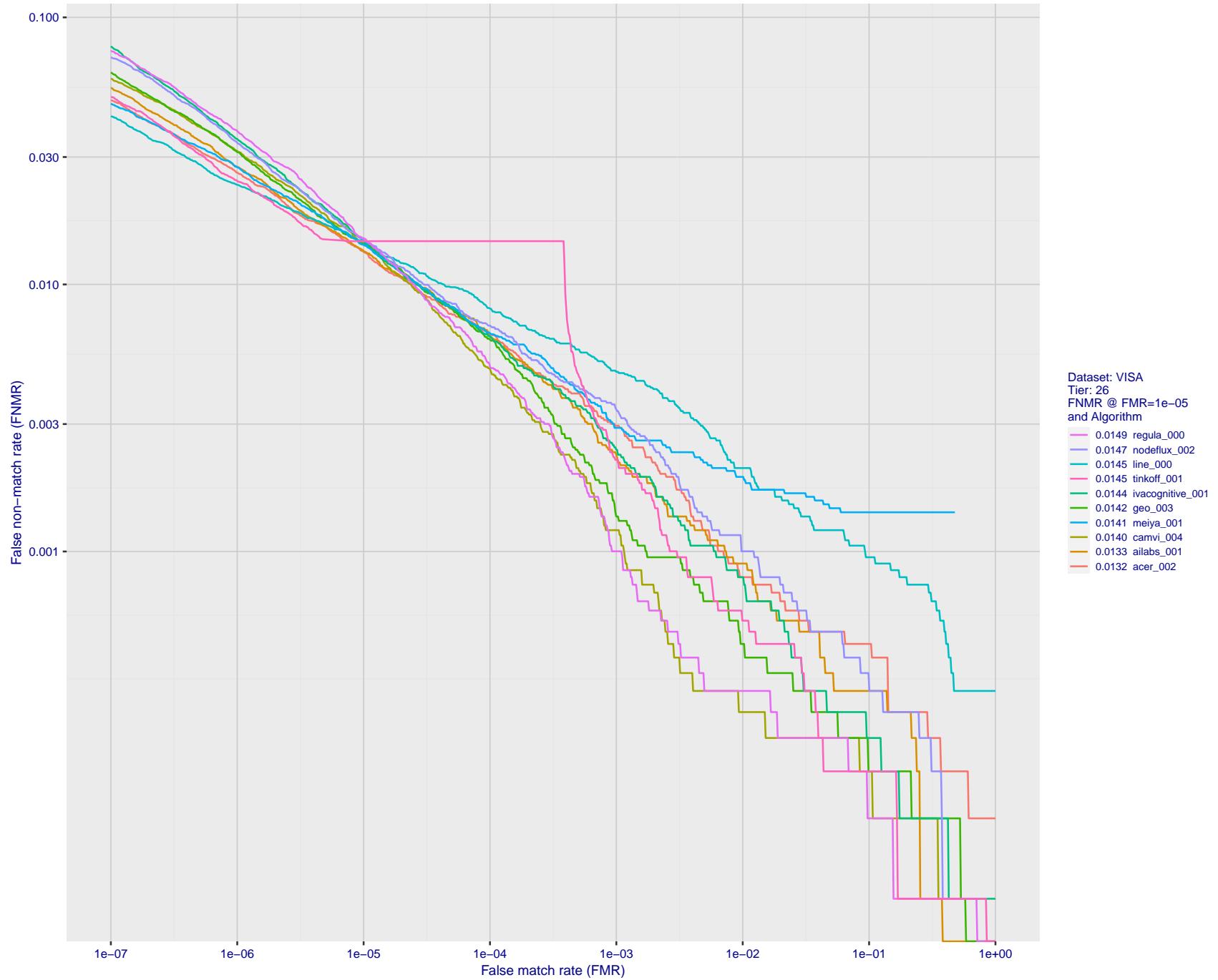


Figure 45: For the visa images, detection error tradeoff (DET) characteristics showing false non-match rate vs. false match rate plotted parametrically on threshold, T . The scales are logarithmic in order to show many decades of FMR.

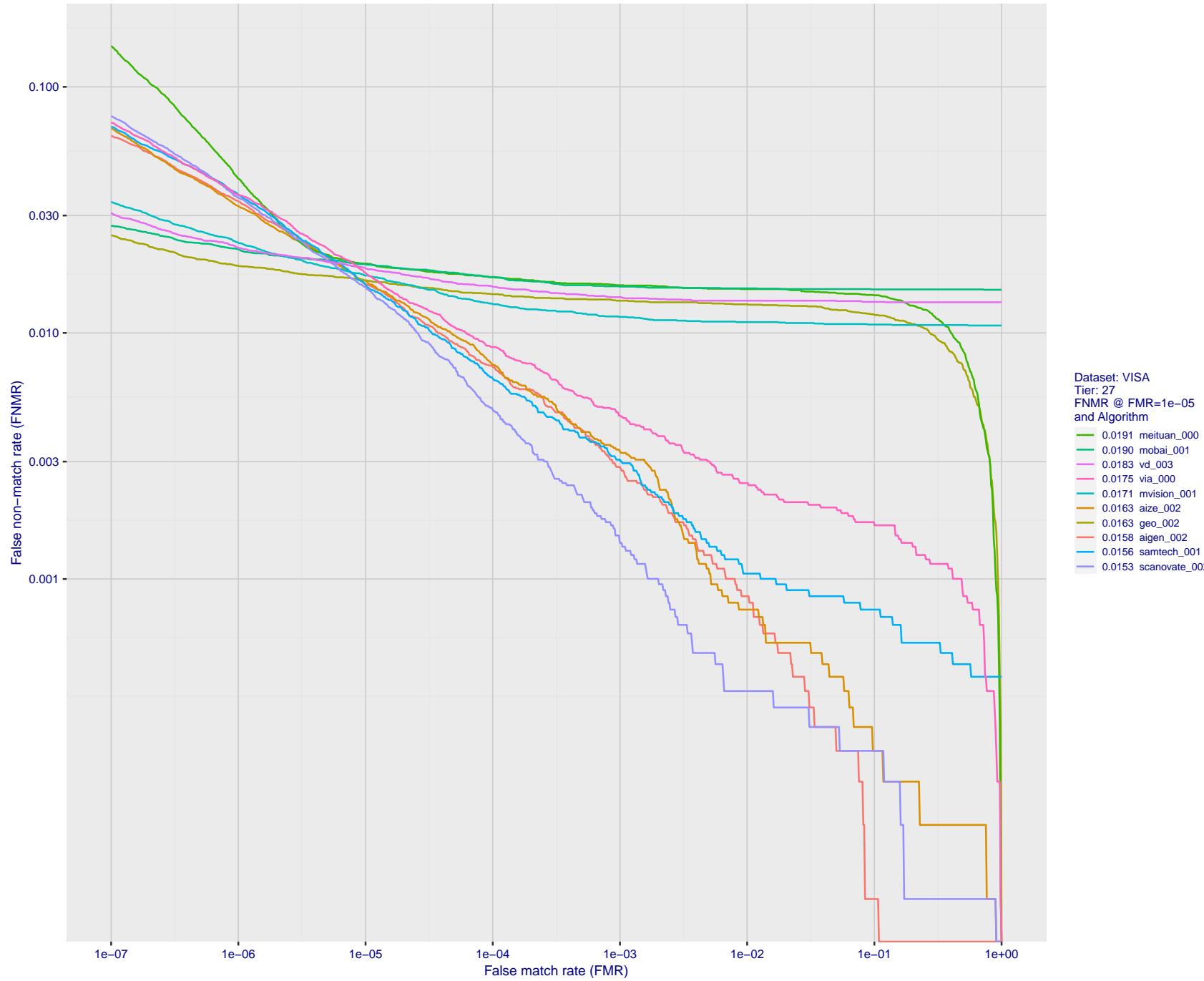


Figure 46: For the visa images, detection error tradeoff (DET) characteristics showing false non-match rate vs. false match rate plotted parametrically on threshold, T . The scales are logarithmic in order to show many decades of FMR.

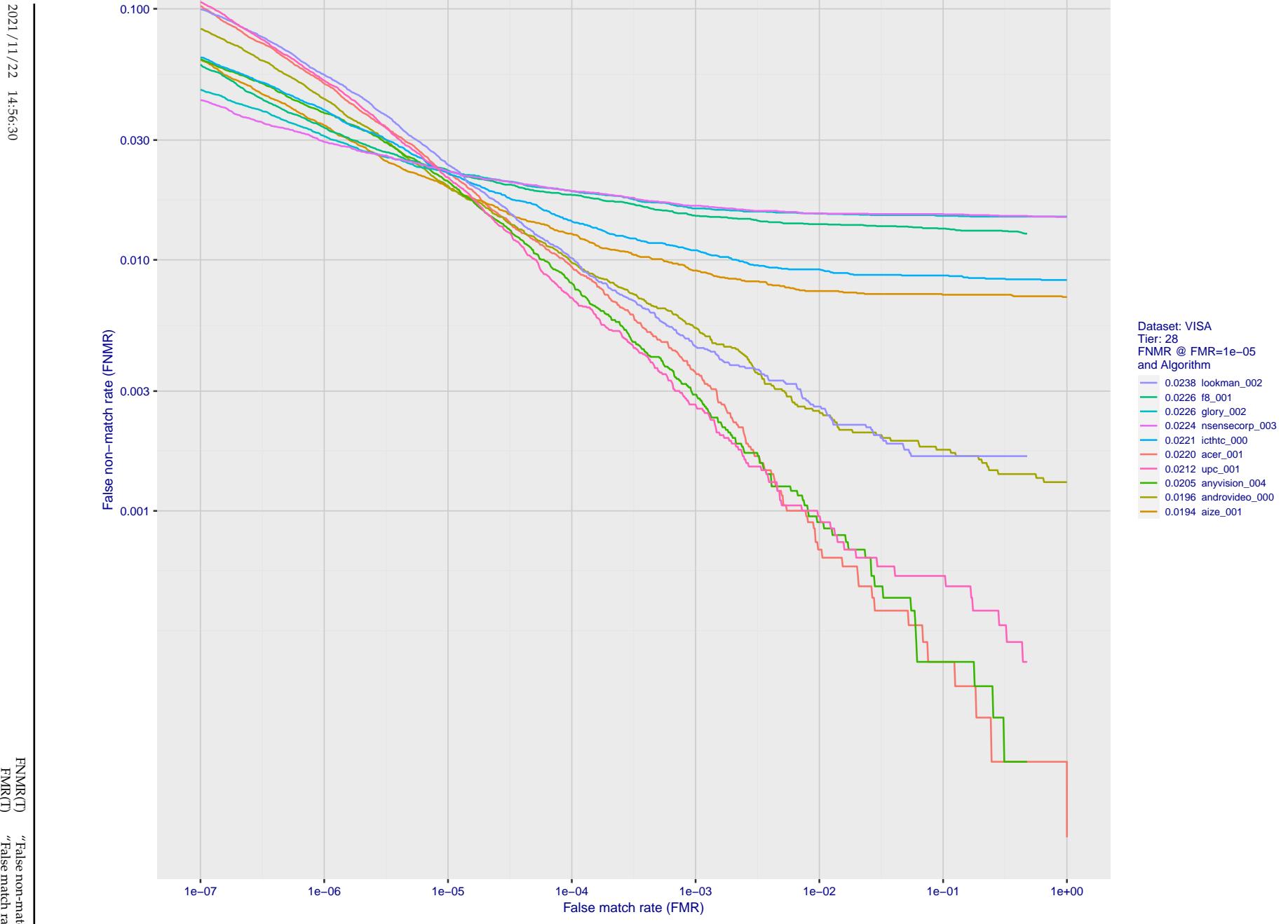


Figure 47: For the visa images, detection error tradeoff (DET) characteristics showing false non-match rate vs. false match rate plotted parametrically on threshold, T . The scales are logarithmic in order to show many decades of FMR.

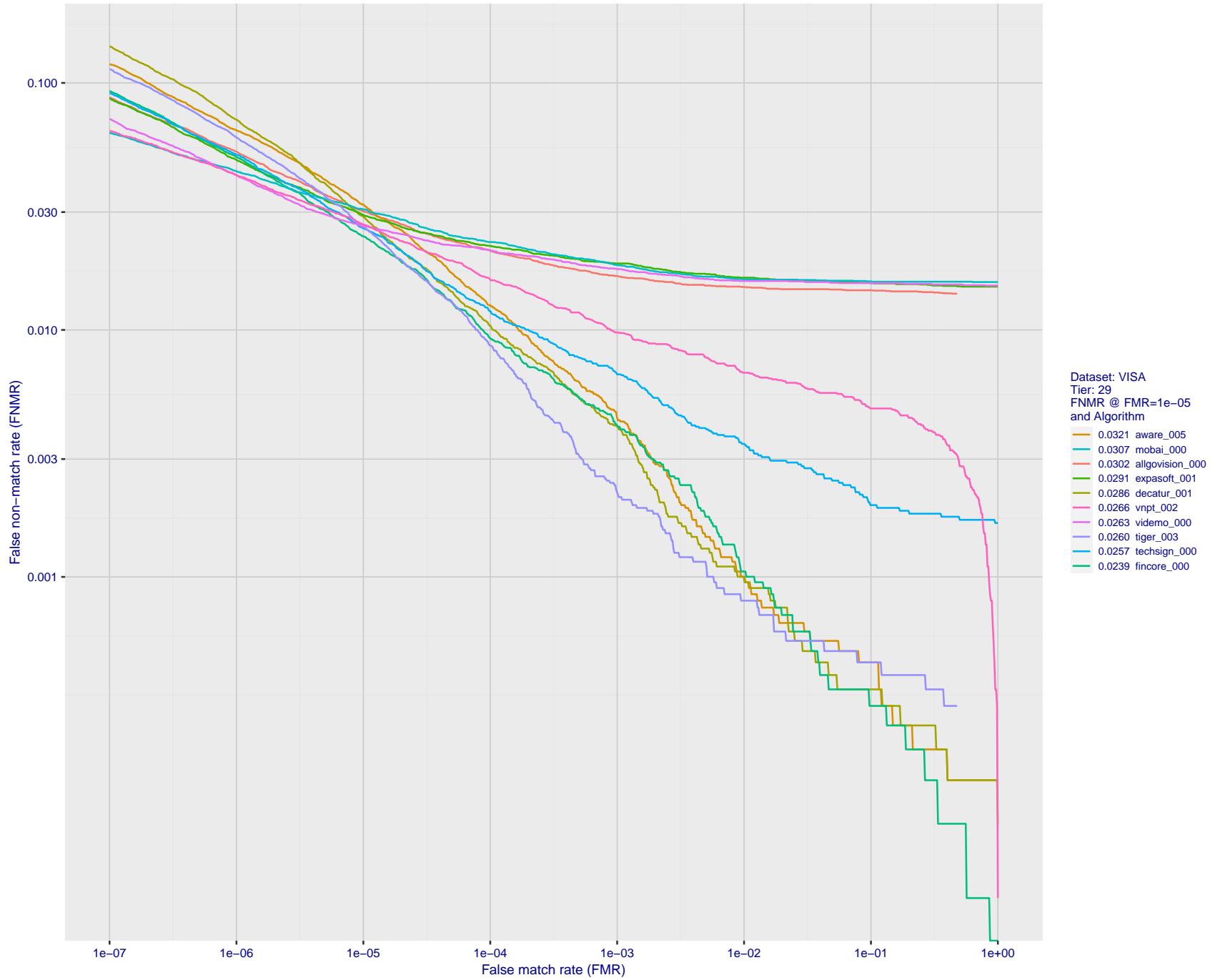


Figure 48: For the visa images, detection error tradeoff (DET) characteristics showing false non-match rate vs. false match rate plotted parametrically on threshold, T . The scales are logarithmic in order to show many decades of FMR.

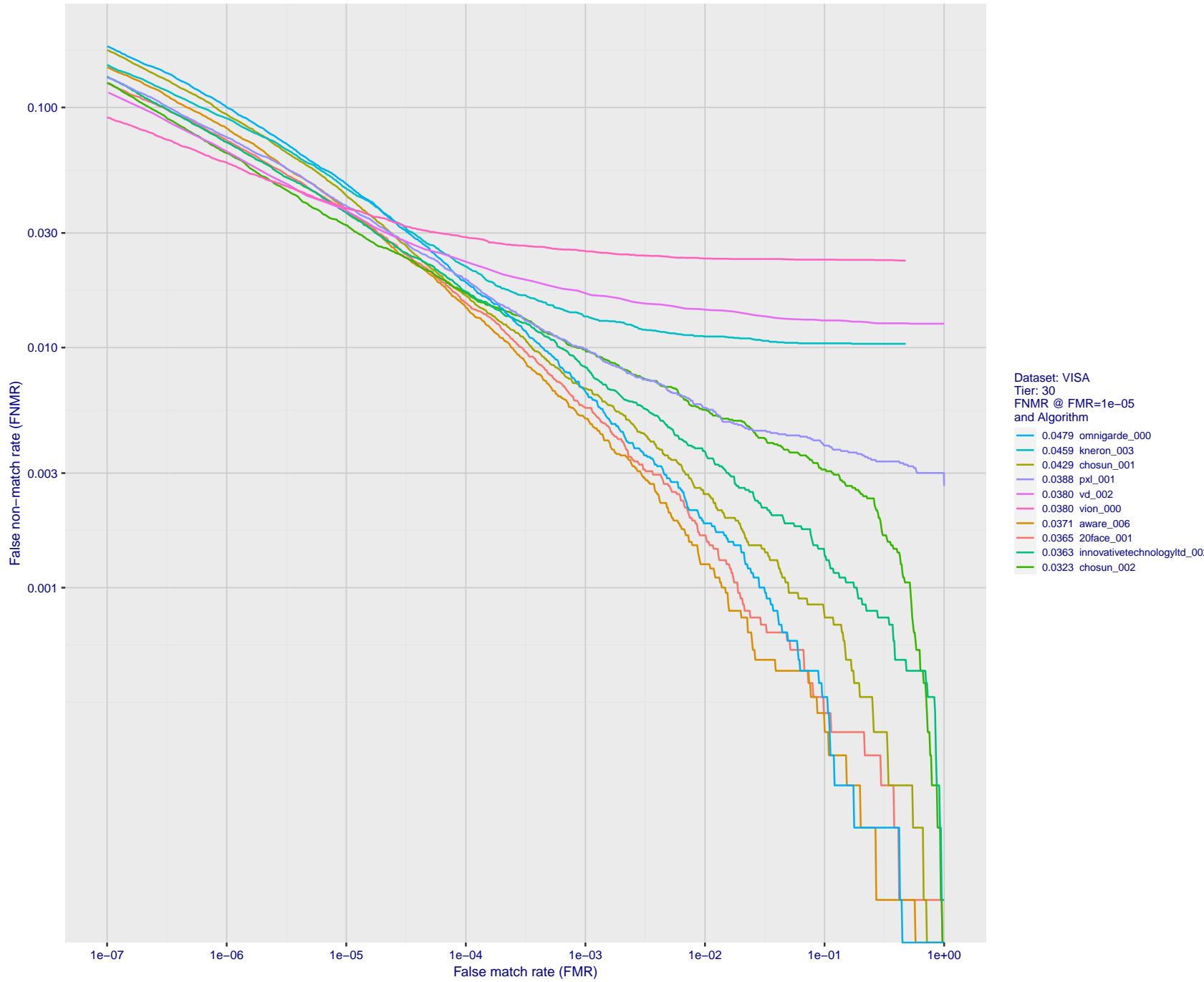


Figure 49: For the visa images, detection error tradeoff (DET) characteristics showing false non-match rate vs. false match rate plotted parametrically on threshold, T . The scales are logarithmic in order to show many decades of FMR.

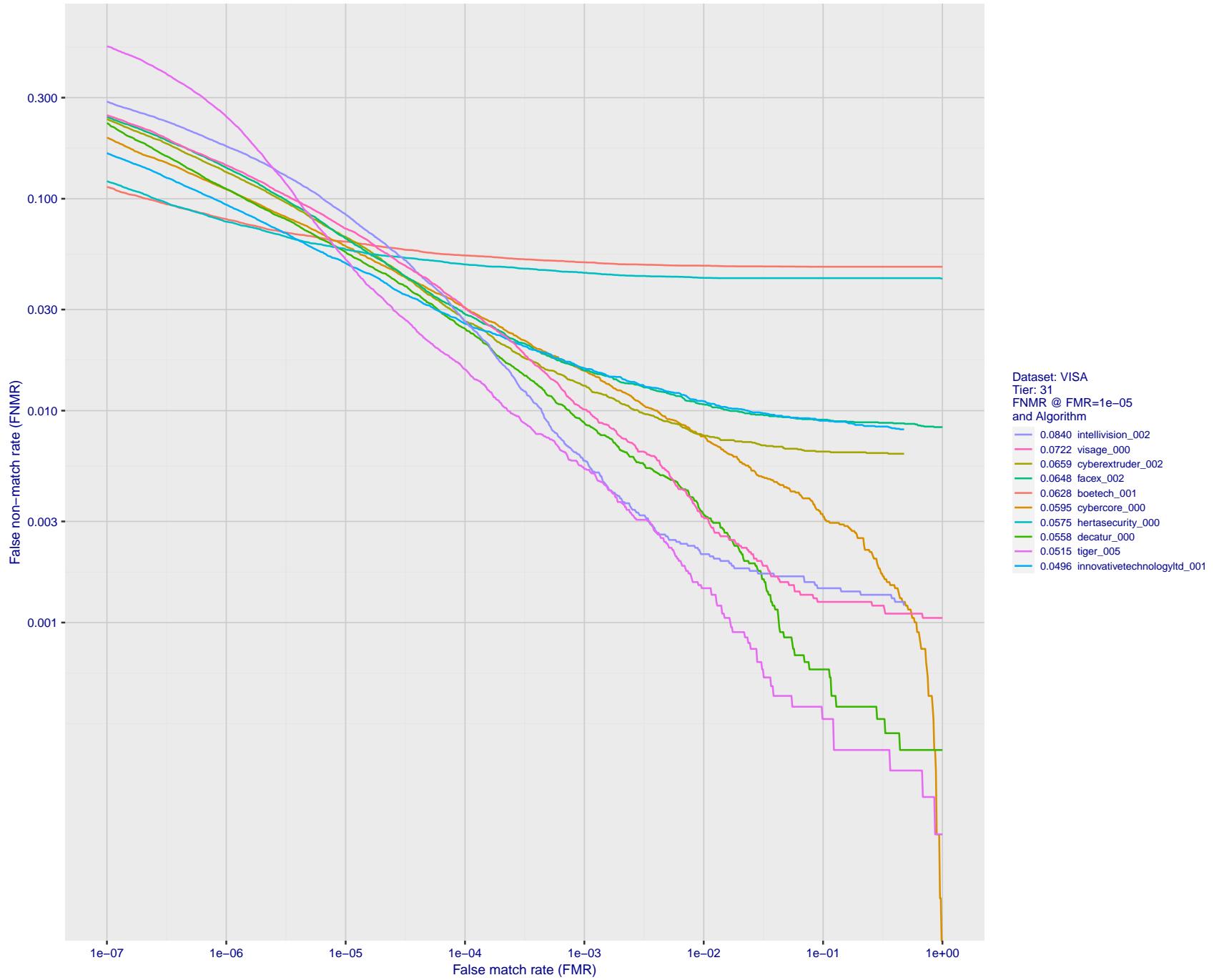


Figure 50: For the visa images, detection error tradeoff (DET) characteristics showing false non-match rate vs. false match rate plotted parametrically on threshold, T . The scales are logarithmic in order to show many decades of FMR.

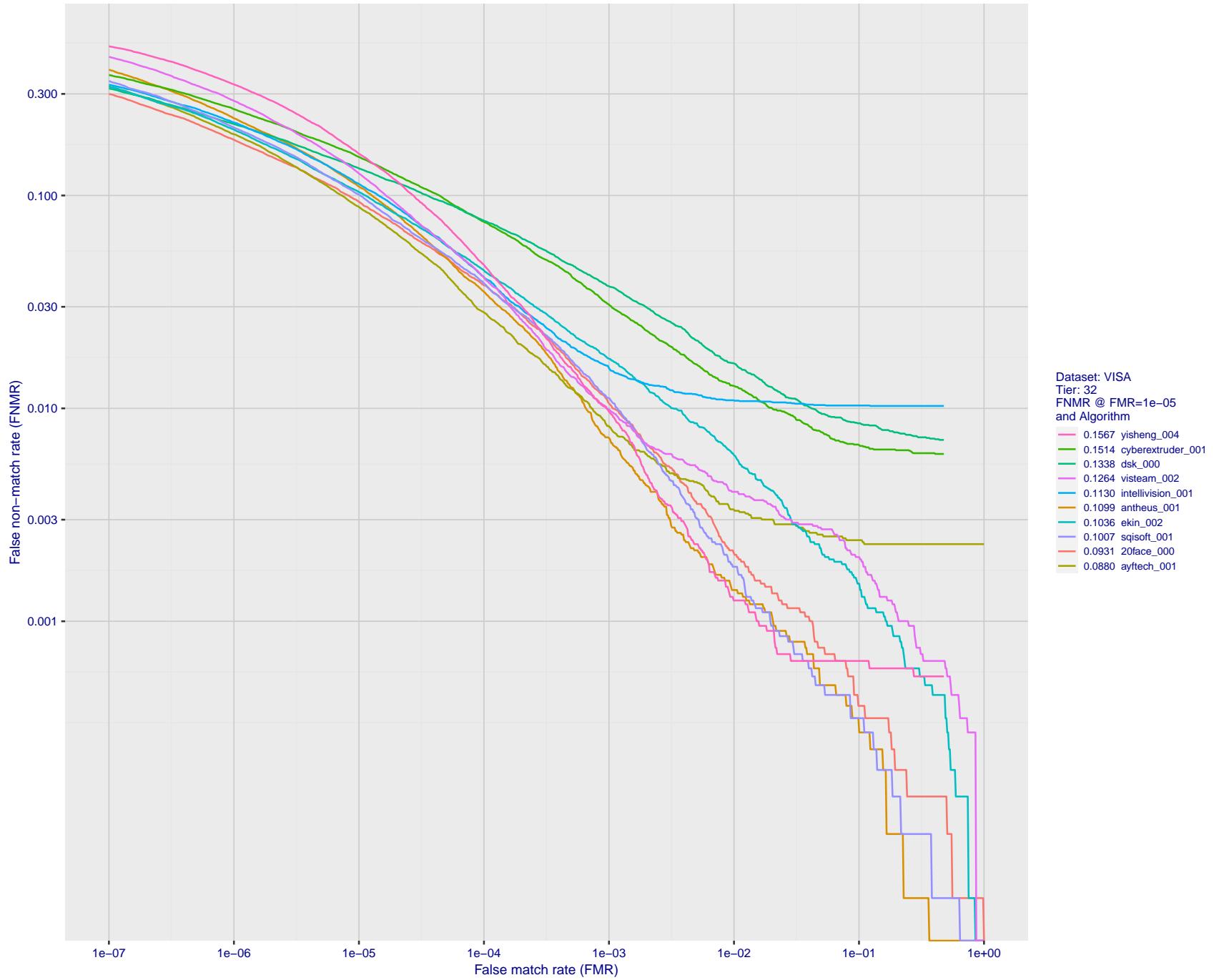


Figure 51: For the visa images, detection error tradeoff (DET) characteristics showing false non-match rate vs. false match rate plotted parametrically on threshold, T . The scales are logarithmic in order to show many decades of FMR.

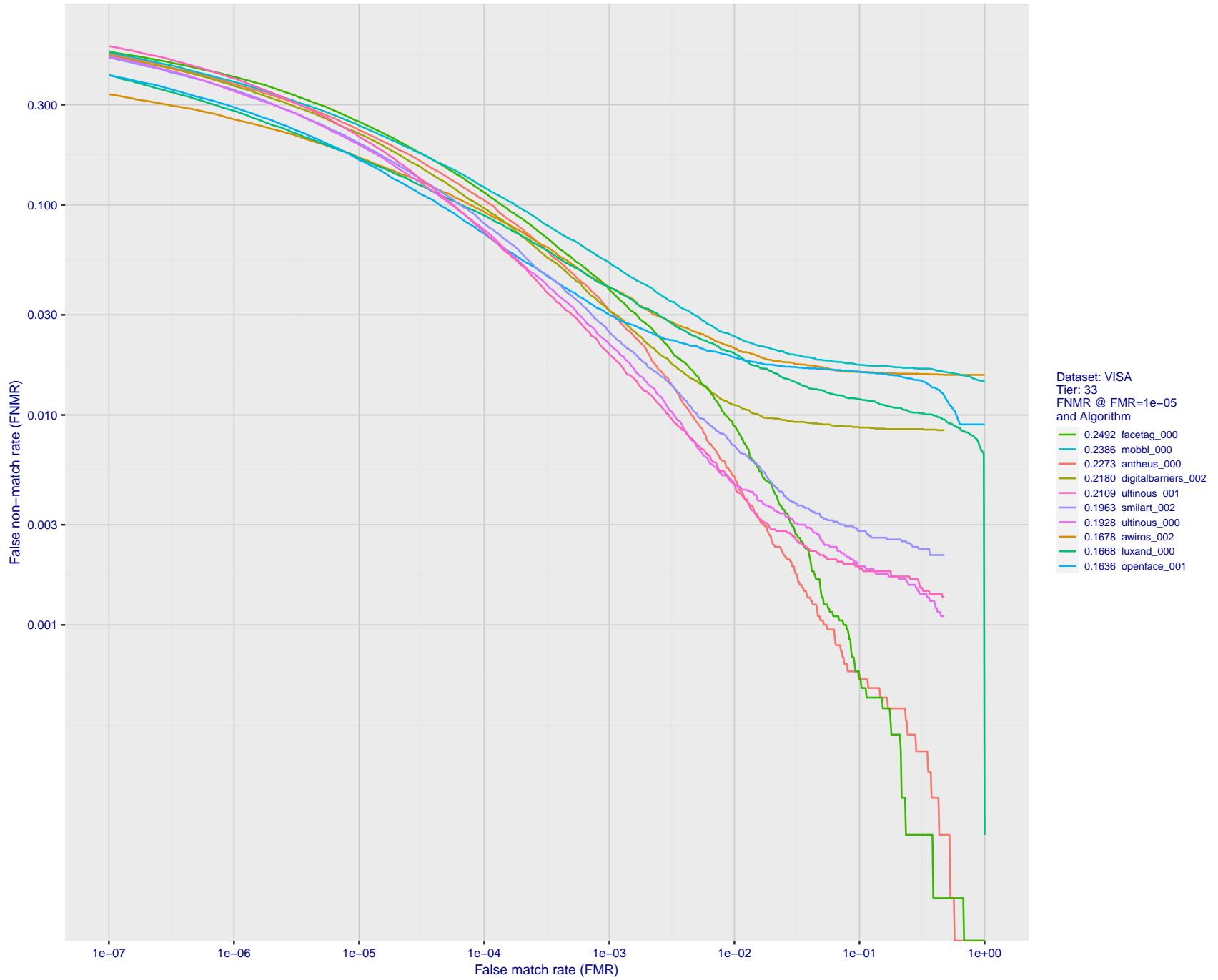


Figure 52: For the visa images, detection error tradeoff (DET) characteristics showing false non-match rate vs. false match rate plotted parametrically on threshold, T . The scales are logarithmic in order to show many decades of FMR.

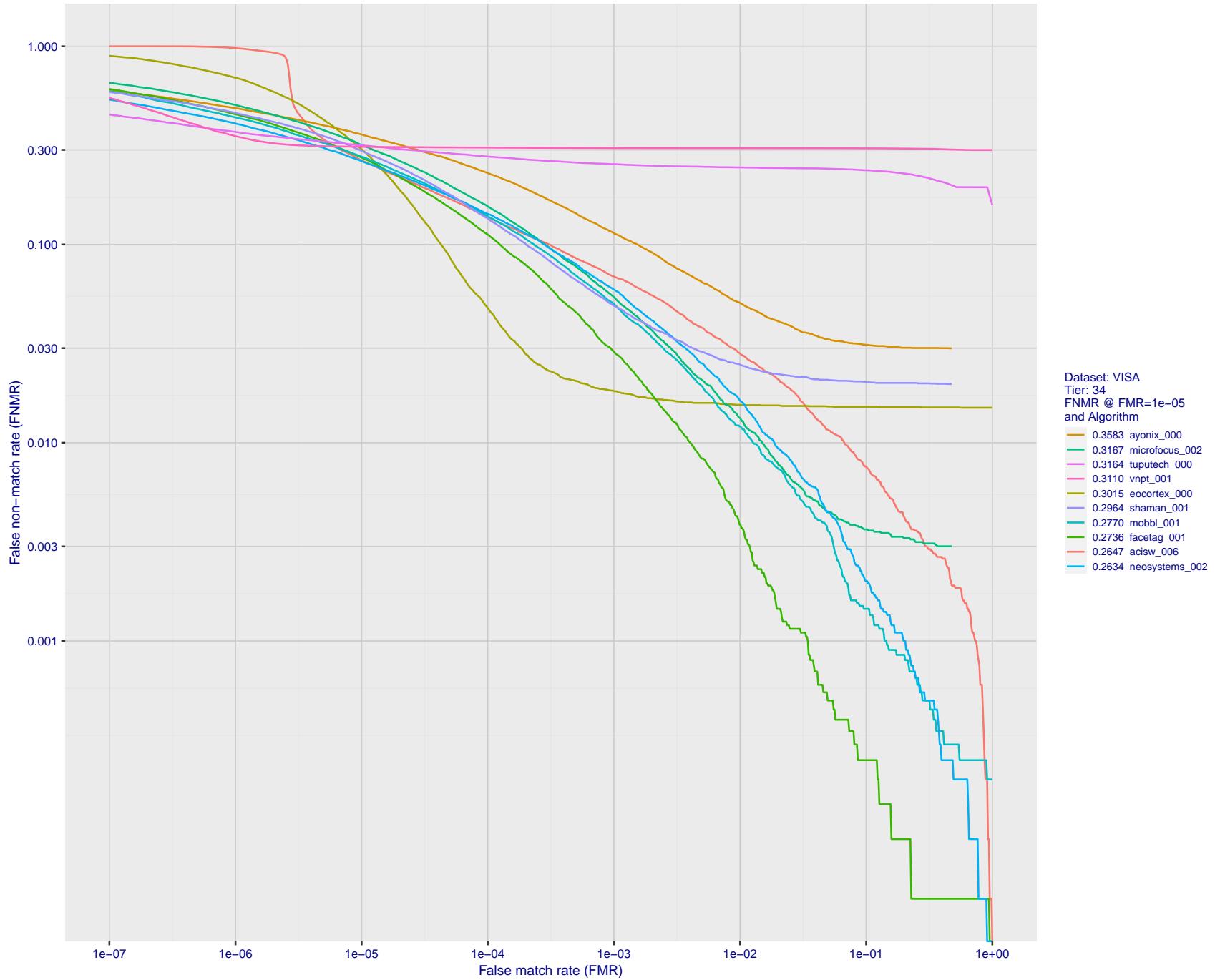


Figure 53: For the visa images, detection error tradeoff (DET) characteristics showing false non-match rate vs. false match rate plotted parametrically on threshold, T . The scales are logarithmic in order to show many decades of FMR.

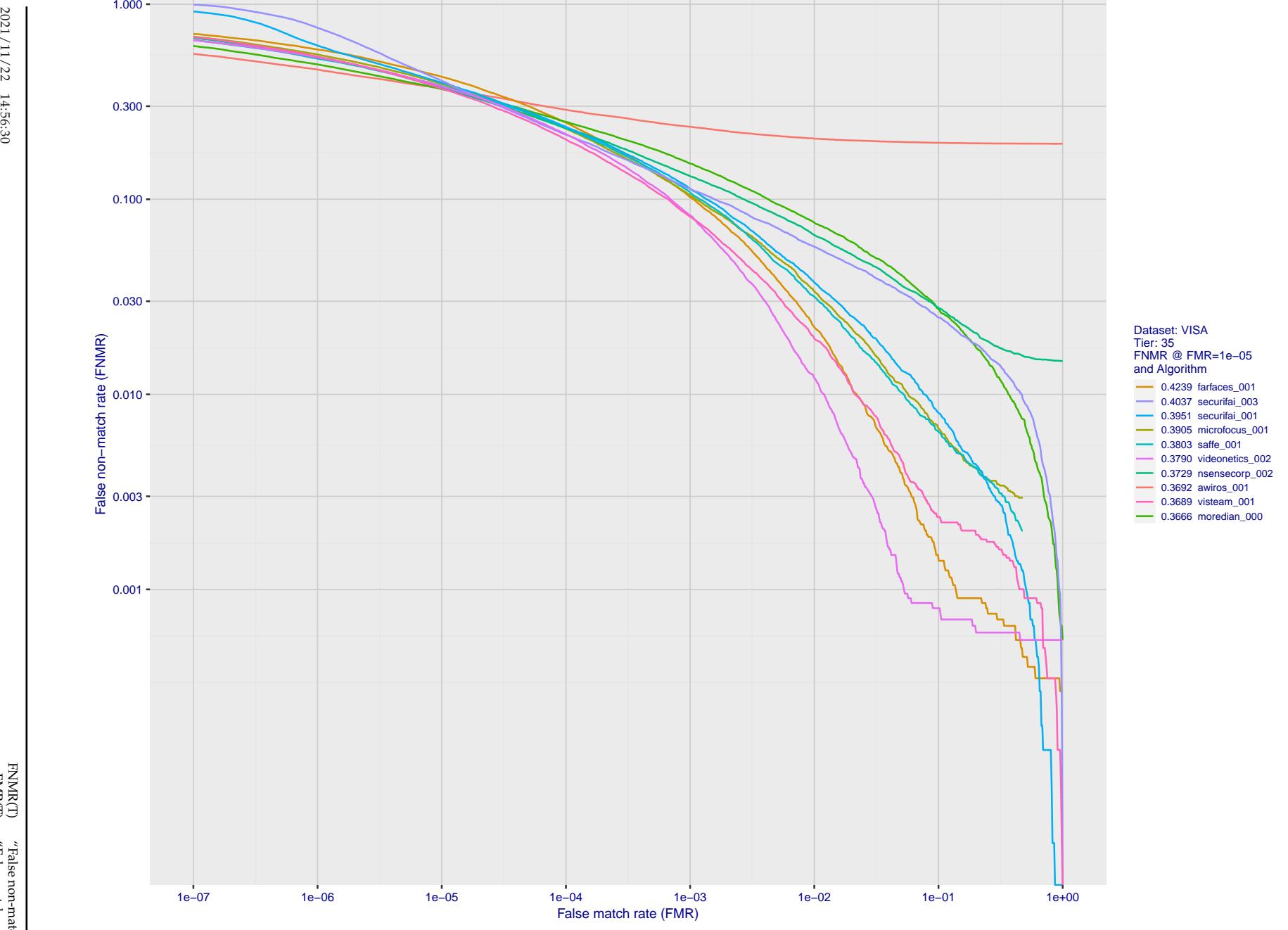


Figure 54: For the visa images, detection error tradeoff (DET) characteristics showing false non-match rate vs. false match rate plotted parametrically on threshold, T . The scales are logarithmic in order to show many decades of FMR.

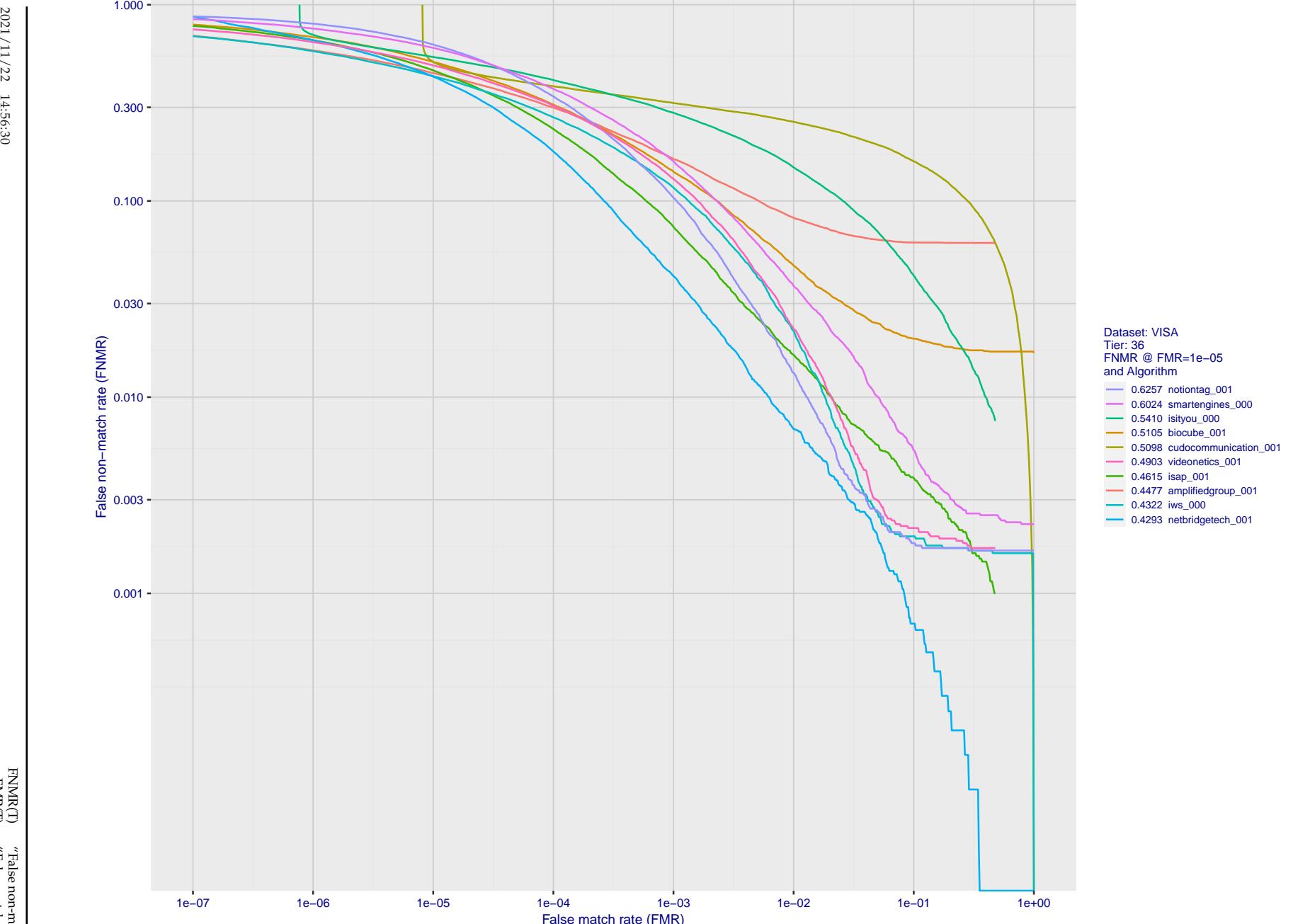


Figure 55: For the visa images, detection error tradeoff (DET) characteristics showing false non-match rate vs. false match rate plotted parametrically on threshold, T . The scales are logarithmic in order to show many decades of FMR.

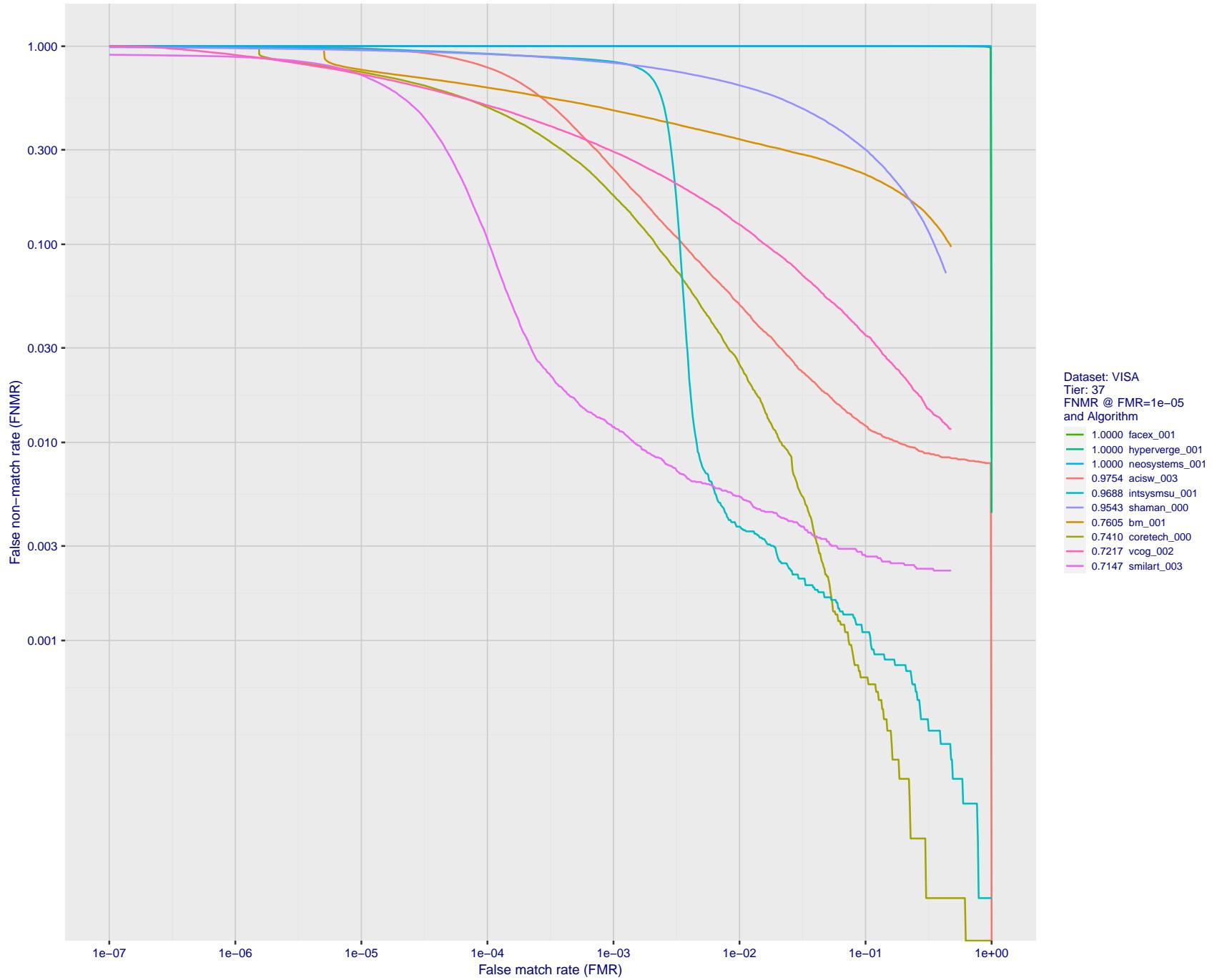


Figure 56: For the visa images, detection error tradeoff (DET) characteristics showing false non-match rate vs. false match rate plotted parametrically on threshold, T . The scales are logarithmic in order to show many decades of FMR.

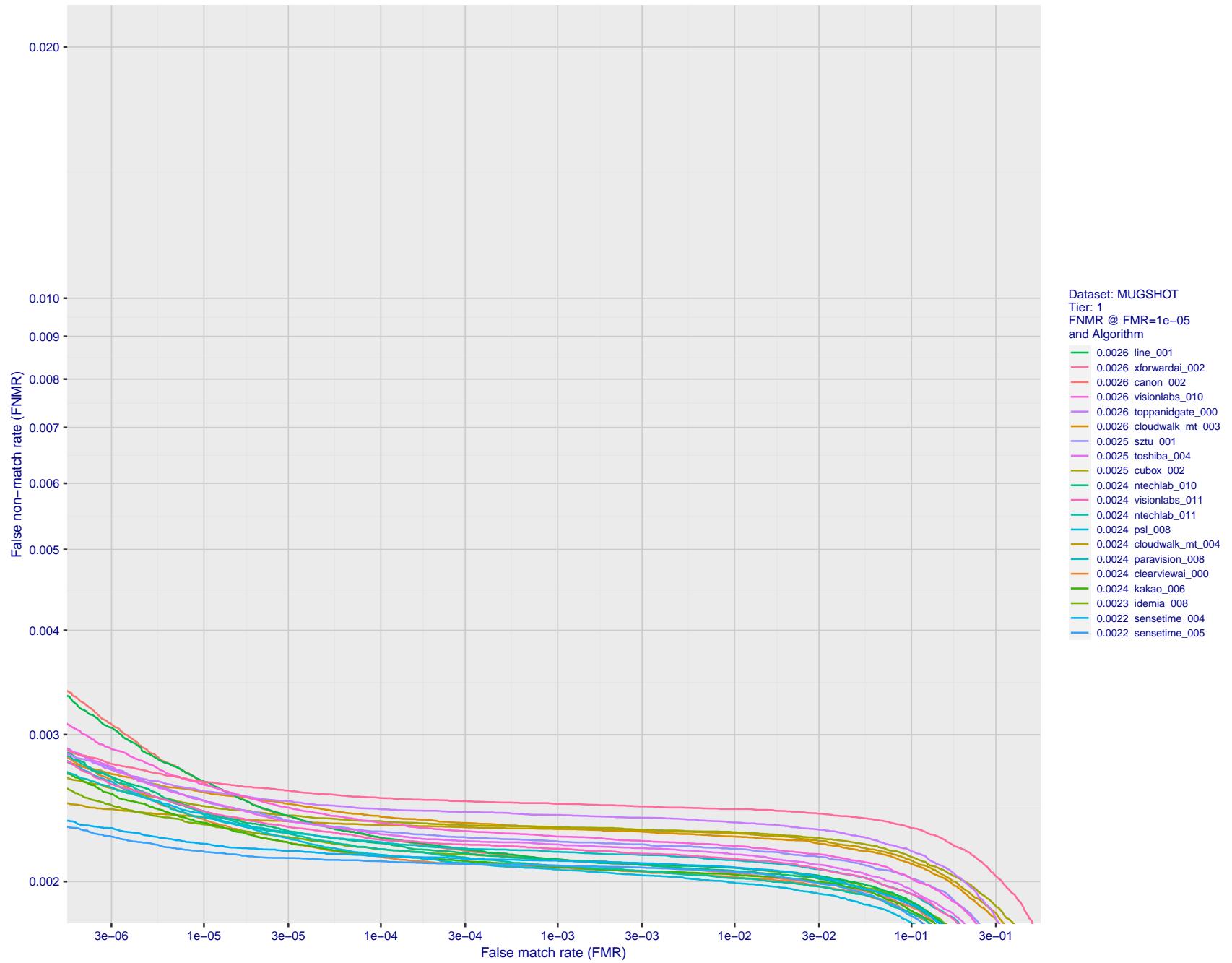


Figure 57: For the mugshot images, detection error tradeoff (DET) characteristics showing false non-match rate vs. false match rate plotted parametrically on threshold, T . The scales are logarithmic in order to show decades of FMR.

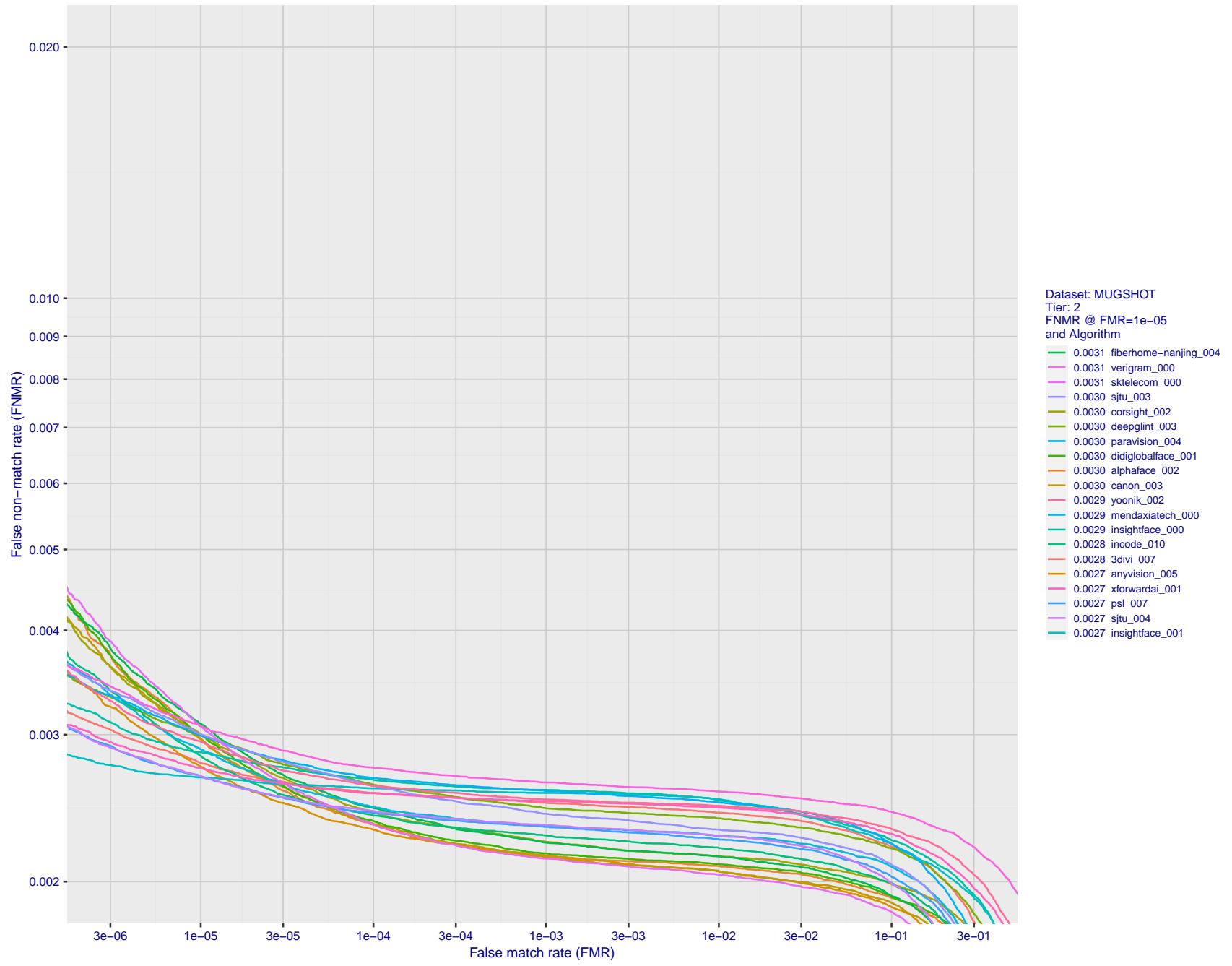


Figure 58: For the mugshot images, detection error tradeoff (DET) characteristics showing false non-match rate vs. false match rate plotted parametrically on threshold, T . The scales are logarithmic in order to show decades of FMR.

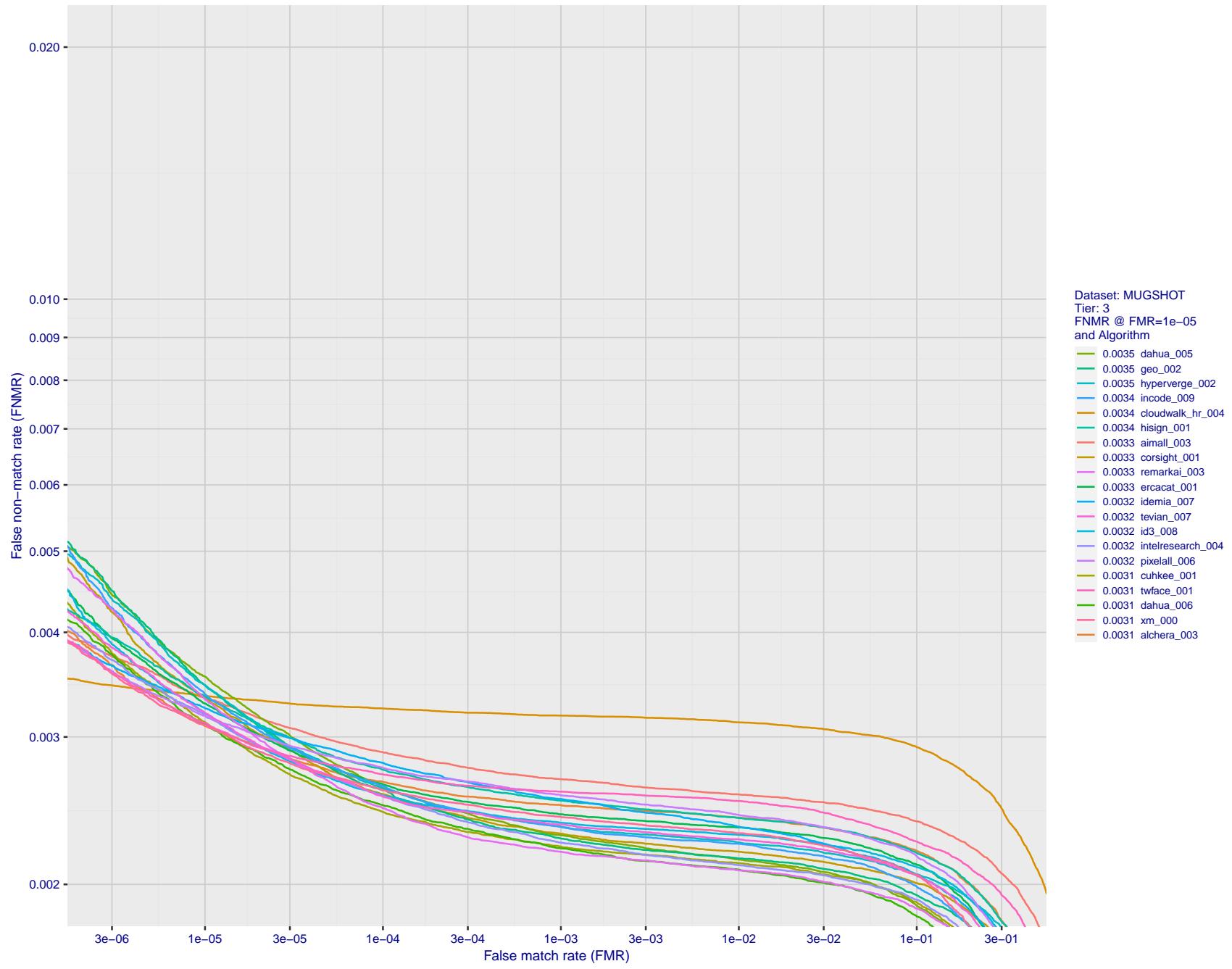


Figure 59: For the mugshot images, detection error tradeoff (DET) characteristics showing false non-match rate vs. false match rate plotted parametrically on threshold, T . The scales are logarithmic in order to show decades of FMR.

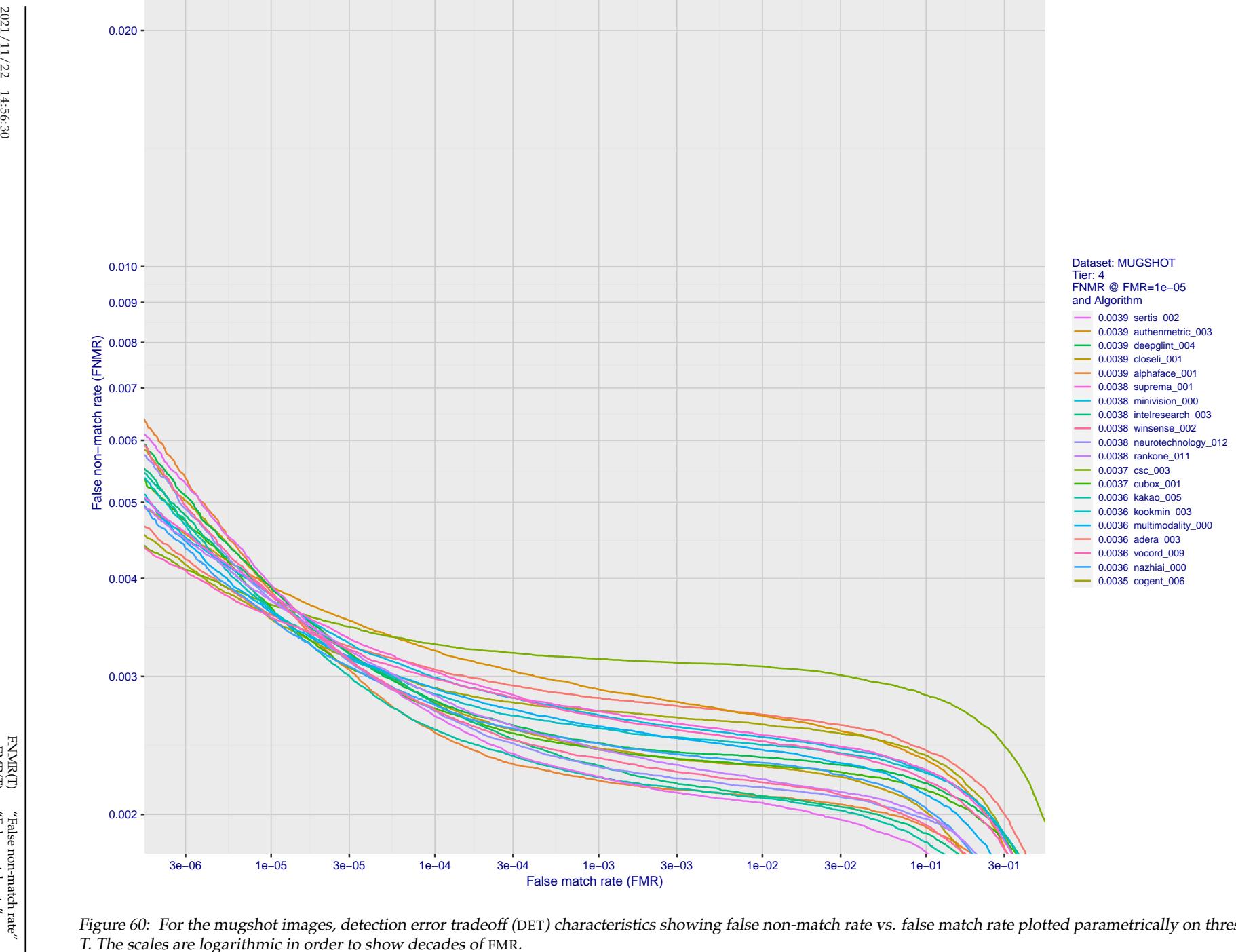


Figure 60: For the mugshot images, detection error tradeoff (DET) characteristics showing false non-match rate vs. false match rate plotted parametrically on threshold, T . The scales are logarithmic in order to show decades of FMR.

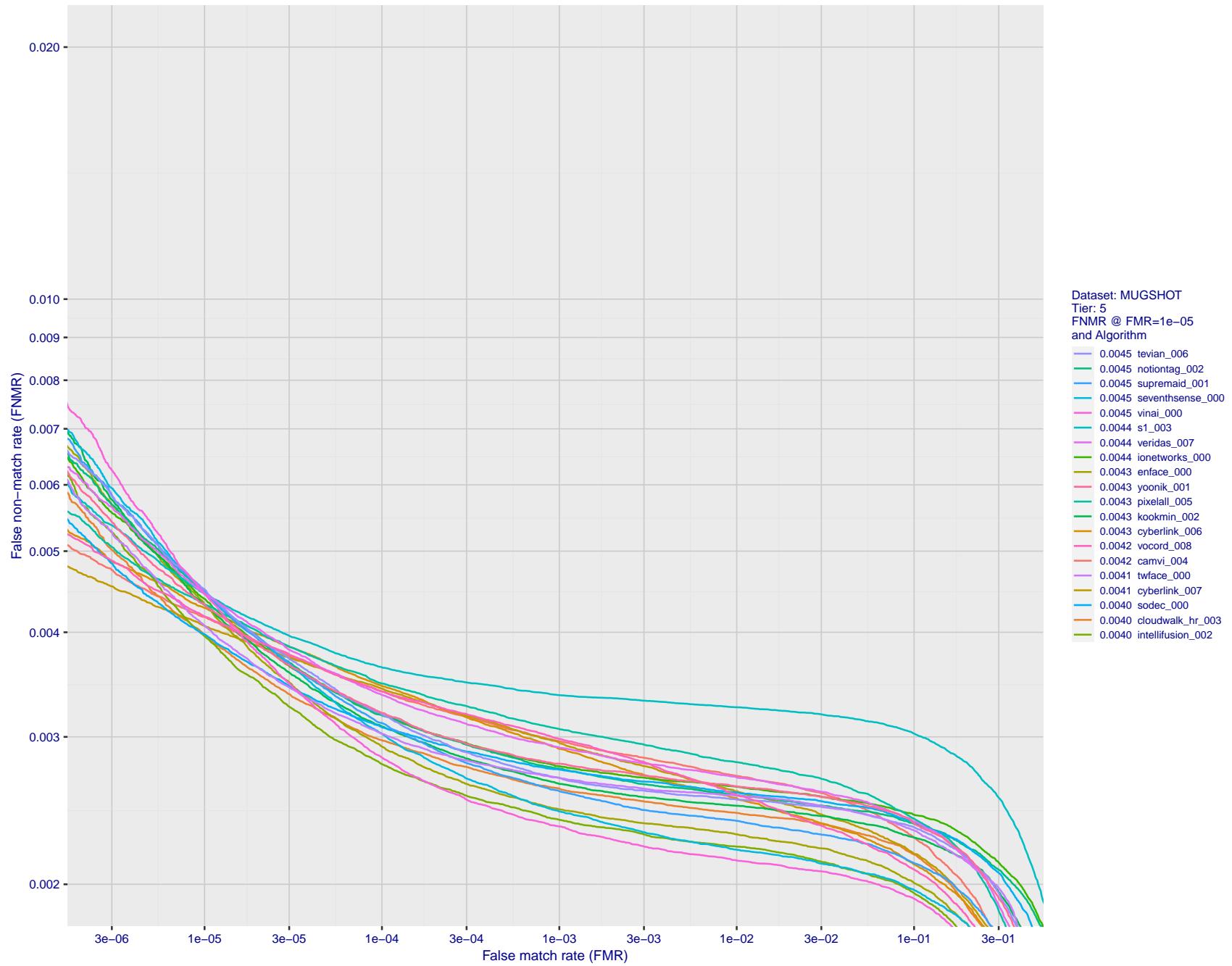


Figure 61: For the mugshot images, detection error tradeoff (DET) characteristics showing false non-match rate vs. false match rate plotted parametrically on threshold, T . The scales are logarithmic in order to show decades of FMR.

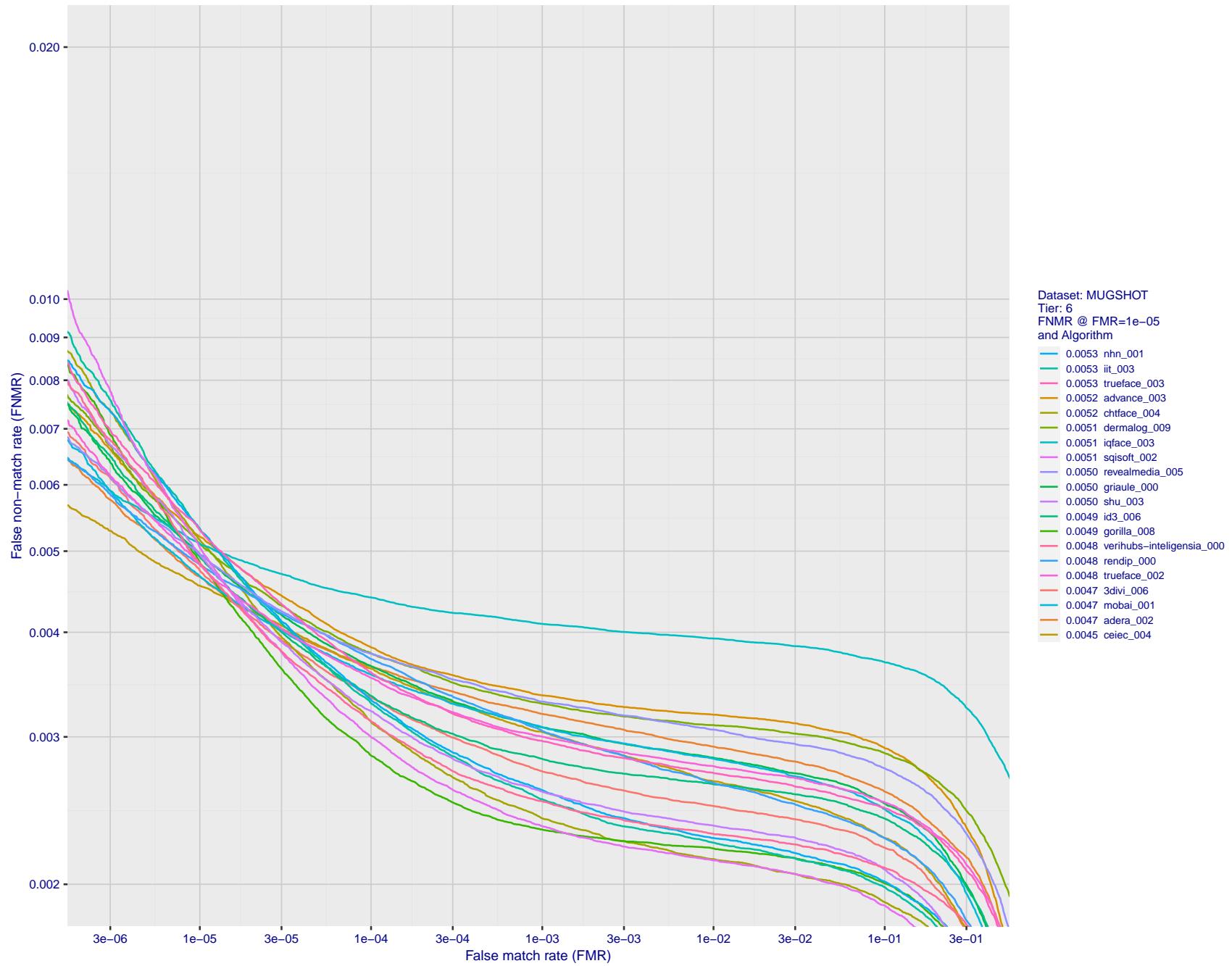


Figure 62: For the mugshot images, detection error tradeoff (DET) characteristics showing false non-match rate vs. false match rate plotted parametrically on threshold, T . The scales are logarithmic in order to show decades of FMR.

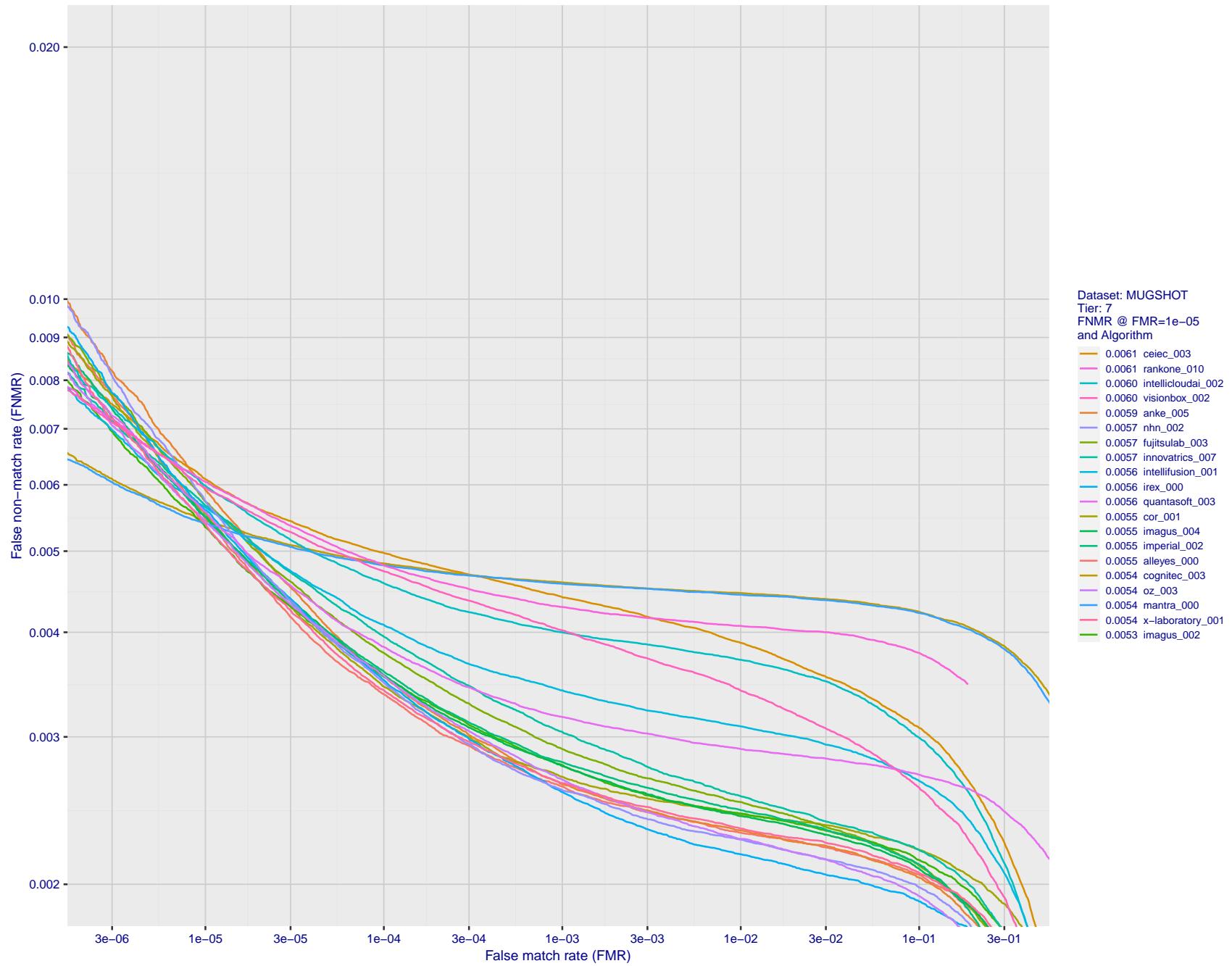
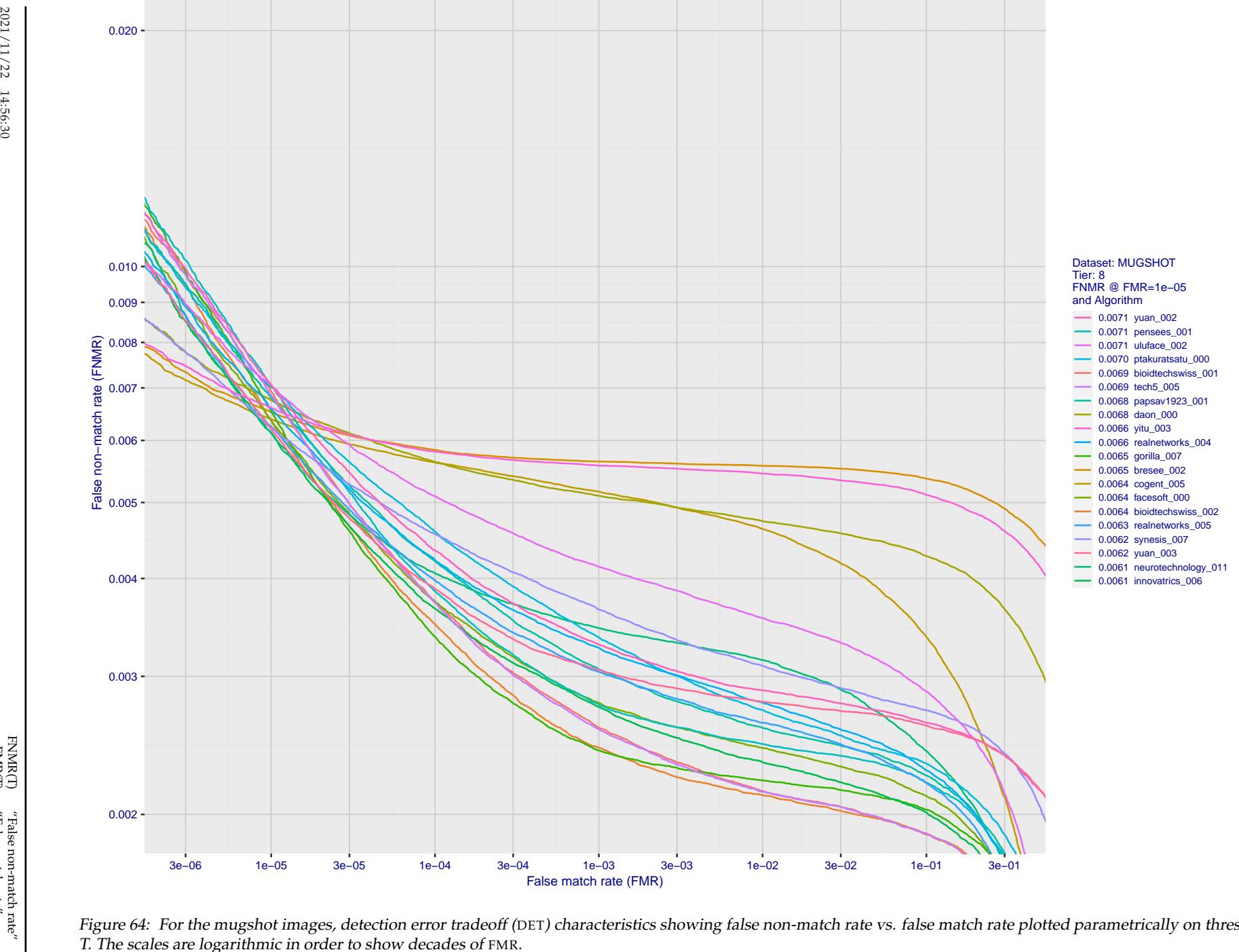


Figure 63: For the mugshot images, detection error tradeoff (DET) characteristics showing false non-match rate vs. false match rate plotted parametrically on threshold, T . The scales are logarithmic in order to show decades of FMR.



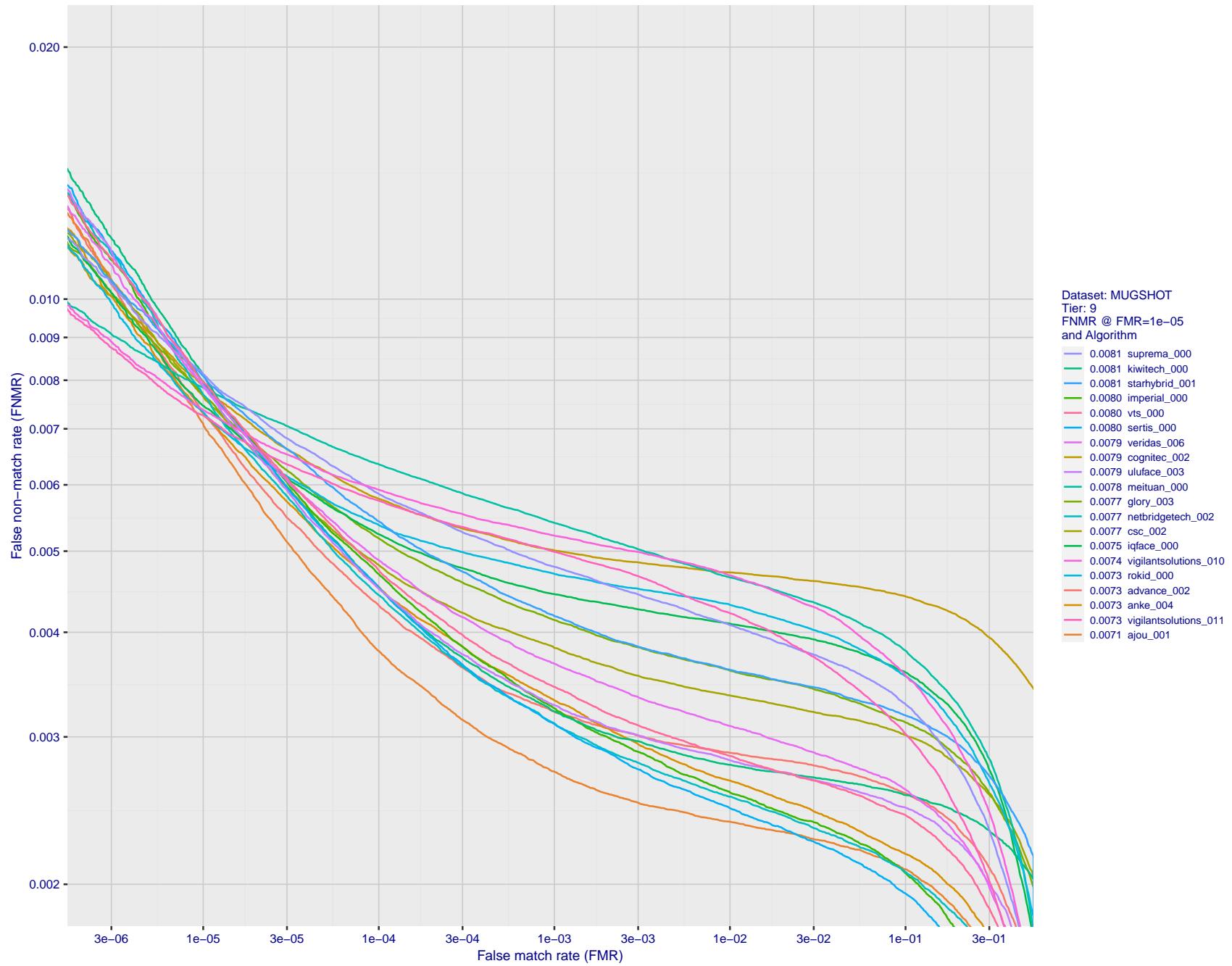


Figure 65: For the mugshot images, detection error tradeoff (DET) characteristics showing false non-match rate vs. false match rate plotted parametrically on threshold, T . The scales are logarithmic in order to show decades of FMR.

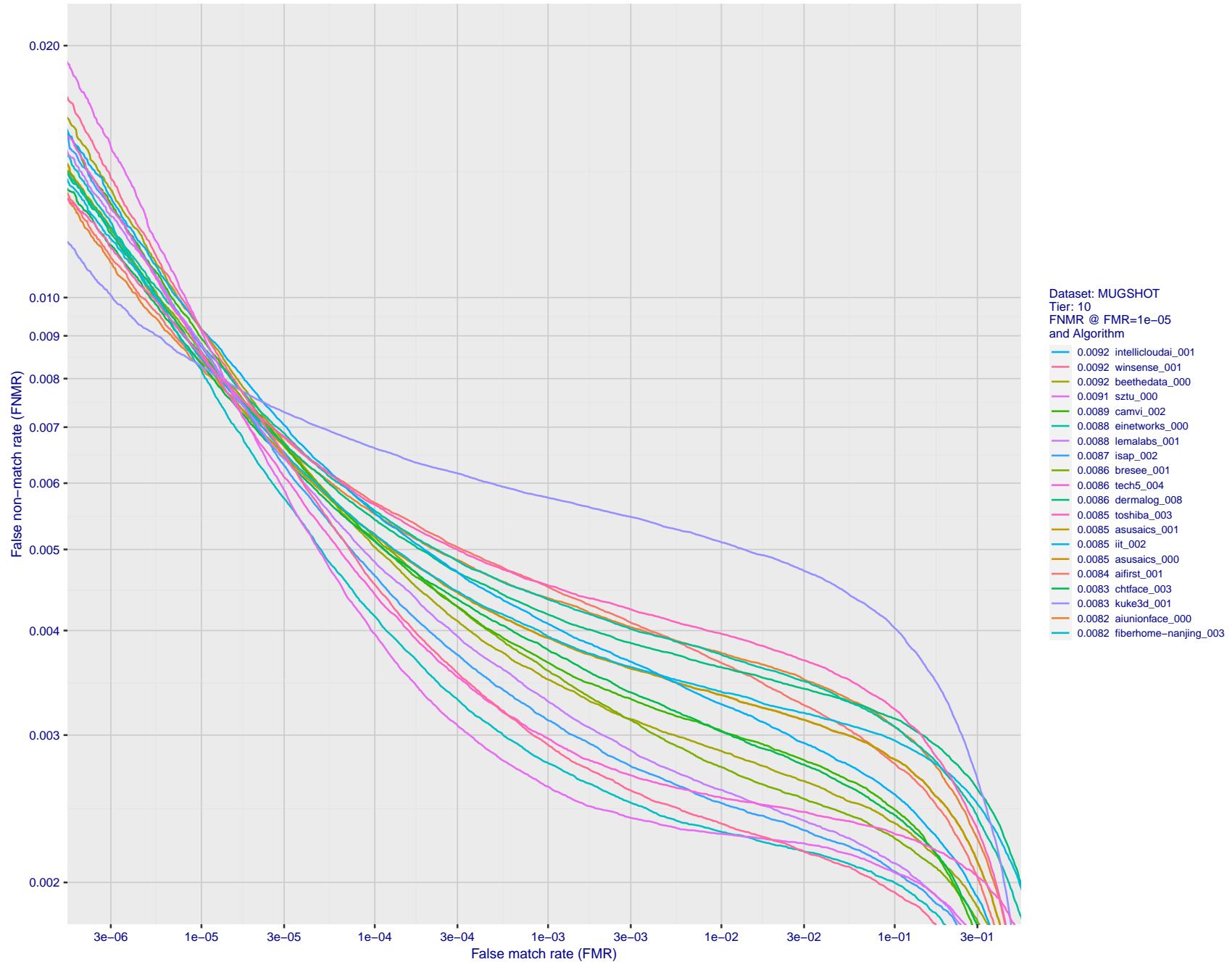


Figure 66: For the mugshot images, detection error tradeoff (DET) characteristics showing false non-match rate vs. false match rate plotted parametrically on threshold, T . The scales are logarithmic in order to show decades of FMR.

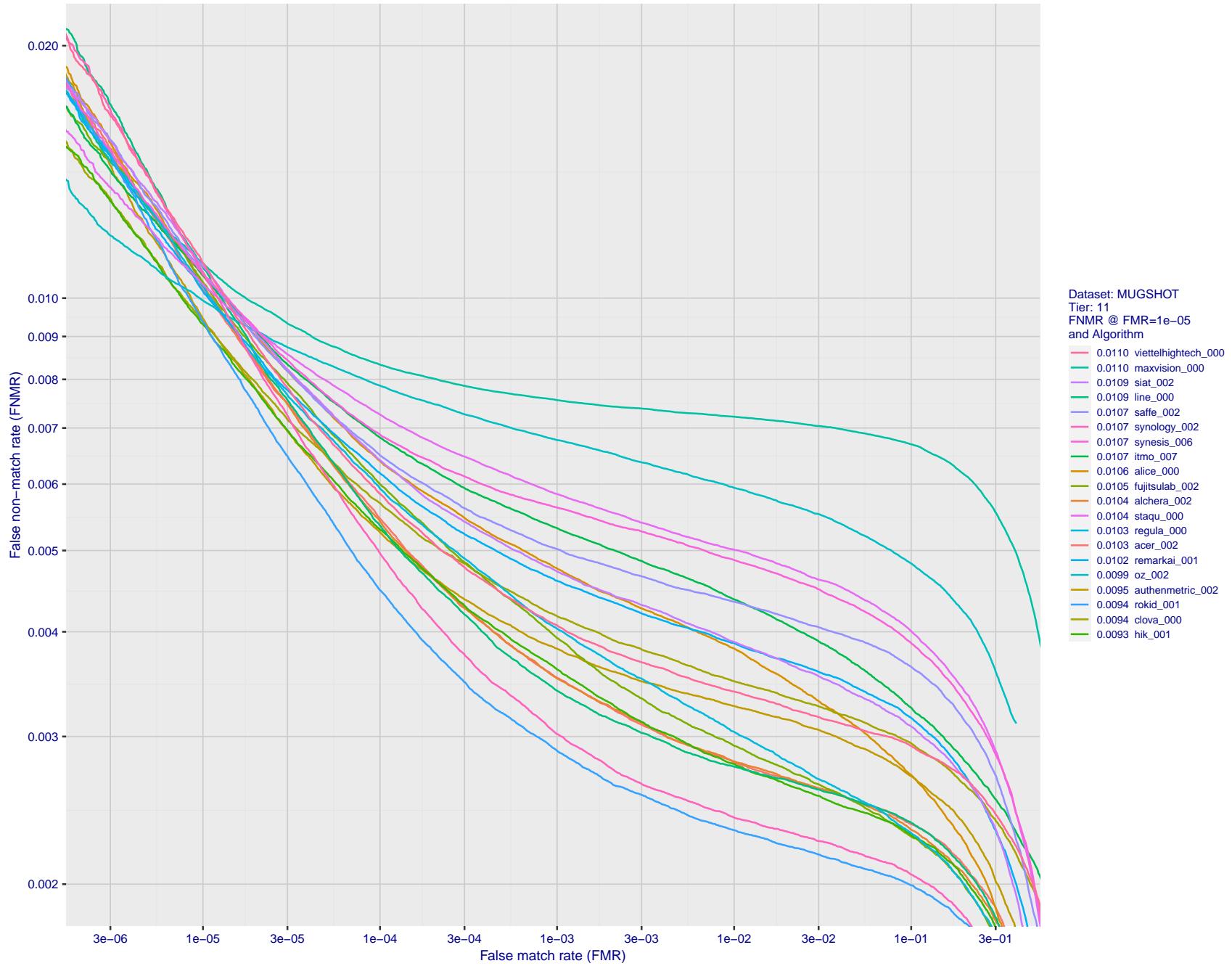


Figure 67: For the mugshot images, detection error tradeoff (DET) characteristics showing false non-match rate vs. false match rate plotted parametrically on threshold, T . The scales are logarithmic in order to show decades of FMR.

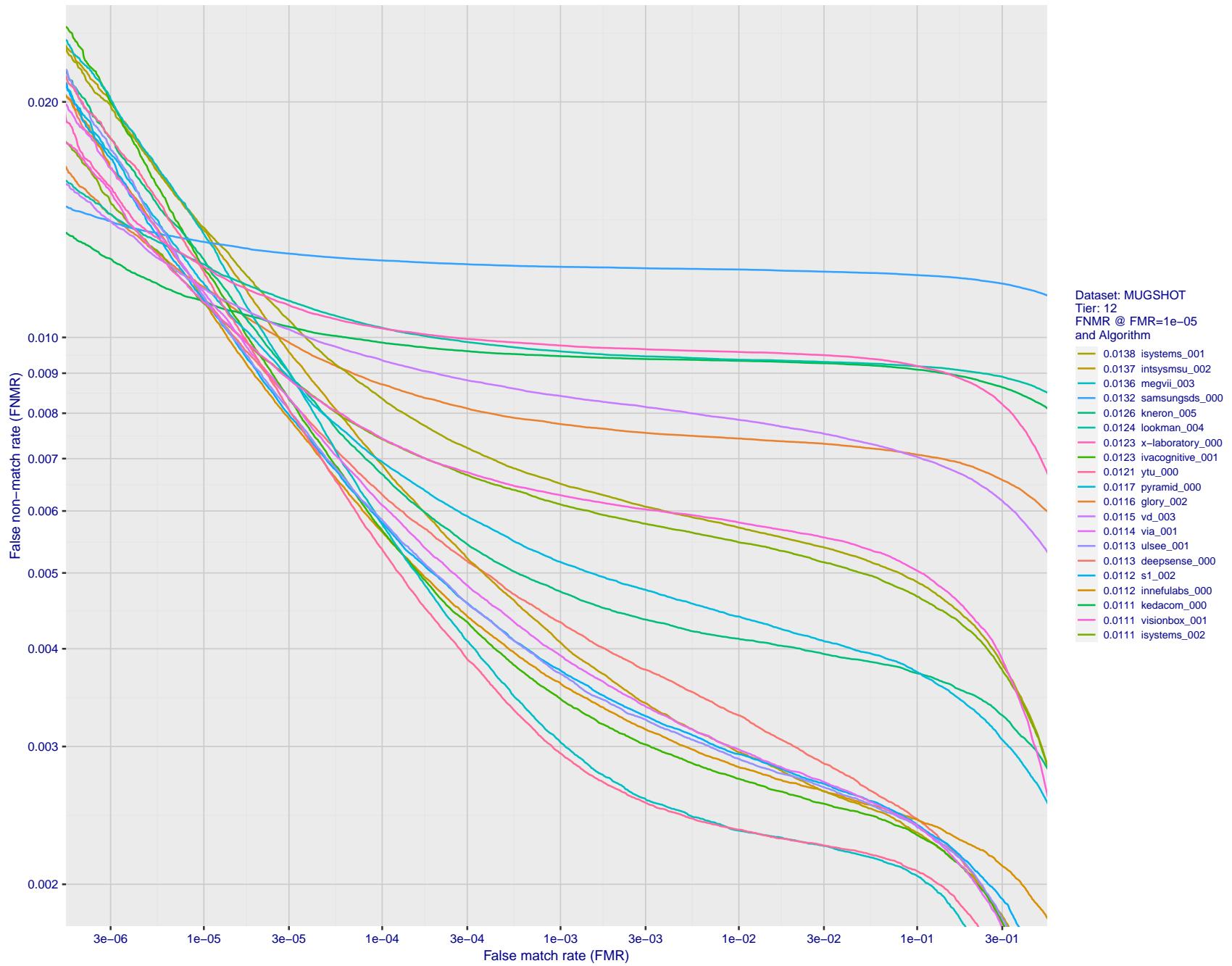


Figure 68: For the mugshot images, detection error tradeoff (DET) characteristics showing false non-match rate vs. false match rate plotted parametrically on threshold, T . The scales are logarithmic in order to show decades of FMR.

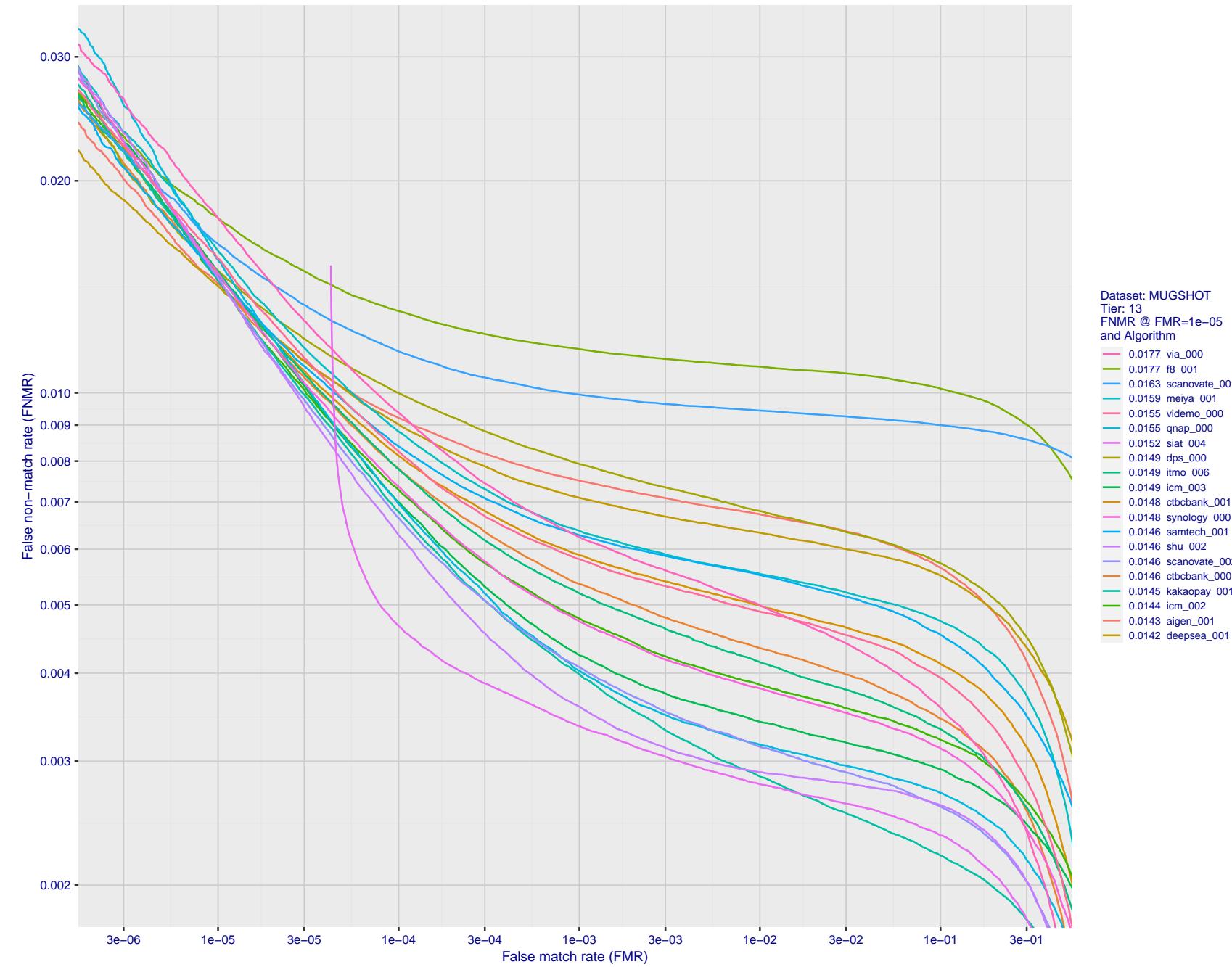


Figure 69: For the mugshot images, detection error tradeoff (DET) characteristics showing false non-match rate vs. false match rate plotted parametrically on threshold, T . The scales are logarithmic in order to show decades of FMR.

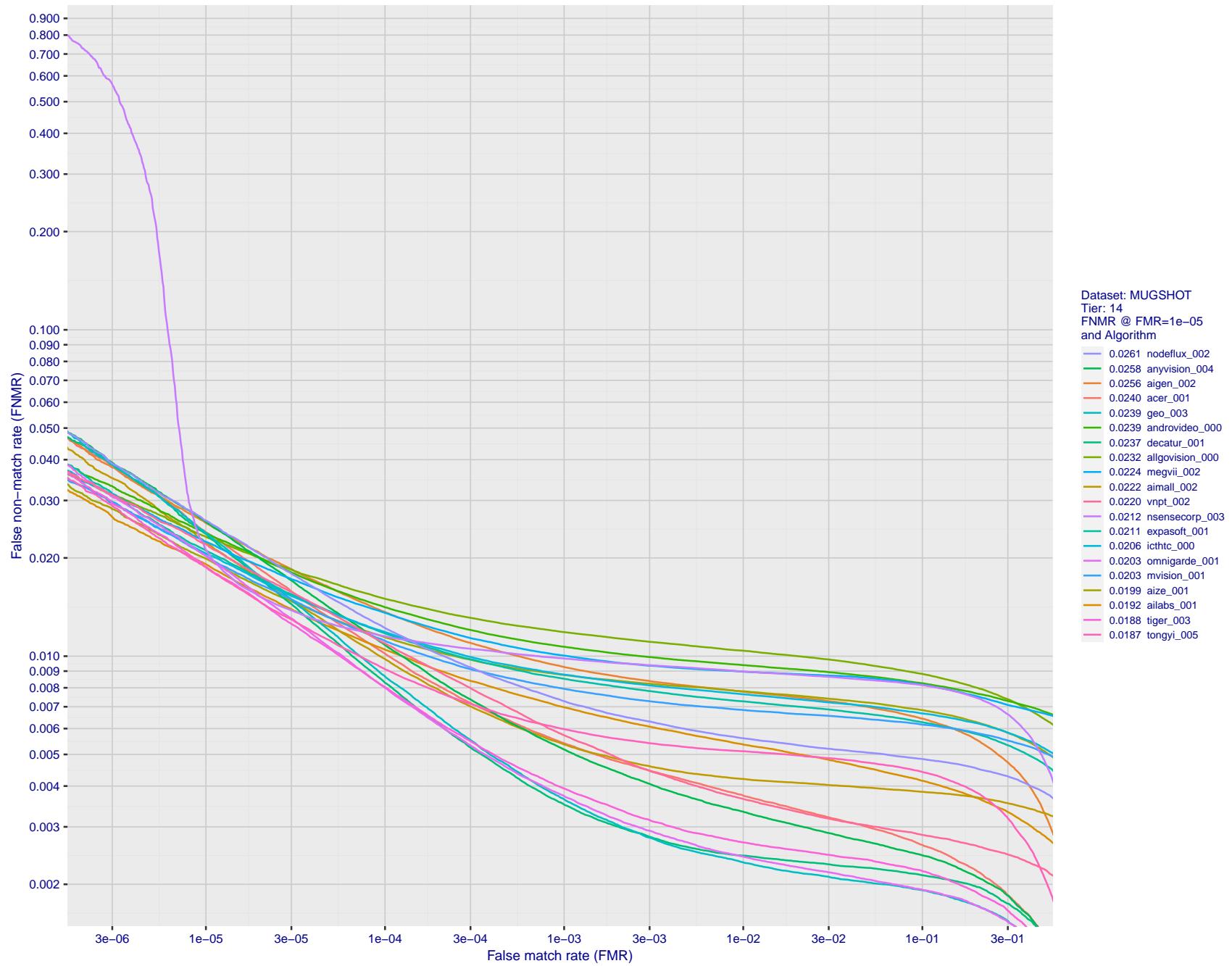


Figure 70: For the mugshot images, detection error tradeoff (DET) characteristics showing false non-match rate vs. false match rate plotted parametrically on threshold, T . The scales are logarithmic in order to show decades of FMR.

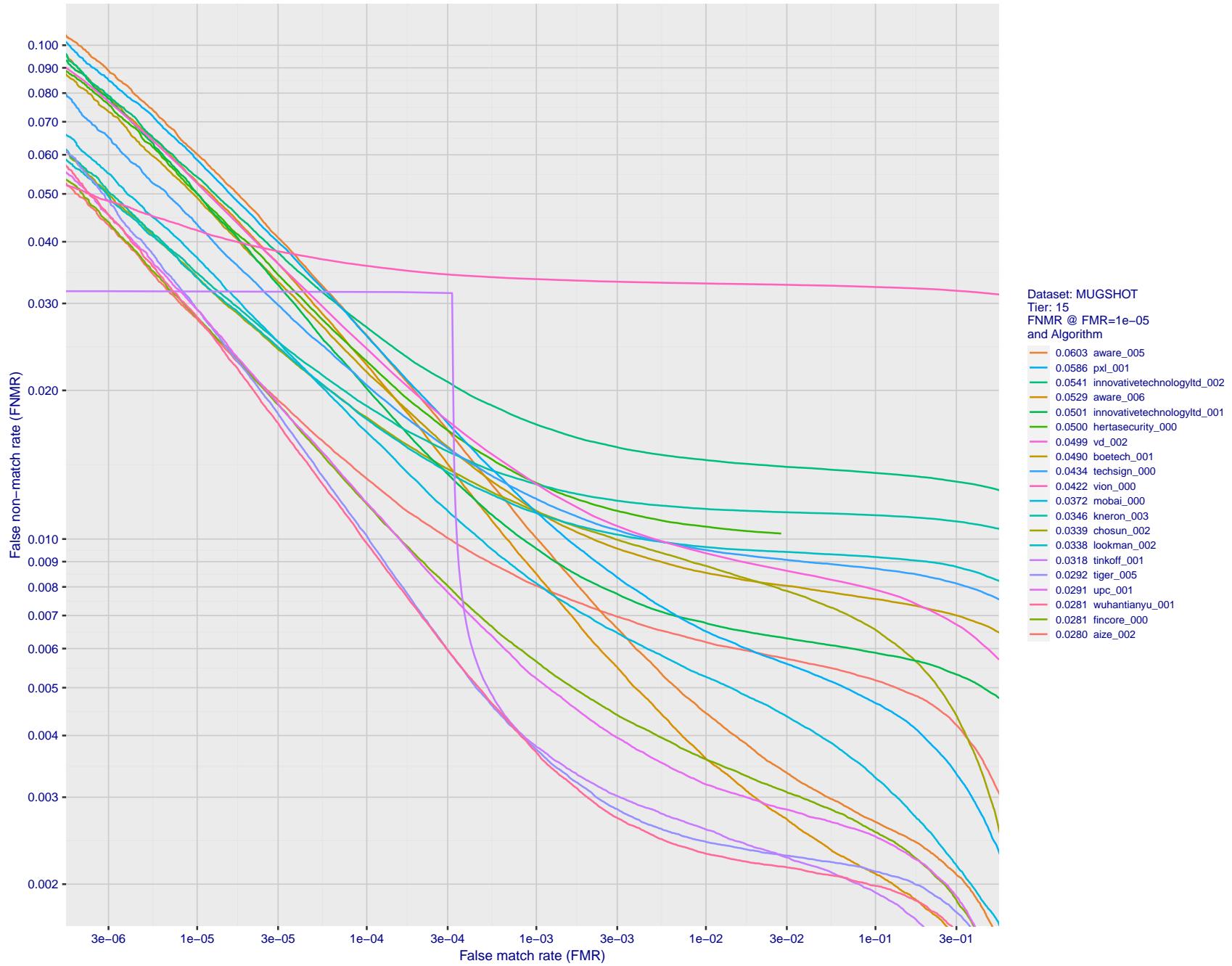


Figure 71: For the mugshot images, detection error tradeoff (DET) characteristics showing false non-match rate vs. false match rate plotted parametrically on threshold, T . The scales are logarithmic in order to show decades of FMR.

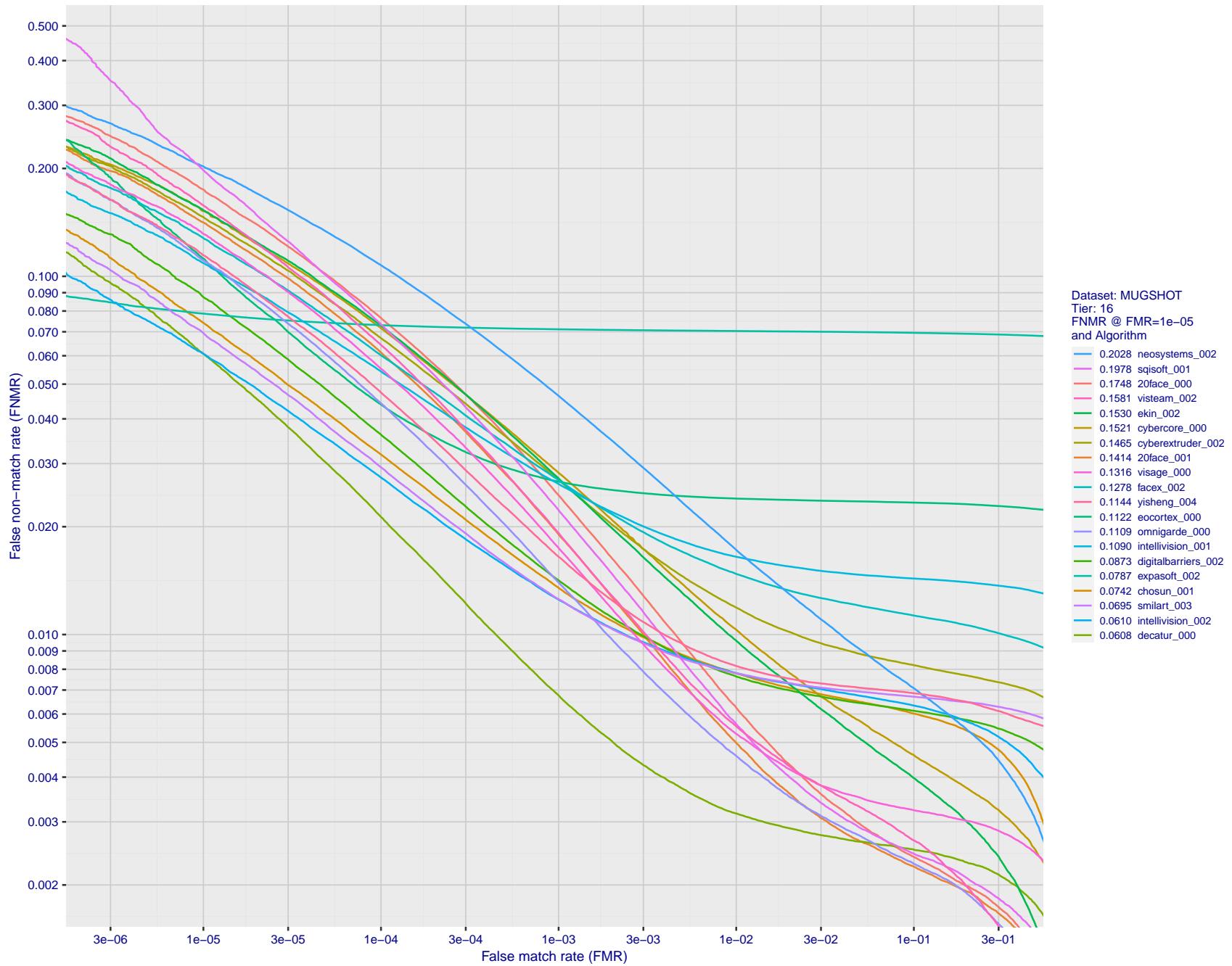


Figure 72: For the mugshot images, detection error tradeoff (DET) characteristics showing false non-match rate vs. false match rate plotted parametrically on threshold, T. The scales are logarithmic in order to show decades of FMR.

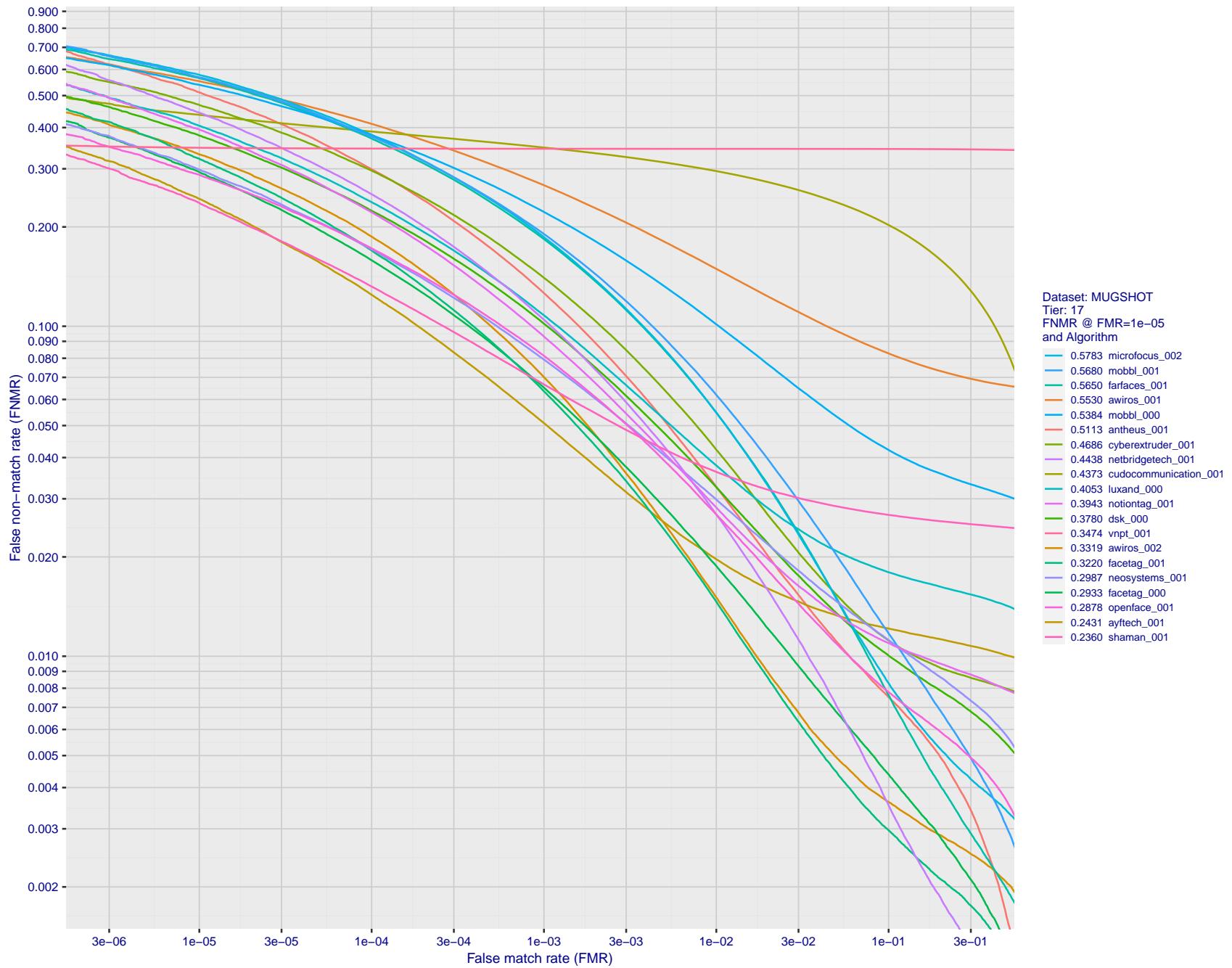


Figure 73: For the mugshot images, detection error tradeoff (DET) characteristics showing false non-match rate vs. false match rate plotted parametrically on threshold, T . The scales are logarithmic in order to show decades of FMR.

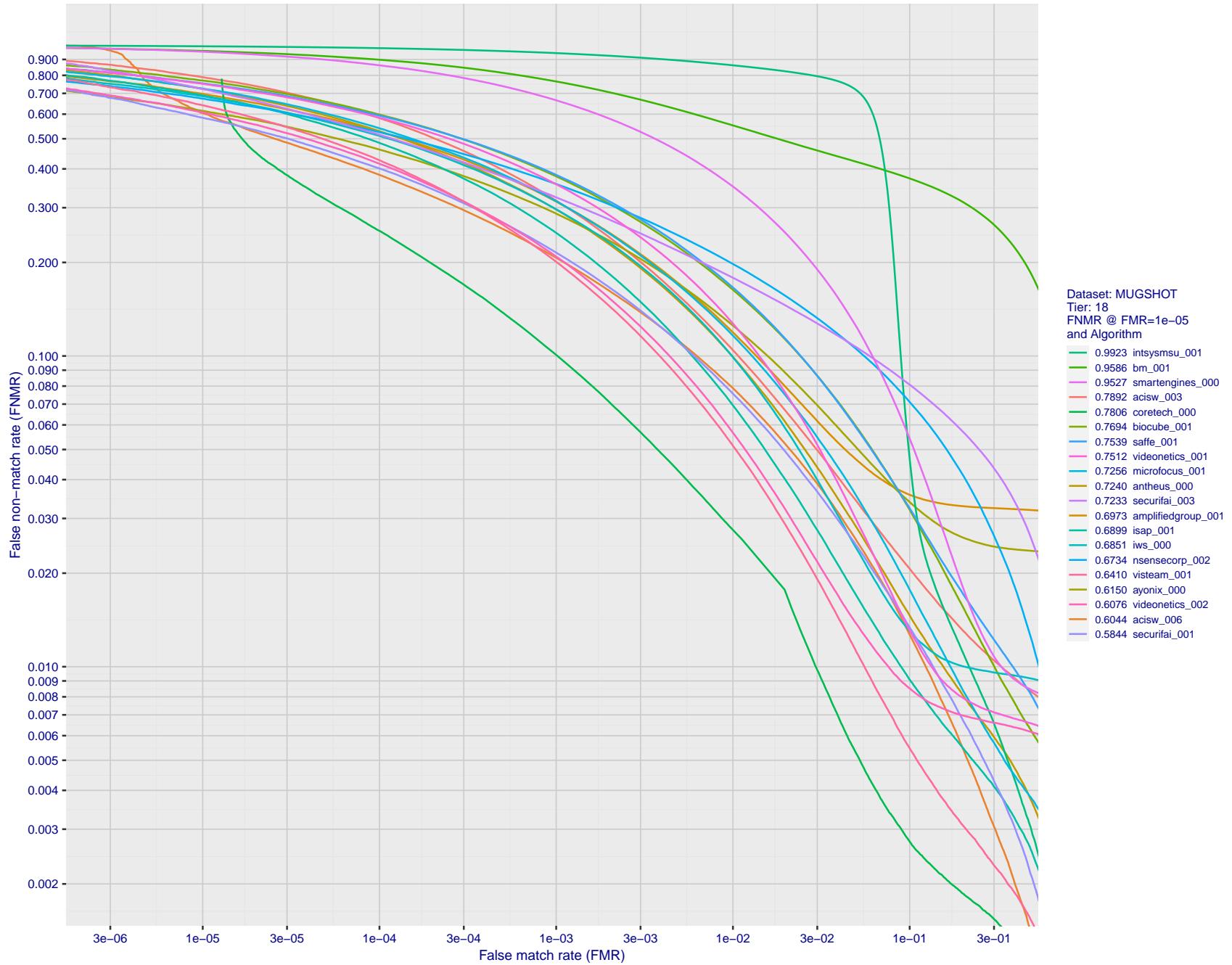


Figure 74: For the mugshot images, detection error tradeoff (DET) characteristics showing false non-match rate vs. false match rate plotted parametrically on threshold, T . The scales are logarithmic in order to show decades of FMR.

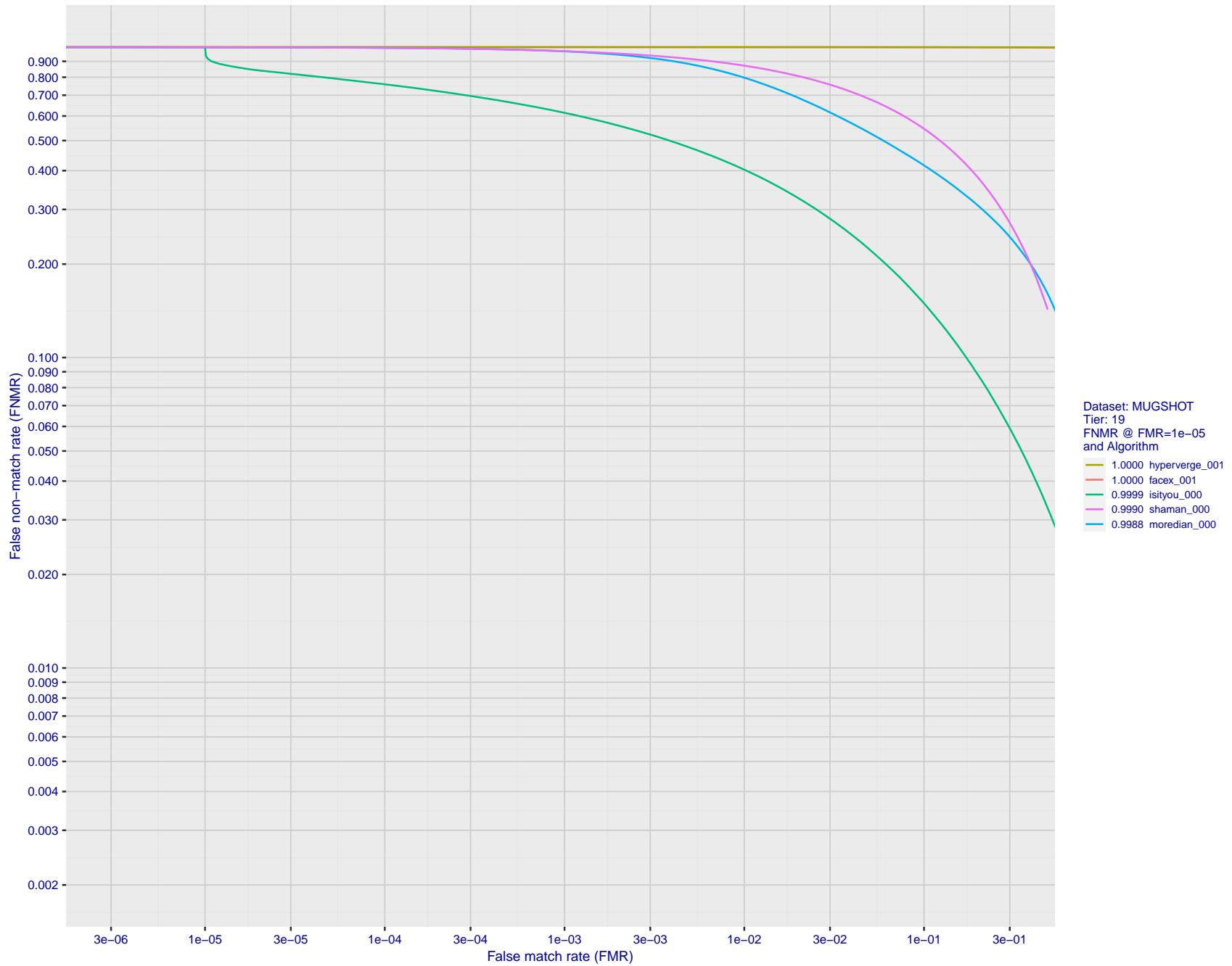


Figure 75: For the mugshot images, detection error tradeoff (DET) characteristics showing false non-match rate vs. false match rate plotted parametrically on threshold, T . The scales are logarithmic in order to show decades of FMR.

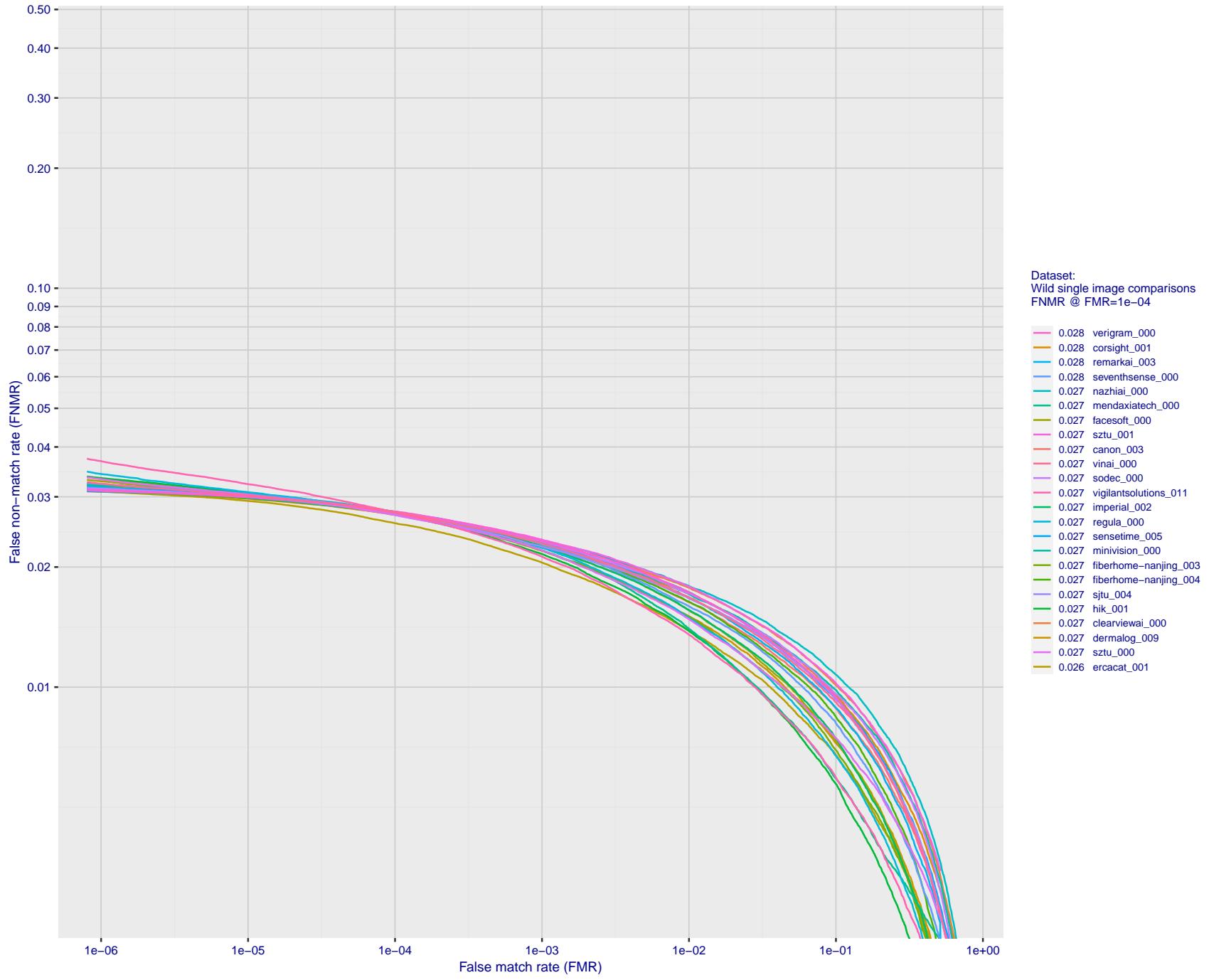


Figure 76: For the 2018 wild image comparisons, detection error tradeoff (DET) characteristics showing false non-match rate vs. false match rate plotted parametrically on threshold, T . The scales are logarithmic in order to show several decades of FMR.

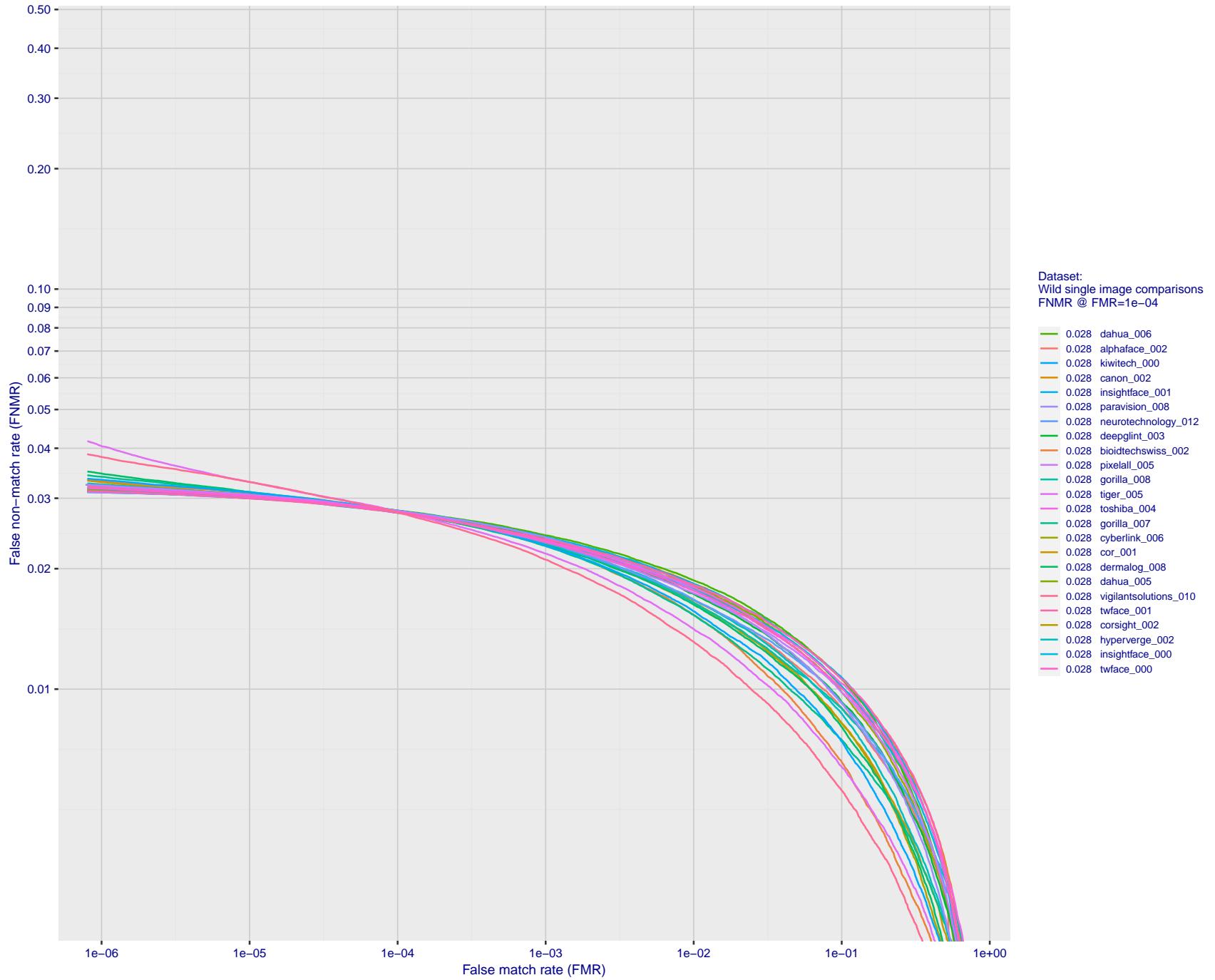


Figure 77: For the 2018 wild image comparisons, detection error tradeoff (DET) characteristics showing false non-match rate vs. false match rate plotted parametrically on threshold, T . The scales are logarithmic in order to show several decades of FMR.

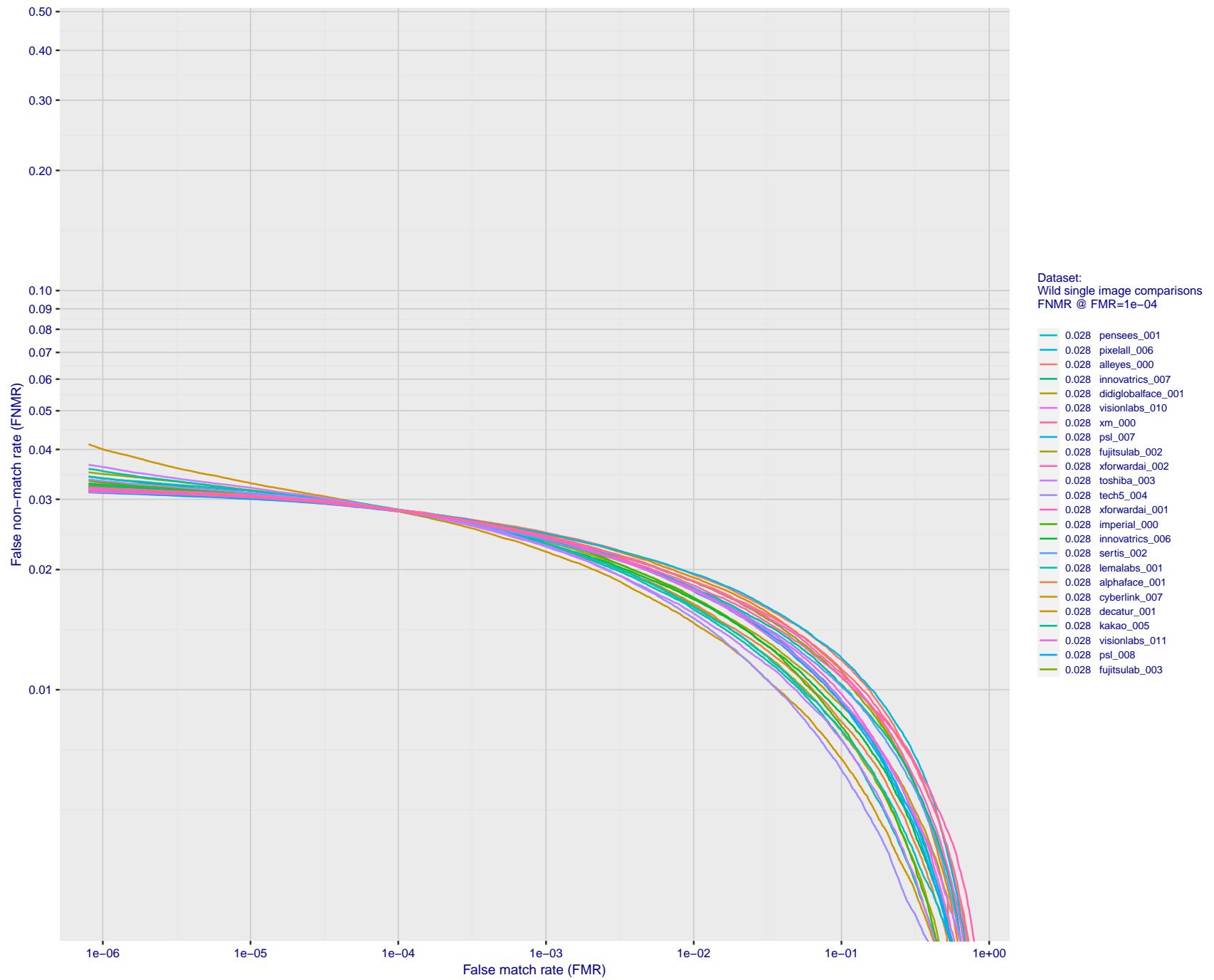


Figure 78: For the 2018 wild image comparisons, detection error tradeoff (DET) characteristics showing false non-match rate vs. false match rate plotted parametrically on threshold, T . The scales are logarithmic in order to show several decades of FMR.

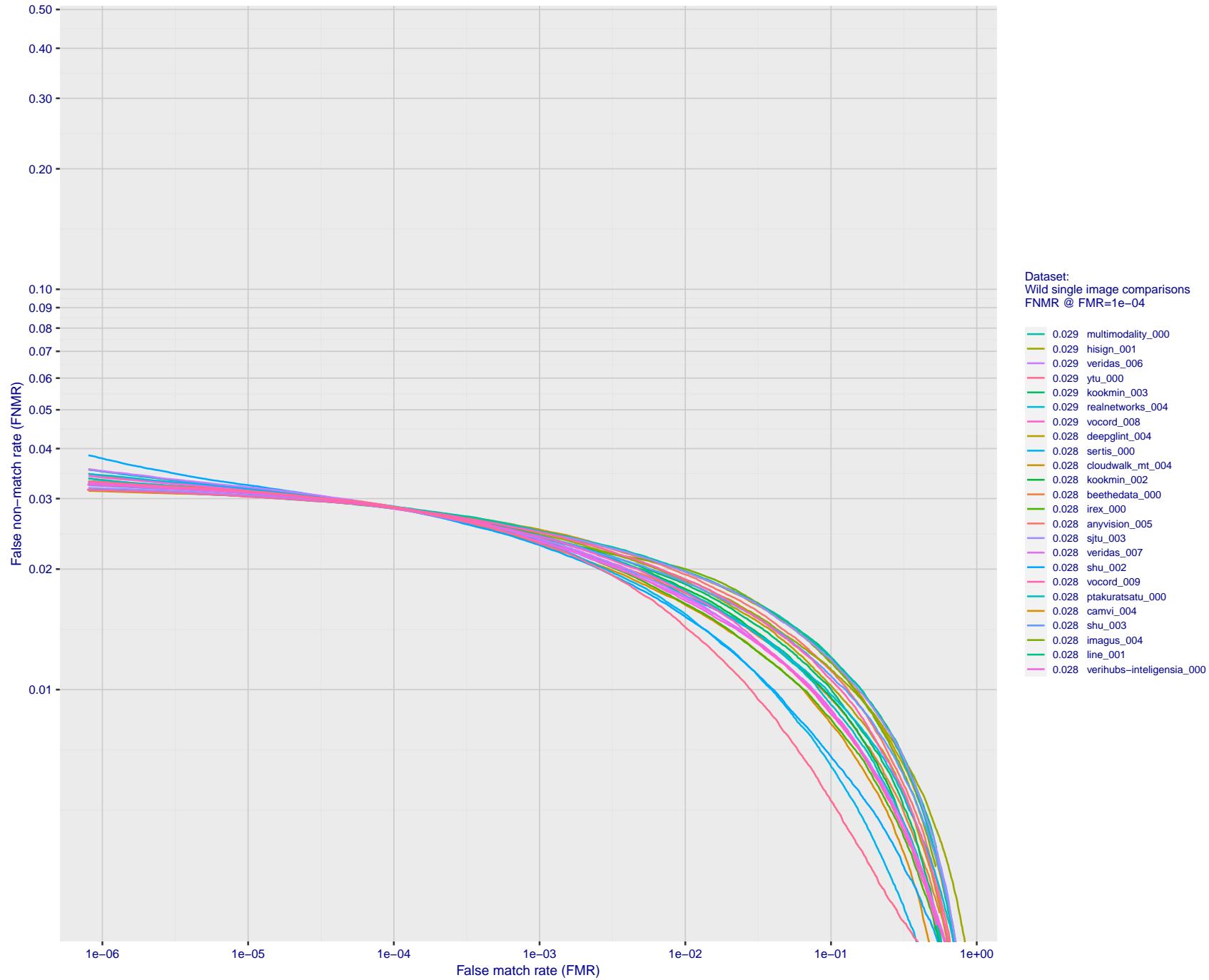


Figure 79: For the 2018 wild image comparisons, detection error tradeoff (DET) characteristics showing false non-match rate vs. false match rate plotted parametrically on threshold, T . The scales are logarithmic in order to show several decades of FMR.

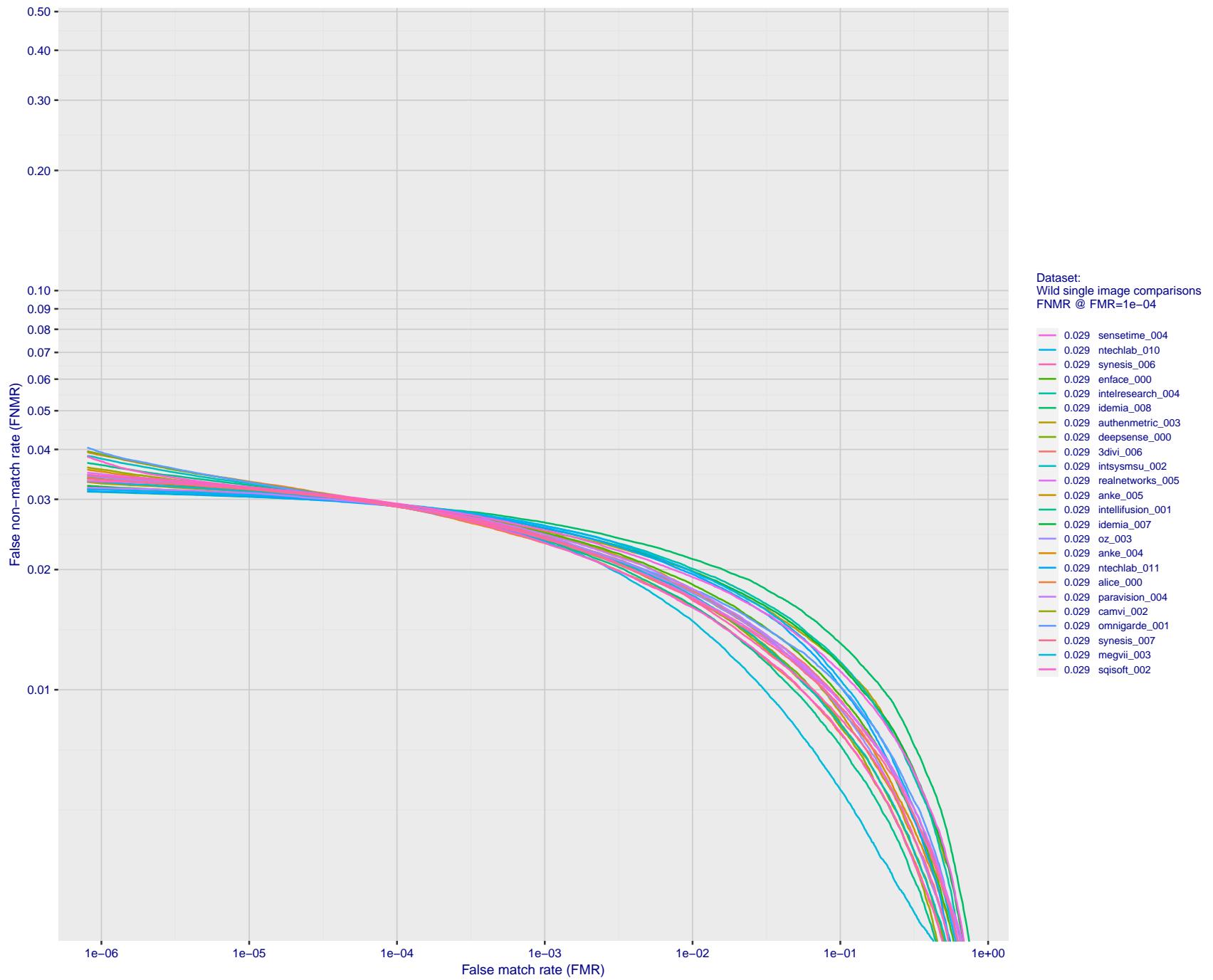


Figure 80: For the 2018 wild image comparisons, detection error tradeoff (DET) characteristics showing false non-match rate vs. false match rate plotted parametrically on threshold, T. The scales are logarithmic in order to show several decades of FMR.

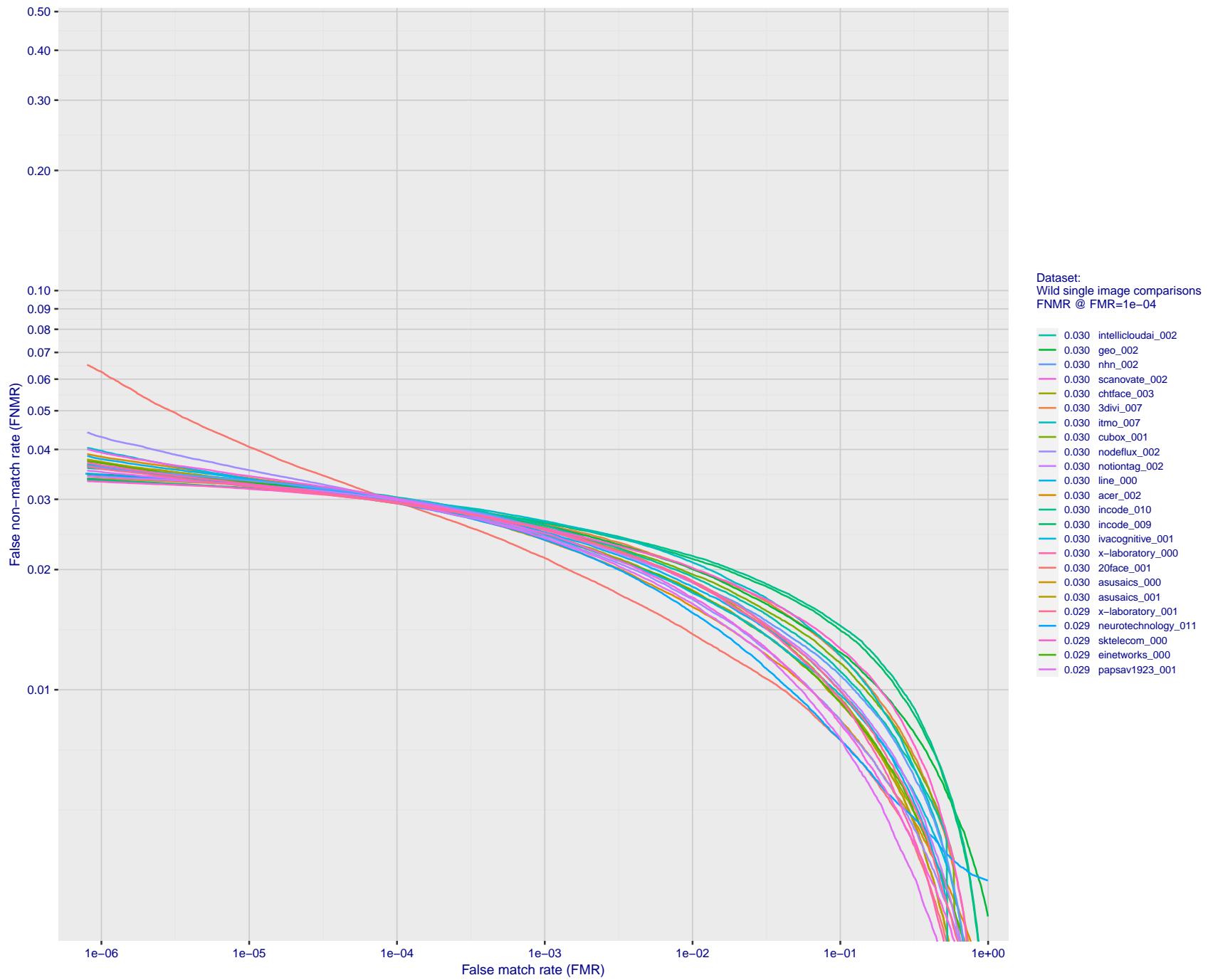


Figure 81: For the 2018 wild image comparisons, detection error tradeoff (DET) characteristics showing false non-match rate vs. false match rate plotted parametrically on threshold, T . The scales are logarithmic in order to show several decades of FMR.

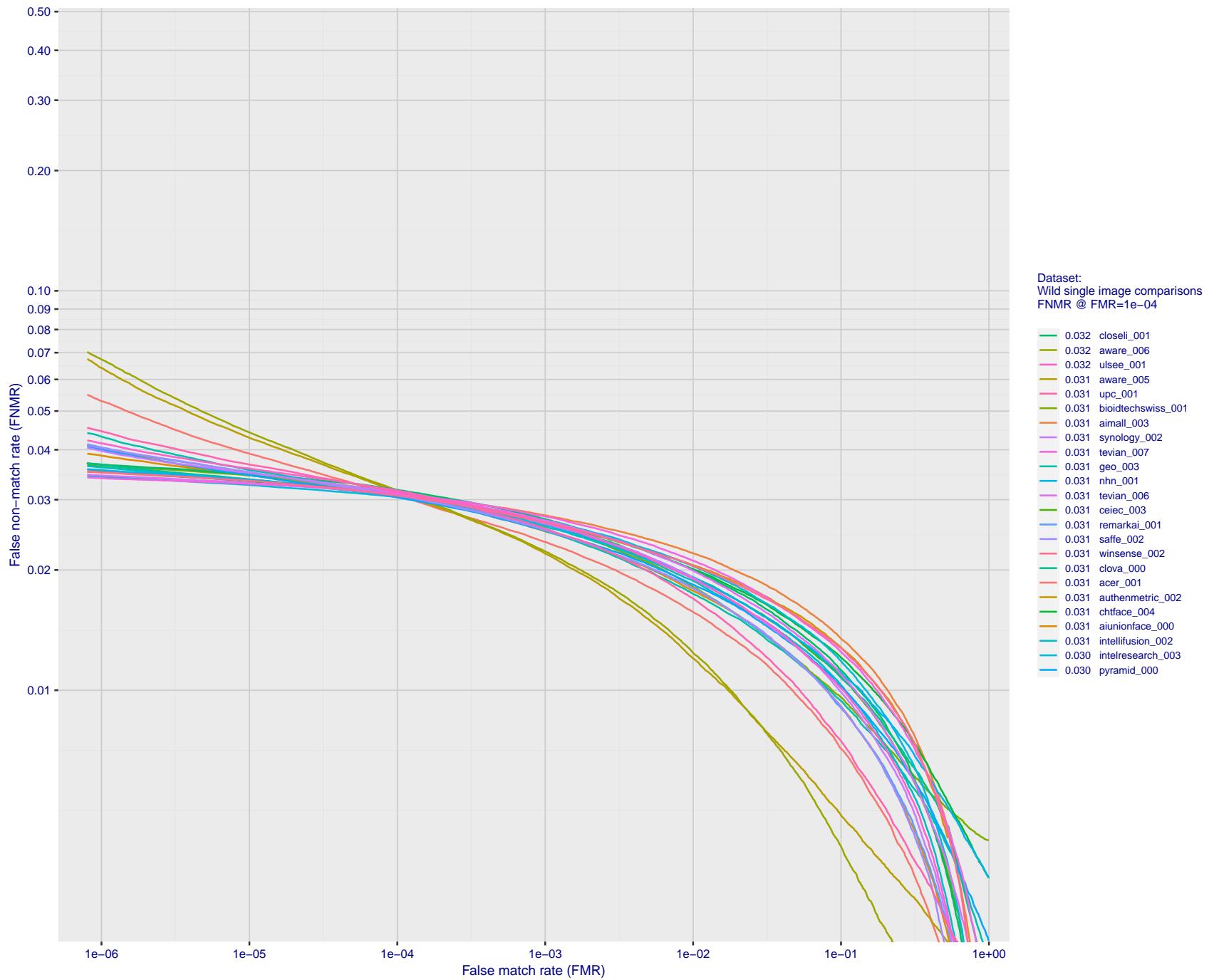


Figure 82: For the 2018 wild image comparisons, detection error tradeoff (DET) characteristics showing false non-match rate vs. false match rate plotted parametrically on threshold, T . The scales are logarithmic in order to show several decades of FMR.

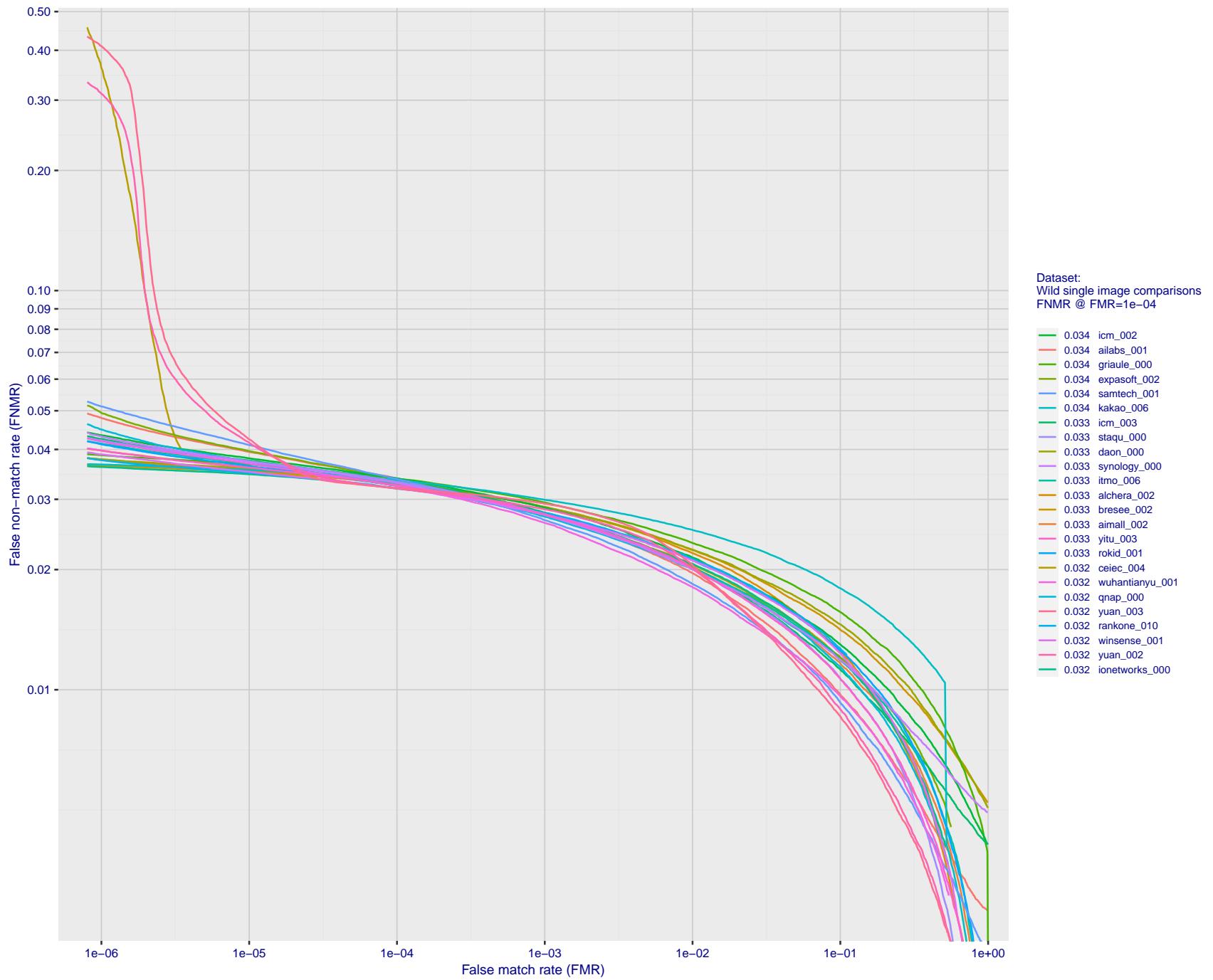
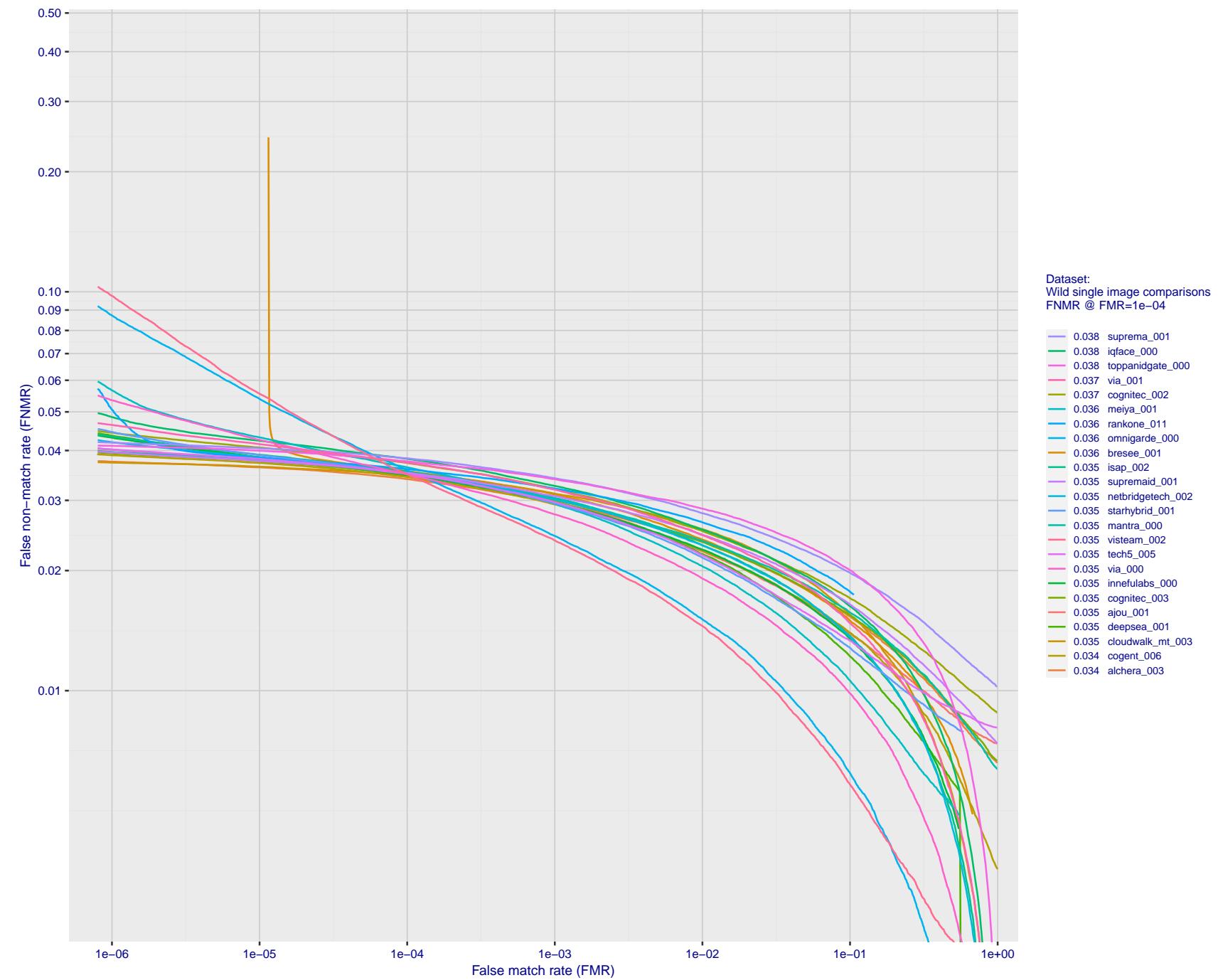


Figure 83: For the 2018 wild image comparisons, detection error tradeoff (DET) characteristics showing false non-match rate vs. false match rate plotted parametrically on threshold, T . The scales are logarithmic in order to show several decades of FMR.

FNMR(T)
"False non-match rate"
"False match rate"Figure 84: For the 2018 wild image comparisons, detection error tradeoff (DET) characteristics showing false non-match rate vs. false match rate plotted parametrically on threshold, T . The scales are logarithmic in order to show several decades of FMR.

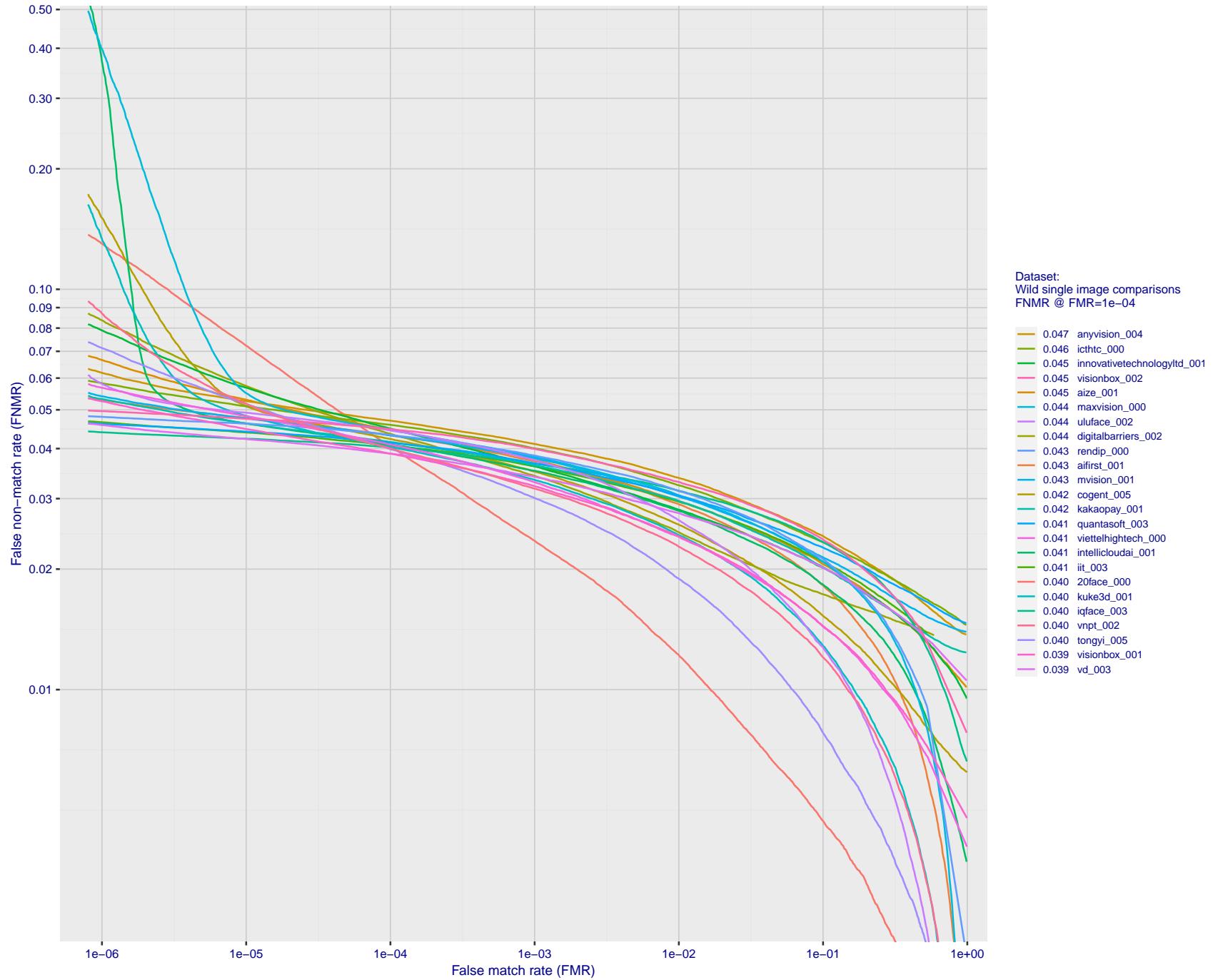


Figure 85: For the 2018 wild image comparisons, detection error tradeoff (DET) characteristics showing false non-match rate vs. false match rate plotted parametrically on threshold, T . The scales are logarithmic in order to show several decades of FMR.

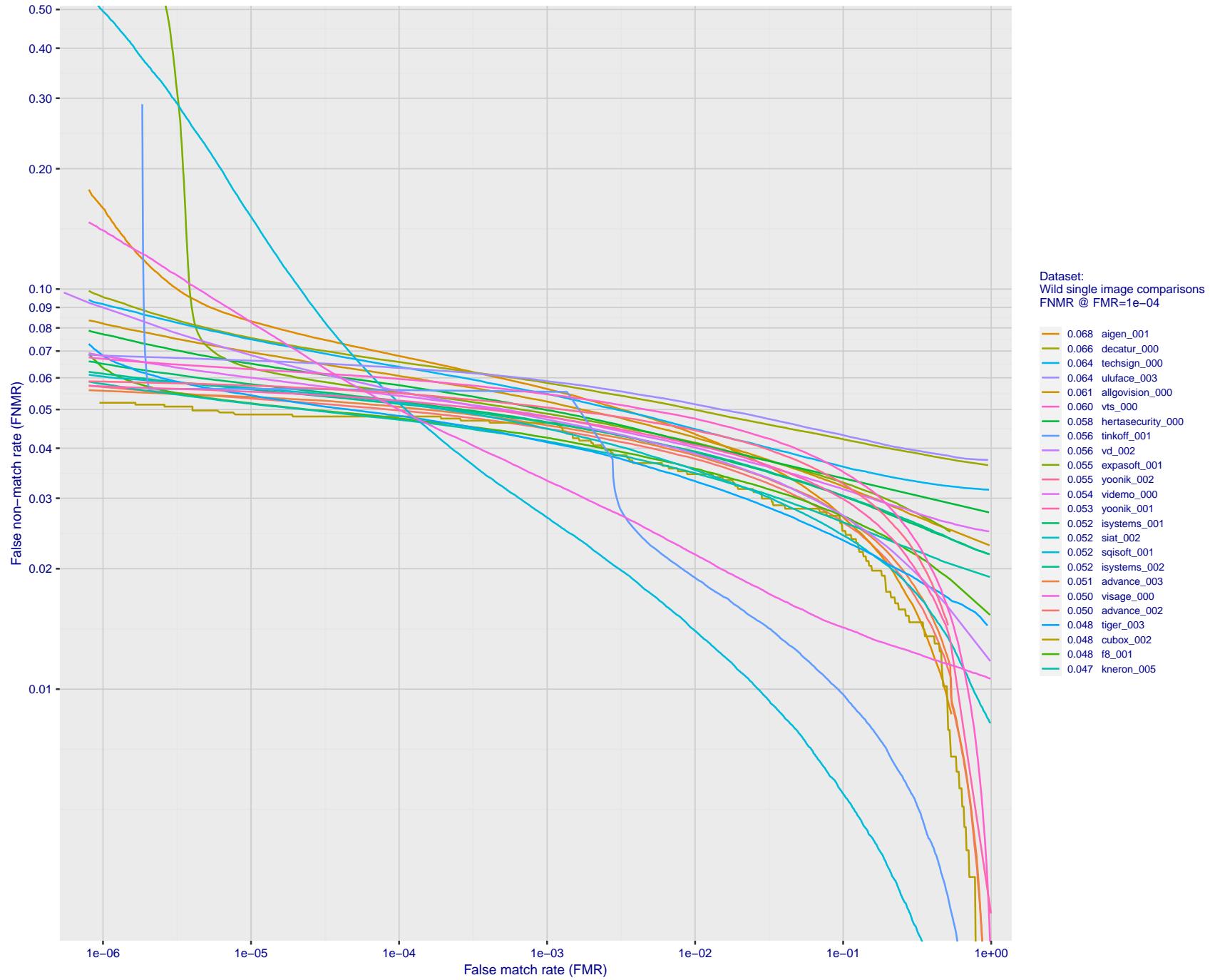


Figure 86: For the 2018 wild image comparisons, detection error tradeoff (DET) characteristics showing false non-match rate vs. false match rate plotted parametrically on threshold, T . The scales are logarithmic in order to show several decades of FMR.

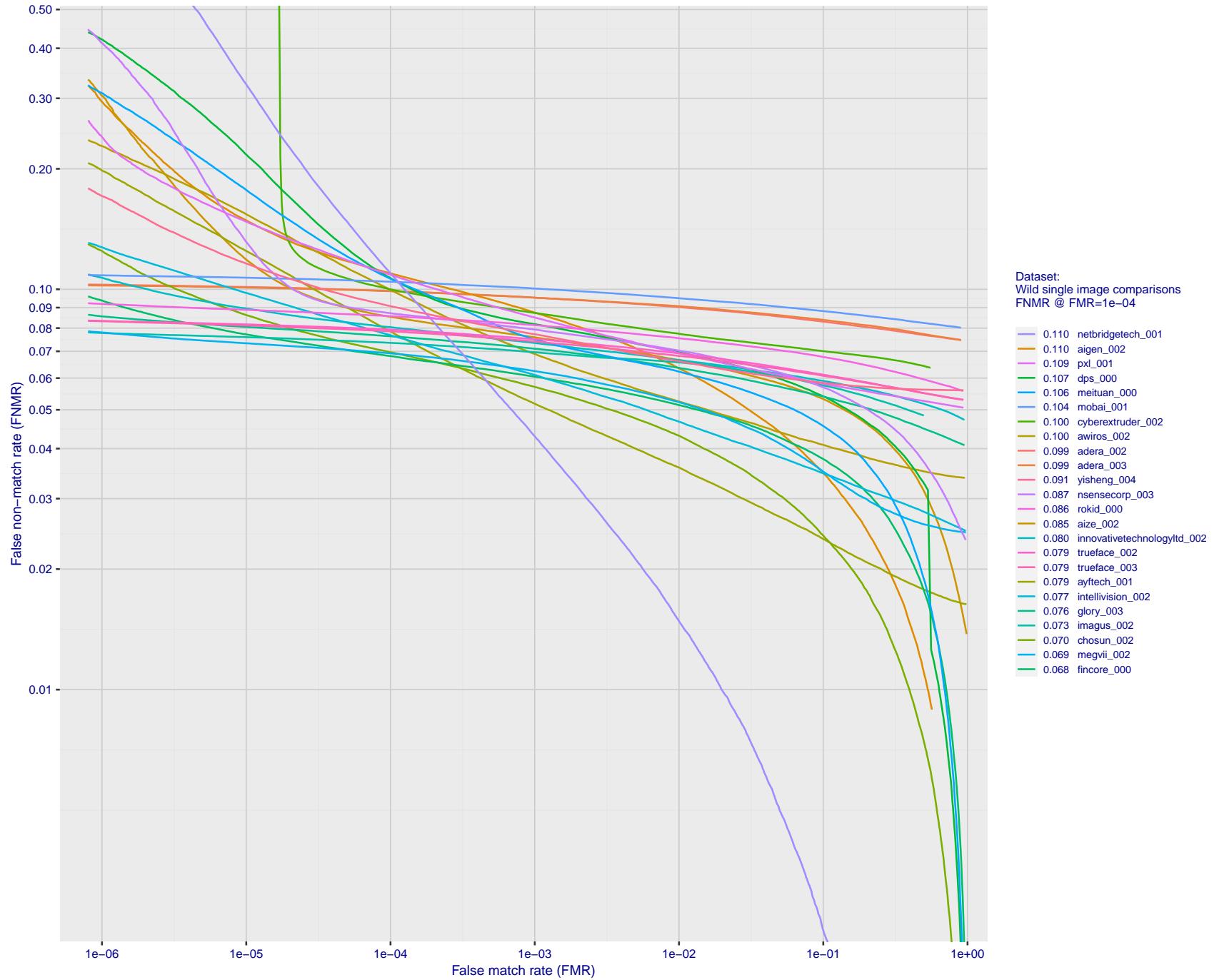


Figure 87: For the 2018 wild image comparisons, detection error tradeoff (DET) characteristics showing false non-match rate vs. false match rate plotted parametrically on threshold, T . The scales are logarithmic in order to show several decades of FMR.

2021/11/22 14:56:30

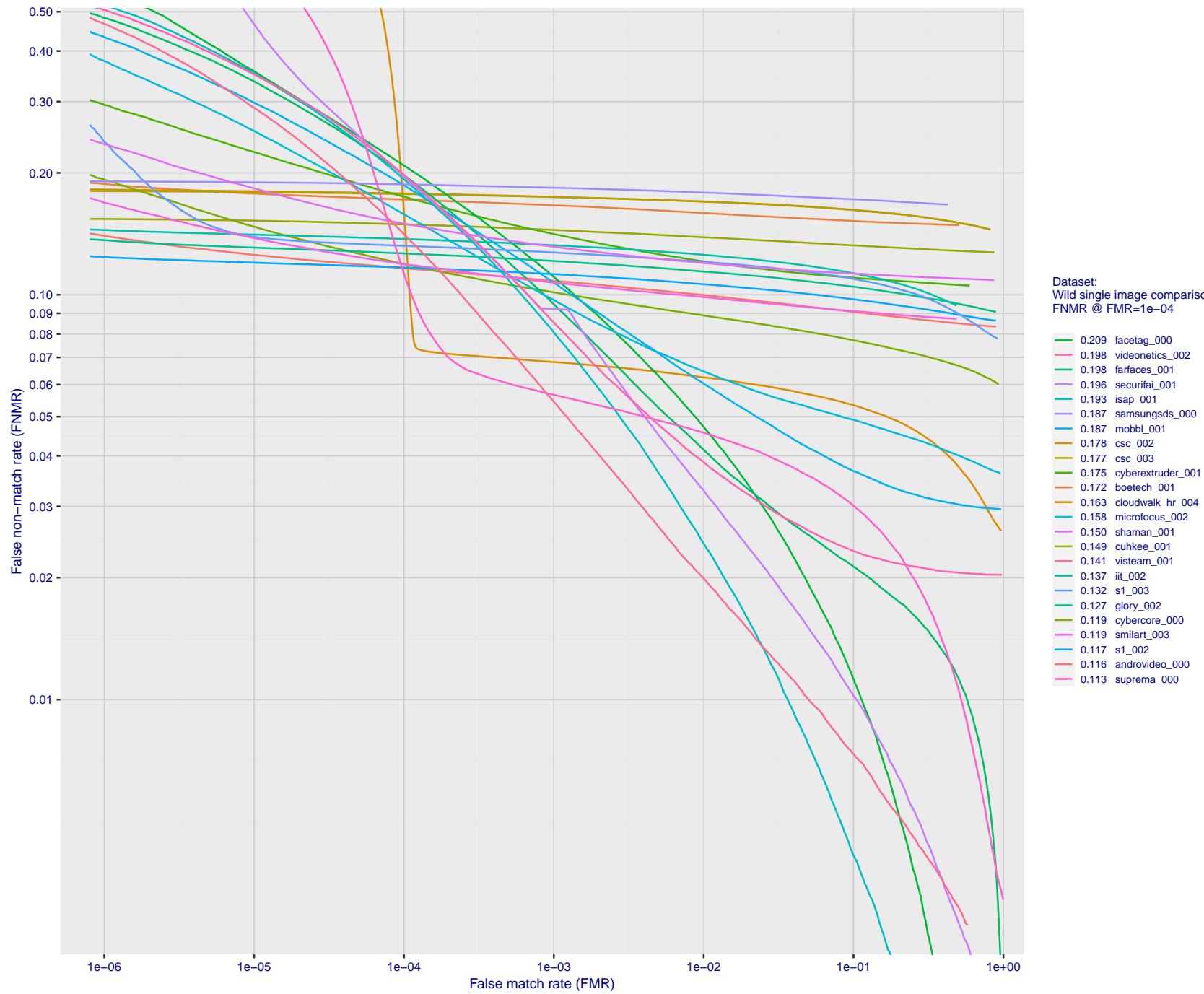
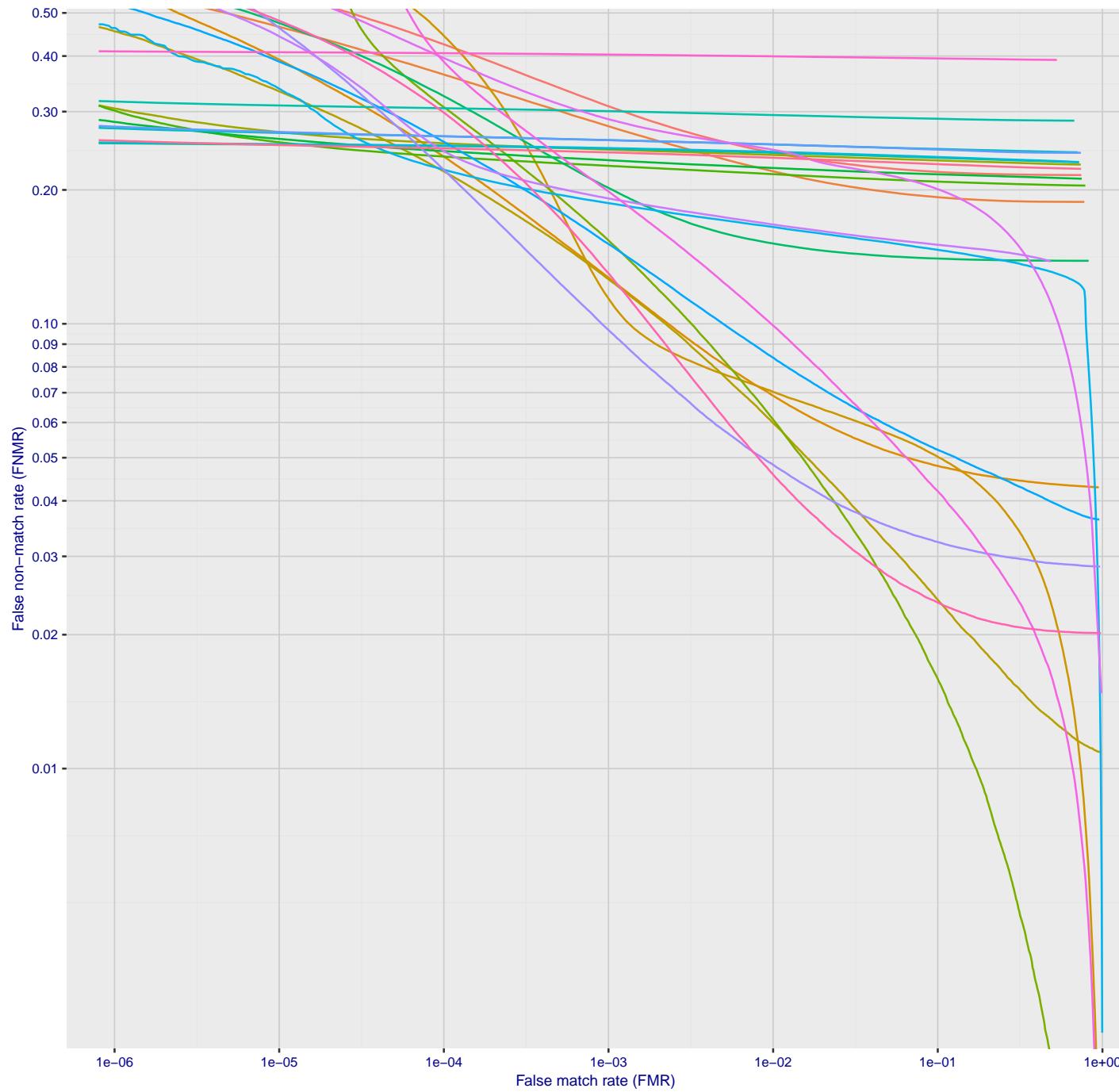


Figure 88: For the 2018 wild image comparisons, detection error tradeoff (DET) characteristics showing false non-match rate vs. false match rate plotted parametrically on threshold, T . The scales are logarithmic in order to show several decades of FMR.

2021/11/22 14:56:30



Dataset:
Wild single image comparisons
FNMR @ FMR=1e-04

FNMR(T)
"False non-match rate"
"False match rate"

Figure 89: For the 2018 wild image comparisons, detection error tradeoff (DET) characteristics showing false non-match rate vs. false match rate plotted parametrically on threshold, T. The scales are logarithmic in order to show several decades of FMR.

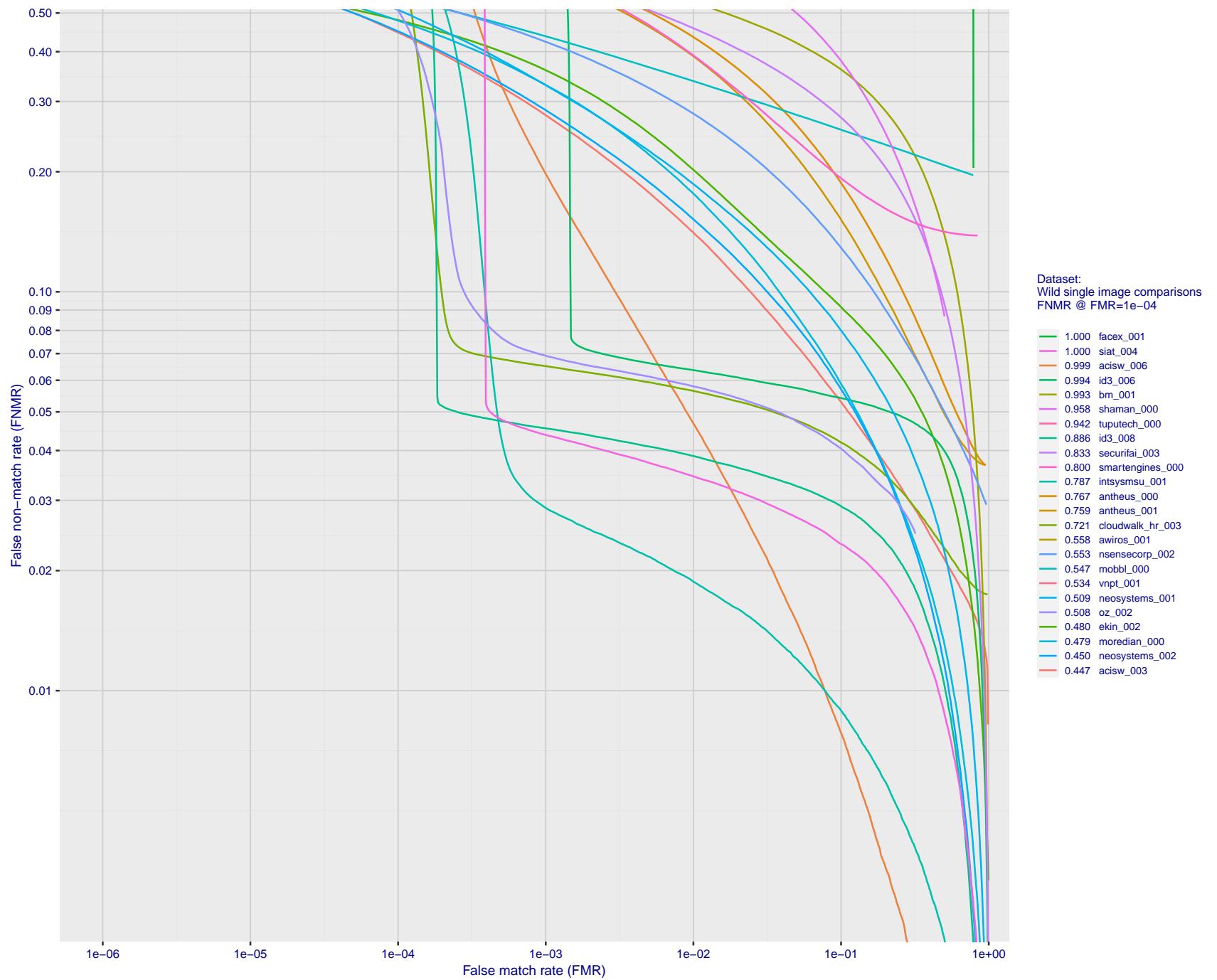


Figure 90: For the 2018 wild image comparisons, detection error tradeoff (DET) characteristics showing false non-match rate vs. false match rate plotted parametrically on threshold, T . The scales are logarithmic in order to show several decades of FMR.

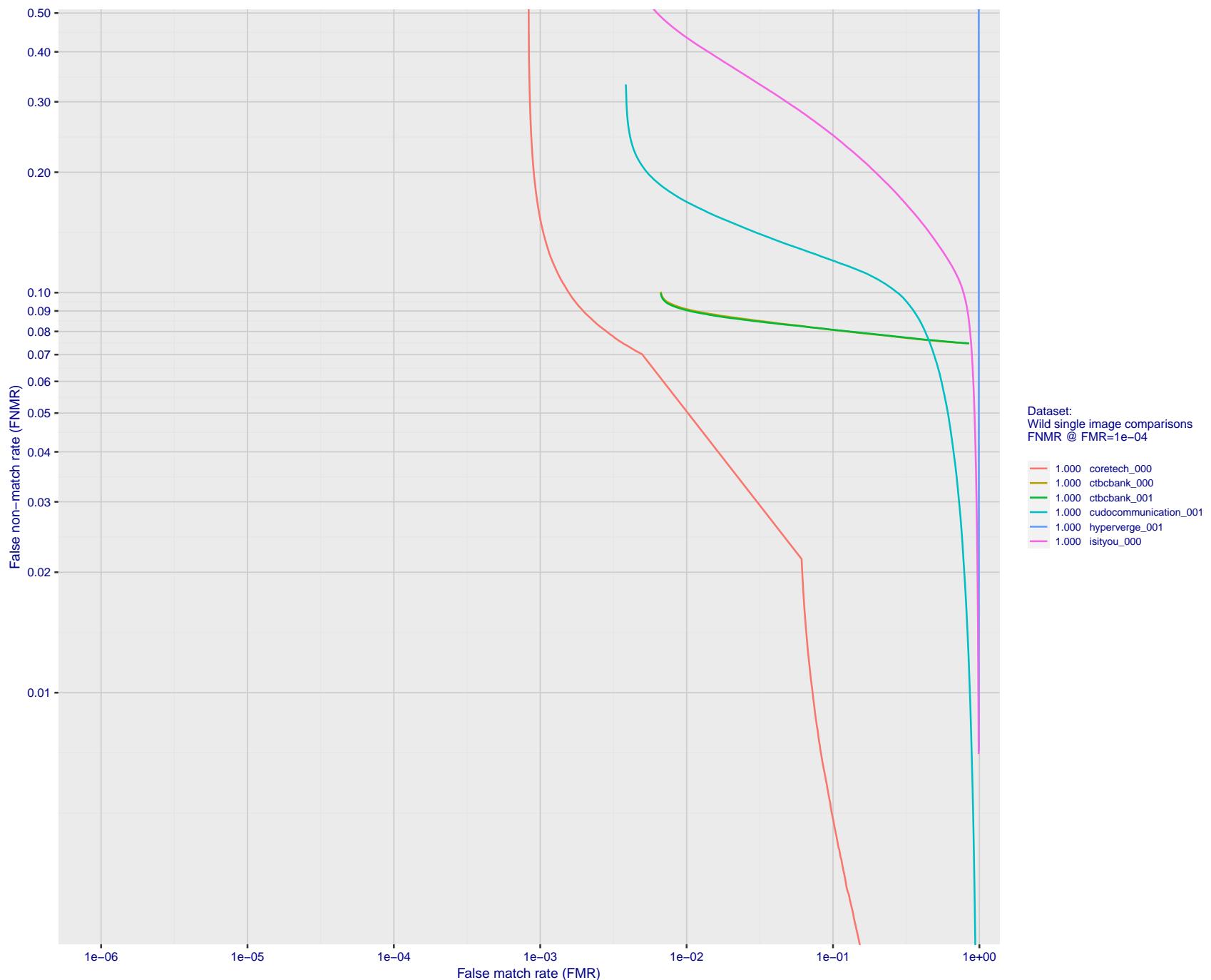


Figure 91: For the 2018 wild image comparisons, detection error tradeoff (DET) characteristics showing false non-match rate vs. false match rate plotted parametrically on threshold, T . The scales are logarithmic in order to show several decades of FMR.

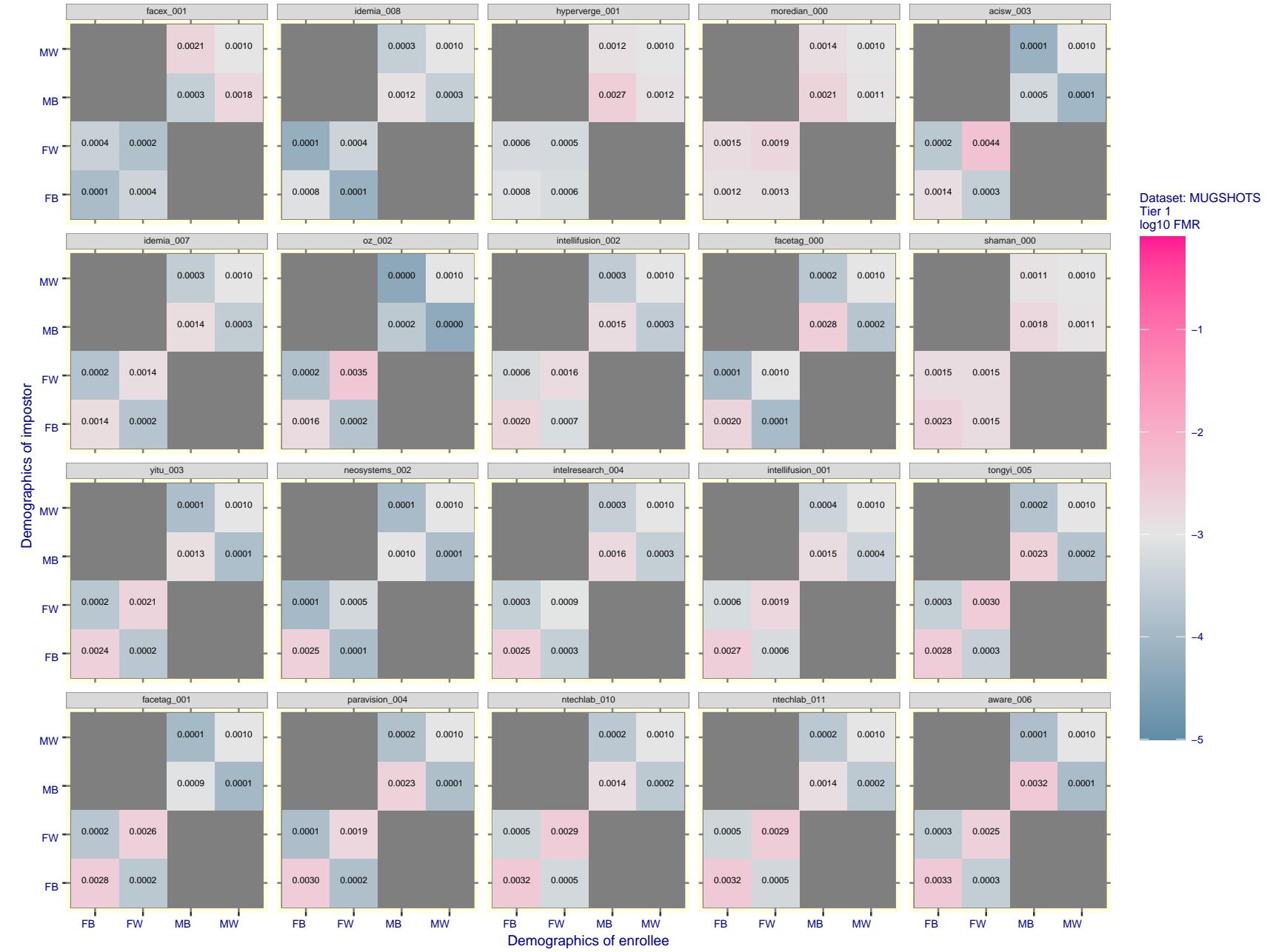


Figure 92: For the mugshot images, FMR for same-sex impostor pairs of images annotated with codes for black female, black male, white female, white male. The threshold is set for each algorithm to give FMR = 0.001 for white males which is the demographic that usually gives the lowest FMR. This means the top right box is the same color in all panels. The panels are sorted over multiple pages in order of FMR on black females, which is the demographic that usually gives the highest FMR.

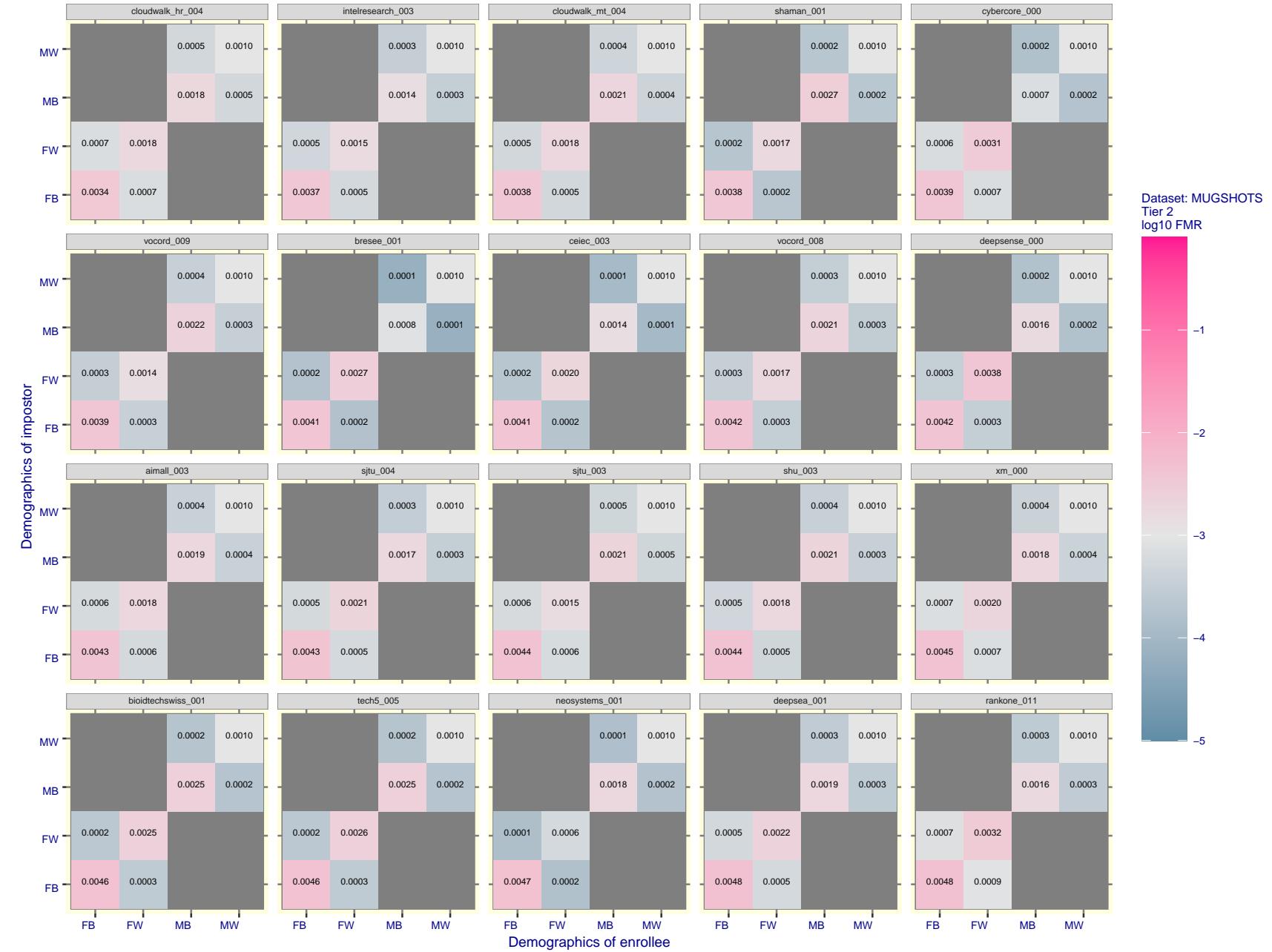


Figure 93: For the mugshot images, FMR for same-sex impostor pairs of images annotated with codes for black female, black male, white female, white male. The threshold is set for each algorithm to give $FMR = 0.001$ for white males which is the demographic that usually gives the lowest FMR. This means the top right box is the same color in all panels. The panels are sorted over multiple pages in order of FMR on black females, which is the demographic that usually gives the highest FMR.

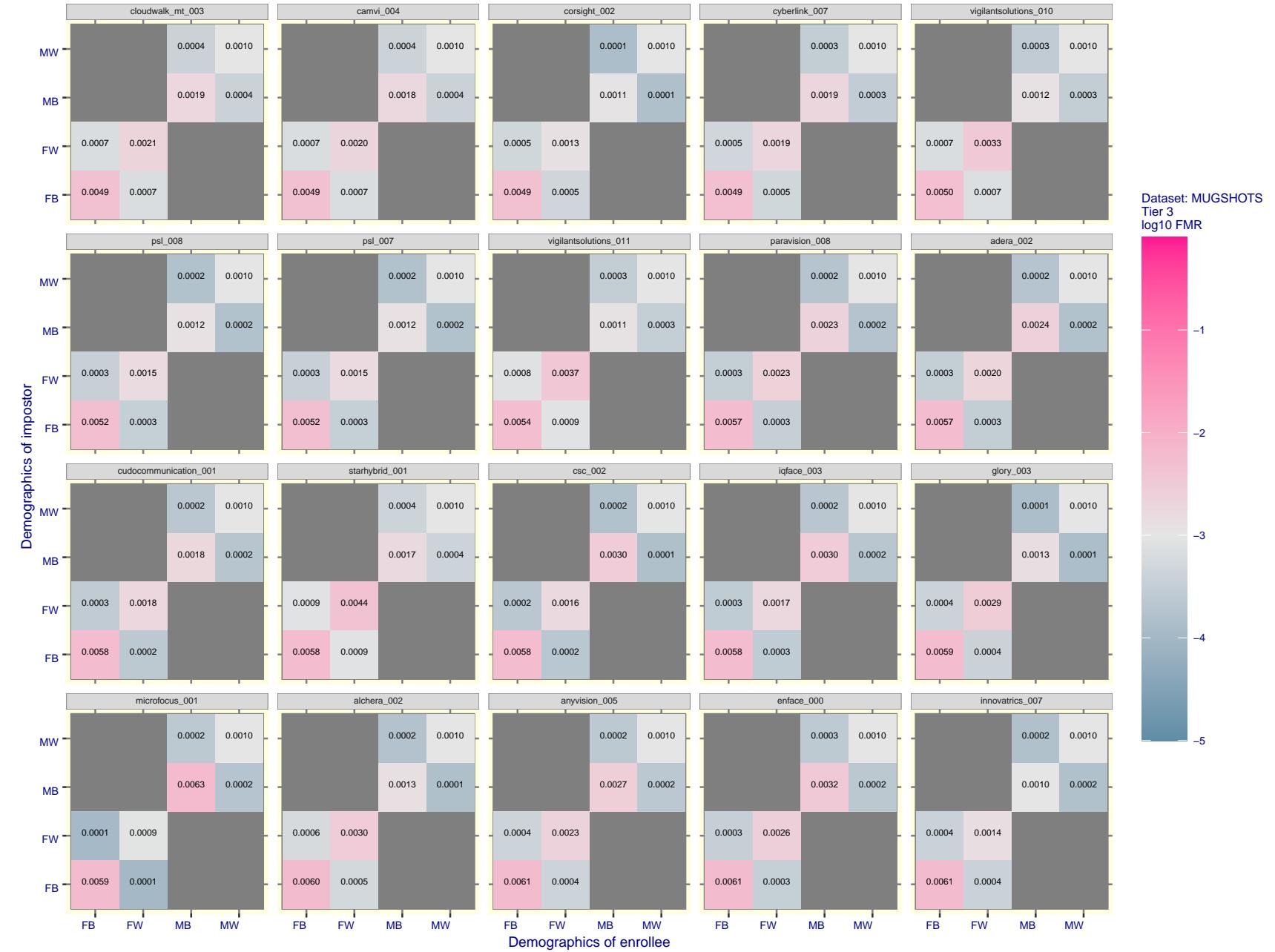


Figure 94: For the mugshot images, FMR for same-sex impostor pairs of images annotated with codes for black female, black male, white female, white male. The threshold is set for each algorithm to give FMR = 0.001 for white males which is the demographic that usually gives the lowest FMR. This means the top right box is the same color in all panels. The panels are sorted over multiple pages in order of FMR on black females, which is the demographic that usually gives the highest FMR.

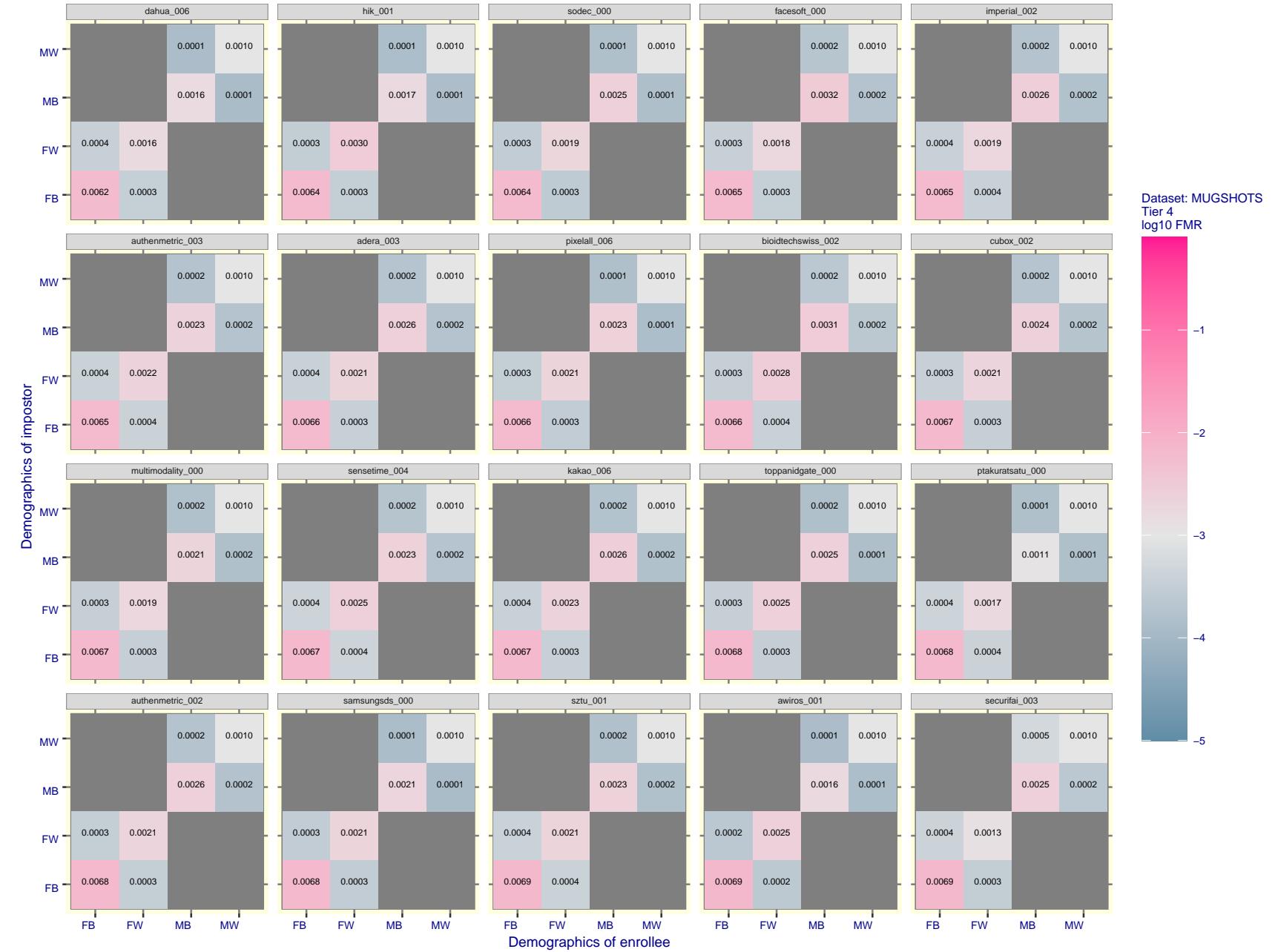


Figure 95: For the mugshot images, FMR for same-sex impostor pairs of images annotated with codes for black female, black male, white female, white male. The threshold is set for each algorithm to give $\text{FMR} = 0.001$ for white males which is the demographic that usually gives the lowest FMR. This means the top right box is the same color in all panels. The panels are sorted over multiple pages in order of FMR on black females, which is the demographic that usually gives the highest FMR.

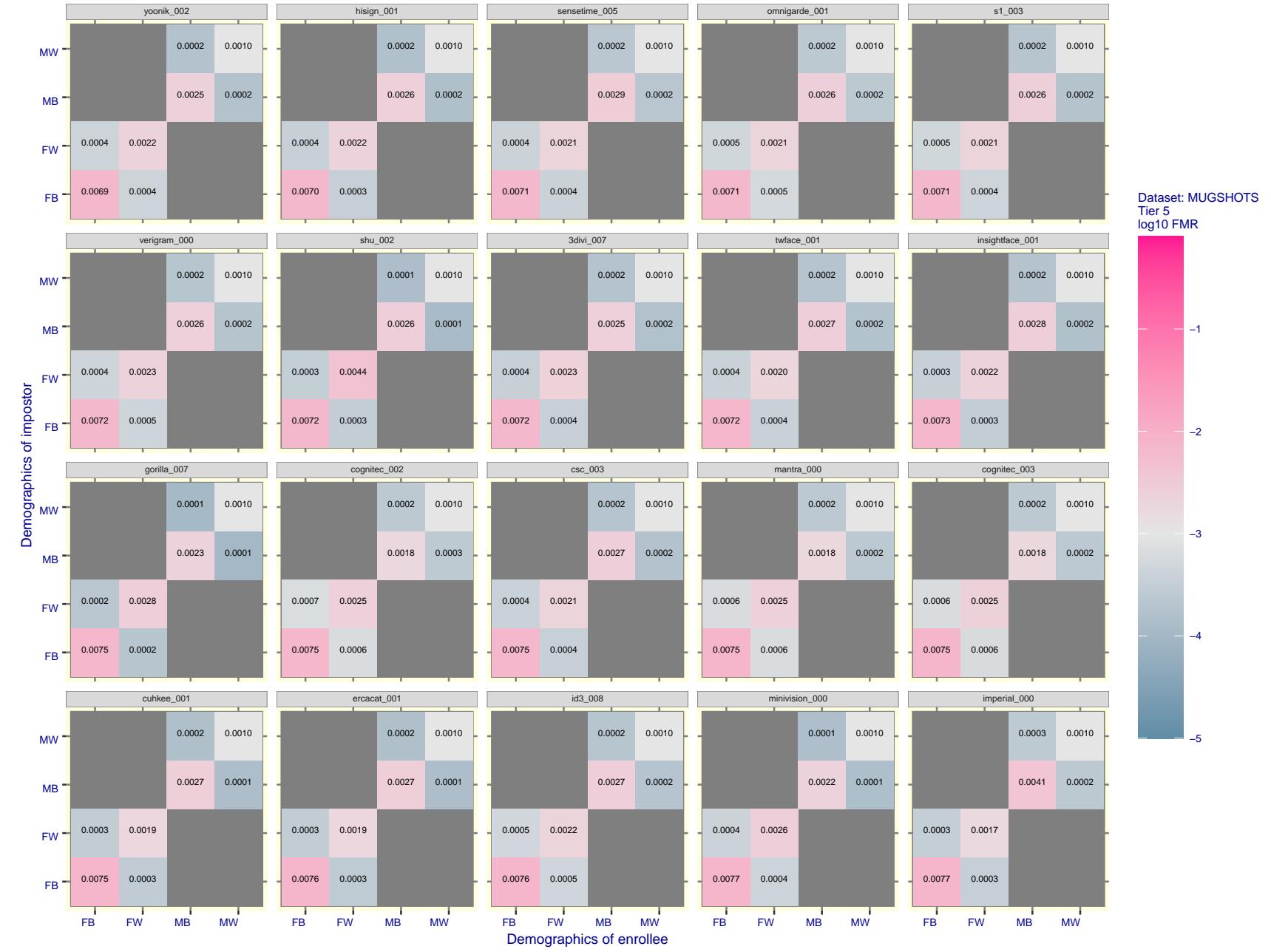


Figure 96: For the mugshot images, FMR for same-sex impostor pairs of images annotated with codes for black female, black male, white female, white male. The threshold is set for each algorithm to give $FMR = 0.001$ for white males which is the demographic that usually gives the lowest FMR. This means the top right box is the same color in all panels. The panels are sorted over multiple pages in order of FMR on black females, which is the demographic that usually gives the highest FMR.

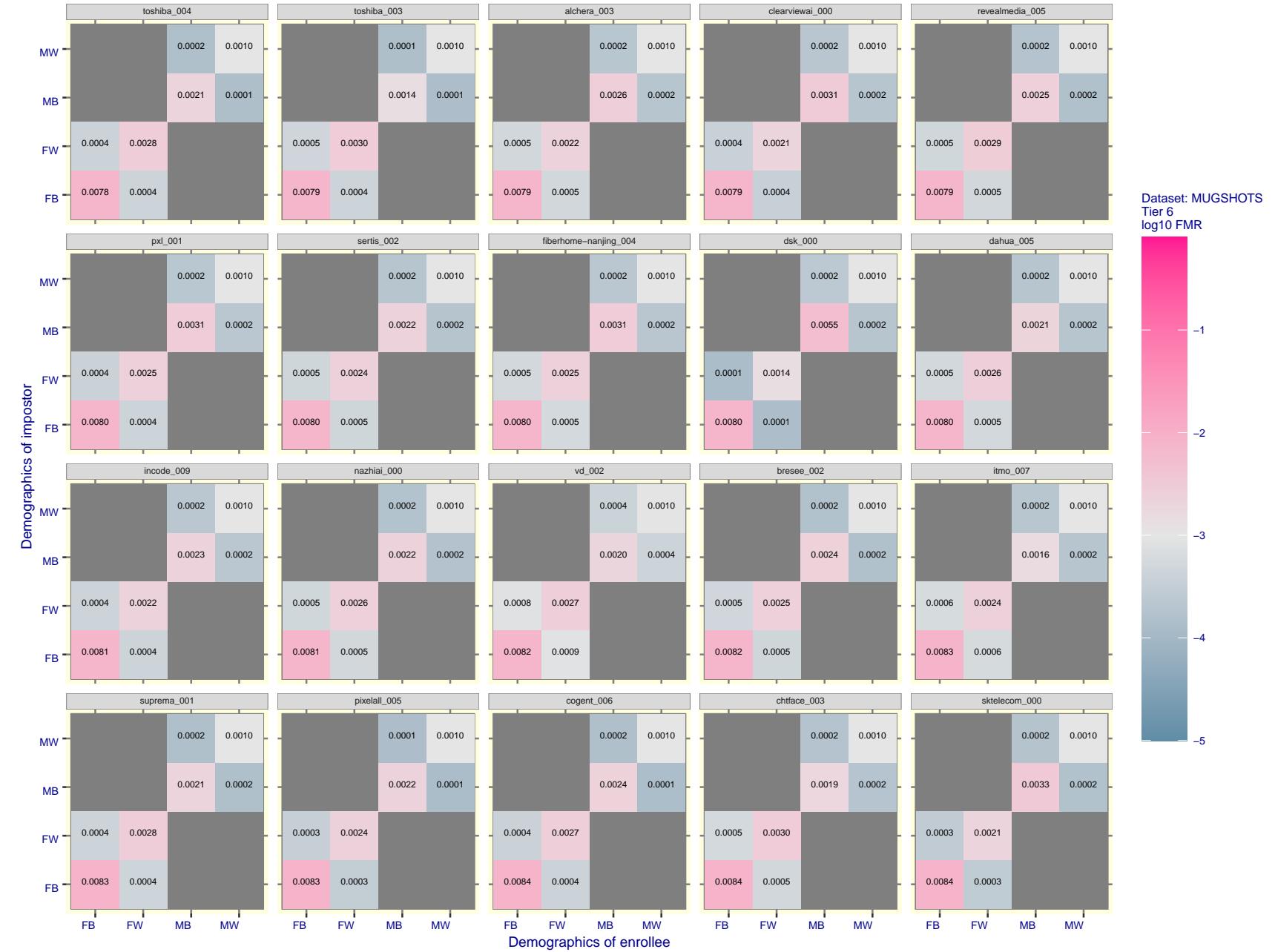


Figure 97: For the mugshot images, FMR for same-sex impostor pairs of images annotated with codes for black female, black male, white female, white male. The threshold is set for each algorithm to give FMR = 0.001 for white males which is the demographic that usually gives the lowest FMR. This means the top right box is the same color in all panels. The panels are sorted over multiple pages in order of FMR on black females, which is the demographic that usually gives the highest FMR.

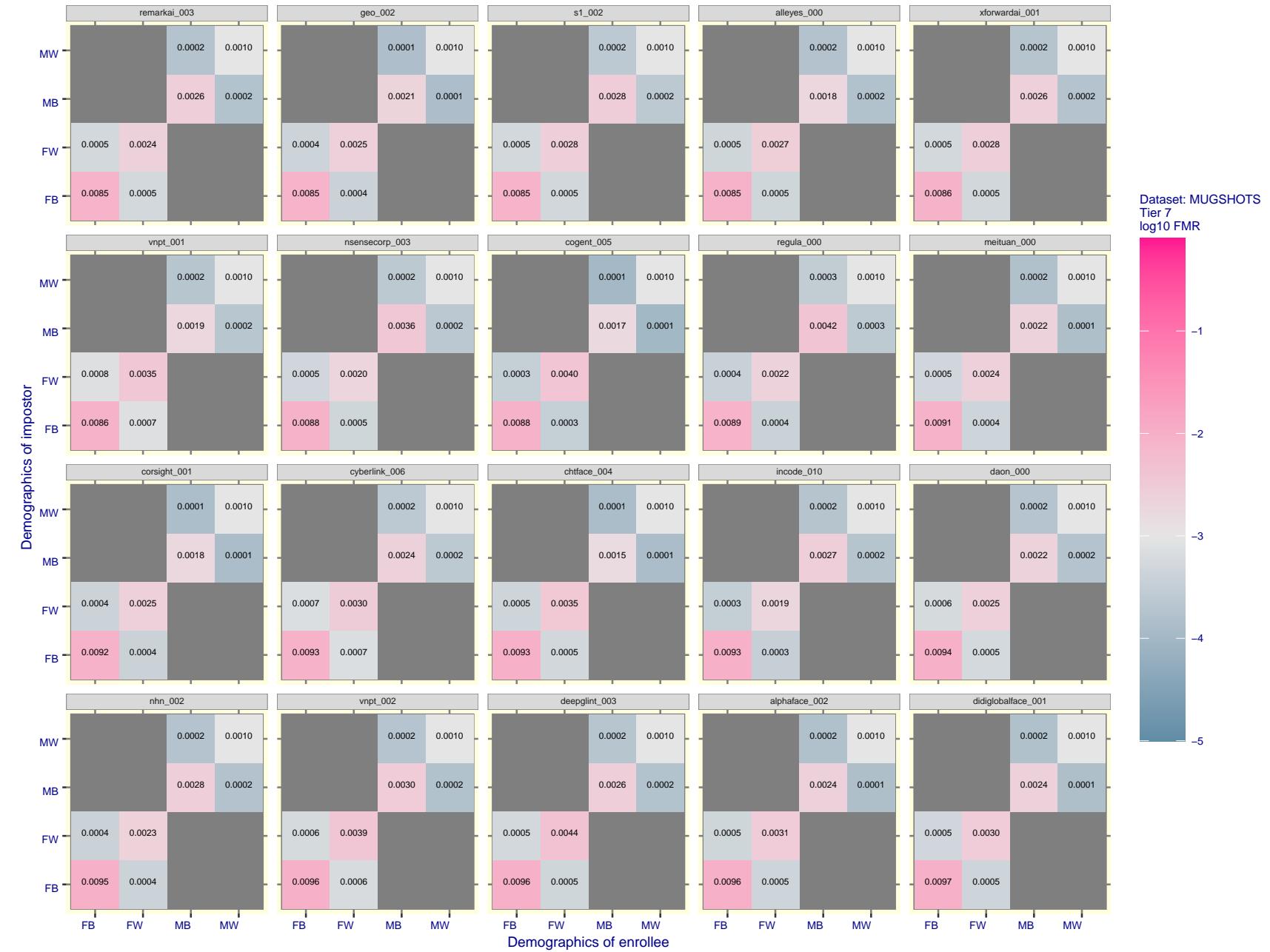


Figure 98: For the mugshot images, FMR for same-sex impostor pairs of images annotated with codes for black female, black male, white female, white male. The threshold is set for each algorithm to give $\text{FMR} = 0.001$ for white males which is the demographic that usually gives the lowest FMR. This means the top right box is the same color in all panels. The panels are sorted over multiple pages in order of FMR on black females, which is the demographic that usually gives the highest FMR.

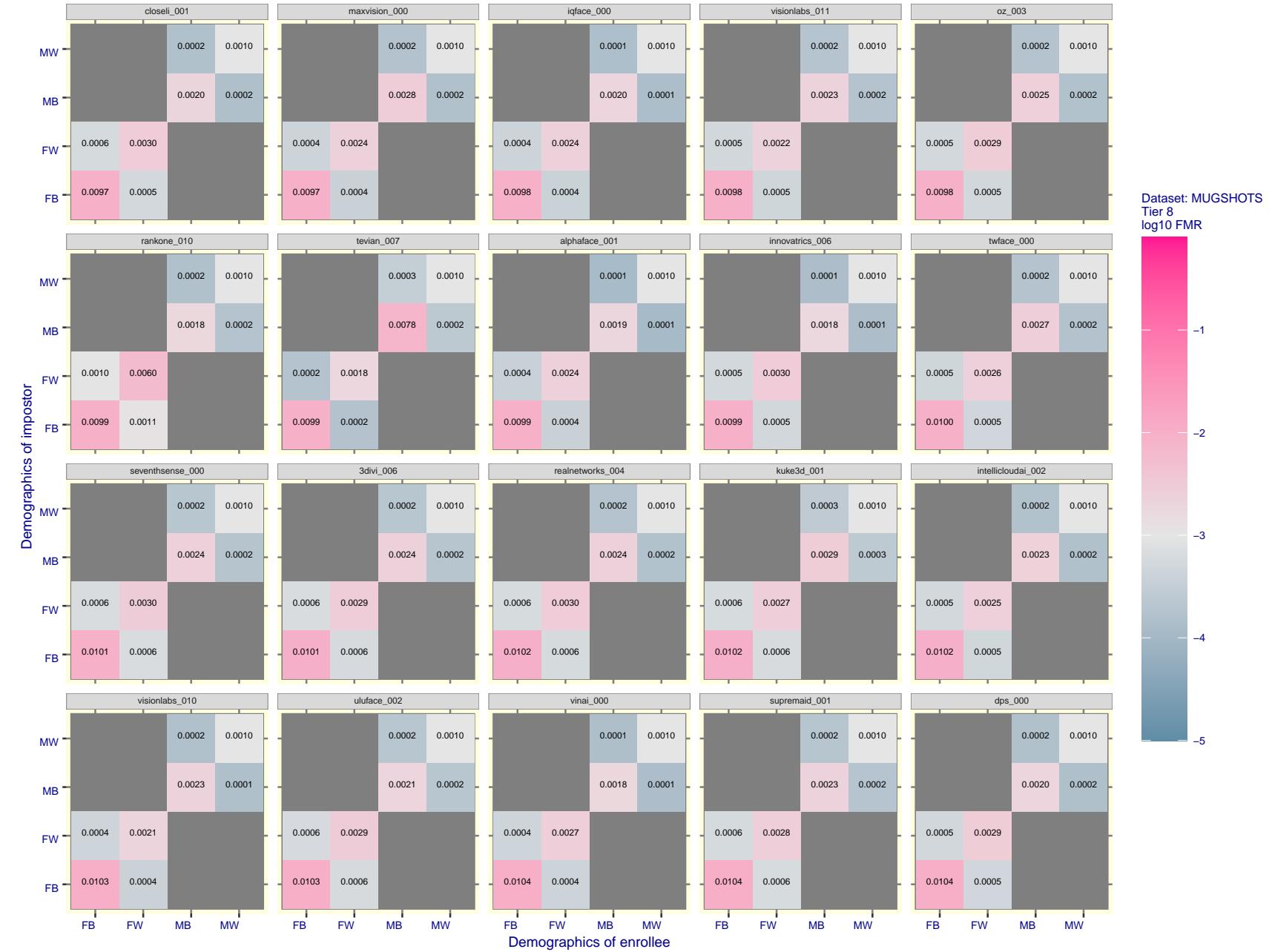


Figure 99: For the mugshot images, FMR for same-sex impostor pairs of images annotated with codes for black female, black male, white female, white male. The threshold is set for each algorithm to give FMR = 0.001 for white males which is the demographic that usually gives the lowest FMR. This means the top right box is the same color in all panels. The panels are sorted over multiple pages in order of FMR on black females, which is the demographic that usually gives the highest FMR.

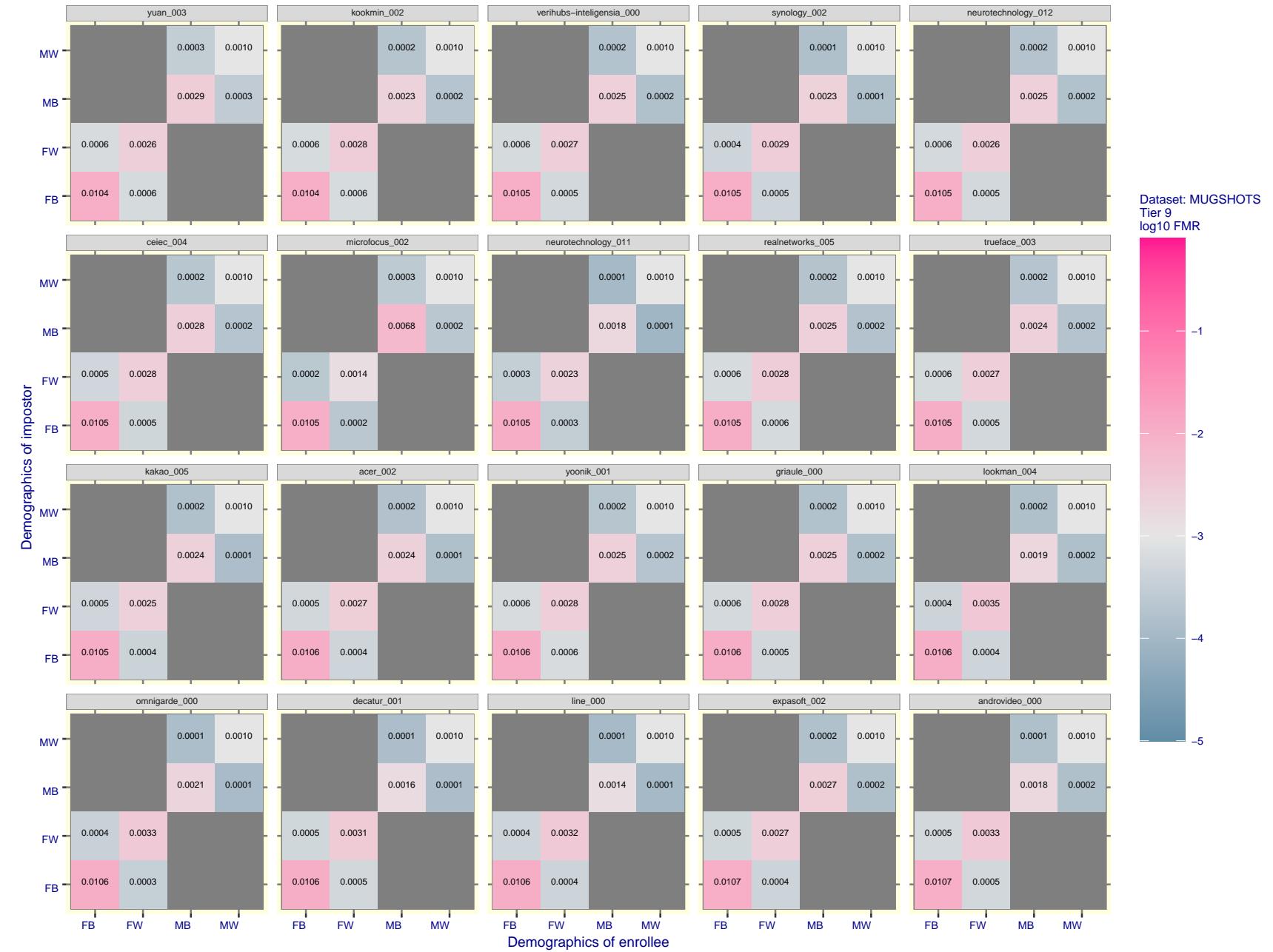


Figure 100: For the mugshot images, FMR for same-sex impostor pairs of images annotated with codes for black female, black male, white female, white male. The threshold is set for each algorithm to give $\text{FMR} = 0.001$ for white males which is the demographic that usually gives the lowest FMR. This means the top right box is the same color in all panels. The panels are sorted over multiple pages in order of FMR on black females, which is the demographic that usually gives the highest FMR.

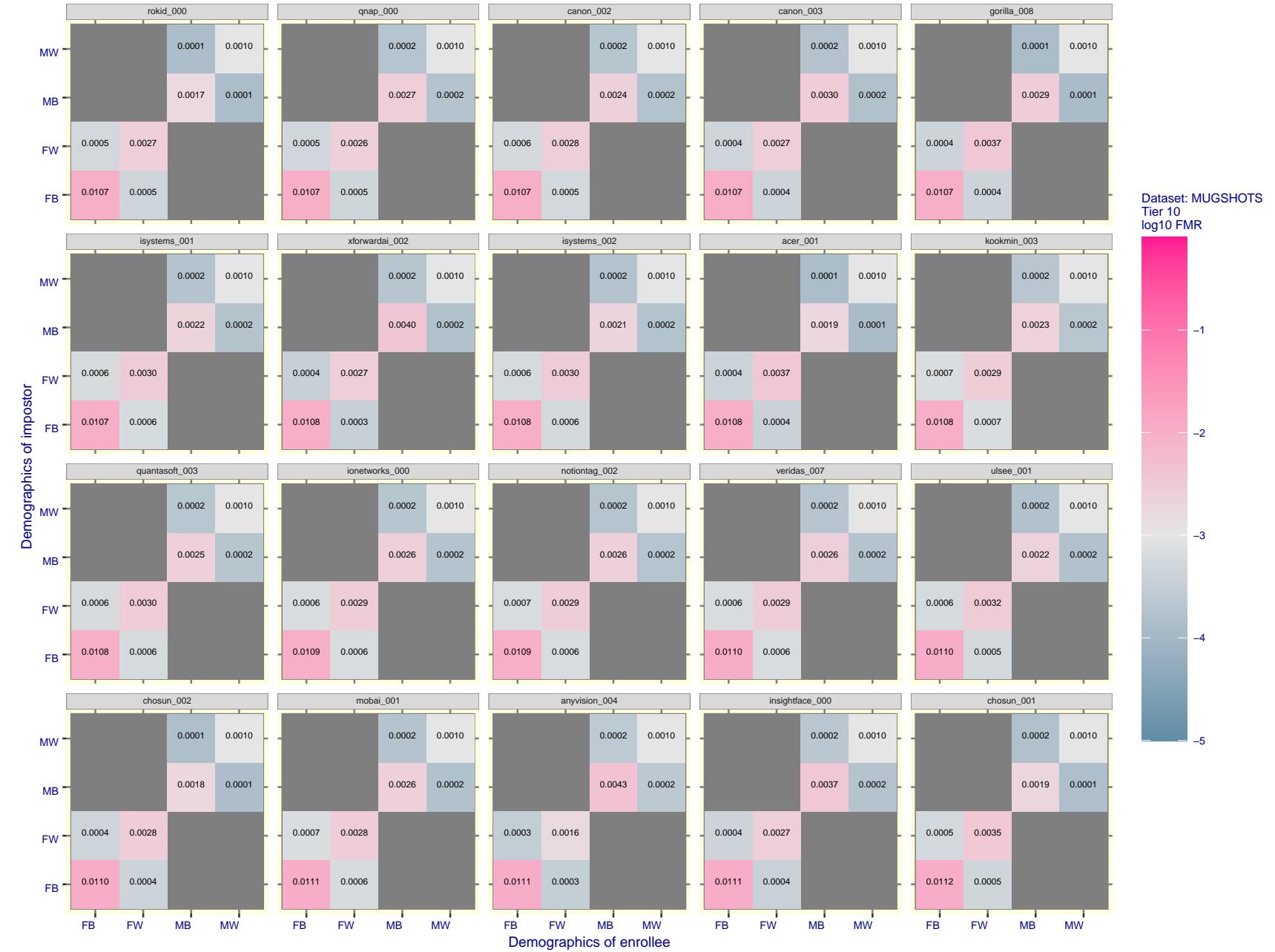


Figure 101: For the mugshot images, FMR for same-sex impostor pairs of images annotated with codes for black female, black male, white female, white male. The threshold is set for each algorithm to give FMR = 0.001 for white males which is the demographic that usually gives the lowest FMR. This means the top right box is the same color in all panels. The panels are sorted over multiple pages in order of FMR on black females, which is the demographic that usually gives the highest FMR.

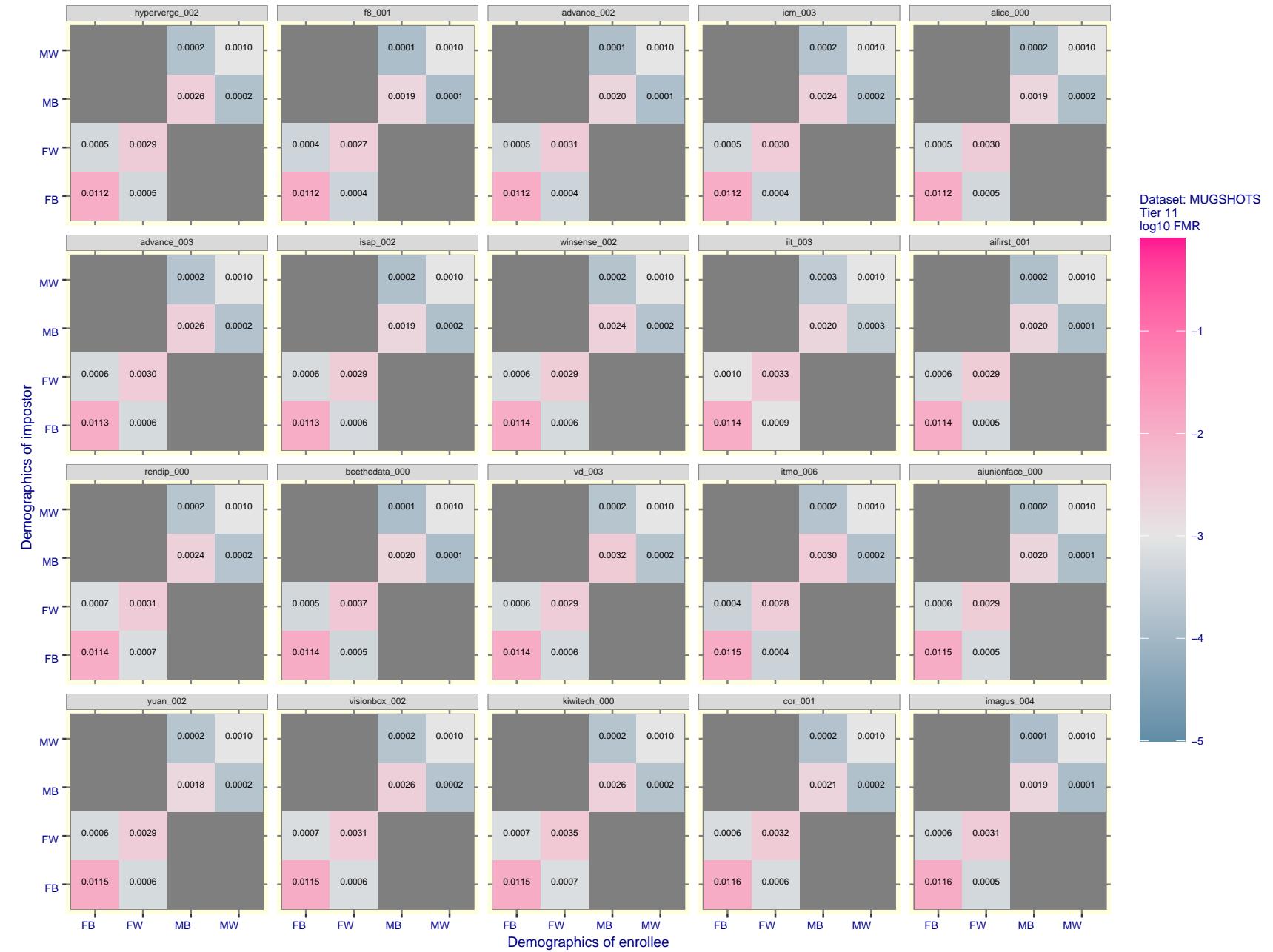


Figure 102: For the mugshot images, FMR for same-sex impostor pairs of images annotated with codes for black female, black male, white female, white male. The threshold is set for each algorithm to give FMR = 0.001 for white males which is the demographic that usually gives the lowest FMR. This means the top right box is the same color in all panels. The panels are sorted over multiple pages in order of FMR on black females, which is the demographic that usually gives the highest FMR.

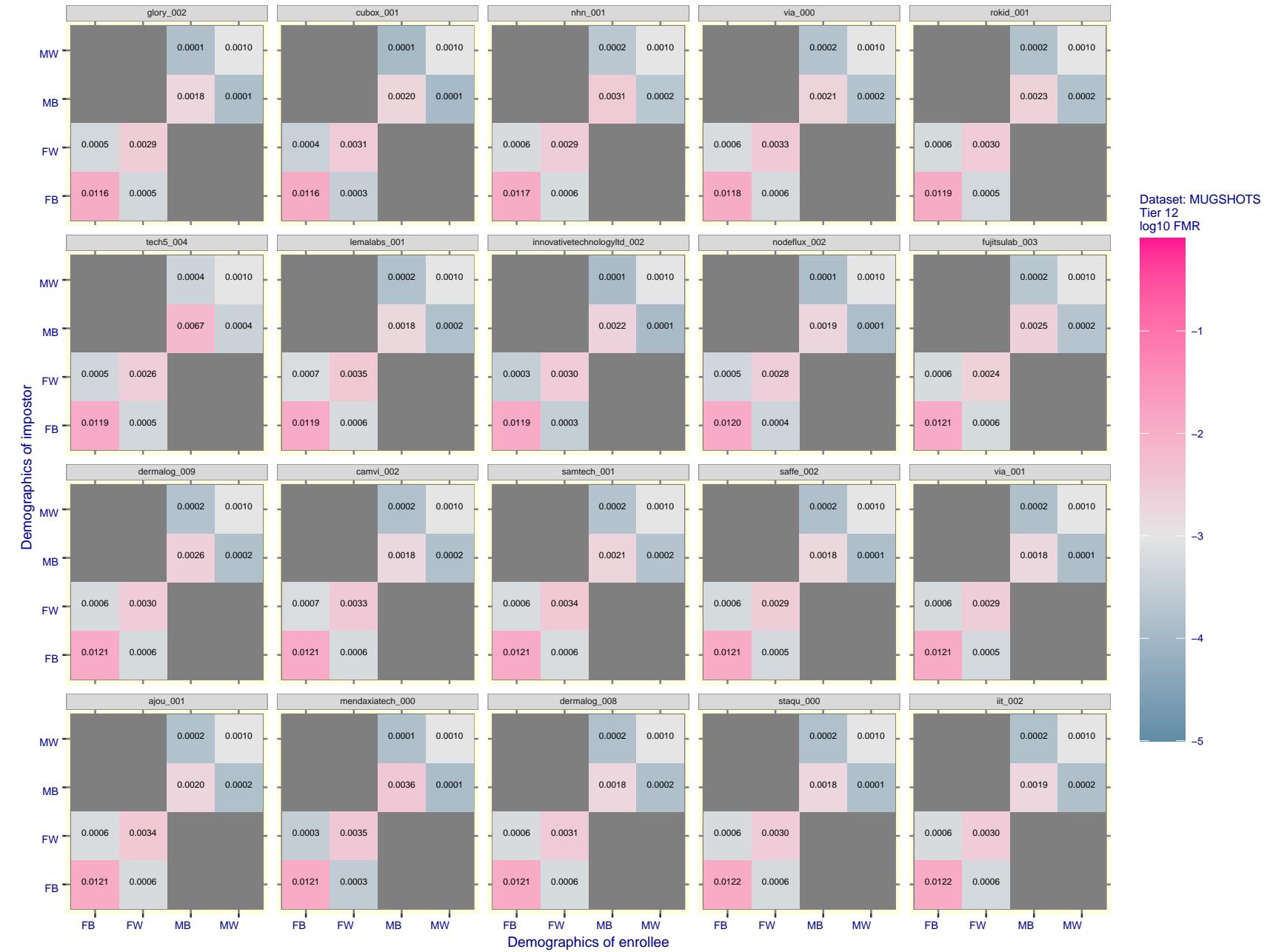


Figure 103: For the mugshot images, FMR for same-sex impostor pairs of images annotated with codes for black female, black male, white female, white male. The threshold is set for each algorithm to give $FMR = 0.001$ for white males which is the demographic that usually gives the lowest FMR. This means the top right box is the same color in all panels. The panels are sorted over multiple pages in order of FMR on black females, which is the demographic that usually gives the highest FMR.

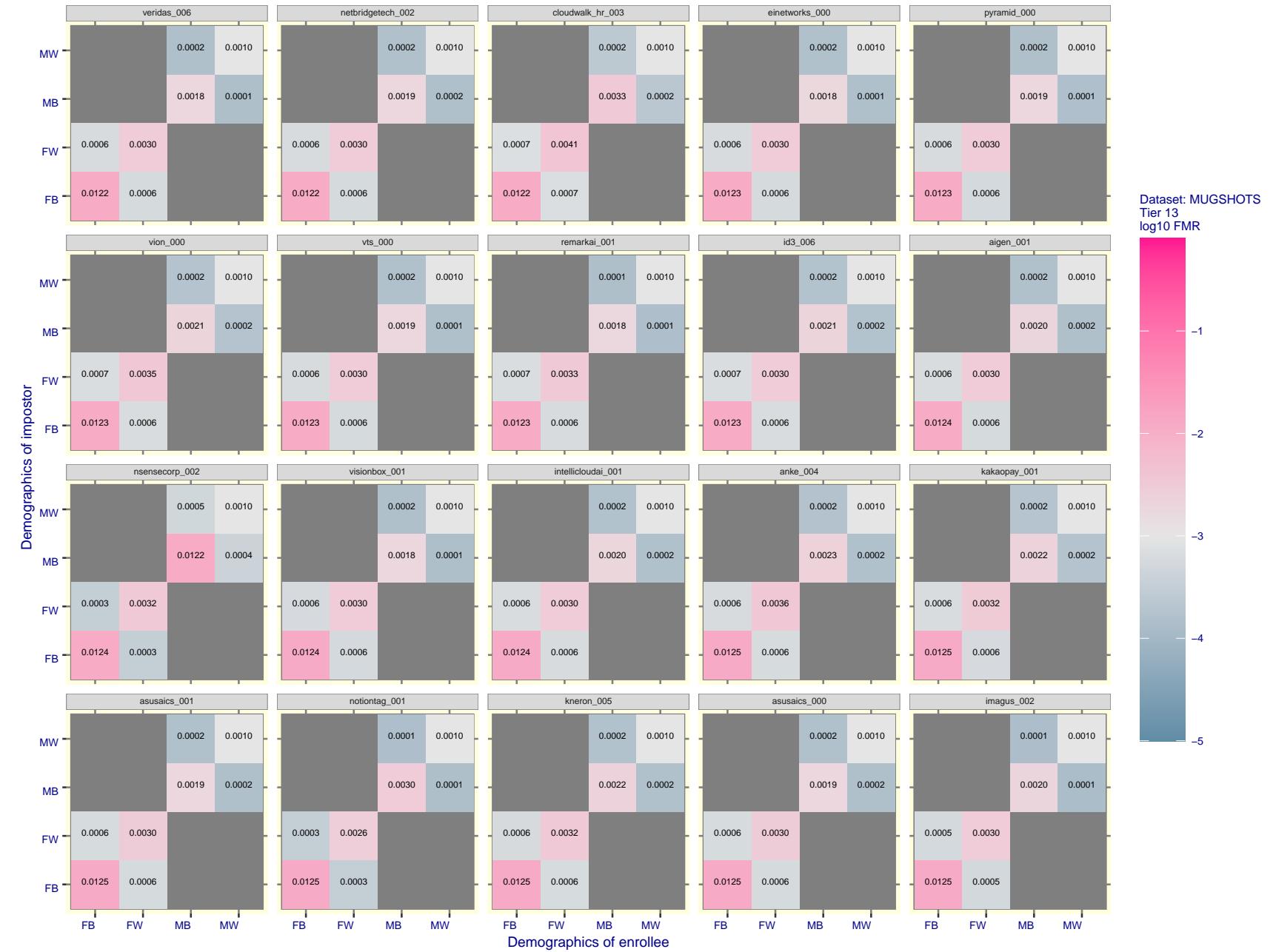


Figure 104: For the mugshot images, FMR for same-sex impostor pairs of images annotated with codes for black female, black male, white female, white male. The threshold is set for each algorithm to give $FMR = 0.001$ for white males which is the demographic that usually gives the lowest FMR. This means the top right box is the same color in all panels. The panels are sorted over multiple pages in order of FMR on black females, which is the demographic that usually gives the highest FMR.

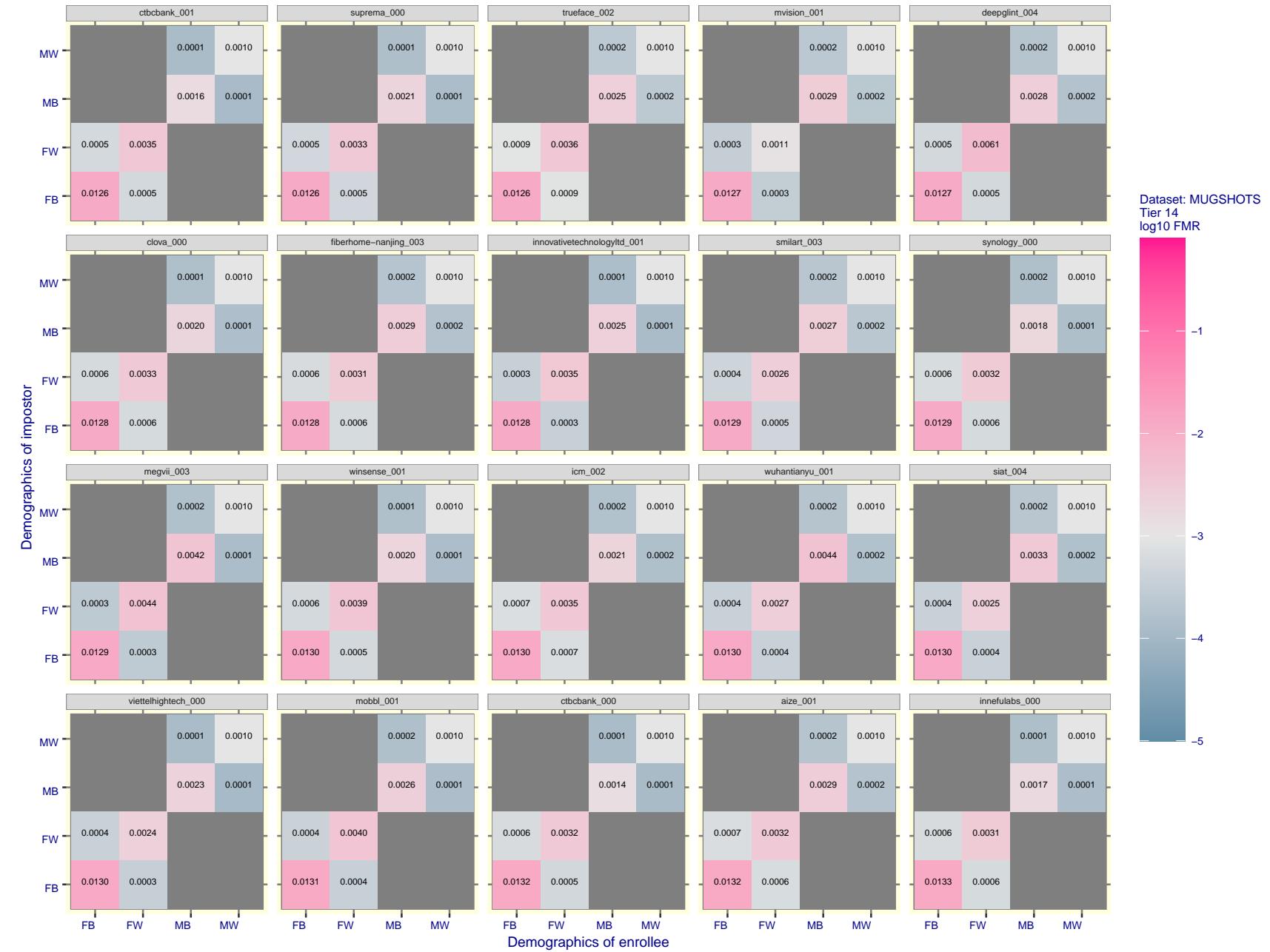


Figure 105: For the mugshot images, FMR for same-sex impostor pairs of images annotated with codes for black female, black male, white female, white male. The threshold is set for each algorithm to give FMR = 0.001 for white males which is the demographic that usually gives the lowest FMR. This means the top right box is the same color in all panels. The panels are sorted over multiple pages in order of FMR on black females, which is the demographic that usually gives the highest FMR.

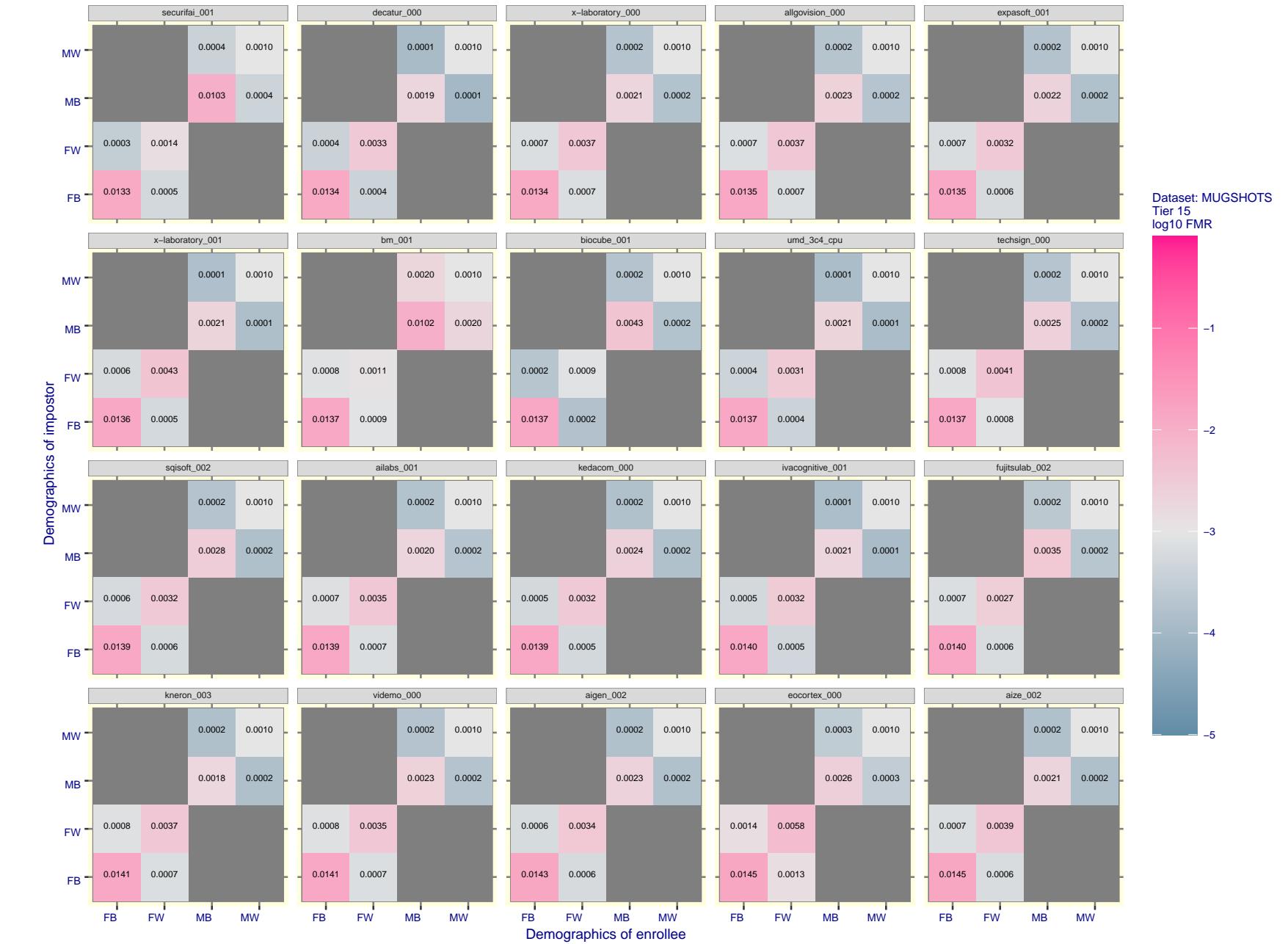


Figure 106: For the mugshot images, FMR for same-sex impostor pairs of images annotated with codes for black female, black male, white female, white male. The threshold is set for each algorithm to give FMR = 0.001 for white males which is the demographic that usually gives the lowest FMR. This means the top right box is the same color in all panels. The panels are sorted over multiple pages in order of FMR on black females, which is the demographic that usually gives the highest FMR.

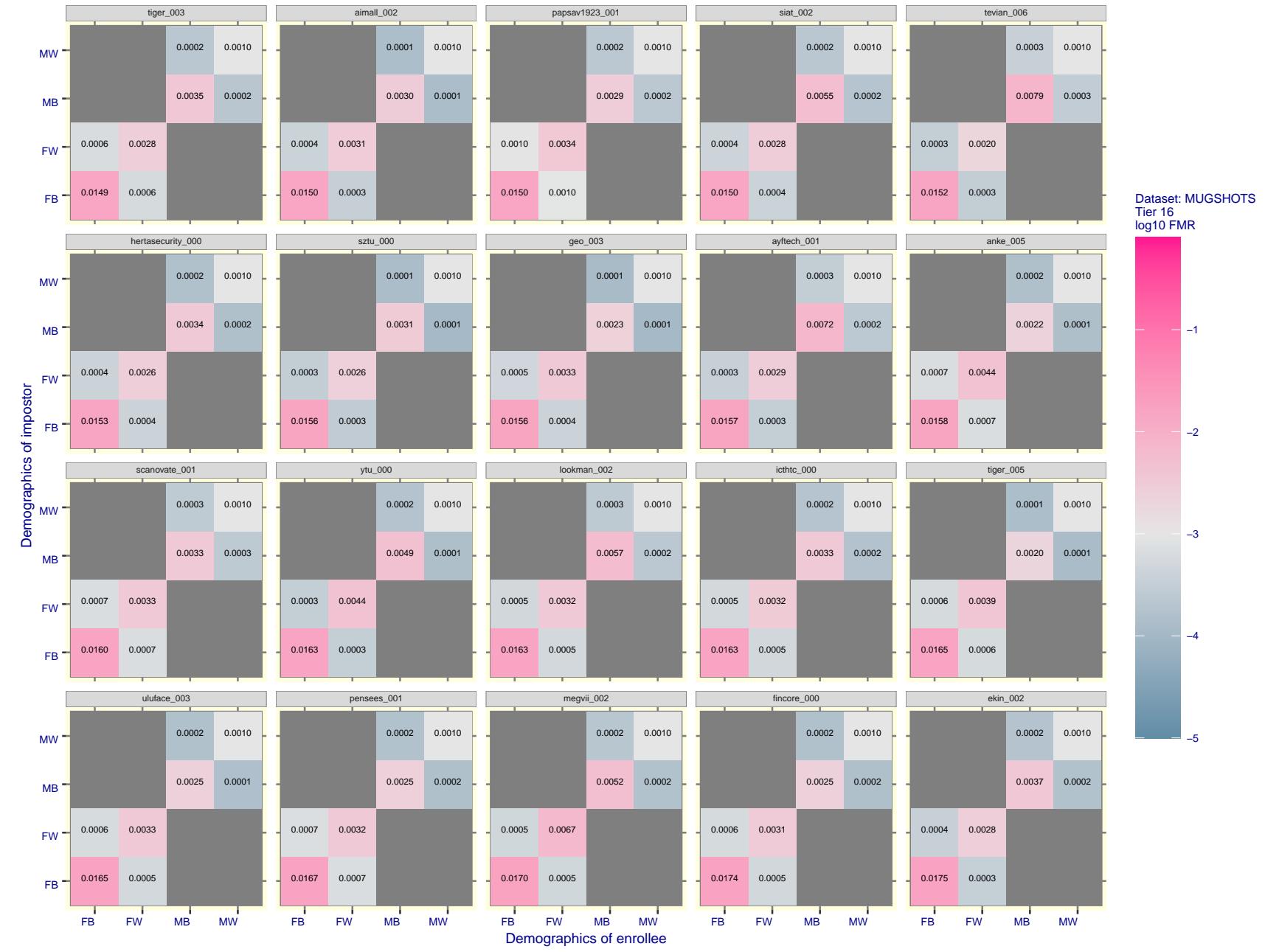


Figure 107: For the mugshot images, FMR for same-sex impostor pairs of images annotated with codes for black female, black male, white female, white male. The threshold is set for each algorithm to give FMR = 0.001 for white males which is the demographic that usually gives the lowest FMR. This means the top right box is the same color in all panels. The panels are sorted over multiple pages in order of FMR on black females, which is the demographic that usually gives the highest FMR.

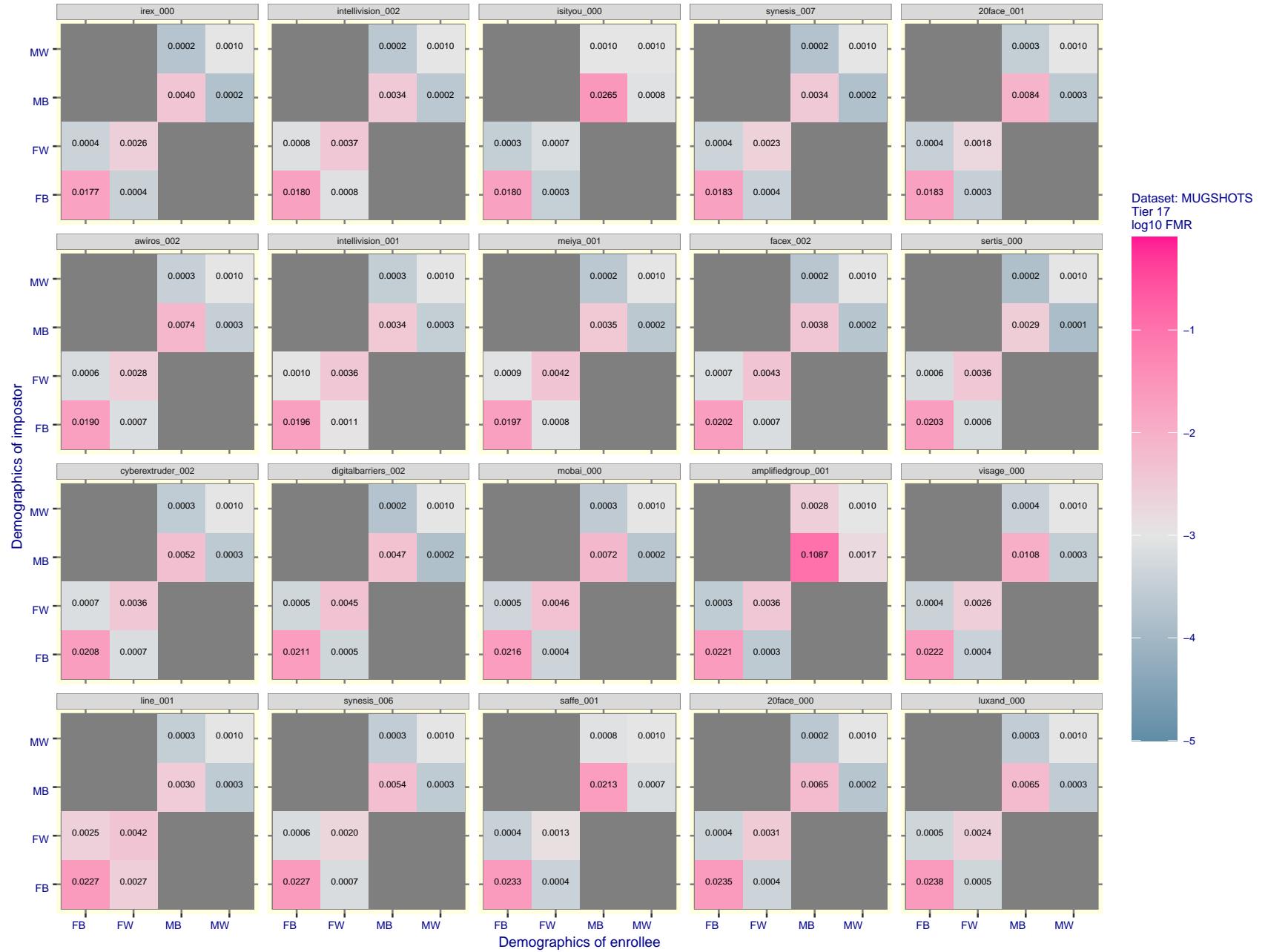


Figure 108: For the mugshot images, FMR for same-sex impostor pairs of images annotated with codes for black female, black male, white female, white male. The threshold is set for each algorithm to give FMR = 0.001 for white males which is the demographic that usually gives the lowest FMR. This means the top right box is the same color in all panels. The panels are sorted over multiple pages in order of FMR on black females, which is the demographic that usually gives the highest FMR.

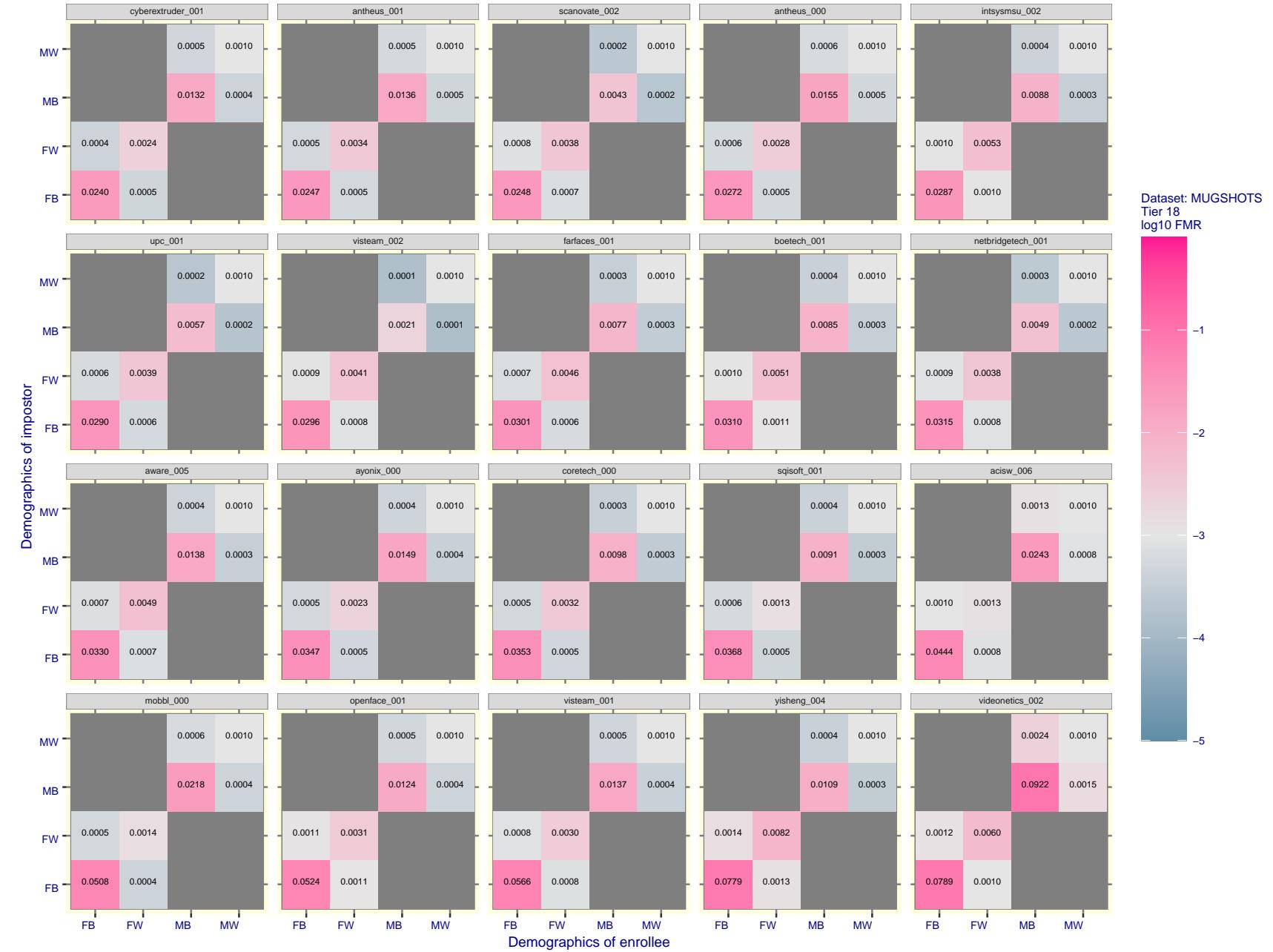


Figure 109: For the mugshot images, FMR for same-sex impostor pairs of images annotated with codes for black female, black male, white female, white male. The threshold is set for each algorithm to give FMR = 0.001 for white males which is the demographic that usually gives the lowest FMR. This means the top right box is the same color in all panels. The panels are sorted over multiple pages in order of FMR on black females, which is the demographic that usually gives the highest FMR.

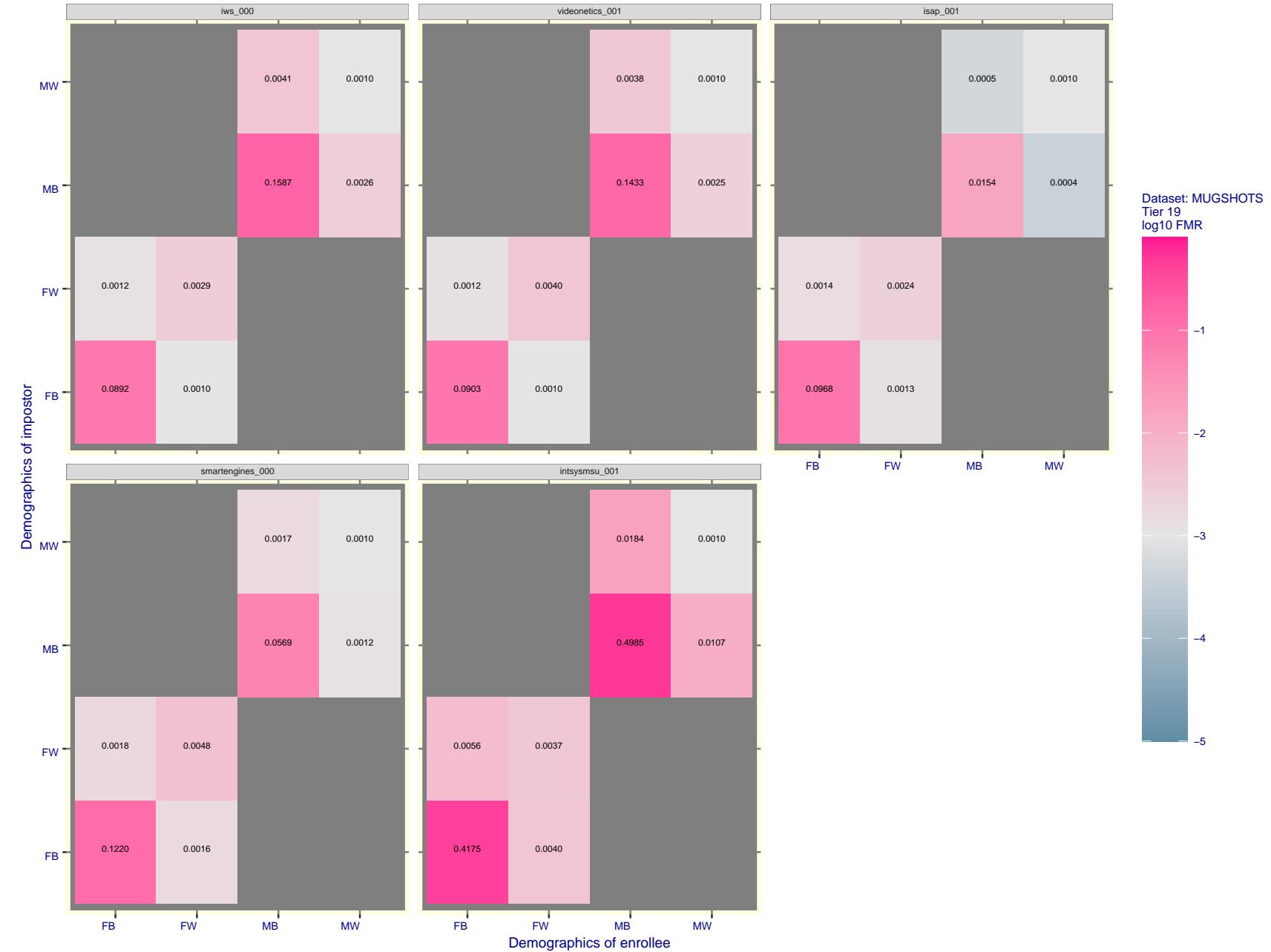


Figure 110: For the mugshot images, FMR for same-sex impostor pairs of images annotated with codes for black female, black male, white female, white male. The threshold is set for each algorithm to give $\text{FMR} = 0.001$ for white males which is the demographic that usually gives the lowest FMR. This means the top right box is the same color in all panels. The panels are sorted over multiple pages in order of FMR on black females, which is the demographic that usually gives the highest FMR.

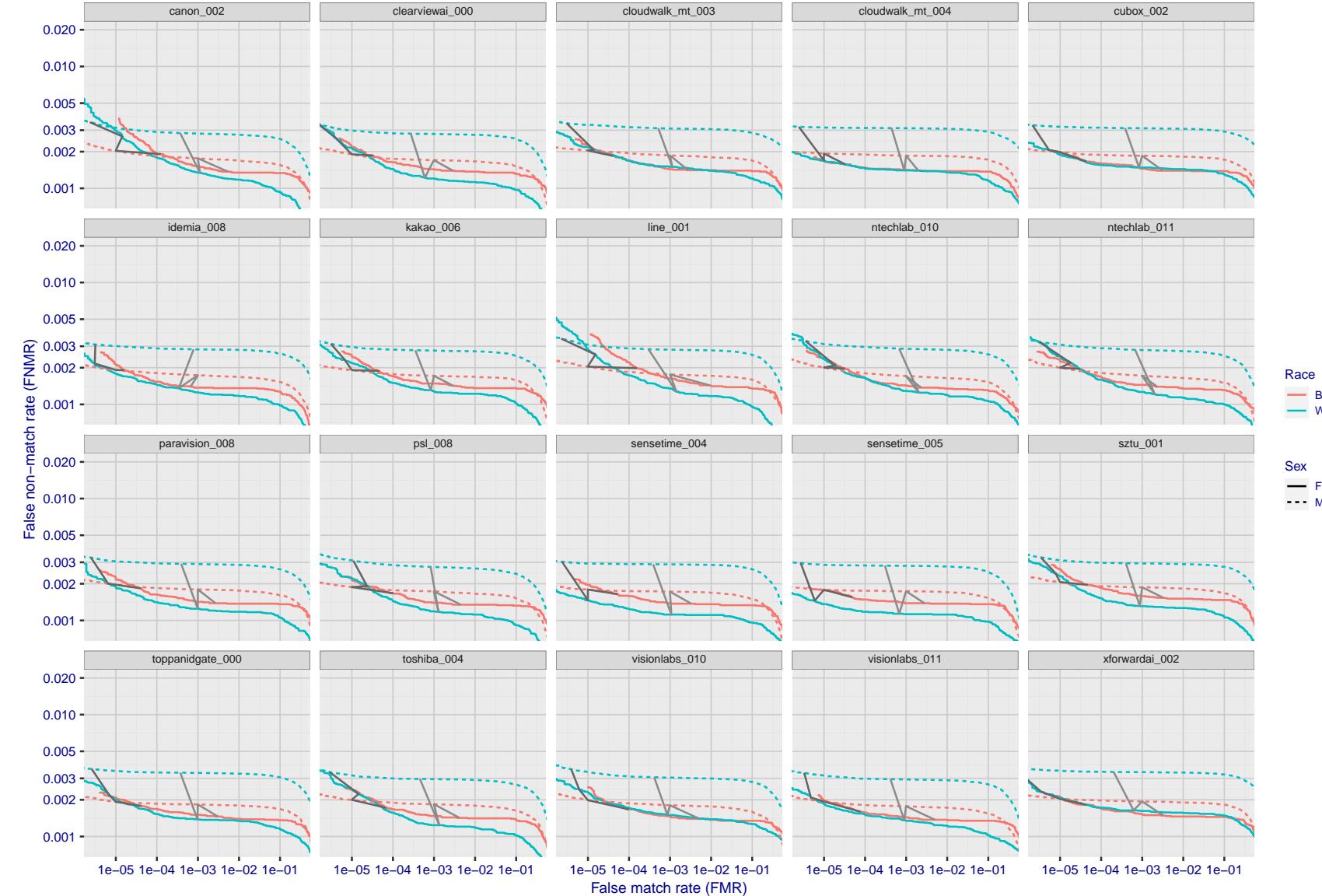


Figure 111: For the mugshot images, error tradeoff characteristics for white females, black females, black males and white males. The Z-shaped grey lines correspond to fixed thresholds, showing both FNMR and FMR vary at one T value. Note: Many of the plots will naively be read as saying women gives worse error rates than men because the solid traces lie above the dotted ones. However, this is misleading and incomplete: The grey lines show the traces reveal horizontal shifts. Thus for the cogent-003 algorithm FNMR for men is higher than for women at a fixed threshold but, at the same time, FMR is higher for women - see Figure 179. As access control systems almost always operate at a fixed threshold, the naive interpretation is incorrect.

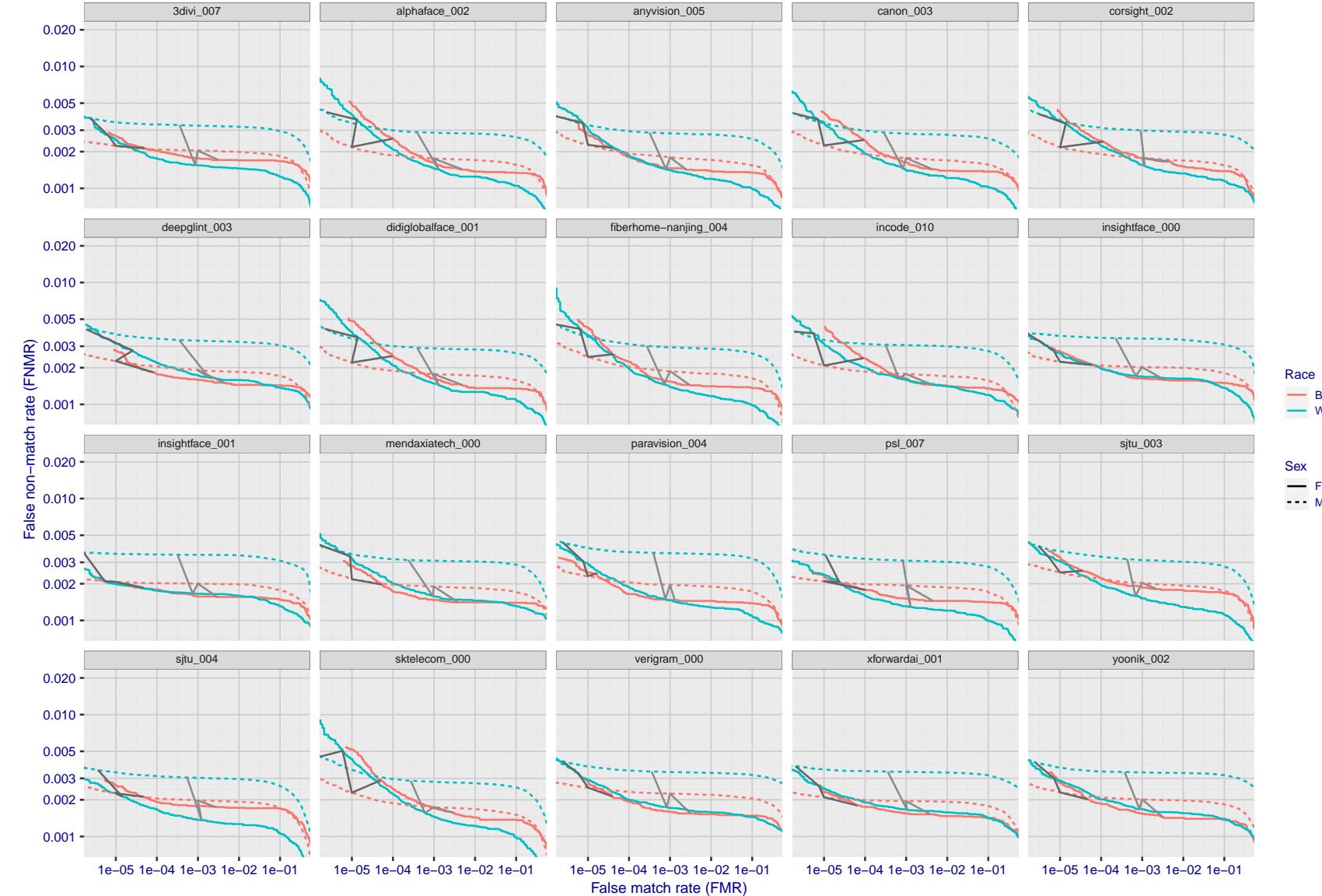


Figure 112: For the mugshot images, error tradeoff characteristics for white females, black females, black males and white males. The Z-shaped grey lines correspond to fixed thresholds, showing both FNMR and FMR vary at one T value. Note: Many of the plots will naively be read as saying women gives worse error rates than men because the solid traces lie above the dotted ones. However, this is misleading and incomplete: The grey lines show the traces reveal horizontal shifts. Thus for the cogent-003 algorithm FNMR for men is higher than for women at a fixed threshold but, at the same time, FMR is higher for women - see Figure 179. As access control systems almost always operate at a fixed threshold, the naive interpretation is incorrect.

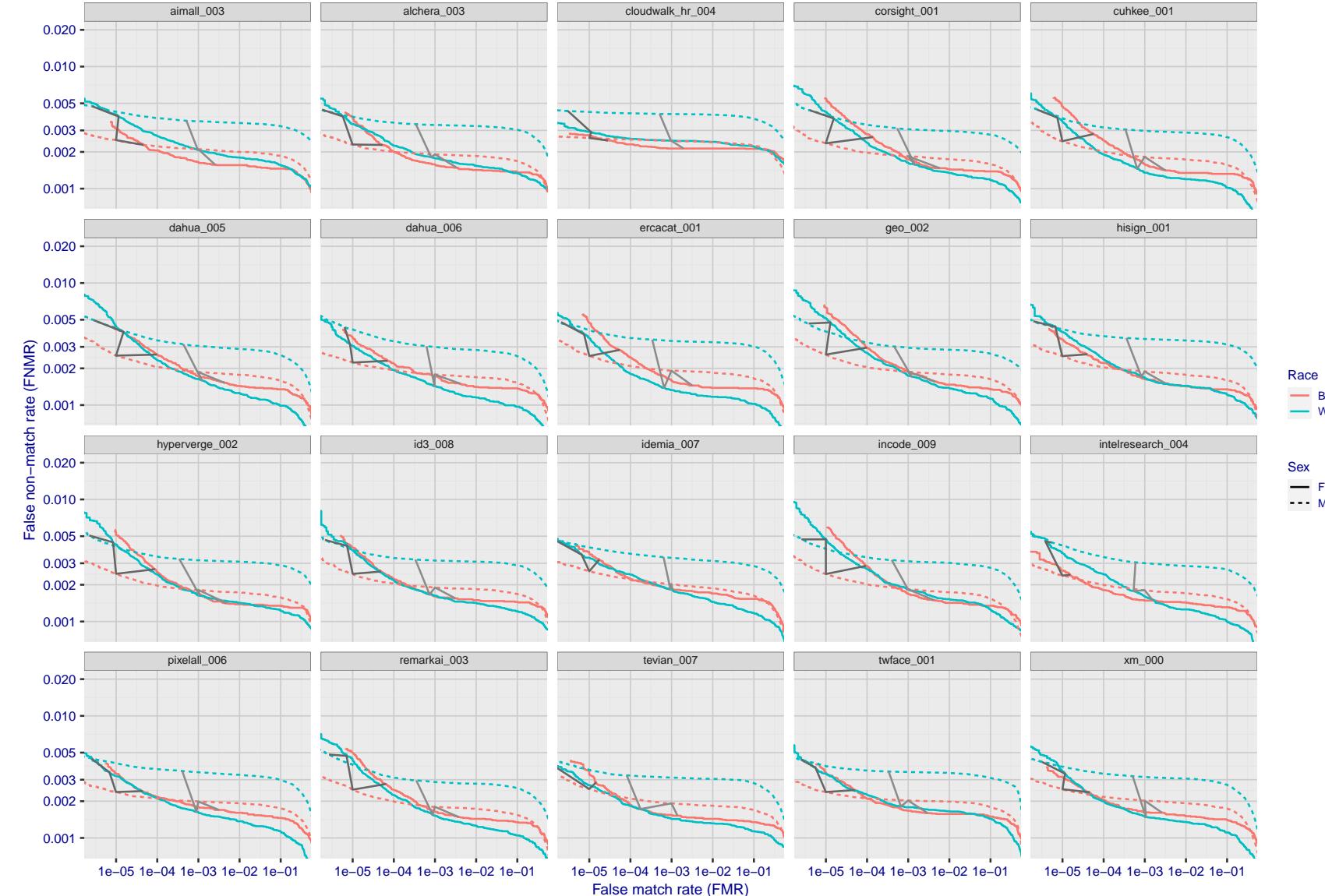


Figure 113: For the mugshot images, error tradeoff characteristics for white females, black females, black males and white males. The Z-shaped grey lines correspond to fixed thresholds, showing both FNMR and FMR vary at one T value. Note: Many of the plots will naively be read as saying women gives worse error rates than men because the solid traces lie above the dotted ones. However, this is misleading and incomplete: The grey lines show the traces reveal horizontal shifts. Thus for the cogent-003 algorithm FNMR for men is higher than for women at a fixed threshold but, at the same time, FMR is higher for women - see Figure 179. As access control systems almost always operate at a fixed threshold, the naive interpretation is incorrect.

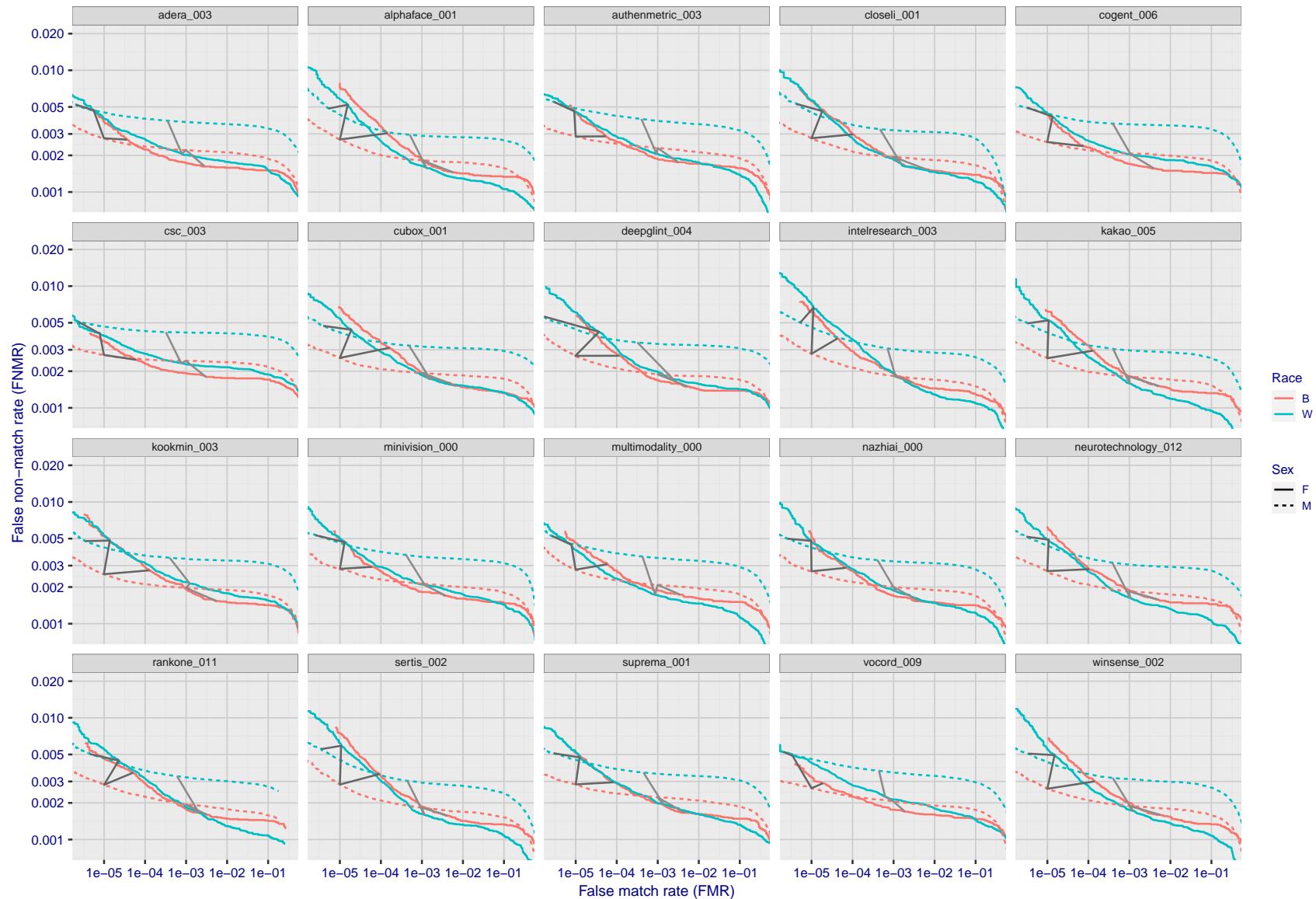


Figure 114: For the mugshot images, error tradeoff characteristics for white females, black females, black males and white males. The Z-shaped grey lines correspond to fixed thresholds, showing both FNMR and FMR vary at one T value. Note: Many of the plots will naively be read as saying women gives worse error rates than men because the solid traces lie above the dotted ones. However, this is misleading and incomplete: The grey lines show the traces reveal horizontal shifts. Thus for the cogent-003 algorithm FNMR for men is higher than for women at a fixed threshold but, at the same time, FMR is higher for women - see Figure 179. As access control systems almost always operate at a fixed threshold, the naive interpretation is incorrect.

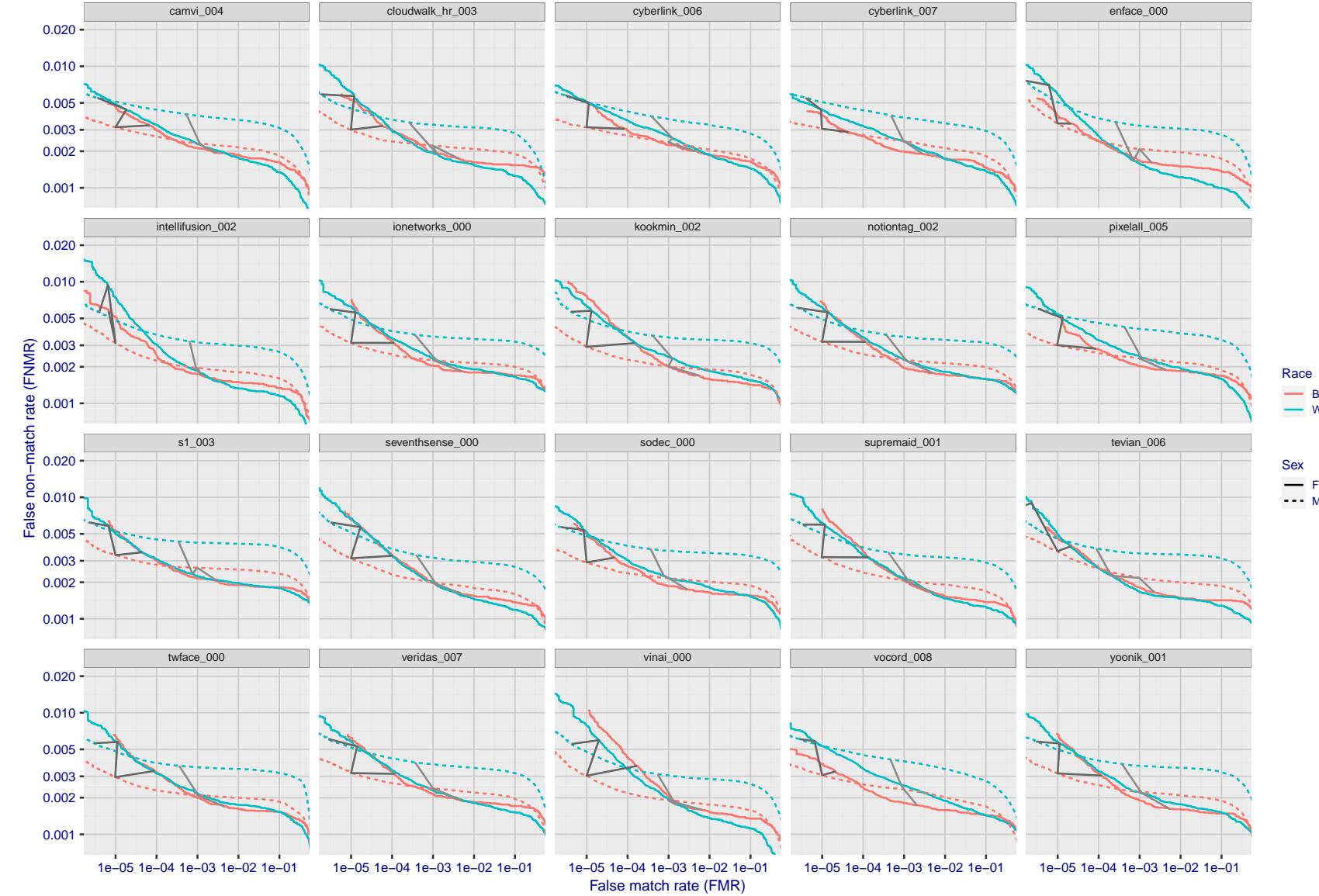


Figure 115: For the mugshot images, error tradeoff characteristics for white females, black females, black males and white males. The Z-shaped grey lines correspond to fixed thresholds, showing both FNMR and FMR vary at one T value. Note: Many of the plots will naively be read as saying women gives worse error rates than men because the solid traces lie above the dotted ones. However, this is misleading and incomplete: The grey lines show the traces reveal horizontal shifts. Thus for the cogent-003 algorithm FNMR for men is higher than for women at a fixed threshold but, at the same time, FMR is higher for women - see Figure 179. As access control systems almost always operate at a fixed threshold, the naive interpretation is incorrect.

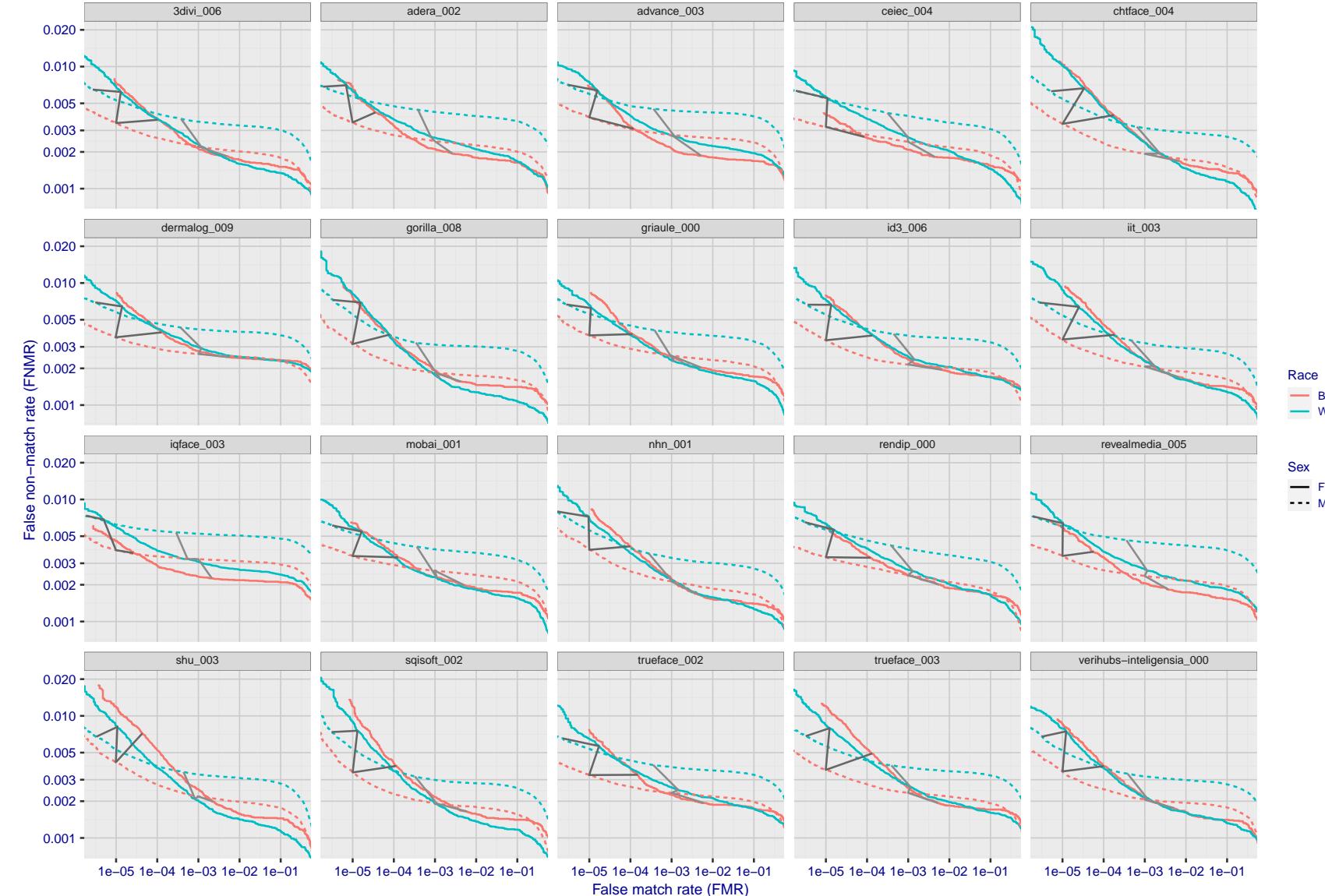


Figure 116: For the mugshot images, error tradeoff characteristics for white females, black females, black males and white males. The Z-shaped grey lines correspond to fixed thresholds, showing both FNMR and FMR vary at one T value. Note: Many of the plots will naively be read as saying women gives worse error rates than men because the solid traces lie above the dotted ones. However, this is misleading and incomplete: The grey lines show the traces reveal horizontal shifts. Thus for the cogent-003 algorithm FNMR for men is higher than for women at a fixed threshold but, at the same time, FMR is higher for women - see Figure 179. As access control systems almost always operate at a fixed threshold, the naive interpretation is incorrect.

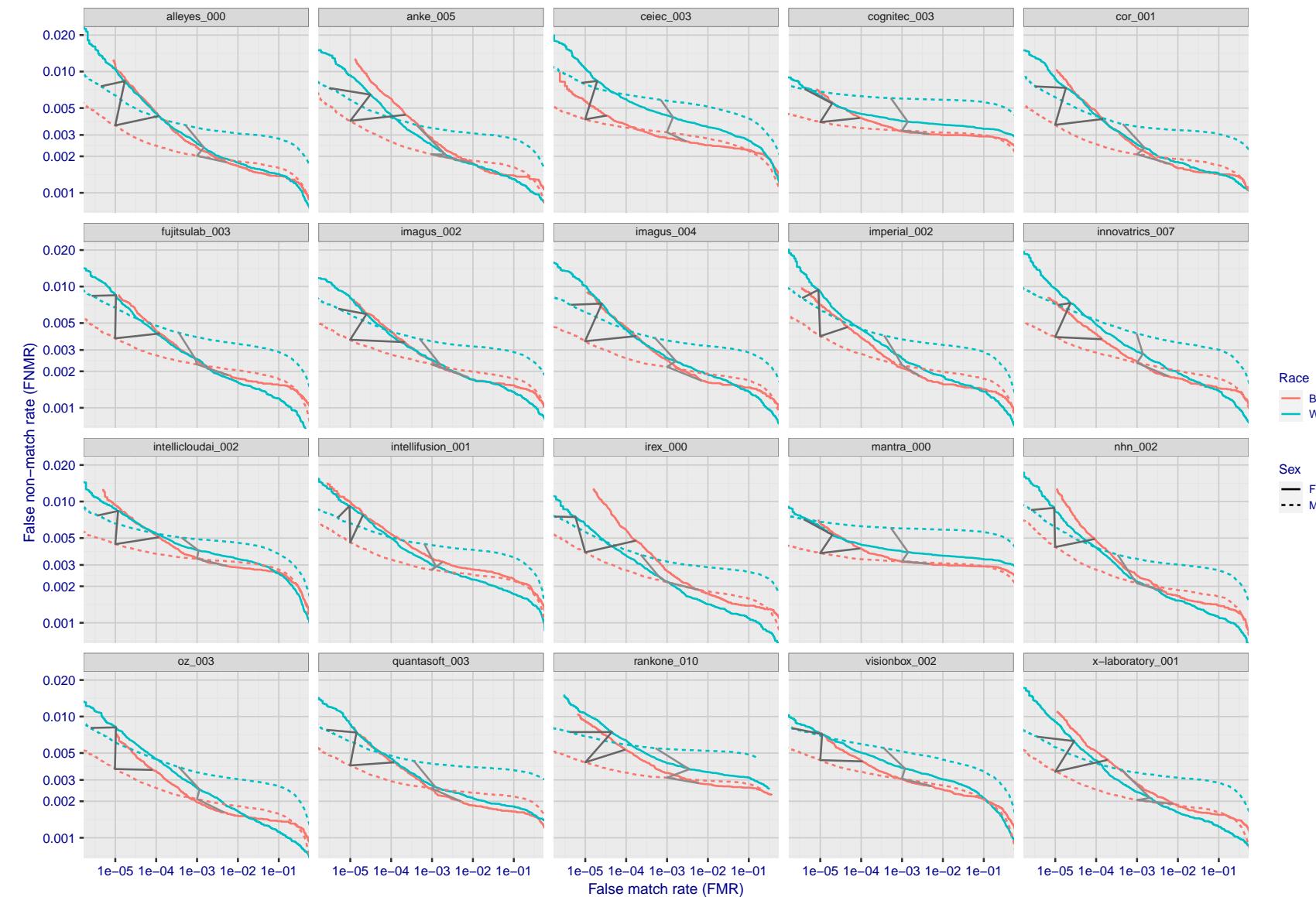


Figure 117: For the mugshot images, error tradeoff characteristics for white females, black females, black males and white males. The Z-shaped grey lines correspond to fixed thresholds, showing both FNMR and FMR vary at one T value. Note: Many of the plots will naively be read as saying women gives worse error rates than men because the solid traces lie above the dotted ones. However, this is misleading and incomplete: The grey lines show the traces reveal horizontal shifts. Thus for the cogent-003 algorithm FNMR for men is higher than for women at a fixed threshold but, at the same time, FMR is higher for women - see Figure 179. As access control systems almost always operate at a fixed threshold, the naive interpretation is incorrect.

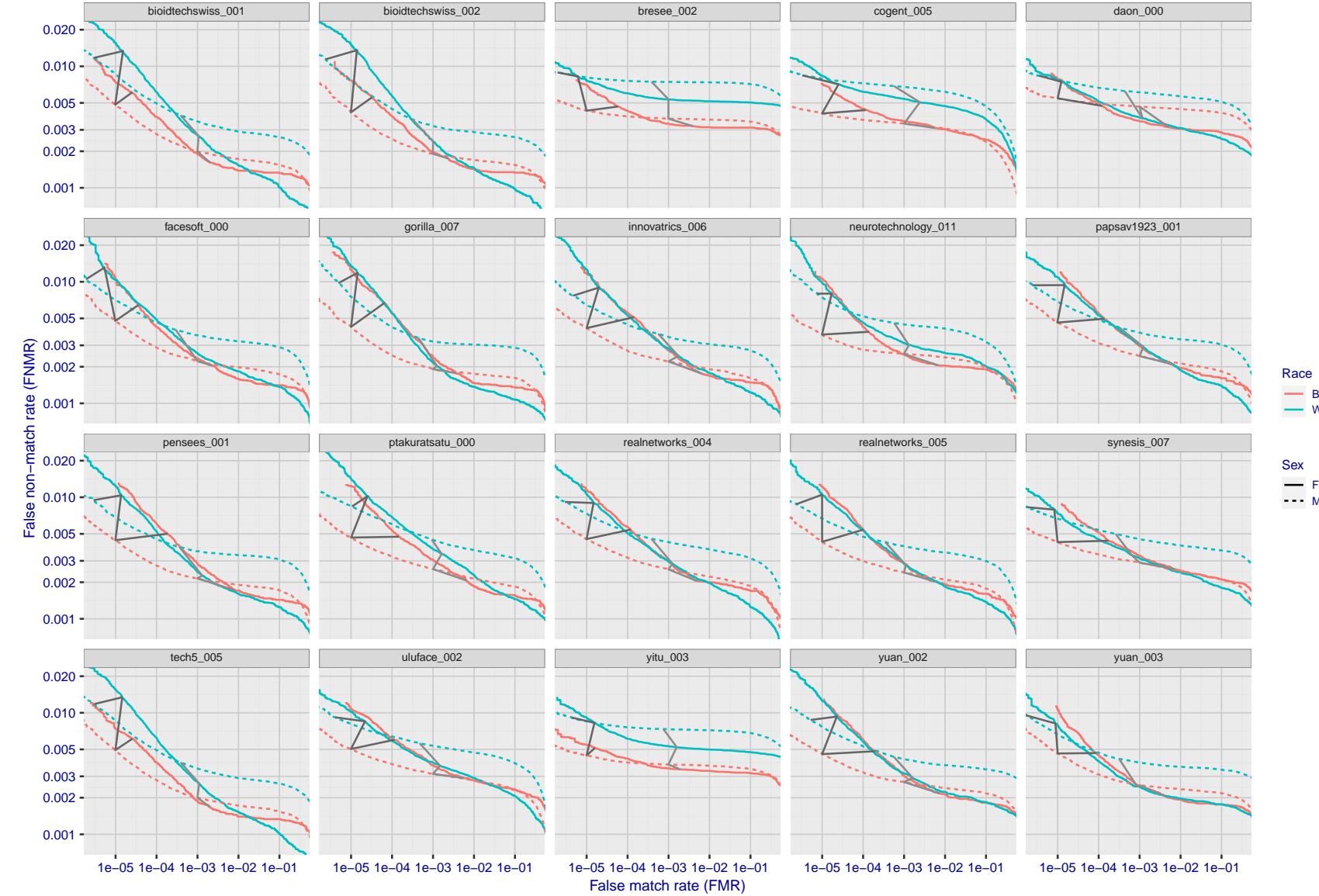


Figure 118: For the mugshot images, error tradeoff characteristics for white females, black females, black males and white males. The Z-shaped grey lines correspond to fixed thresholds, showing both FNMR and FMR vary at one T value. Note: Many of the plots will naively be read as saying women gives worse error rates than men because the solid traces lie above the dotted ones. However, this is misleading and incomplete: The grey lines show the traces reveal horizontal shifts. Thus for the cogent-003 algorithm FNMR for men is higher than for women at a fixed threshold but, at the same time, FMR is higher for women - see Figure 179. As access control systems almost always operate at a fixed threshold, the naive interpretation is incorrect.

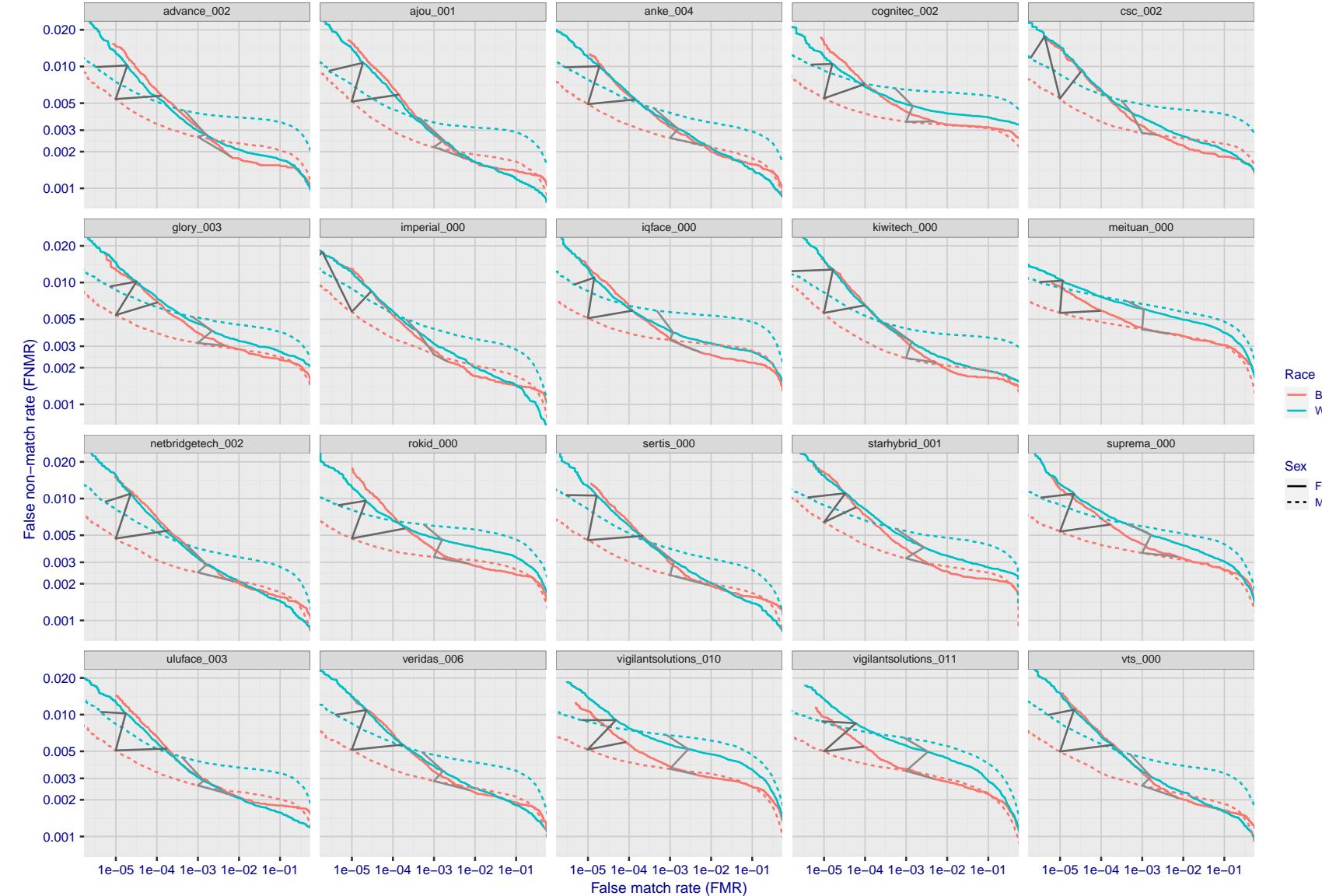


Figure 119: For the mugshot images, error tradeoff characteristics for white females, black females, black males and white males. The Z-shaped grey lines correspond to fixed thresholds, showing both FNMR and FMR vary at one T value. Note: Many of the plots will naively be read as saying women gives worse error rates than men because the solid traces lie above the dotted ones. However, this is misleading and incomplete: The grey lines show the traces reveal horizontal shifts. Thus for the cogent-003 algorithm FNMR for men is higher than for women at a fixed threshold but, at the same time, FMR is higher for women - see Figure 179. As access control systems almost always operate at a fixed threshold, the naive interpretation is incorrect.

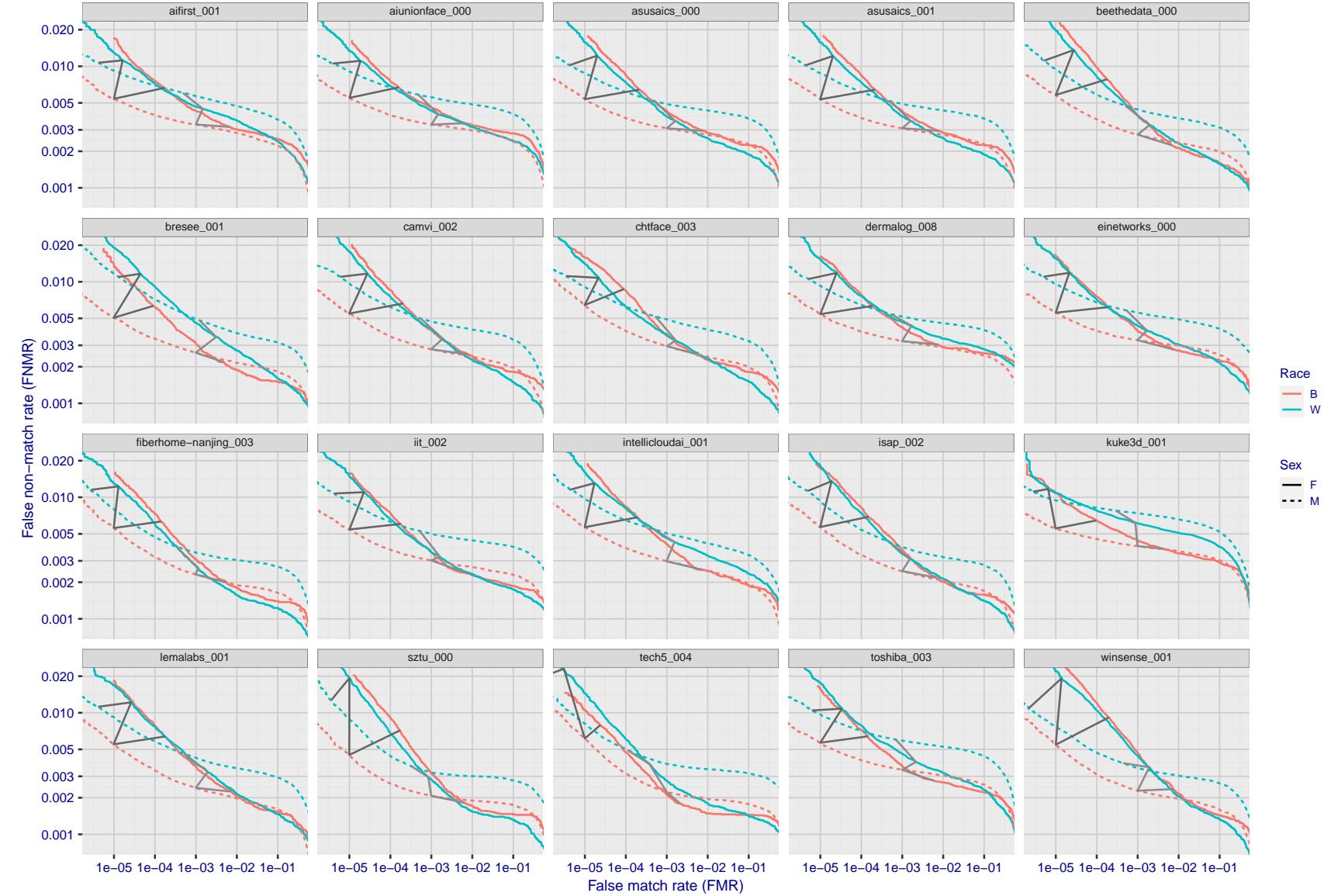


Figure 120: For the mugshot images, error tradeoff characteristics for white females, black females, black males and white males. The Z-shaped grey lines correspond to fixed thresholds, showing both FNMR and FMR vary at one T value. Note: Many of the plots will naively be read as saying women gives worse error rates than men because the solid traces lie above the dotted ones. However, this is misleading and incomplete: The grey lines show the traces reveal horizontal shifts. Thus for the cogent-003 algorithm FNMR for men is higher than for women at a fixed threshold but, at the same time, FMR is higher for women - see Figure 179. As access control systems almost always operate at a fixed threshold, the naive interpretation is incorrect.

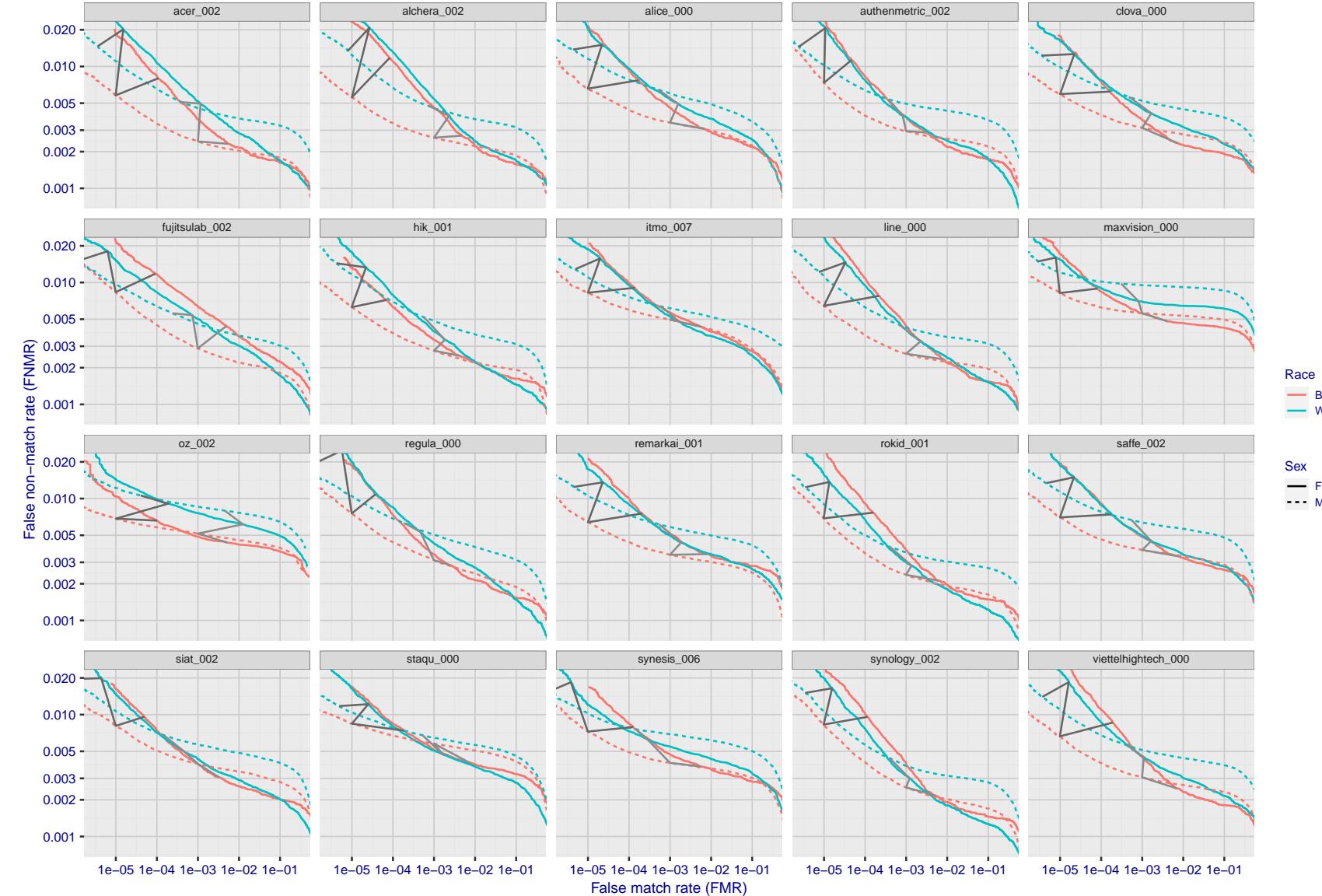


Figure 121: For the mugshot images, error tradeoff characteristics for white females, black females, black males and white males. The Z-shaped grey lines correspond to fixed thresholds, showing both FNMR and FMR vary at one T value. Note: Many of the plots will naively be read as saying women gives worse error rates than men because the solid traces lie above the dotted ones. However, this is misleading and incomplete: The grey lines show the traces reveal horizontal shifts. Thus for the cogent-003 algorithm FNMR for men is higher than for women at a fixed threshold but, at the same time, FMR is higher for women - see Figure 179. As access control systems almost always operate at a fixed threshold, the naive interpretation is incorrect.

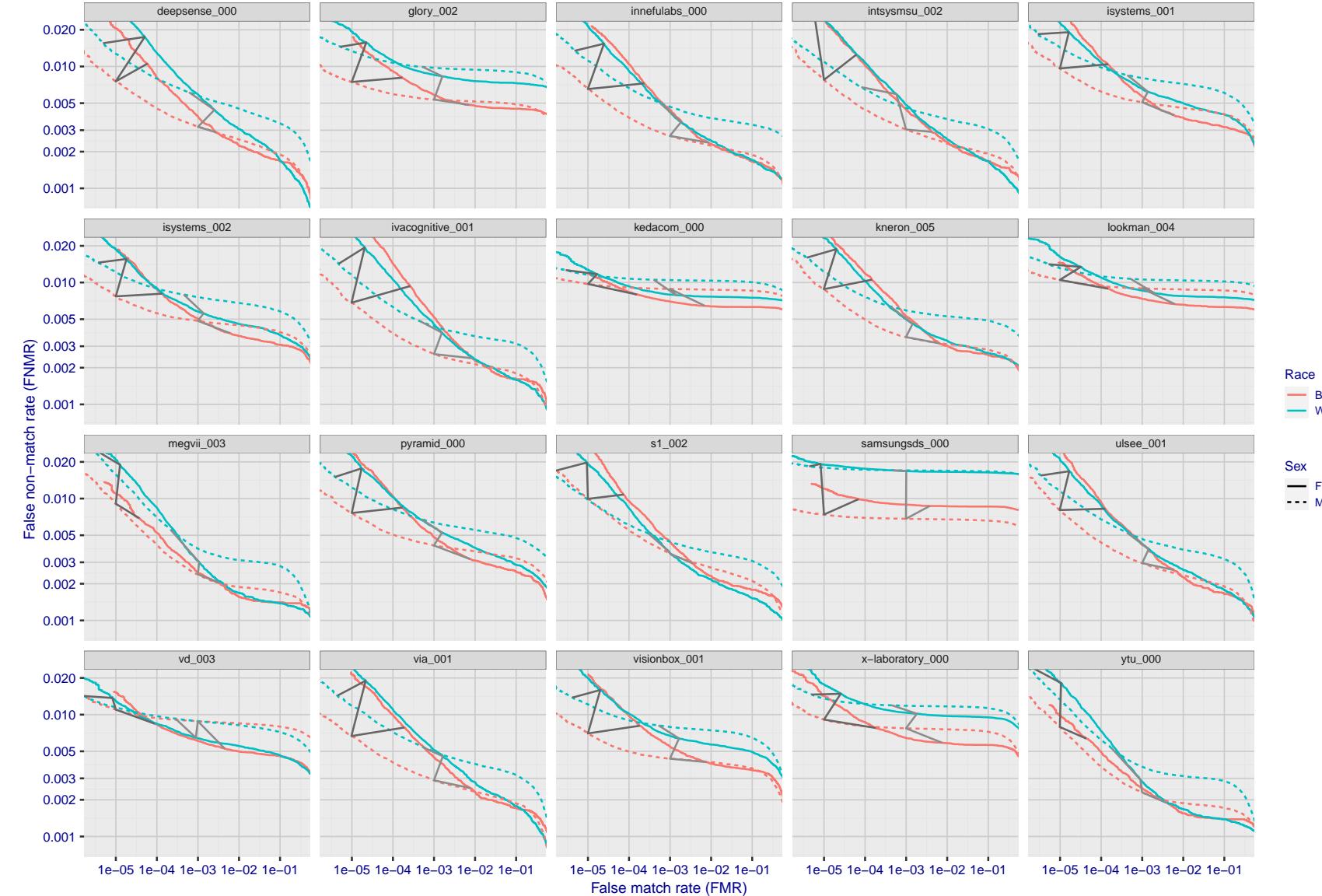


Figure 122: For the mugshot images, error tradeoff characteristics for white females, black females, black males and white males. The Z-shaped grey lines correspond to fixed thresholds, showing both FNMR and FMR vary at one T value. Note: Many of the plots will naively be read as saying women gives worse error rates than men because the solid traces lie above the dotted ones. However, this is misleading and incomplete: The grey lines show the traces reveal horizontal shifts. Thus for the cogent-003 algorithm FNMR for men is higher than for women at a fixed threshold but, at the same time, FMR is higher for women - see Figure 179. As access control systems almost always operate at a fixed threshold, the naive interpretation is incorrect.

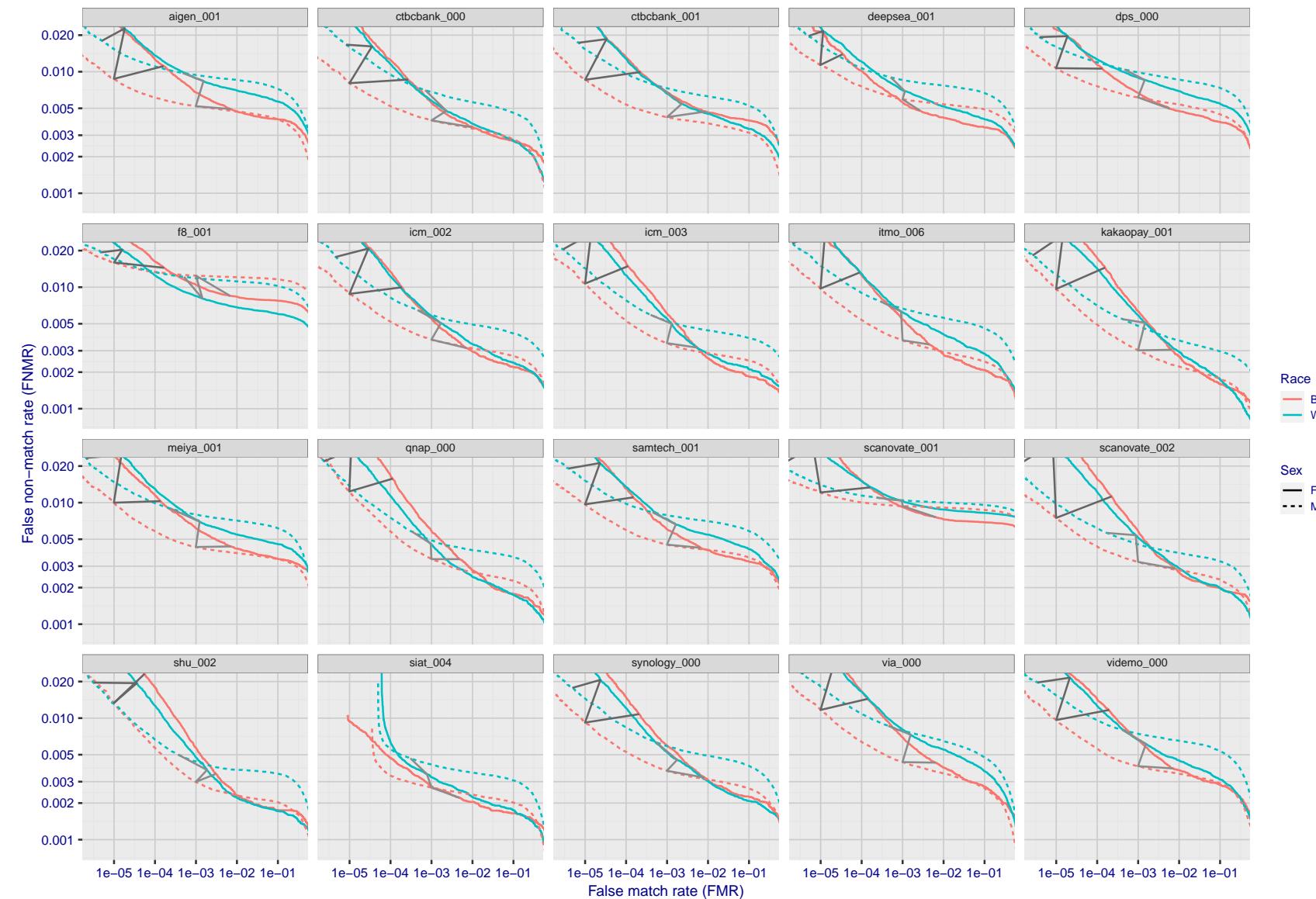


Figure 123: For the mugshot images, error tradeoff characteristics for white females, black females, black males and white males. The Z-shaped grey lines correspond to fixed thresholds, showing both FNMR and FMR vary at one T value. Note: Many of the plots will naively be read as saying women gives worse error rates than men because the solid traces lie above the dotted ones. However, this is misleading and incomplete: The grey lines show the traces reveal horizontal shifts. Thus for the cogent-003 algorithm FNMR for men is higher than for women at a fixed threshold but, at the same time, FMR is higher for women - see Figure 179. As access control systems almost always operate at a fixed threshold, the naive interpretation is incorrect.

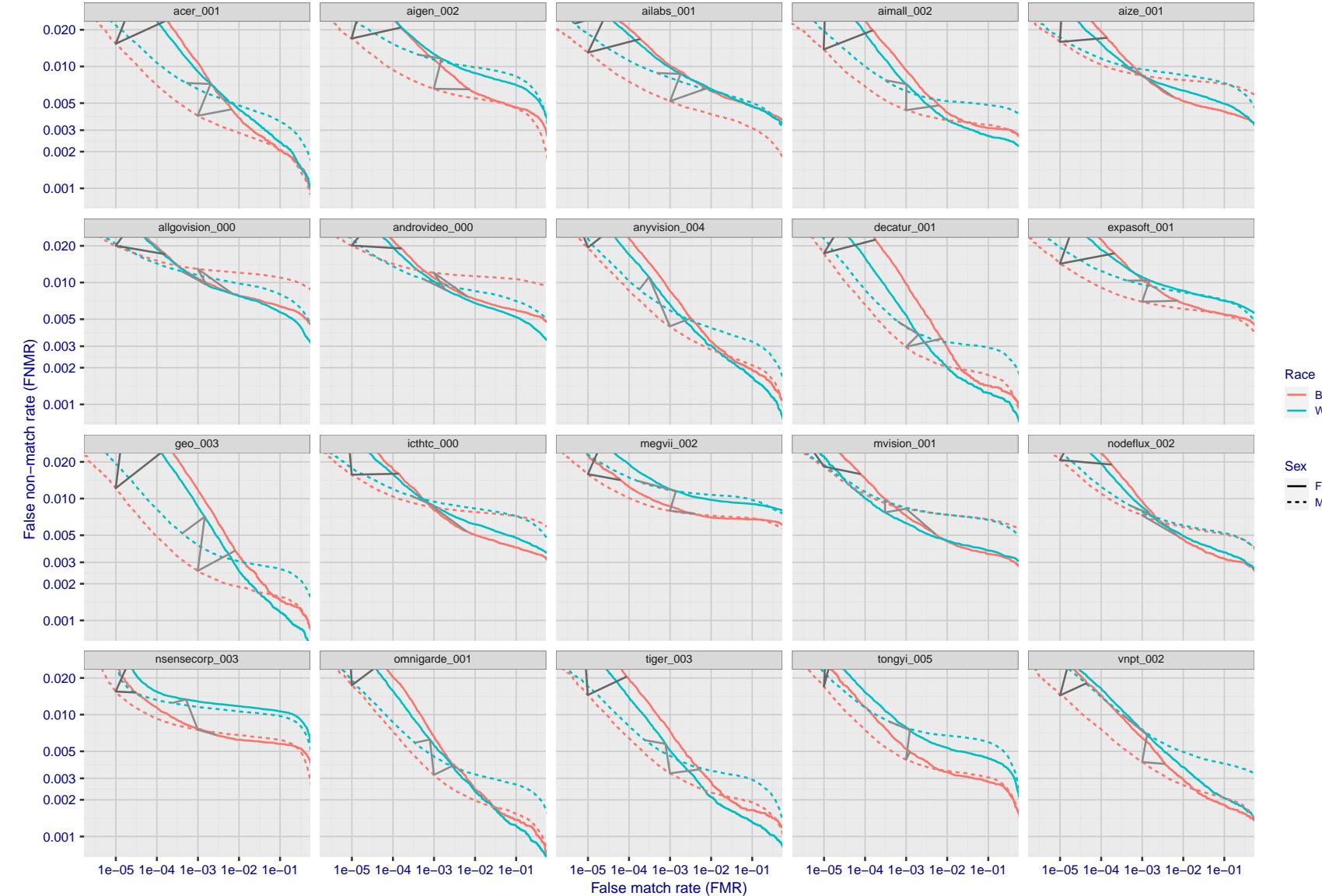


Figure 124: For the mugshot images, error tradeoff characteristics for white females, black females, black males and white males. The Z-shaped grey lines correspond to fixed thresholds, showing both FNMR and FMR vary at one T value. Note: Many of the plots will naively be read as saying women gives worse error rates than men because the solid traces lie above the dotted ones. However, this is misleading and incomplete: The grey lines show the traces reveal horizontal shifts. Thus for the cogent-003 algorithm FNMR for men is higher than for women at a fixed threshold but, at the same time, FMR is higher for women - see Figure 179. As access control systems almost always operate at a fixed threshold, the naive interpretation is incorrect.

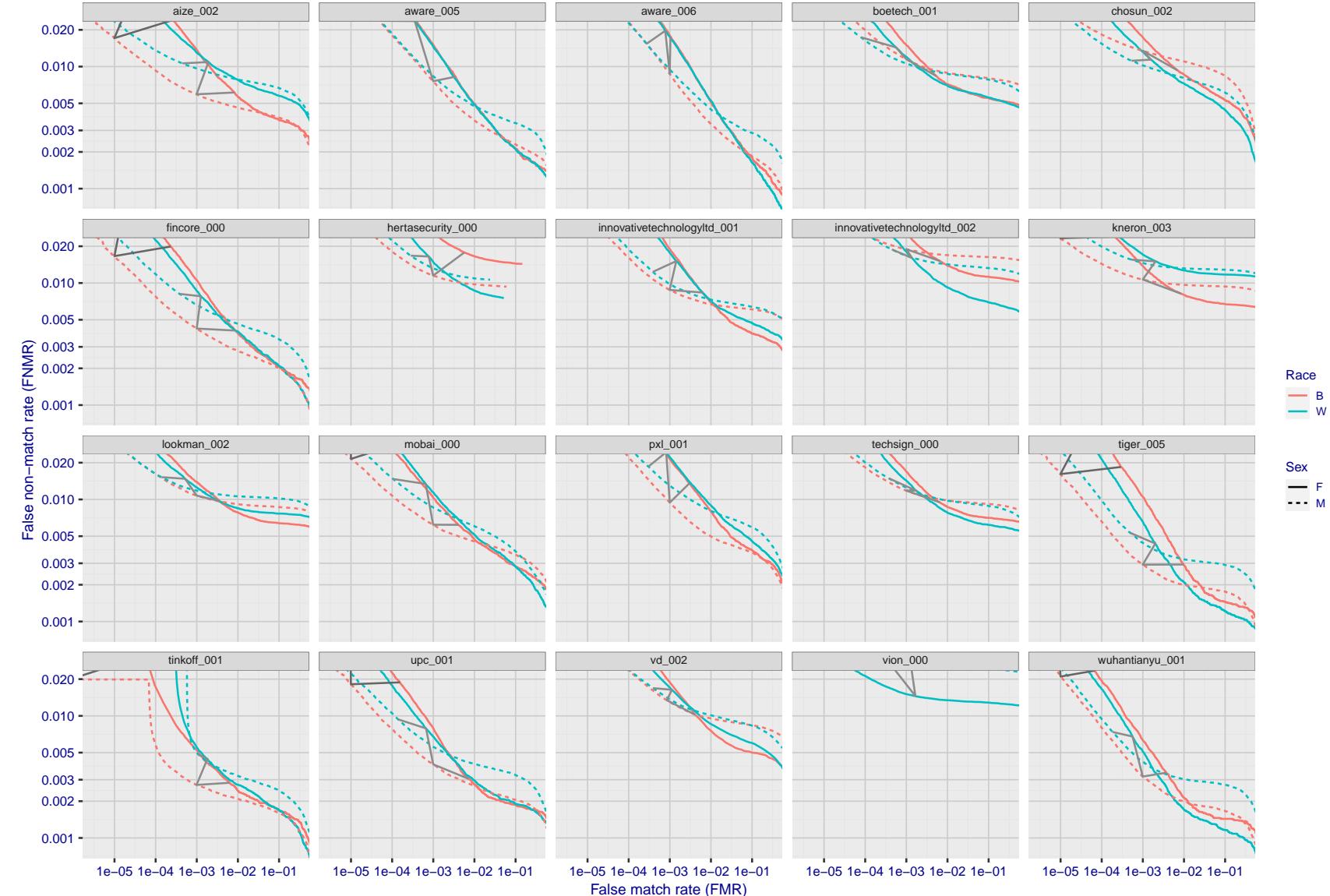


Figure 125: For the mugshot images, error tradeoff characteristics for white females, black females, black males and white males. The Z-shaped grey lines correspond to fixed thresholds, showing both FNMR and FMR vary at one T value. Note: Many of the plots will naively be read as saying women gives worse error rates than men because the solid traces lie above the dotted ones. However, this is misleading and incomplete: The grey lines show the traces reveal horizontal shifts. Thus for the cogent-003 algorithm FNMR for men is higher than for women at a fixed threshold but, at the same time, FMR is higher for women - see Figure 179. As access control systems almost always operate at a fixed threshold, the naive interpretation is incorrect.

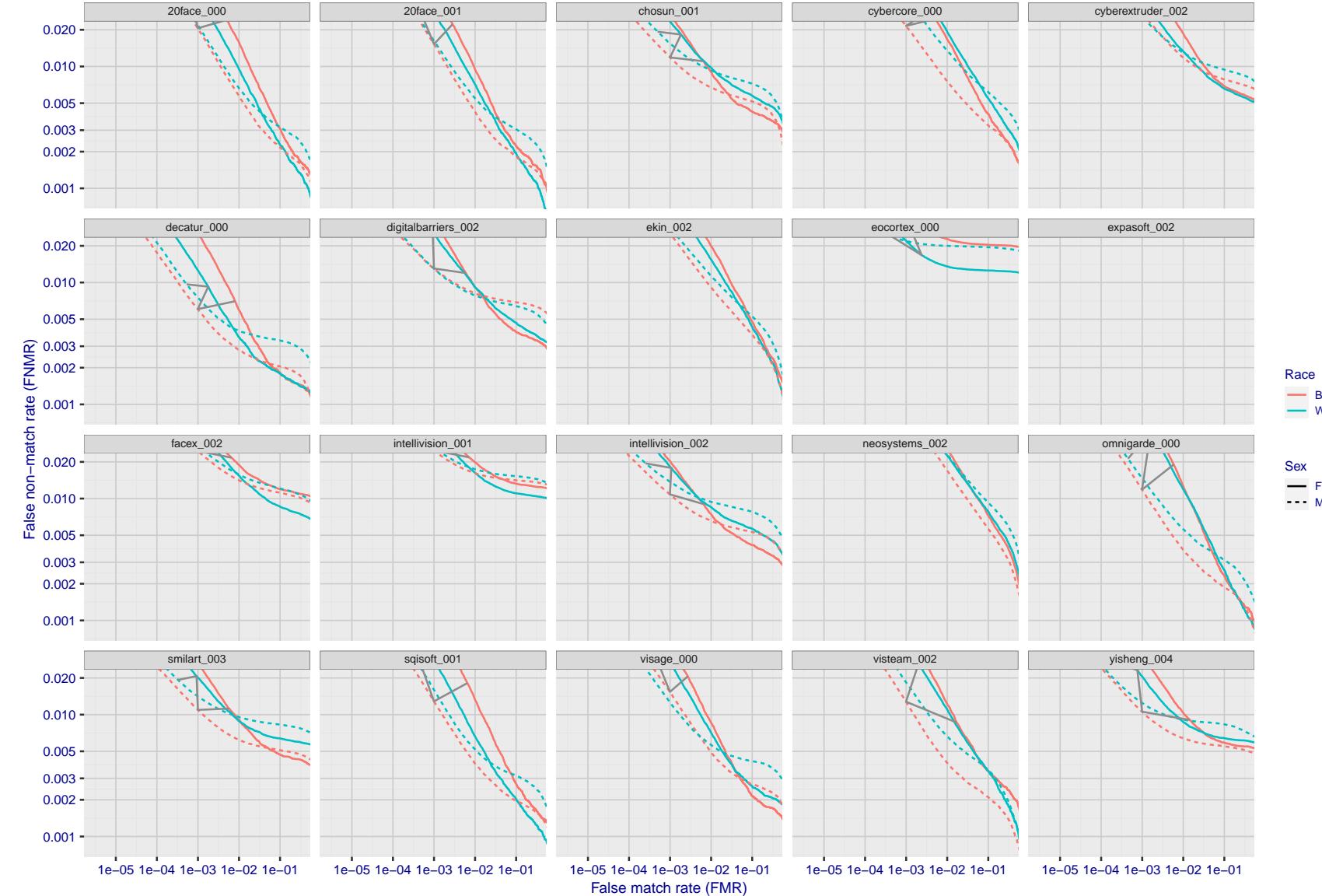


Figure 126: For the mugshot images, error tradeoff characteristics for white females, black females, black males and white males. The Z-shaped grey lines correspond to fixed thresholds, showing both FNMR and FMR vary at one T value. Note: Many of the plots will naively be read as saying women gives worse error rates than men because the solid traces lie above the dotted ones. However, this is misleading and incomplete: The grey lines show the traces reveal horizontal shifts. Thus for the cogent-003 algorithm FNMR for men is higher than for women at a fixed threshold but, at the same time, FMR is higher for women - see Figure 179. As access control systems almost always operate at a fixed threshold, the naive interpretation is incorrect.

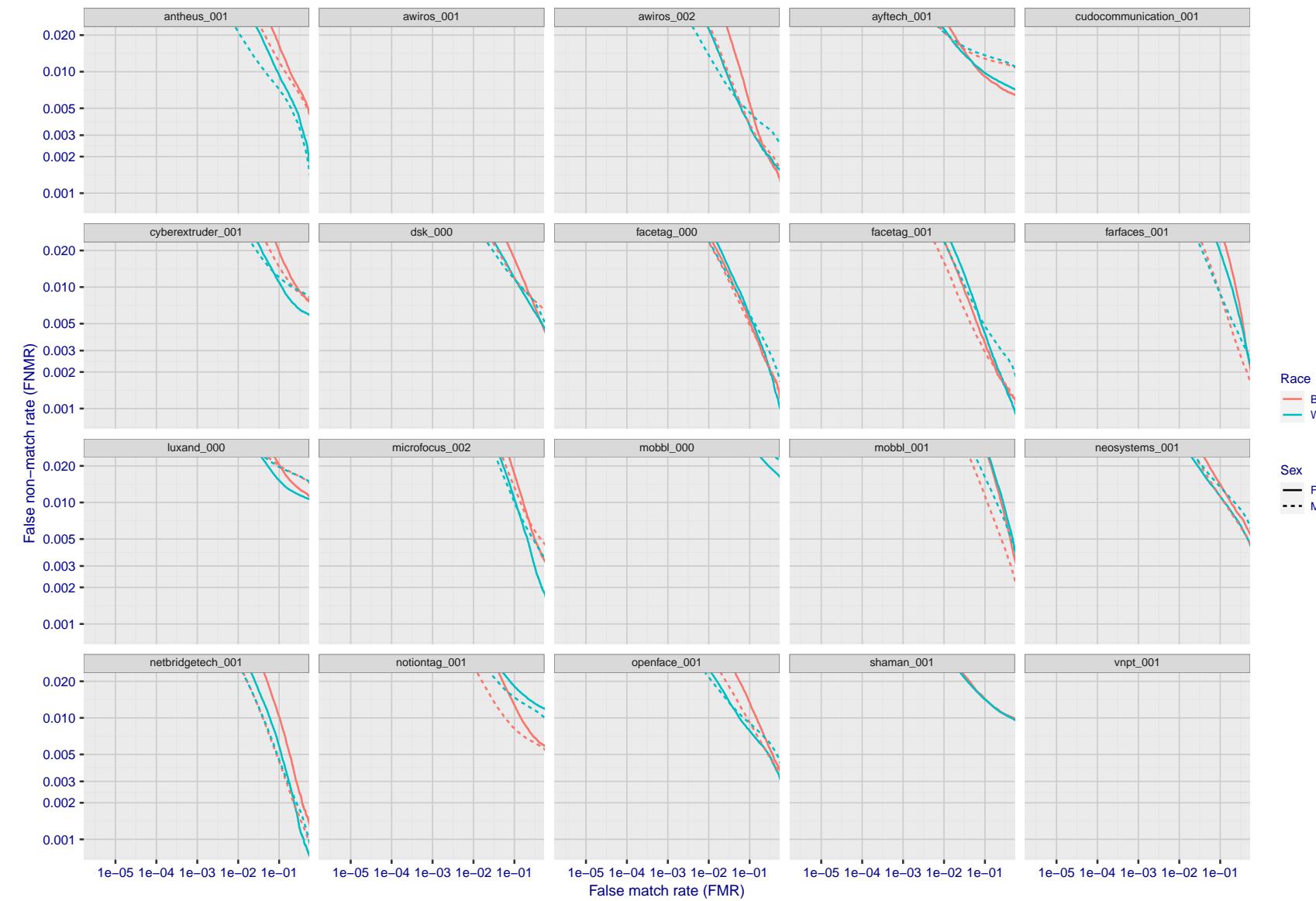


Figure 127: For the mugshot images, error tradeoff characteristics for white females, black females, black males and white males. The Z-shaped grey lines correspond to fixed thresholds, showing both FNMR and FMR vary at one T value. Note: Many of the plots will naively be read as saying women gives worse error rates than men because the solid traces lie above the dotted ones. However, this is misleading and incomplete: The grey lines show the traces reveal horizontal shifts. Thus for the cogent-003 algorithm FNMR for men is higher than for women at a fixed threshold but, at the same time, FMR is higher for women - see Figure 179. As access control systems almost always operate at a fixed threshold, the naive interpretation is incorrect.

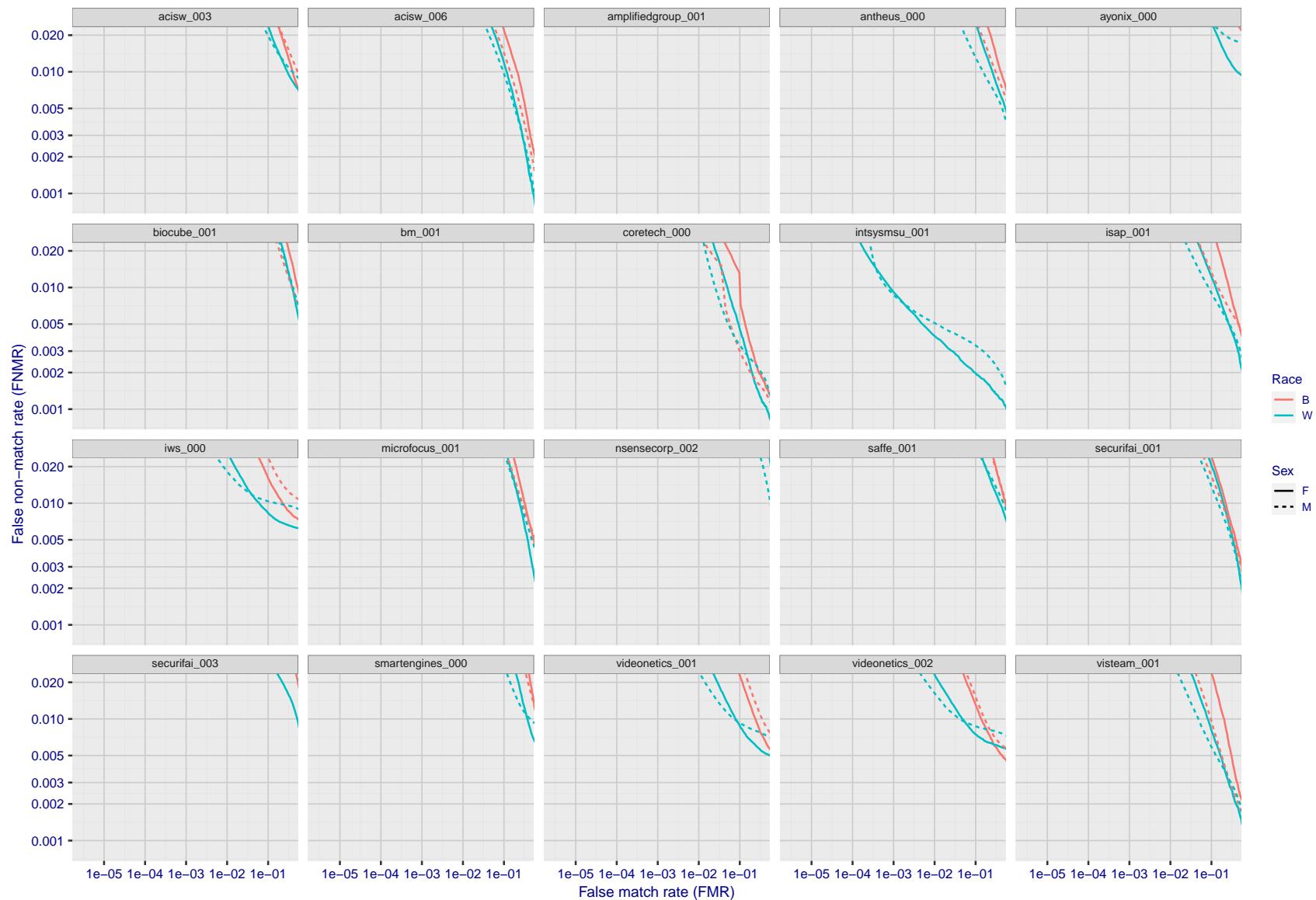


Figure 128: For the mugshot images, error tradeoff characteristics for white females, black females, black males and white males. The Z-shaped grey lines correspond to fixed thresholds, showing both FNMR and FMR vary at one T value. Note: Many of the plots will naively be read as saying women gives worse error rates than men because the solid traces lie above the dotted ones. However, this is misleading and incomplete: The grey lines show the traces reveal horizontal shifts. Thus for the cogent-003 algorithm FNMR for men is higher than for women at a fixed threshold but, at the same time, FMR is higher for women - see Figure 179. As access control systems almost always operate at a fixed threshold, the naive interpretation is incorrect.

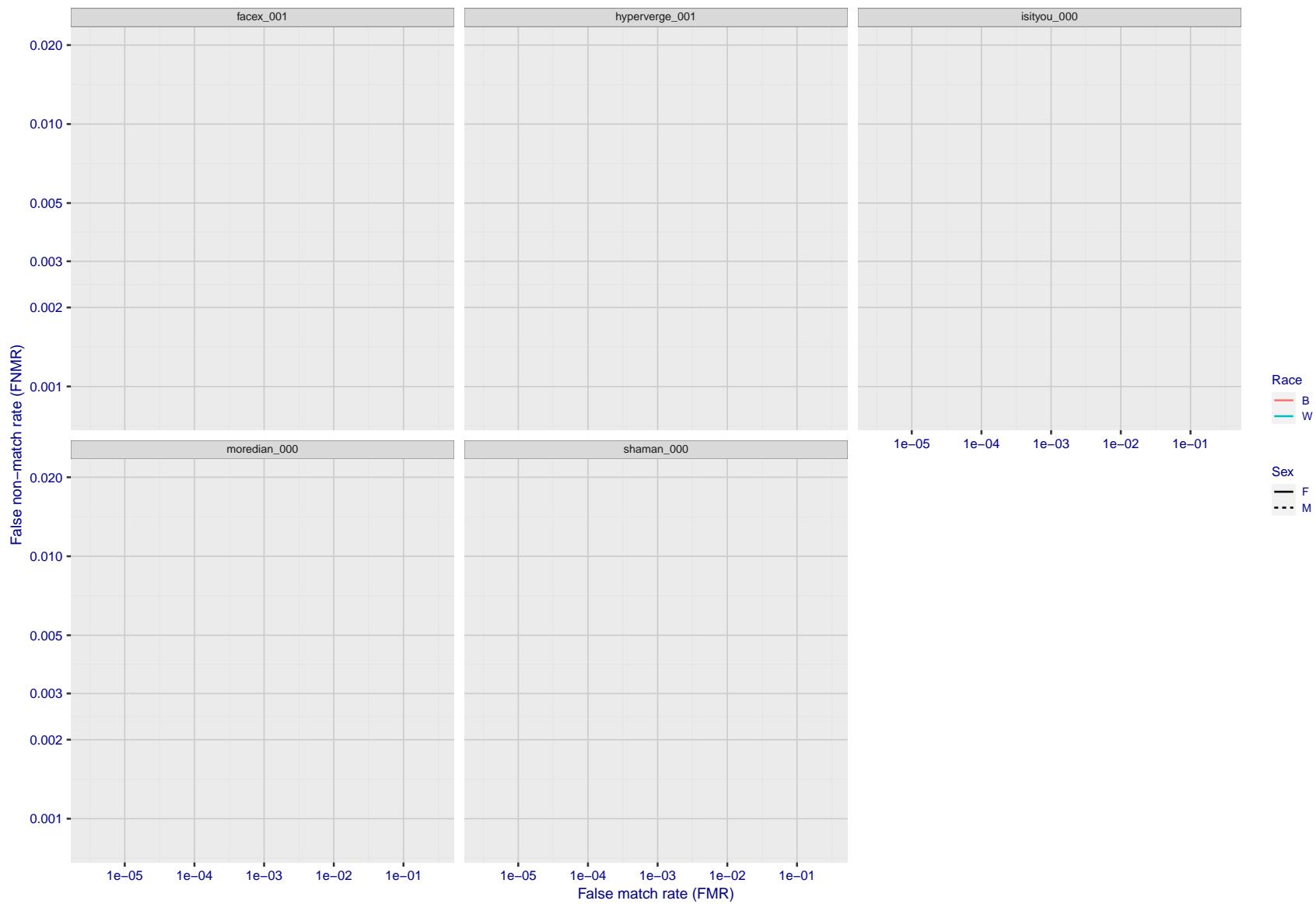


Figure 129: For the mugshot images, error tradeoff characteristics for white females, black females, black males and white males. The Z-shaped grey lines correspond to fixed thresholds, showing both FNMR and FMR vary at one T value. Note: Many of the plots will naively be read as saying women gives worse error rates than men because the solid traces lie above the dotted ones. However, this is misleading and incomplete: The grey lines show the traces reveal horizontal shifts. Thus for the cogent-003 algorithm FNMR for men is higher than for women at a fixed threshold but, at the same time, FMR is higher for women - see Figure 179. As access control systems almost always operate at a fixed threshold, the naive interpretation is incorrect.

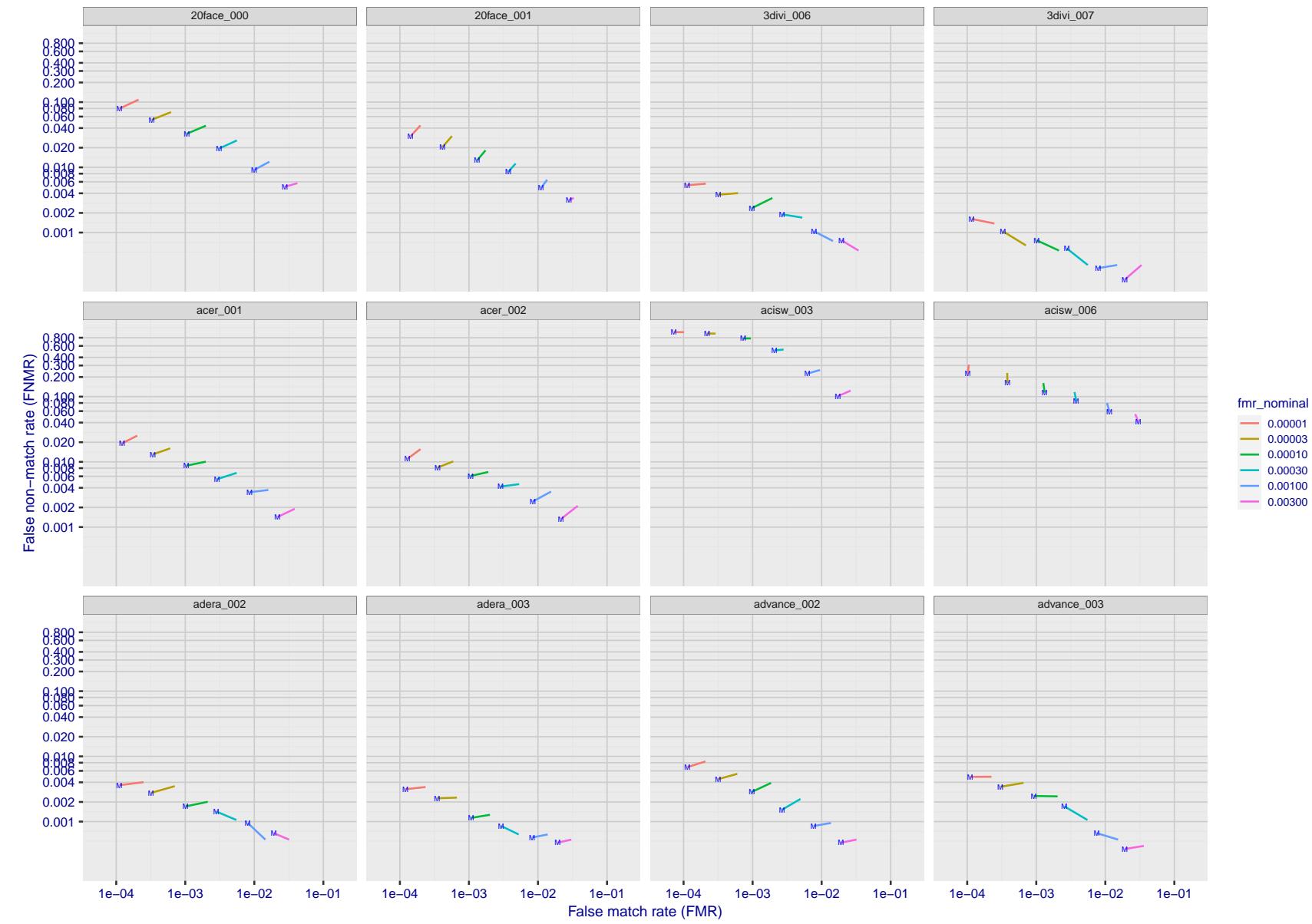


Figure 130: For the visa images, FNMR and FMR at six operating points along the DET characteristic. At each point a line is drawn between $(FMR, FNMR)_{MALE}$ and $(FMR, FNMR)_{FEMALE}$ showing how which sex has lower FMR and/or FNMR. The "M" label denotes male, the other end of the line corresponds to female. The six operating thresholds are selected to give the nominal false match rates given in the legend, and are computed over all impostor pairs regardless of age, sex, and place of birth. The plotted FMR values are broadly an order of magnitude larger than the nominal rates because FMR is computed over demographically-matched impostor pairs i.e individuals of the same sex, from the same geographic region (see section 3.6.1), and the same age group (see section 3.6.2).

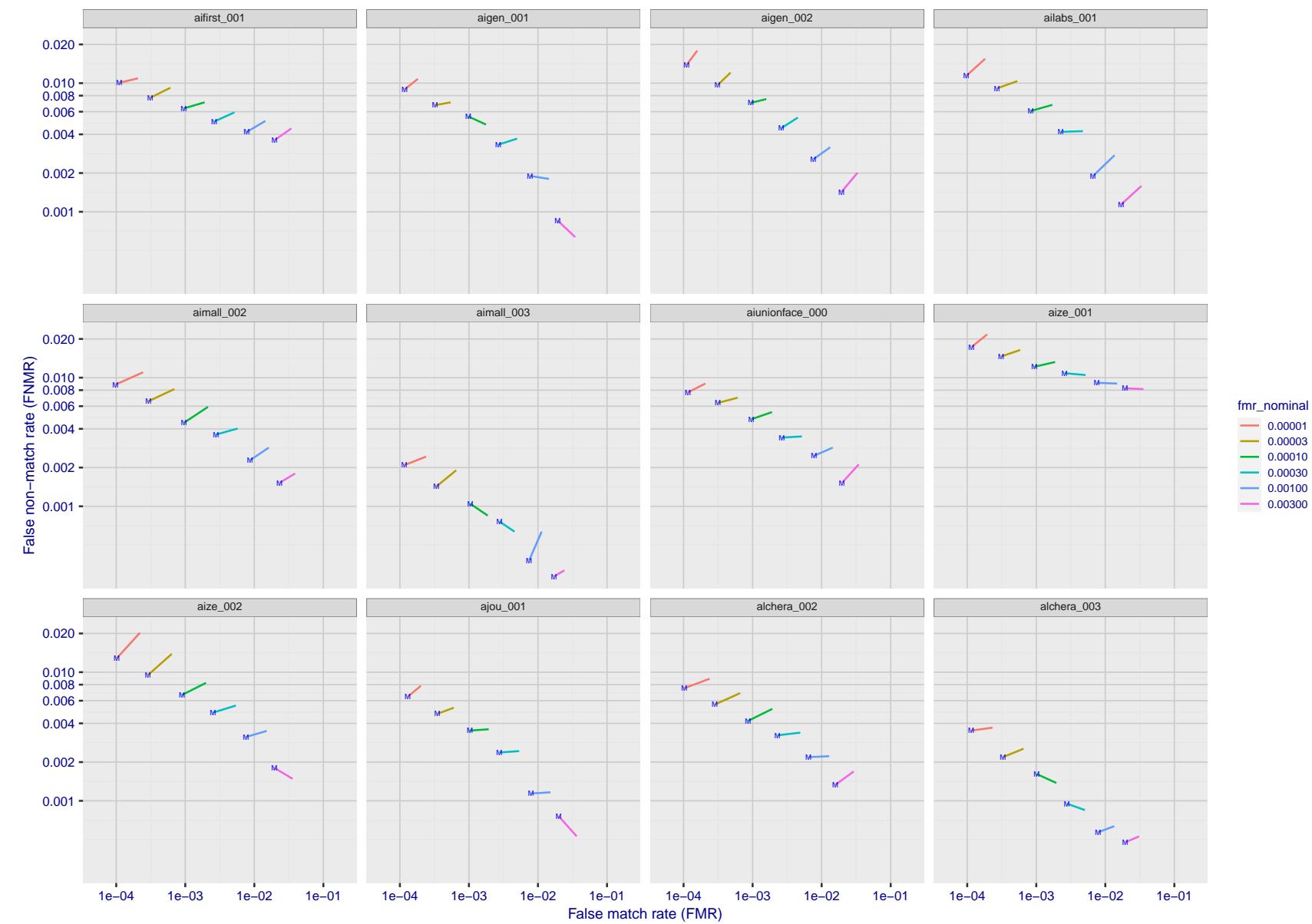


Figure 131: For the visa images, FNMR and FMR at six operating points along the DET characteristic. At each point a line is drawn between $(FMR, FNMR)_{MALE}$ and $(FMR, FNMR)_{FEMALE}$ showing how which sex has lower FMR and/or FNMR. The "M" label denotes male, the other end of the line corresponds to female. The six operating thresholds are selected to give the nominal false match rates given in the legend, and are computed over all impostor pairs regardless of age, sex, and place of birth. The plotted FMR values are broadly an order of magnitude larger than the nominal rates because FMR is computed over demographically-matched impostor pairs i.e individuals of the same sex, from the same geographic region (see section 3.6.1), and the same age group (see section 3.6.2).

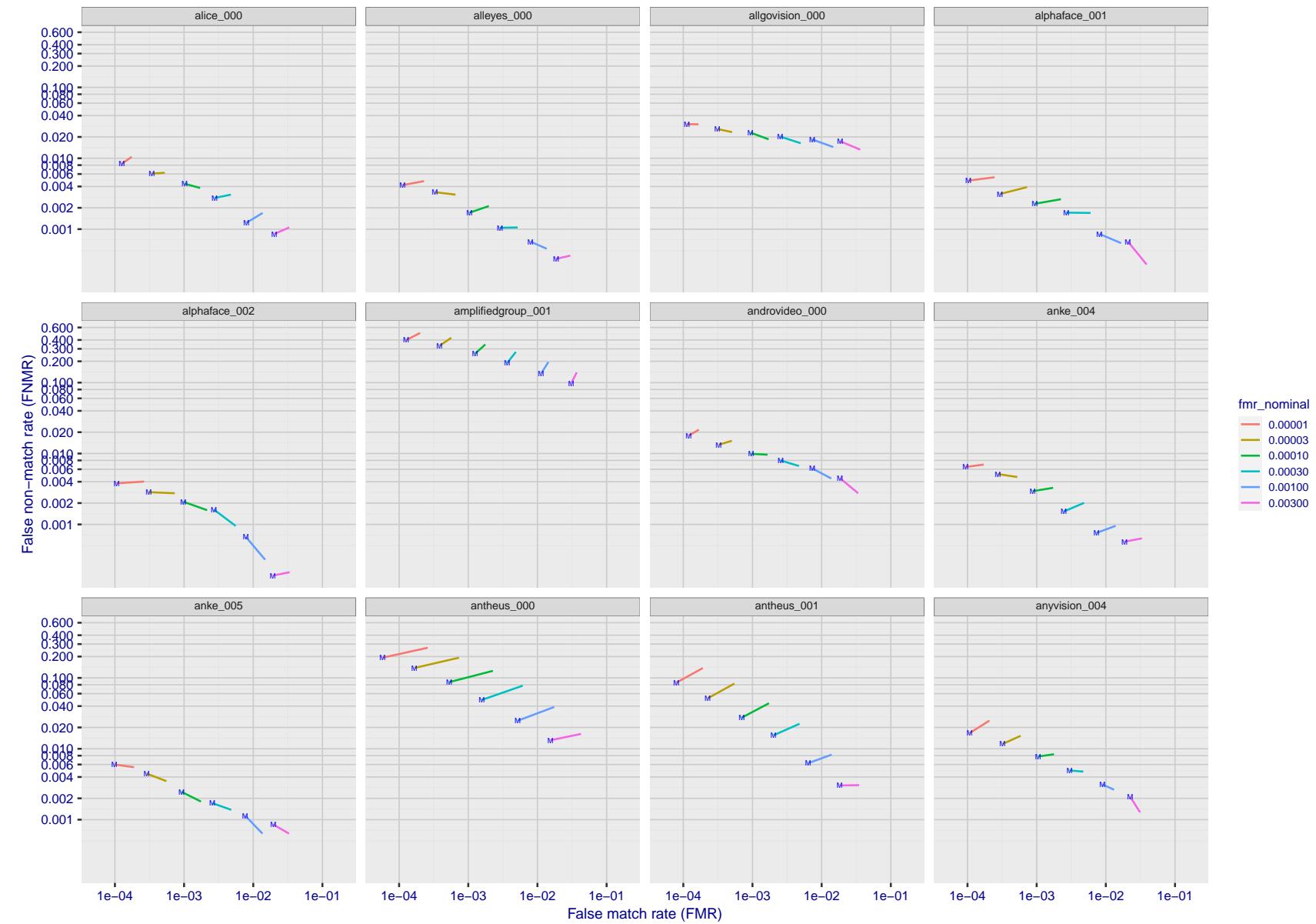


Figure 132: For the visa images, FNMR and FMR at six operating points along the DET characteristic. At each point a line is drawn between $(FMR, FNMR)_{MALE}$ and $(FMR, FNMR)_{FEMALE}$ showing how which sex has lower FMR and/or FNMR. The "M" label denotes male, the other end of the line corresponds to female. The six operating thresholds are selected to give the nominal false match rates given in the legend, and are computed over all impostor pairs regardless of age, sex, and place of birth. The plotted FMR values are broadly an order of magnitude larger than the nominal rates because FMR is computed over demographically-matched impostor pairs i.e individuals of the same sex, from the same geographic region (see section 3.6.1), and the same age group (see section 3.6.2).

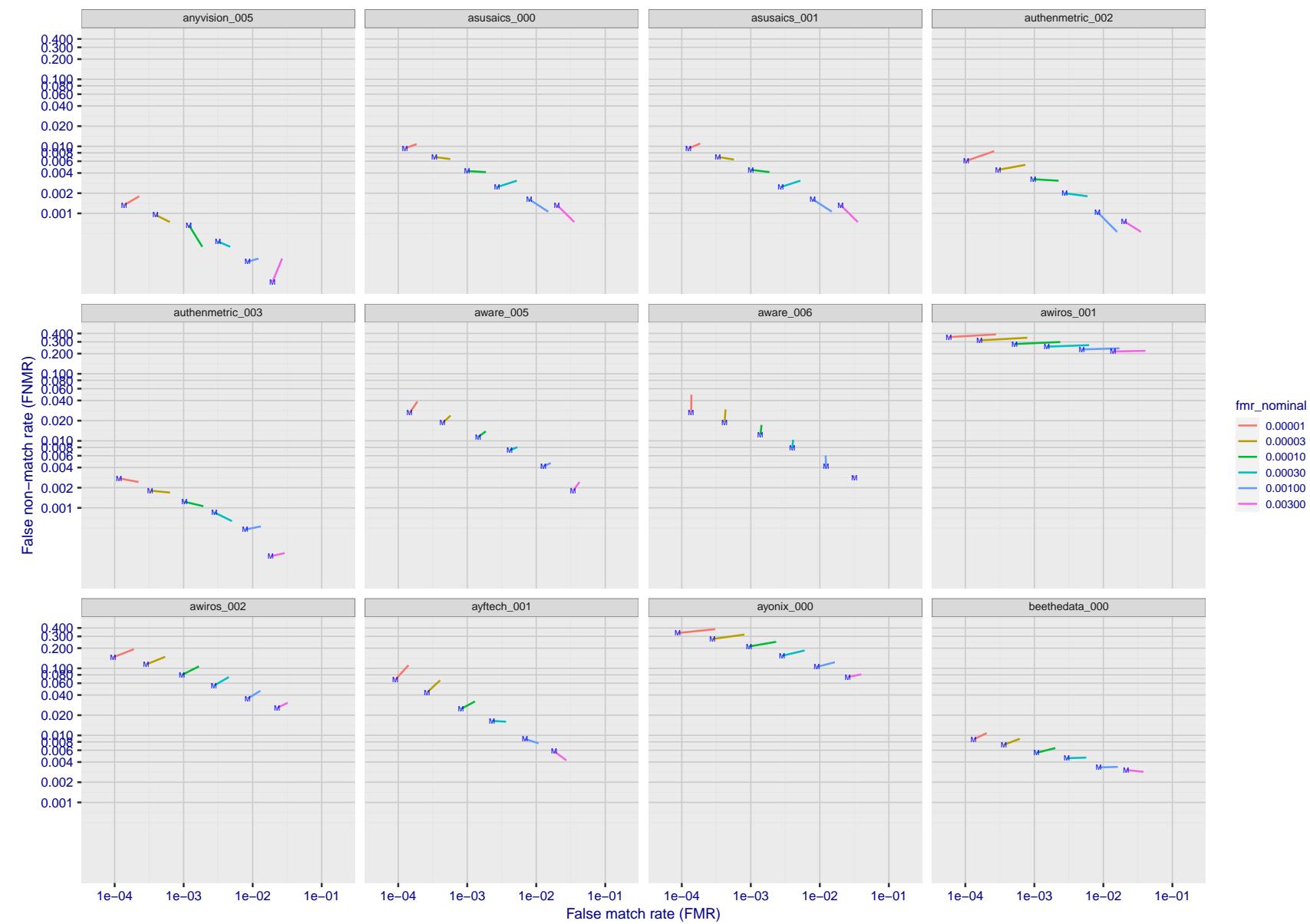


Figure 133: For the visa images, FNMR and FMR at six operating points along the DET characteristic. At each point a line is drawn between $(FMR, FNMR)_{MALE}$ and $(FMR, FNMR)_{FEMALE}$ showing how which sex has lower FMR and/or FNMR. The "M" label denotes male, the other end of the line corresponds to female. The six operating thresholds are selected to give the nominal false match rates given in the legend, and are computed over all impostor pairs regardless of age, sex, and place of birth. The plotted FMR values are broadly an order of magnitude larger than the nominal rates because FMR is computed over demographically-matched impostor pairs i.e individuals of the same sex, from the same geographic region (see section 3.6.1), and the same age group (see section 3.6.2).

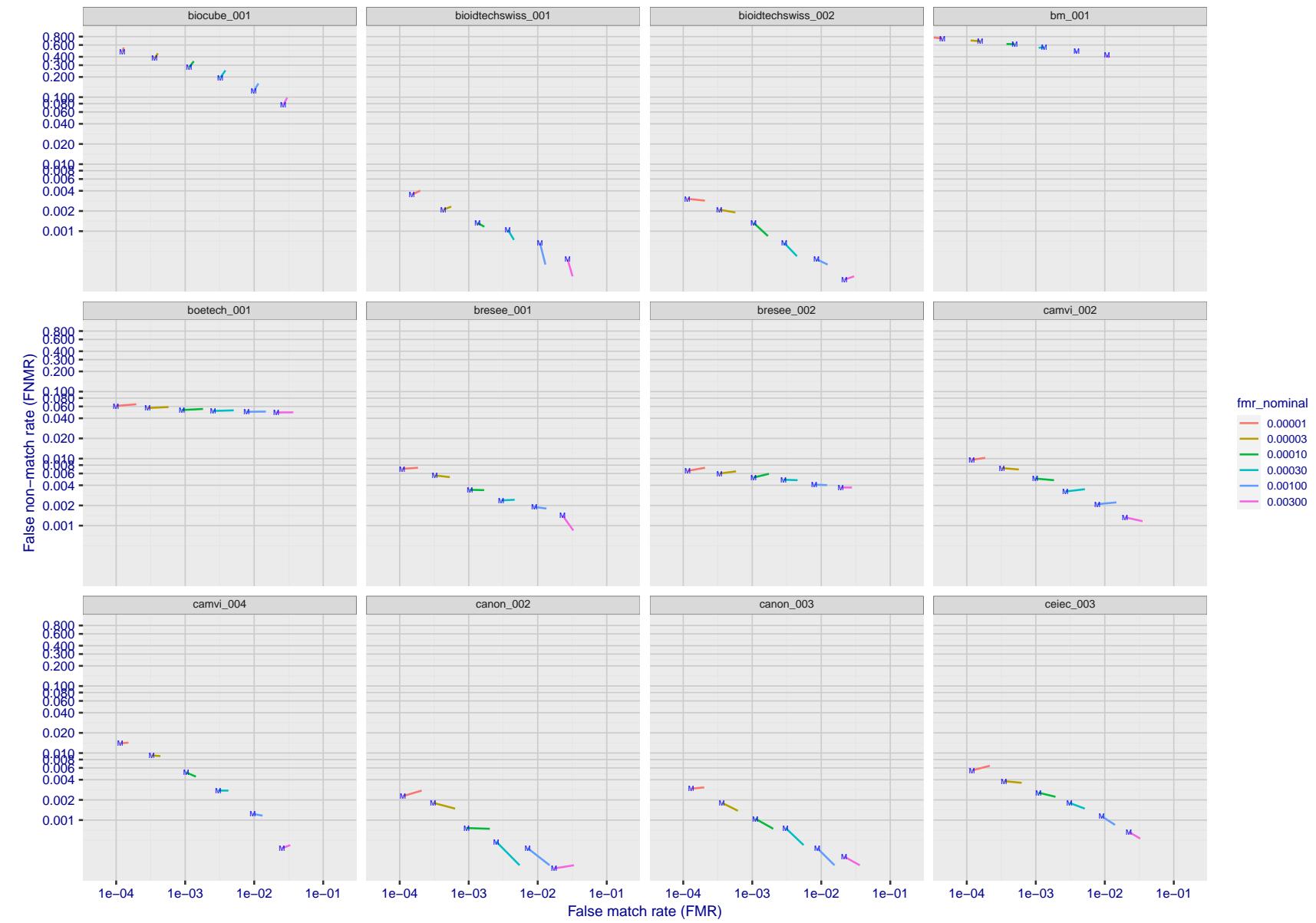


Figure 134: For the visa images, FNMR and FMR at six operating points along the DET characteristic. At each point a line is drawn between $(FMR, FNMR)_{MALE}$ and $(FMR, FNMR)_{FEMALE}$ showing how which sex has lower FMR and/or FNMR. The "M" label denotes male, the other end of the line corresponds to female. The six operating thresholds are selected to give the nominal false match rates given in the legend, and are computed over all impostor pairs regardless of age, sex, and place of birth. The plotted FMR values are broadly an order of magnitude larger than the nominal rates because FMR is computed over demographically-matched impostor pairs i.e individuals of the same sex, from the same geographic region (see section 3.6.1), and the same age group (see section 3.6.2).

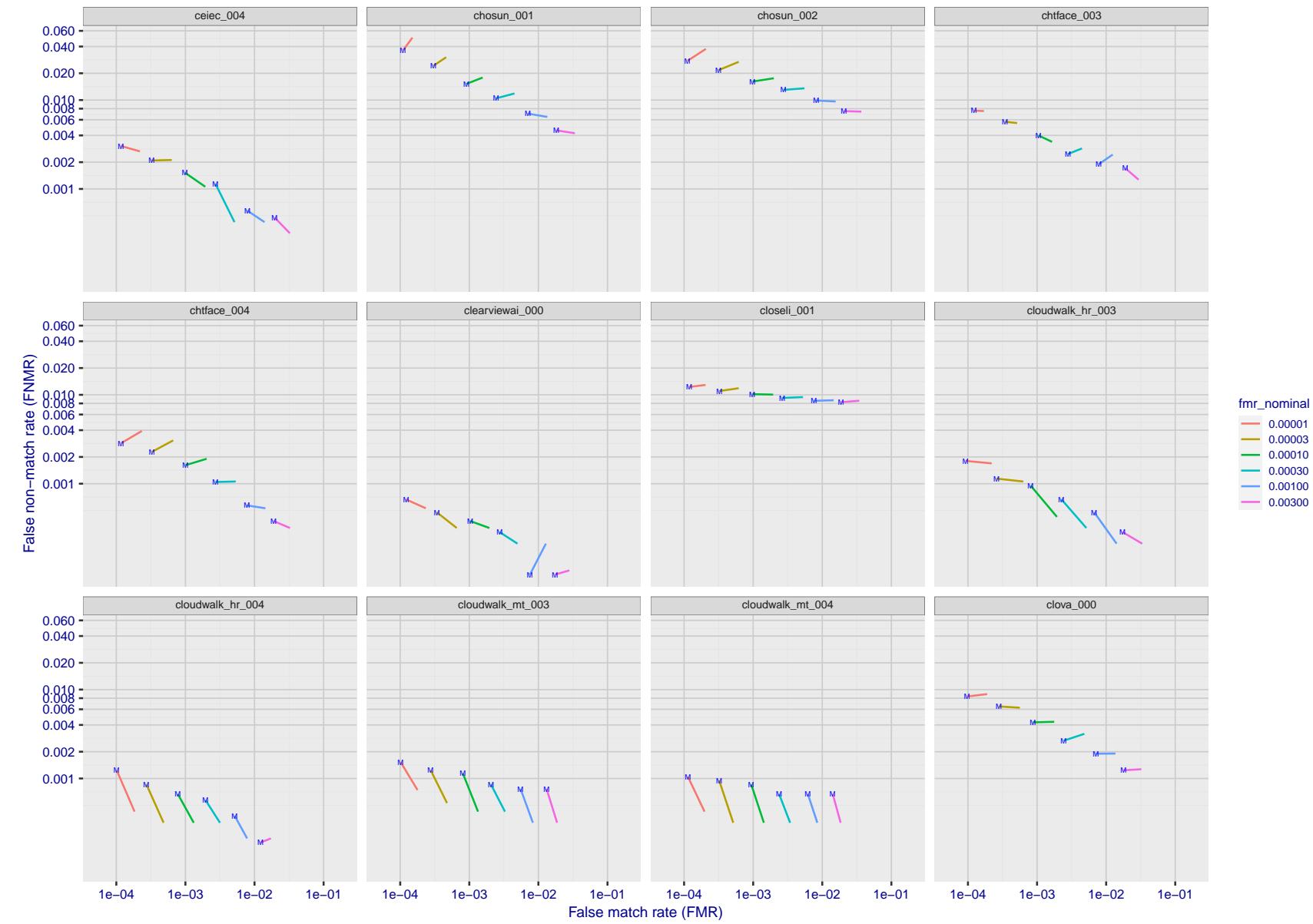


Figure 135: For the visa images, FNMR and FMR at six operating points along the DET characteristic. At each point a line is drawn between $(FMR, FNMR)_{MALE}$ and $(FMR, FNMR)_{FEMALE}$ showing how which sex has lower FMR and/or FNMR. The "M" label denotes male, the other end of the line corresponds to female. The six operating thresholds are selected to give the nominal false match rates given in the legend, and are computed over all impostor pairs regardless of age, sex, and place of birth. The plotted FMR values are broadly an order of magnitude larger than the nominal rates because FMR is computed over demographically-matched impostor pairs i.e individuals of the same sex, from the same geographic region (see section 3.6.1), and the same age group (see section 3.6.2).

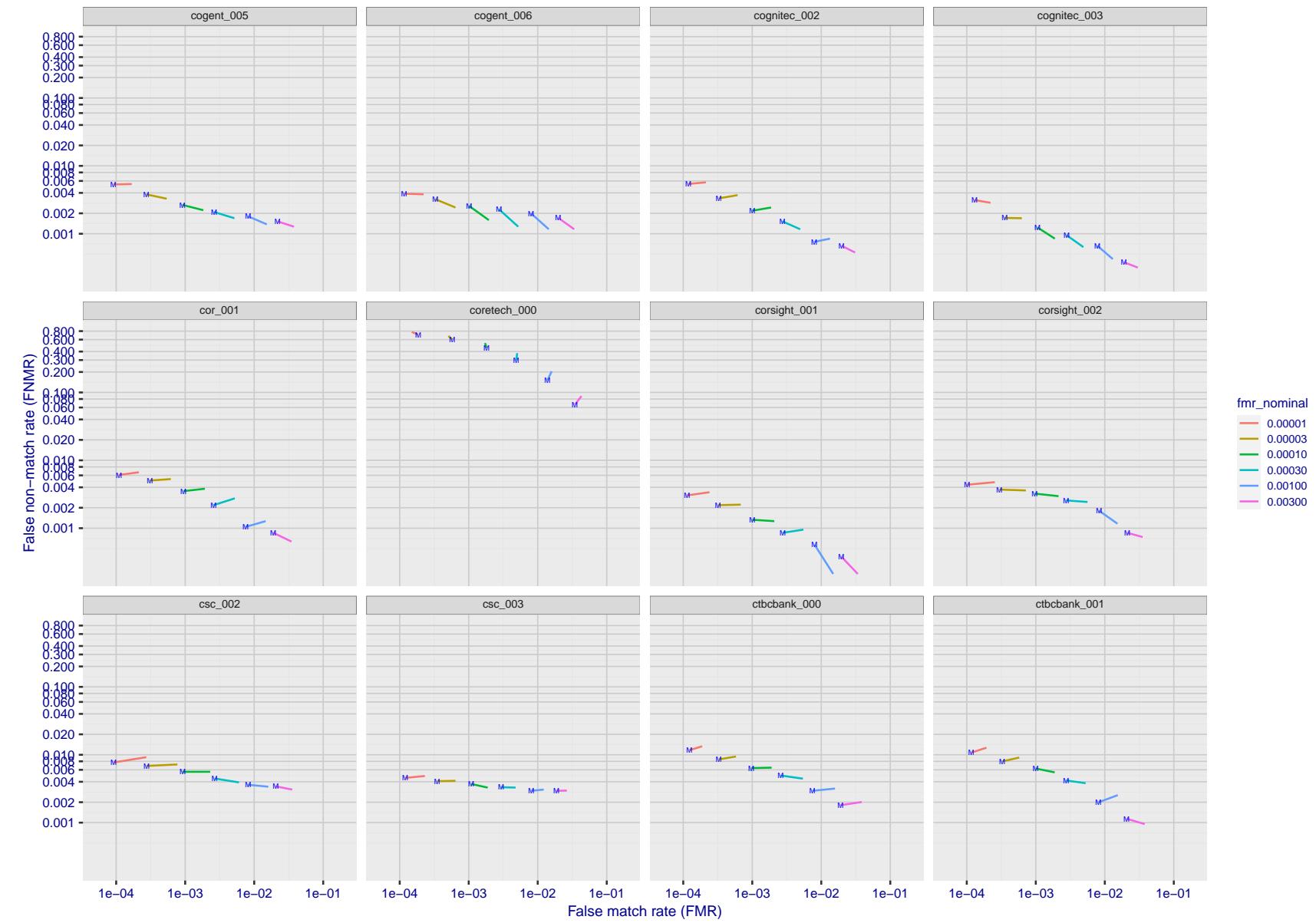


Figure 136: For the visa images, FNMR and FMR at six operating points along the DET characteristic. At each point a line is drawn between $(FMR, FNMR)_{MALE}$ and $(FMR, FNMR)_{FEMALE}$ showing how which sex has lower FMR and/or FNMR. The "M" label denotes male, the other end of the line corresponds to female. The six operating thresholds are selected to give the nominal false match rates given in the legend, and are computed over all impostor pairs regardless of age, sex, and place of birth. The plotted FMR values are broadly an order of magnitude larger than the nominal rates because FMR is computed over demographically-matched impostor pairs i.e individuals of the same sex, from the same geographic region (see section 3.6.1), and the same age group (see section 3.6.2).

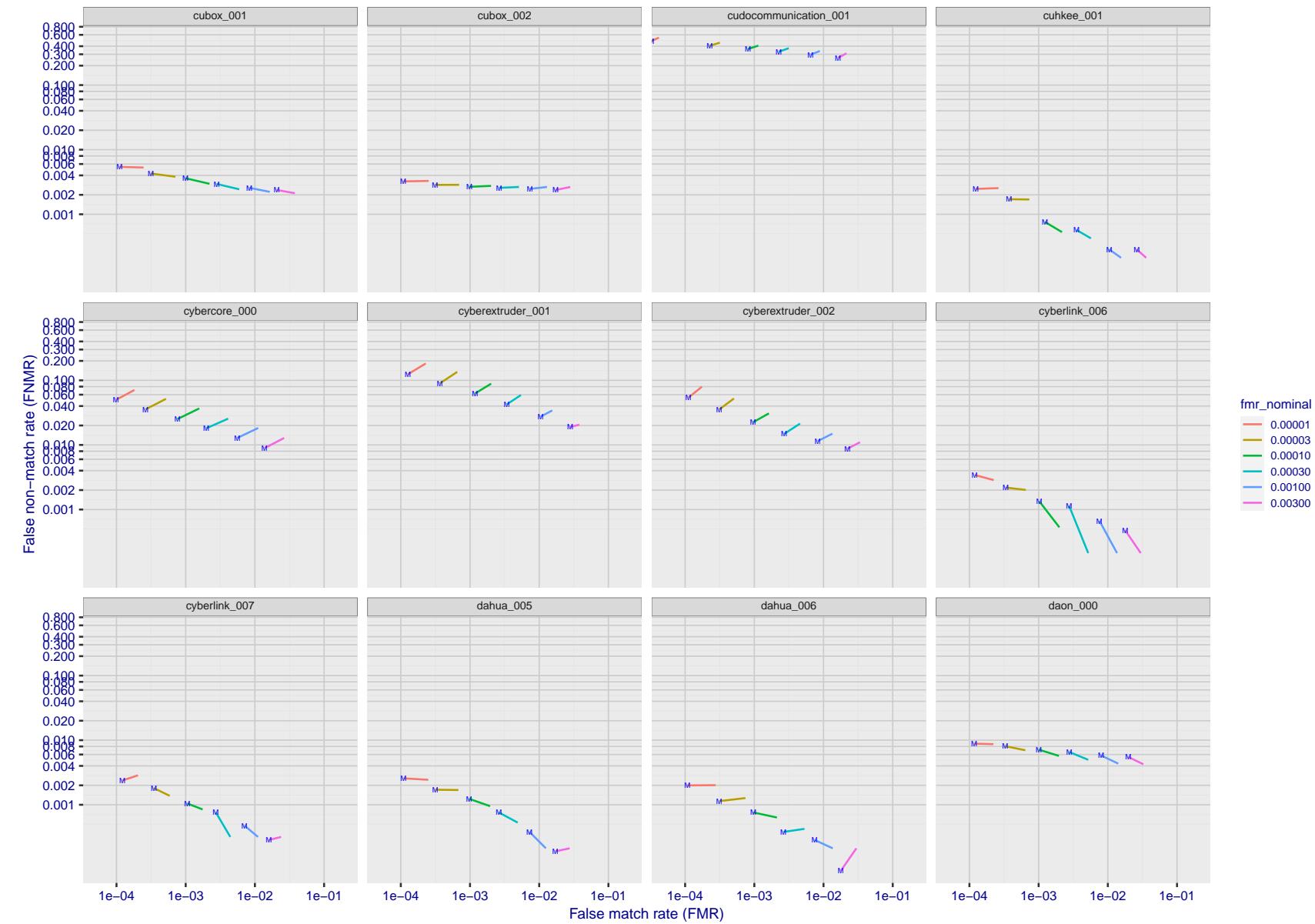


Figure 137: For the visa images, FNMR and FMR at six operating points along the DET characteristic. At each point a line is drawn between $(FMR, FNMR)_{MALE}$ and $(FMR, FNMR)_{FEMALE}$ showing how which sex has lower FMR and/or FNMR. The "M" label denotes male, the other end of the line corresponds to female. The six operating thresholds are selected to give the nominal false match rates given in the legend, and are computed over all impostor pairs regardless of age, sex, and place of birth. The plotted FMR values are broadly an order of magnitude larger than the nominal rates because FMR is computed over demographically-matched impostor pairs i.e individuals of the same sex, from the same geographic region (see section 3.6.1), and the same age group (see section 3.6.2).

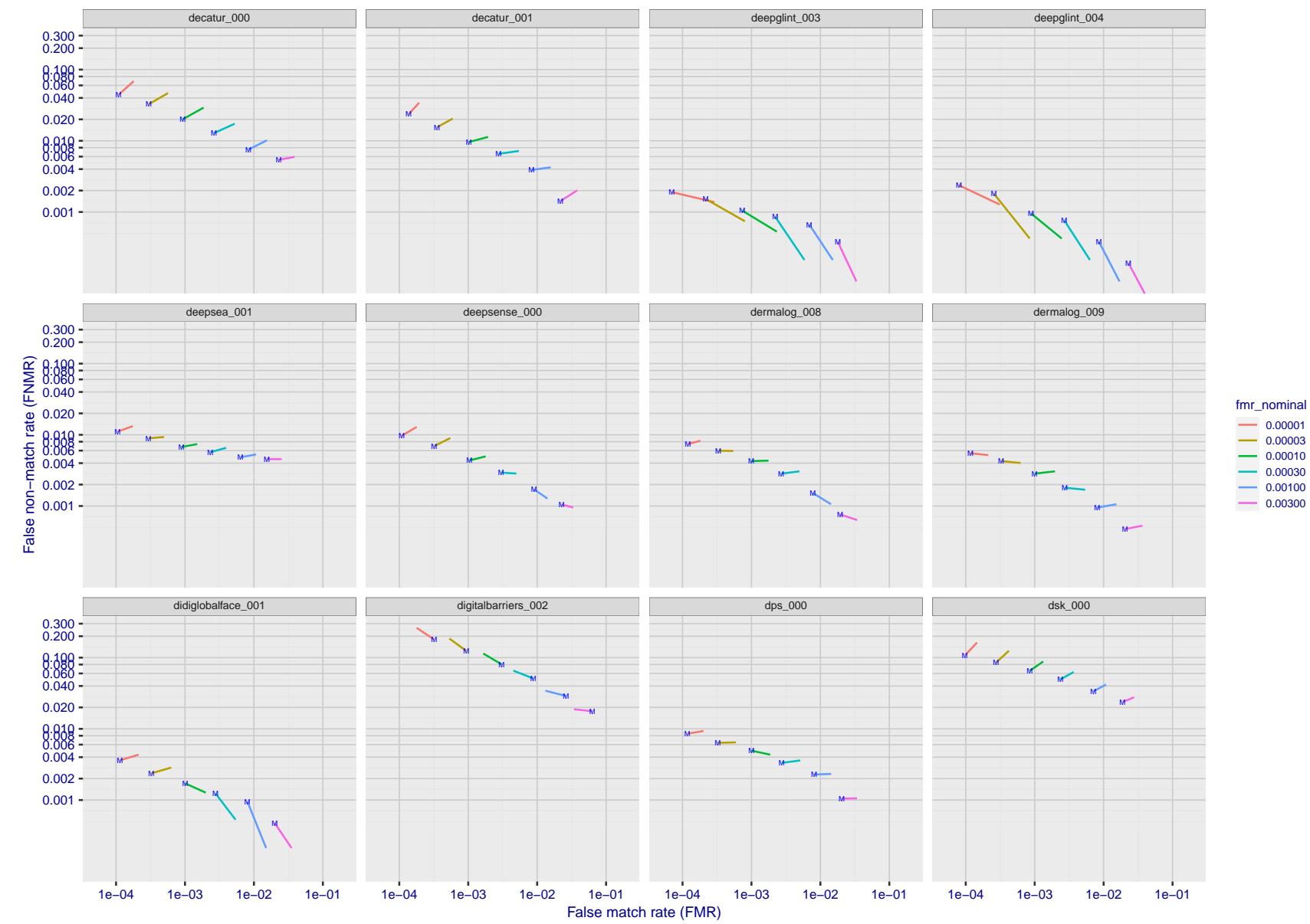


Figure 138: For the visa images, FNMR and FMR at six operating points along the DET characteristic. At each point a line is drawn between $(FMR, FNMR)_{MALE}$ and $(FMR, FNMR)_{FEMALE}$ showing how which sex has lower FMR and/or FNMR. The "M" label denotes male, the other end of the line corresponds to female. The six operating thresholds are selected to give the nominal false match rates given in the legend, and are computed over all impostor pairs regardless of age, sex, and place of birth. The plotted FMR values are broadly an order of magnitude larger than the nominal rates because FMR is computed over demographically-matched impostor pairs i.e individuals of the same sex, from the same geographic region (see section 3.6.1), and the same age group (see section 3.6.2).

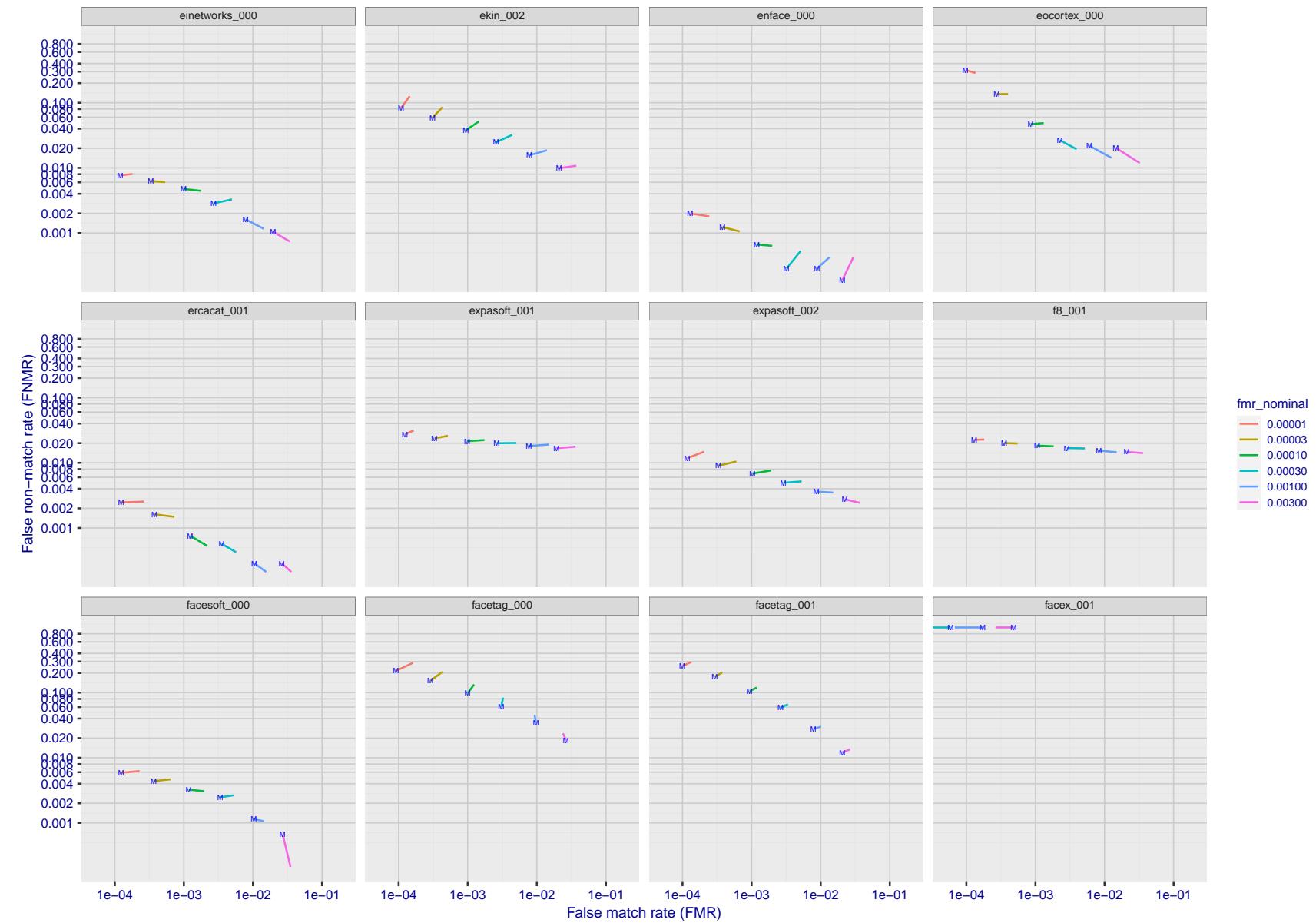


Figure 139: For the visa images, FNMR and FMR at six operating points along the DET characteristic. At each point a line is drawn between $(FMR, FNMR)_{MALE}$ and $(FMR, FNMR)_{FEMALE}$ showing how which sex has lower FMR and/or FNMR. The "M" label denotes male, the other end of the line corresponds to female. The six operating thresholds are selected to give the nominal false match rates given in the legend, and are computed over all impostor pairs regardless of age, sex, and place of birth. The plotted FMR values are broadly an order of magnitude larger than the nominal rates because FMR is computed over demographically-matched impostor pairs i.e individuals of the same sex, from the same geographic region (see section 3.6.1), and the same age group (see section 3.6.2).

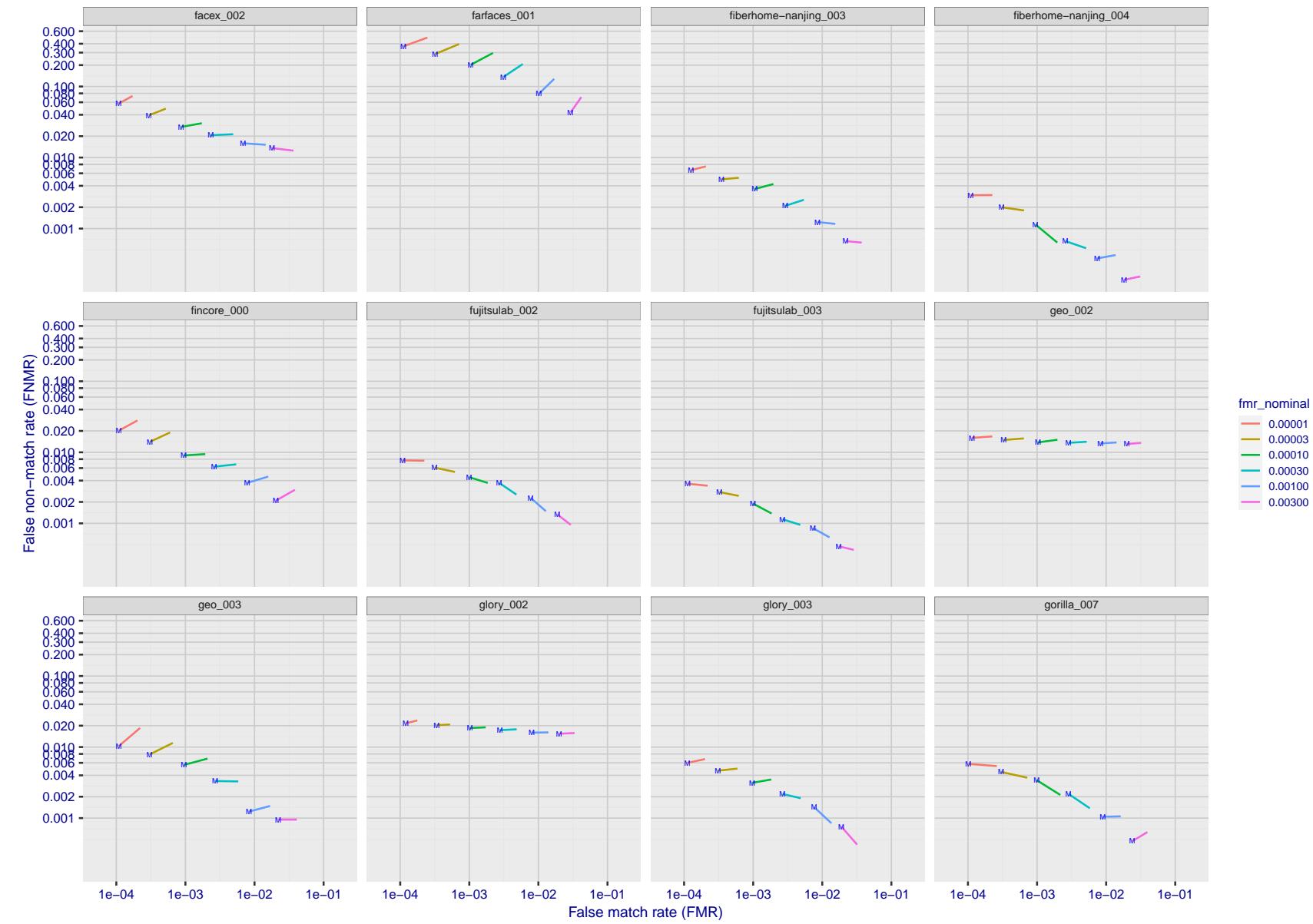


Figure 140: For the visa images, FNMR and FMR at six operating points along the DET characteristic. At each point a line is drawn between $(FMR, FNMR)_{MALE}$ and $(FMR, FNMR)_{FEMALE}$ showing how which sex has lower FMR and/or FNMR. The "M" label denotes male, the other end of the line corresponds to female. The six operating thresholds are selected to give the nominal false match rates given in the legend, and are computed over all impostor pairs regardless of age, sex, and place of birth. The plotted FMR values are broadly an order of magnitude larger than the nominal rates because FMR is computed over demographically-matched impostor pairs i.e individuals of the same sex, from the same geographic region (see section 3.6.1), and the same age group (see section 3.6.2).

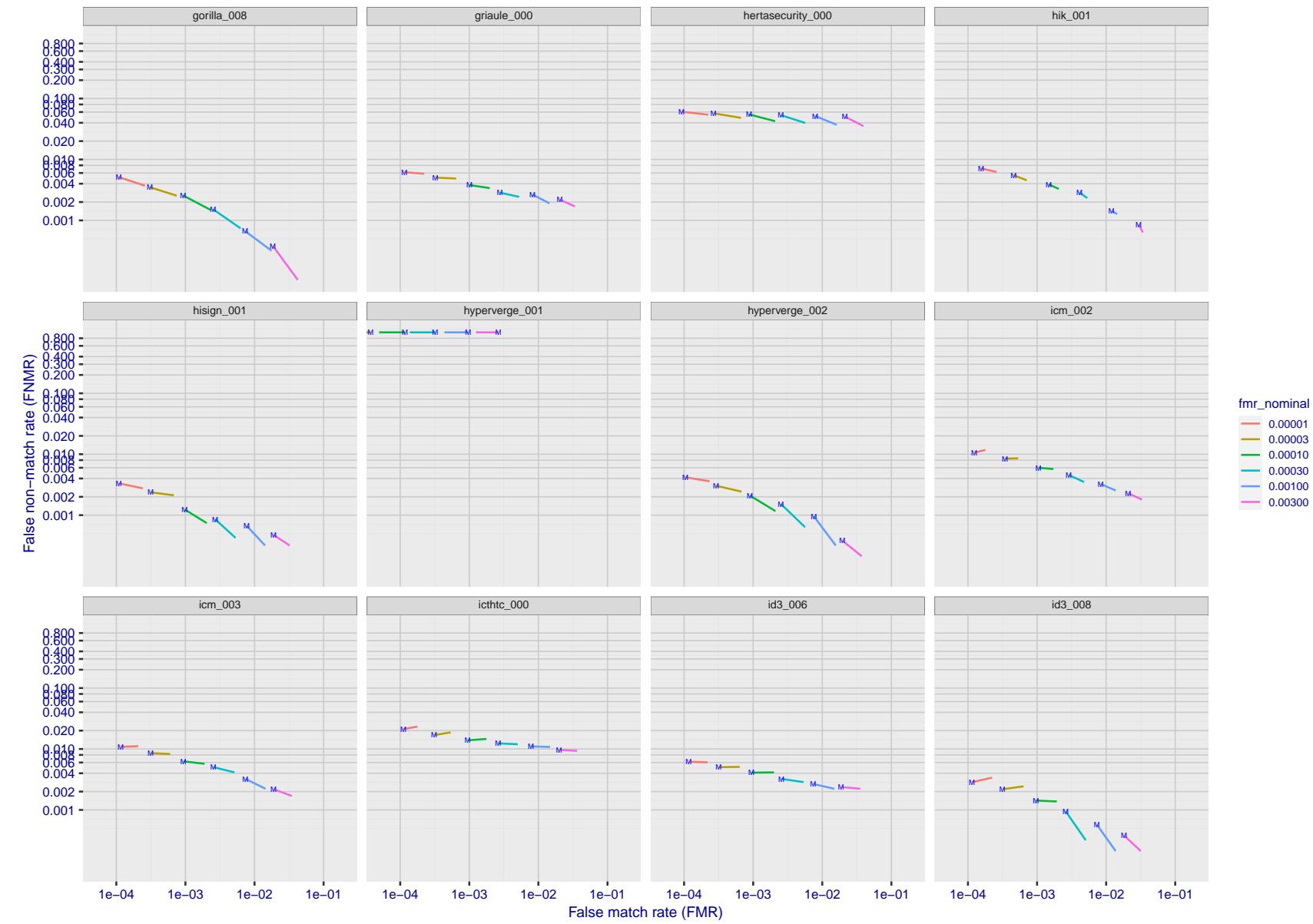


Figure 141: For the visa images, FNMR and FMR at six operating points along the DET characteristic. At each point a line is drawn between $(FMR, FNMR)_{MALE}$ and $(FMR, FNMR)_{FEMALE}$ showing how which sex has lower FMR and/or FNMR. The "M" label denotes male, the other end of the line corresponds to female. The six operating thresholds are selected to give the nominal false match rates given in the legend, and are computed over all impostor pairs regardless of age, sex, and place of birth. The plotted FMR values are broadly an order of magnitude larger than the nominal rates because FMR is computed over demographically-matched impostor pairs i.e individuals of the same sex, from the same geographic region (see section 3.6.1), and the same age group (see section 3.6.2).

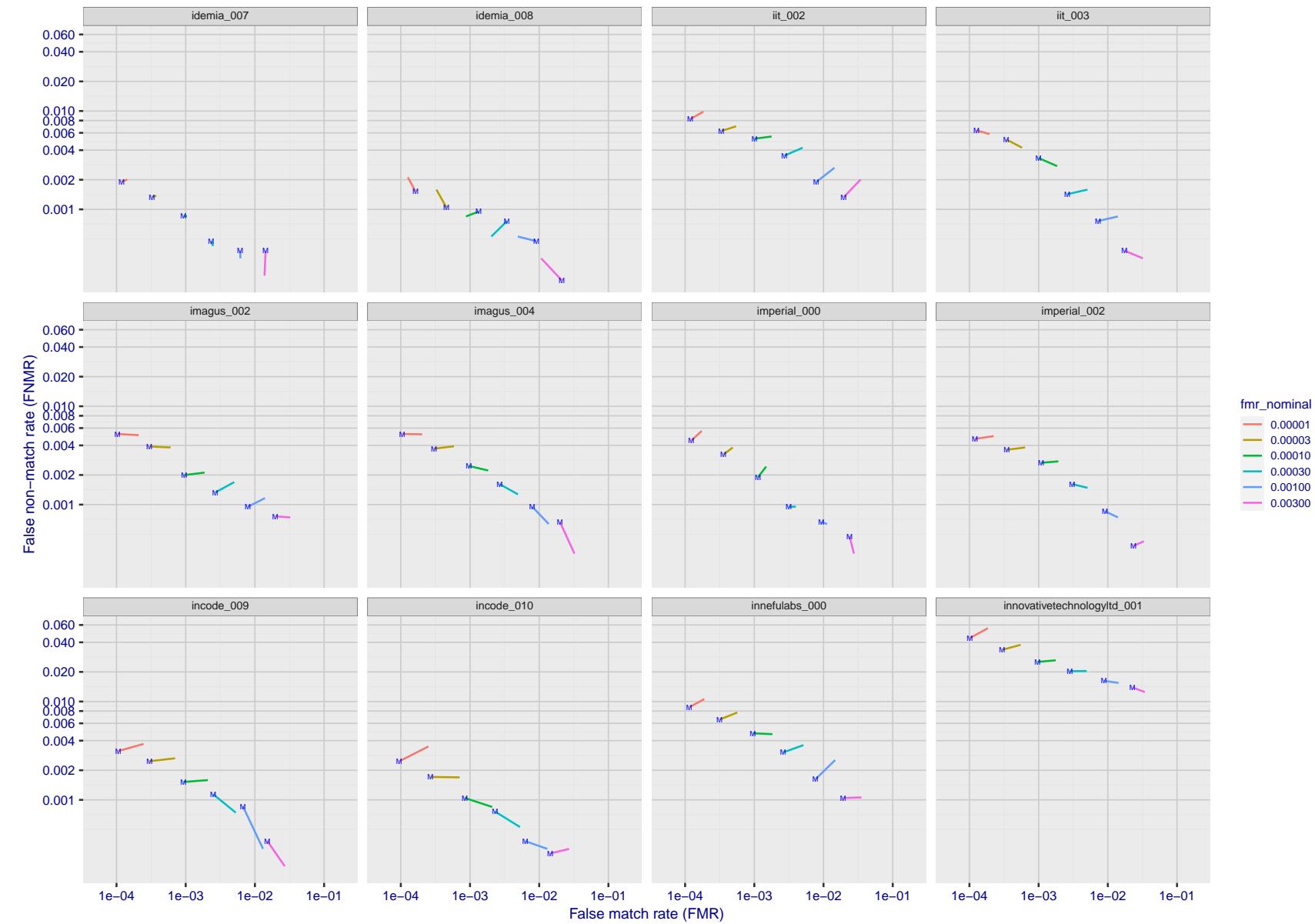


Figure 142: For the visa images, FNMR and FMR at six operating points along the DET characteristic. At each point a line is drawn between $(FMR, FNMR)_{MALE}$ and $(FMR, FNMR)_{FEMALE}$ showing how which sex has lower FMR and/or FNMR. The "M" label denotes male, the other end of the line corresponds to female. The six operating thresholds are selected to give the nominal false match rates given in the legend, and are computed over all impostor pairs regardless of age, sex, and place of birth. The plotted FMR values are broadly an order of magnitude larger than the nominal rates because FMR is computed over demographically-matched impostor pairs i.e individuals of the same sex, from the same geographic region (see section 3.6.1), and the same age group (see section 3.6.2).

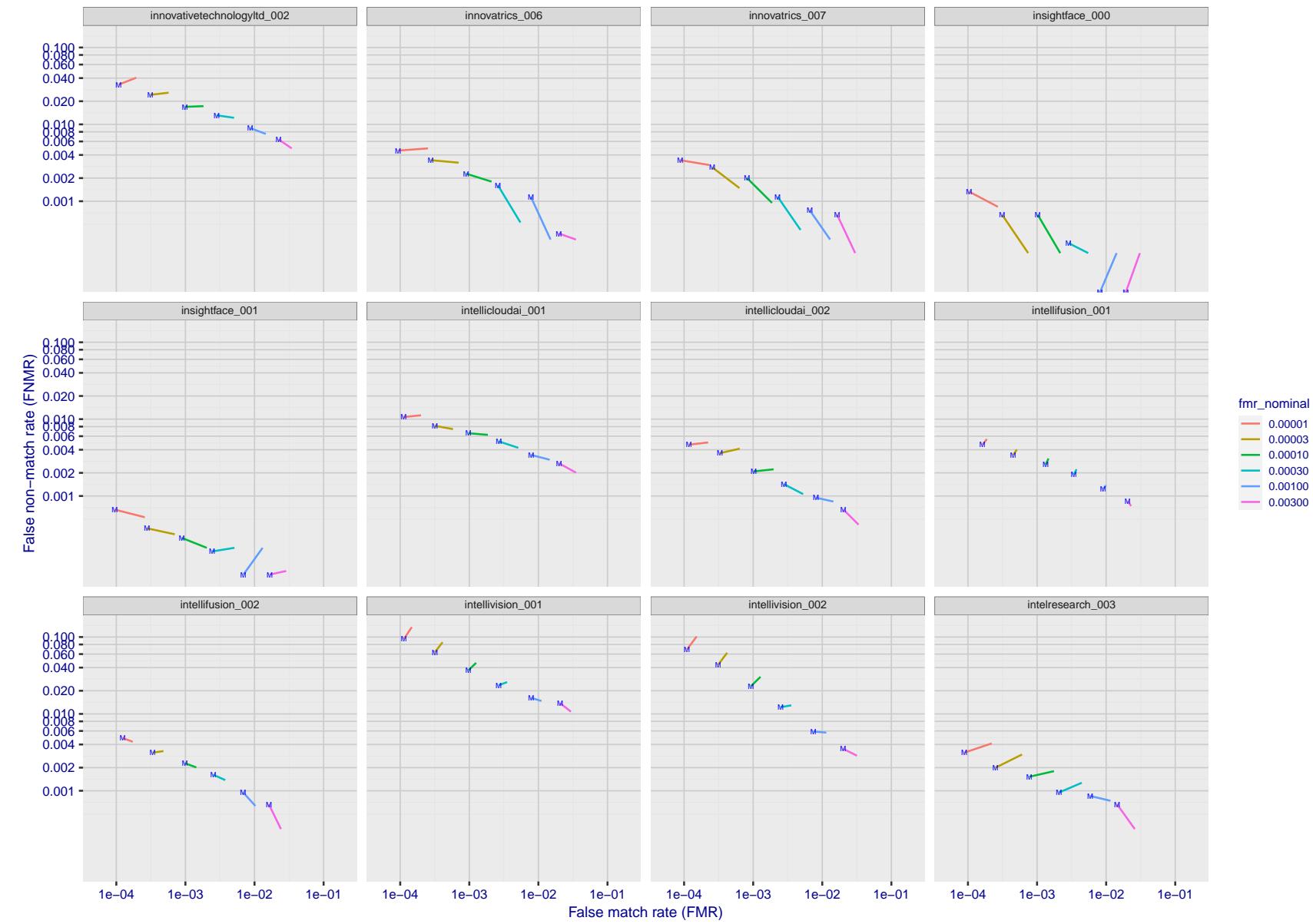


Figure 143: For the visa images, FNMR and FMR at six operating points along the DET characteristic. At each point a line is drawn between $(FMR, FNMR)_{MALE}$ and $(FMR, FNMR)_{FEMALE}$ showing how which sex has lower FMR and/or FNMR. The "M" label denotes male, the other end of the line corresponds to female. The six operating thresholds are selected to give the nominal false match rates given in the legend, and are computed over all impostor pairs regardless of age, sex, and place of birth. The plotted FMR values are broadly an order of magnitude larger than the nominal rates because FMR is computed over demographically-matched impostor pairs i.e individuals of the same sex, from the same geographic region (see section 3.6.1), and the same age group (see section 3.6.2).

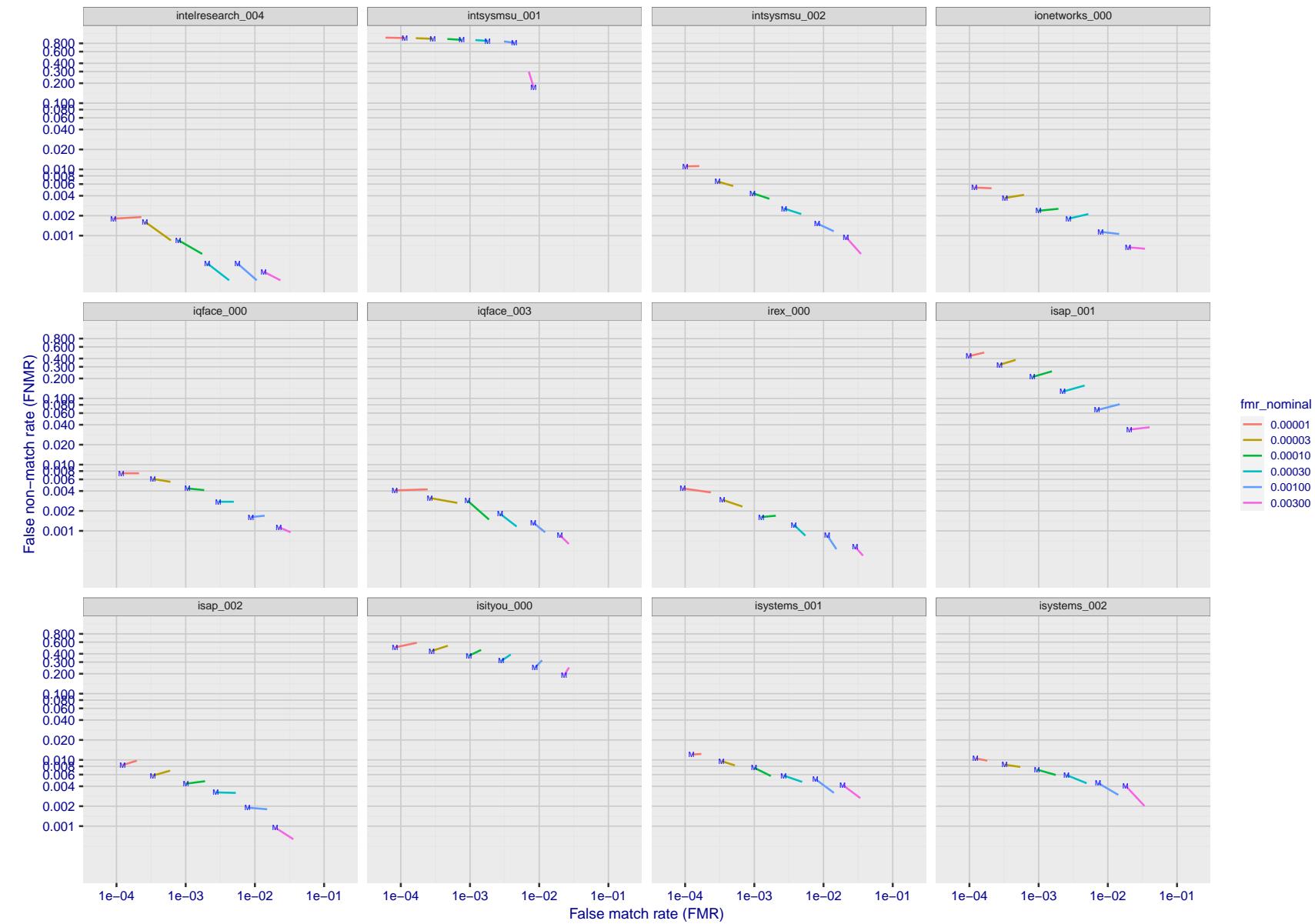


Figure 144: For the visa images, FNMR and FMR at six operating points along the DET characteristic. At each point a line is drawn between $(FMR, FNMR)_{MALE}$ and $(FMR, FNMR)_{FEMALE}$ showing how which sex has lower FMR and/or FNMR. The "M" label denotes male, the other end of the line corresponds to female. The six operating thresholds are selected to give the nominal false match rates given in the legend, and are computed over all impostor pairs regardless of age, sex, and place of birth. The plotted FMR values are broadly an order of magnitude larger than the nominal rates because FMR is computed over demographically-matched impostor pairs i.e individuals of the same sex, from the same geographic region (see section 3.6.1), and the same age group (see section 3.6.2).

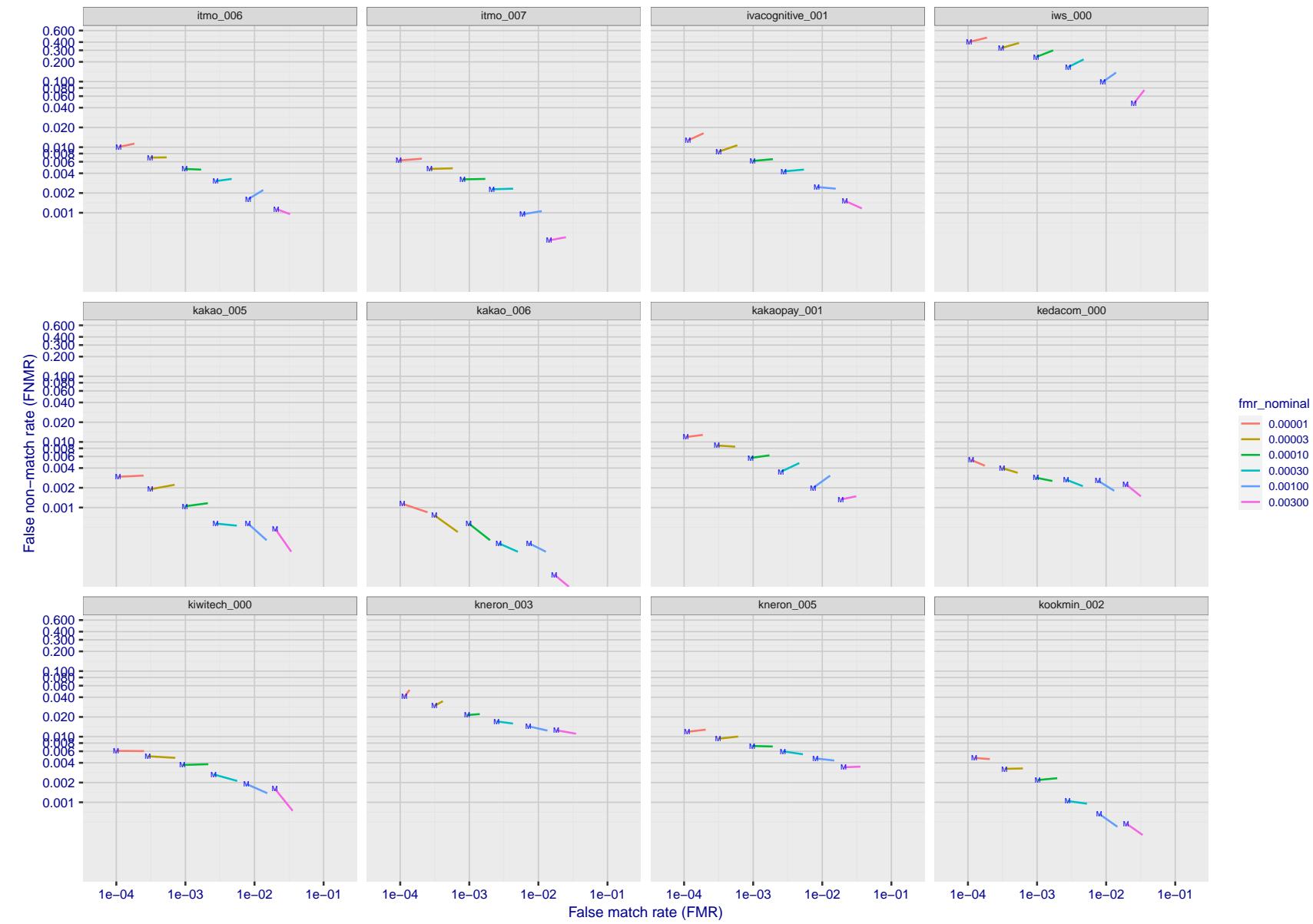


Figure 145: For the visa images, FNMR and FMR at six operating points along the DET characteristic. At each point a line is drawn between $(FMR, FNMR)_{MALE}$ and $(FMR, FNMR)_{FEMALE}$ showing how which sex has lower FMR and/or FNMR. The "M" label denotes male, the other end of the line corresponds to female. The six operating thresholds are selected to give the nominal false match rates given in the legend, and are computed over all impostor pairs regardless of age, sex, and place of birth. The plotted FMR values are broadly an order of magnitude larger than the nominal rates because FMR is computed over demographically-matched impostor pairs i.e individuals of the same sex, from the same geographic region (see section 3.6.1), and the same age group (see section 3.6.2).

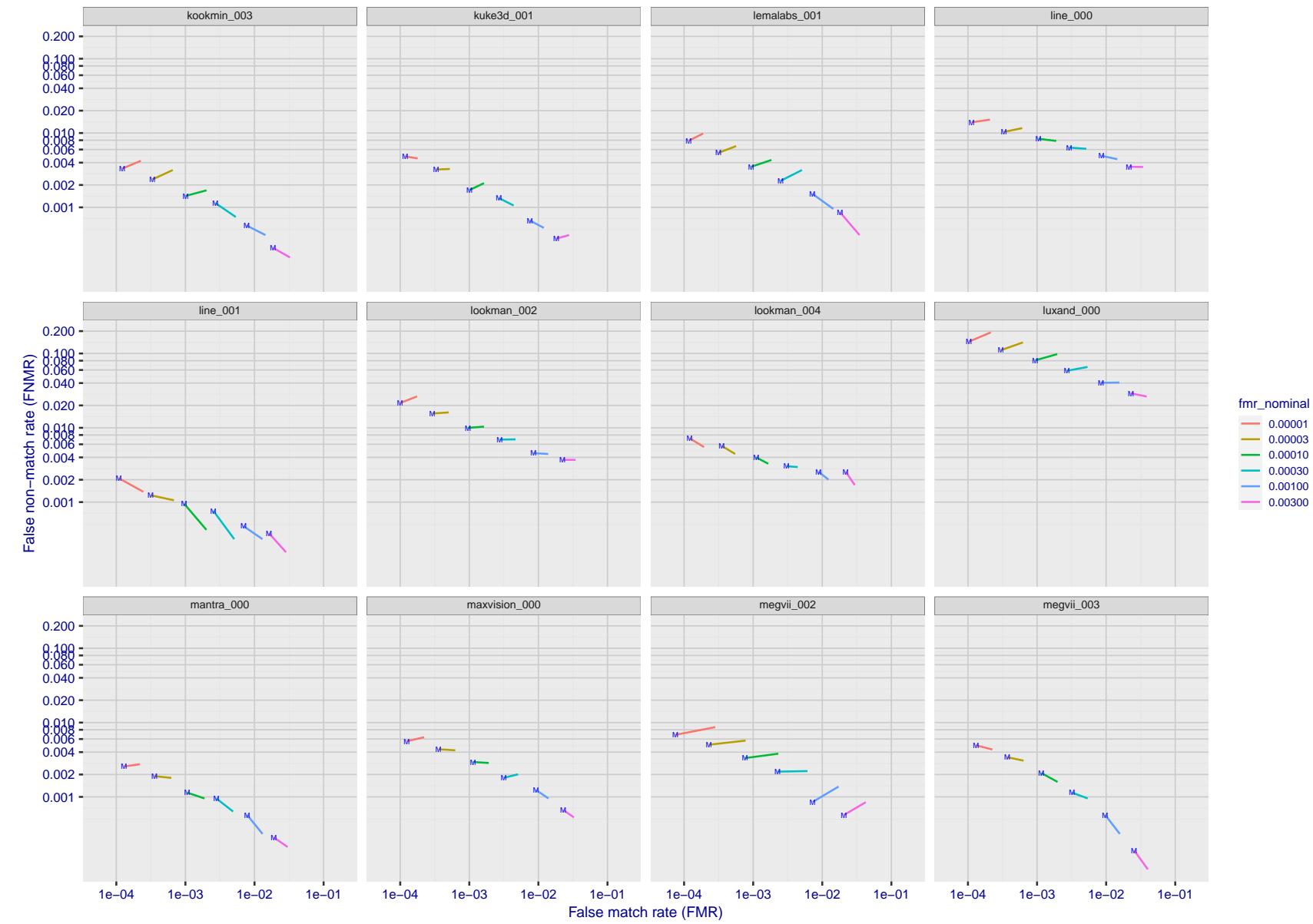


Figure 146: For the visa images, FNMR and FMR at six operating points along the DET characteristic. At each point a line is drawn between $(FMR, FNMR)_{MALE}$ and $(FMR, FNMR)_{FEMALE}$ showing how which sex has lower FMR and/or FNMR. The "M" label denotes male, the other end of the line corresponds to female. The six operating thresholds are selected to give the nominal false match rates given in the legend, and are computed over all impostor pairs regardless of age, sex, and place of birth. The plotted FMR values are broadly an order of magnitude larger than the nominal rates because FMR is computed over demographically-matched impostor pairs i.e individuals of the same sex, from the same geographic region (see section 3.6.1), and the same age group (see section 3.6.2).

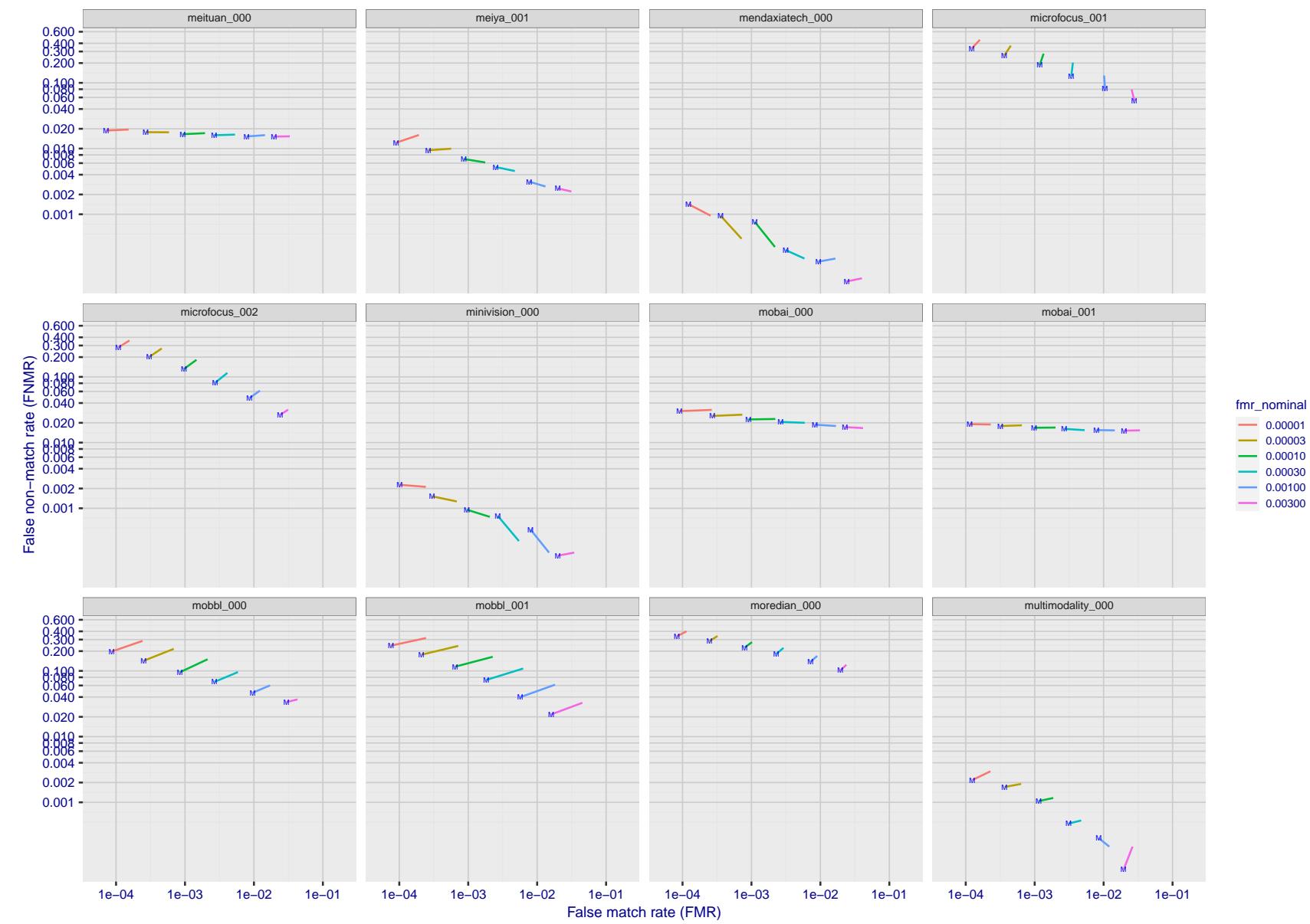


Figure 147: For the visa images, FNMR and FMR at six operating points along the DET characteristic. At each point a line is drawn between $(FMR, FNMR)_{MALE}$ and $(FMR, FNMR)_{FEMALE}$ showing how which sex has lower FMR and/or FNMR. The "M" label denotes male, the other end of the line corresponds to female. The six operating thresholds are selected to give the nominal false match rates given in the legend, and are computed over all impostor pairs regardless of age, sex, and place of birth. The plotted FMR values are broadly an order of magnitude larger than the nominal rates because FMR is computed over demographically-matched impostor pairs i.e individuals of the same sex, from the same geographic region (see section 3.6.1), and the same age group (see section 3.6.2).

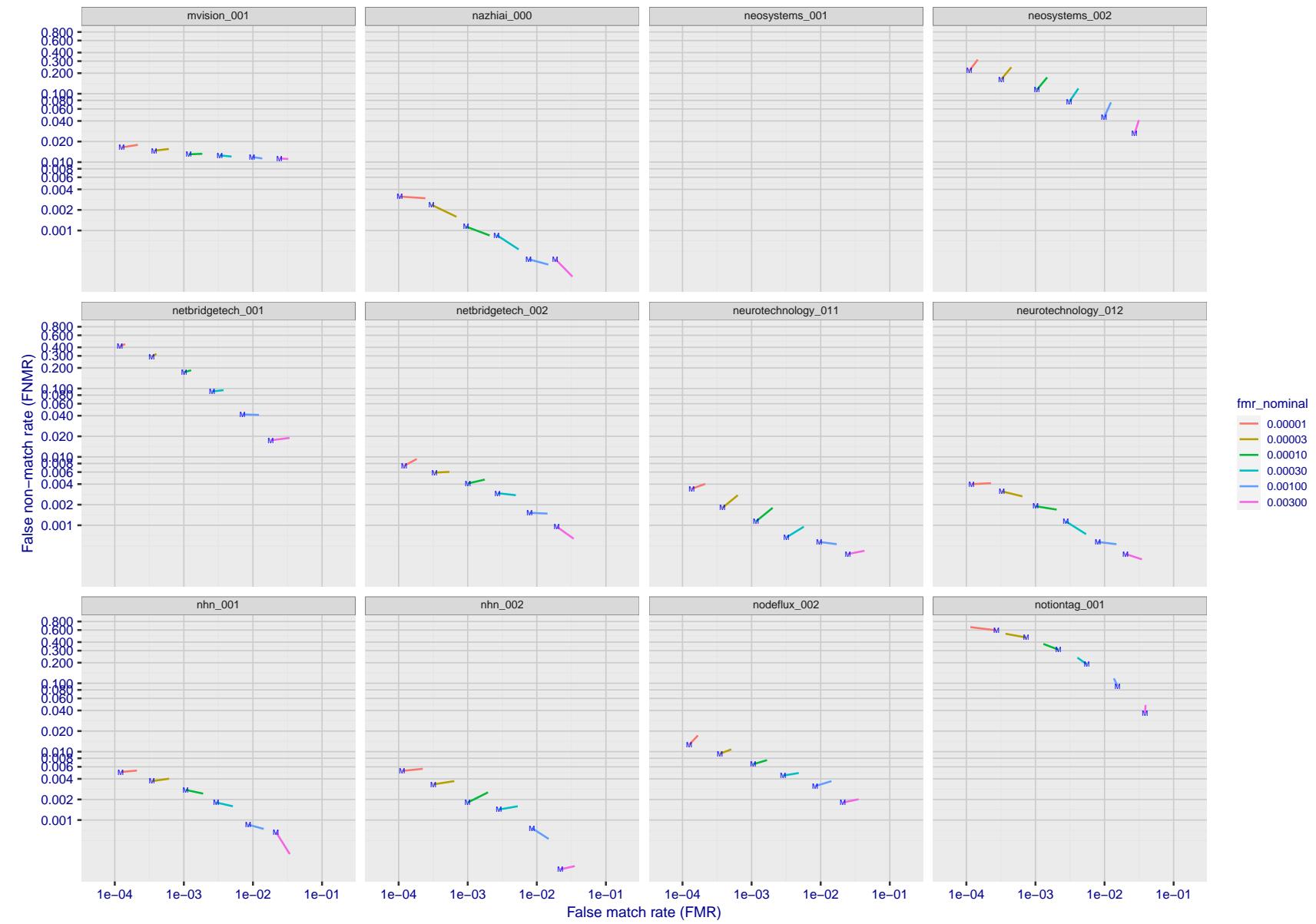


Figure 148: For the visa images, FNMR and FMR at six operating points along the DET characteristic. At each point a line is drawn between $(FMR, FNMR)_{MALE}$ and $(FMR, FNMR)_{FEMALE}$ showing how which sex has lower FMR and/or FNMR. The "M" label denotes male, the other end of the line corresponds to female. The six operating thresholds are selected to give the nominal false match rates given in the legend, and are computed over all impostor pairs regardless of age, sex, and place of birth. The plotted FMR values are broadly an order of magnitude larger than the nominal rates because FMR is computed over demographically-matched impostor pairs i.e individuals of the same sex, from the same geographic region (see section 3.6.1), and the same age group (see section 3.6.2).

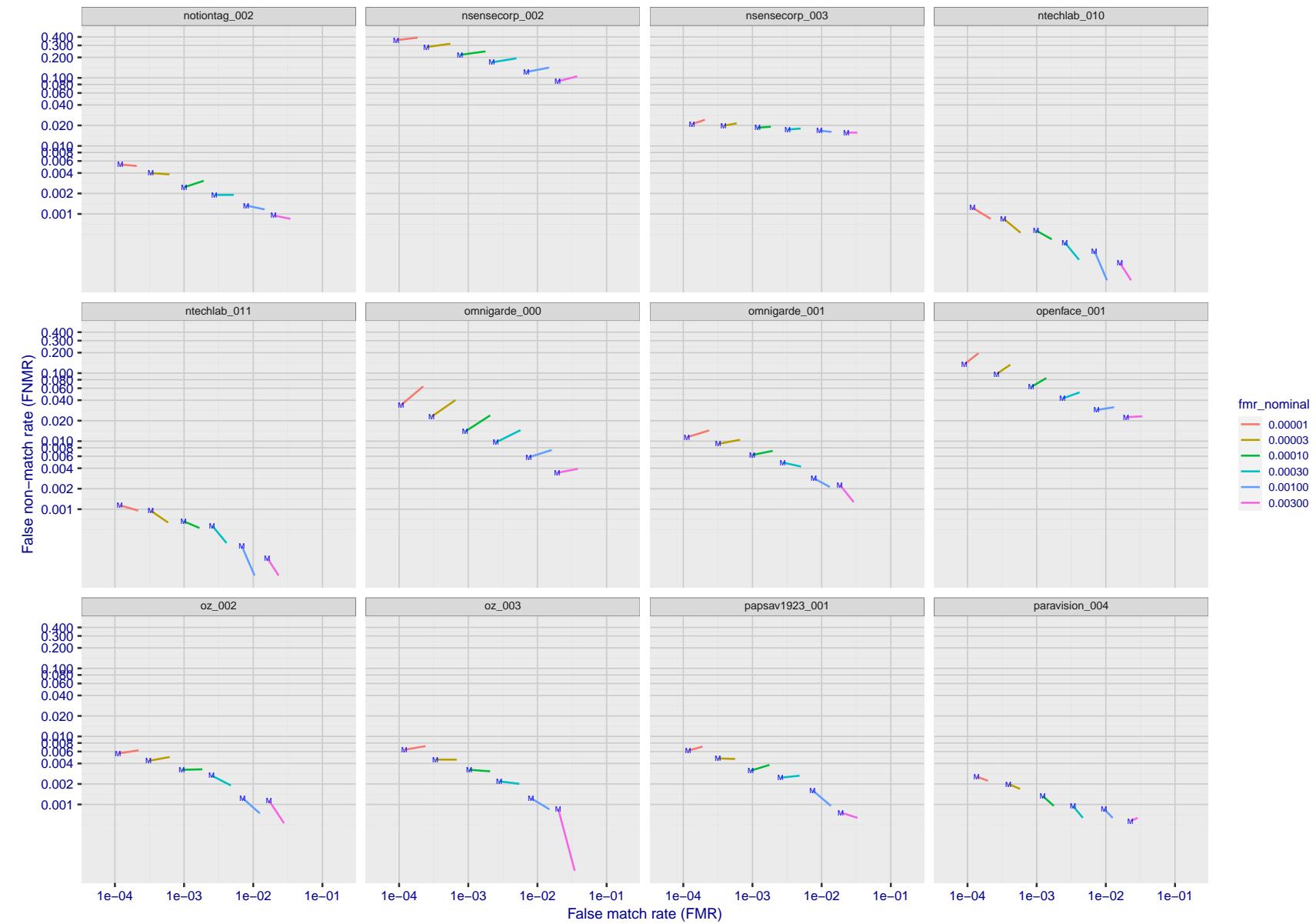


Figure 149: For the visa images, FNMR and FMR at six operating points along the DET characteristic. At each point a line is drawn between $(FMR, FNMR)_{MALE}$ and $(FMR, FNMR)_{FEMALE}$ showing how which sex has lower FMR and/or FNMR. The "M" label denotes male, the other end of the line corresponds to female. The six operating thresholds are selected to give the nominal false match rates given in the legend, and are computed over all impostor pairs regardless of age, sex, and place of birth. The plotted FMR values are broadly an order of magnitude larger than the nominal rates because FMR is computed over demographically-matched impostor pairs i.e individuals of the same sex, from the same geographic region (see section 3.6.1), and the same age group (see section 3.6.2).

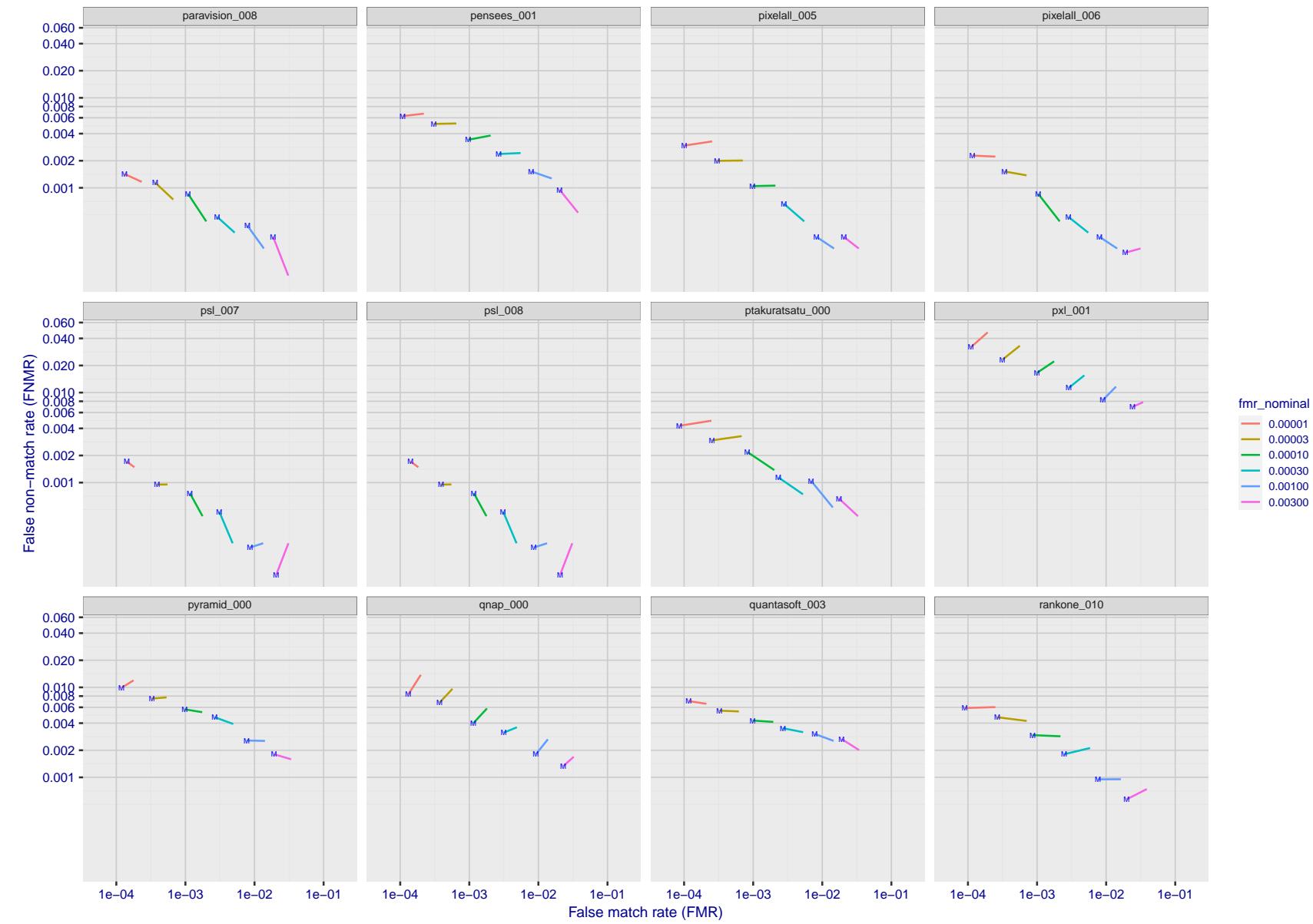


Figure 150: For the visa images, FNMR and FMR at six operating points along the DET characteristic. At each point a line is drawn between $(FMR, FNMR)_{MALE}$ and $(FMR, FNMR)_{FEMALE}$ showing how which sex has lower FMR and/or FNMR. The "M" label denotes male, the other end of the line corresponds to female. The six operating thresholds are selected to give the nominal false match rates given in the legend, and are computed over all impostor pairs regardless of age, sex, and place of birth. The plotted FMR values are broadly an order of magnitude larger than the nominal rates because FMR is computed over demographically-matched impostor pairs i.e individuals of the same sex, from the same geographic region (see section 3.6.1), and the same age group (see section 3.6.2).

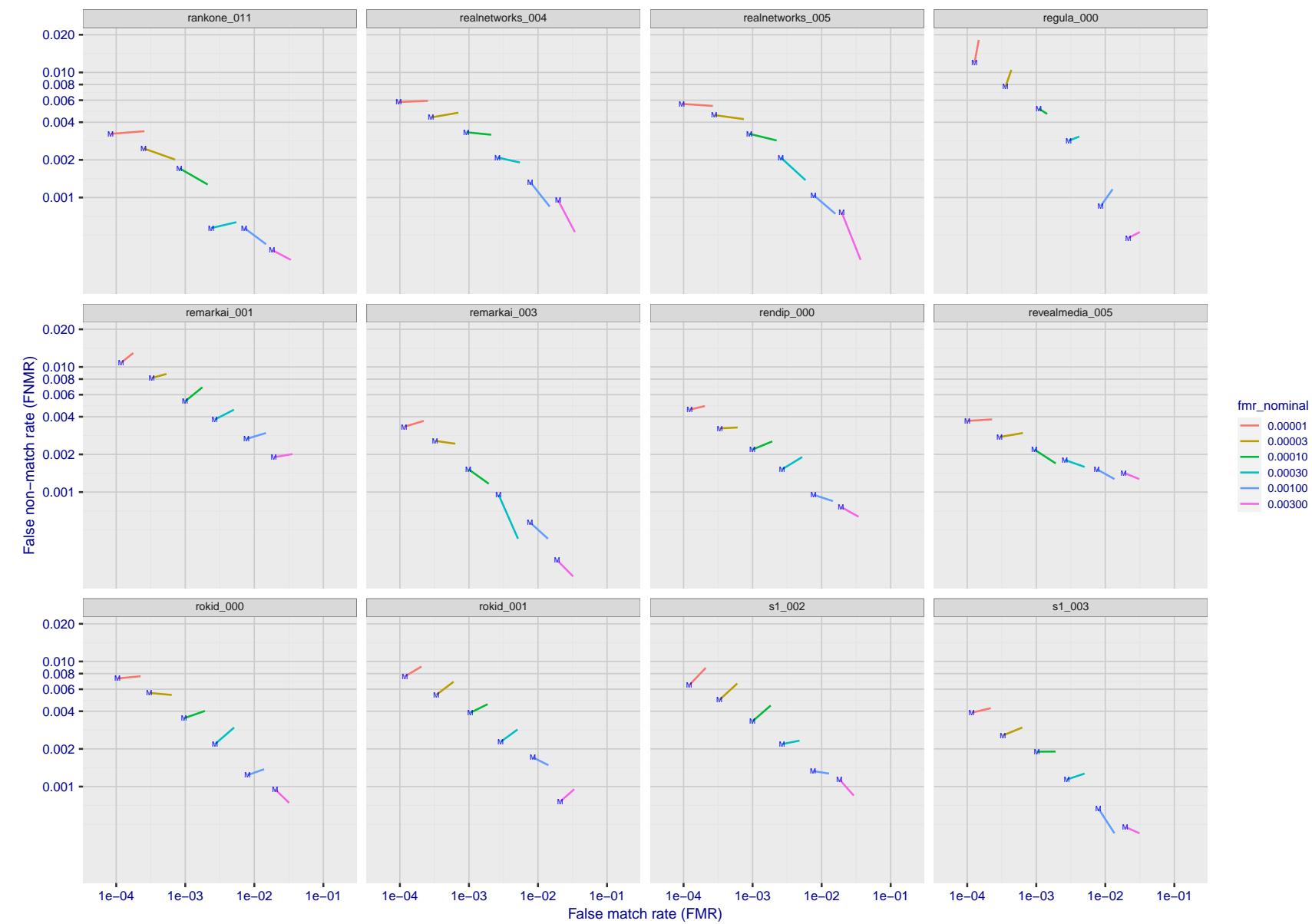


Figure 151: For the visa images, FNMR and FMR at six operating points along the DET characteristic. At each point a line is drawn between $(FMR, FNMR)_{MALE}$ and $(FMR, FNMR)_{FEMALE}$ showing how which sex has lower FMR and/or FNMR. The "M" label denotes male, the other end of the line corresponds to female. The six operating thresholds are selected to give the nominal false match rates given in the legend, and are computed over all impostor pairs regardless of age, sex, and place of birth. The plotted FMR values are broadly an order of magnitude larger than the nominal rates because FMR is computed over demographically-matched impostor pairs i.e individuals of the same sex, from the same geographic region (see section 3.6.1), and the same age group (see section 3.6.2).

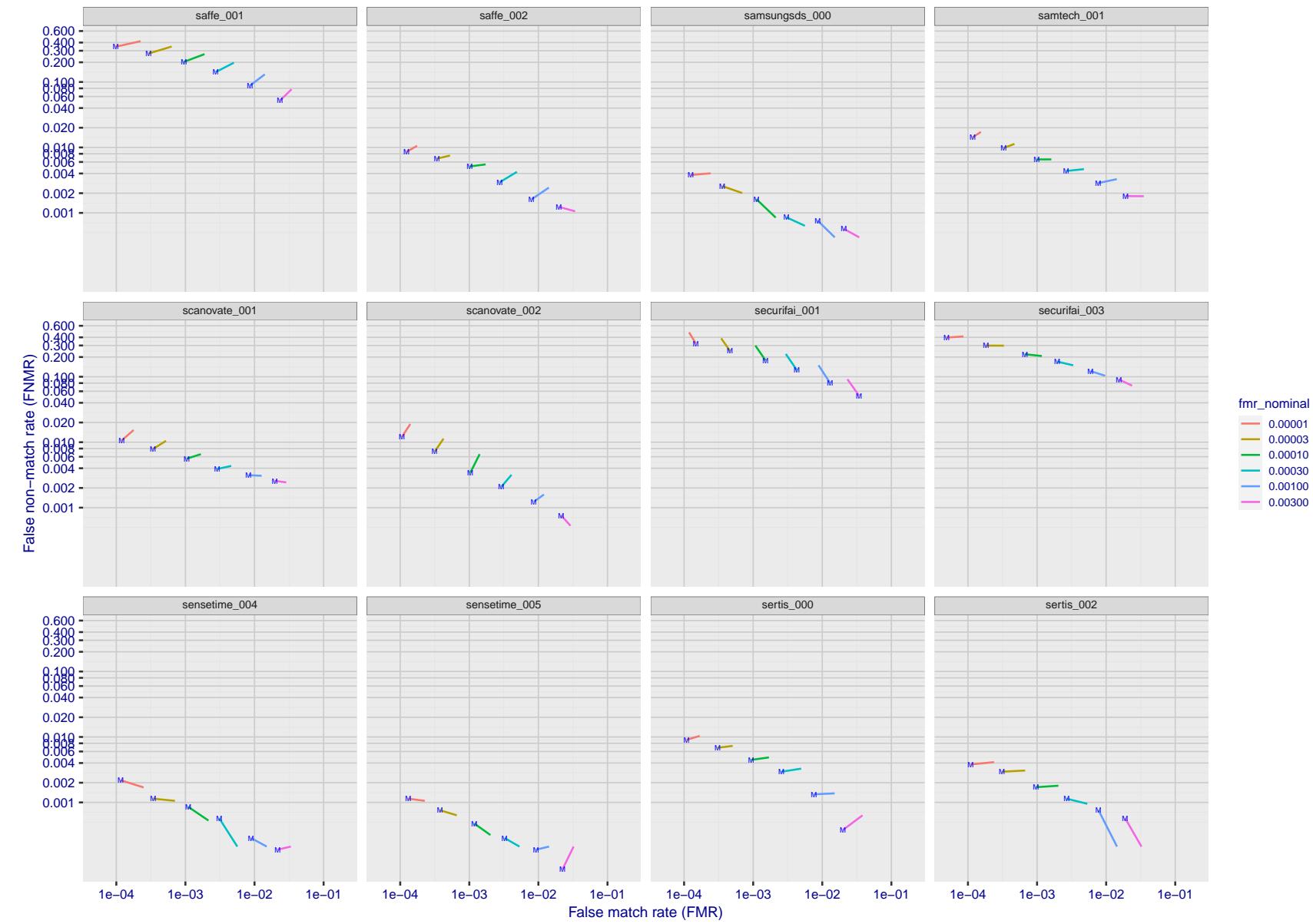


Figure 152: For the visa images, FNMR and FMR at six operating points along the DET characteristic. At each point a line is drawn between $(FMR, FNMR)_{MALE}$ and $(FMR, FNMR)_{FEMALE}$ showing how which sex has lower FMR and/or FNMR. The "M" label denotes male, the other end of the line corresponds to female. The six operating thresholds are selected to give the nominal false match rates given in the legend, and are computed over all impostor pairs regardless of age, sex, and place of birth. The plotted FMR values are broadly an order of magnitude larger than the nominal rates because FMR is computed over demographically-matched impostor pairs i.e individuals of the same sex, from the same geographic region (see section 3.6.1), and the same age group (see section 3.6.2).

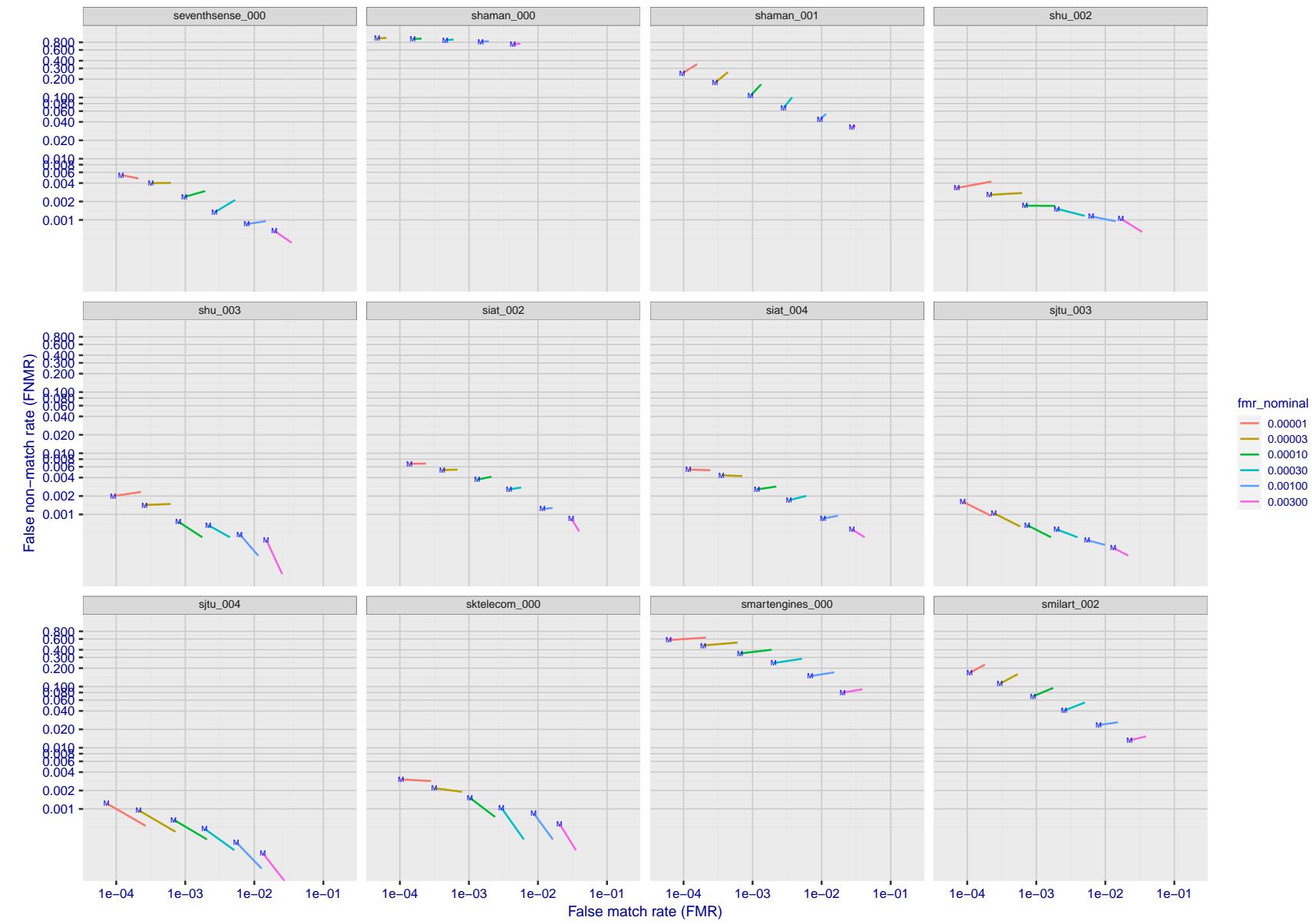


Figure 153: For the visa images, FNMR and FMR at six operating points along the DET characteristic. At each point a line is drawn between $(FMR, FNMR)_{MALE}$ and $(FMR, FNMR)_{FEMALE}$ showing how which sex has lower FMR and/or FNMR. The "M" label denotes male, the other end of the line corresponds to female. The six operating thresholds are selected to give the nominal false match rates given in the legend, and are computed over all impostor pairs regardless of age, sex, and place of birth. The plotted FMR values are broadly an order of magnitude larger than the nominal rates because FMR is computed over demographically-matched impostor pairs i.e individuals of the same sex, from the same geographic region (see section 3.6.1), and the same age group (see section 3.6.2).

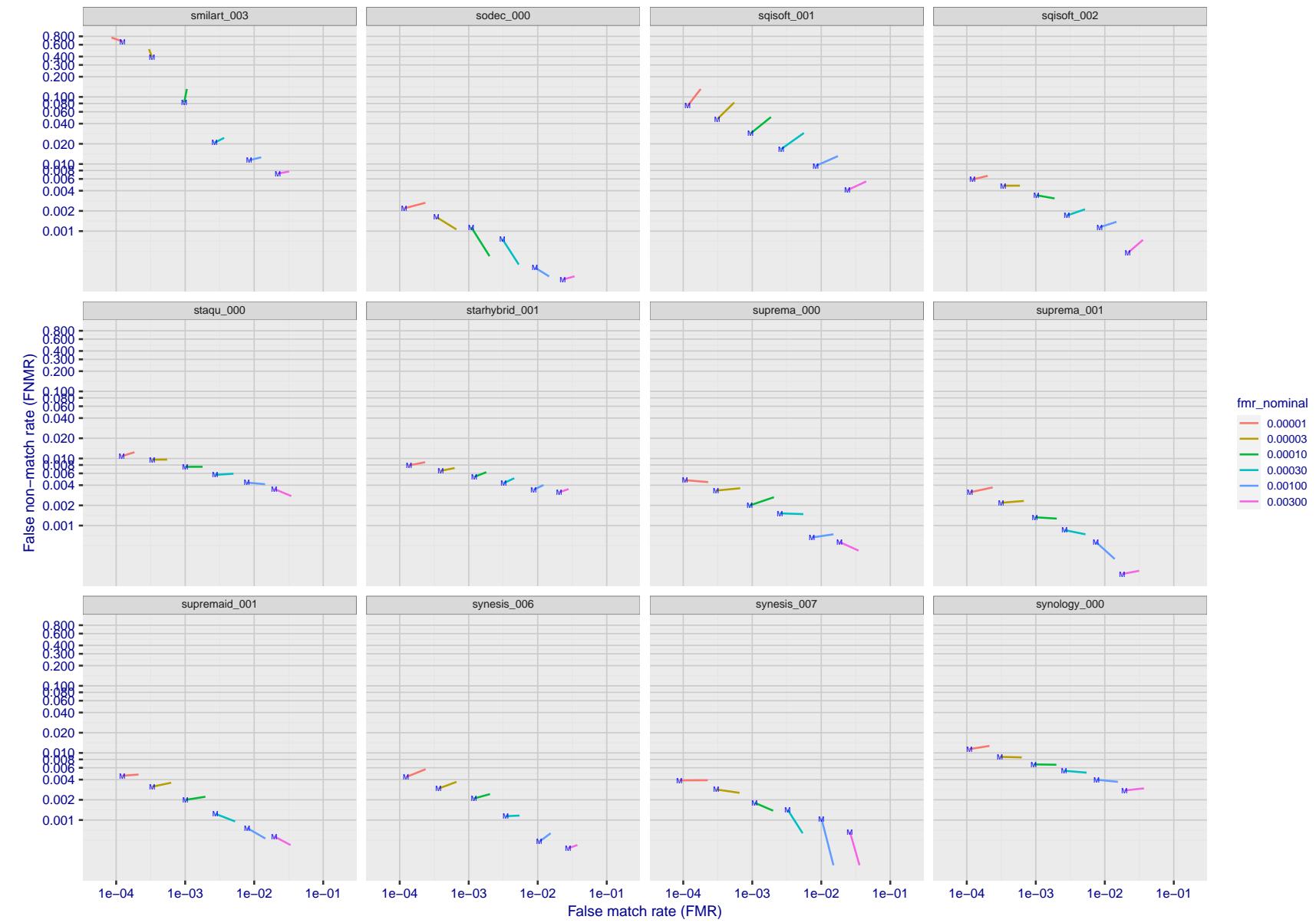


Figure 154: For the visa images, FNMR and FMR at six operating points along the DET characteristic. At each point a line is drawn between $(FMR, FNMR)_{MALE}$ and $(FMR, FNMR)_{FEMALE}$ showing how which sex has lower FMR and/or FNMR. The "M" label denotes male, the other end of the line corresponds to female. The six operating thresholds are selected to give the nominal false match rates given in the legend, and are computed over all impostor pairs regardless of age, sex, and place of birth. The plotted FMR values are broadly an order of magnitude larger than the nominal rates because FMR is computed over demographically-matched impostor pairs i.e individuals of the same sex, from the same geographic region (see section 3.6.1), and the same age group (see section 3.6.2).

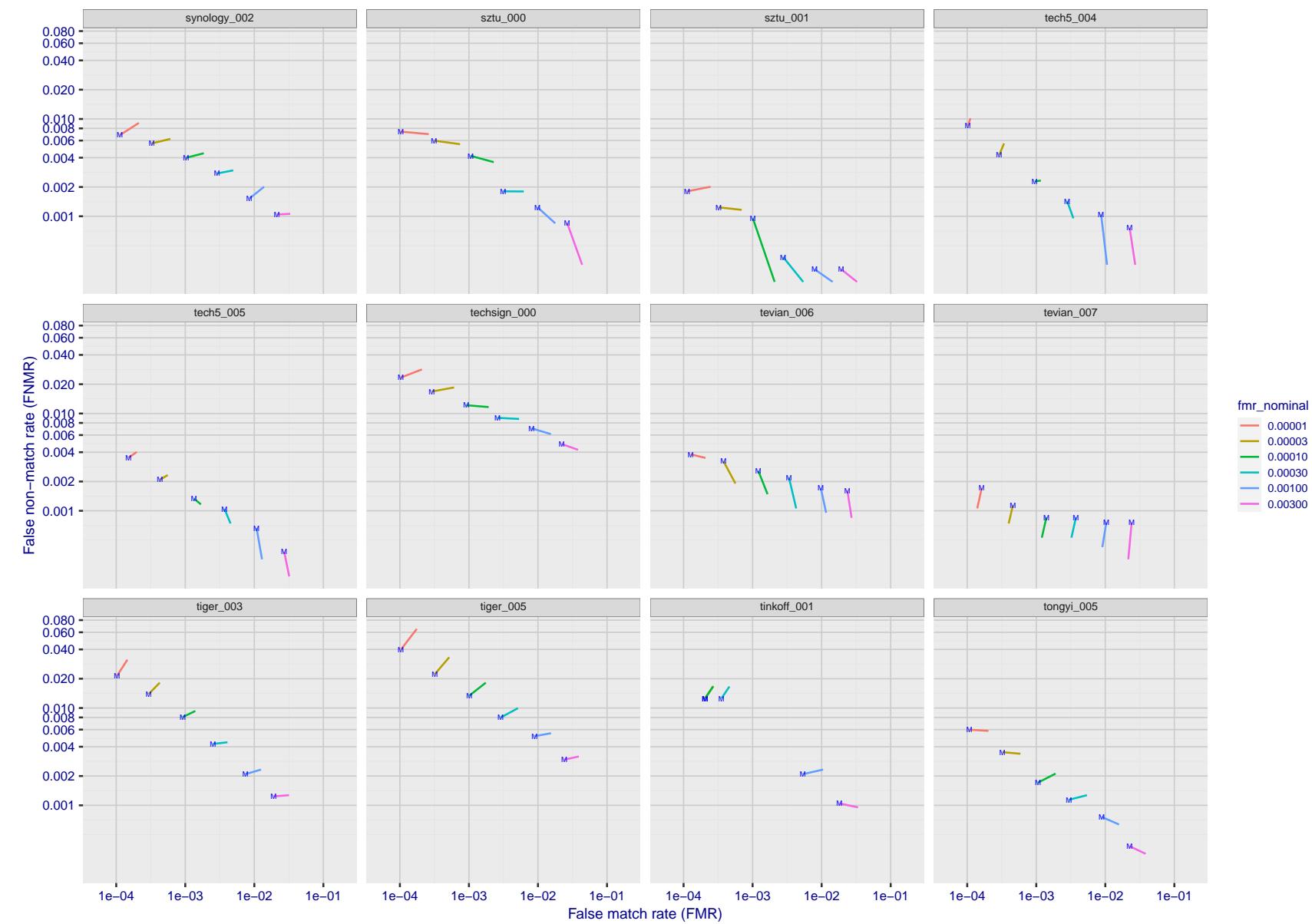


Figure 155: For the visa images, FNMR and FMR at six operating points along the DET characteristic. At each point a line is drawn between $(FMR, FNMR)_{MALE}$ and $(FMR, FNMR)_{FEMALE}$ showing how which sex has lower FMR and/or FNMR. The "M" label denotes male, the other end of the line corresponds to female. The six operating thresholds are selected to give the nominal false match rates given in the legend, and are computed over all impostor pairs regardless of age, sex, and place of birth. The plotted FMR values are broadly an order of magnitude larger than the nominal rates because FMR is computed over demographically-matched impostor pairs i.e individuals of the same sex, from the same geographic region (see section 3.6.1), and the same age group (see section 3.6.2).

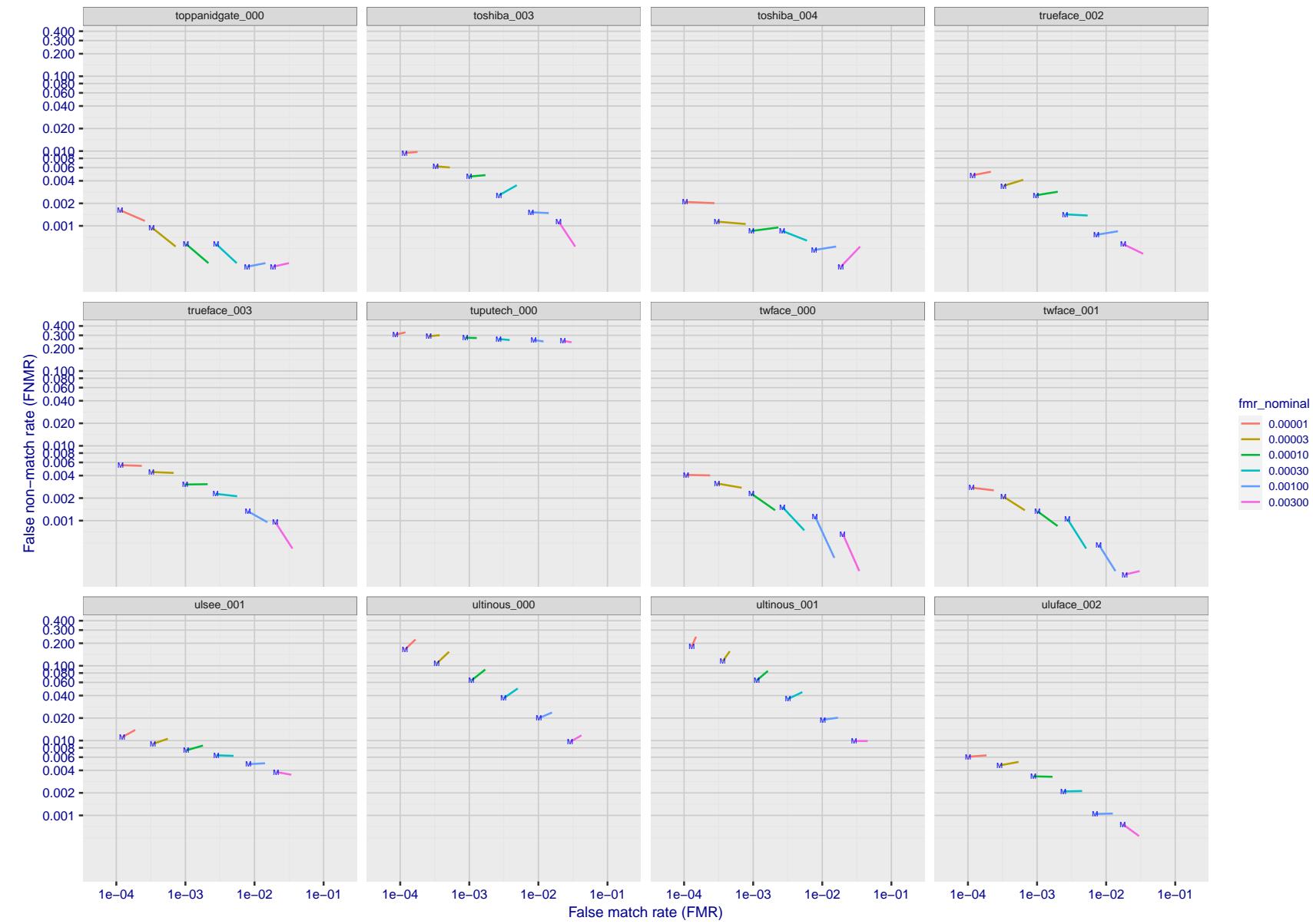


Figure 156: For the visa images, FNMR and FMR at six operating points along the DET characteristic. At each point a line is drawn between $(FMR, FNMR)_{MALE}$ and $(FMR, FNMR)_{FEMALE}$ showing how which sex has lower FMR and/or FNMR. The "M" label denotes male, the other end of the line corresponds to female. The six operating thresholds are selected to give the nominal false match rates given in the legend, and are computed over all impostor pairs regardless of age, sex, and place of birth. The plotted FMR values are broadly an order of magnitude larger than the nominal rates because FMR is computed over demographically-matched impostor pairs i.e individuals of the same sex, from the same geographic region (see section 3.6.1), and the same age group (see section 3.6.2).

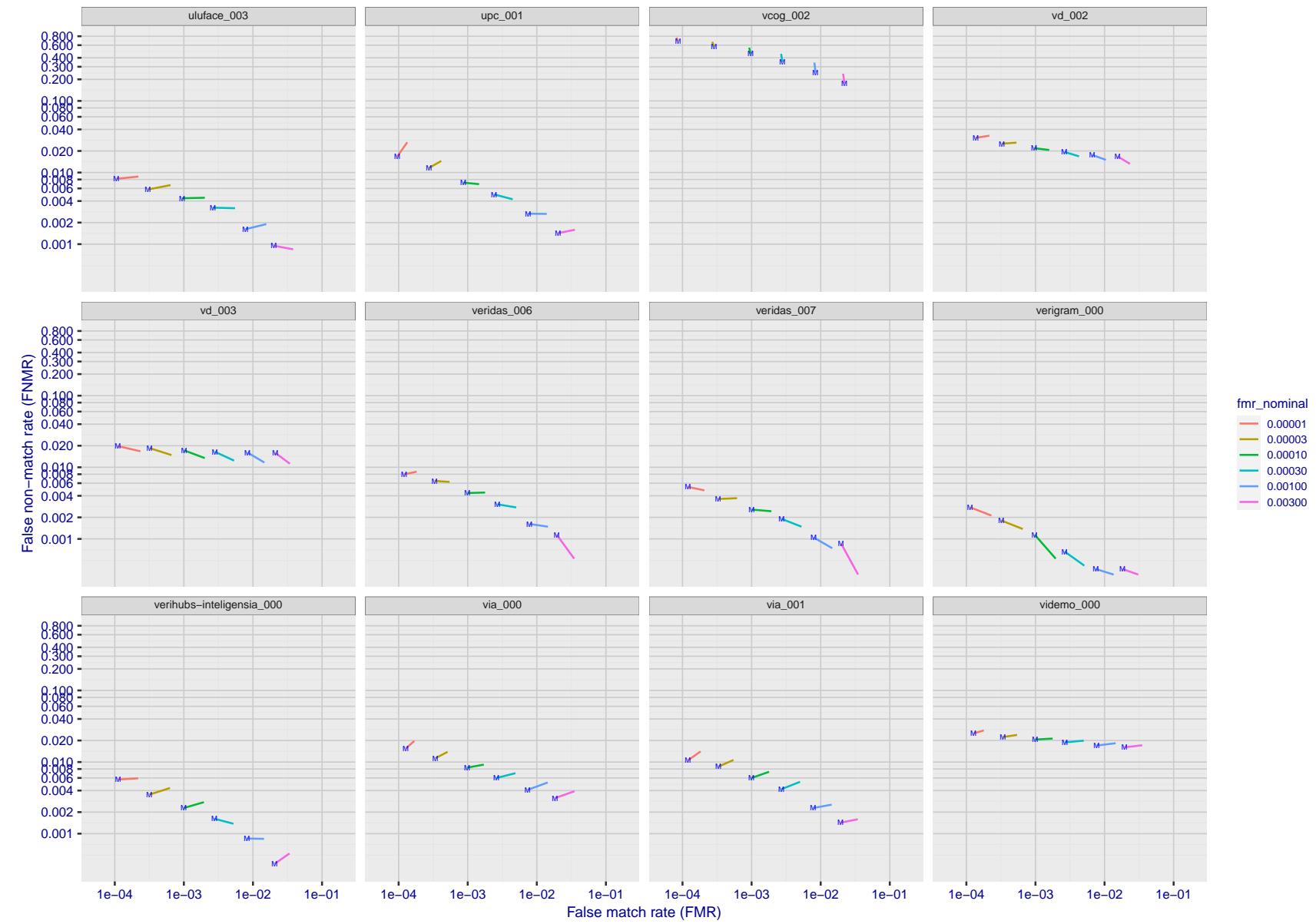


Figure 157: For the visa images, FNMR and FMR at six operating points along the DET characteristic. At each point a line is drawn between $(FMR, FNMR)_{MALE}$ and $(FMR, FNMR)_{FEMALE}$ showing how which sex has lower FMR and/or FNMR. The "M" label denotes male, the other end of the line corresponds to female. The six operating thresholds are selected to give the nominal false match rates given in the legend, and are computed over all impostor pairs regardless of age, sex, and place of birth. The plotted FMR values are broadly an order of magnitude larger than the nominal rates because FMR is computed over demographically-matched impostor pairs i.e individuals of the same sex, from the same geographic region (see section 3.6.1), and the same age group (see section 3.6.2).

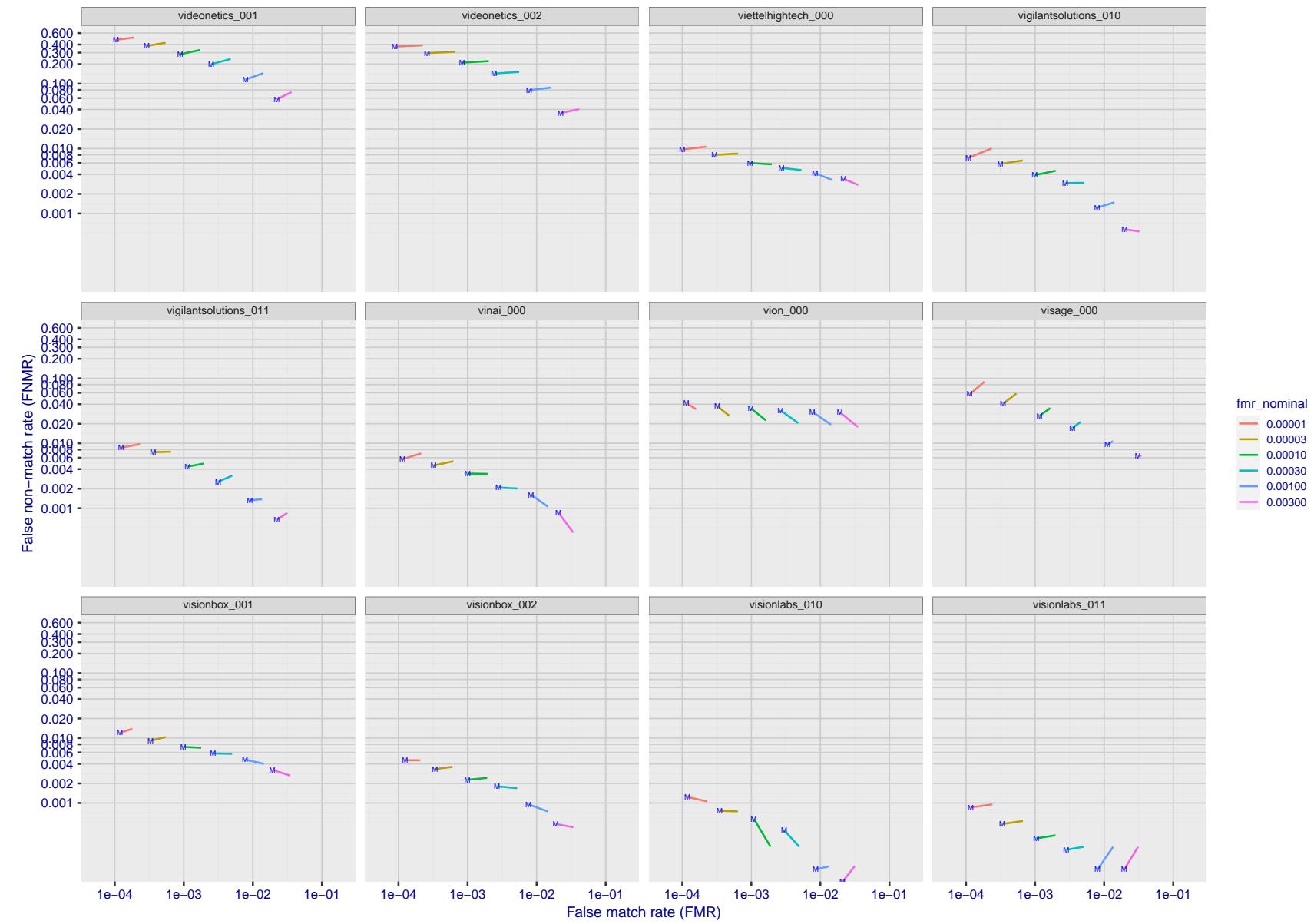


Figure 158: For the visa images, FNMR and FMR at six operating points along the DET characteristic. At each point a line is drawn between $(FMR, FNMR)_{MALE}$ and $(FMR, FNMR)_{FEMALE}$ showing how which sex has lower FMR and/or FNMR. The "M" label denotes male, the other end of the line corresponds to female. The six operating thresholds are selected to give the nominal false match rates given in the legend, and are computed over all impostor pairs regardless of age, sex, and place of birth. The plotted FMR values are broadly an order of magnitude larger than the nominal rates because FMR is computed over demographically-matched impostor pairs i.e individuals of the same sex, from the same geographic region (see section 3.6.1), and the same age group (see section 3.6.2).

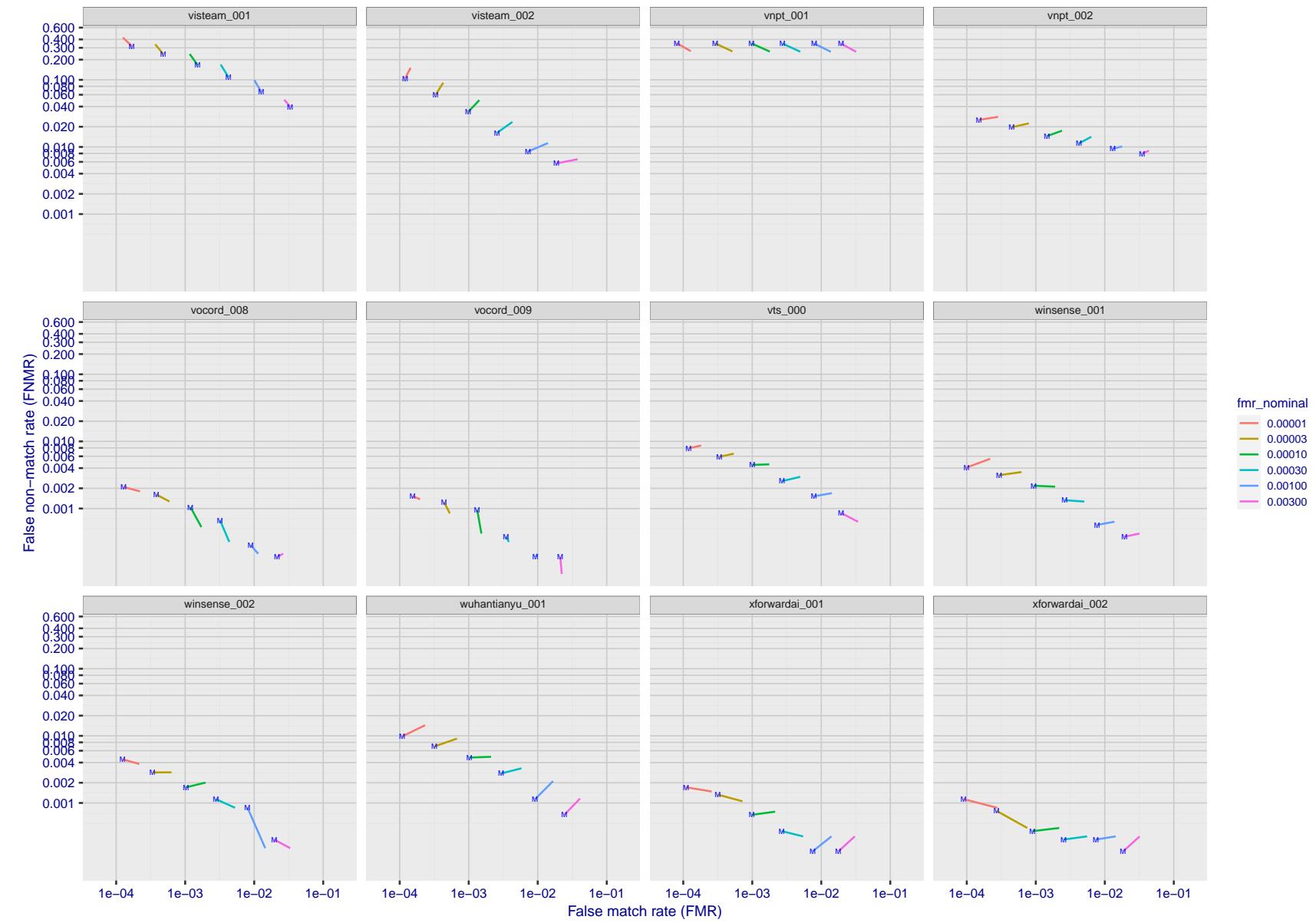


Figure 159: For the visa images, FNMR and FMR at six operating points along the DET characteristic. At each point a line is drawn between $(FMR, FNMR)_{MALE}$ and $(FMR, FNMR)_{FEMALE}$ showing how which sex has lower FMR and/or FNMR. The "M" label denotes male, the other end of the line corresponds to female. The six operating thresholds are selected to give the nominal false match rates given in the legend, and are computed over all impostor pairs regardless of age, sex, and place of birth. The plotted FMR values are broadly an order of magnitude larger than the nominal rates because FMR is computed over demographically-matched impostor pairs i.e individuals of the same sex, from the same geographic region (see section 3.6.1), and the same age group (see section 3.6.2).

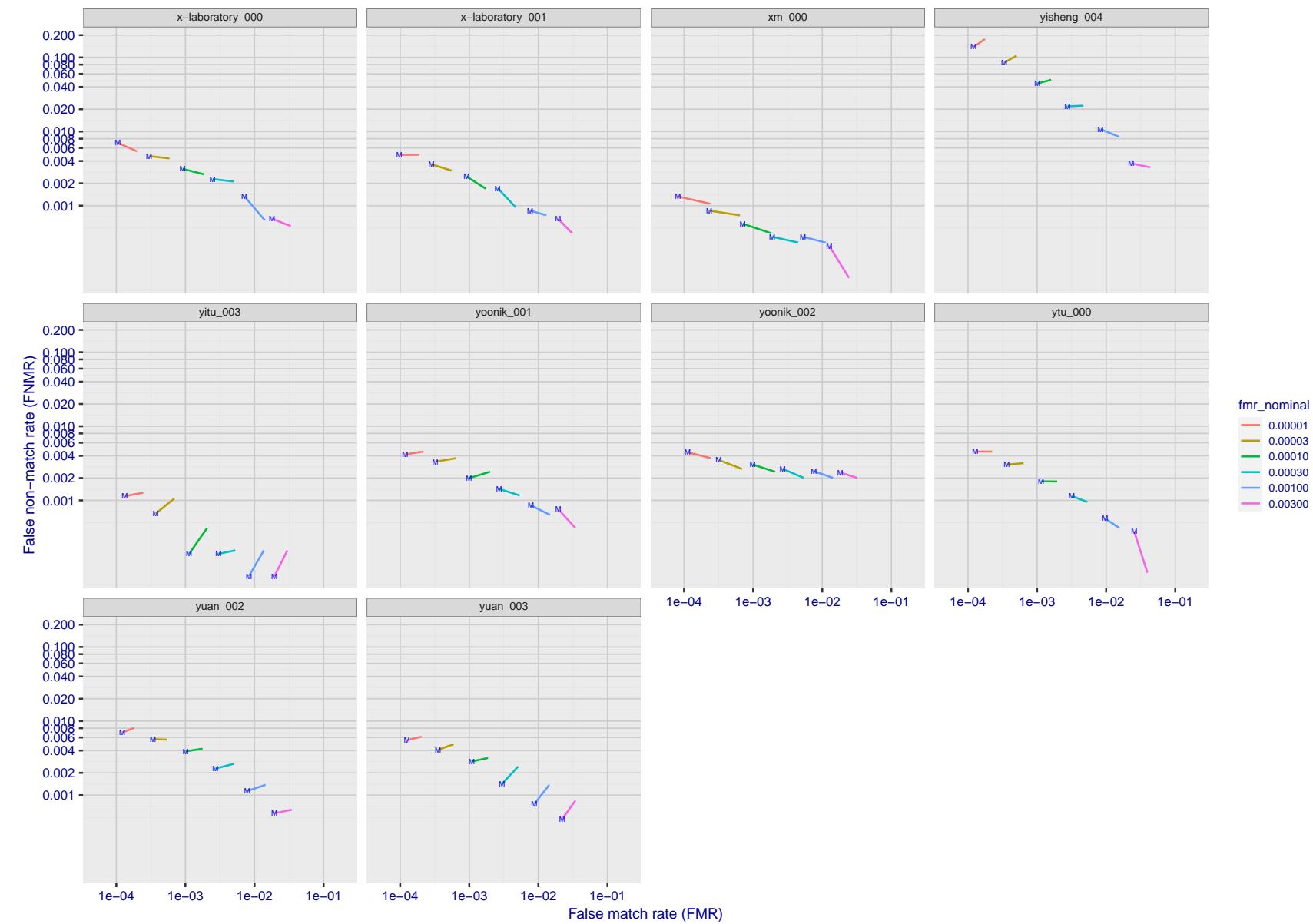


Figure 160: For the visa images, FNMR and FMR at six operating points along the DET characteristic. At each point a line is drawn between $(FMR, FNMR)_{MALE}$ and $(FMR, FNMR)_{FEMALE}$ showing how which sex has lower FMR and/or FNMR. The "M" label denotes male, the other end of the line corresponds to female. The six operating thresholds are selected to give the nominal false match rates given in the legend, and are computed over all impostor pairs regardless of age, sex, and place of birth. The plotted FMR values are broadly an order of magnitude larger than the nominal rates because FMR is computed over demographically-matched impostor pairs i.e individuals of the same sex, from the same geographic region (see section 3.6.1), and the same age group (see section 3.6.2).

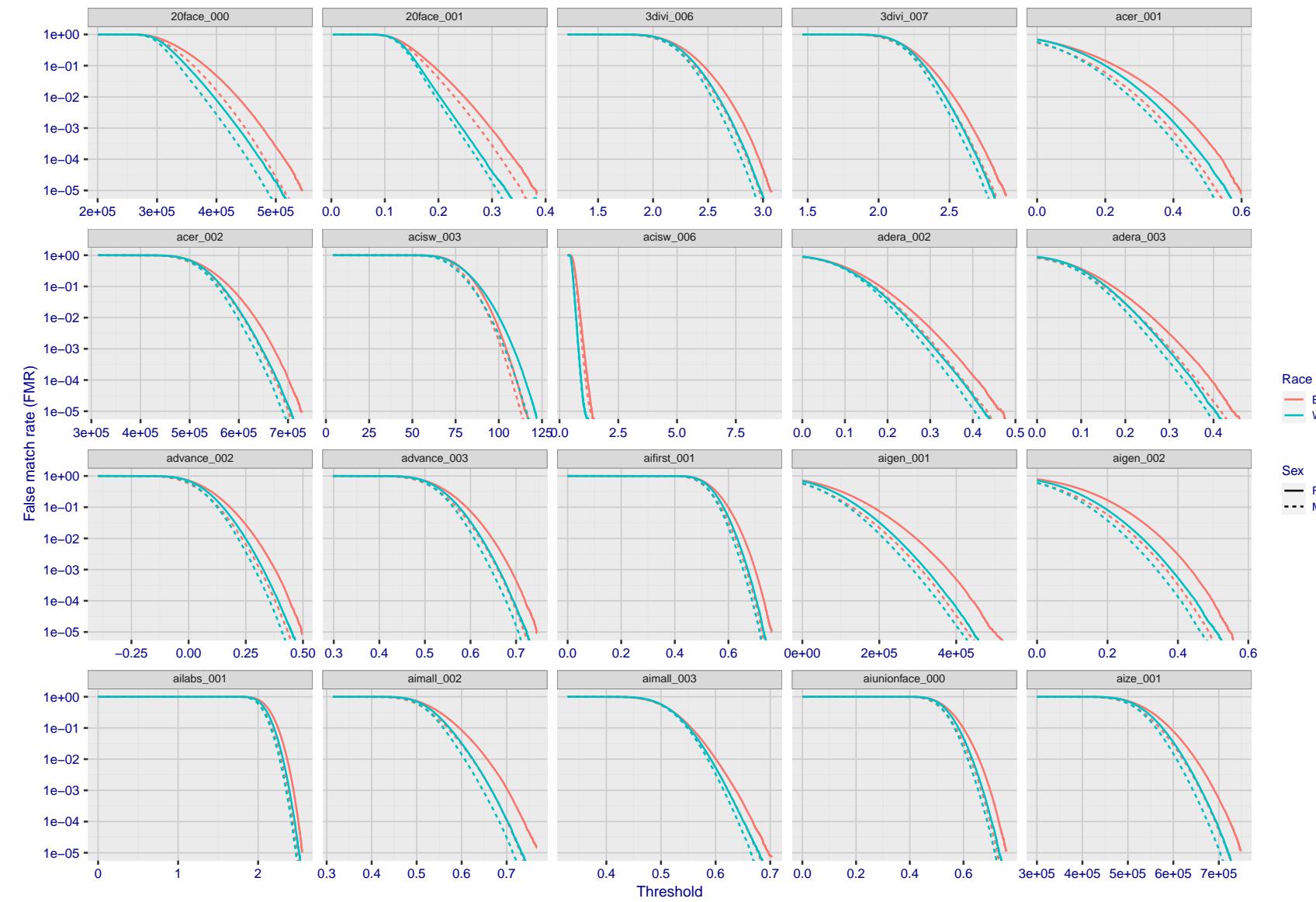


Figure 161: For the mugshot images, the false match calibration curves show false match rate vs. threshold. Separate curves appear for white females, black females, black males and white males.

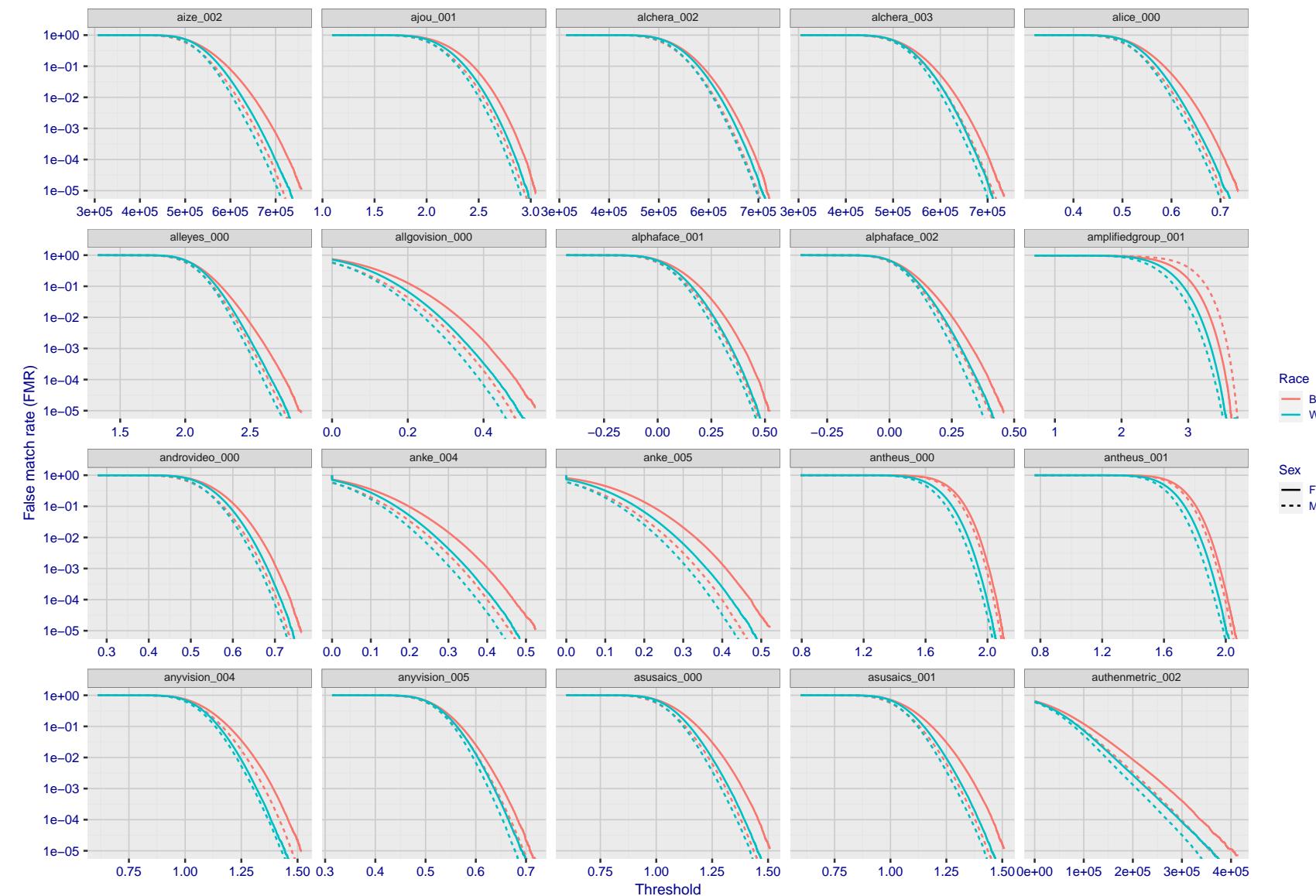


Figure 162: For the mugshot images, the false match calibration curves show false match rate vs. threshold. Separate curves appear for white females, black females, black males and white males.

2021/11/22 14:56:30

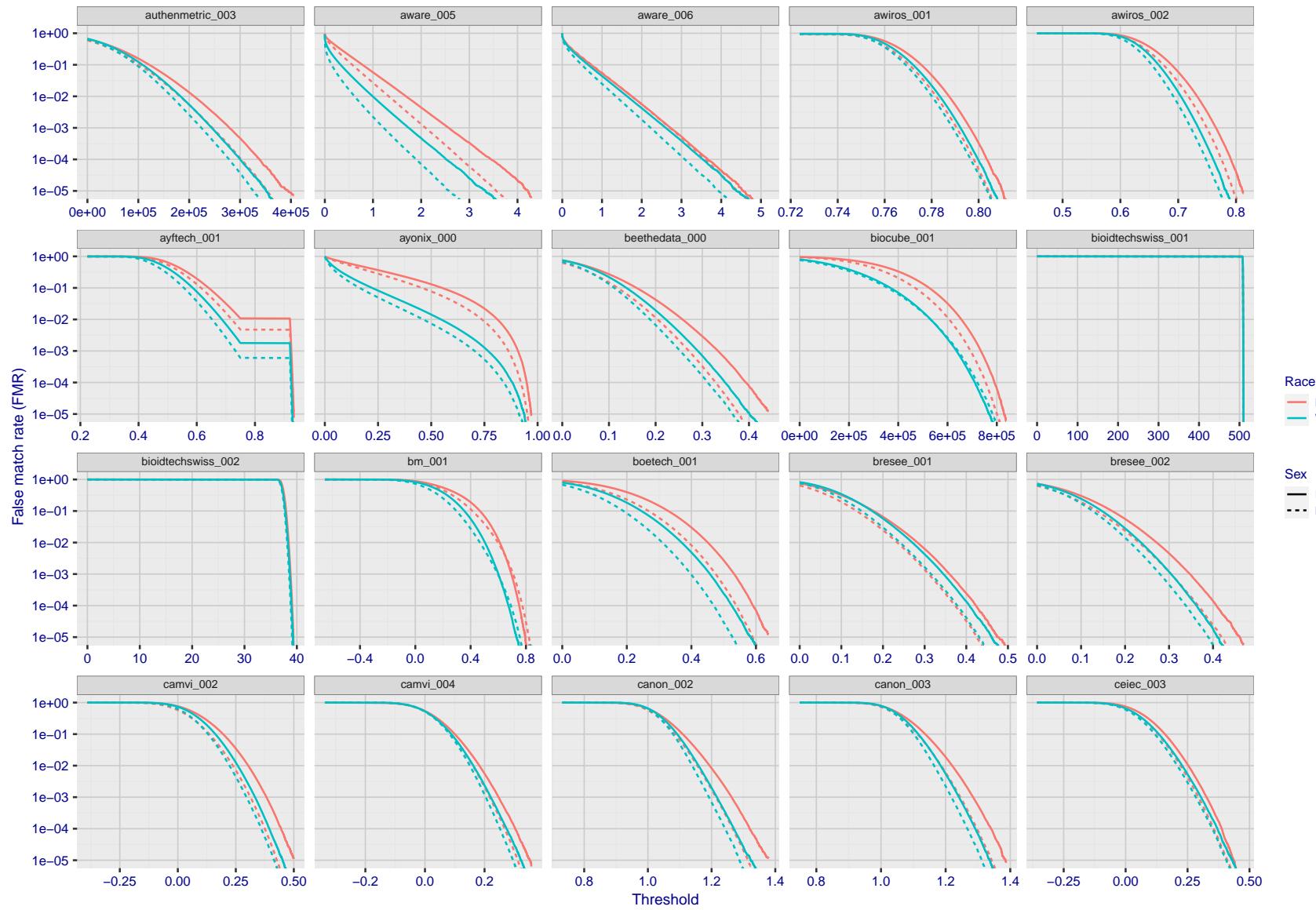


Figure 163: For the mugshot images, the false match calibration curves show false match rate vs. threshold. Separate curves appear for white females, black females, black males and white males.

FNMR(T)
"False non-match rate"
"False match rate"

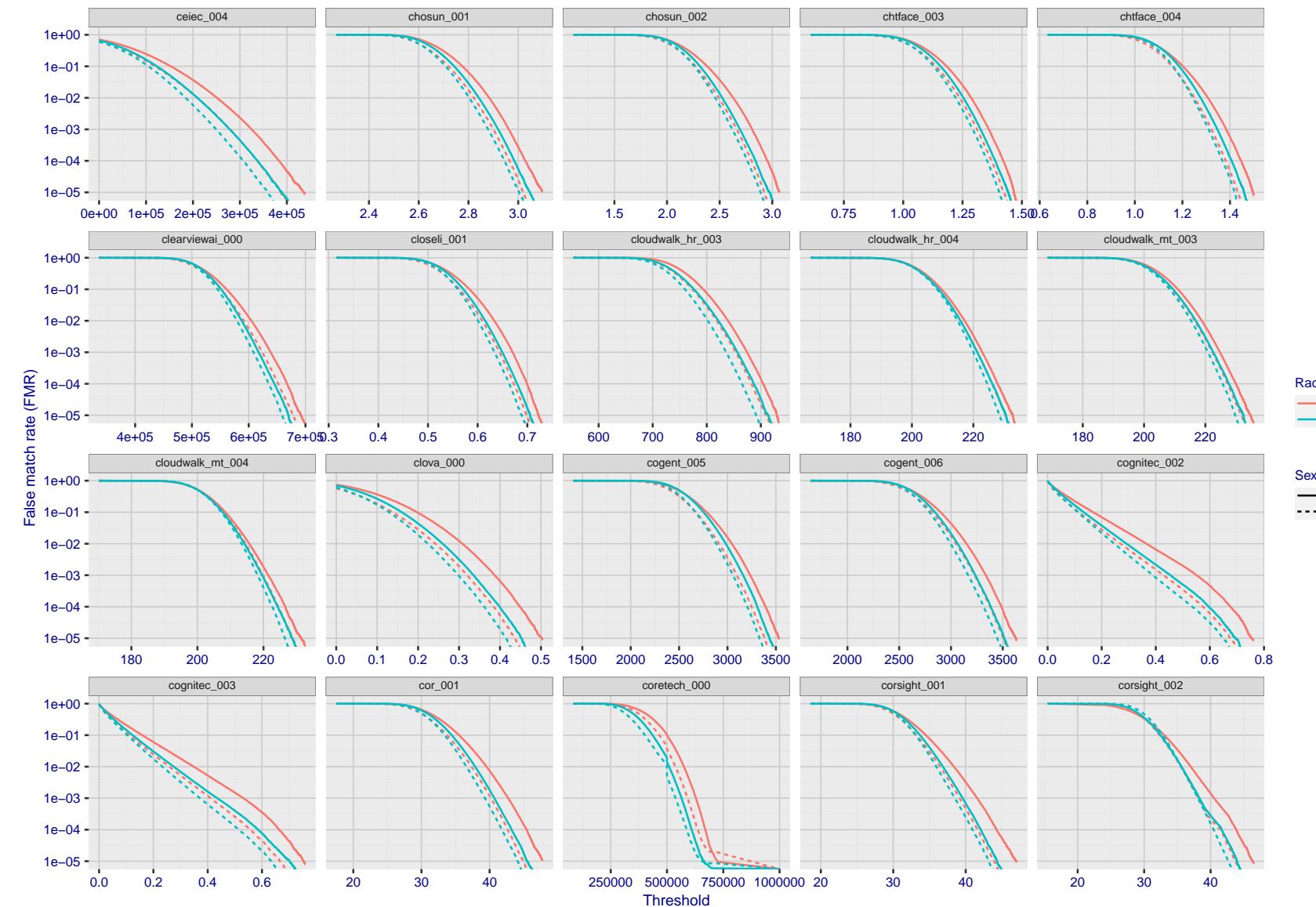


Figure 164: For the mugshot images, the false match calibration curves show false match rate vs. threshold. Separate curves appear for white females, black females, black males and white males.

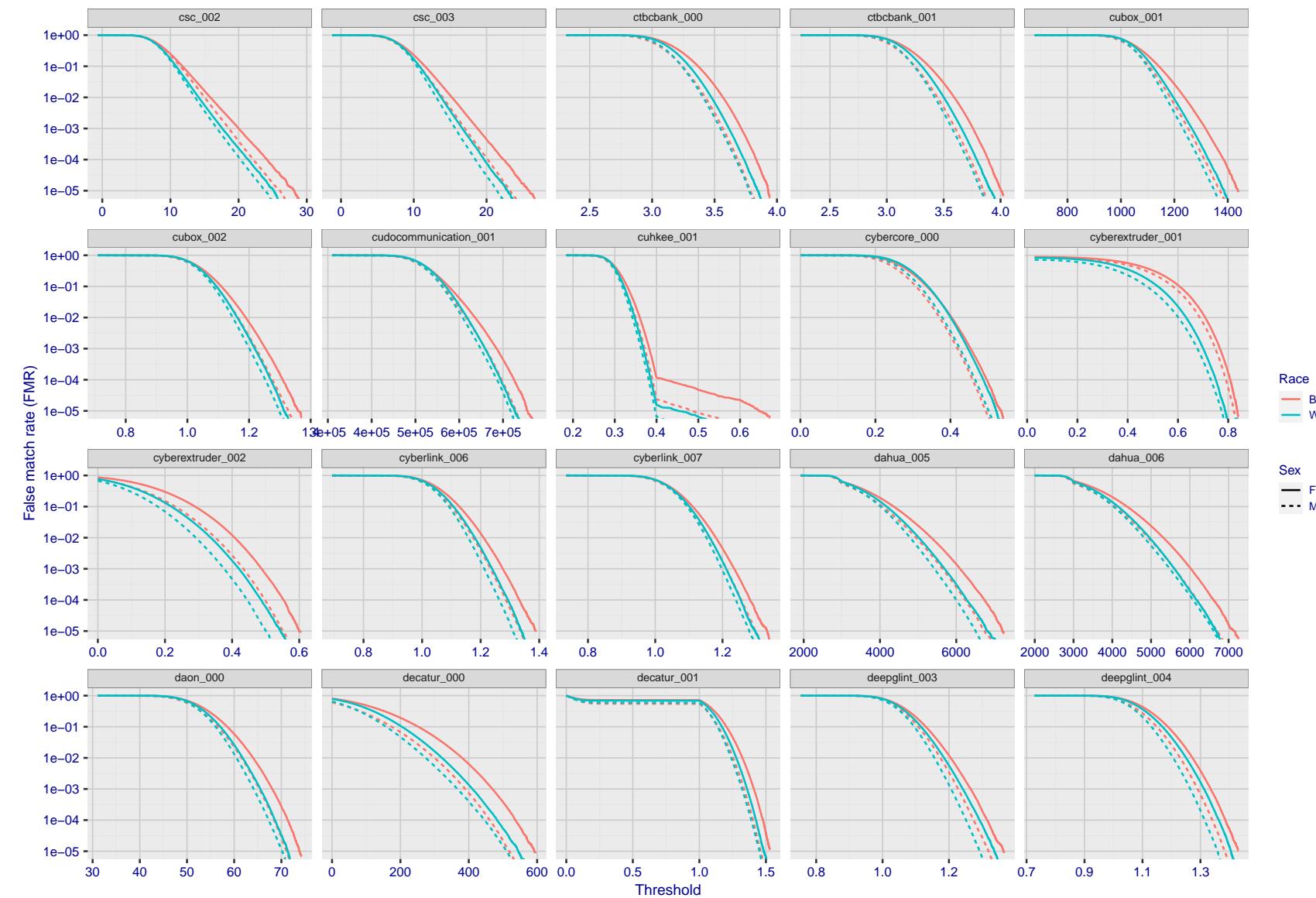


Figure 165: For the mugshot images, the false match calibration curves show false match rate vs. threshold. Separate curves appear for white females, black females, black males and white males.

2021/11/22 14:56:30

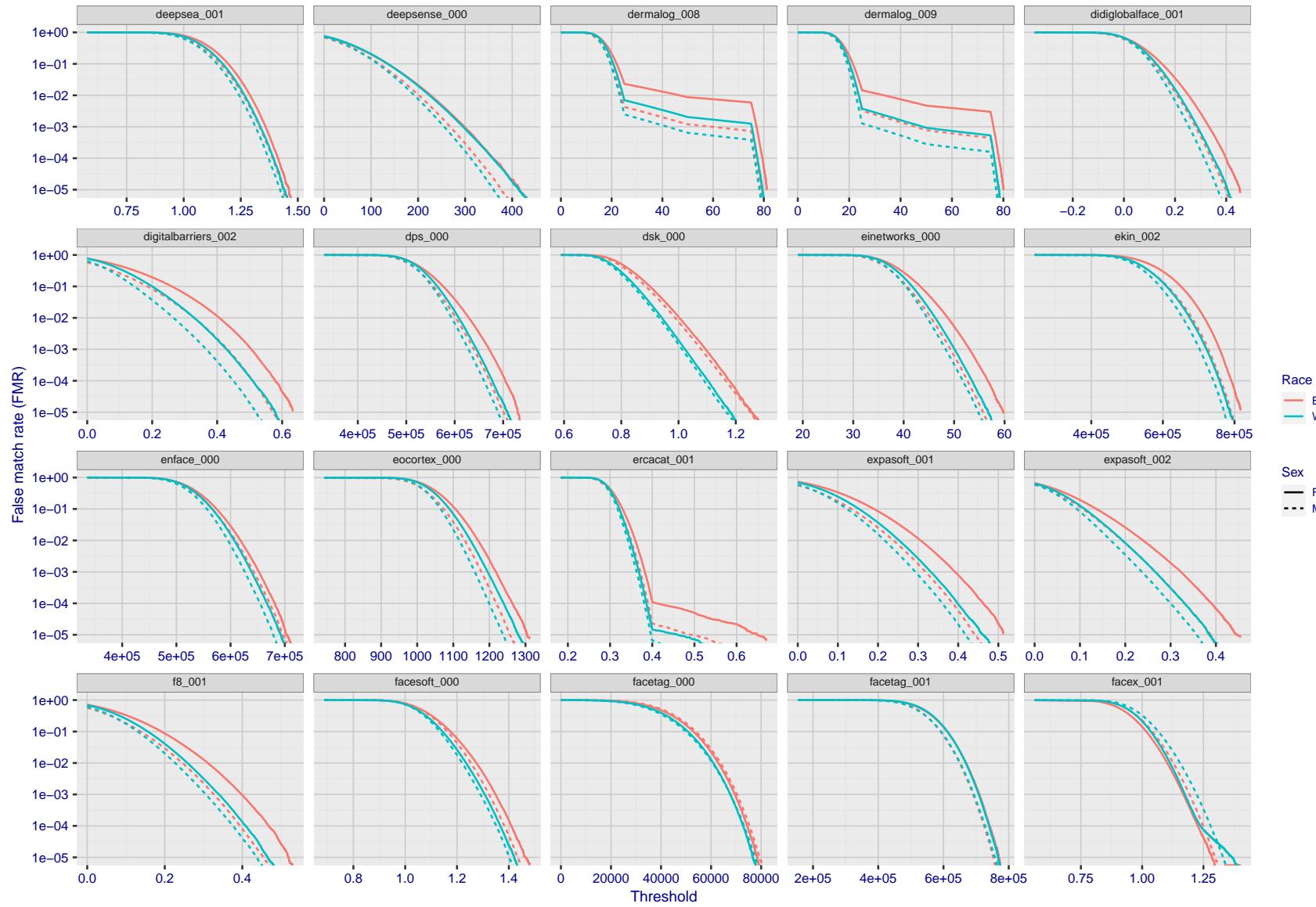


Figure 166: For the mugshot images, the false match calibration curves show false match rate vs. threshold. Separate curves appear for white females, black females, black males and white males.

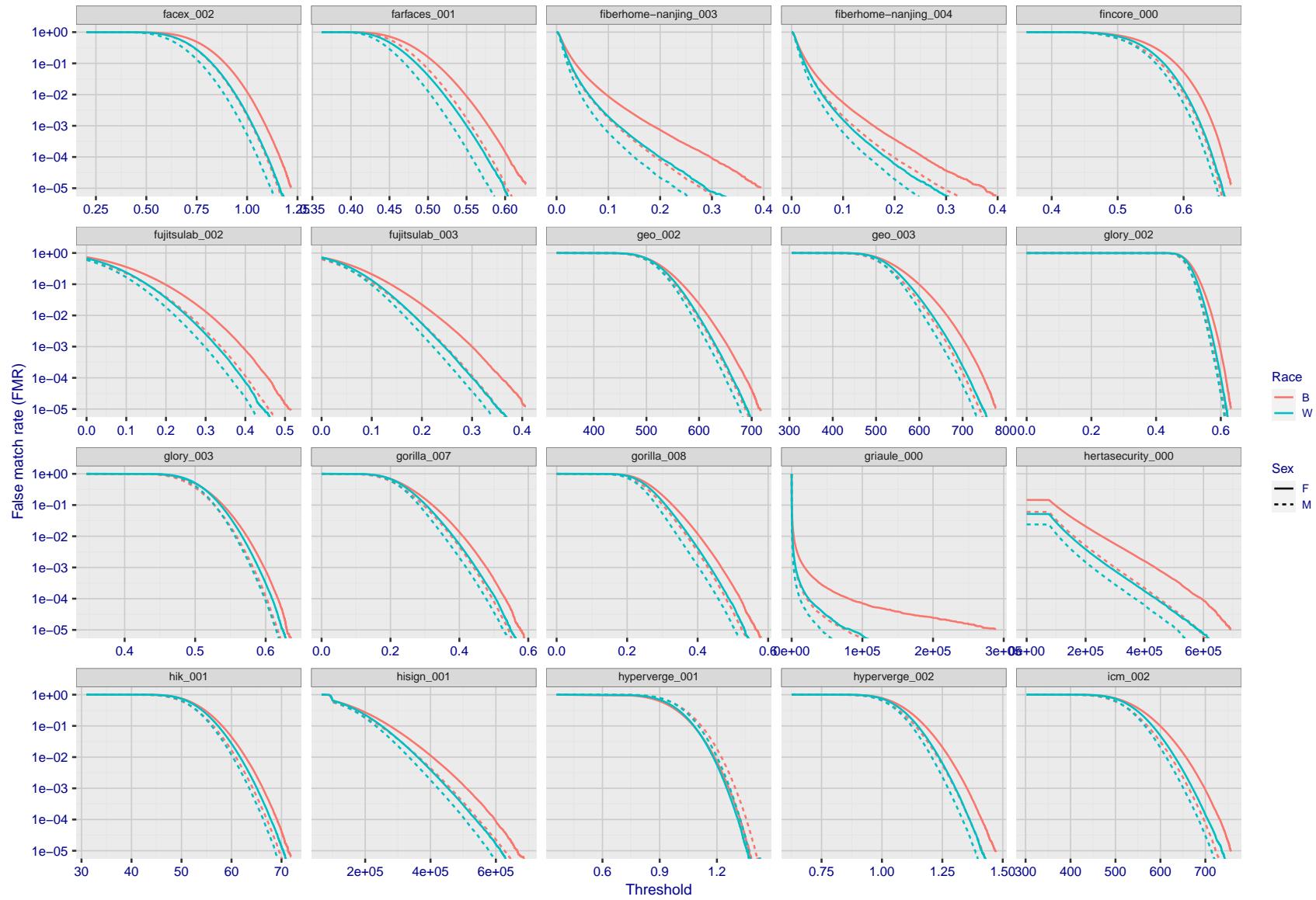


Figure 167: For the mugshot images, the false match calibration curves show false match rate vs. threshold. Separate curves appear for white females, black females, black males and white males.

2021/11/22 14:56:30

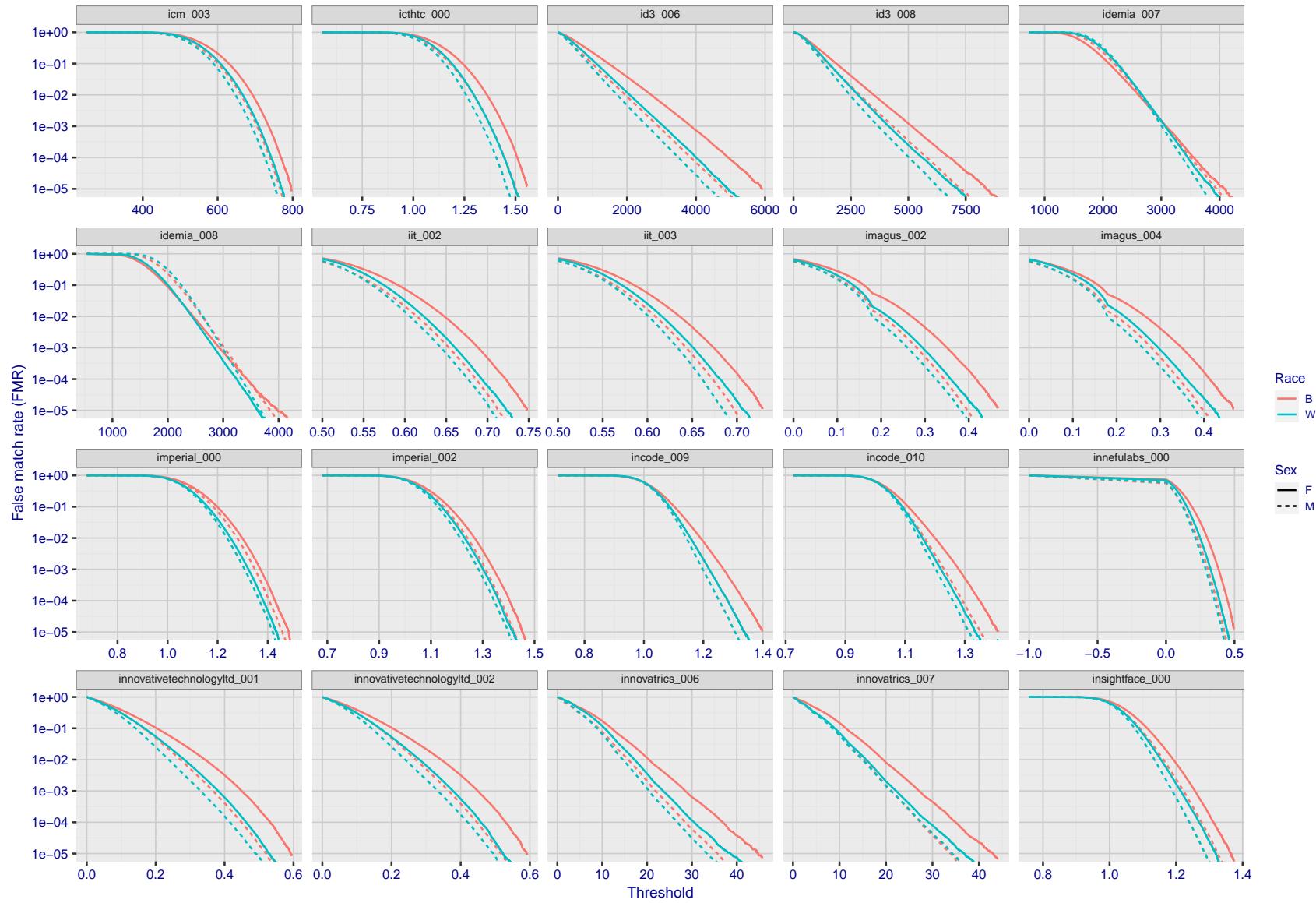


Figure 168: For the mugshot images, the false match calibration curves show false match rate vs. threshold. Separate curves appear for white females, black females, black males and white males.

2021/11/22 14:56:30

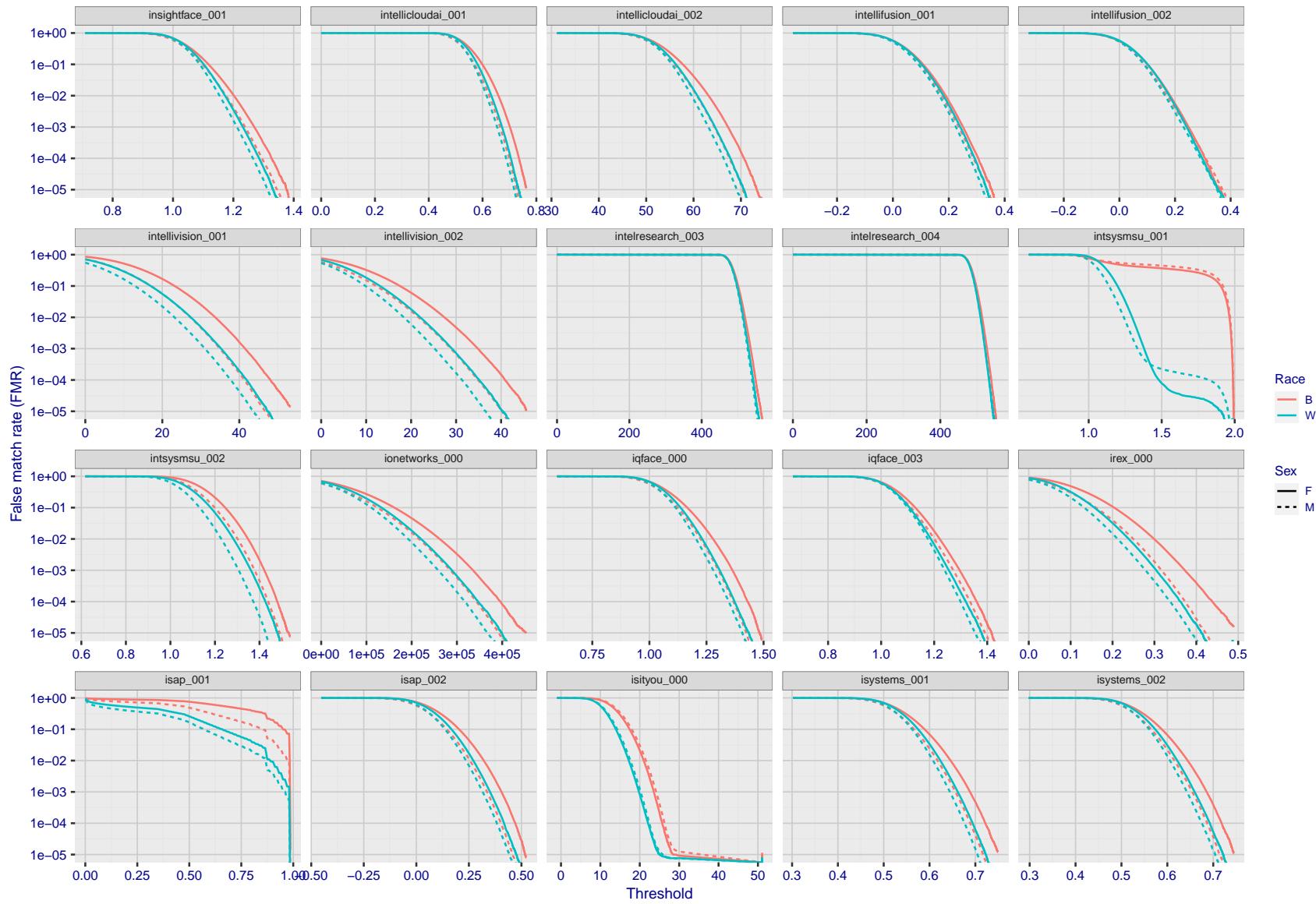


Figure 169: For the mugshot images, the false match calibration curves show false match rate vs. threshold. Separate curves appear for white females, black females, black males and white males.

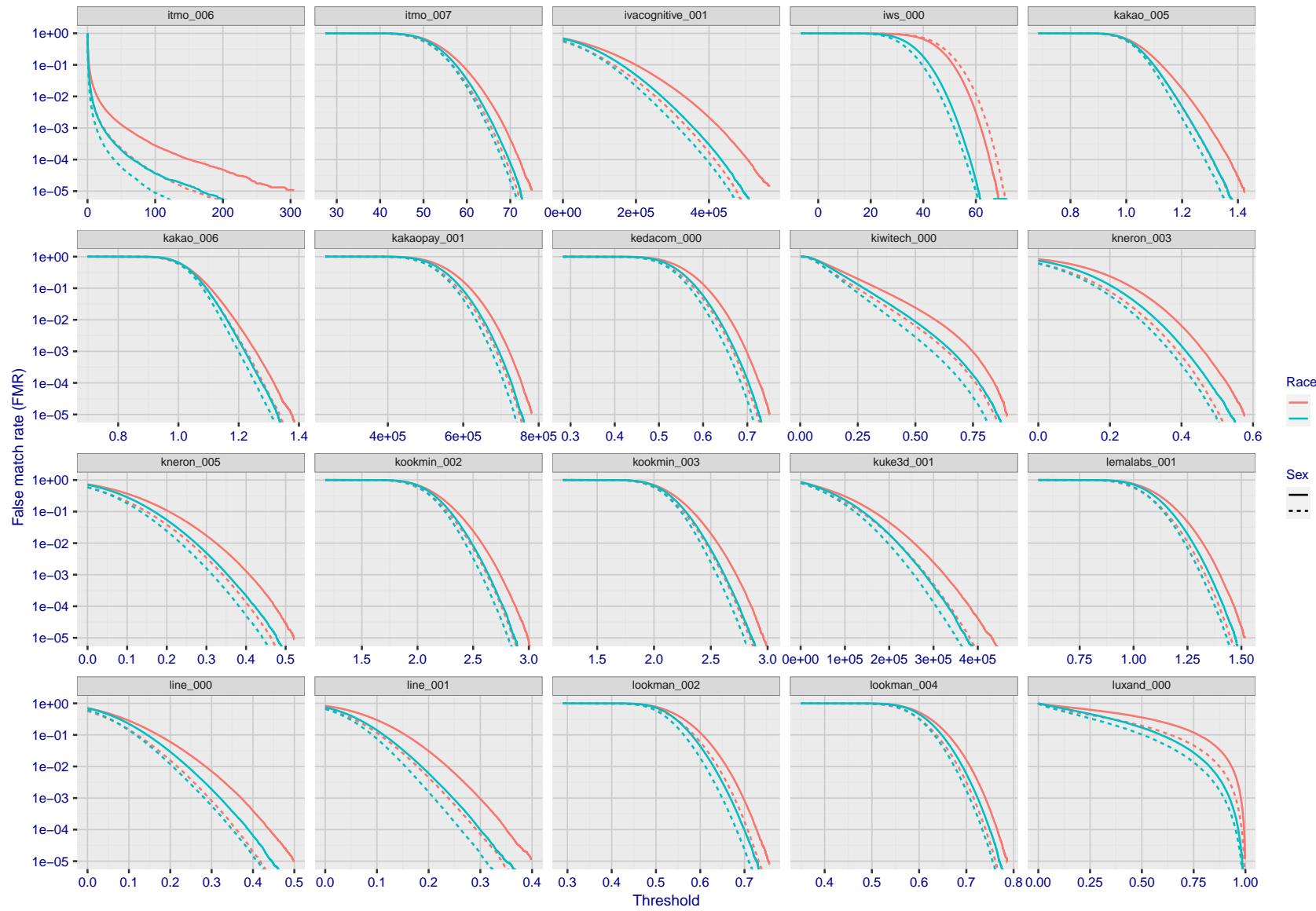


Figure 170: For the mugshot images, the false match calibration curves show false match rate vs. threshold. Separate curves appear for white females, black females, black males and white males.

2021/11/22 14:56:30

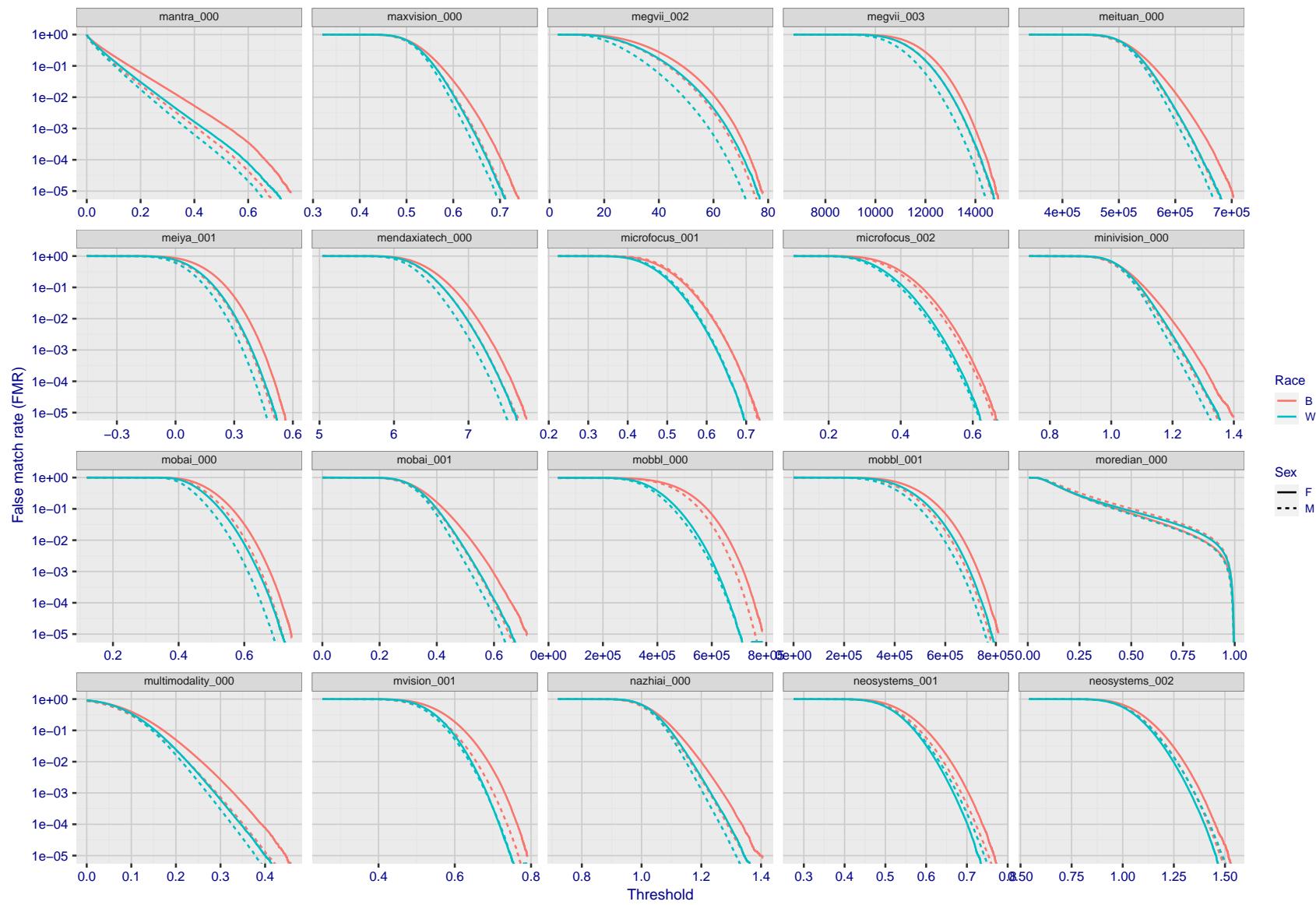


Figure 171: For the mugshot images, the false match calibration curves show false match rate vs. threshold. Separate curves appear for white females, black females, black males and white males.

2021/11/22 14:56:30

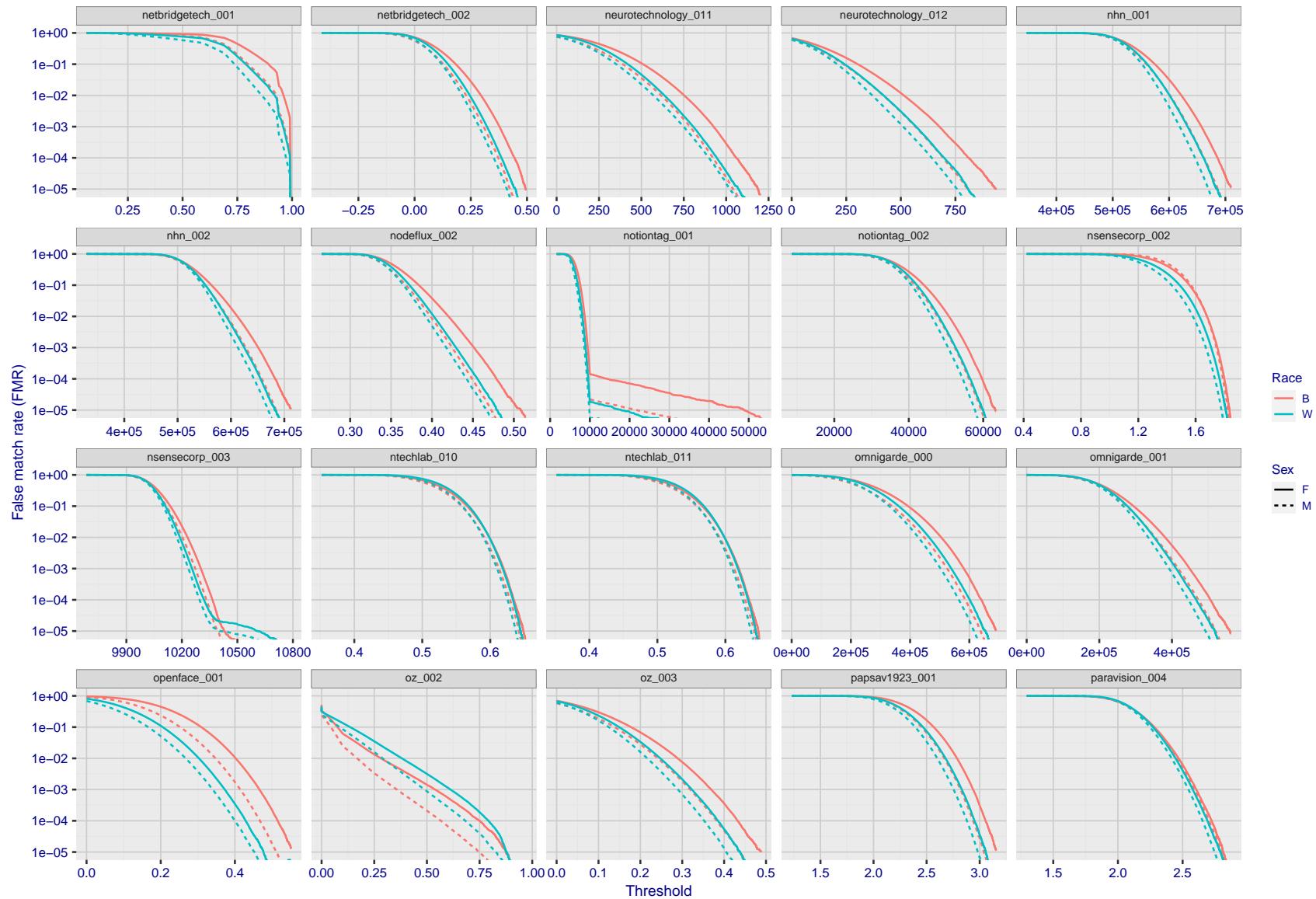


Figure 172: For the mugshot images, the false match calibration curves show false match rate vs. threshold. Separate curves appear for white females, black females, black males and white males.

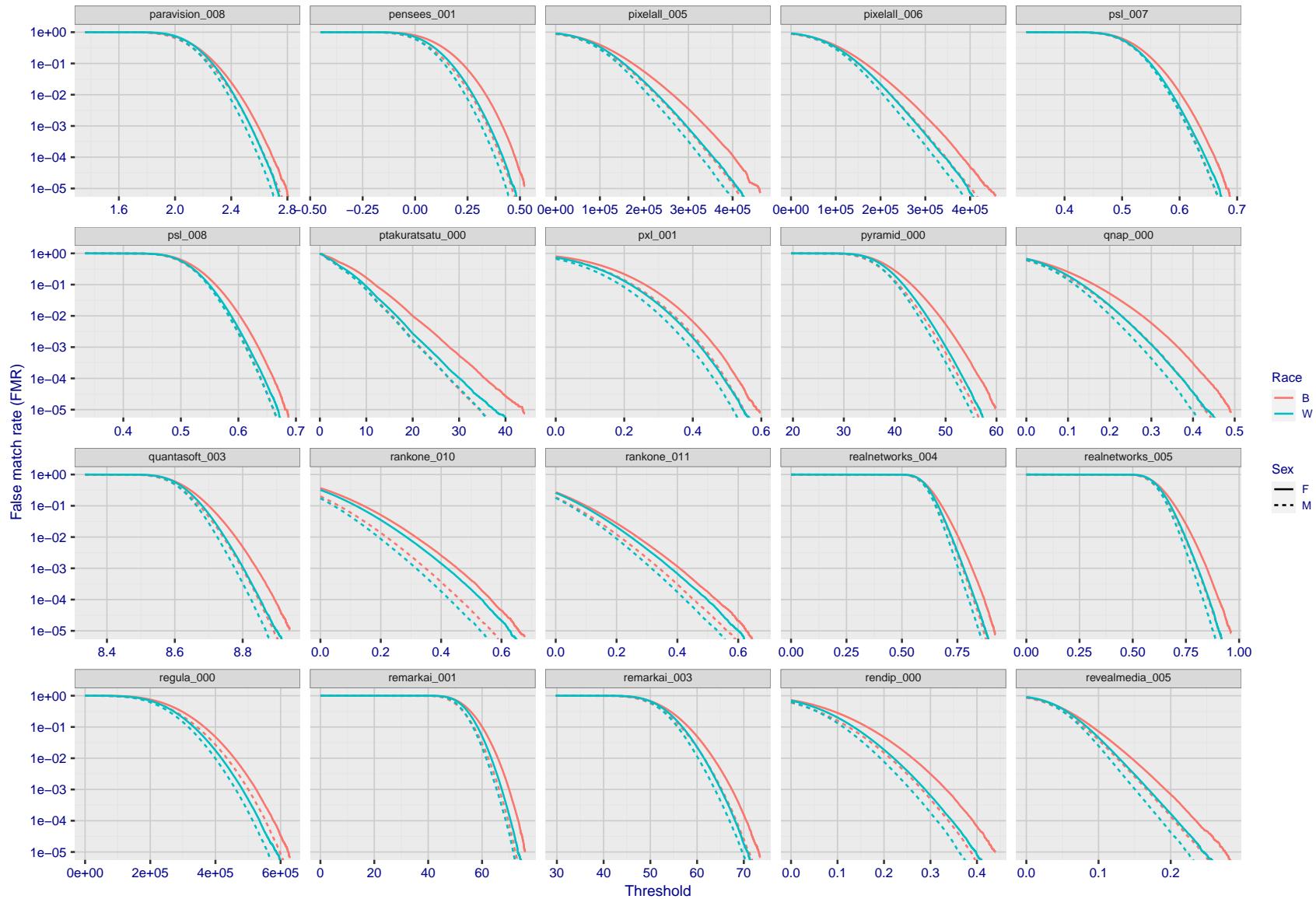


Figure 173: For the mugshot images, the false match calibration curves show false match rate vs. threshold. Separate curves appear for white females, black females, black males and white males.

2021/11/22 14:56:30

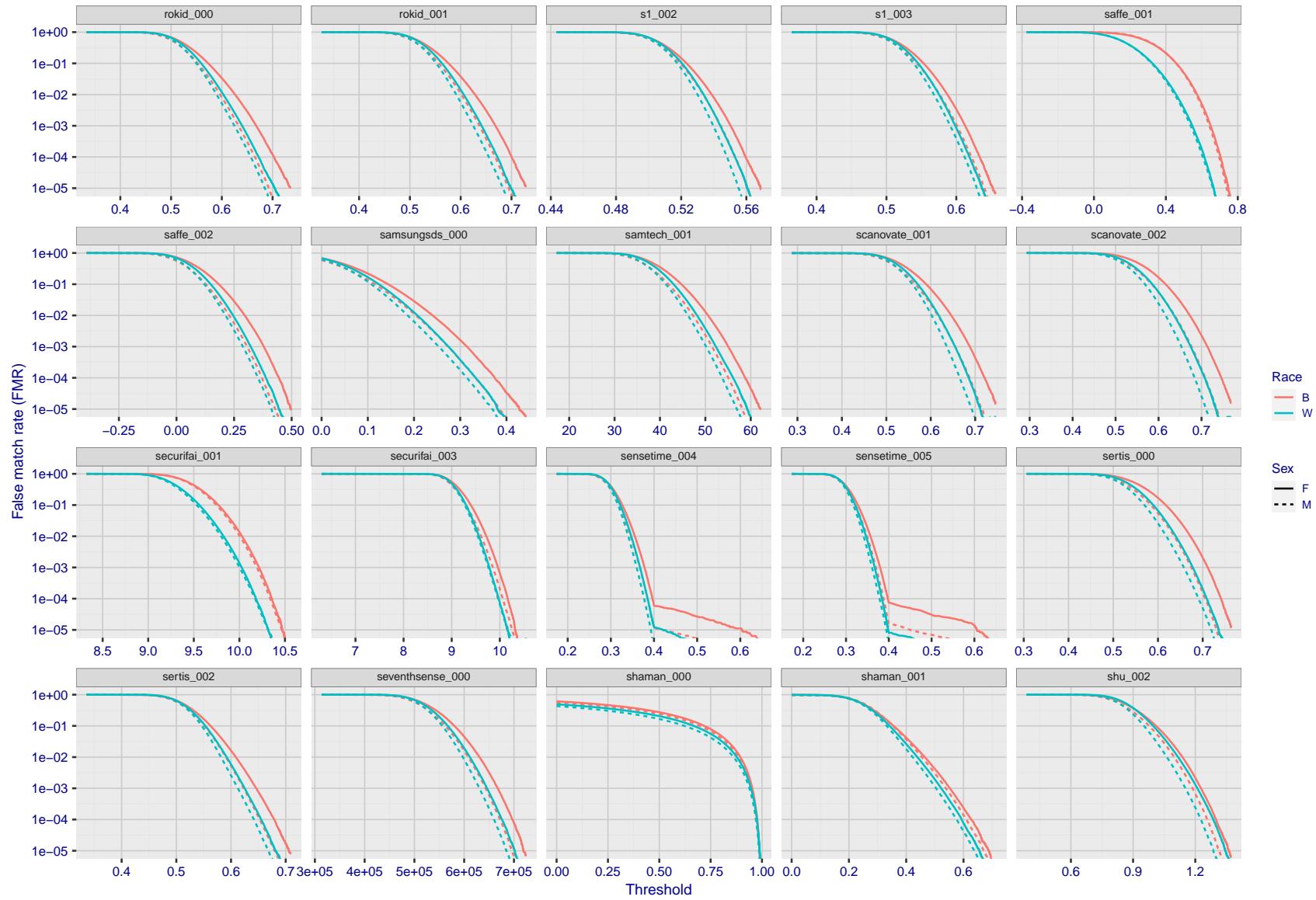


Figure 174: For the mugshot images, the false match calibration curves show false match rate vs. threshold. Separate curves appear for white females, black females, black males and white males.

2021/11/22 14:56:30

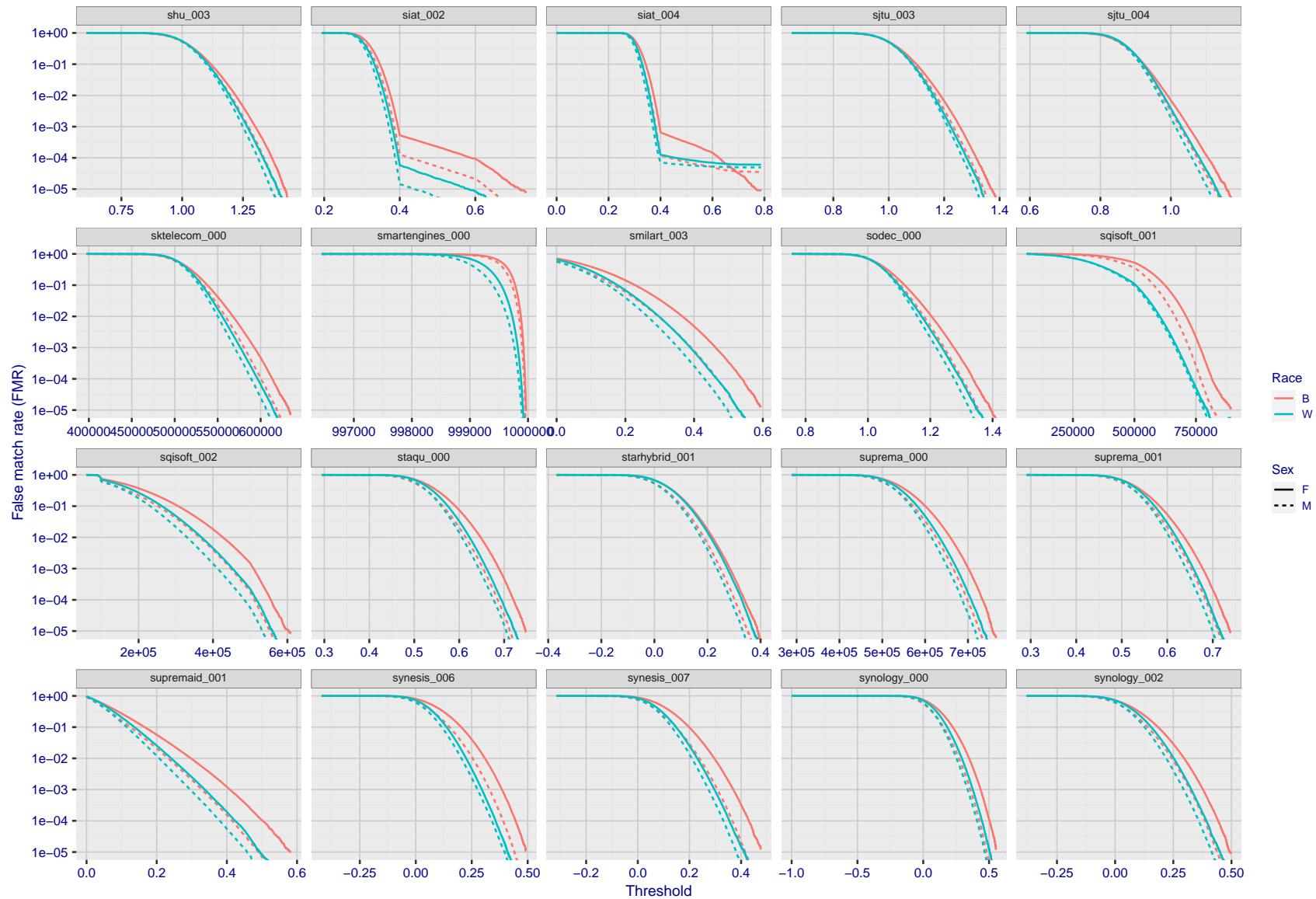


Figure 175: For the mugshot images, the false match calibration curves show false match rate vs. threshold. Separate curves appear for white females, black females, black males and white males.

2021/11/22 14:56:30

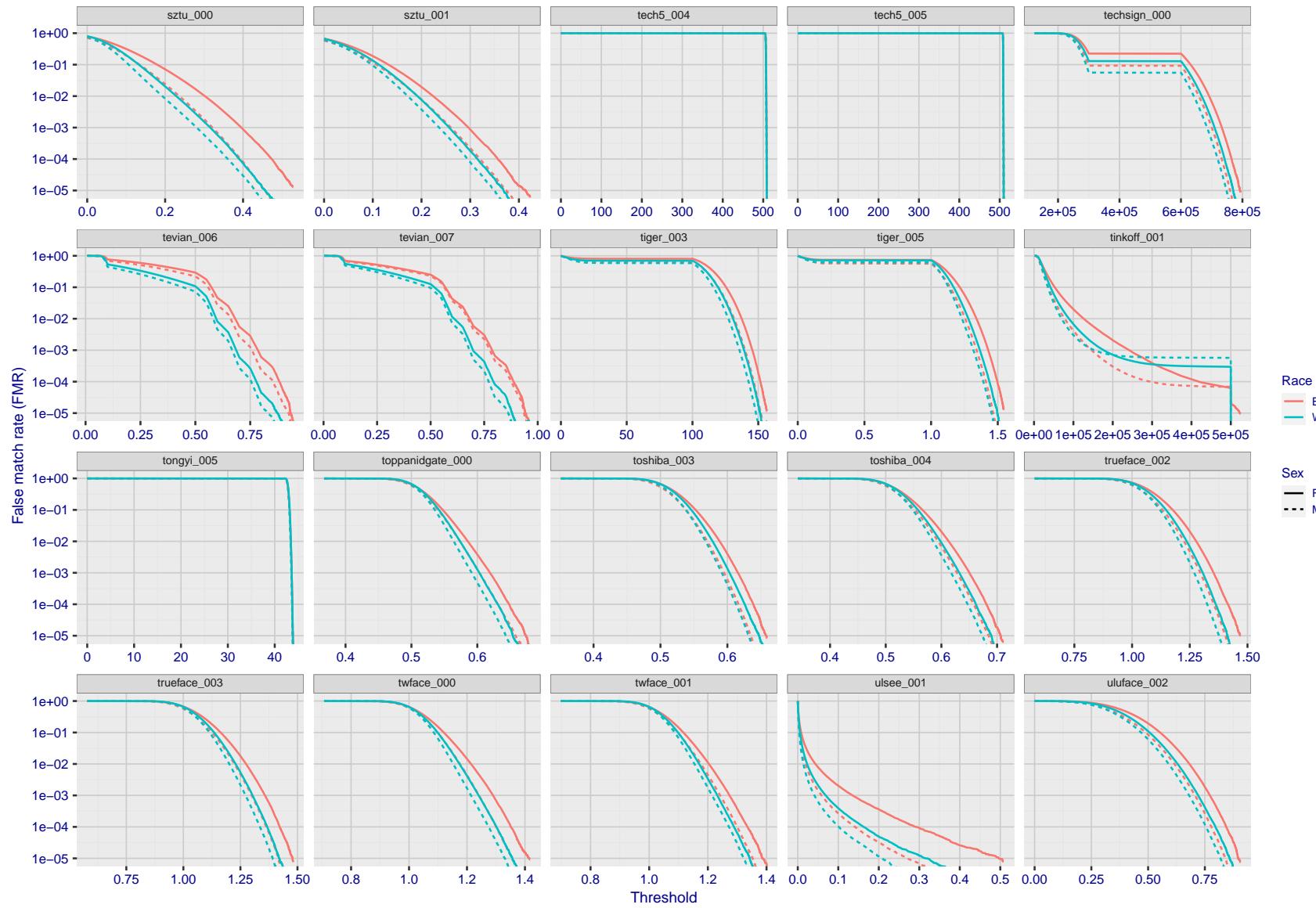


Figure 176: For the mugshot images, the false match calibration curves show false match rate vs. threshold. Separate curves appear for white females, black females, black males and white males.

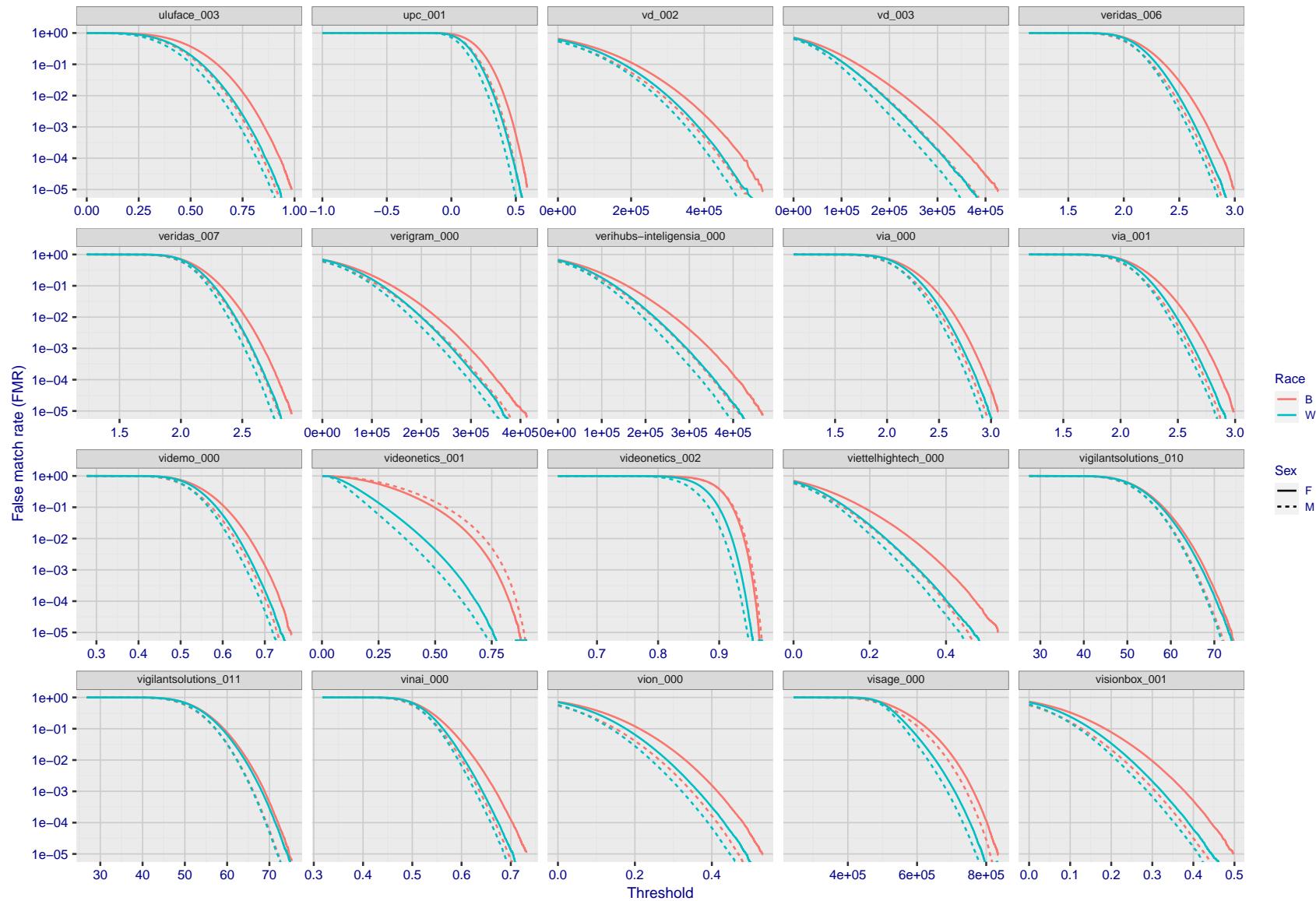


Figure 177: For the mugshot images, the false match calibration curves show false match rate vs. threshold. Separate curves appear for white females, black females, black males and white males.

2021/11/22 14:56:30

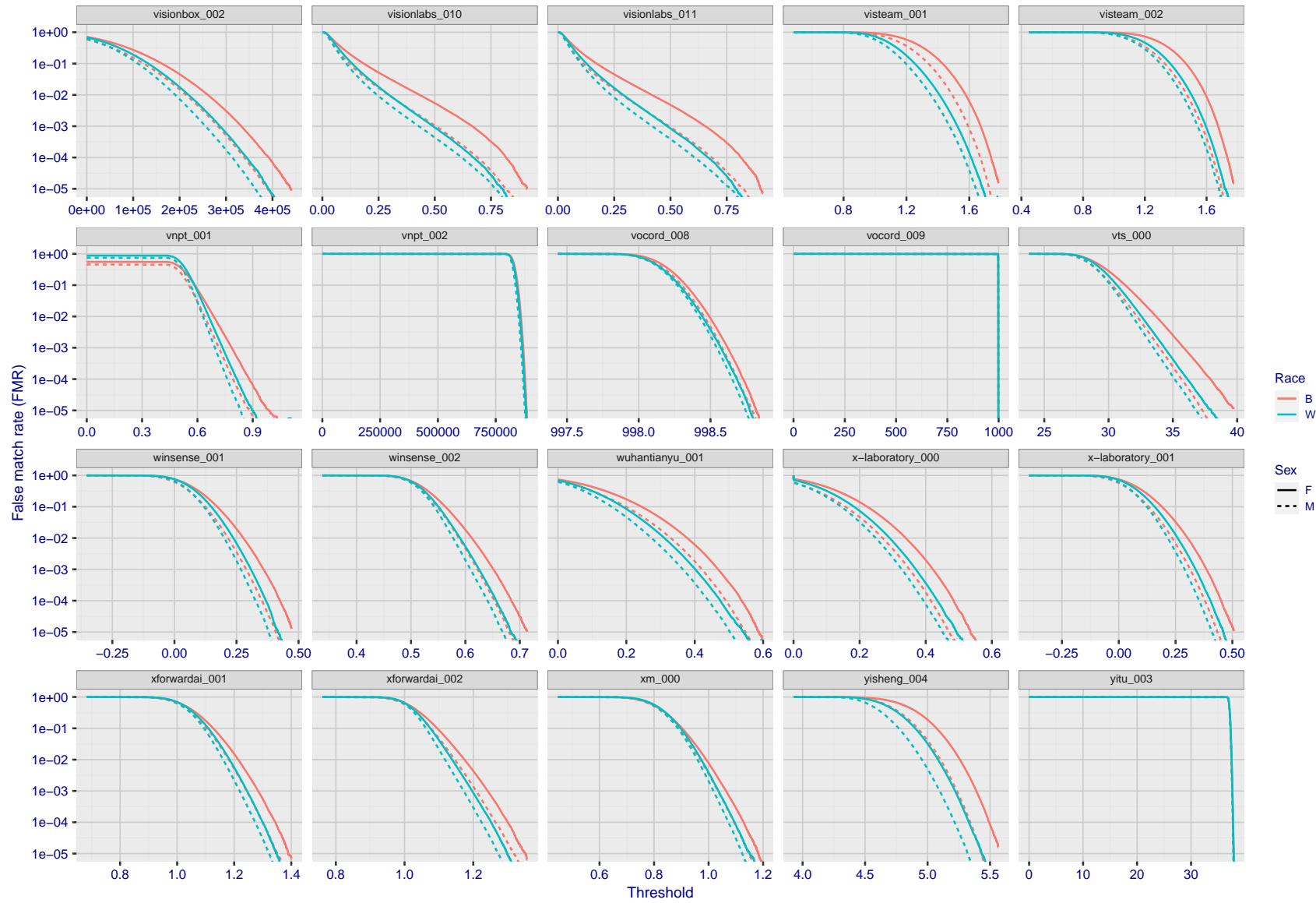


Figure 178: For the mugshot images, the false match calibration curves show false match rate vs. threshold. Separate curves appear for white females, black females, black males and white males.

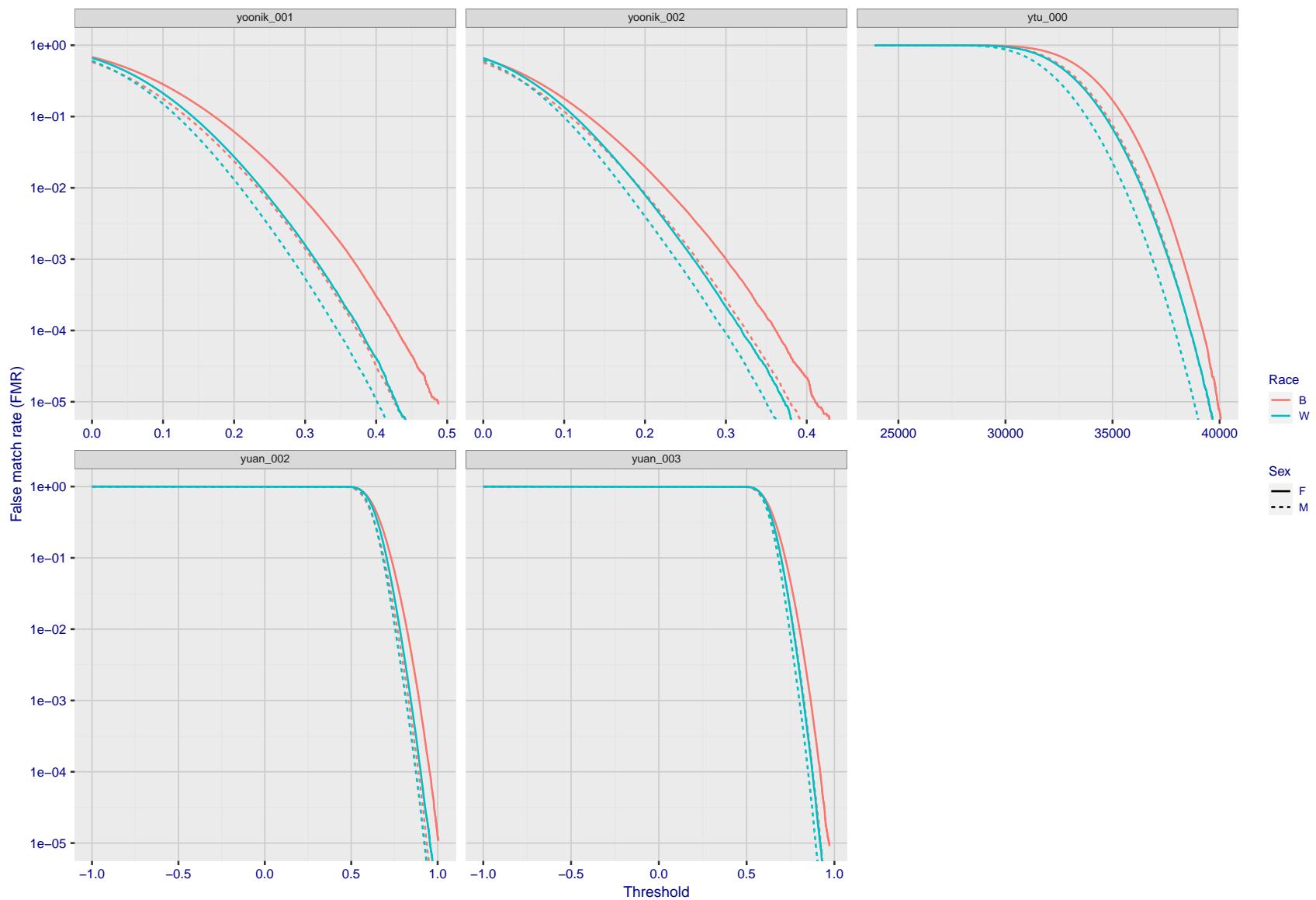


Figure 179: For the mugshot images, the false match calibration curves show false match rate vs. threshold. Separate curves appear for white females, black females, black males and white males.

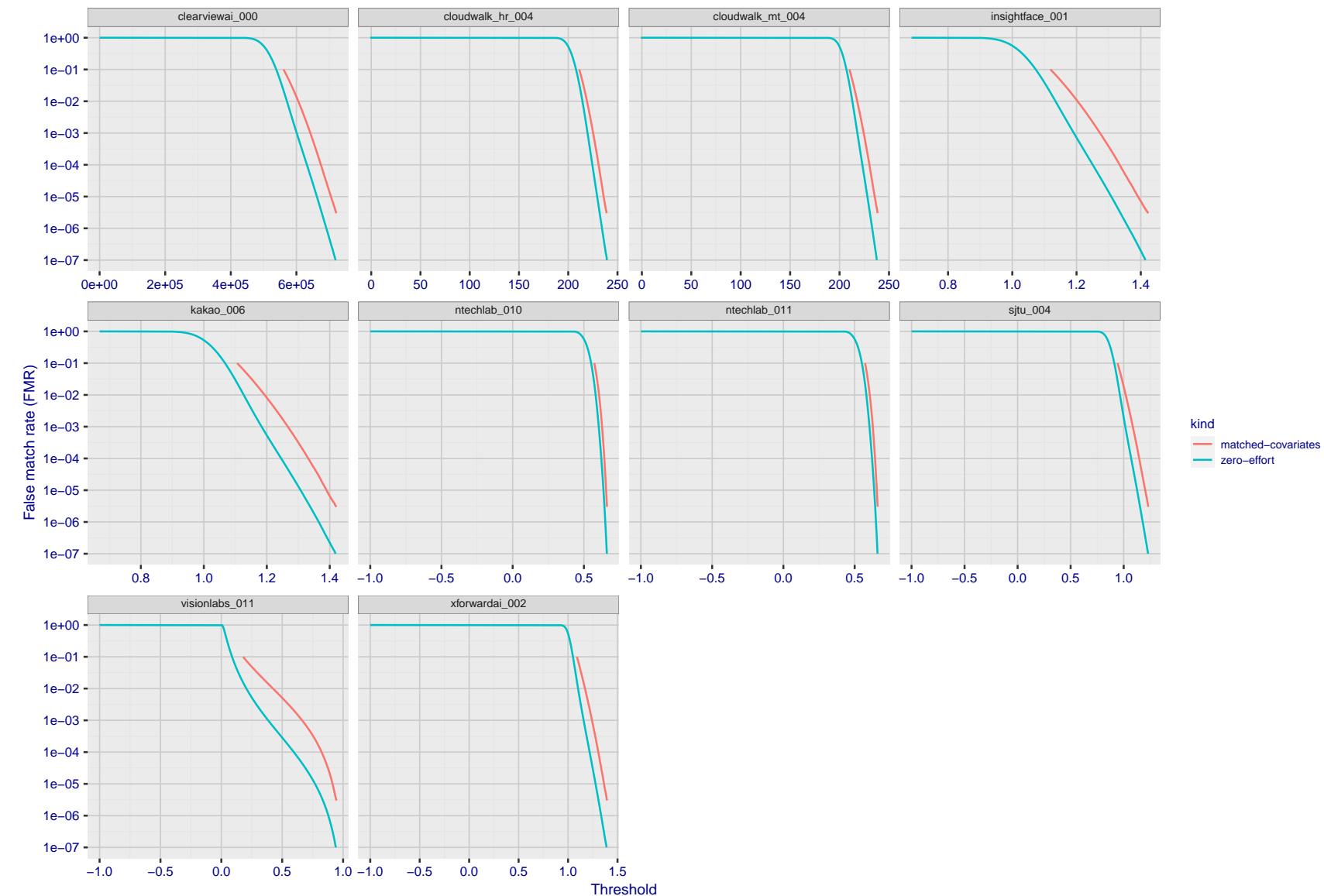


Figure 180: For the visa images, the false match calibration curves show FMR vs. threshold, T . The blue (lower) curves are for zero-effort impostors (i.e. comparing all images against all). The red (upper) curves are for persons of the same-sex, same-age, and same national-origin. This shows that FMR is underestimated (by a factor of 10 or more) by using a zero-effort impostor calculation to calibrate T . As shown later (sec. 3.6), FMR is higher for demographic-matched impostors.

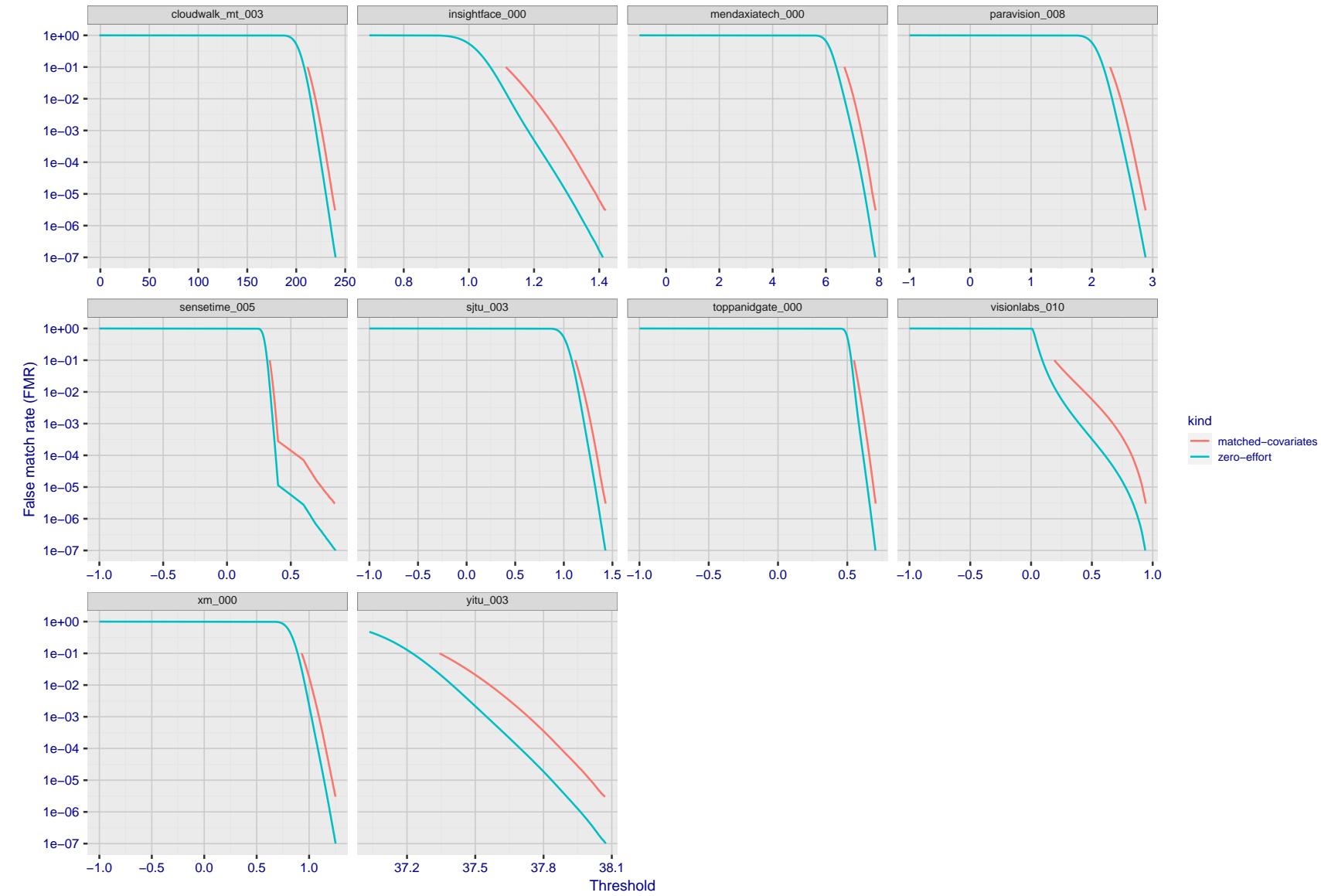


Figure 181: For the visa images, the false match calibration curves show FMR vs. threshold, T . The blue (lower) curves are for zero-effort impostors (i.e. comparing all images against all). The red (upper) curves are for persons of the same-sex, same-age, and same national-origin. This shows that FMR is underestimated (by a factor of 10 or more) by using a zero-effort impostor calculation to calibrate T . As shown later (sec. 3.6), FMR is higher for demographic-matched impostors.

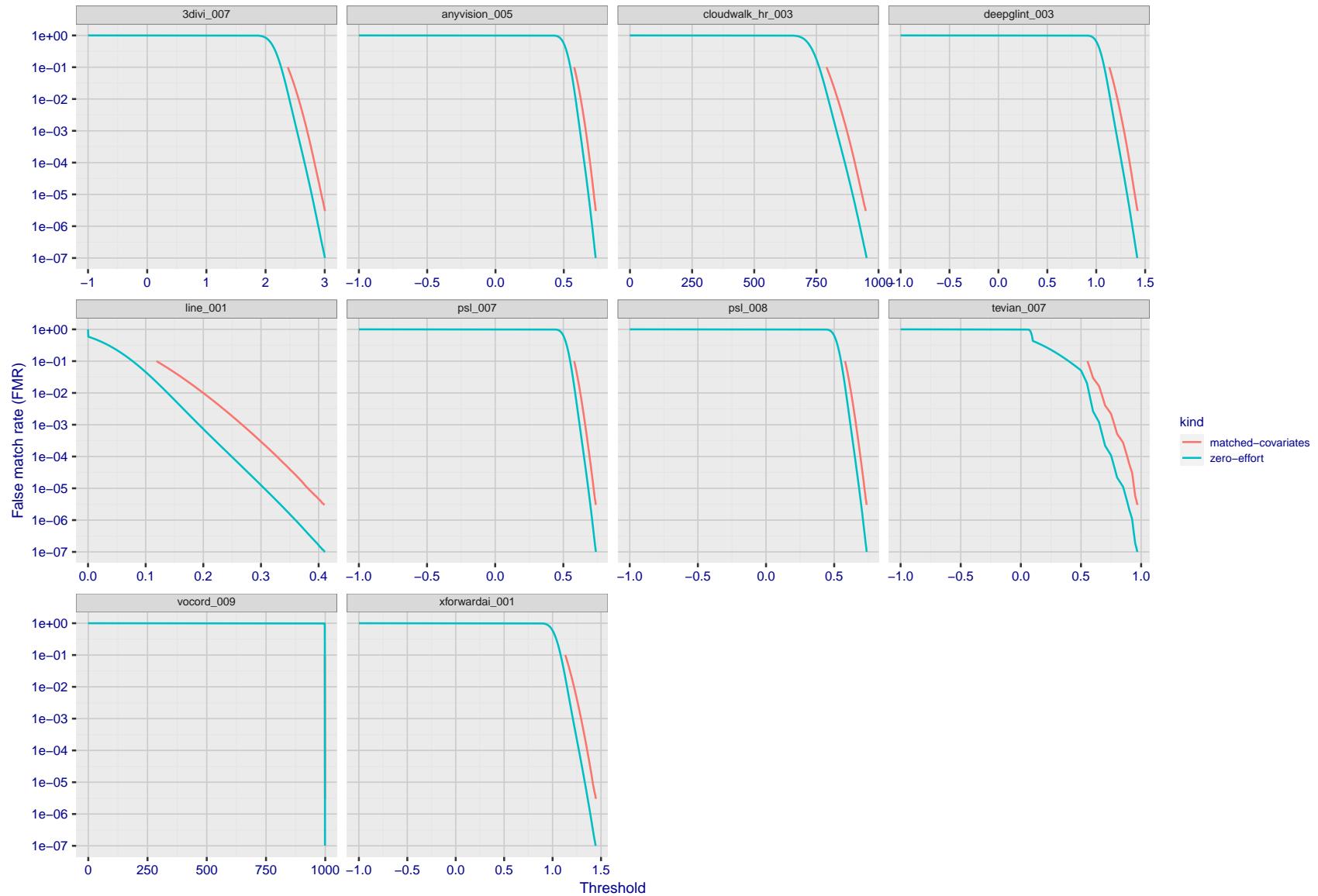


Figure 182: For the visa images, the false match calibration curves show FMR vs. threshold, T . The blue (lower) curves are for zero-effort impostors (i.e. comparing all images against all). The red (upper) curves are for persons of the same-sex, same-age, and same national-origin. This shows that FMR is underestimated (by a factor of 10 or more) by using a zero-effort impostor calculation to calibrate T . As shown later (sec. 3.6), FMR is higher for demographic-matched impostors.

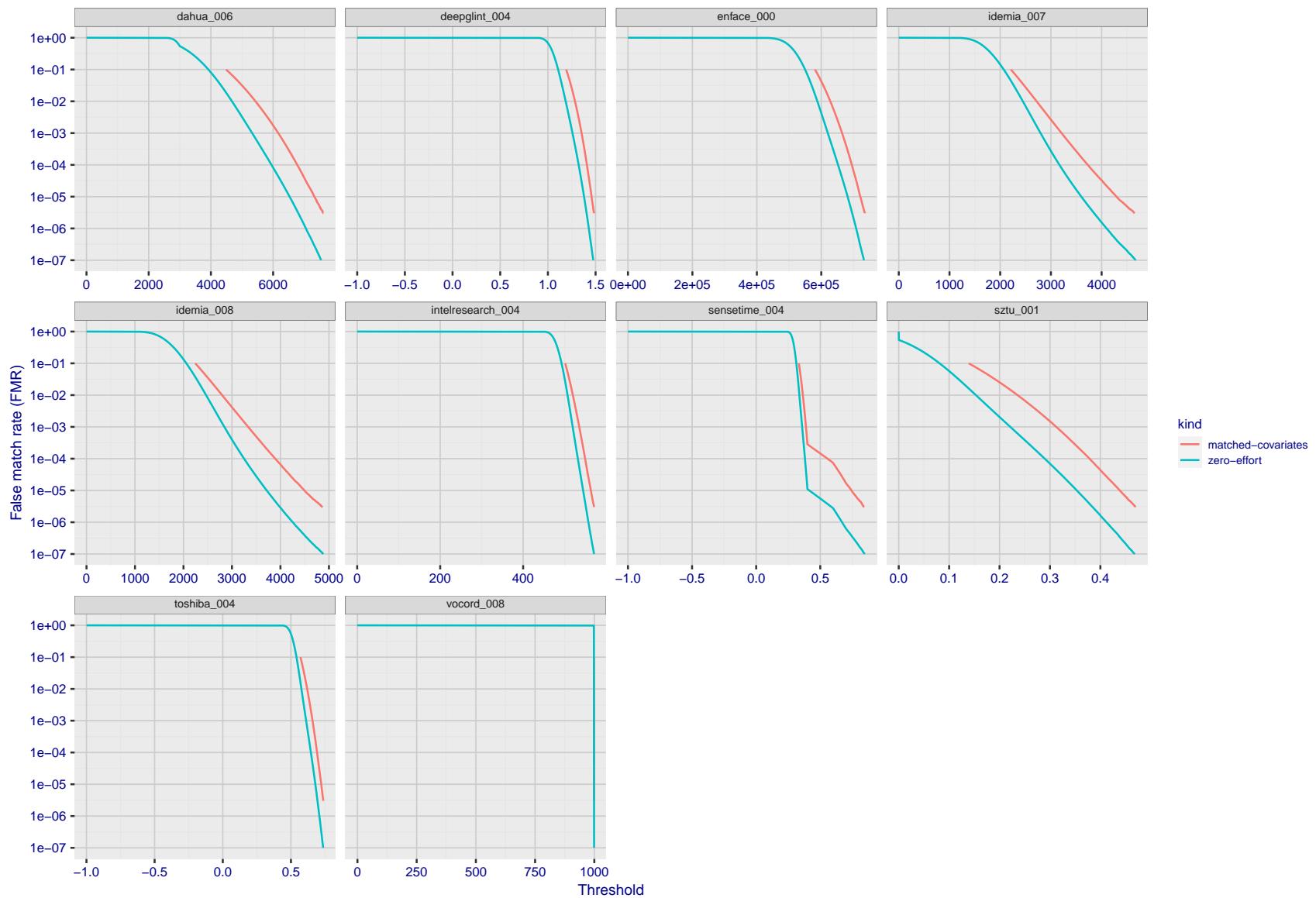


Figure 183: For the visa images, the false match calibration curves show FMR vs. threshold, T . The blue (lower) curves are for zero-effort impostors (i.e. comparing all images against all). The red (upper) curves are for persons of the same-sex, same-age, and same national-origin. This shows that FMR is underestimated (by a factor of 10 or more) by using a zero-effort impostor calculation to calibrate T . As shown later (sec. 3.6), FMR is higher for demographic-matched impostors.

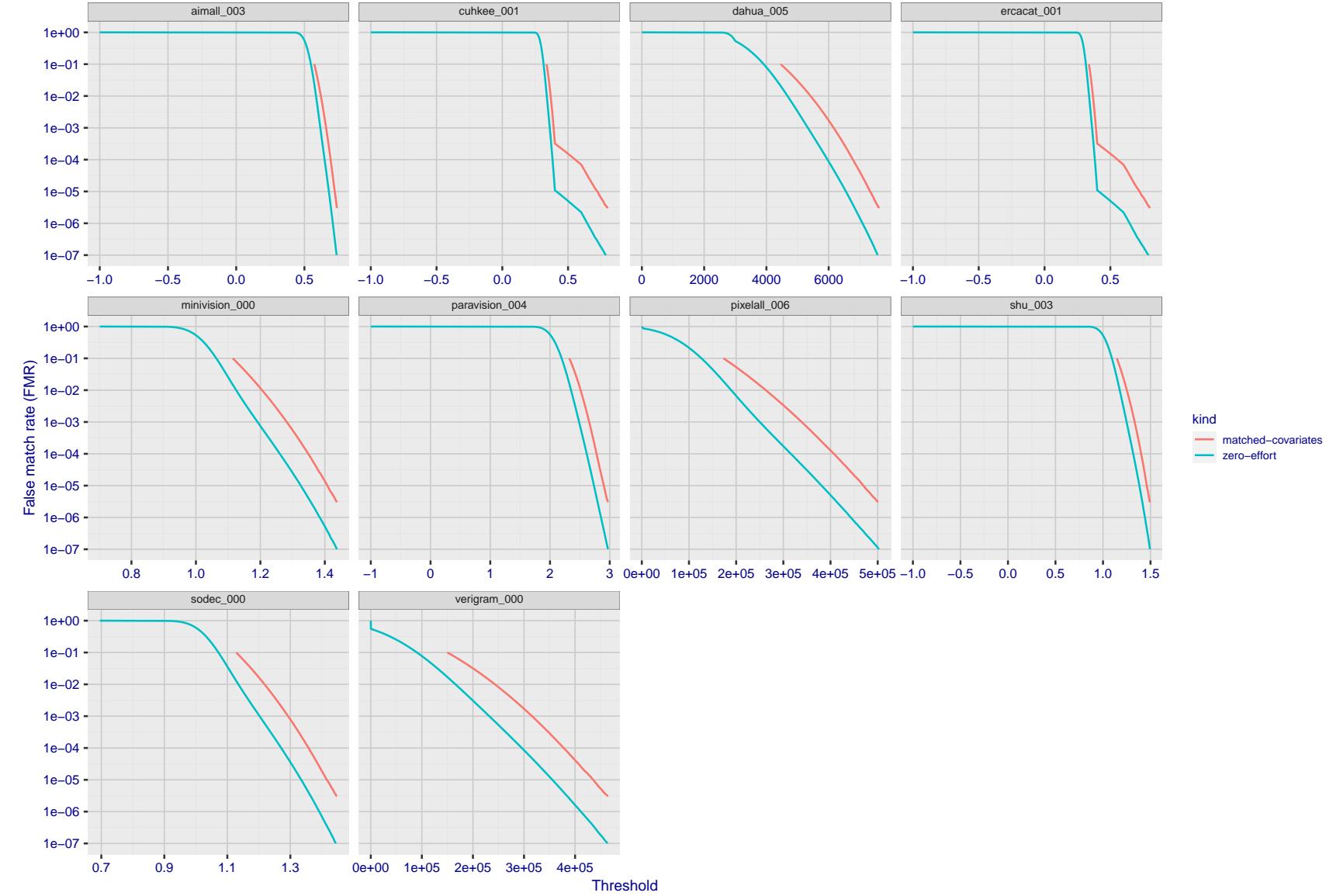


Figure 184: For the visa images, the false match calibration curves show FMR vs. threshold, T . The blue (lower) curves are for zero-effort impostors (i.e. comparing all images against all). The red (upper) curves are for persons of the same-sex, same-age, and same national-origin. This shows that FMR is underestimated (by a factor of 10 or more) by using a zero-effort impostor calculation to calibrate T . As shown later (sec. 3.6), FMR is higher for demographic-matched impostors.

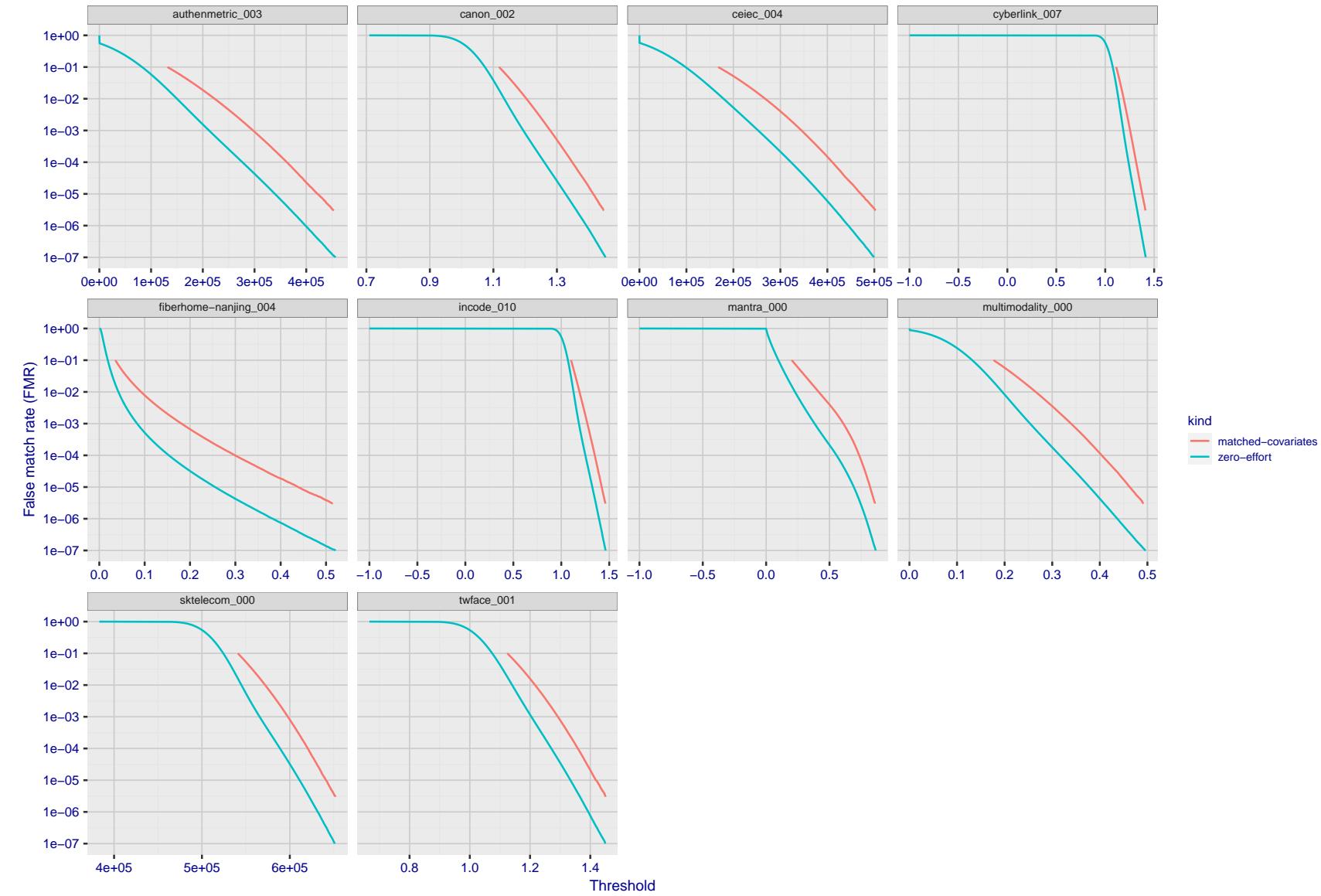


Figure 185: For the visa images, the false match calibration curves show FMR vs. threshold, T . The blue (lower) curves are for zero-effort impostors (i.e. comparing all images against all). The red (upper) curves are for persons of the same-sex, same-age, and same national-origin. This shows that FMR is underestimated (by a factor of 10 or more) by using a zero-effort impostor calculation to calibrate T . As shown later (sec. 3.6), FMR is higher for demographic-matched impostors.

2021/11/22 14:56:30

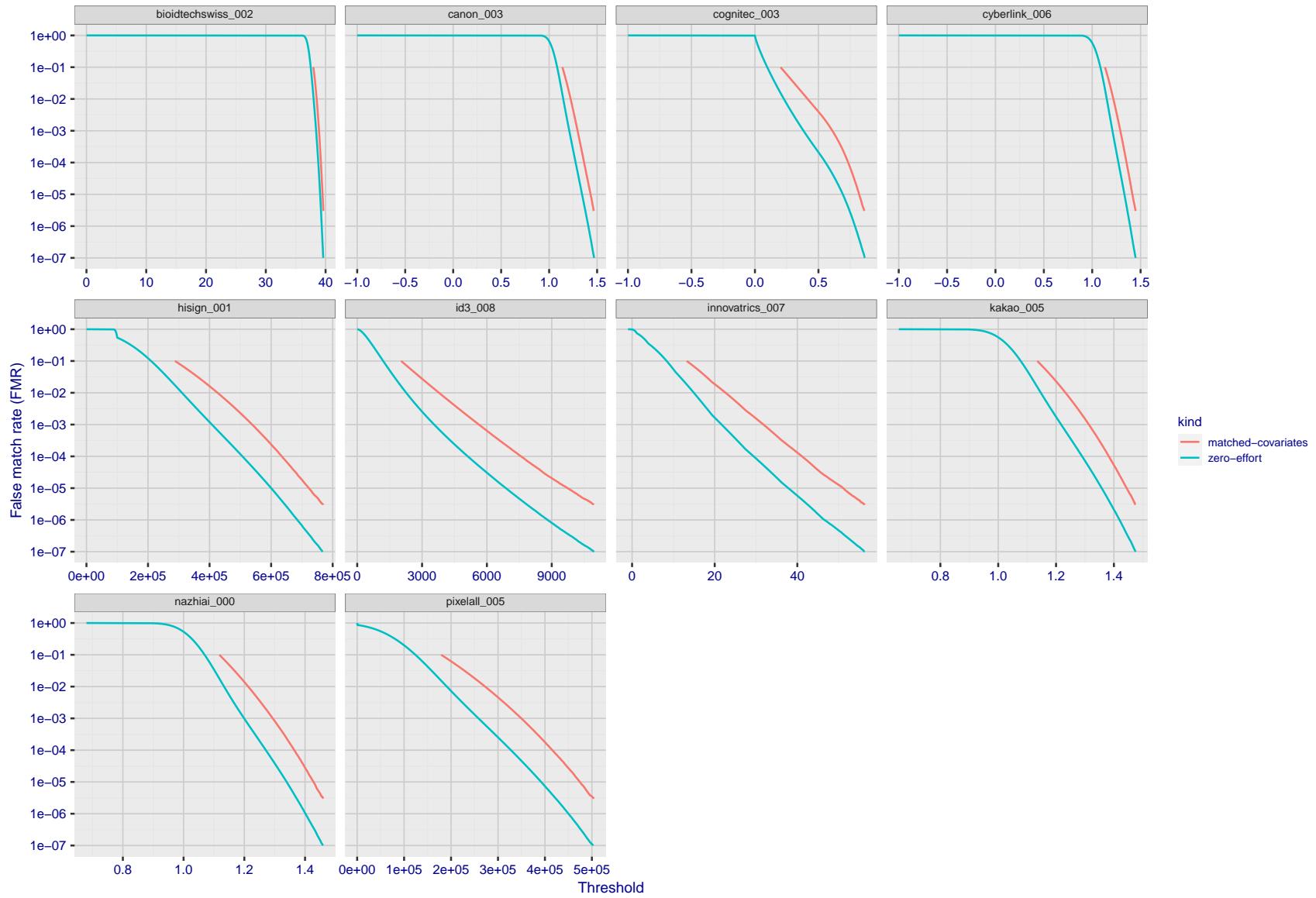


Figure 186: For the visa images, the false match calibration curves show FMR vs. threshold, T . The blue (lower) curves are for zero-effort impostors (i.e. comparing all images against all). The red (upper) curves are for persons of the same-sex, same-age, and same national-origin. This shows that FMR is underestimated (by a factor of 10 or more) by using a zero-effort impostor calculation to calibrate T . As shown later (sec. 3.6), FMR is higher for demographic-matched impostors.

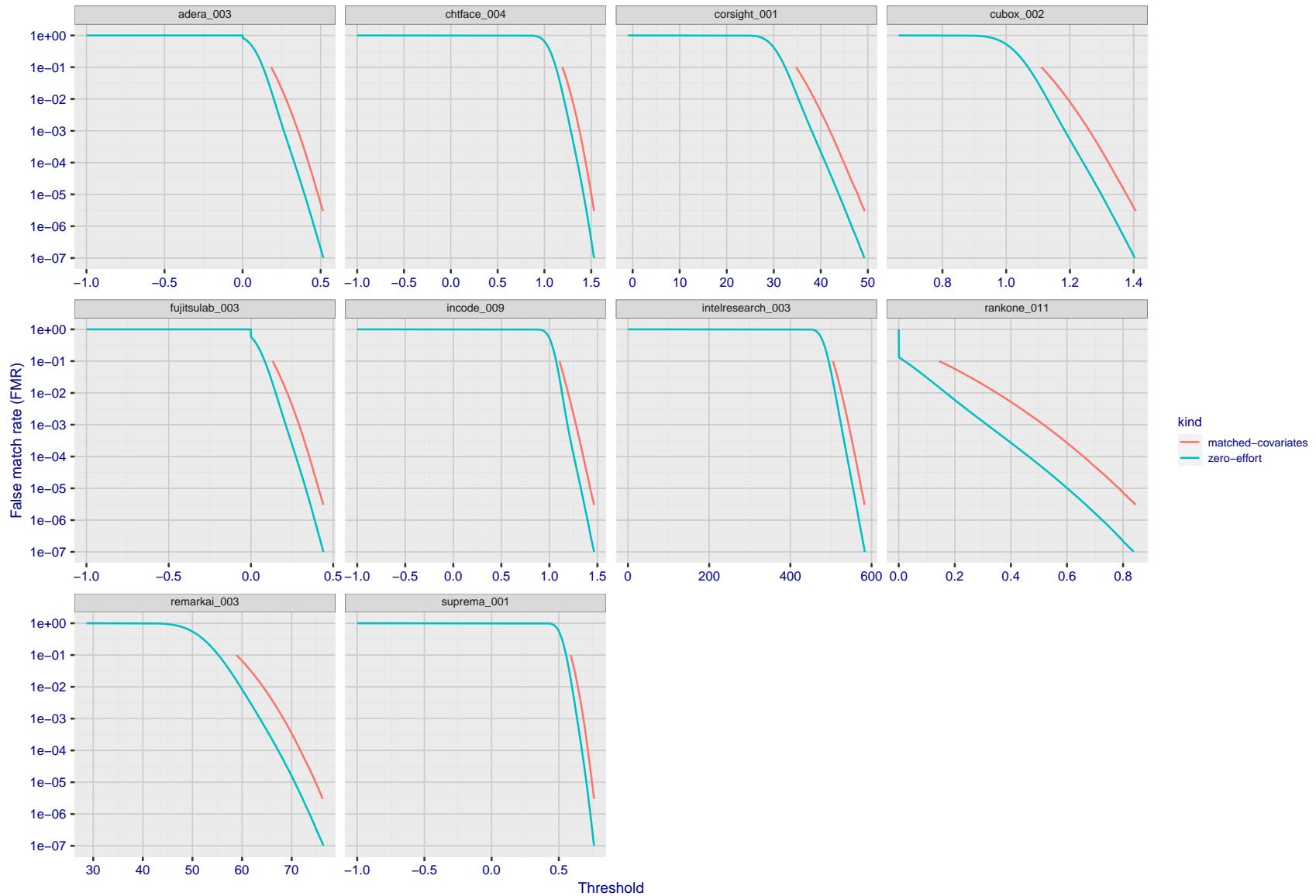


Figure 187: For the visa images, the false match calibration curves show FMR vs. threshold, T . The blue (lower) curves are for zero-effort impostors (i.e. comparing all images against all). The red (upper) curves are for persons of the same-sex, same-age, and same national-origin. This shows that FMR is underestimated (by a factor of 10 or more) by using a zero-effort impostor calculation to calibrate T . As shown later (sec. 3.6), FMR is higher for demographic-matched impostors.

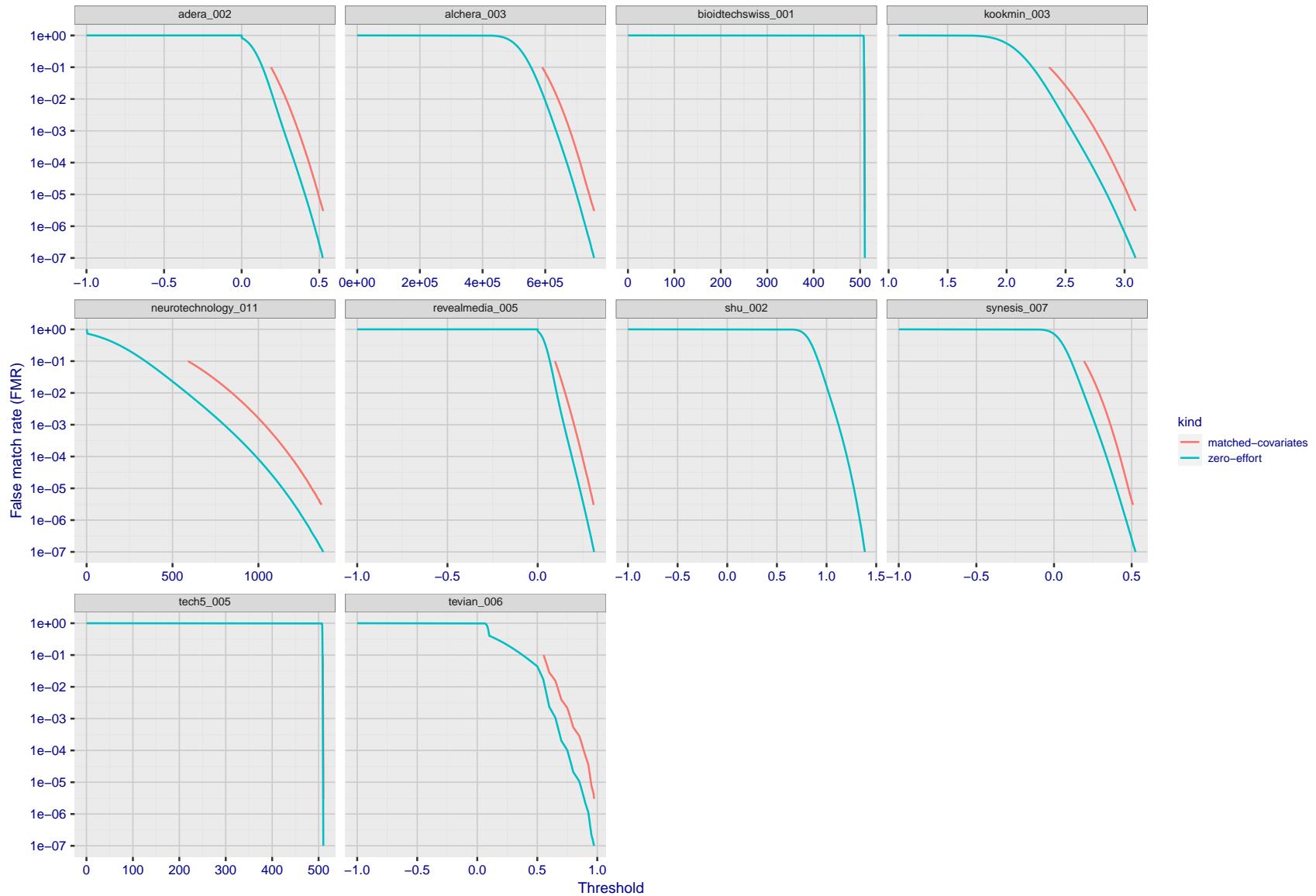


Figure 188: For the visa images, the false match calibration curves show FMR vs. threshold, T . The blue (lower) curves are for zero-effort impostors (i.e. comparing all images against all). The red (upper) curves are for persons of the same-sex, same-age, and same national-origin. This shows that FMR is underestimated (by a factor of 10 or more) by using a zero-effort impostor calculation to calibrate T . As shown later (sec. 3.6), FMR is higher for demographic-matched impostors.

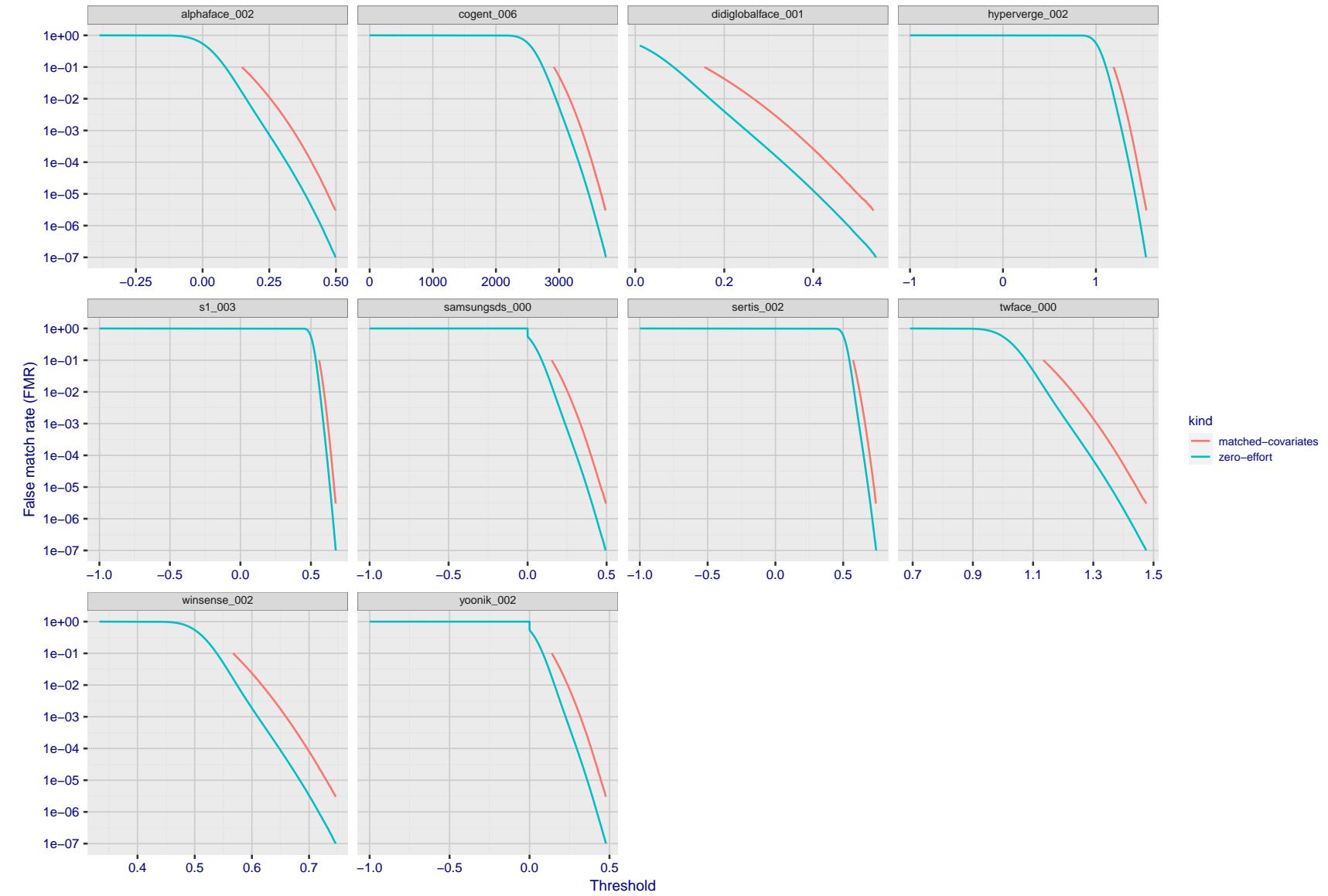


Figure 189: For the visa images, the false match calibration curves show FMR vs. threshold, T . The blue (lower) curves are for zero-effort impostors (i.e. comparing all images against all). The red (upper) curves are for persons of the same-sex, same-age, and same national-origin. This shows that FMR is underestimated (by a factor of 10 or more) by using a zero-effort impostor calculation to calibrate T . As shown later (sec. 3.6), FMR is higher for demographic-matched impostors.

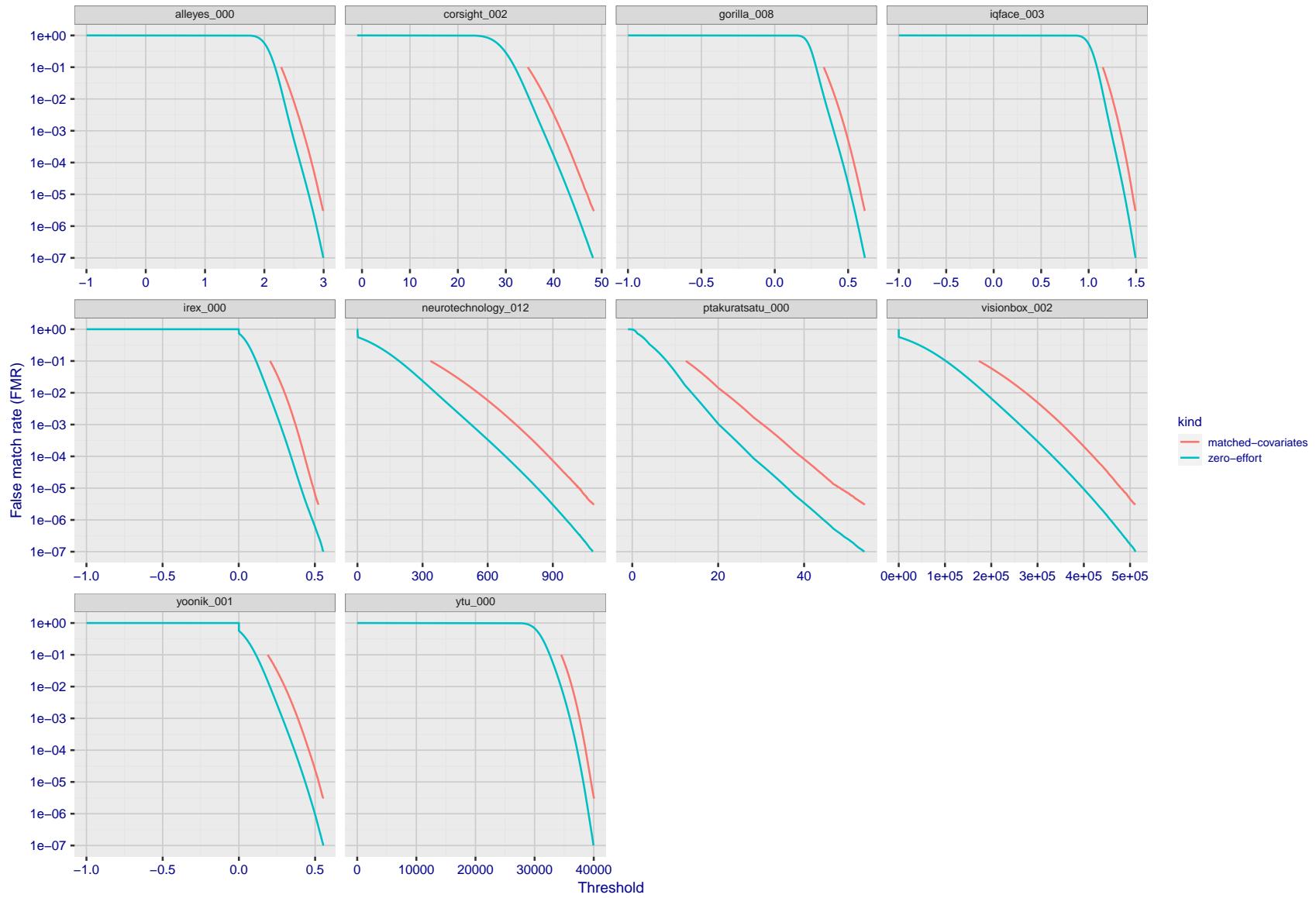


Figure 190: For the visa images, the false match calibration curves show FMR vs. threshold, T . The blue (lower) curves are for zero-effort impostors (i.e. comparing all images against all). The red (upper) curves are for persons of the same-sex, same-age, and same national-origin. This shows that FMR is underestimated (by a factor of 10 or more) by using a zero-effort impostor calculation to calibrate T . As shown later (sec. 3.6), FMR is higher for demographic-matched impostors.

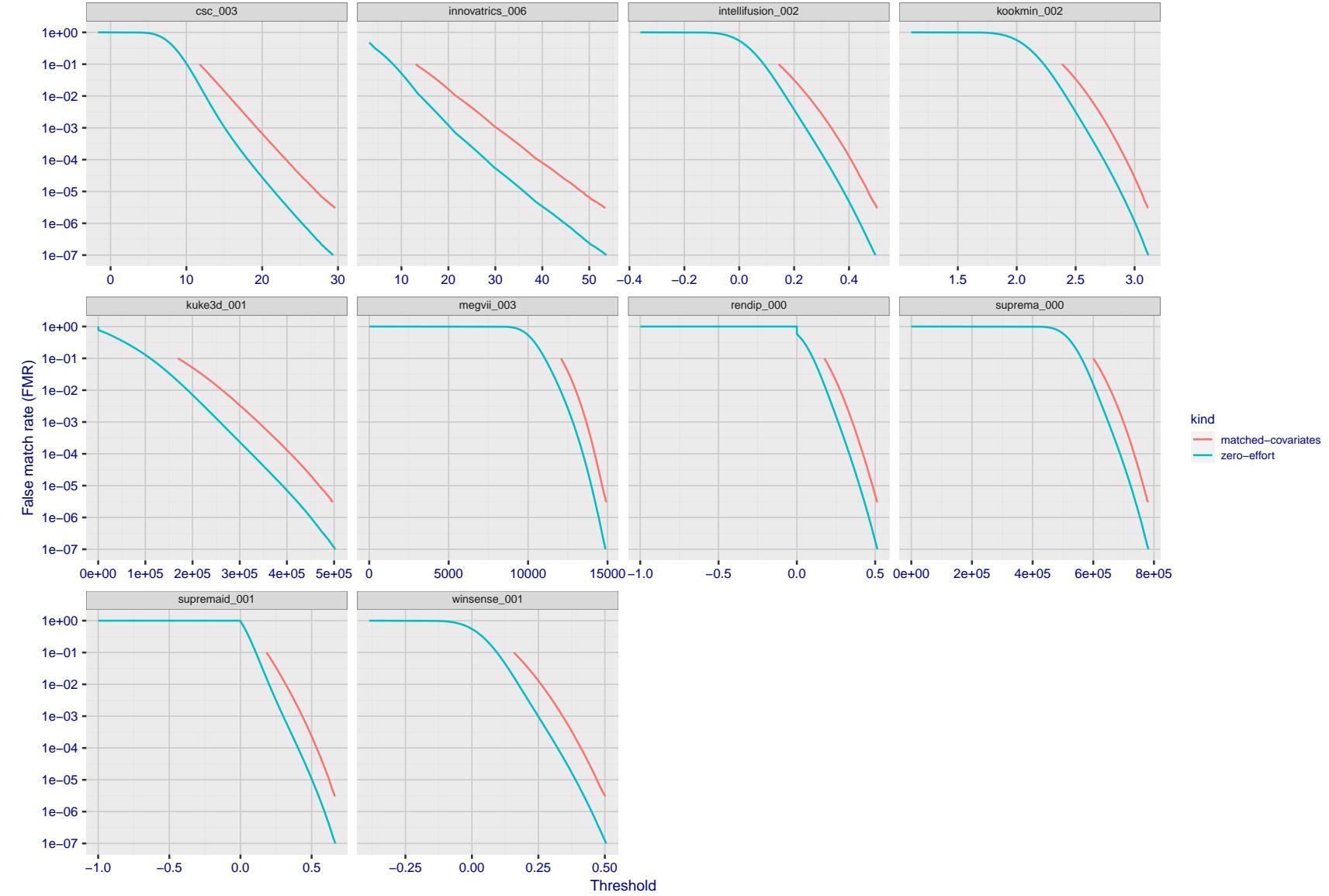


Figure 191: For the visa images, the false match calibration curves show FMR vs. threshold, T . The blue (lower) curves are for zero-effort impostors (i.e. comparing all images against all). The red (upper) curves are for persons of the same-sex, same-age, and same national-origin. This shows that FMR is underestimated (by a factor of 10 or more) by using a zero-effort impostor calculation to calibrate T . As shown later (sec. 3.6), FMR is higher for demographic-matched impostors.

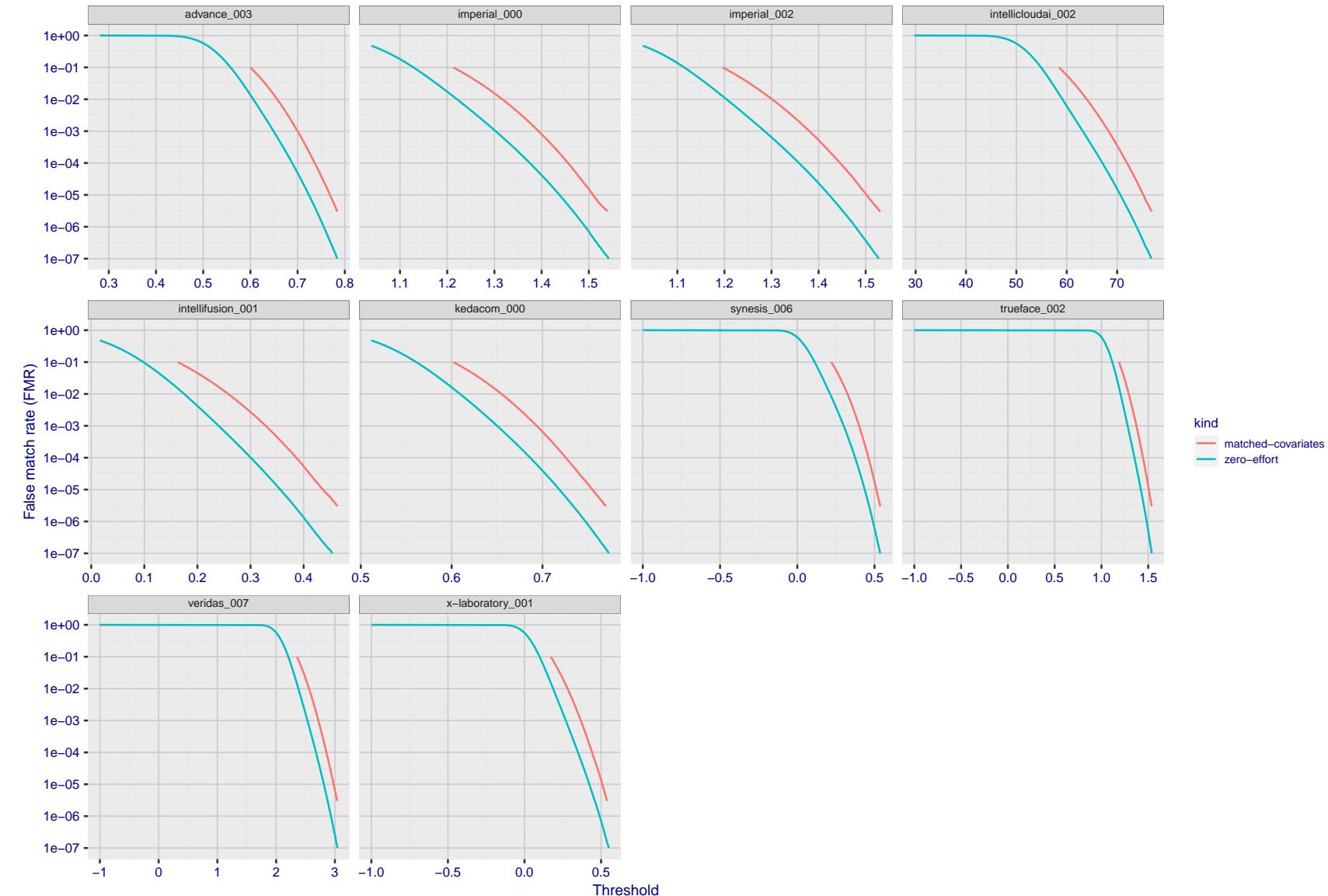


Figure 192: For the visa images, the false match calibration curves show FMR vs. threshold, T . The blue (lower) curves are for zero-effort impostors (i.e. comparing all images against all). The red (upper) curves are for persons of the same-sex, same-age, and same national-origin. This shows that FMR is underestimated (by a factor of 10 or more) by using a zero-effort impostor calculation to calibrate T . As shown later (sec. 3.6), FMR is higher for demographic-matched impostors.

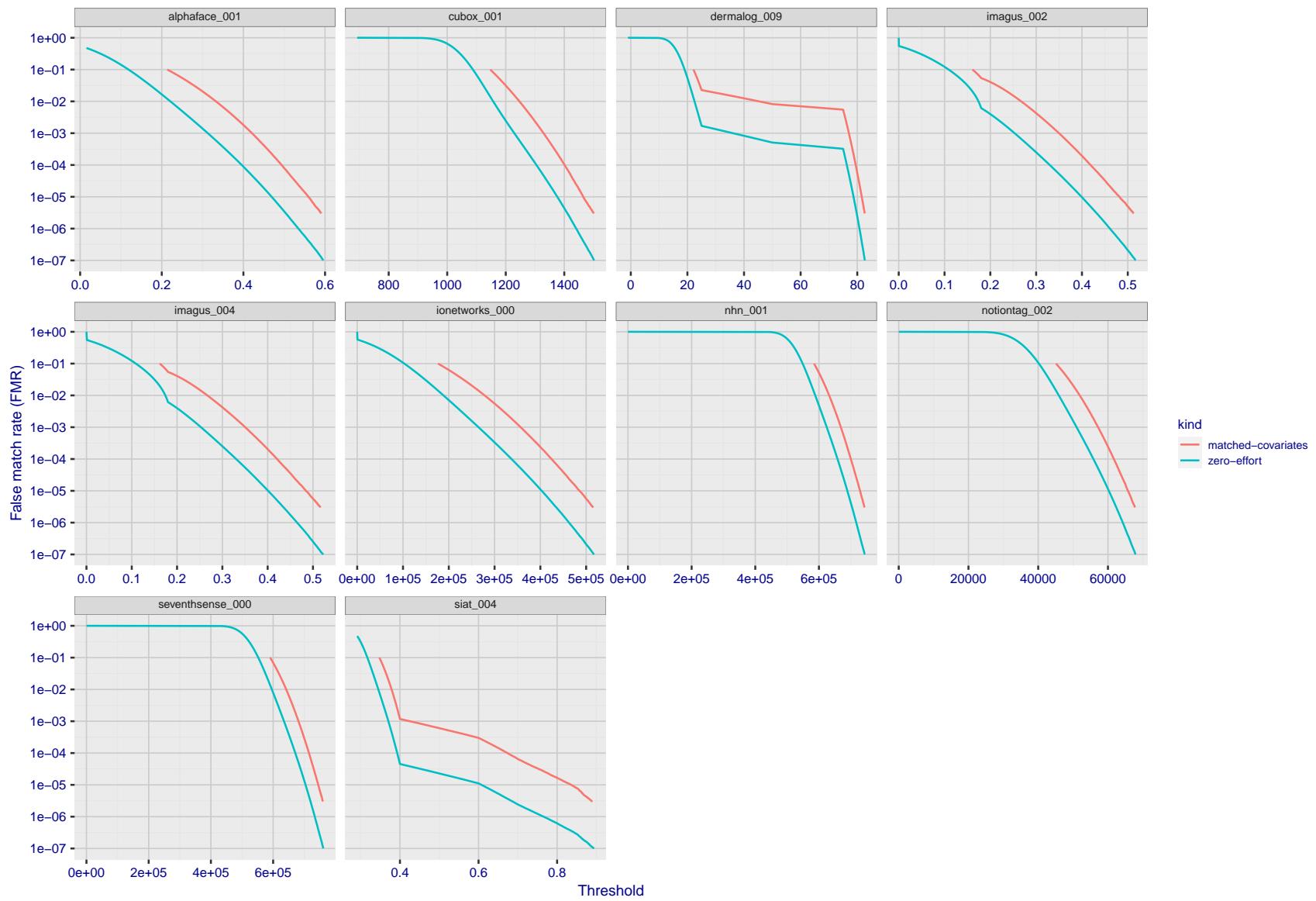


Figure 193: For the visa images, the false match calibration curves show FMR vs. threshold, T . The blue (lower) curves are for zero-effort impostors (i.e. comparing all images against all). The red (upper) curves are for persons of the same-sex, same-age, and same national-origin. This shows that FMR is underestimated (by a factor of 10 or more) by using a zero-effort impostor calculation to calibrate T . As shown later (sec. 3.6), FMR is higher for demographic-matched impostors.

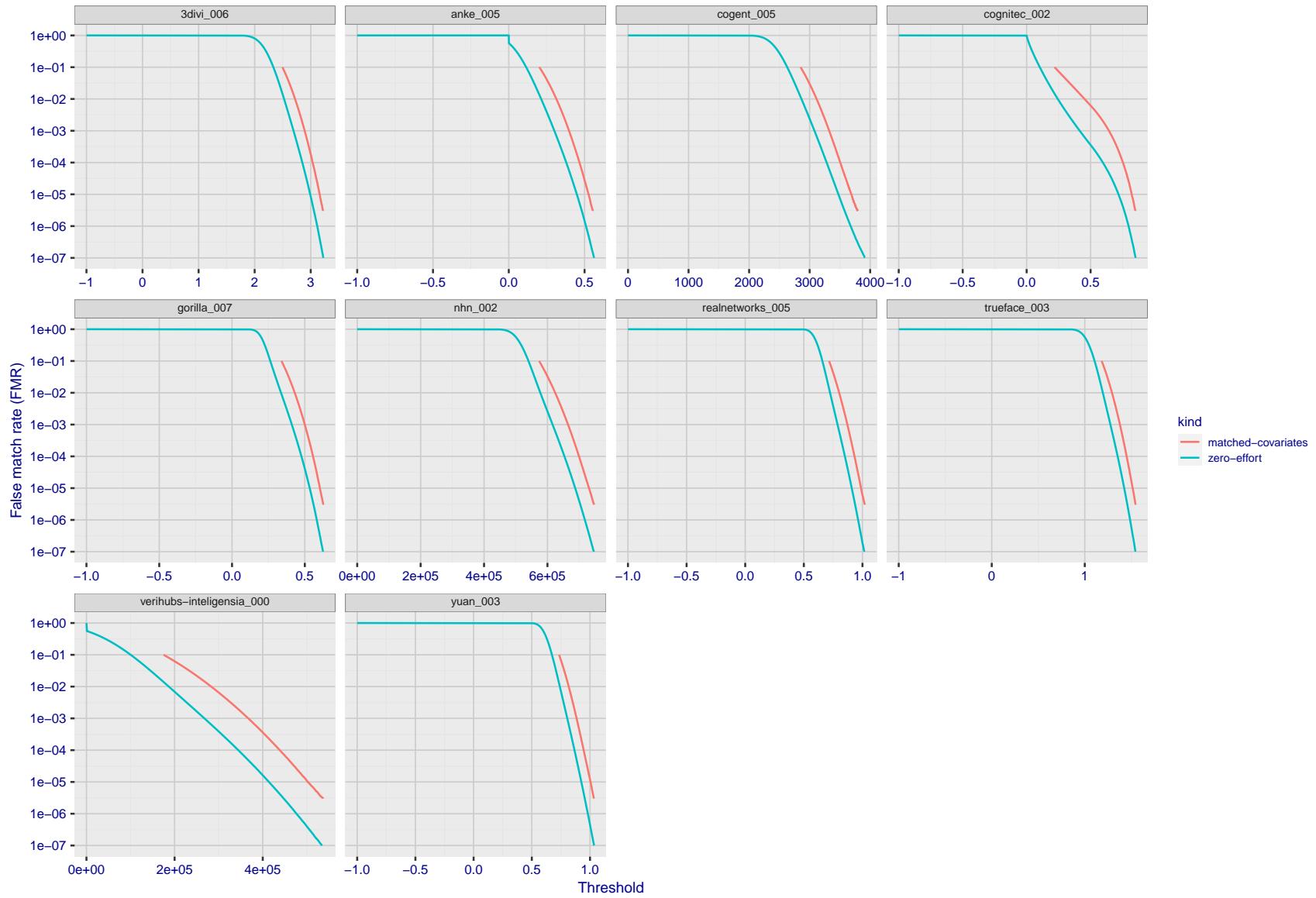


Figure 194: For the visa images, the false match calibration curves show FMR vs. threshold, T . The blue (lower) curves are for zero-effort impostors (i.e. comparing all images against all). The red (upper) curves are for persons of the same-sex, same-age, and same national-origin. This shows that FMR is underestimated (by a factor of 10 or more) by using a zero-effort impostor calculation to calibrate T . As shown later (sec. 3.6), FMR is higher for demographic-matched impostors.

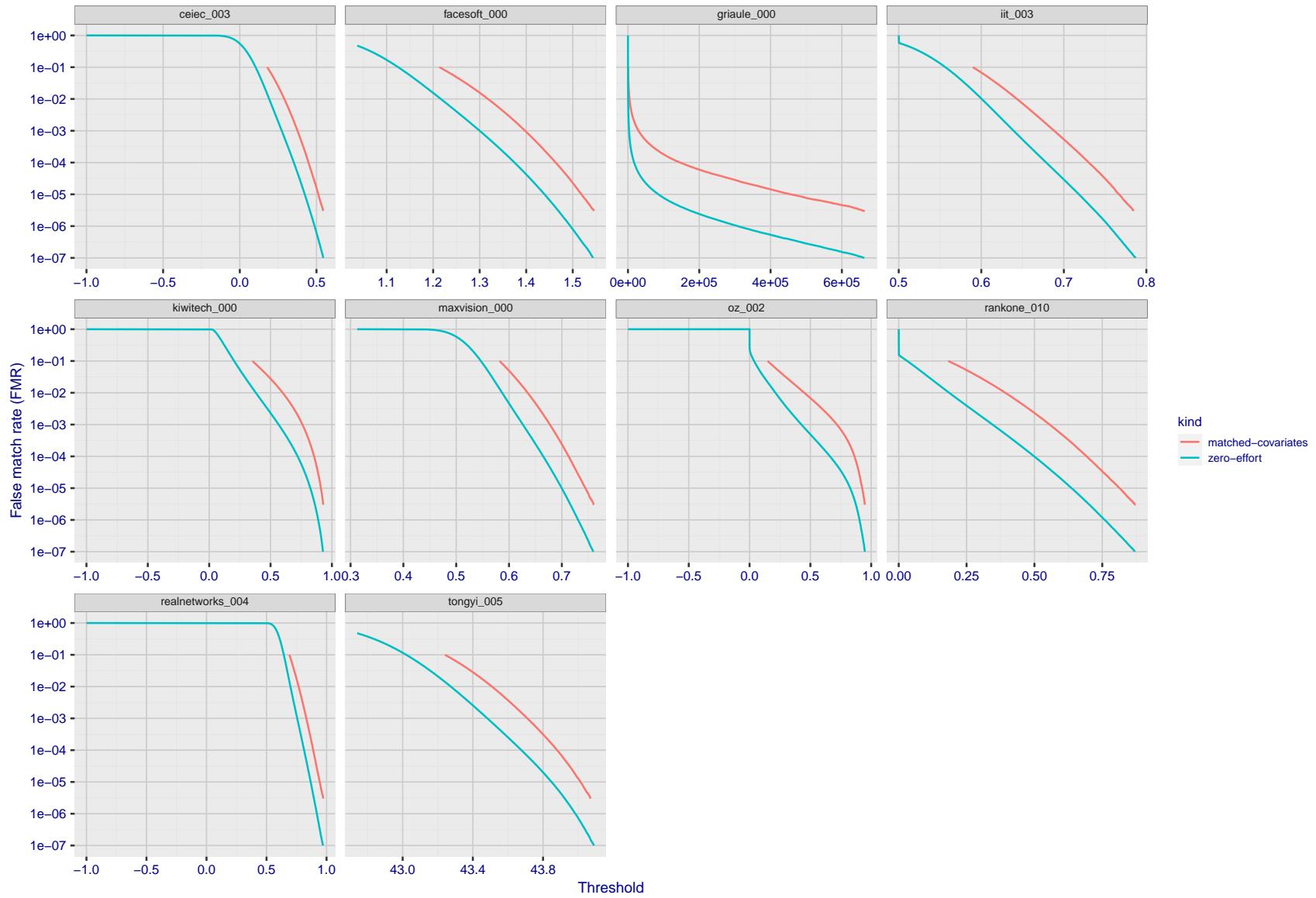


Figure 195: For the visa images, the false match calibration curves show FMR vs. threshold, T . The blue (lower) curves are for zero-effort impostors (i.e. comparing all images against all). The red (upper) curves are for persons of the same-sex, same-age, and same national-origin. This shows that FMR is underestimated (by a factor of 10 or more) by using a zero-effort impostor calculation to calibrate T . As shown later (sec. 3.6), FMR is higher for demographic-matched impostors.

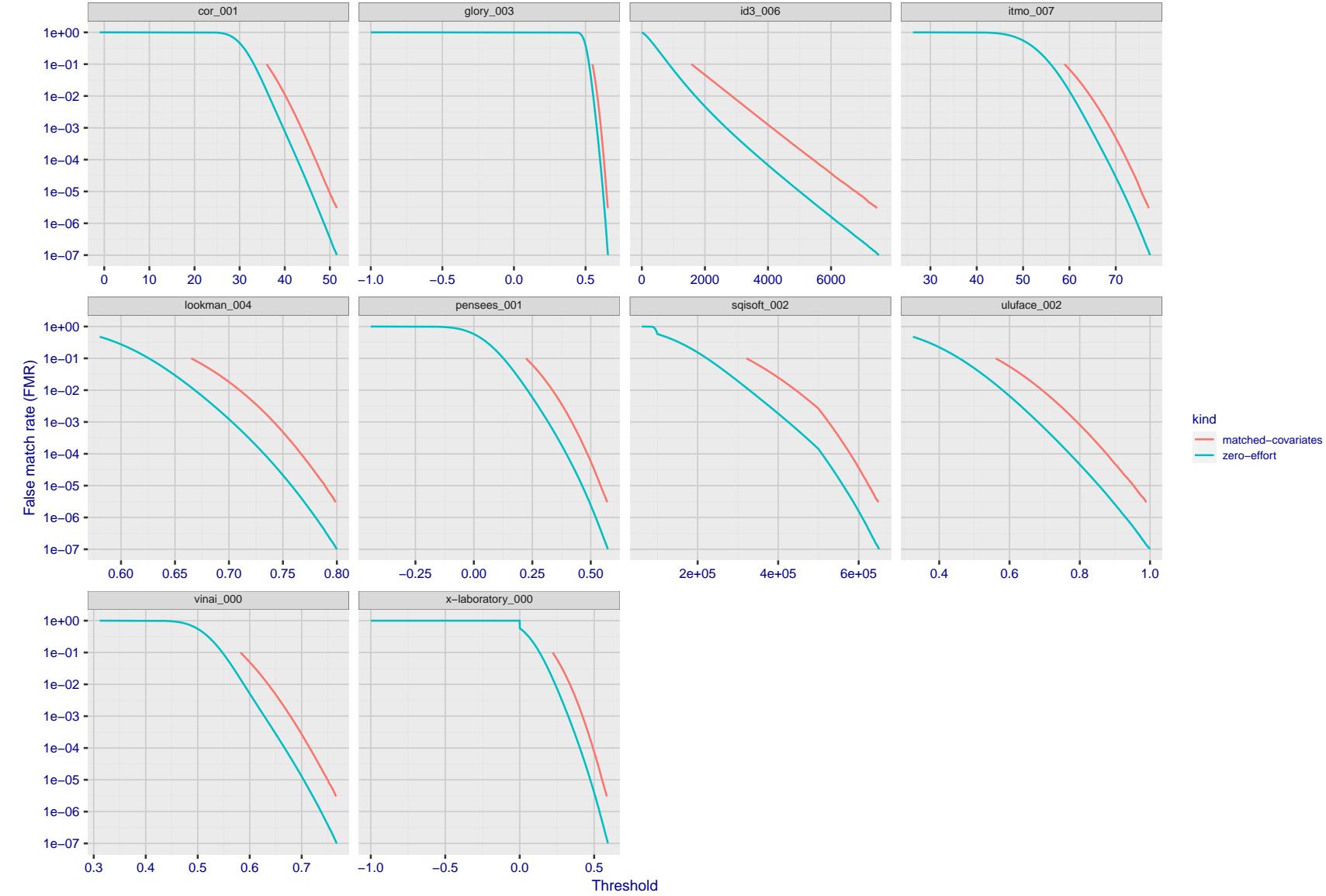


Figure 196: For the visa images, the false match calibration curves show FMR vs. threshold, T . The blue (lower) curves are for zero-effort impostors (i.e. comparing all images against all). The red (upper) curves are for persons of the same-sex, same-age, and same national-origin. This shows that FMR is underestimated (by a factor of 10 or more) by using a zero-effort impostor calculation to calibrate T . As shown later (sec. 3.6), FMR is higher for demographic-matched impostors.

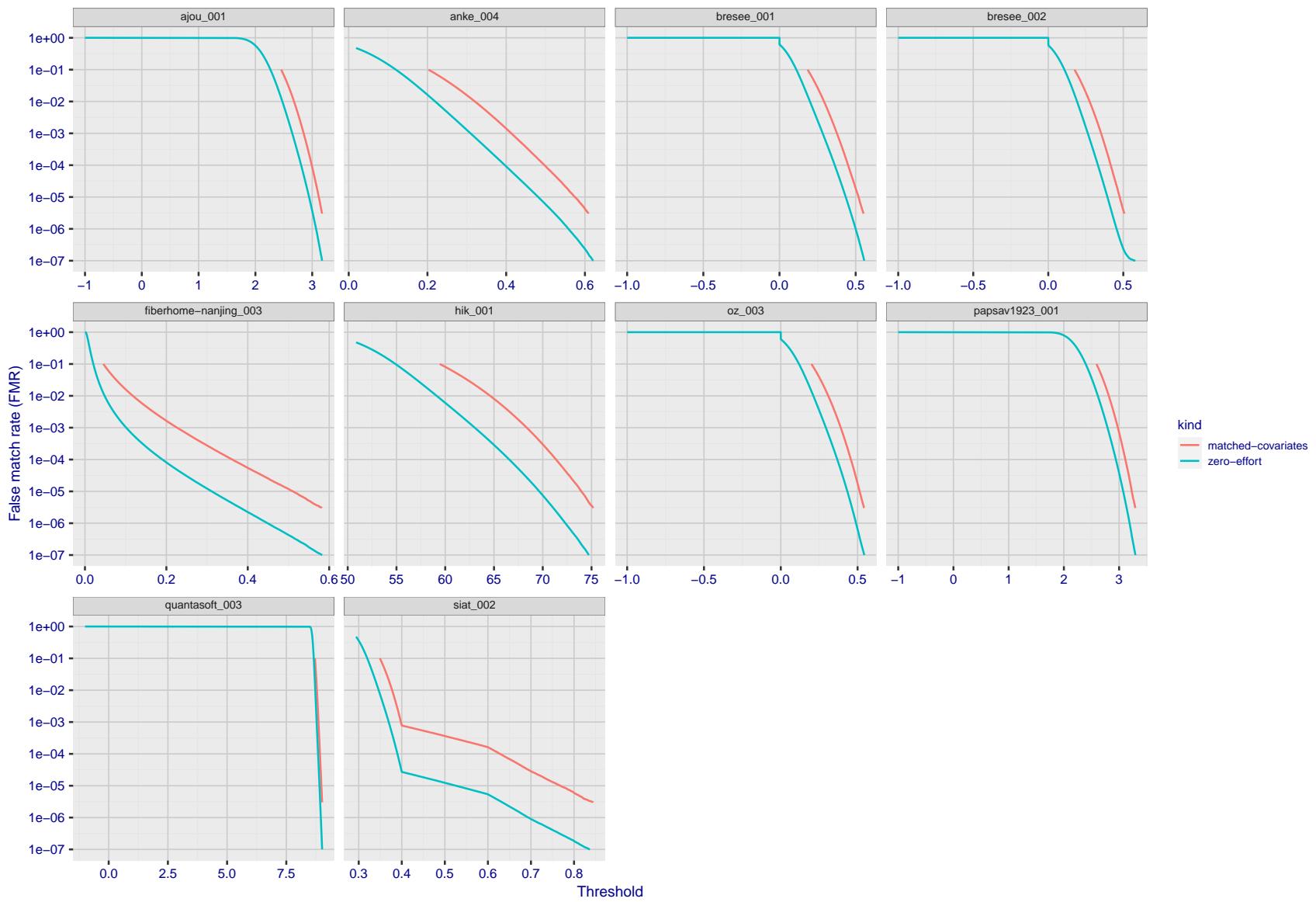


Figure 197: For the visa images, the false match calibration curves show FMR vs. threshold, T . The blue (lower) curves are for zero-effort impostors (i.e. comparing all images against all). The red (upper) curves are for persons of the same-sex, same-age, and same national-origin. This shows that FMR is underestimated (by a factor of 10 or more) by using a zero-effort impostor calculation to calibrate T . As shown later (sec. 3.6), FMR is higher for demographic-matched impostors.

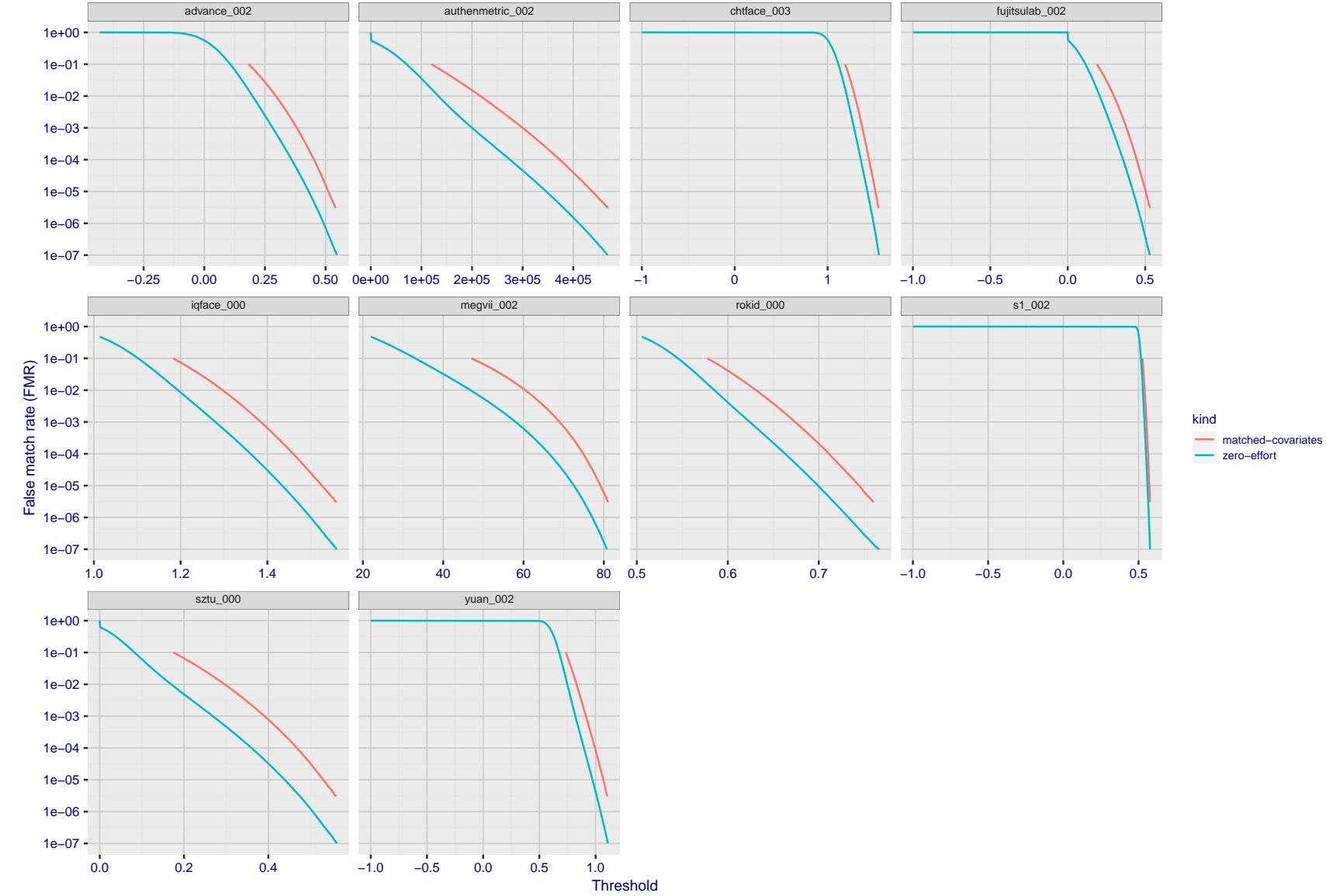


Figure 198: For the visa images, the false match calibration curves show FMR vs. threshold, T . The blue (lower) curves are for zero-effort impostors (i.e. comparing all images against all). The red (upper) curves are for persons of the same-sex, same-age, and same national-origin. This shows that FMR is underestimated (by a factor of 10 or more) by using a zero-effort impostor calculation to calibrate T . As shown later (sec. 3.6), FMR is higher for demographic-matched impostors.

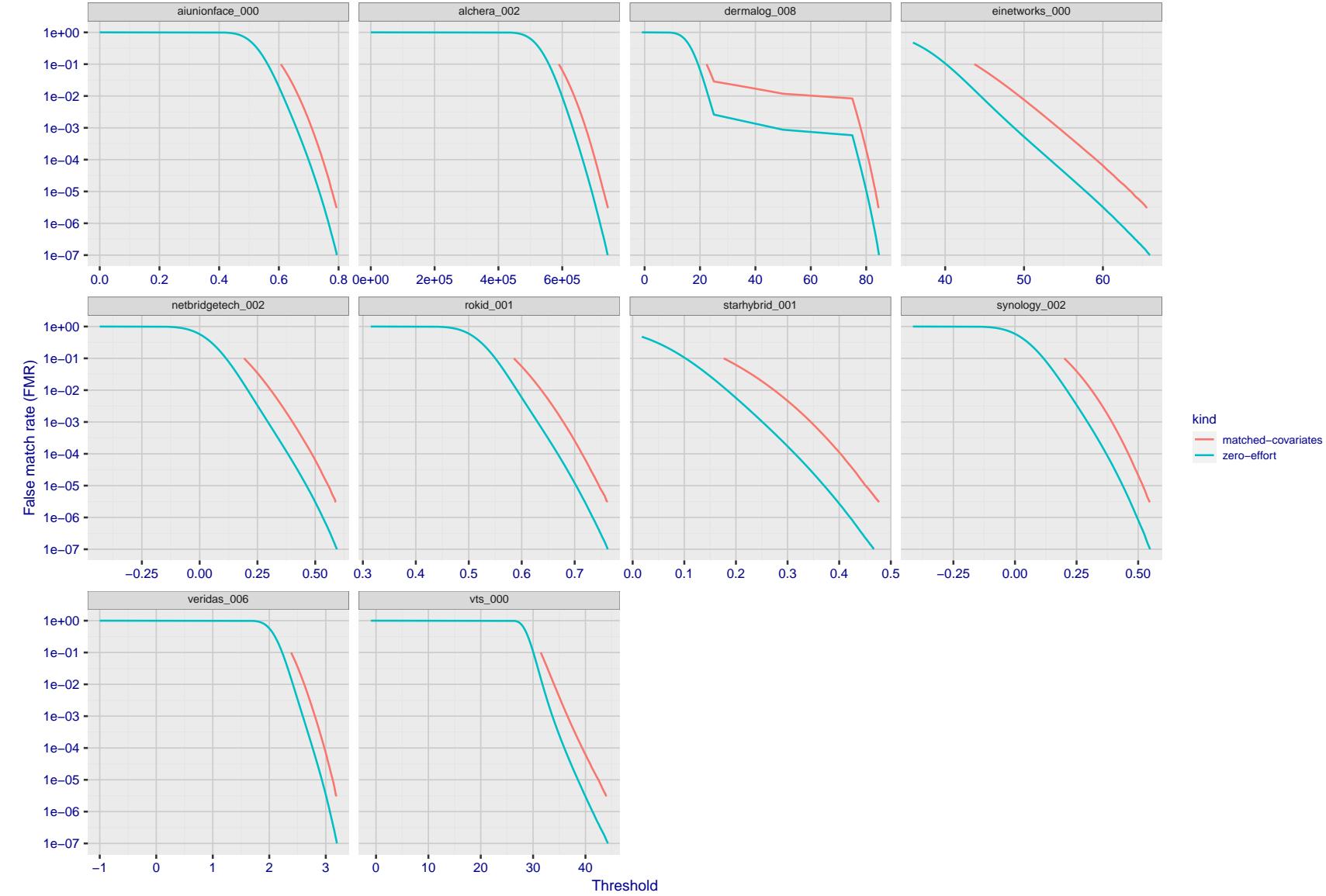


Figure 199: For the visa images, the false match calibration curves show FMR vs. threshold, T . The blue (lower) curves are for zero-effort impostors (i.e. comparing all images against all). The red (upper) curves are for persons of the same-sex, same-age, and same national-origin. This shows that FMR is underestimated (by a factor of 10 or more) by using a zero-effort impostor calculation to calibrate T . As shown later (sec. 3.6), FMR is higher for demographic-matched impostors.

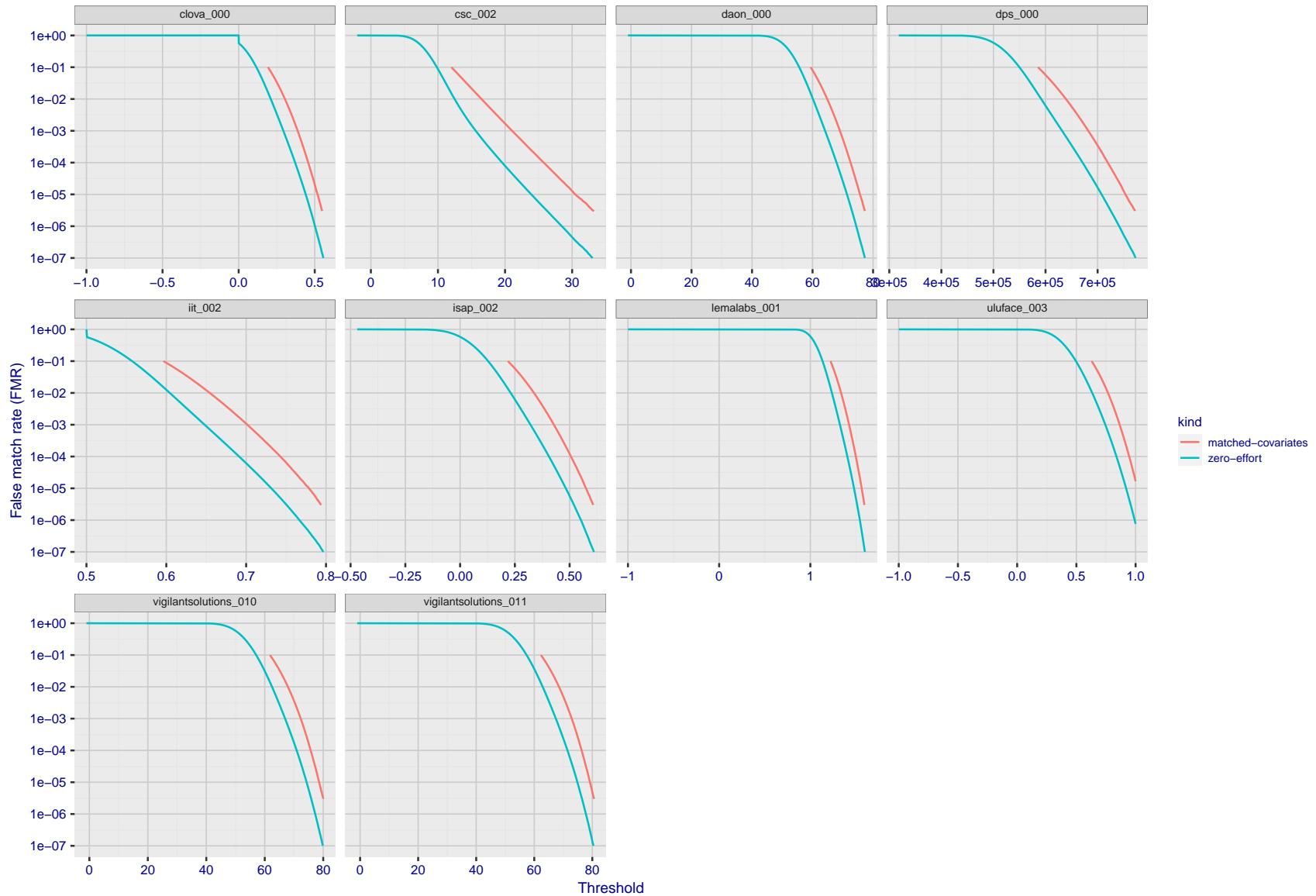


Figure 200: For the visa images, the false match calibration curves show FMR vs. threshold, T . The blue (lower) curves are for zero-effort impostors (i.e. comparing all images against all). The red (upper) curves are for persons of the same-sex, same-age, and same national-origin. This shows that FMR is underestimated (by a factor of 10 or more) by using a zero-effort impostor calculation to calibrate T . As shown later (sec. 3.6), FMR is higher for demographic-matched impostors.

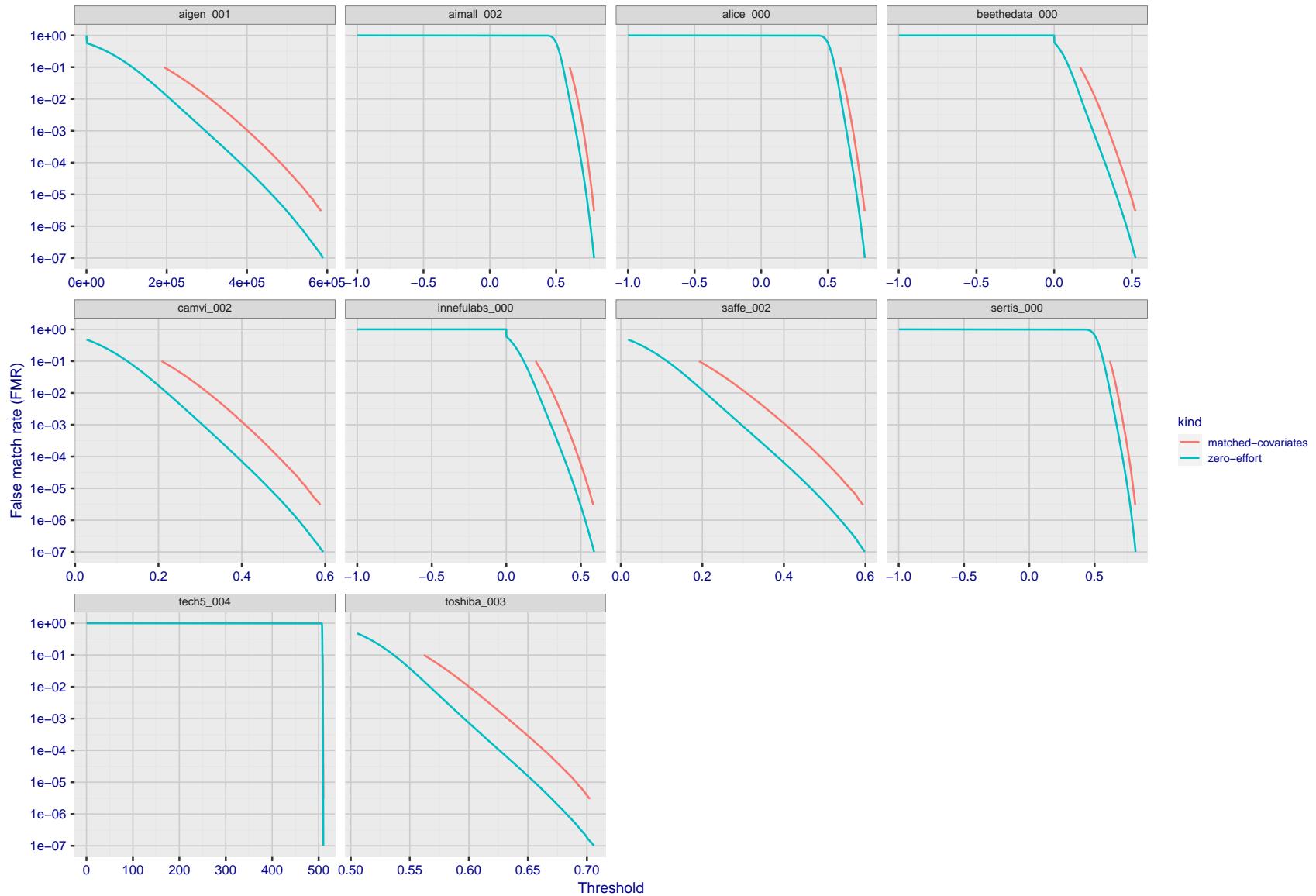


Figure 201: For the visa images, the false match calibration curves show FMR vs. threshold, T . The blue (lower) curves are for zero-effort impostors (i.e. comparing all images against all). The red (upper) curves are for persons of the same-sex, same-age, and same national-origin. This shows that FMR is underestimated (by a factor of 10 or more) by using a zero-effort impostor calculation to calibrate T . As shown later (sec. 3.6), FMR is higher for demographic-matched impostors.

2021/11/22 14:56:30

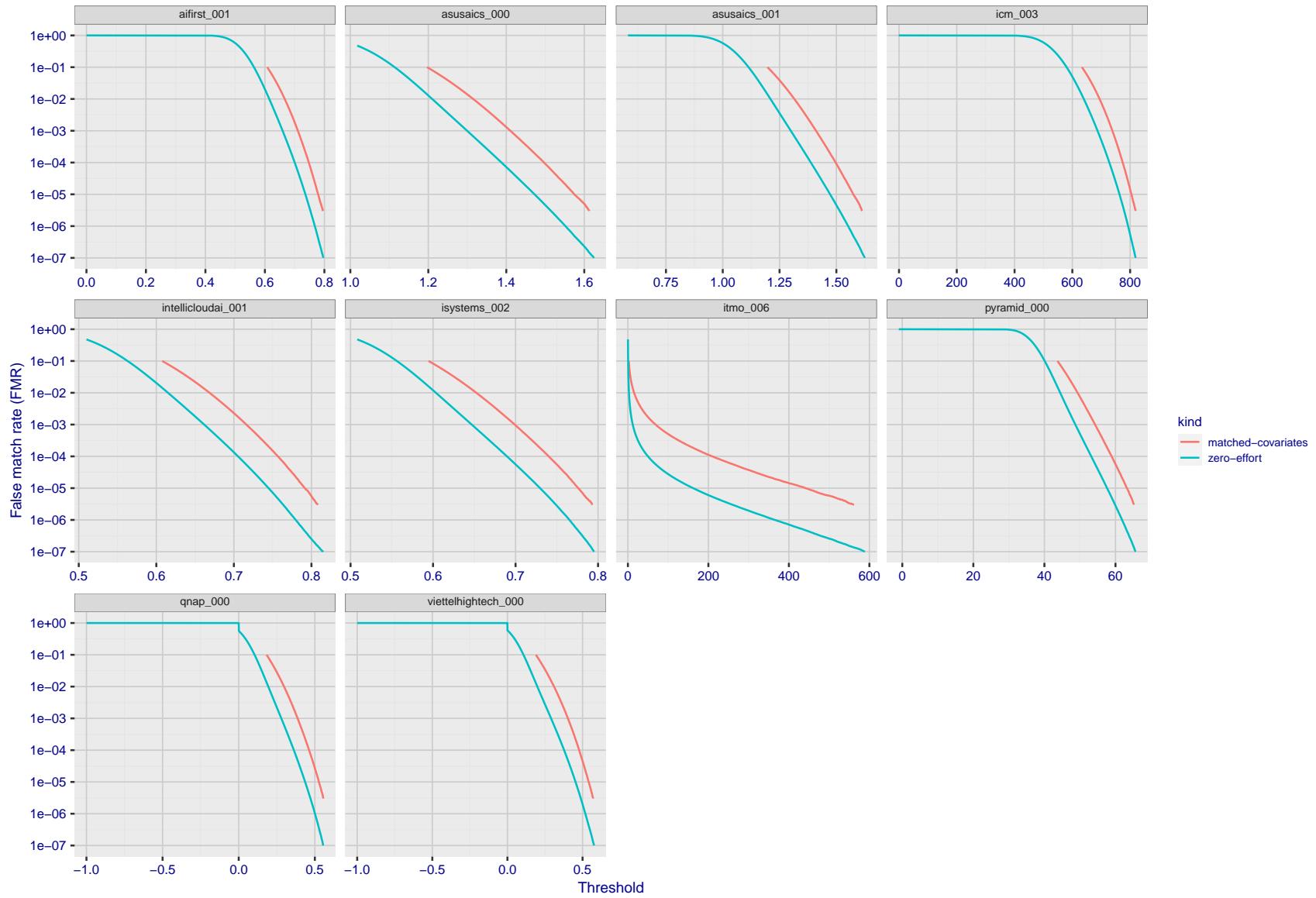


Figure 202: For the visa images, the false match calibration curves show FMR vs. threshold, T . The blue (lower) curves are for zero-effort impostors (i.e. comparing all images against all). The red (upper) curves are for persons of the same-sex, same-age, and same national-origin. This shows that FMR is underestimated (by a factor of 10 or more) by using a zero-effort impostor calculation to calibrate T . As shown later (sec. 3.6), FMR is higher for demographic-matched impostors.

FNMR(T)
"False non-match rate"
"False match rate"

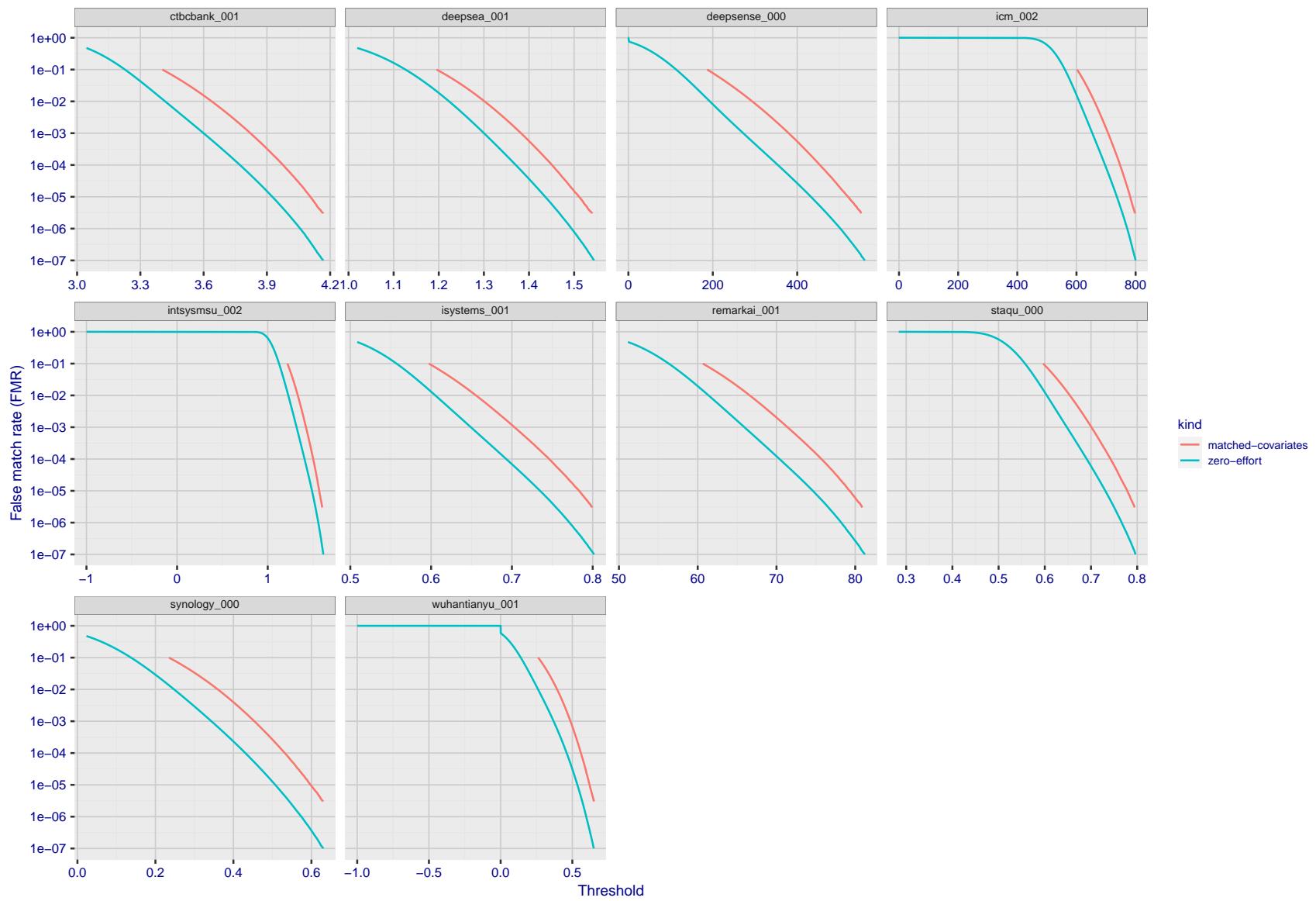


Figure 203: For the visa images, the false match calibration curves show FMR vs. threshold, T . The blue (lower) curves are for zero-effort impostors (i.e. comparing all images against all). The red (upper) curves are for persons of the same-sex, same-age, and same national-origin. This shows that FMR is underestimated (by a factor of 10 or more) by using a zero-effort impostor calculation to calibrate T . As shown later (sec. 3.6), FMR is higher for demographic-matched impostors.

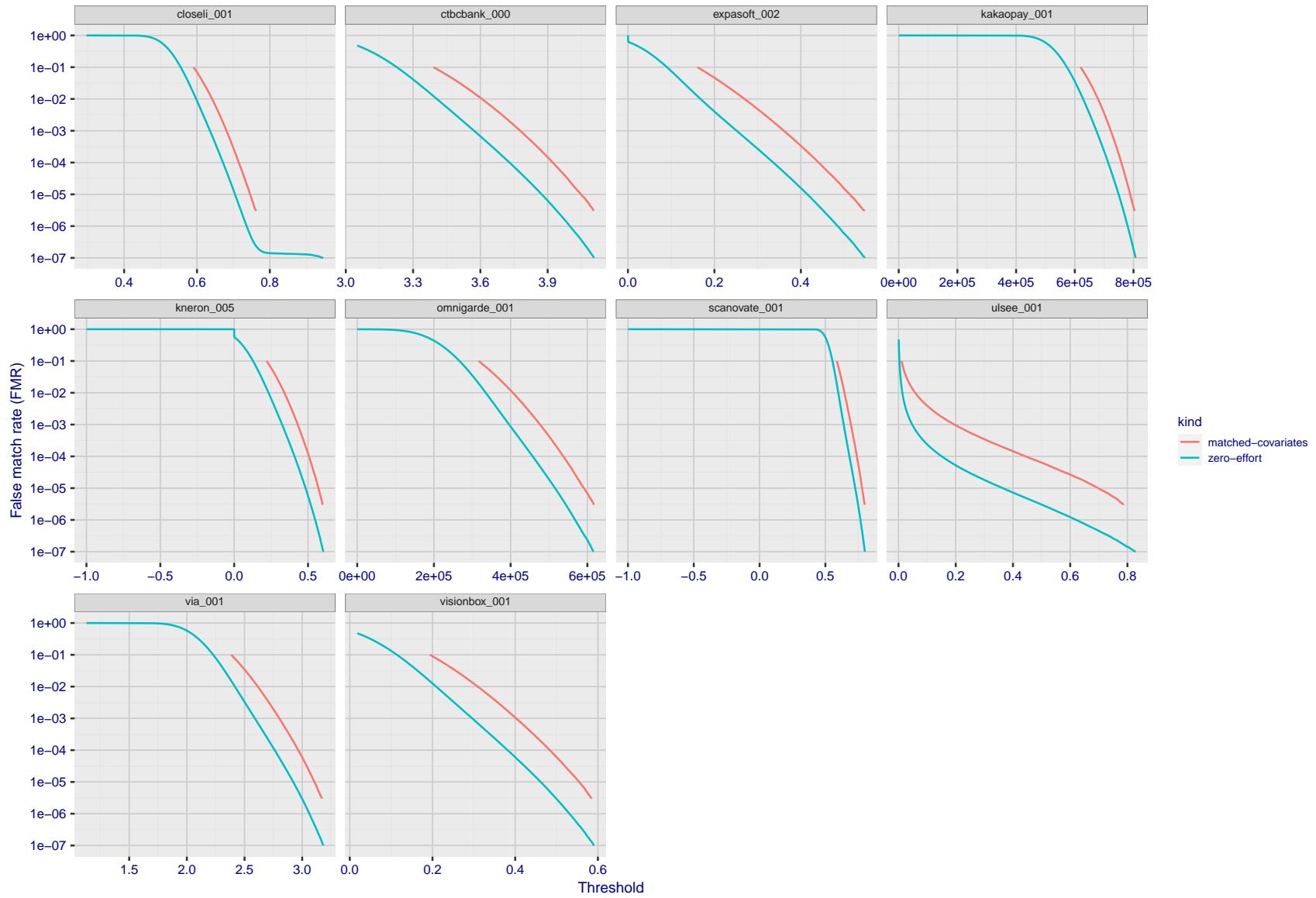


Figure 204: For the visa images, the false match calibration curves show FMR vs. threshold, T . The blue (lower) curves are for zero-effort impostors (i.e. comparing all images against all). The red (upper) curves are for persons of the same-sex, same-age, and same national-origin. This shows that FMR is underestimated (by a factor of 10 or more) by using a zero-effort impostor calculation to calibrate T . As shown later (sec. 3.6), FMR is higher for demographic-matched impostors.

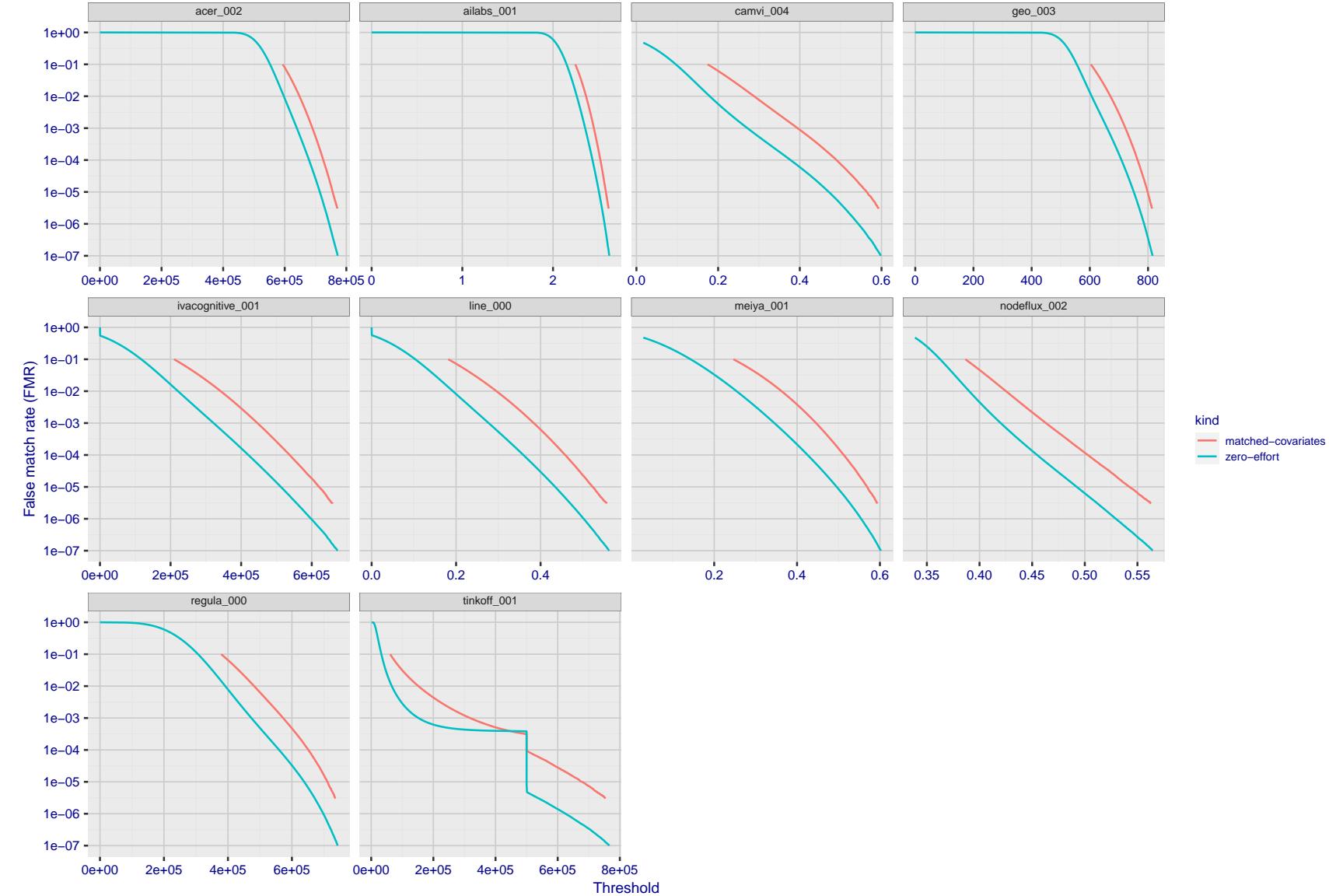


Figure 205: For the visa images, the false match calibration curves show FMR vs. threshold, T . The blue (lower) curves are for zero-effort impostors (i.e. comparing all images against all). The red (upper) curves are for persons of the same-sex, same-age, and same national-origin. This shows that FMR is underestimated (by a factor of 10 or more) by using a zero-effort impostor calculation to calibrate T . As shown later (sec. 3.6), FMR is higher for demographic-matched impostors.

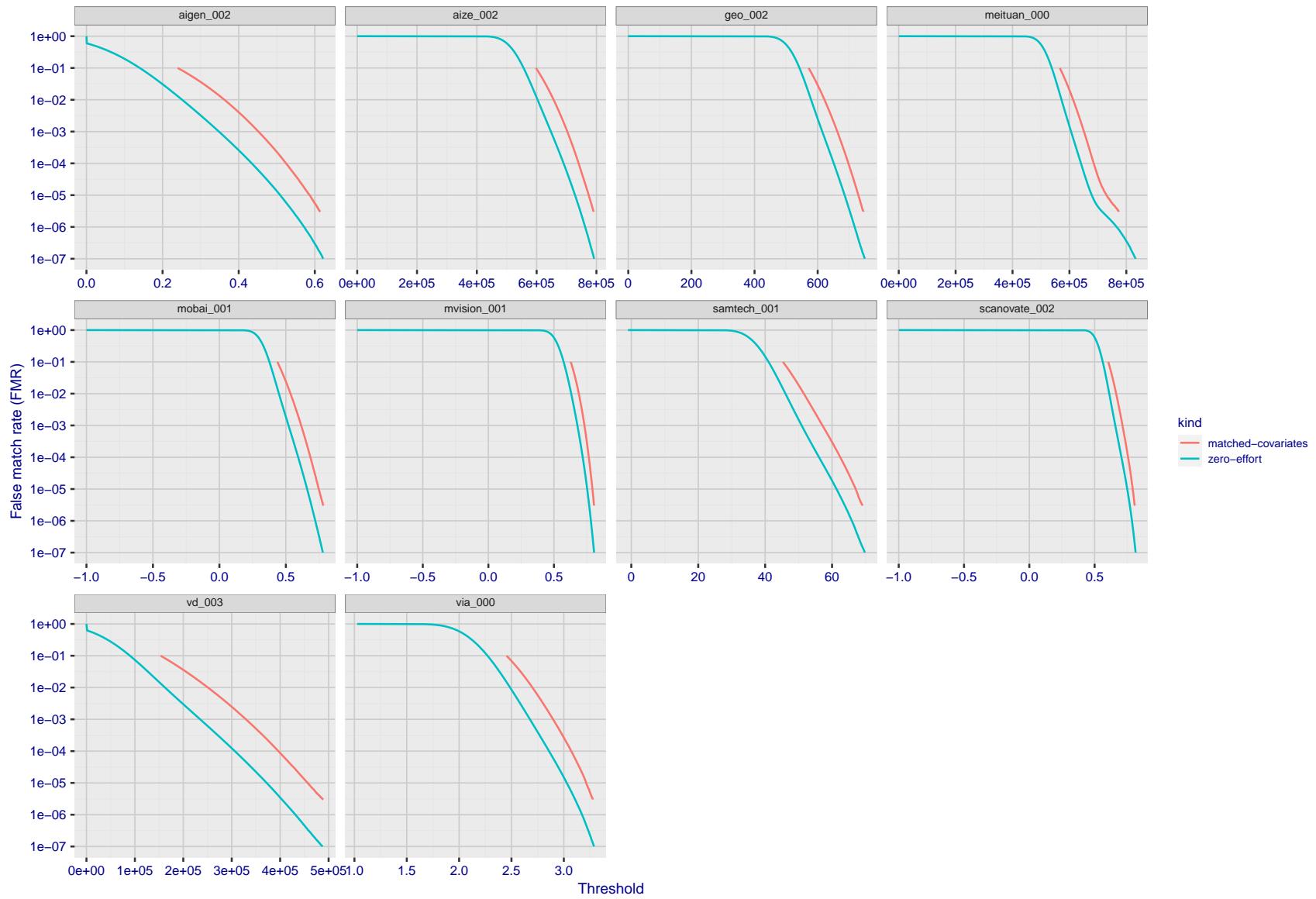


Figure 206: For the visa images, the false match calibration curves show FMR vs. threshold, T . The blue (lower) curves are for zero-effort impostors (i.e. comparing all images against all). The red (upper) curves are for persons of the same-sex, same-age, and same national-origin. This shows that FMR is underestimated (by a factor of 10 or more) by using a zero-effort impostor calculation to calibrate T . As shown later (sec. 3.6), FMR is higher for demographic-matched impostors.

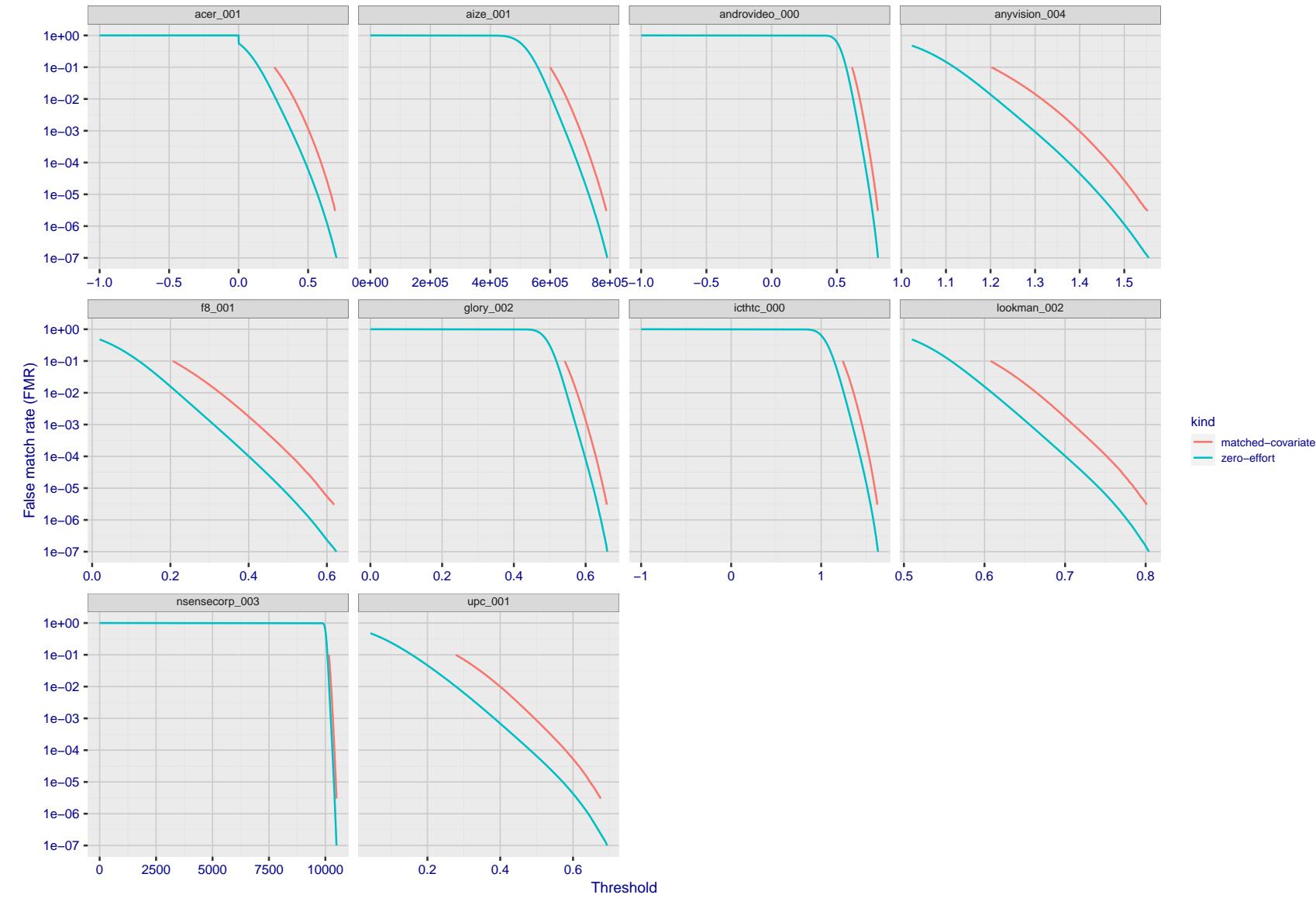


Figure 207: For the visa images, the false match calibration curves show FMR vs. threshold, T . The blue (lower) curves are for zero-effort impostors (i.e. comparing all images against all). The red (upper) curves are for persons of the same-sex, same-age, and same national-origin. This shows that FMR is underestimated (by a factor of 10 or more) by using a zero-effort impostor calculation to calibrate T . As shown later (sec. 3.6), FMR is higher for demographic-matched impostors.

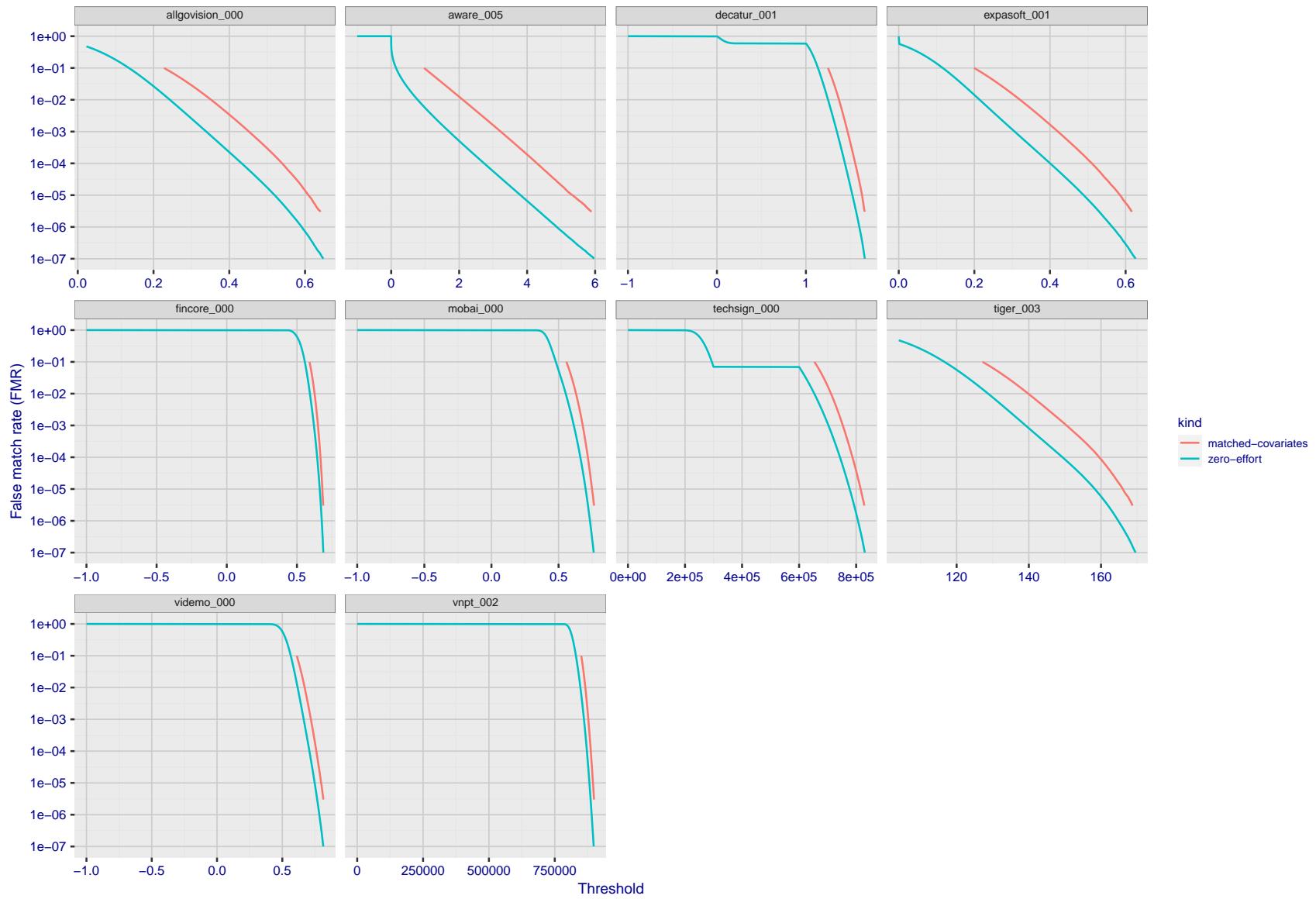


Figure 208: For the visa images, the false match calibration curves show FMR vs. threshold, T . The blue (lower) curves are for zero-effort impostors (i.e. comparing all images against all). The red (upper) curves are for persons of the same-sex, same-age, and same national-origin. This shows that FMR is underestimated (by a factor of 10 or more) by using a zero-effort impostor calculation to calibrate T . As shown later (sec. 3.6), FMR is higher for demographic-matched impostors.

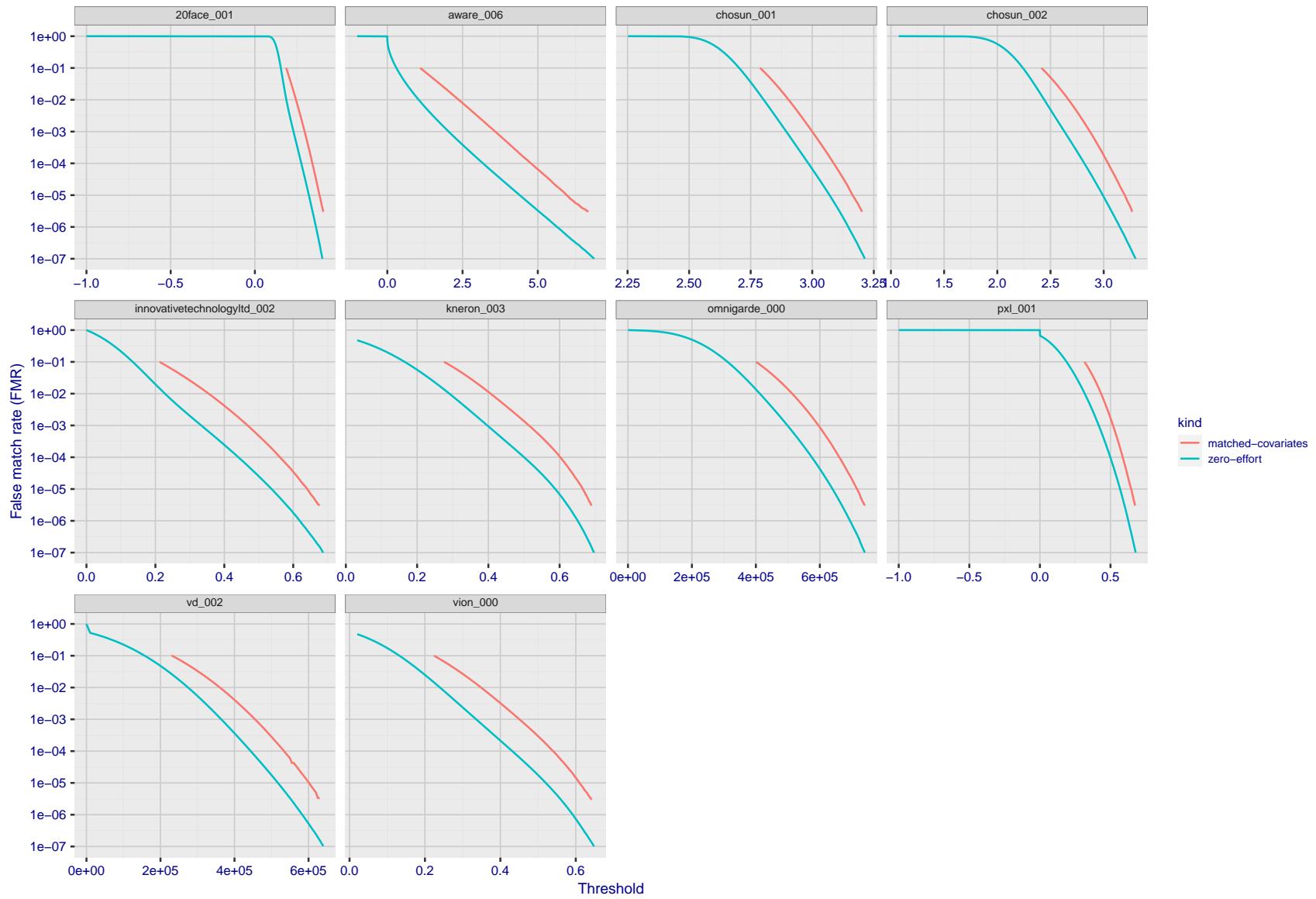


Figure 209: For the visa images, the false match calibration curves show FMR vs. threshold, T . The blue (lower) curves are for zero-effort impostors (i.e. comparing all images against all). The red (upper) curves are for persons of the same-sex, same-age, and same national-origin. This shows that FMR is underestimated (by a factor of 10 or more) by using a zero-effort impostor calculation to calibrate T . As shown later (sec. 3.6), FMR is higher for demographic-matched impostors.

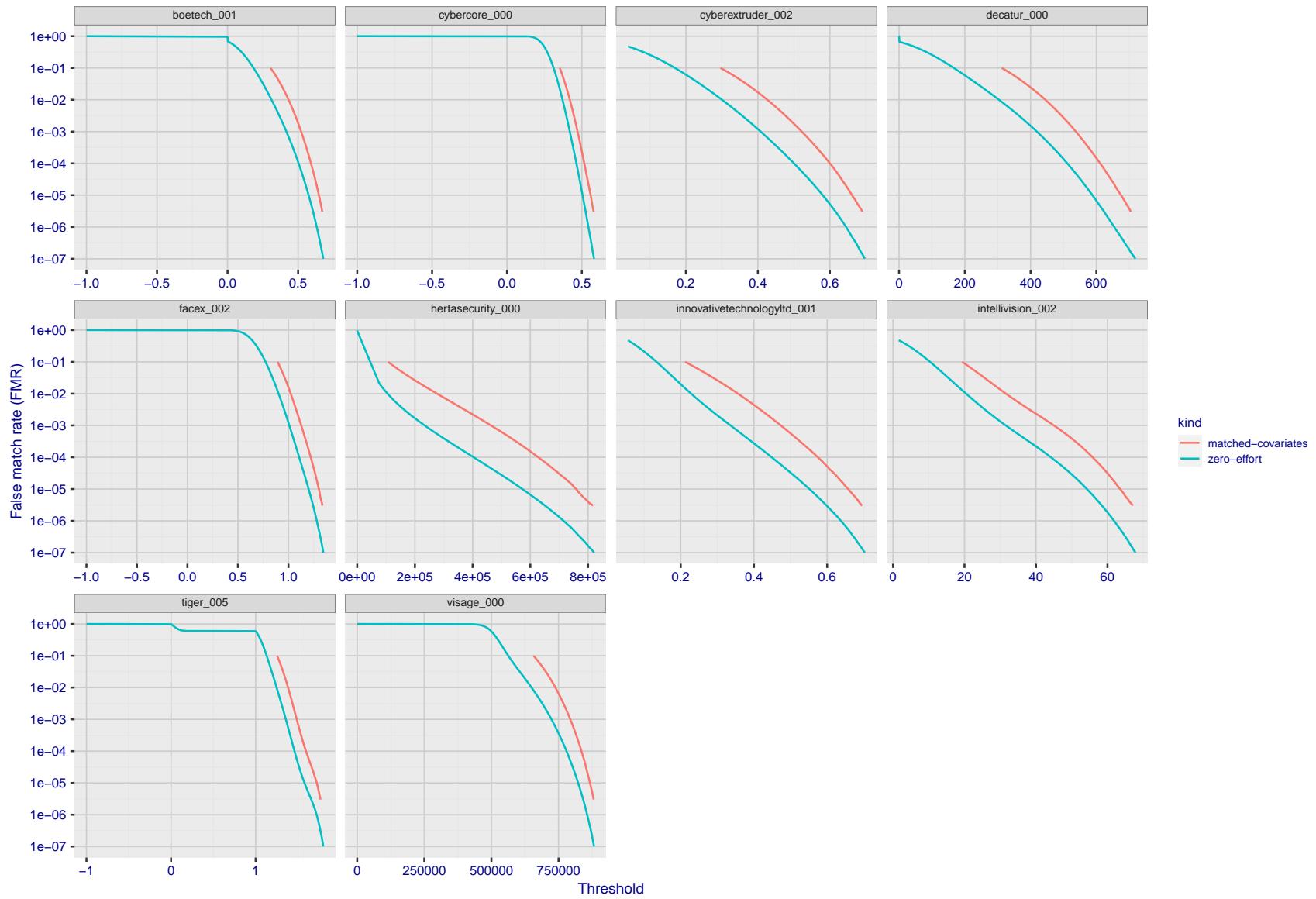


Figure 210: For the visa images, the false match calibration curves show FMR vs. threshold, T . The blue (lower) curves are for zero-effort impostors (i.e. comparing all images against all). The red (upper) curves are for persons of the same-sex, same-age, and same national-origin. This shows that FMR is underestimated (by a factor of 10 or more) by using a zero-effort impostor calculation to calibrate T . As shown later (sec. 3.6), FMR is higher for demographic-matched impostors.

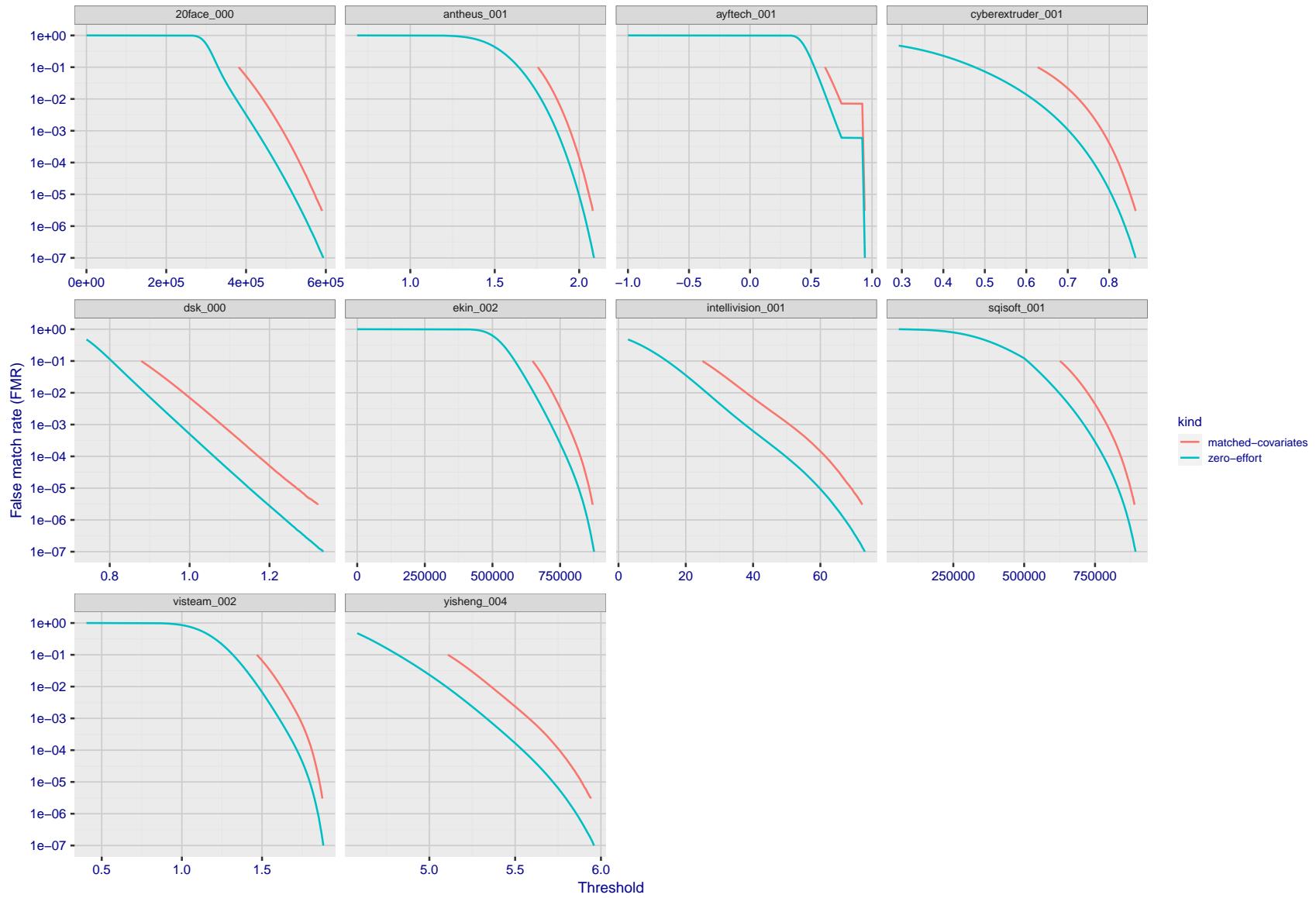


Figure 211: For the visa images, the false match calibration curves show FMR vs. threshold, T . The blue (lower) curves are for zero-effort impostors (i.e. comparing all images against all). The red (upper) curves are for persons of the same-sex, same-age, and same national-origin. This shows that FMR is underestimated (by a factor of 10 or more) by using a zero-effort impostor calculation to calibrate T . As shown later (sec. 3.6), FMR is higher for demographic-matched impostors.

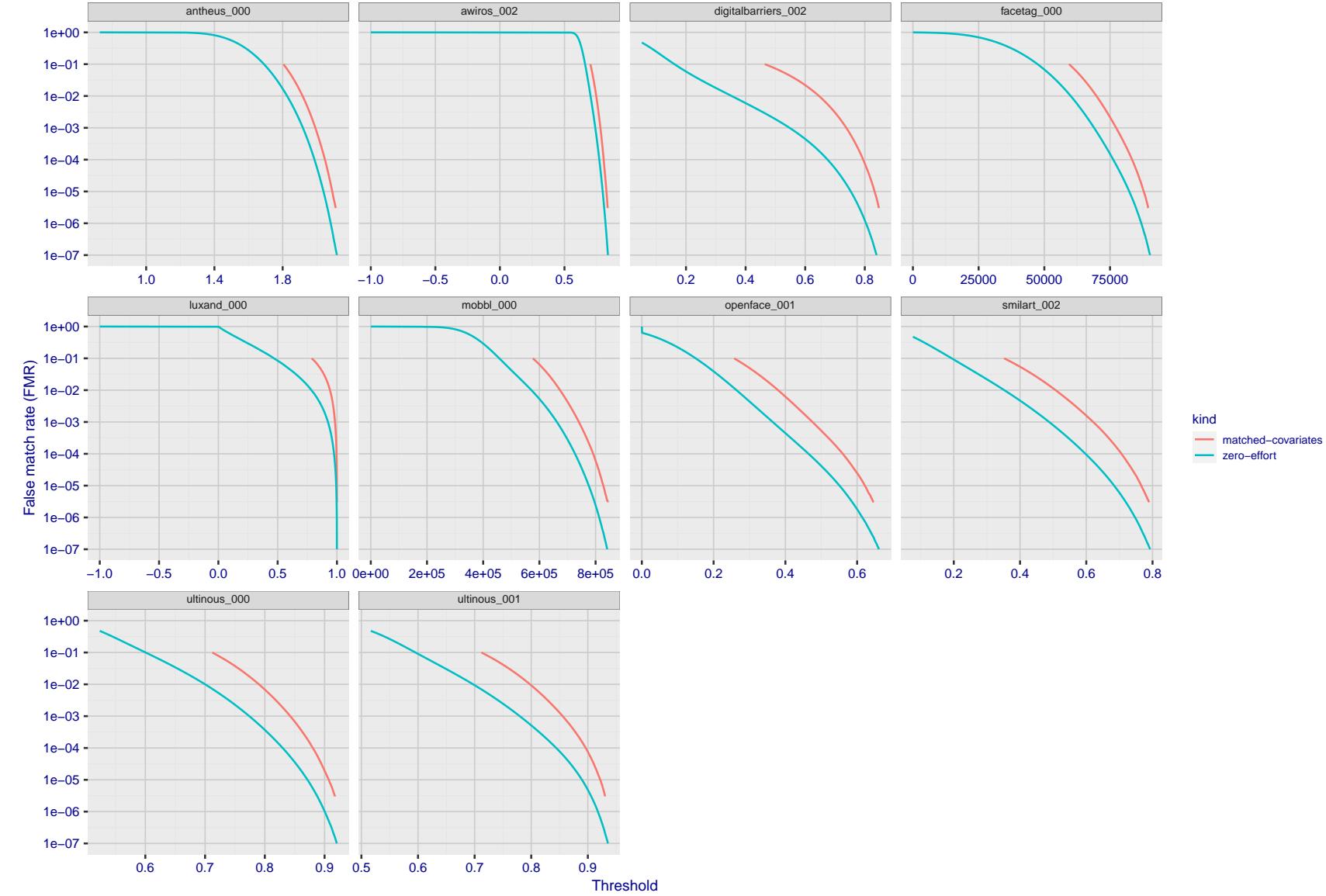


Figure 212: For the visa images, the false match calibration curves show FMR vs. threshold, T . The blue (lower) curves are for zero-effort impostors (i.e. comparing all images against all). The red (upper) curves are for persons of the same-sex, same-age, and same national-origin. This shows that FMR is underestimated (by a factor of 10 or more) by using a zero-effort impostor calculation to calibrate T . As shown later (sec. 3.6), FMR is higher for demographic-matched impostors.

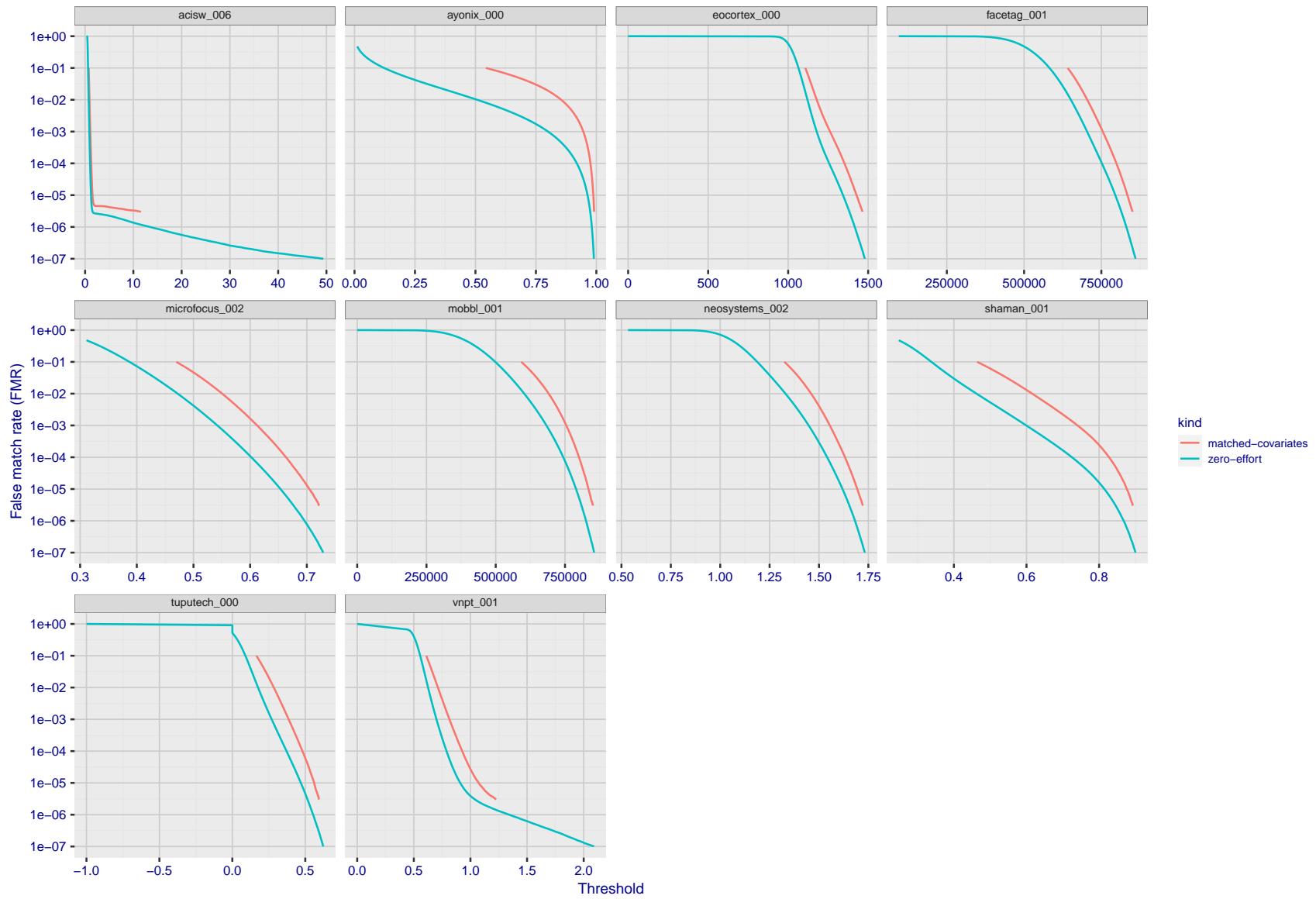


Figure 213: For the visa images, the false match calibration curves show FMR vs. threshold, T . The blue (lower) curves are for zero-effort impostors (i.e. comparing all images against all). The red (upper) curves are for persons of the same-sex, same-age, and same national-origin. This shows that FMR is underestimated (by a factor of 10 or more) by using a zero-effort impostor calculation to calibrate T . As shown later (sec. 3.6), FMR is higher for demographic-matched impostors.

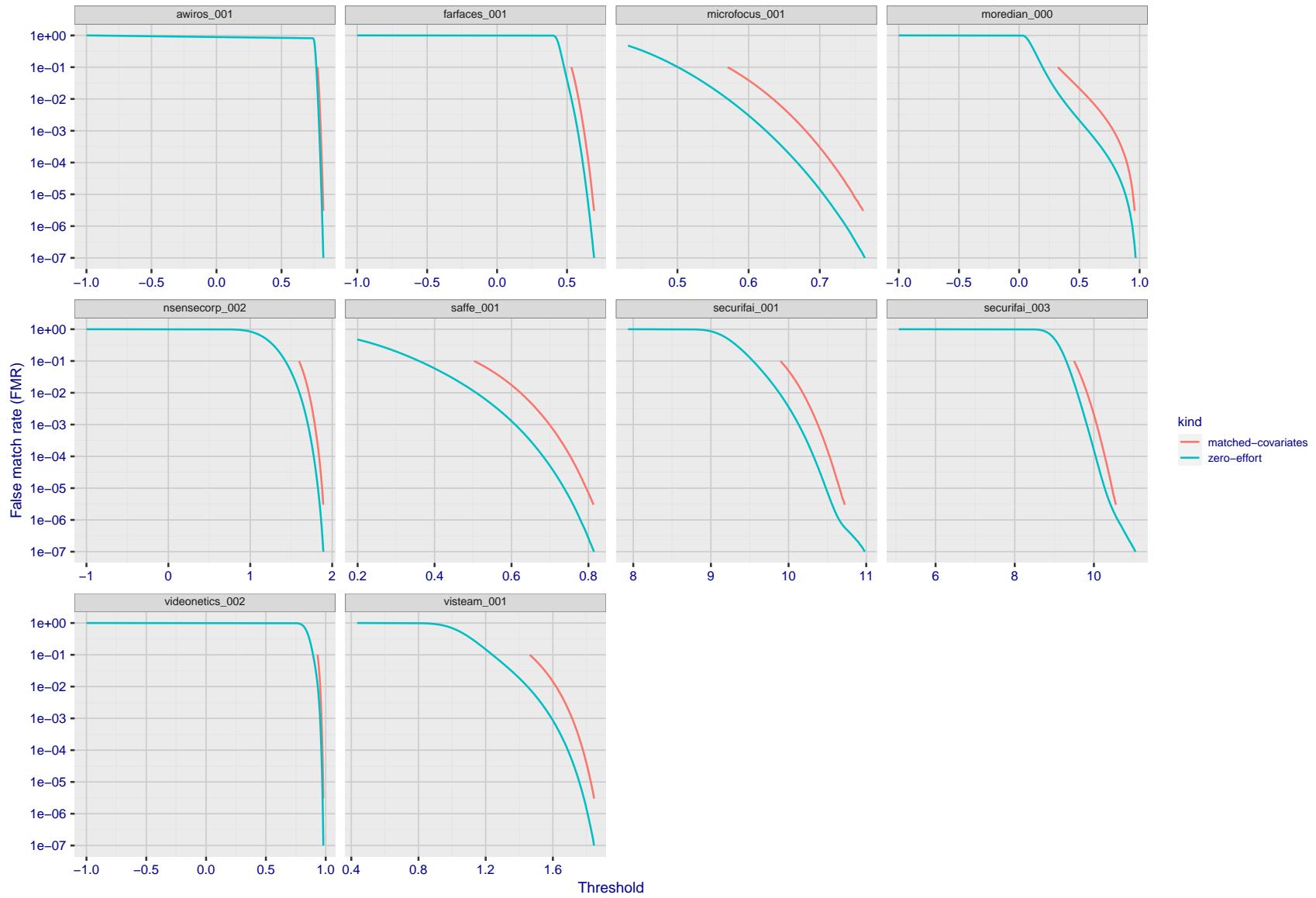


Figure 214: For the visa images, the false match calibration curves show FMR vs. threshold, T . The blue (lower) curves are for zero-effort impostors (i.e. comparing all images against all). The red (upper) curves are for persons of the same-sex, same-age, and same national-origin. This shows that FMR is underestimated (by a factor of 10 or more) by using a zero-effort impostor calculation to calibrate T . As shown later (sec. 3.6), FMR is higher for demographic-matched impostors.

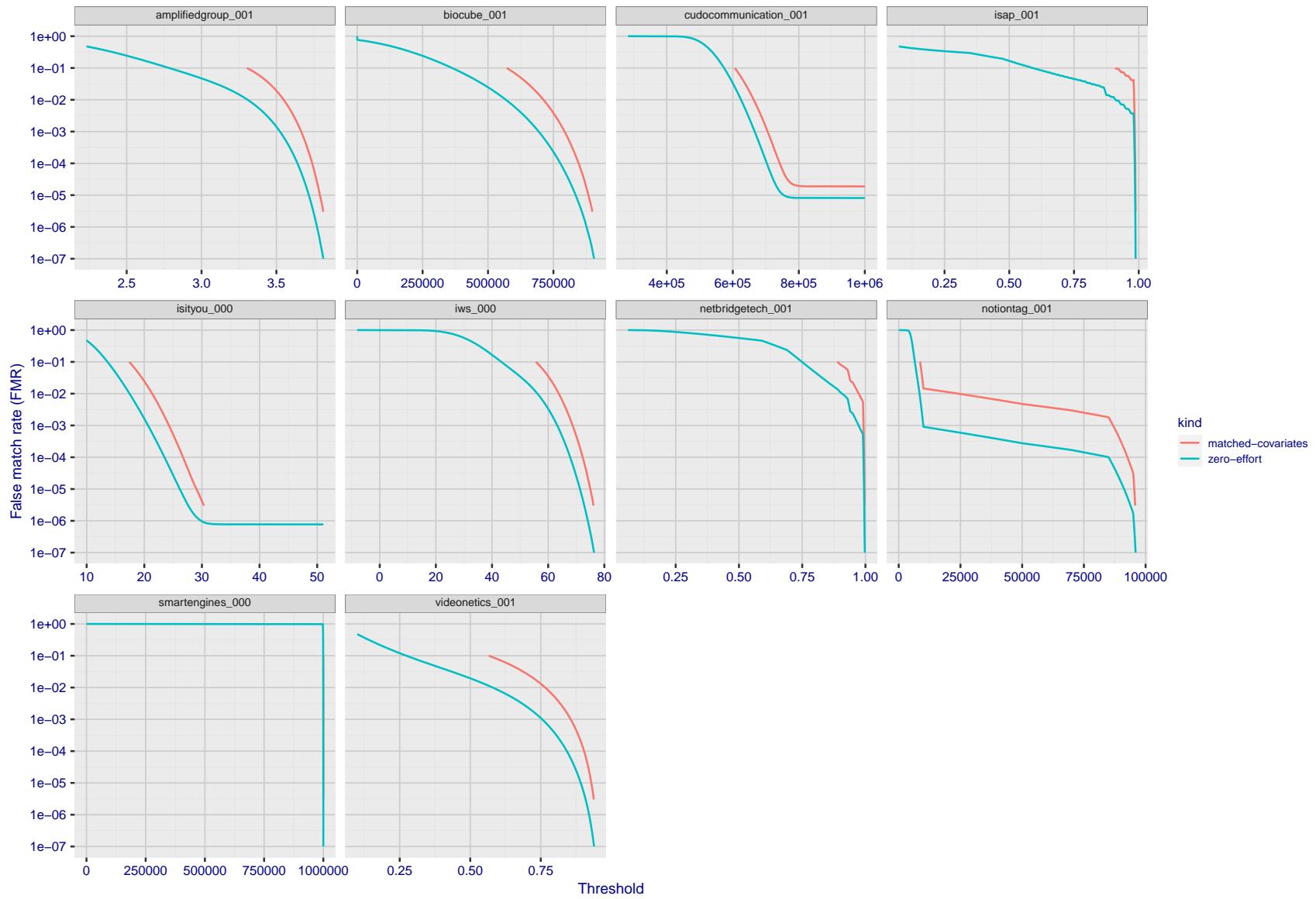


Figure 215: For the visa images, the false match calibration curves show FMR vs. threshold, T . The blue (lower) curves are for zero-effort impostors (i.e. comparing all images against all). The red (upper) curves are for persons of the same-sex, same-age, and same national-origin. This shows that FMR is underestimated (by a factor of 10 or more) by using a zero-effort impostor calculation to calibrate T . As shown later (sec. 3.6), FMR is higher for demographic-matched impostors.

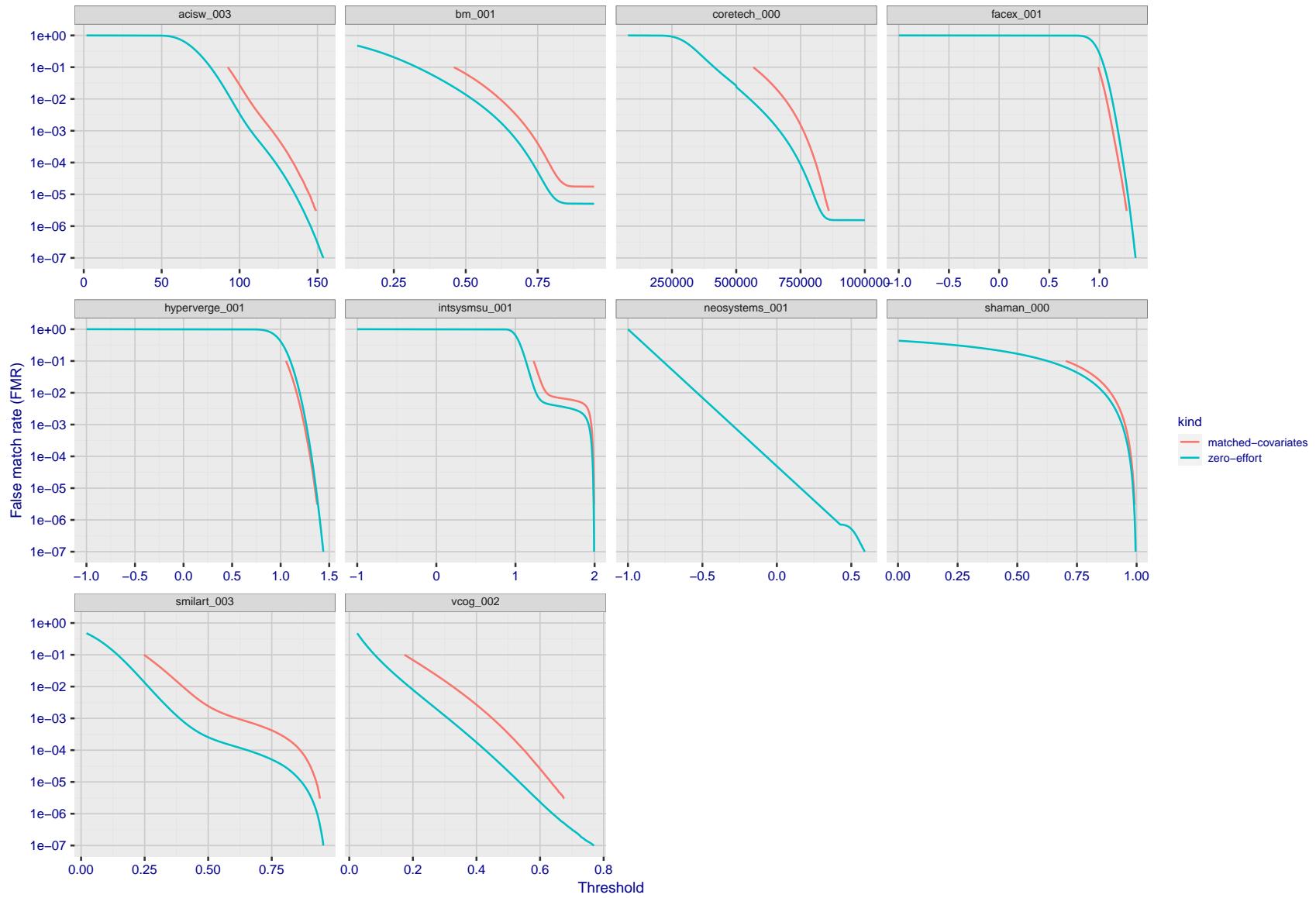


Figure 216: For the visa images, the false match calibration curves show FMR vs. threshold, T . The blue (lower) curves are for zero-effort impostors (i.e. comparing all images against all). The red (upper) curves are for persons of the same-sex, same-age, and same national-origin. This shows that FMR is underestimated (by a factor of 10 or more) by using a zero-effort impostor calculation to calibrate T . As shown later (sec. 3.6), FMR is higher for demographic-matched impostors.

3.5 Genuine distribution stability

3.5.1 Effect of birth place on the genuine distribution

Background: Both skin tone and bone structure vary geographically. Prior studies have reported variations in FNMR and FMR.

Goal: To measure false non-match rate (FNMR) variation with country of birth.

Methods: Thresholds are determined that give $FMR = \{0.001, 0.0001\}$ over the entire impostor set. Then FNMR is measured over 1000 bootstrap replications of the genuine scores. Only those countries with at least 140 individuals are included in the analysis.

Results: Figure 247 shows FNMR by country of birth for the two thresholds.

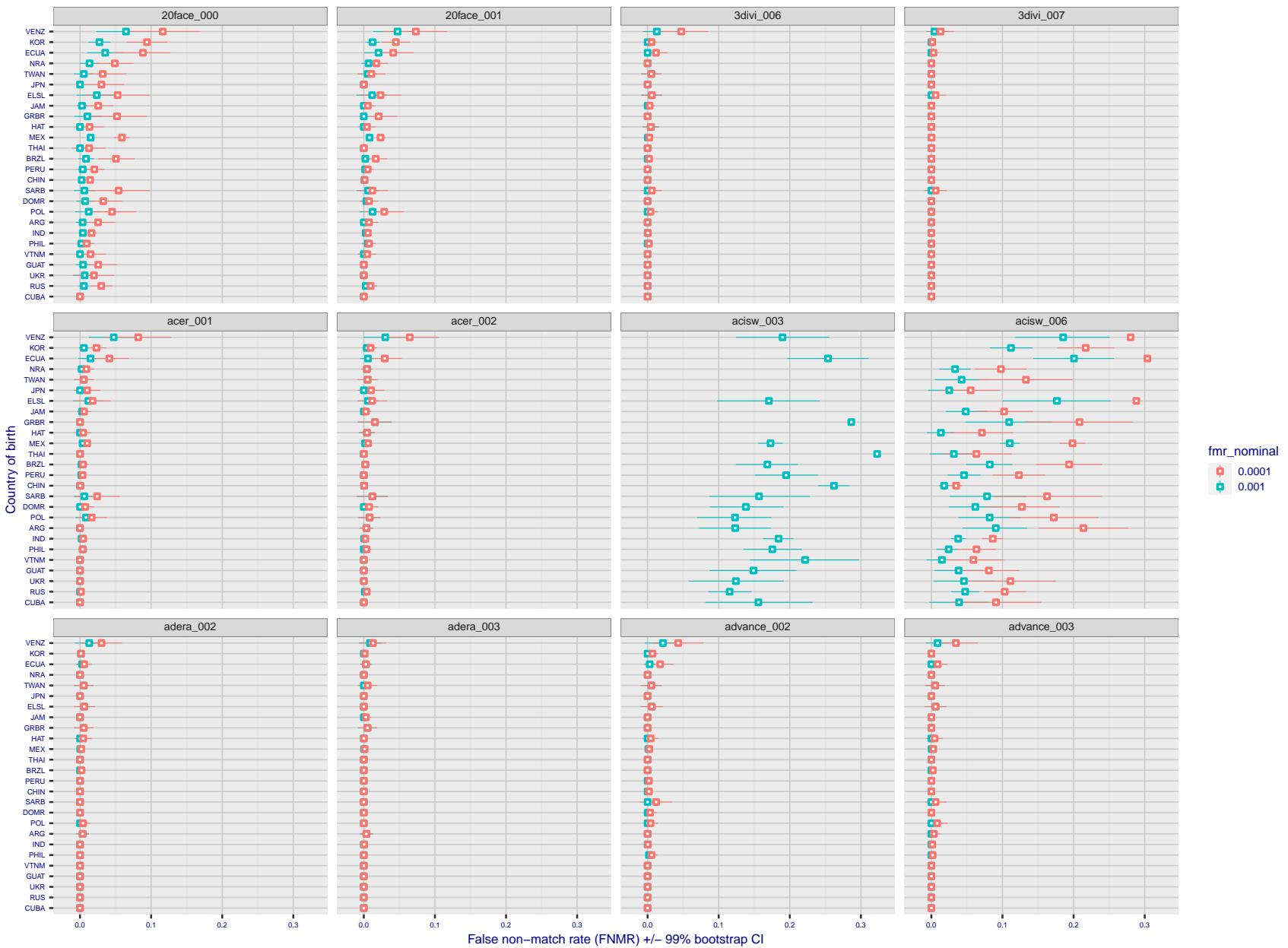


Figure 217: For the visa images, the dots show FNMR by country of birth for two globally set operating thresholds corresponding to $FMR = \{0.001, 0.0001\}$ computed over all on the order of 10^{10} impostor scores. The FMR in each bin will vary also - see subsequent impostor heatmaps in sec. 3.6.1. The figures shows an order of magnitude variation in FNMR across country of birth; these effects are likely due quality variations, then demographics like age and race. The error rates in some cases are zero, and in others the DET is flat so the error rates at the two thresholds are identical. The lines span 1% and 99% of bootstrap replicated FNMR estimates.

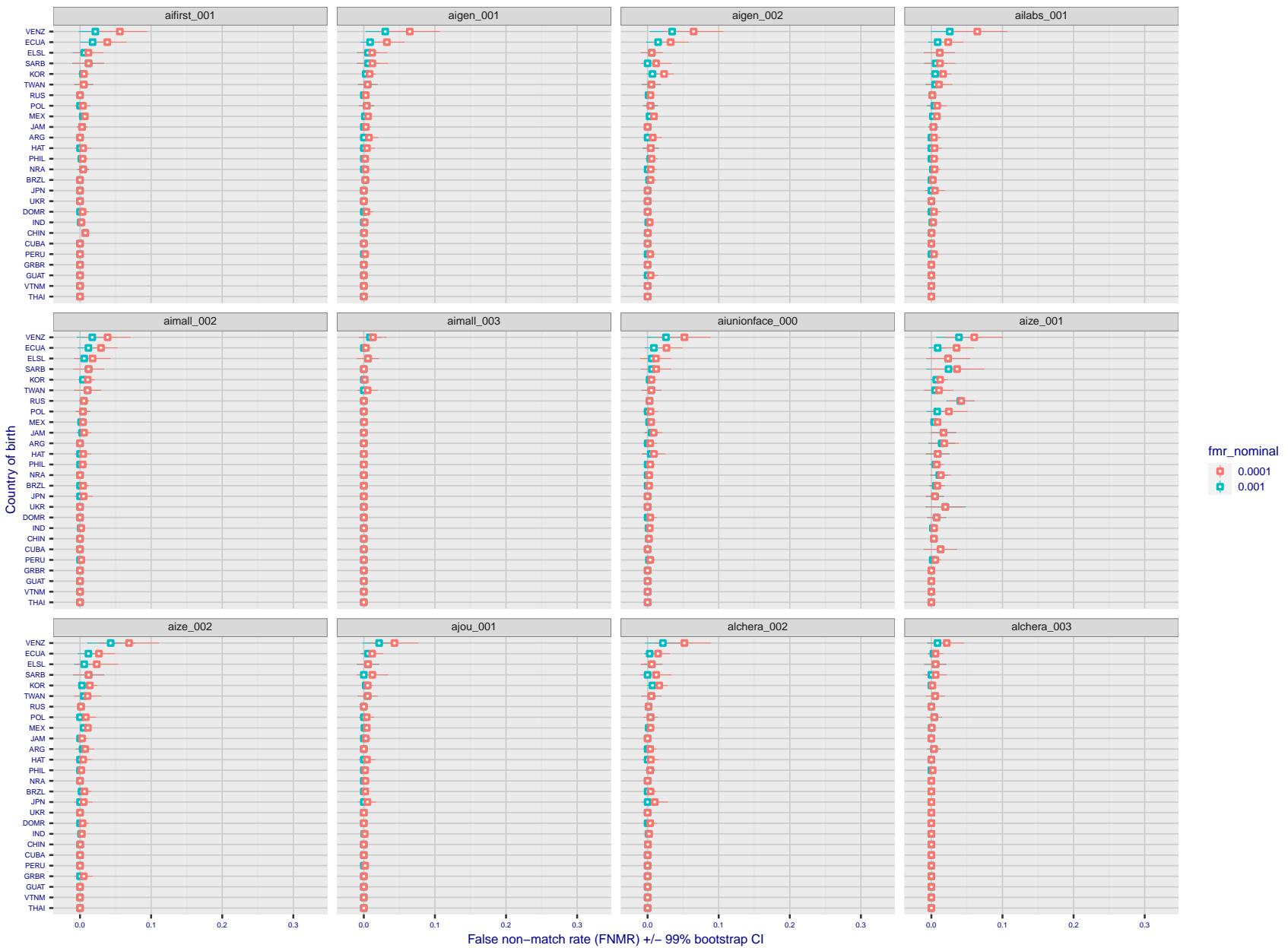


Figure 218: For the visa images, the dots show FNMR by country of birth for two globally set operating thresholds corresponding to $FMR = \{0.001, 0.0001\}$ computed over all on the order of 10^{10} impostor scores. The FMR in each bin will vary also - see subsequent impostor heatmaps in sec. 3.6.1. The figures shows an order of magnitude variation in FNMR across country of birth; these effects are likely due quality variations, then demographics like age and race. The error rates in some cases are zero, and in others the DET is flat so the error rates at the two thresholds are identical. The lines span 1% and 99% of bootstrap replicated FNMR estimates.

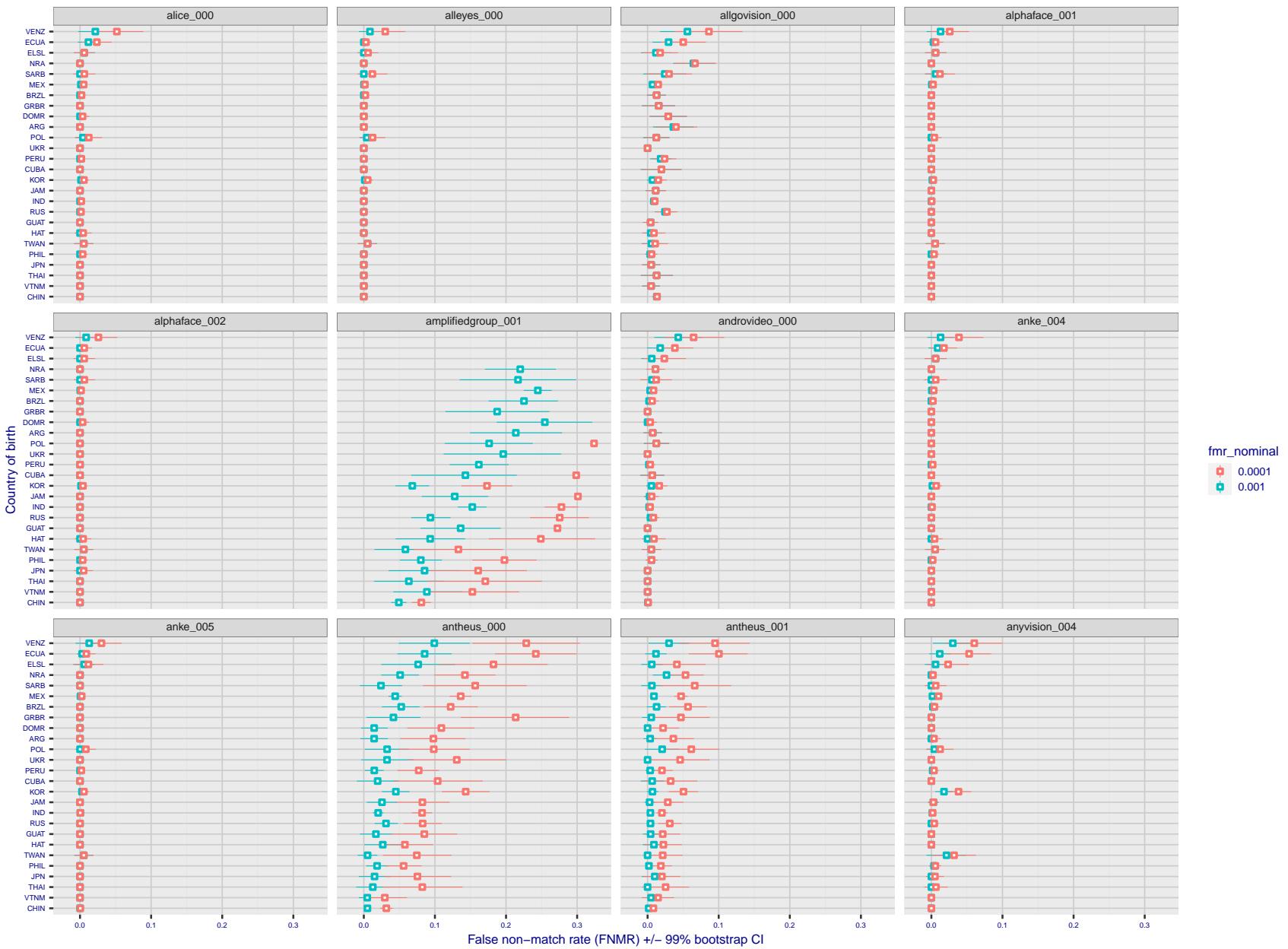


Figure 219: For the visa images, the dots show FNMR by country of birth for two globally set operating thresholds corresponding to $FMR = \{0.001, 0.0001\}$ computed over all on the order of 10^{10} impostor scores. The FMR in each bin will vary also - see subsequent impostor heatmaps in sec. 3.6.1. The figures shows an order of magnitude variation in FNMR across country of birth; these effects are likely due quality variations, then demographics like age and race. The error rates in some cases are zero, and in others the DET is flat so the error rates at the two thresholds are identical. The lines span 1% and 99% of bootstrap replicated FNMR estimates.

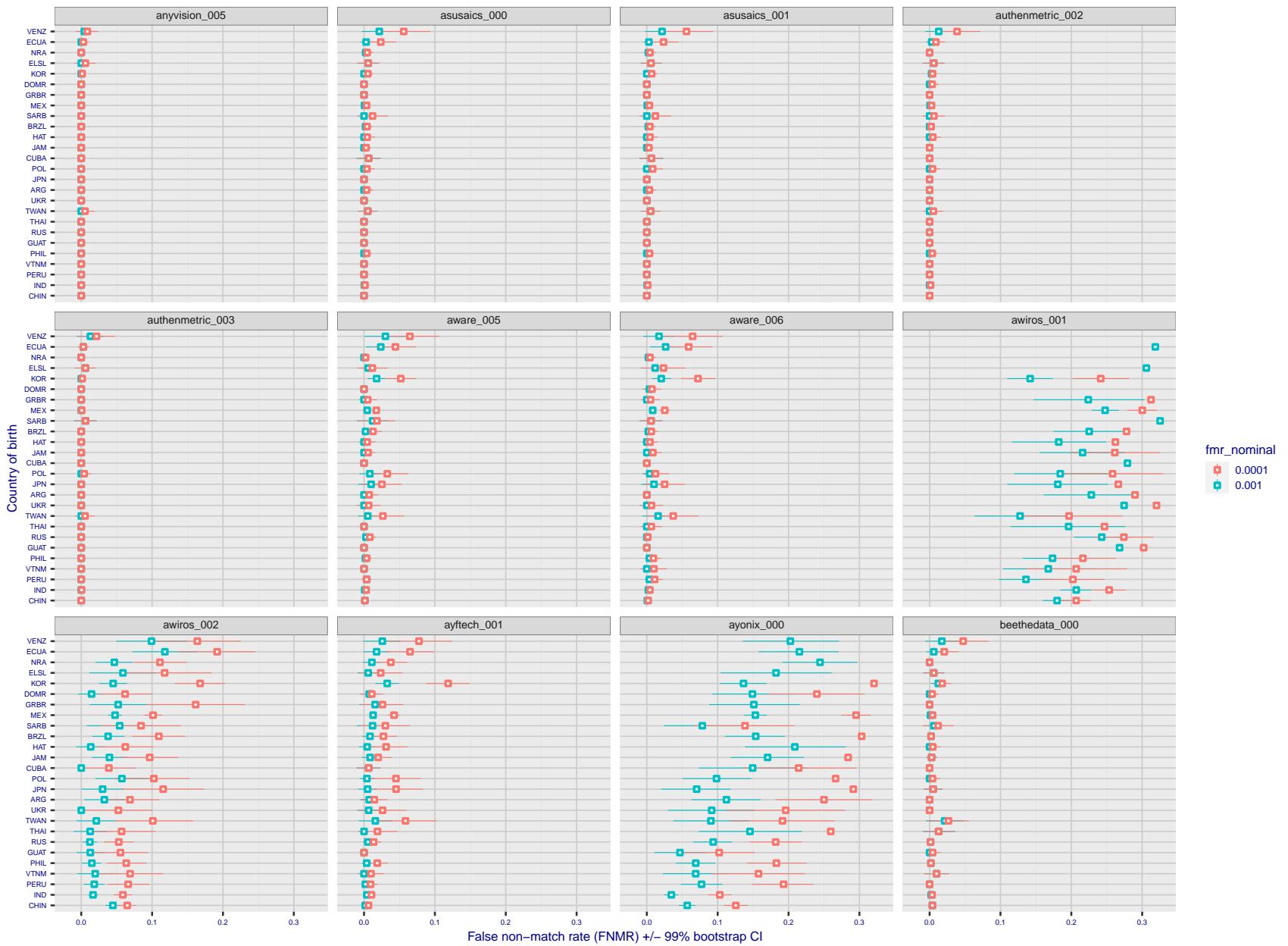


Figure 220: For the visa images, the dots show FNMR by country of birth for two globally set operating thresholds corresponding to $FMR = \{0.001, 0.0001\}$ computed over all on the order of 10^{10} impostor scores. The FMR in each bin will vary also - see subsequent impostor heatmaps in sec. 3.6.1. The figures shows an order of magnitude variation in FNMR across country of birth; these effects are likely due quality variations, then demographics like age and race. The error rates in some cases are zero, and in others the DET is flat so the error rates at the two thresholds are identical. The lines span 1% and 99% of bootstrap replicated FNMR estimates.

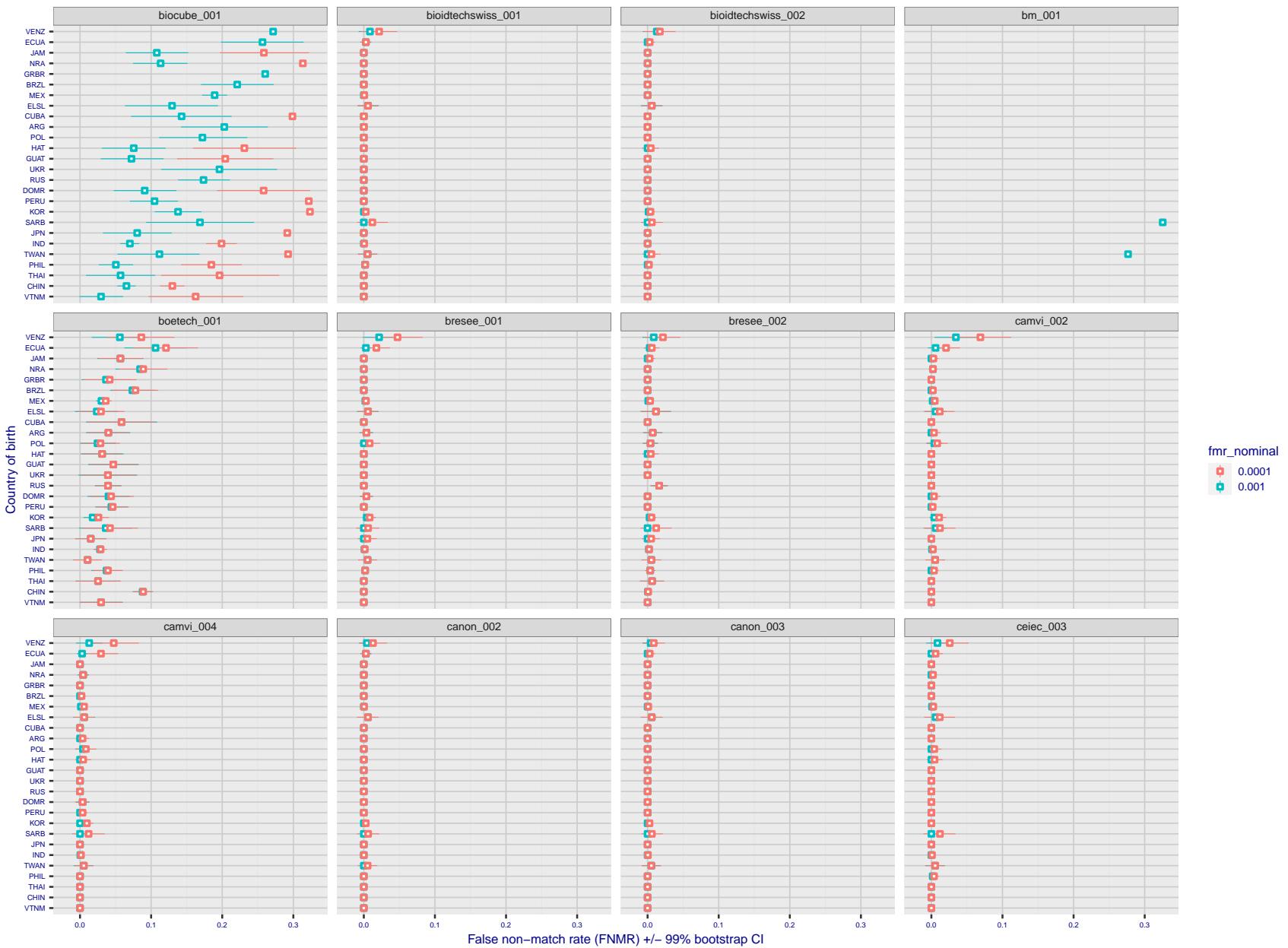


Figure 221: For the visa images, the dots show FNMR by country of birth for two globally set operating thresholds corresponding to $FMR = \{0.001, 0.0001\}$ computed over all on the order of 10^{10} impostor scores. The FMR in each bin will vary also - see subsequent impostor heatmaps in sec. 3.6.1. The figures shows an order of magnitude variation in FNMR across country of birth; these effects are likely due quality variations, then demographics like age and race. The error rates in some cases are zero, and in others the DET is flat so the error rates at the two thresholds are identical. The lines span 1% and 99% of bootstrap replicated FNMR estimates.

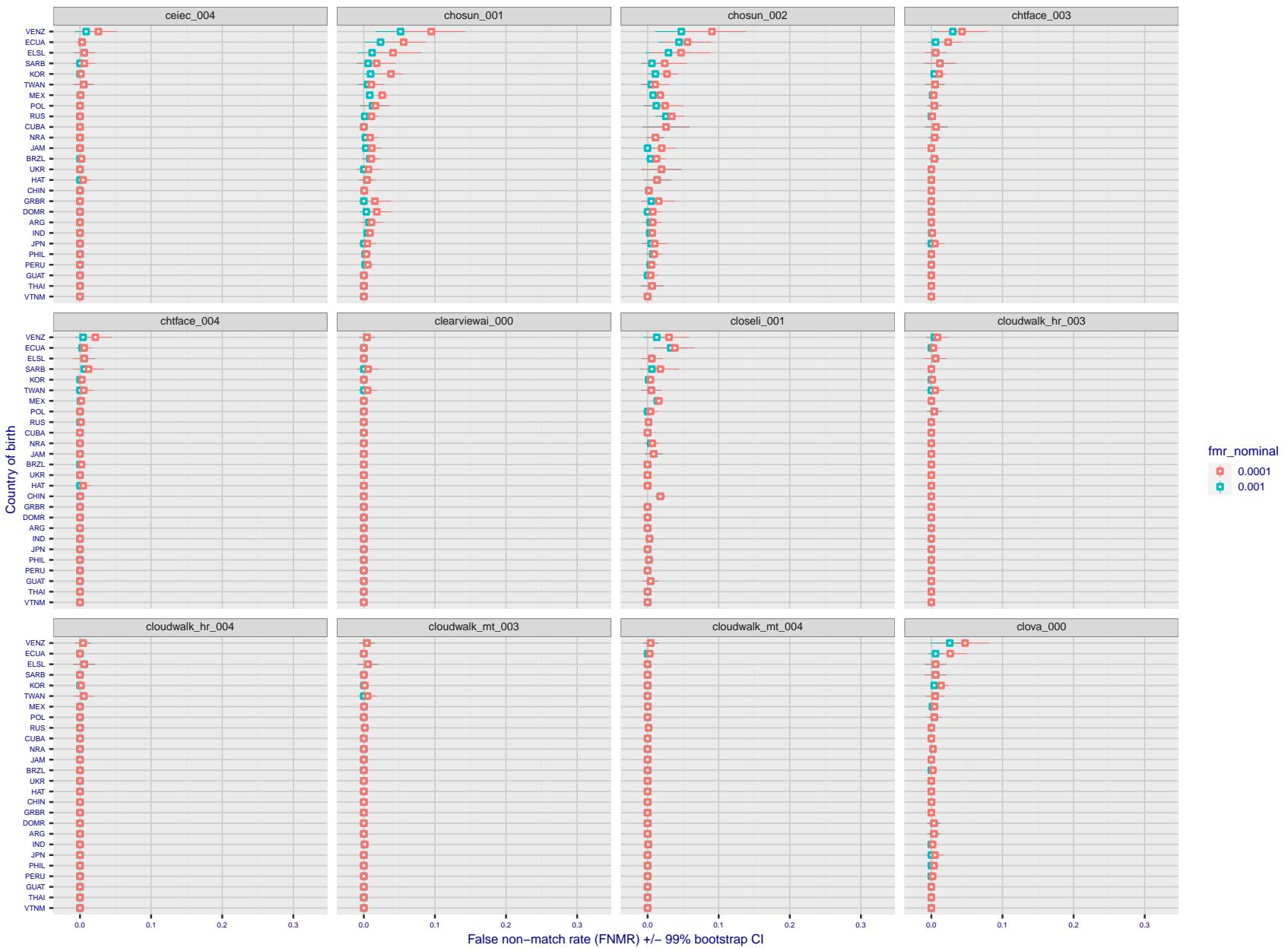


Figure 222: For the visa images, the dots show FNMR by country of birth for two globally set operating thresholds corresponding to $FMR = \{0.001, 0.0001\}$ computed over all on the order of 10^{10} impostor scores. The FMR in each bin will vary also - see subsequent impostor heatmaps in sec. 3.6.1. The figures shows an order of magnitude variation in FNMR across country of birth; these effects are likely due quality variations, then demographics like age and race. The error rates in some cases are zero, and in others the DET is flat so the error rates at the two thresholds are identical. The lines span 1% and 99% of bootstrap replicated FNMR estimates.

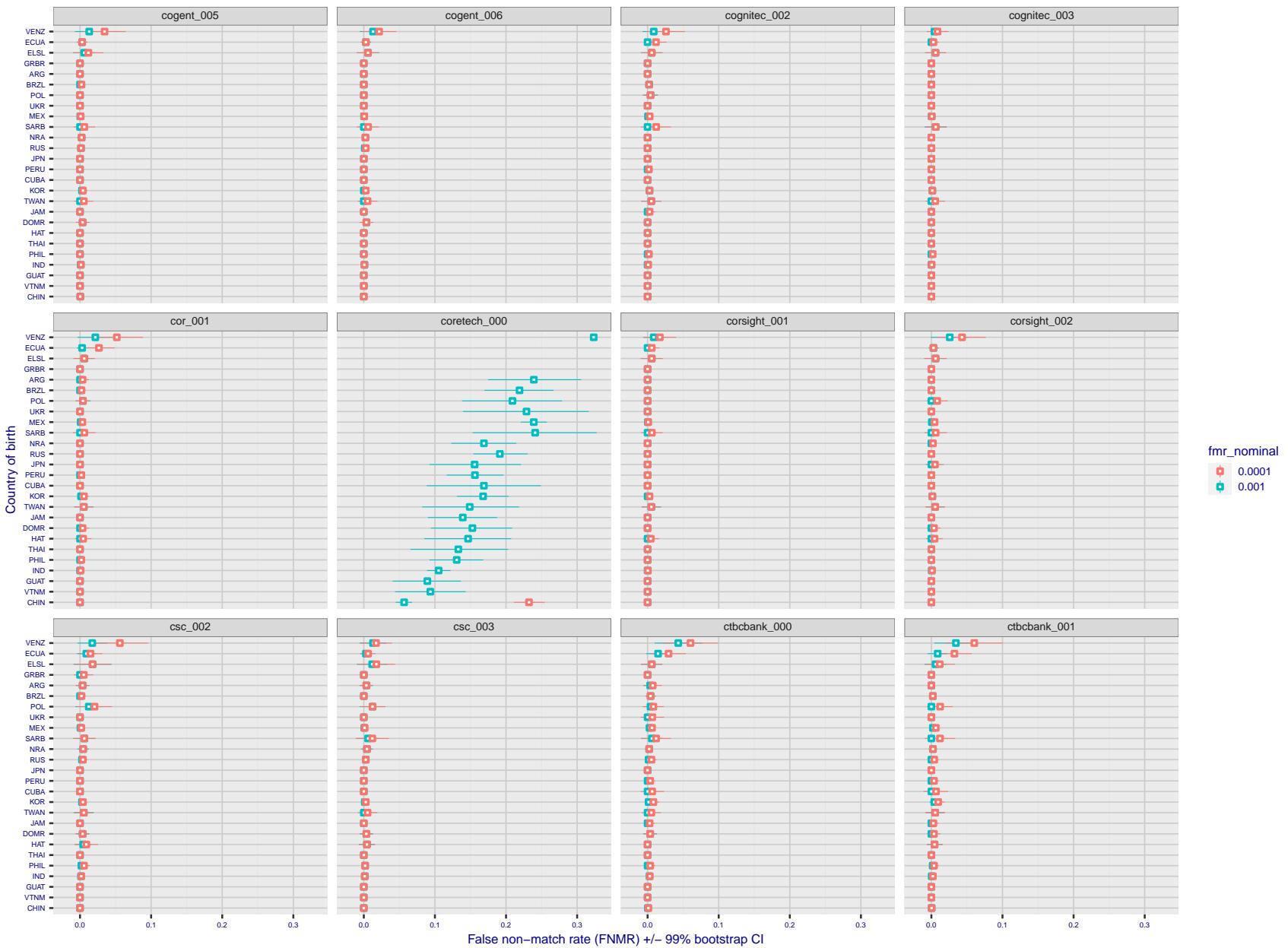


Figure 223: For the visa images, the dots show FNMR by country of birth for two globally set operating thresholds corresponding to $FMR = \{0.001, 0.0001\}$ computed over all on the order of 10^{10} impostor scores. The FMR in each bin will vary also - see subsequent impostor heatmaps in sec. 3.6.1. The figures shows an order of magnitude variation in FNMR across country of birth; these effects are likely due quality variations, then demographics like age and race. The error rates in some cases are zero, and in others the DET is flat so the error rates at the two thresholds are identical. The lines span 1% and 99% of bootstrap replicated FNMR estimates.

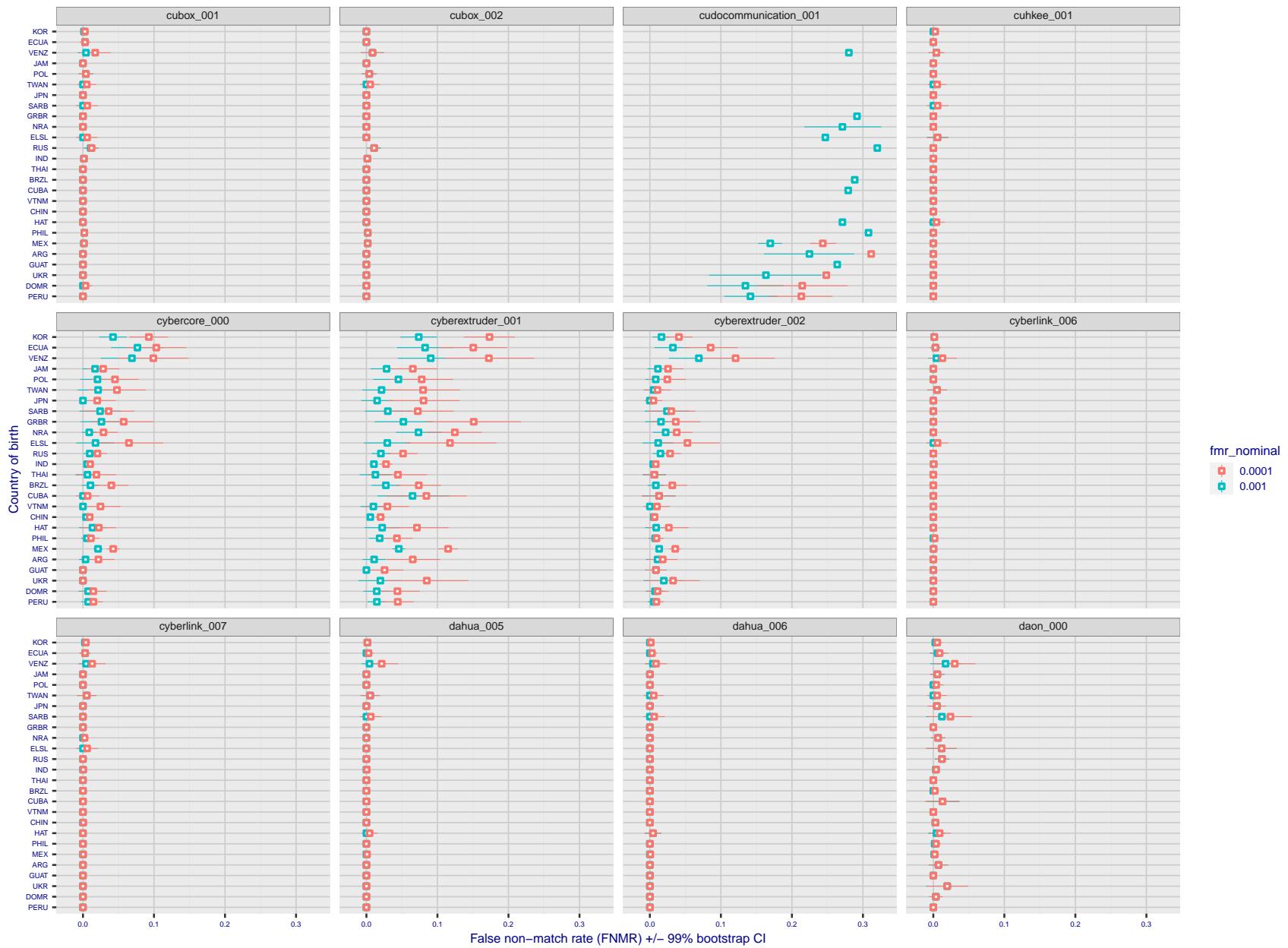


Figure 224: For the visa images, the dots show FNMR by country of birth for two globally set operating thresholds corresponding to $FMR = \{0.001, 0.0001\}$ computed over all on the order of 10^{10} impostor scores. The FMR in each bin will vary also - see subsequent impostor heatmaps in sec. 3.6.1. The figures shows an order of magnitude variation in FNMR across country of birth; these effects are likely due quality variations, then demographics like age and race. The error rates in some cases are zero, and in others the DET is flat so the error rates at the two thresholds are identical. The lines span 1% and 99% of bootstrap replicated FNMR estimates.

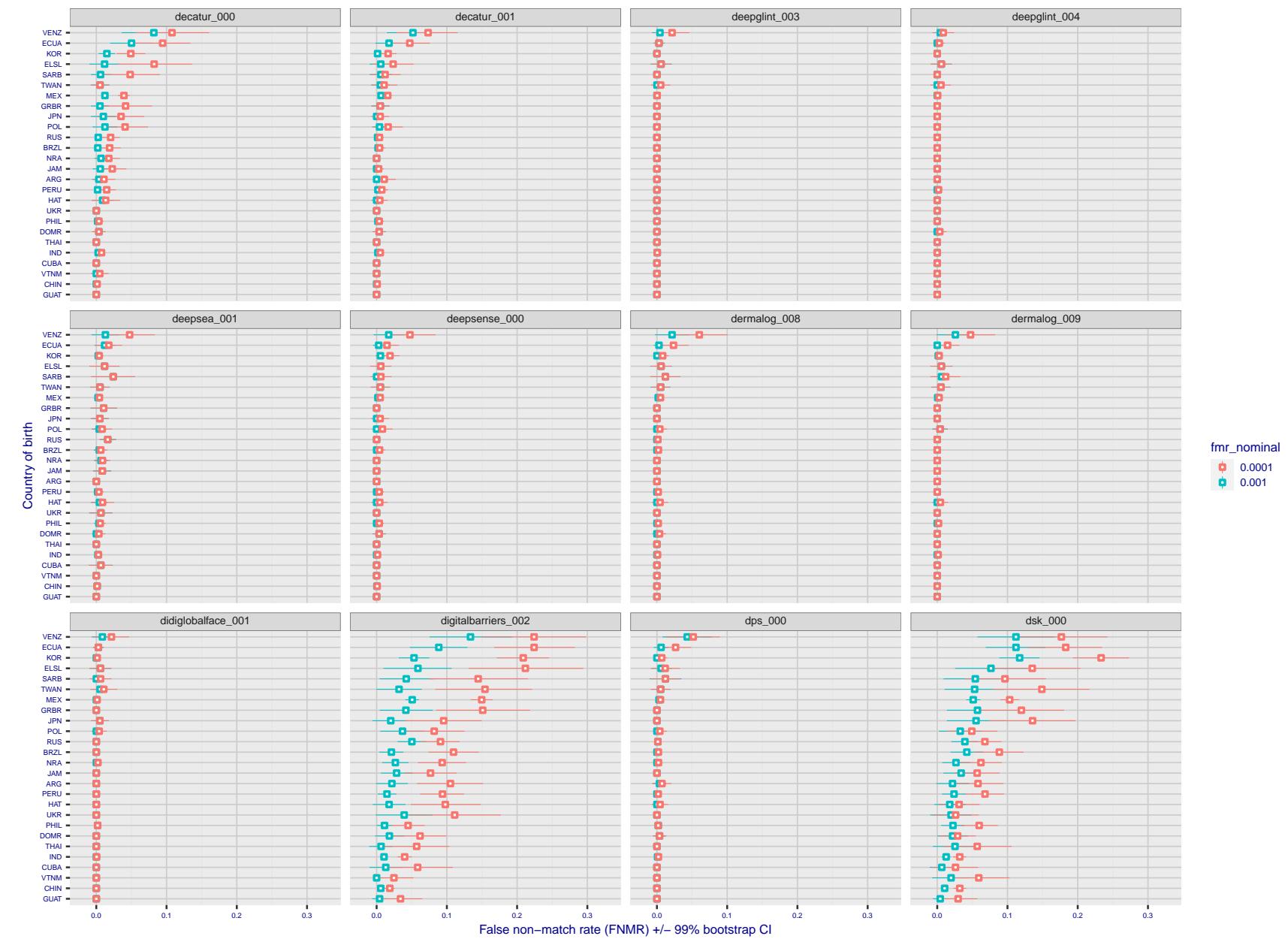


Figure 225: For the visa images, the dots show FNMR by country of birth for two globally set operating thresholds corresponding to $FMR = \{0.001, 0.0001\}$ computed over all on the order of 10^{10} impostor scores. The FMR in each bin will vary also - see subsequent impostor heatmaps in sec. 3.6.1. The figures shows an order of magnitude variation in FNMR across country of birth; these effects are likely due quality variations, then demographics like age and race. The error rates in some cases are zero, and in others the DET is flat so the error rates at the two thresholds are identical. The lines span 1% and 99% of bootstrap replicated FNMR estimates.

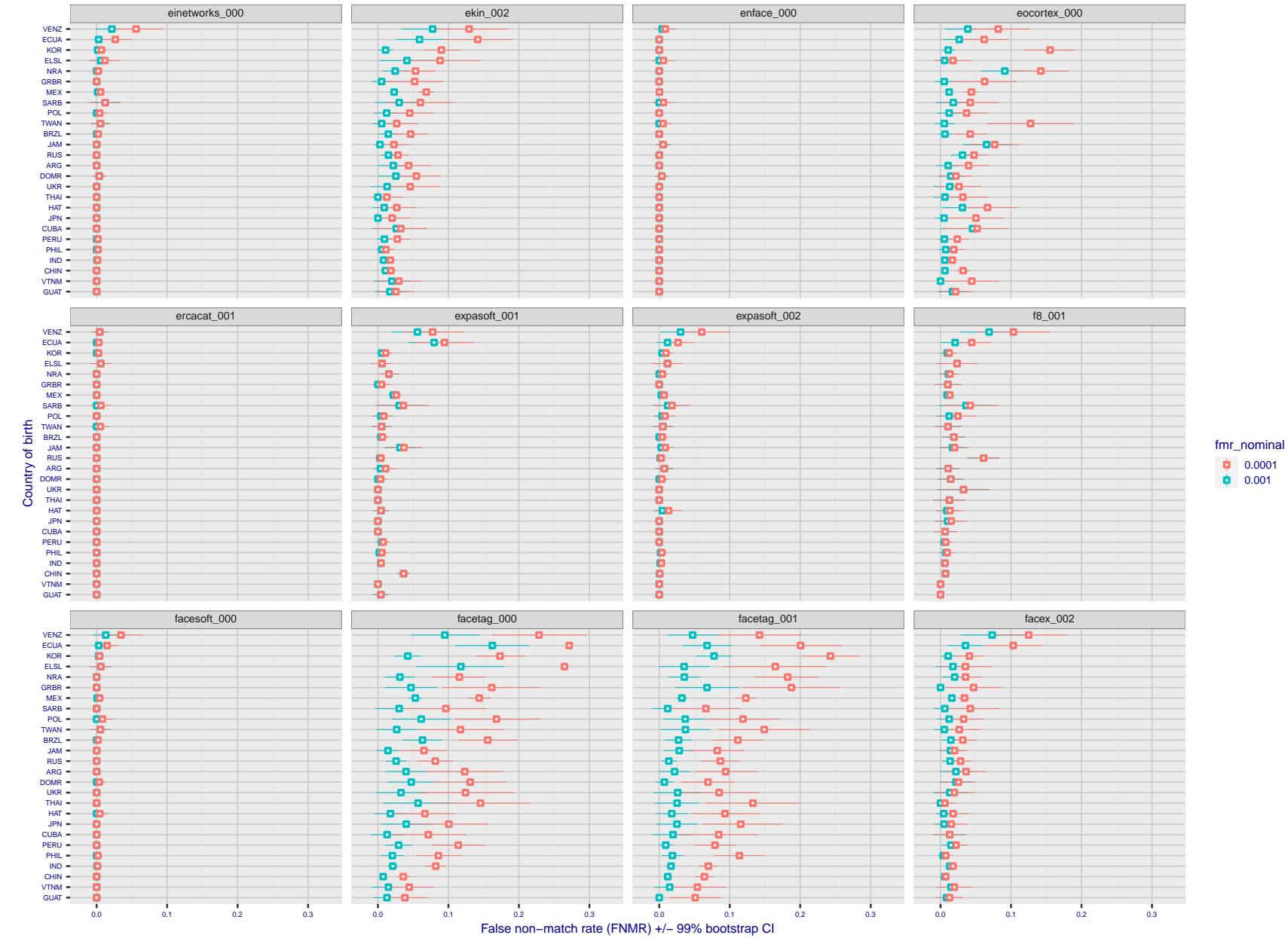


Figure 226: For the visa images, the dots show FNMR by country of birth for two globally set operating thresholds corresponding to $FMR = \{0.001, 0.0001\}$ computed over all on the order of 10^{10} impostor scores. The FMR in each bin will vary also - see subsequent impostor heatmaps in sec. 3.6.1. The figures shows an order of magnitude variation in FNMR across country of birth; these effects are likely due quality variations, then demographics like age and race. The error rates in some cases are zero, and in others the DET is flat so the error rates at the two thresholds are identical. The lines span 1% and 99% of bootstrap replicated FNMR estimates.

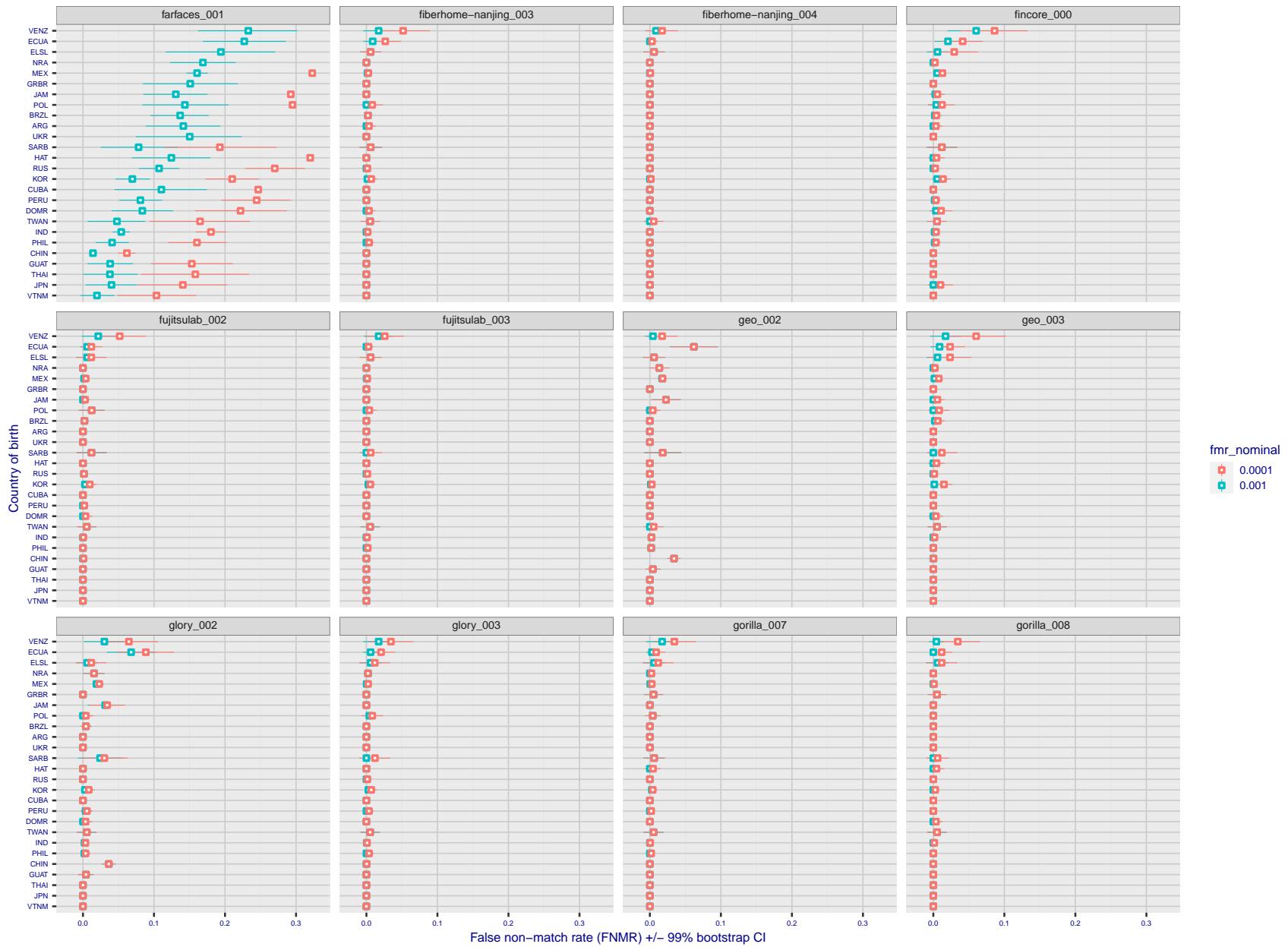


Figure 227: For the visa images, the dots show FNMR by country of birth for two globally set operating thresholds corresponding to $FMR = \{0.001, 0.0001\}$ computed over all on the order of 10^{10} impostor scores. The FMR in each bin will vary also - see subsequent impostor heatmaps in sec. 3.6.1. The figures shows an order of magnitude variation in FNMR across country of birth; these effects are likely due quality variations, then demographics like age and race. The error rates in some cases are zero, and in others the DET is flat so the error rates at the two thresholds are identical. The lines span 1% and 99% of bootstrap replicated FNMR estimates.

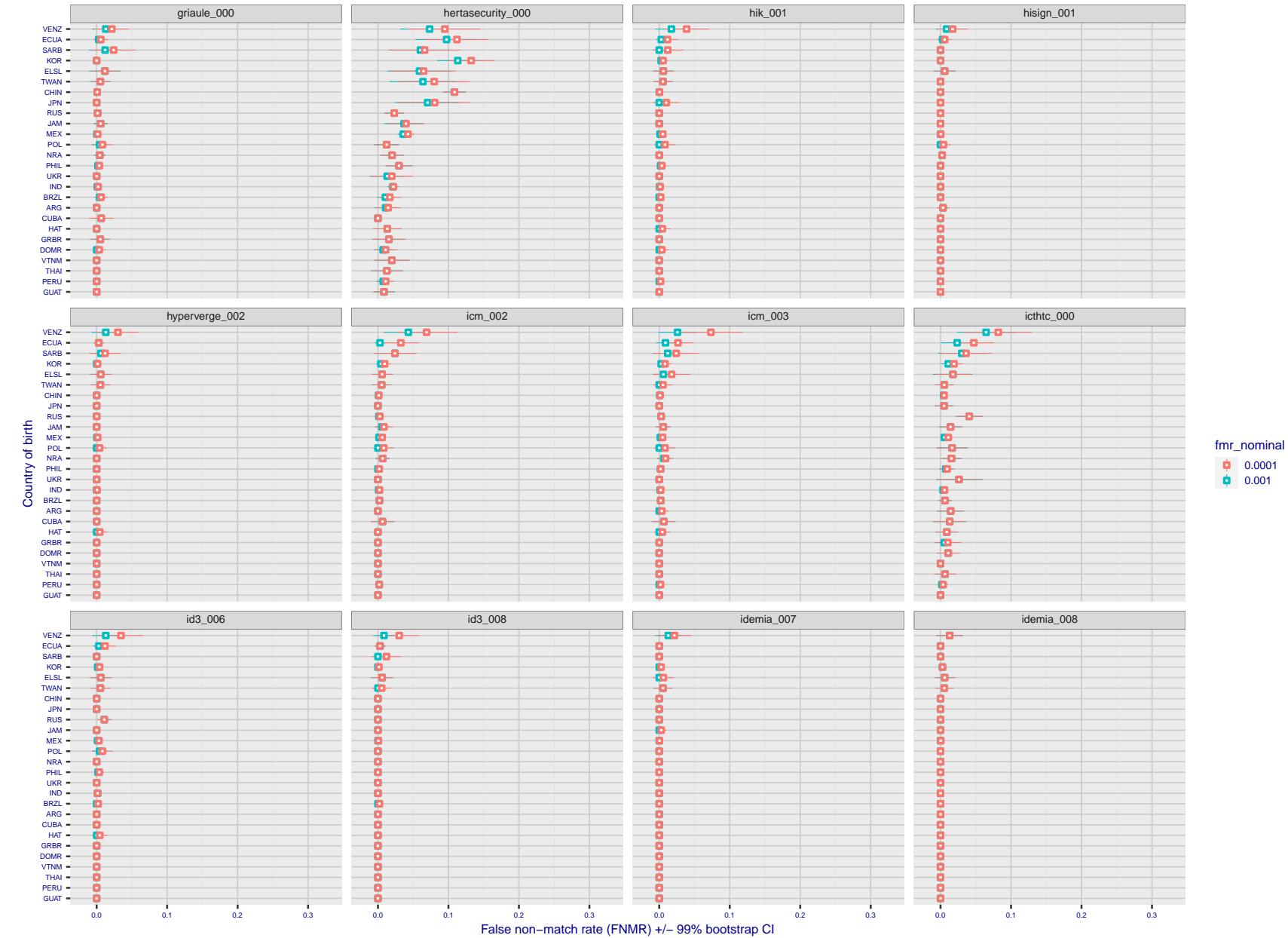


Figure 228: For the visa images, the dots show FNMR by country of birth for two globally set operating thresholds corresponding to $FMR = \{0.001, 0.0001\}$ computed over all on the order of 10^{10} impostor scores. The FMR in each bin will vary also - see subsequent impostor heatmaps in sec. 3.6.1. The figures shows an order of magnitude variation in FNMR across country of birth; these effects are likely due quality variations, then demographics like age and race. The error rates in some cases are zero, and in others the DET is flat so the error rates at the two thresholds are identical. The lines span 1% and 99% of bootstrap replicated FNMR estimates.

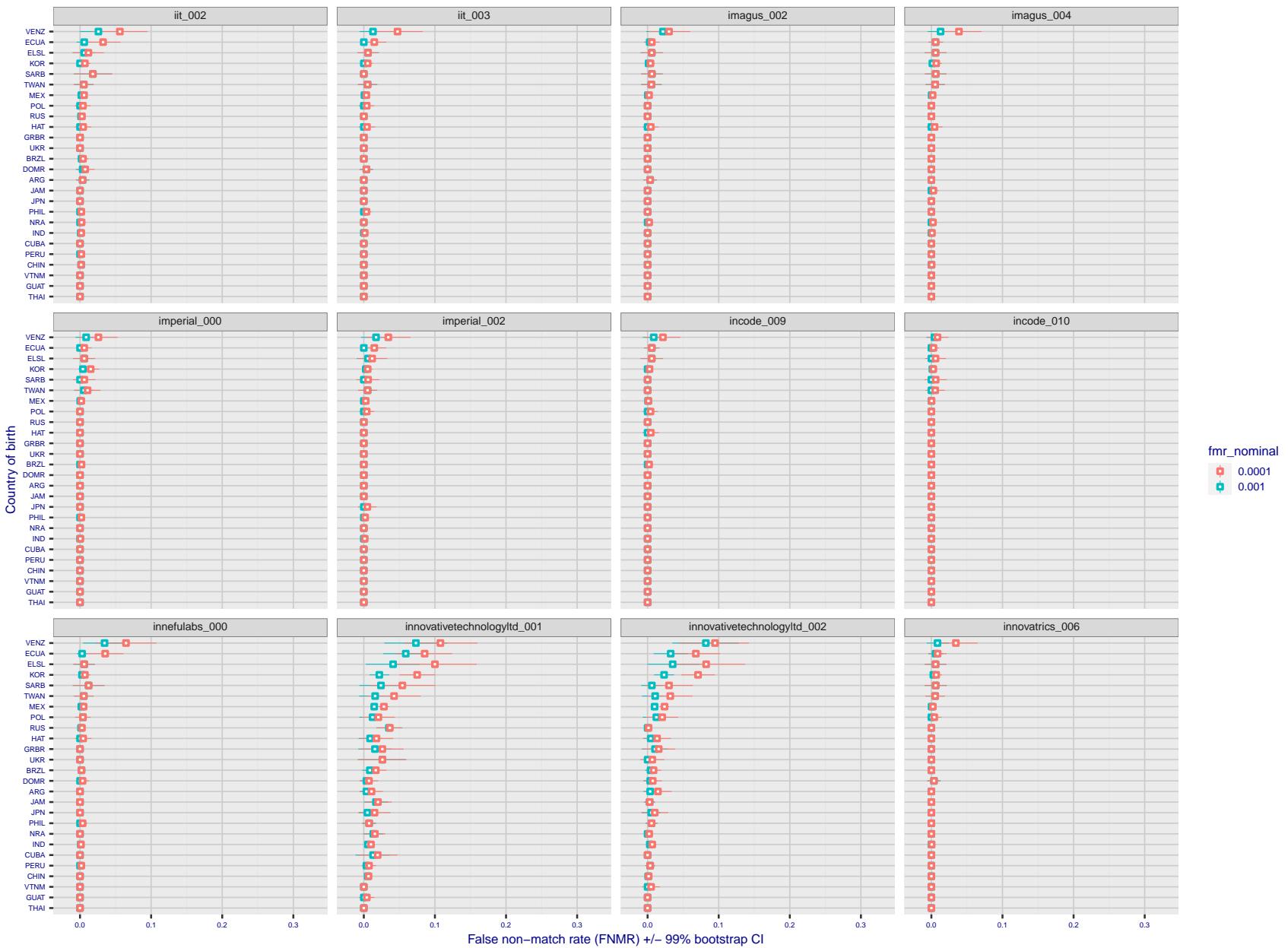


Figure 229: For the visa images, the dots show FNMR by country of birth for two globally set operating thresholds corresponding to $FMR = \{0.001, 0.0001\}$ computed over all on the order of 10^{10} impostor scores. The FMR in each bin will vary also - see subsequent impostor heatmaps in sec. 3.6.1. The figures shows an order of magnitude variation in FNMR across country of birth; these effects are likely due quality variations, then demographics like age and race. The error rates in some cases are zero, and in others the DET is flat so the error rates at the two thresholds are identical. The lines span 1% and 99% of bootstrap replicated FNMR estimates.

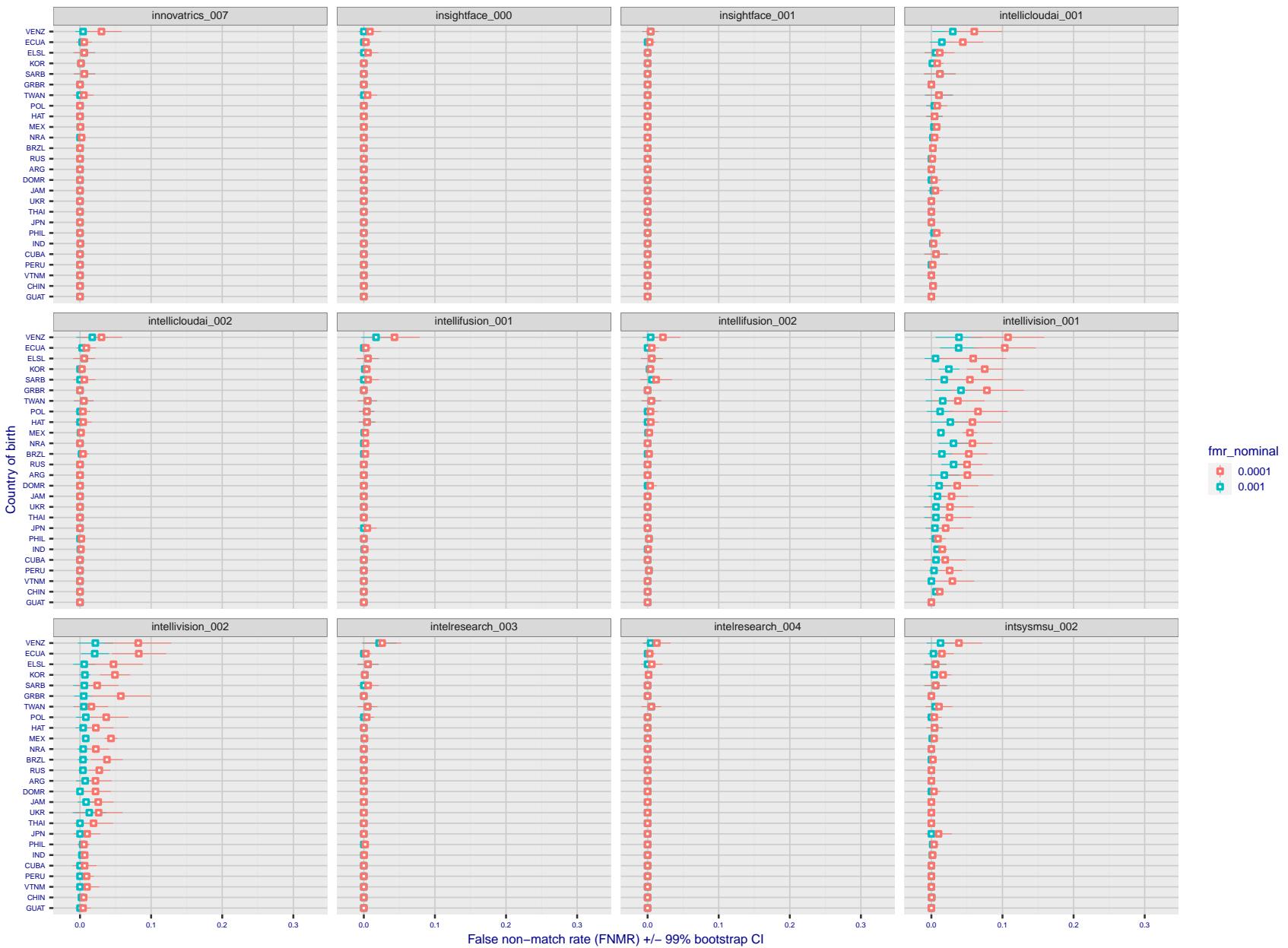


Figure 230: For the visa images, the dots show FNMR by country of birth for two globally set operating thresholds corresponding to $FMR = \{0.001, 0.0001\}$ computed over all on the order of 10^{10} impostor scores. The FMR in each bin will vary also - see subsequent impostor heatmaps in sec. 3.6.1. The figures shows an order of magnitude variation in FNMR across country of birth; these effects are likely due quality variations, then demographics like age and race. The error rates in some cases are zero, and in others the DET is flat so the error rates at the two thresholds are identical. The lines span 1% and 99% of bootstrap replicated FNMR estimates.

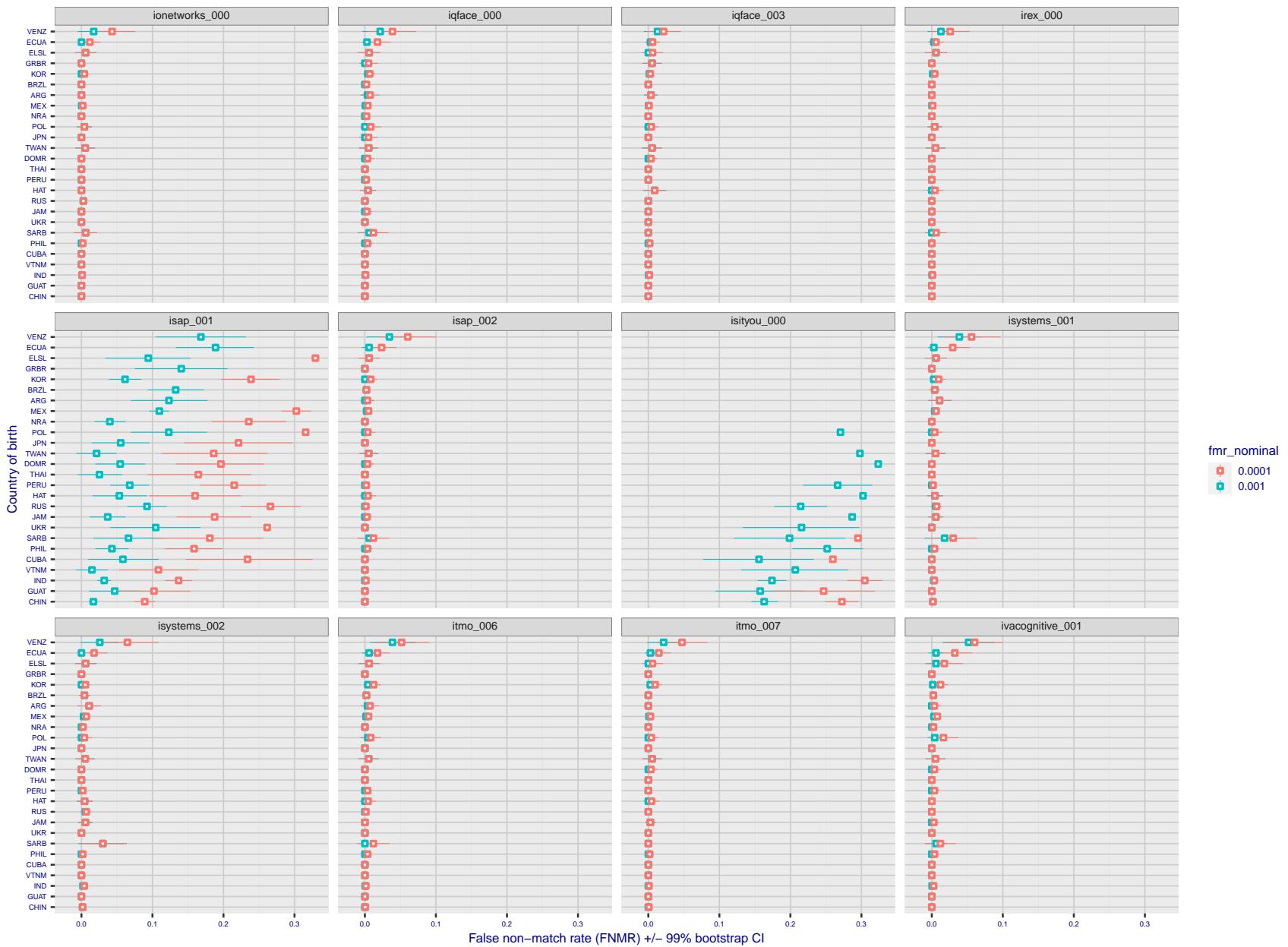


Figure 231: For the visa images, the dots show FNMR by country of birth for two globally set operating thresholds corresponding to $FMR = \{0.001, 0.0001\}$ computed over all on the order of 10^{10} impostor scores. The FMR in each bin will vary also - see subsequent impostor heatmaps in sec. 3.6.1. The figures shows an order of magnitude variation in FNMR across country of birth; these effects are likely due quality variations, then demographics like age and race. The error rates in some cases are zero, and in others the DET is flat so the error rates at the two thresholds are identical. The lines span 1% and 99% of bootstrap replicated FNMR estimates.

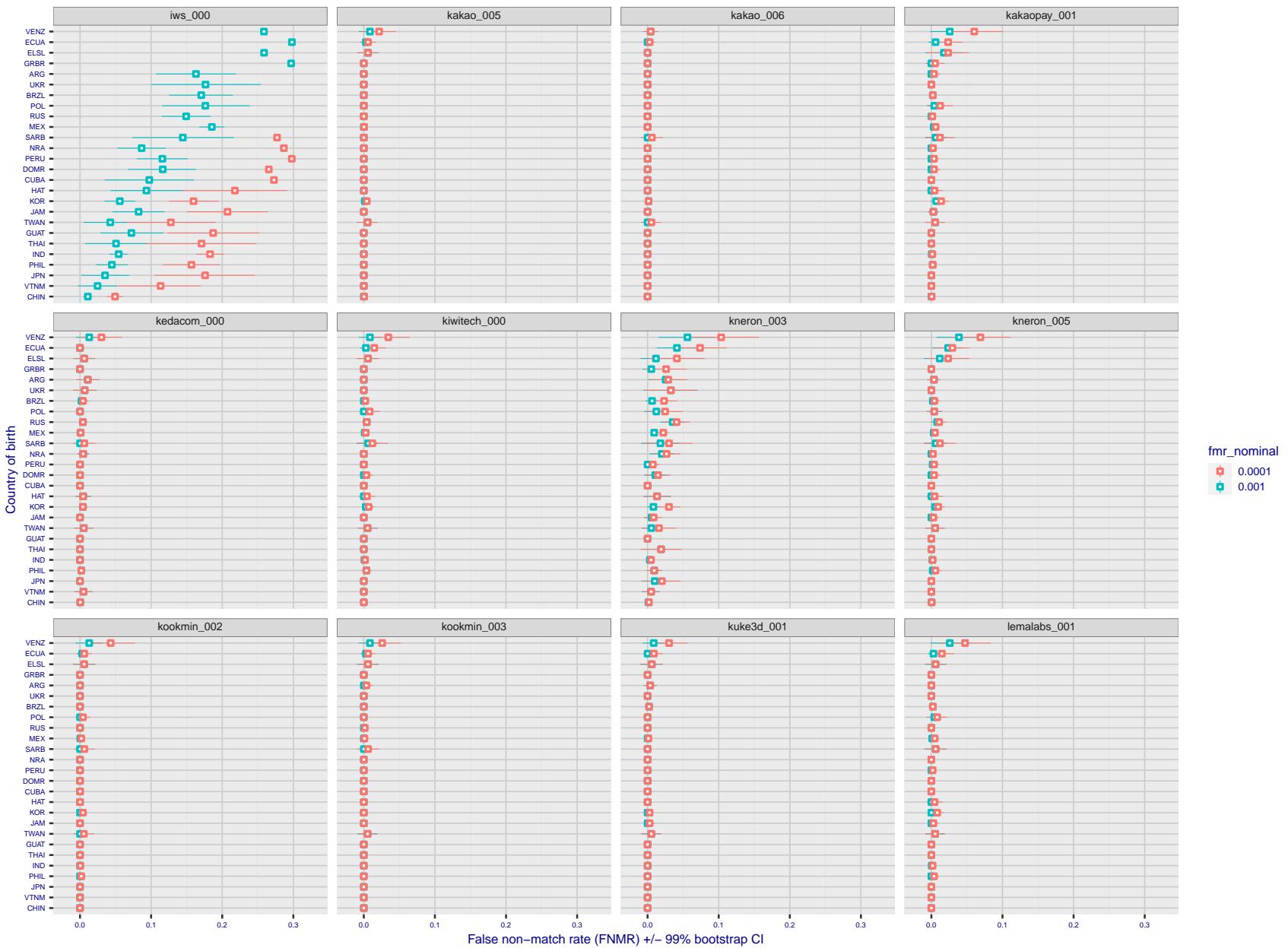


Figure 232: For the visa images, the dots show FNMR by country of birth for two globally set operating thresholds corresponding to $FMR = \{0.001, 0.0001\}$ computed over all on the order of 10^{10} impostor scores. The FMR in each bin will vary also - see subsequent impostor heatmaps in sec. 3.6.1. The figures shows an order of magnitude variation in FNMR across country of birth; these effects are likely due quality variations, then demographics like age and race. The error rates in some cases are zero, and in others the DET is flat so the error rates at the two thresholds are identical. The lines span 1% and 99% of bootstrap replicated FNMR estimates.

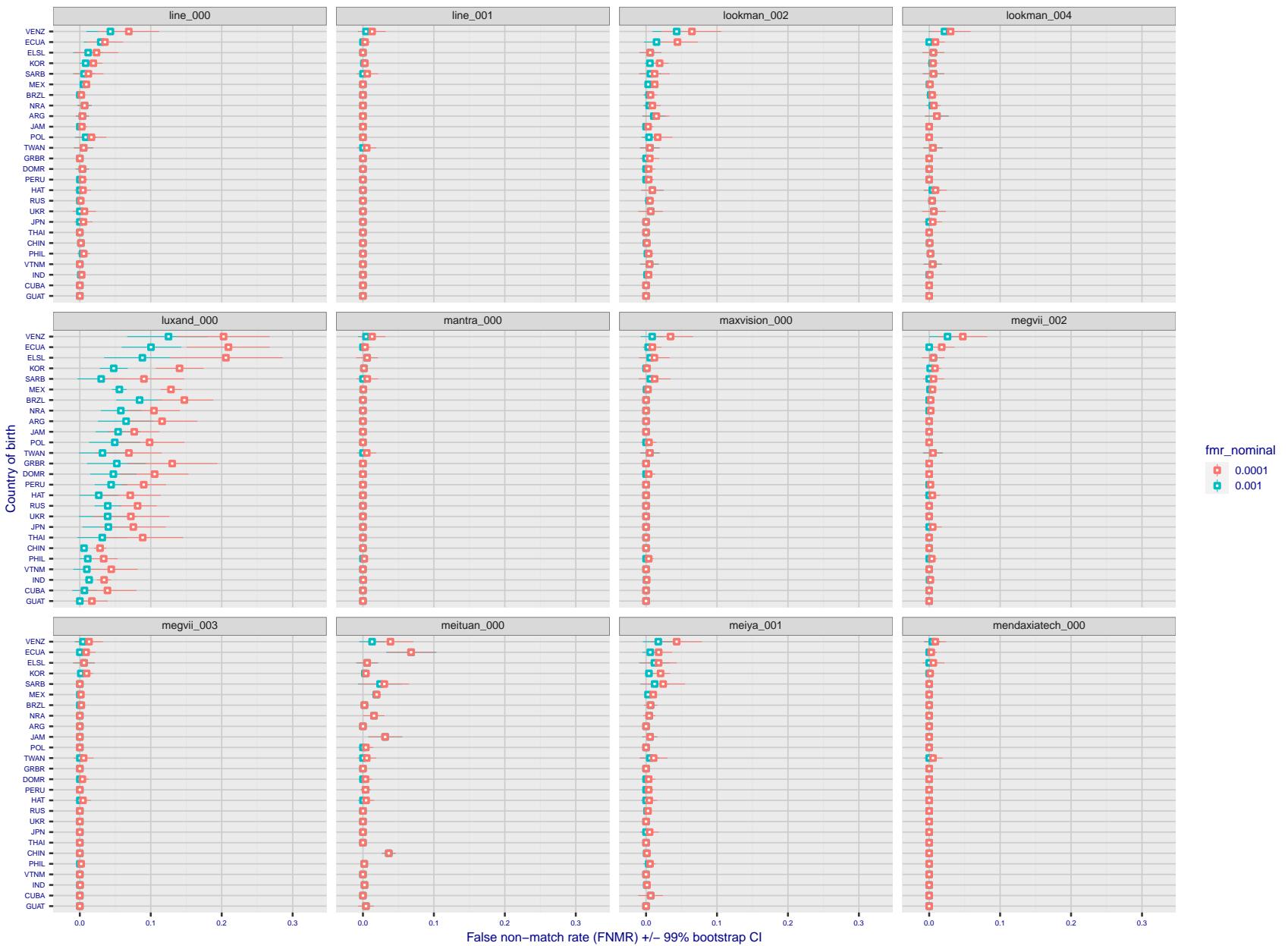


Figure 233: For the visa images, the dots show FNMR by country of birth for two globally set operating thresholds corresponding to $FMR = \{0.001, 0.0001\}$ computed over all on the order of 10^{10} impostor scores. The FMR in each bin will vary also - see subsequent impostor heatmaps in sec. 3.6.1. The figures shows an order of magnitude variation in FNMR across country of birth; these effects are likely due quality variations, then demographics like age and race. The error rates in some cases are zero, and in others the DET is flat so the error rates at the two thresholds are identical. The lines span 1% and 99% of bootstrap replicated FNMR estimates.

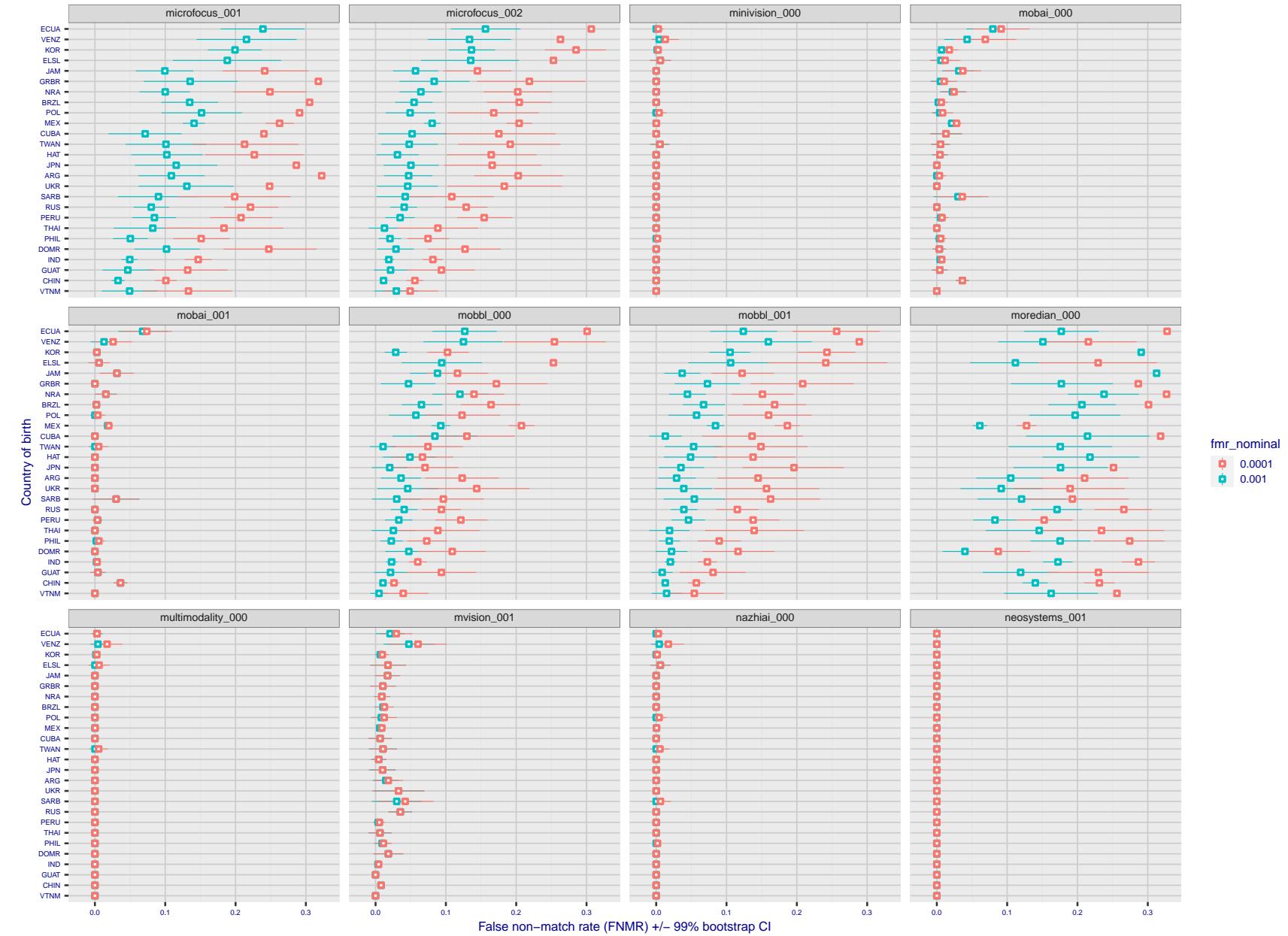


Figure 234: For the visa images, the dots show FNMR by country of birth for two globally set operating thresholds corresponding to $FMR = \{0.001, 0.0001\}$ computed over all on the order of 10^{10} impostor scores. The FMR in each bin will vary also - see subsequent impostor heatmaps in sec. 3.6.1. The figures shows an order of magnitude variation in FNMR across country of birth; these effects are likely due quality variations, then demographics like age and race. The error rates in some cases are zero, and in others the DET is flat so the error rates at the two thresholds are identical. The lines span 1% and 99% of bootstrap replicated FNMR estimates.

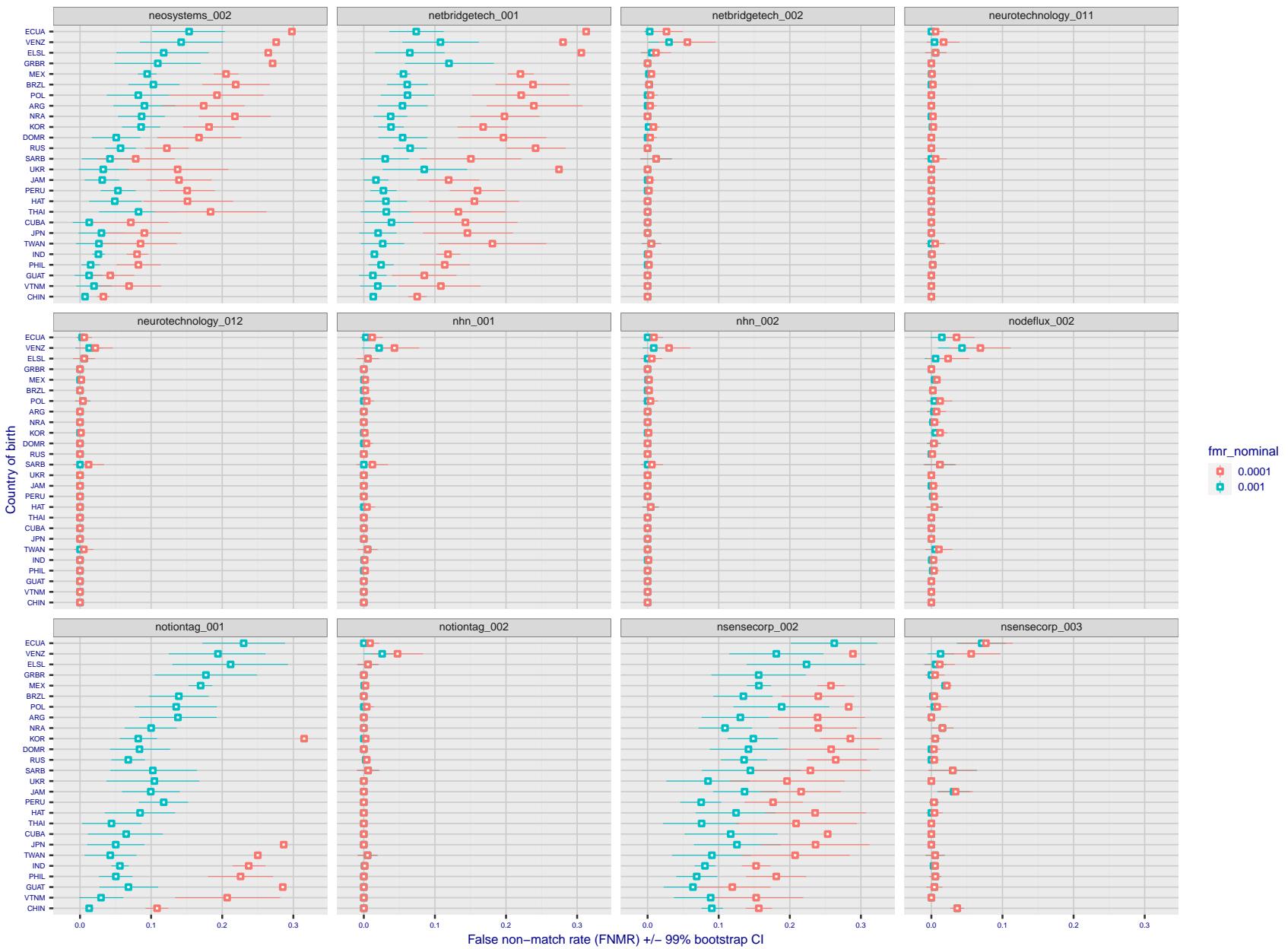


Figure 235: For the visa images, the dots show FNMR by country of birth for two globally set operating thresholds corresponding to $FMR = \{0.001, 0.0001\}$ computed over all on the order of 10^{10} impostor scores. The FMR in each bin will vary also - see subsequent impostor heatmaps in sec. 3.6.1. The figures shows an order of magnitude variation in FNMR across country of birth; these effects are likely due quality variations, then demographics like age and race. The error rates in some cases are zero, and in others the DET is flat so the error rates at the two thresholds are identical. The lines span 1% and 99% of bootstrap replicated FNMR estimates.

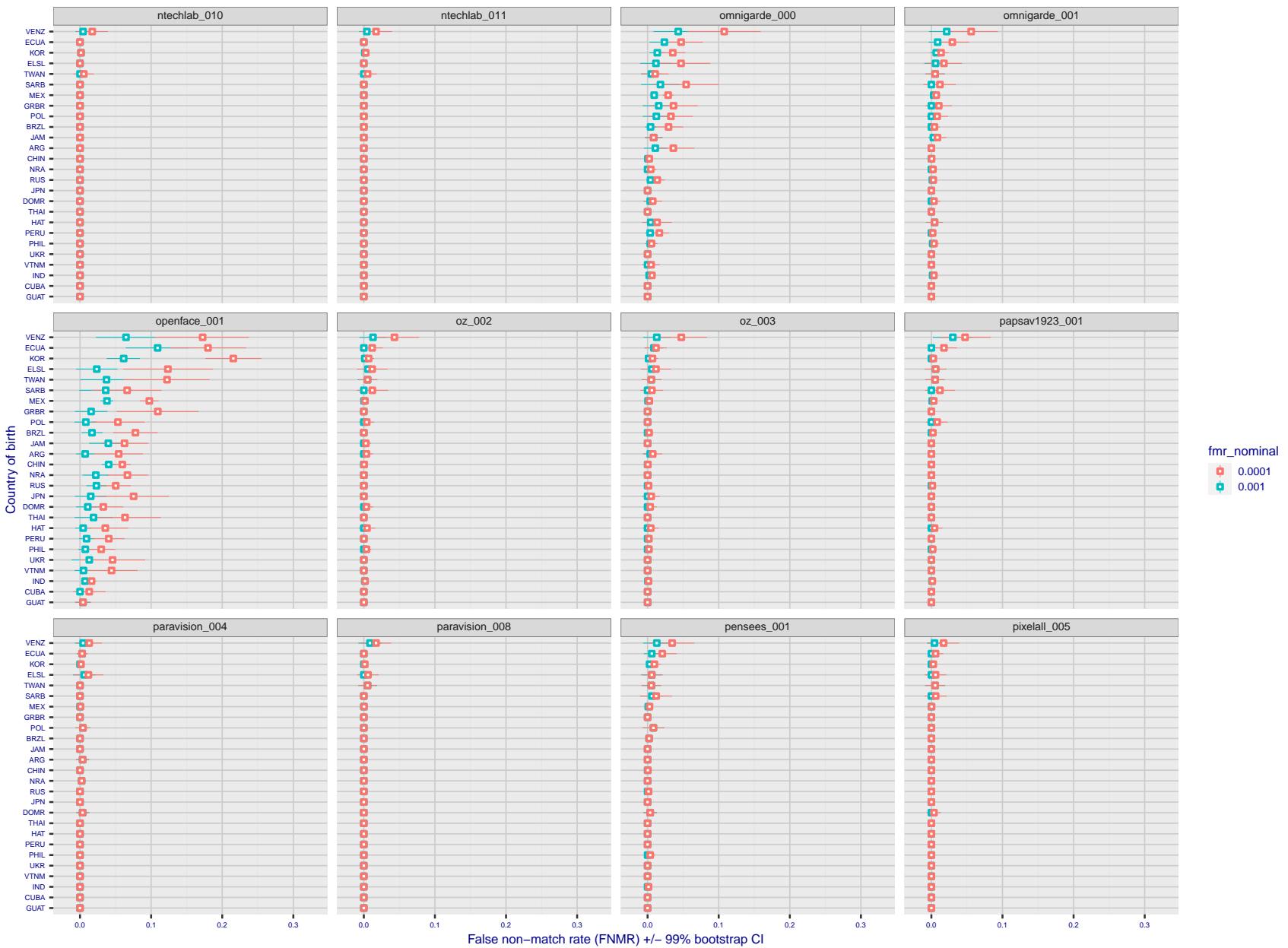


Figure 236: For the visa images, the dots show FNMR by country of birth for two globally set operating thresholds corresponding to $FMR = \{0.001, 0.0001\}$ computed over all on the order of 10^{10} impostor scores. The FMR in each bin will vary also - see subsequent impostor heatmaps in sec. 3.6.1. The figures shows an order of magnitude variation in FNMR across country of birth; these effects are likely due quality variations, then demographics like age and race. The error rates in some cases are zero, and in others the DET is flat so the error rates at the two thresholds are identical. The lines span 1% and 99% of bootstrap replicated FNMR estimates.

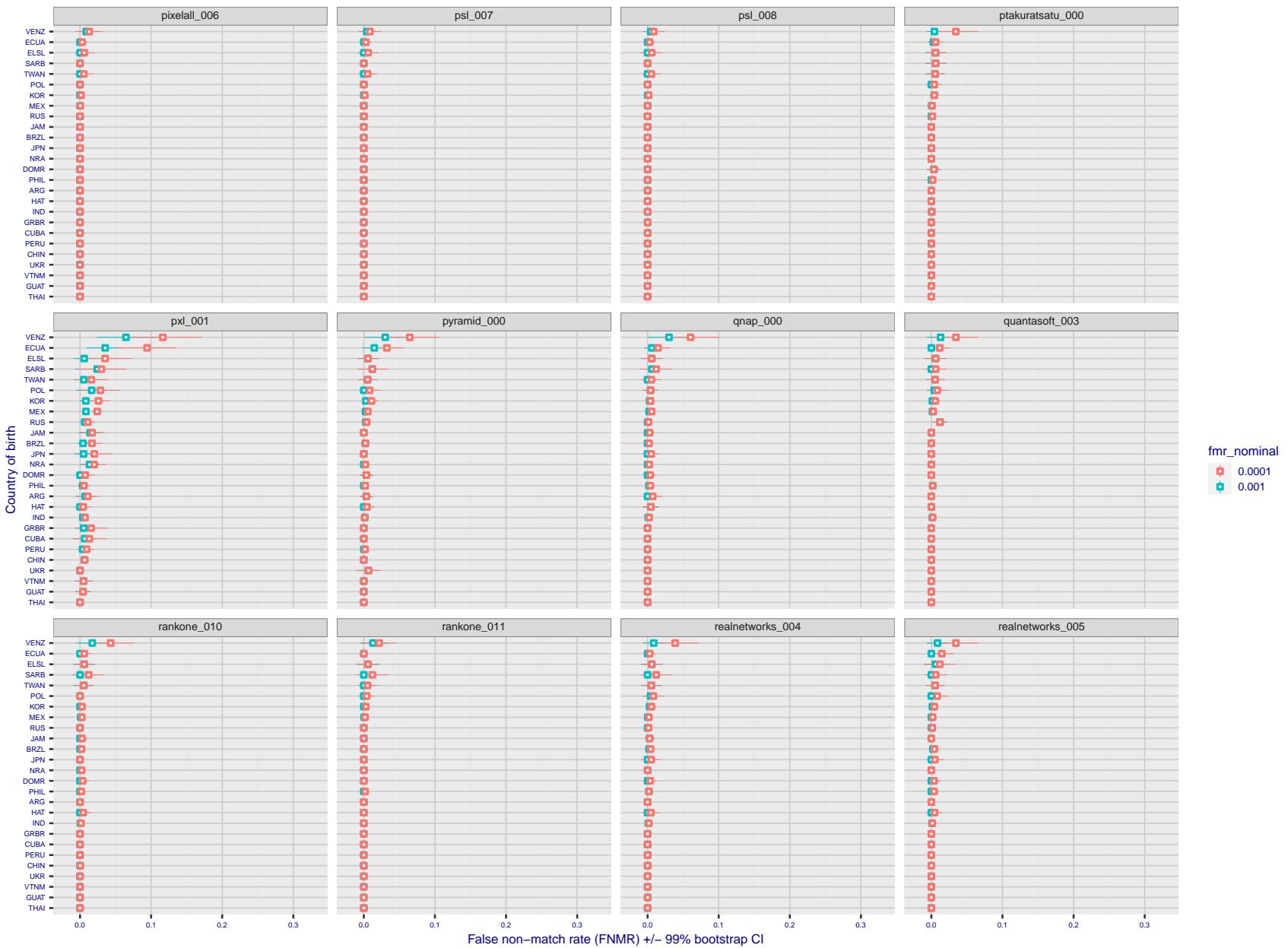


Figure 237: For the visa images, the dots show FNMR by country of birth for two globally set operating thresholds corresponding to $FMR = \{0.001, 0.0001\}$ computed over all on the order of 10^{10} impostor scores. The FMR in each bin will vary also - see subsequent impostor heatmaps in sec. 3.6.1. The figures shows an order of magnitude variation in FNMR across country of birth; these effects are likely due quality variations, then demographics like age and race. The error rates in some cases are zero, and in others the DET is flat so the error rates at the two thresholds are identical. The lines span 1% and 99% of bootstrap replicated FNMR estimates.

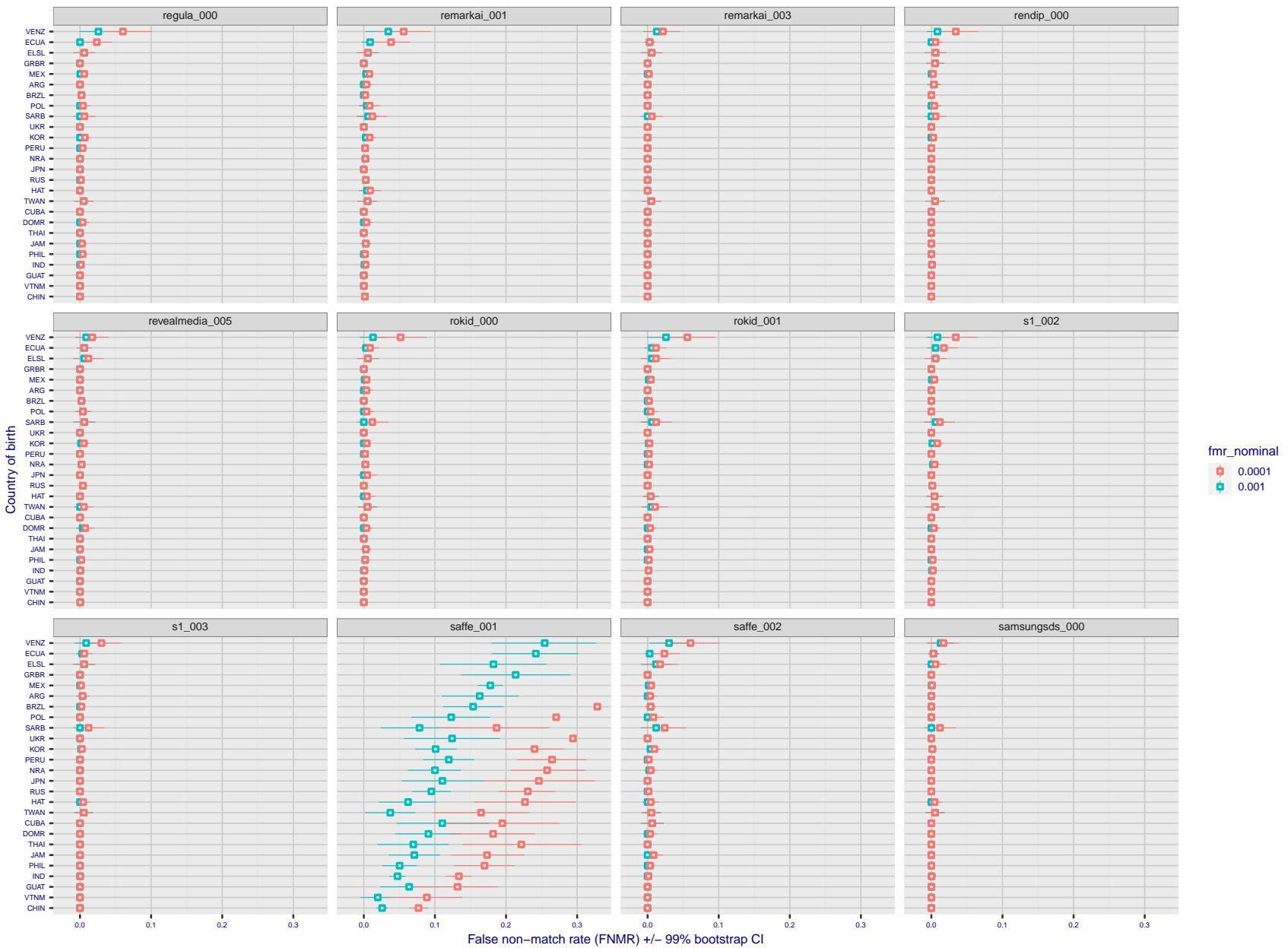


Figure 238: For the visa images, the dots show FNMR by country of birth for two globally set operating thresholds corresponding to $FMR = \{0.001, 0.0001\}$ computed over all on the order of 10^{10} impostor scores. The FMR in each bin will vary also - see subsequent impostor heatmaps in sec. 3.6.1. The figures shows an order of magnitude variation in FNMR across country of birth; these effects are likely due quality variations, then demographics like age and race. The error rates in some cases are zero, and in others the DET is flat so the error rates at the two thresholds are identical. The lines span 1% and 99% of bootstrap replicated FNMR estimates.

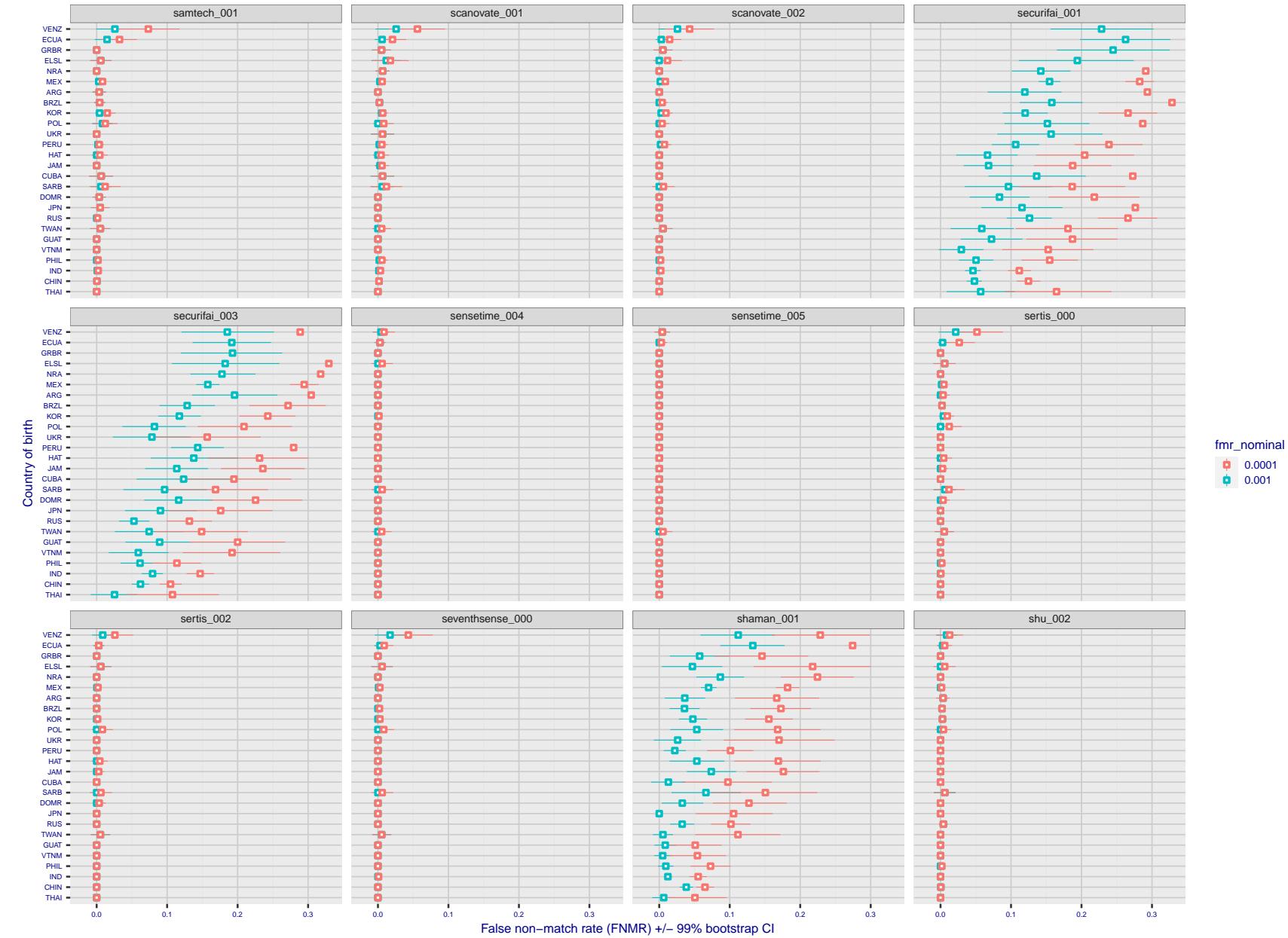


Figure 239: For the visa images, the dots show FNMR by country of birth for two globally set operating thresholds corresponding to $FMR = \{0.001, 0.0001\}$ computed over all on the order of 10^{10} impostor scores. The FMR in each bin will vary also - see subsequent impostor heatmaps in sec. 3.6.1. The figures shows an order of magnitude variation in FNMR across country of birth; these effects are likely due quality variations, then demographics like age and race. The error rates in some cases are zero, and in others the DET is flat so the error rates at the two thresholds are identical. The lines span 1% and 99% of bootstrap replicated FNMR estimates.

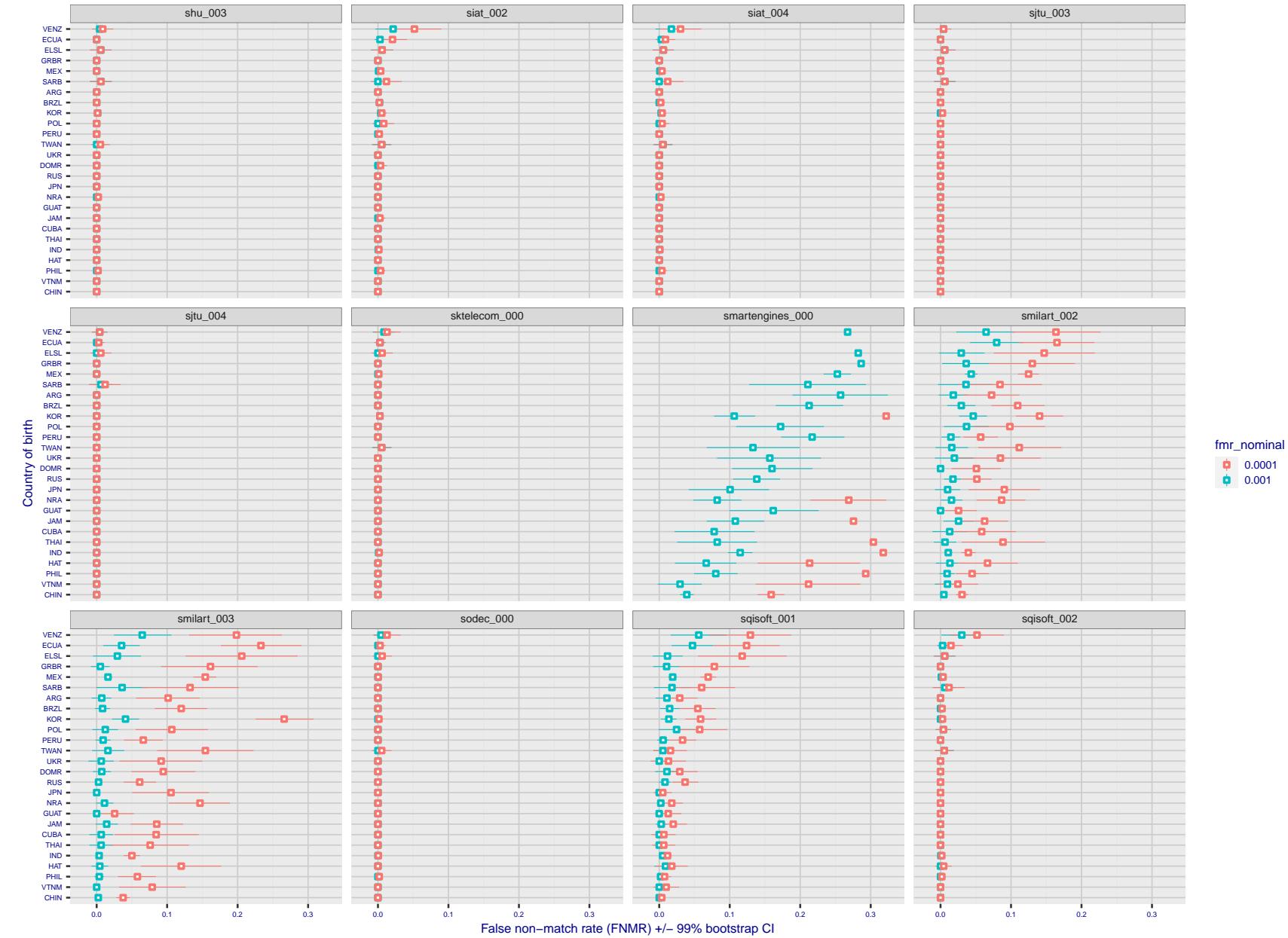


Figure 240: For the visa images, the dots show FNMR by country of birth for two globally set operating thresholds corresponding to $FMR = \{0.001, 0.0001\}$ computed over all on the order of 10^{10} impostor scores. The FMR in each bin will vary also - see subsequent impostor heatmaps in sec. 3.6.1. The figures shows an order of magnitude variation in FNMR across country of birth; these effects are likely due quality variations, then demographics like age and race. The error rates in some cases are zero, and in others the DET is flat so the error rates at the two thresholds are identical. The lines span 1% and 99% of bootstrap replicated FNMR estimates.

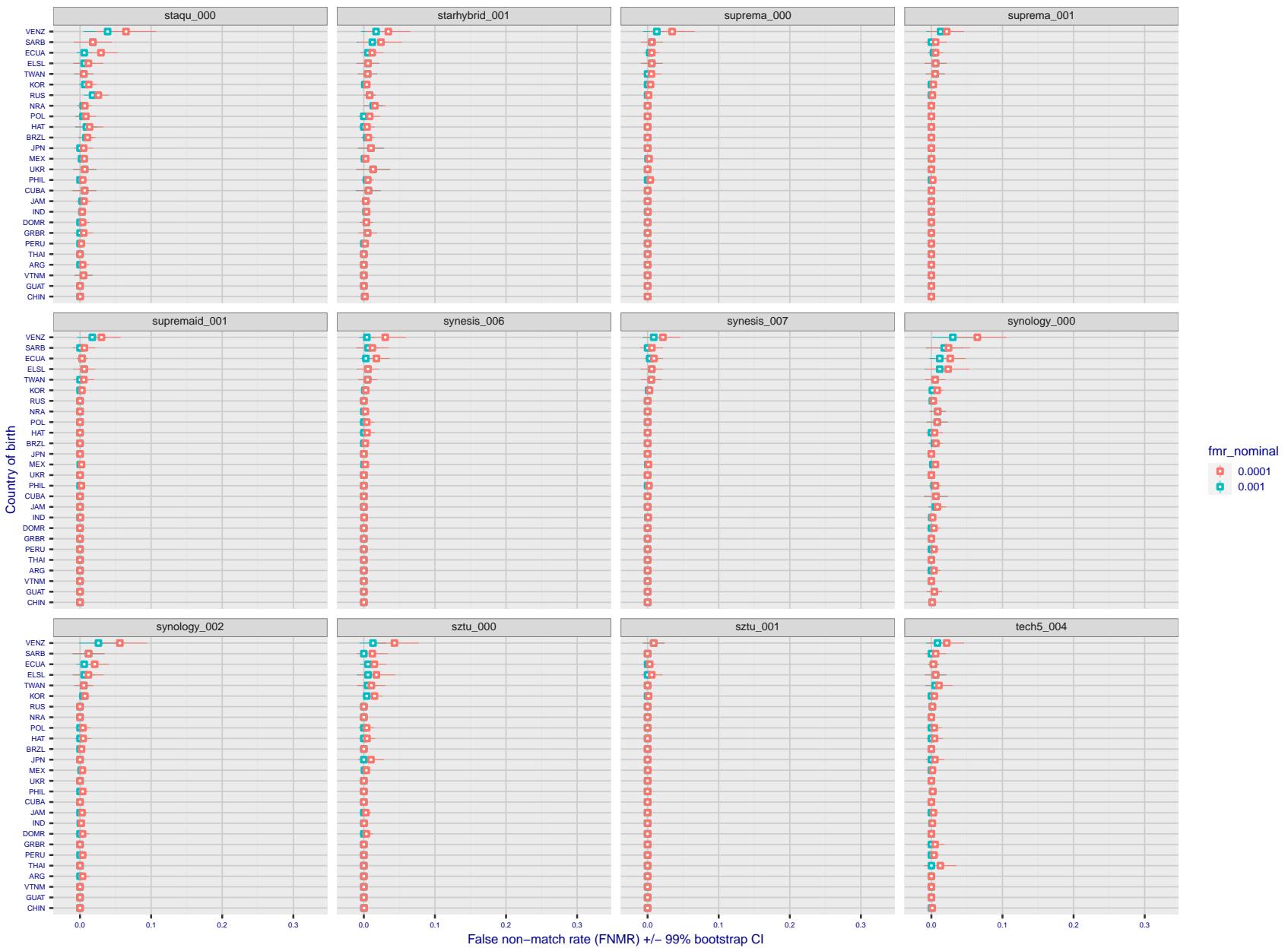


Figure 241: For the visa images, the dots show FNMR by country of birth for two globally set operating thresholds corresponding to $FMR = \{0.001, 0.0001\}$ computed over all on the order of 10^{10} impostor scores. The FMR in each bin will vary also - see subsequent impostor heatmaps in sec. 3.6.1. The figures shows an order of magnitude variation in FNMR across country of birth; these effects are likely due quality variations, then demographics like age and race. The error rates in some cases are zero, and in others the DET is flat so the error rates at the two thresholds are identical. The lines span 1% and 99% of bootstrap replicated FNMR estimates.

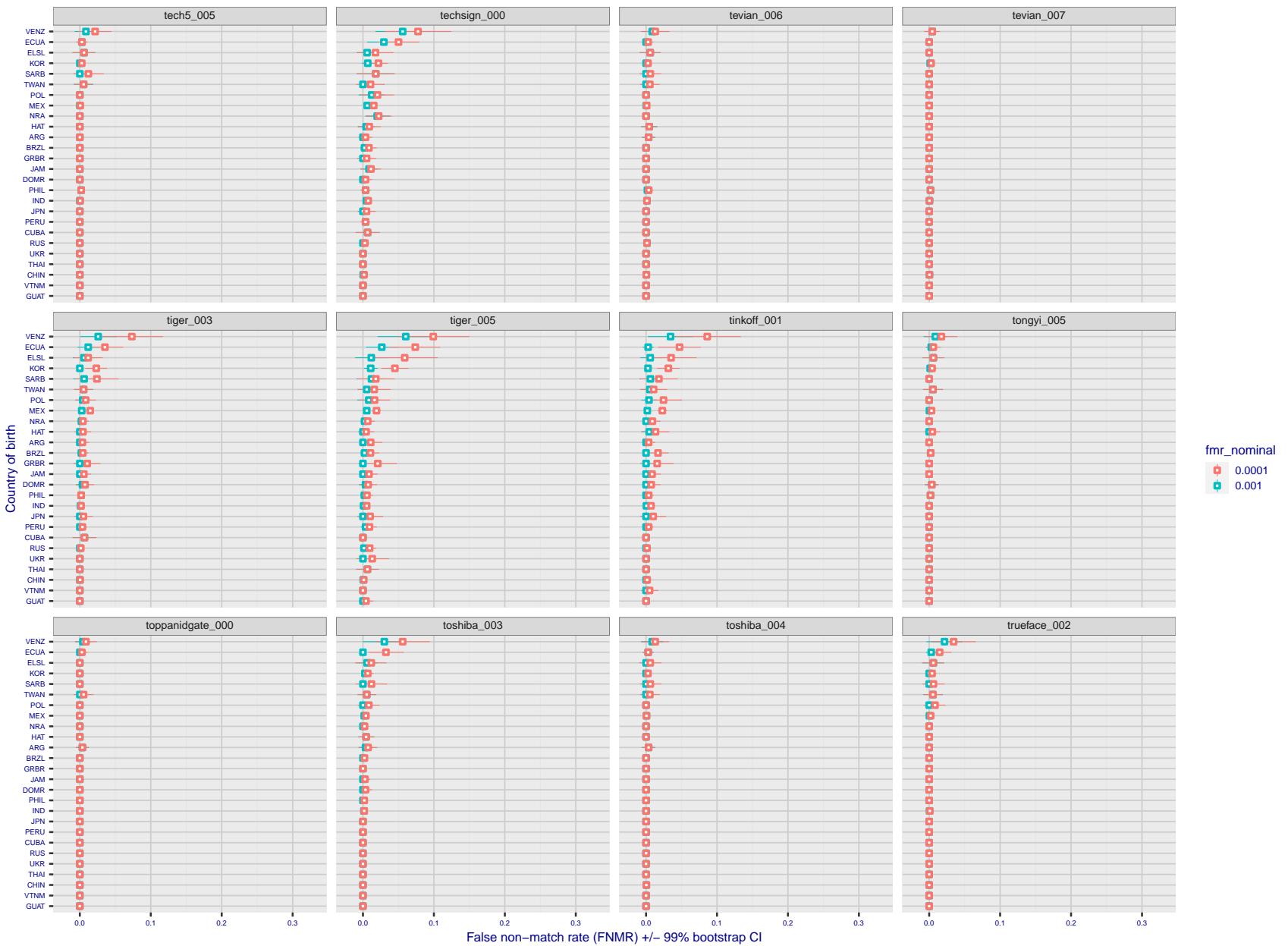


Figure 242: For the visa images, the dots show FNMR by country of birth for two globally set operating thresholds corresponding to $FMR = \{0.001, 0.0001\}$ computed over all on the order of 10^{10} impostor scores. The FMR in each bin will vary also - see subsequent impostor heatmaps in sec. 3.6.1. The figures shows an order of magnitude variation in FNMR across country of birth; these effects are likely due quality variations, then demographics like age and race. The error rates in some cases are zero, and in others the DET is flat so the error rates at the two thresholds are identical. The lines span 1% and 99% of bootstrap replicated FNMR estimates.

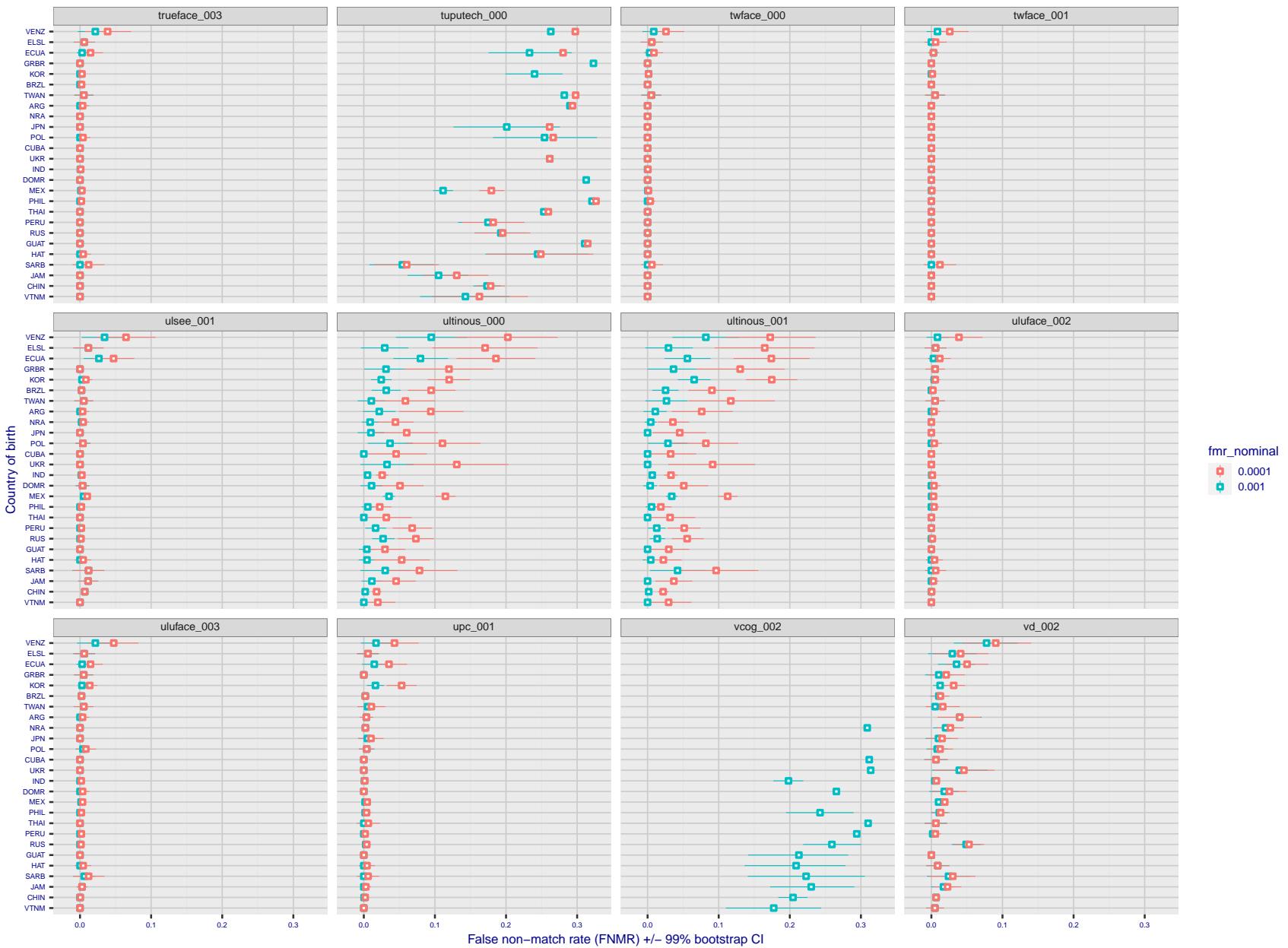


Figure 243: For the visa images, the dots show FNMR by country of birth for two globally set operating thresholds corresponding to $FMR = \{0.001, 0.0001\}$ computed over all on the order of 10^{10} impostor scores. The FMR in each bin will vary also - see subsequent impostor heatmaps in sec. 3.6.1. The figures shows an order of magnitude variation in FNMR across country of birth; these effects are likely due quality variations, then demographics like age and race. The error rates in some cases are zero, and in others the DET is flat so the error rates at the two thresholds are identical. The lines span 1% and 99% of bootstrap replicated FNMR estimates.

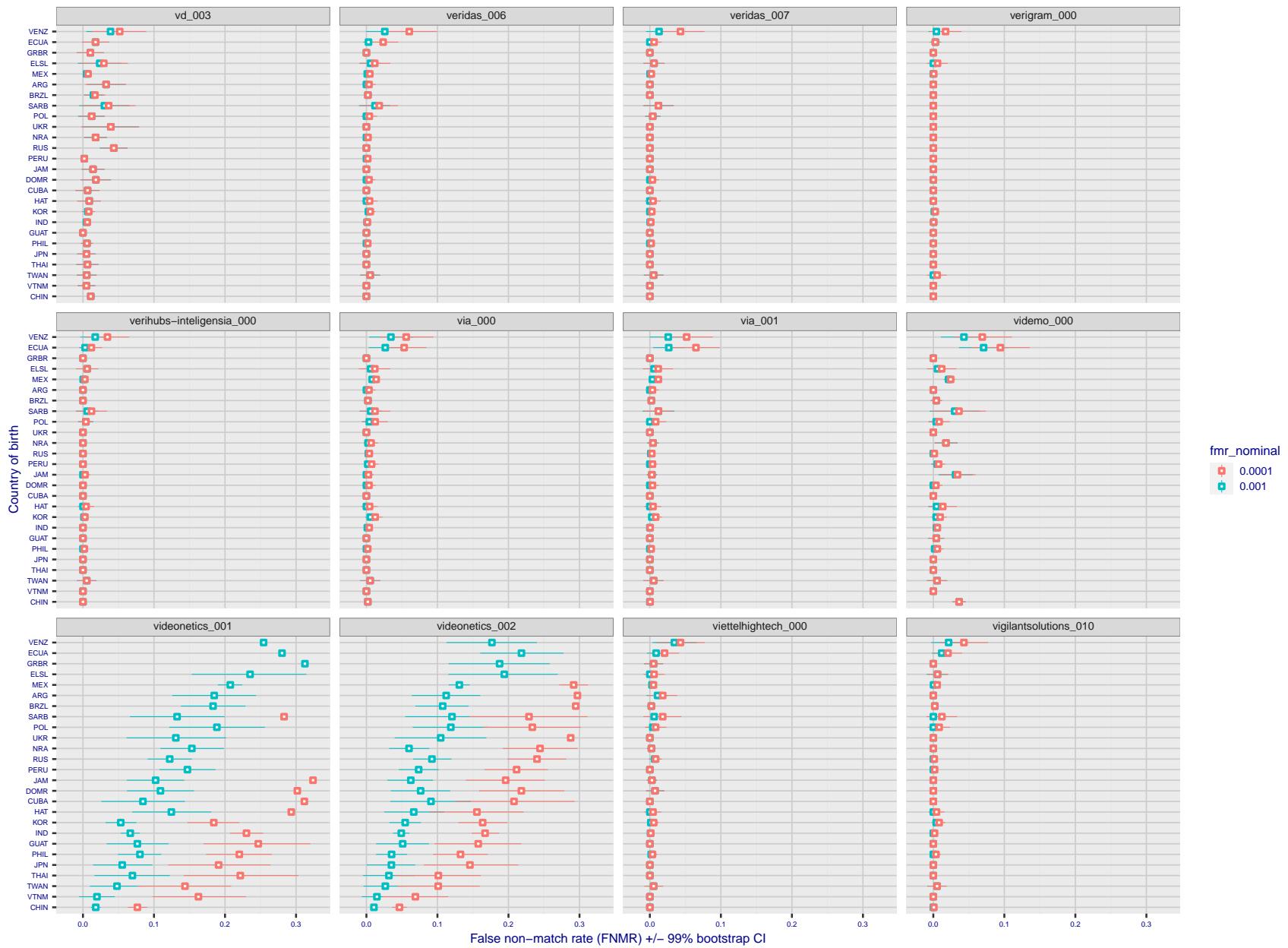


Figure 244: For the visa images, the dots show FNMR by country of birth for two globally set operating thresholds corresponding to $FMR = \{0.001, 0.0001\}$ computed over all on the order of 10^{10} impostor scores. The FMR in each bin will vary also - see subsequent impostor heatmaps in sec. 3.6.1. The figures shows an order of magnitude variation in FNMR across country of birth; these effects are likely due quality variations, then demographics like age and race. The error rates in some cases are zero, and in others the DET is flat so the error rates at the two thresholds are identical. The lines span 1% and 99% of bootstrap replicated FNMR estimates.

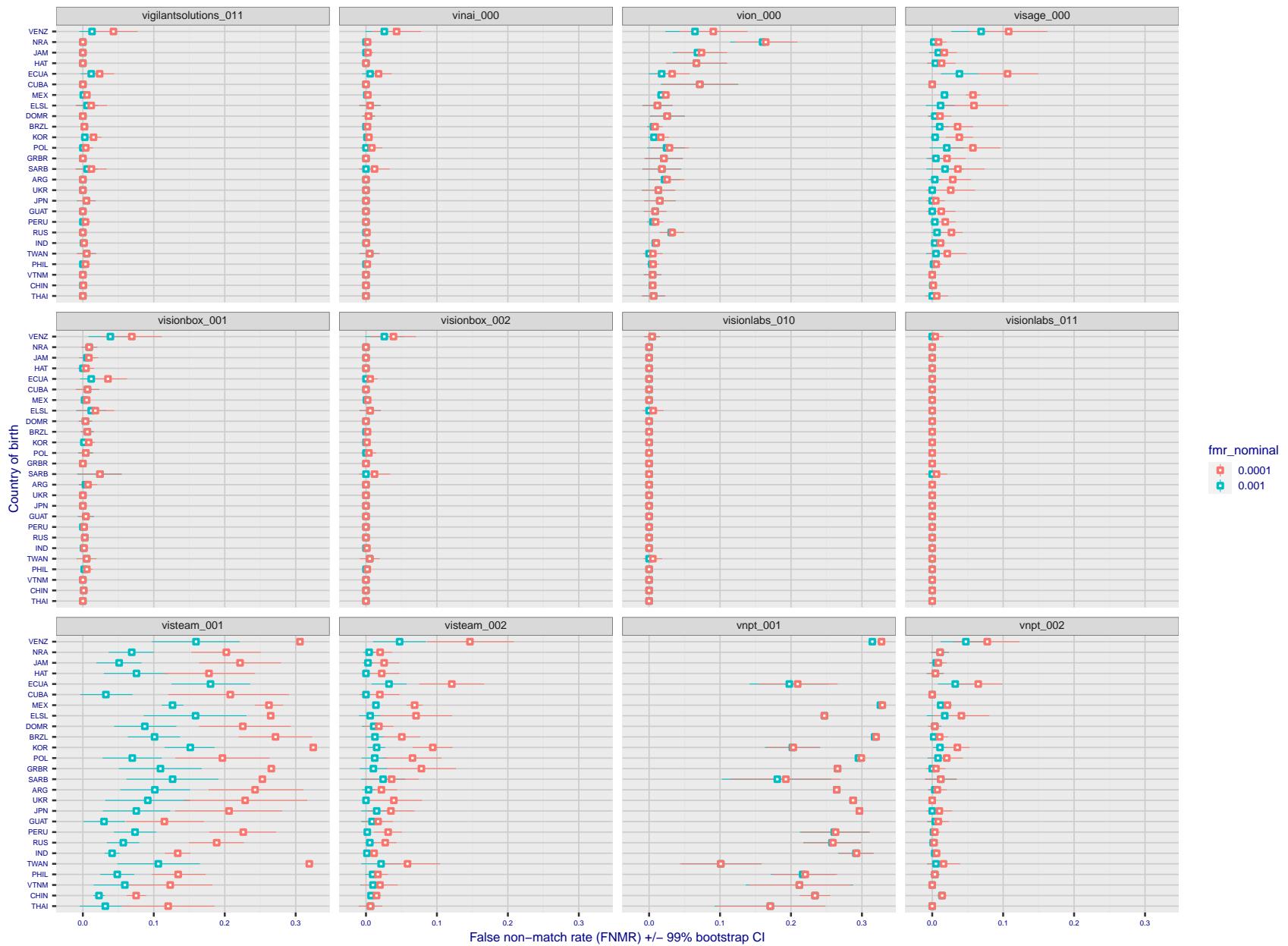


Figure 245: For the visa images, the dots show FNMR by country of birth for two globally set operating thresholds corresponding to $FMR = \{0.001, 0.0001\}$ computed over all on the order of 10^{10} impostor scores. The FMR in each bin will vary also - see subsequent impostor heatmaps in sec. 3.6.1. The figures shows an order of magnitude variation in FNMR across country of birth; these effects are likely due quality variations, then demographics like age and race. The error rates in some cases are zero, and in others the DET is flat so the error rates at the two thresholds are identical. The lines span 1% and 99% of bootstrap replicated FNMR estimates.

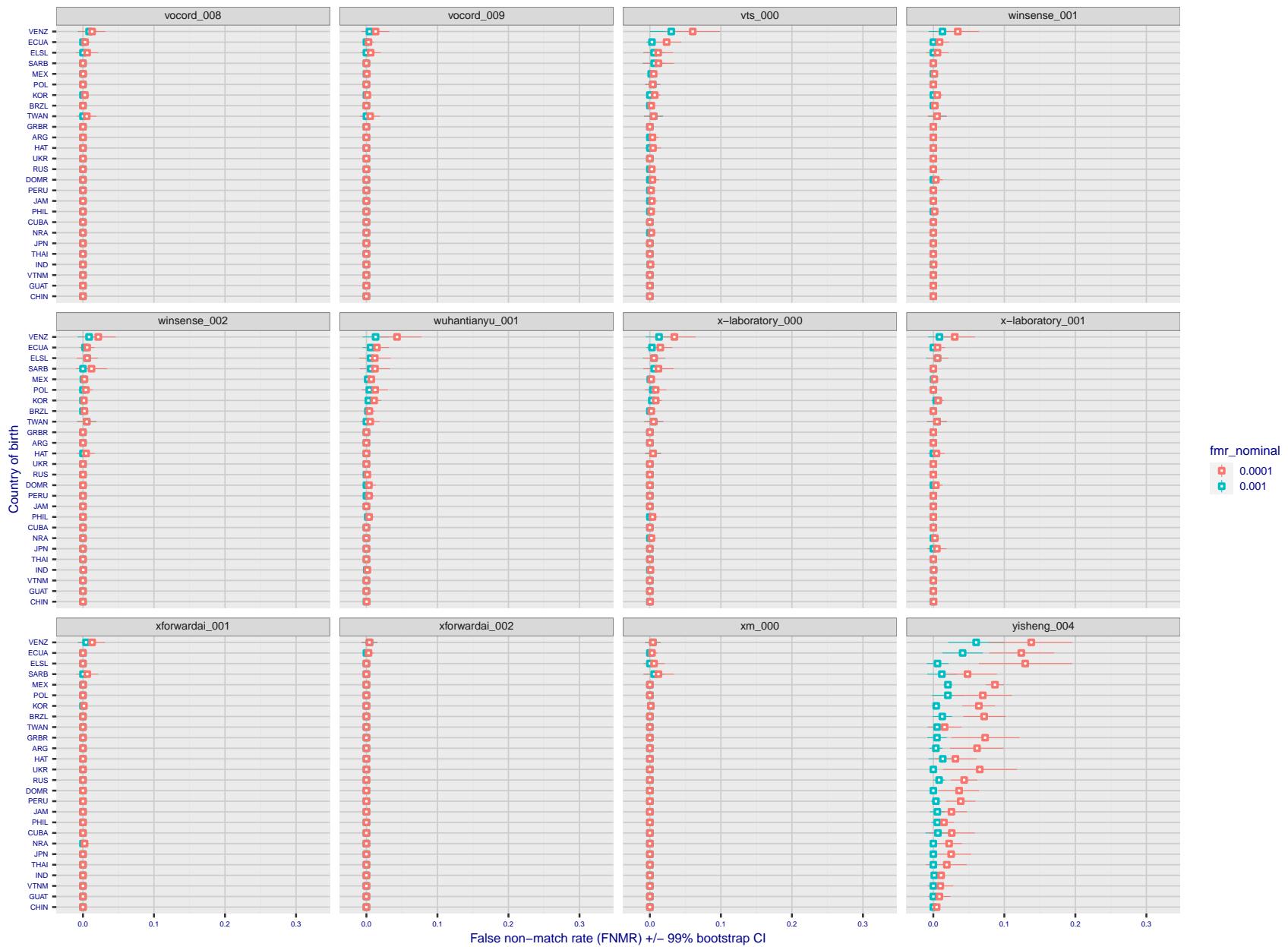


Figure 246: For the visa images, the dots show FNMR by country of birth for two globally set operating thresholds corresponding to $FMR = \{0.001, 0.0001\}$ computed over all on the order of 10^{10} impostor scores. The FMR in each bin will vary also - see subsequent impostor heatmaps in sec. 3.6.1. The figures shows an order of magnitude variation in FNMR across country of birth; these effects are likely due quality variations, then demographics like age and race. The error rates in some cases are zero, and in others the DET is flat so the error rates at the two thresholds are identical. The lines span 1% and 99% of bootstrap replicated FNMR estimates.

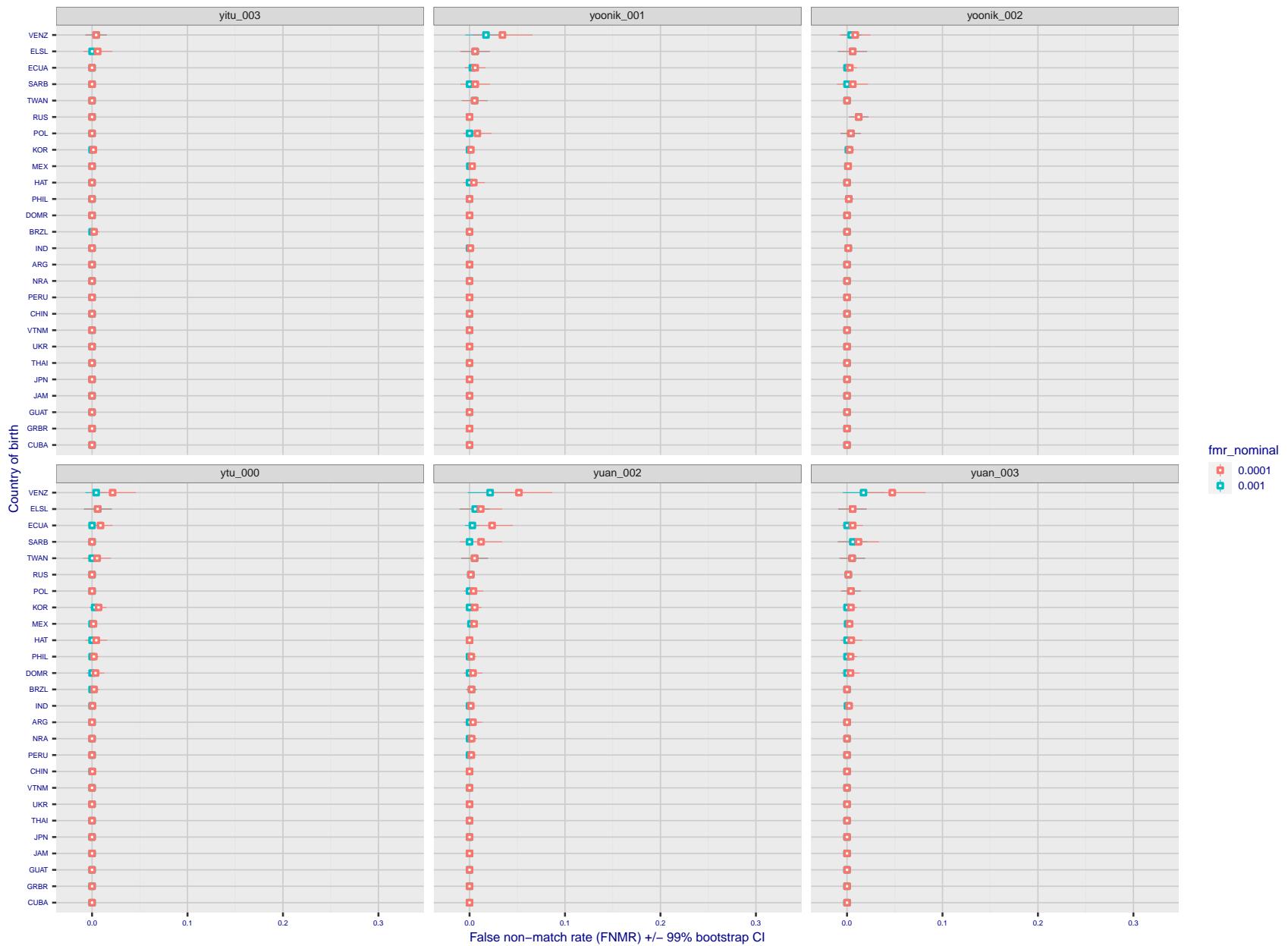


Figure 247: For the visa images, the dots show FNMR by country of birth for two globally set operating thresholds corresponding to $FMR = \{0.001, 0.0001\}$ computed over all on the order of 10^{10} impostor scores. The FMR in each bin will vary also - see subsequent impostor heatmaps in sec. 3.6.1. The figures shows an order of magnitude variation in FNMR across country of birth; these effects are likely due quality variations, then demographics like age and race. The error rates in some cases are zero, and in others the DET is flat so the error rates at the two thresholds are identical. The lines span 1% and 99% of bootstrap replicated FNMR estimates.

Caveats: The results may not relate to subject-specific properties. Instead they could reflect image-specific quality differences, which could occur due to collection protocol or software processing variations.

3.5.2 Effect of ageing

Background: Faces change appearance throughout life. This change gradually reduces similarity of a new image to an earlier image. Face recognition algorithms give reduced similarity scores and more frequent false rejections.

Goal: To quantify false non-match rates (FNMR) as a function of elapsed time in an adult population.

Methods: Using the mugshot images, a threshold is set to give FMR = 0.00001 over the entire impostor set. Then FNMR is measured over 1000 bootstrap replications of the genuine scores.

Results: For the visa images, Figure 270 shows how false non-match rates for genuine users, as a function of age group.

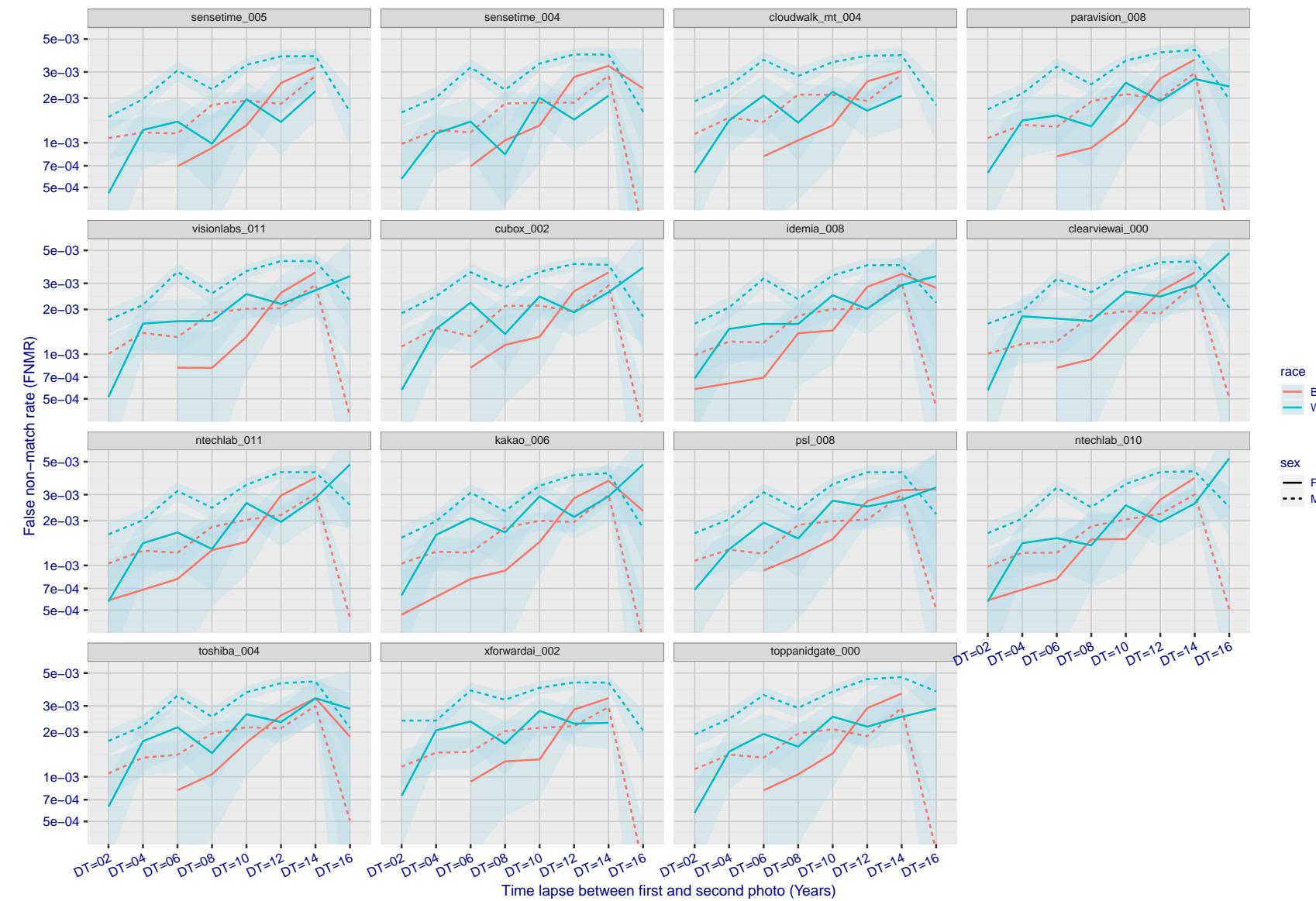


Figure 248: For the mugshot images, FNMR as a function of elapsed time between initial enrollment and second verification images. The panels appear most accurate first, and vertical scale changes on each page. The four traces correspond to images annotated with codes for black female, black male, white female, white male. The threshold is fixed for each algorithm to give FMR = 0.00001 over all (10^8) impostor comparisons. For short time-lapses, the most accurate algorithms give very few errors (FNMR < 0.001) so that the uncertainty estimates are high.

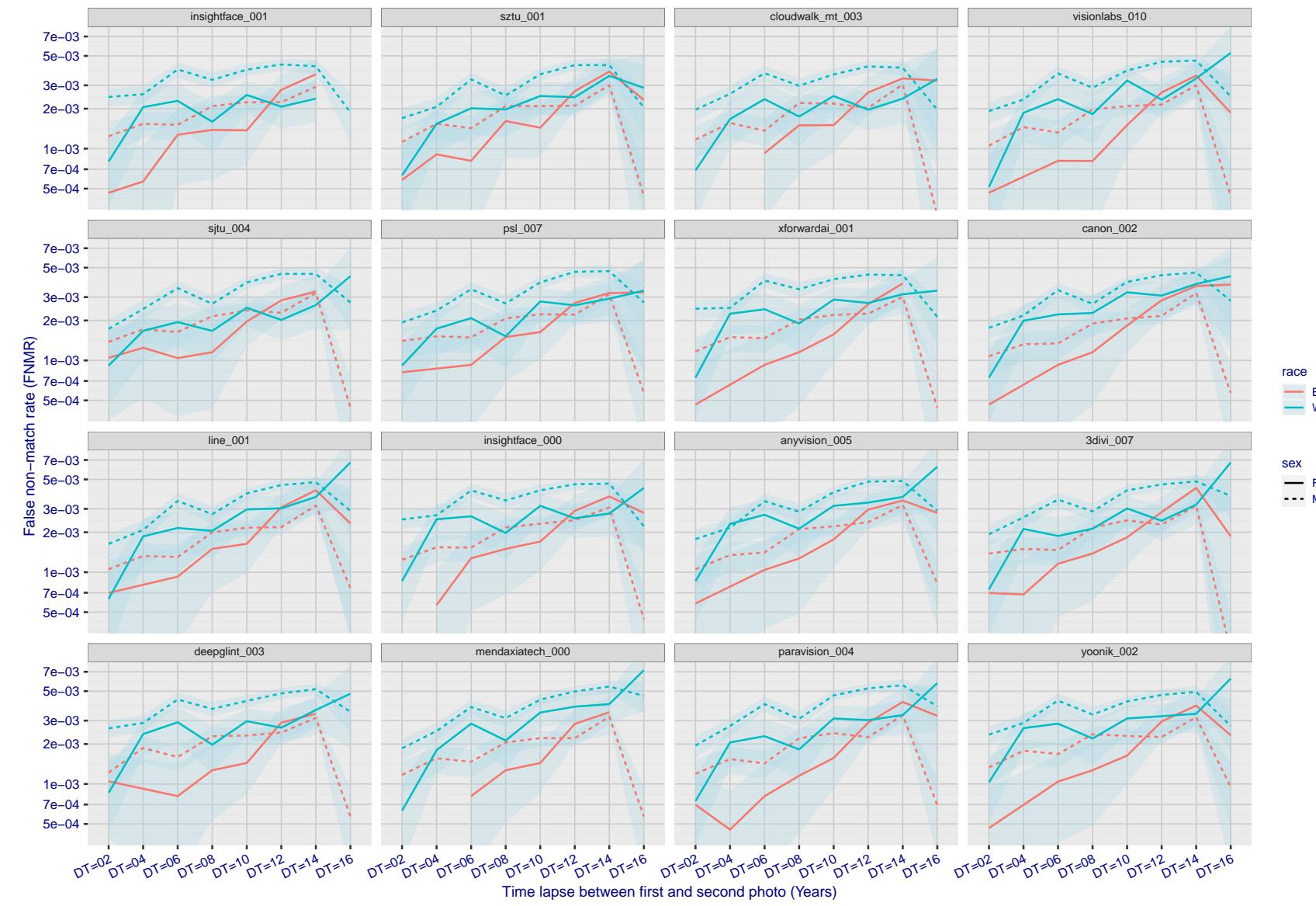


Figure 249: For the mugshot images, FNMR as a function of elapsed time between initial enrollment and second verification images. The panels appear most accurate first, and vertical scale changes on each page. The four traces correspond to images annotated with codes for black female, black male, white female, white male. The threshold is fixed for each algorithm to give FMR = 0.00001 over all (10^8) impostor comparisons. For short time-lapses, the most accurate algorithms give very few errors (FNMR < 0.001) so that the uncertainty estimates are high.

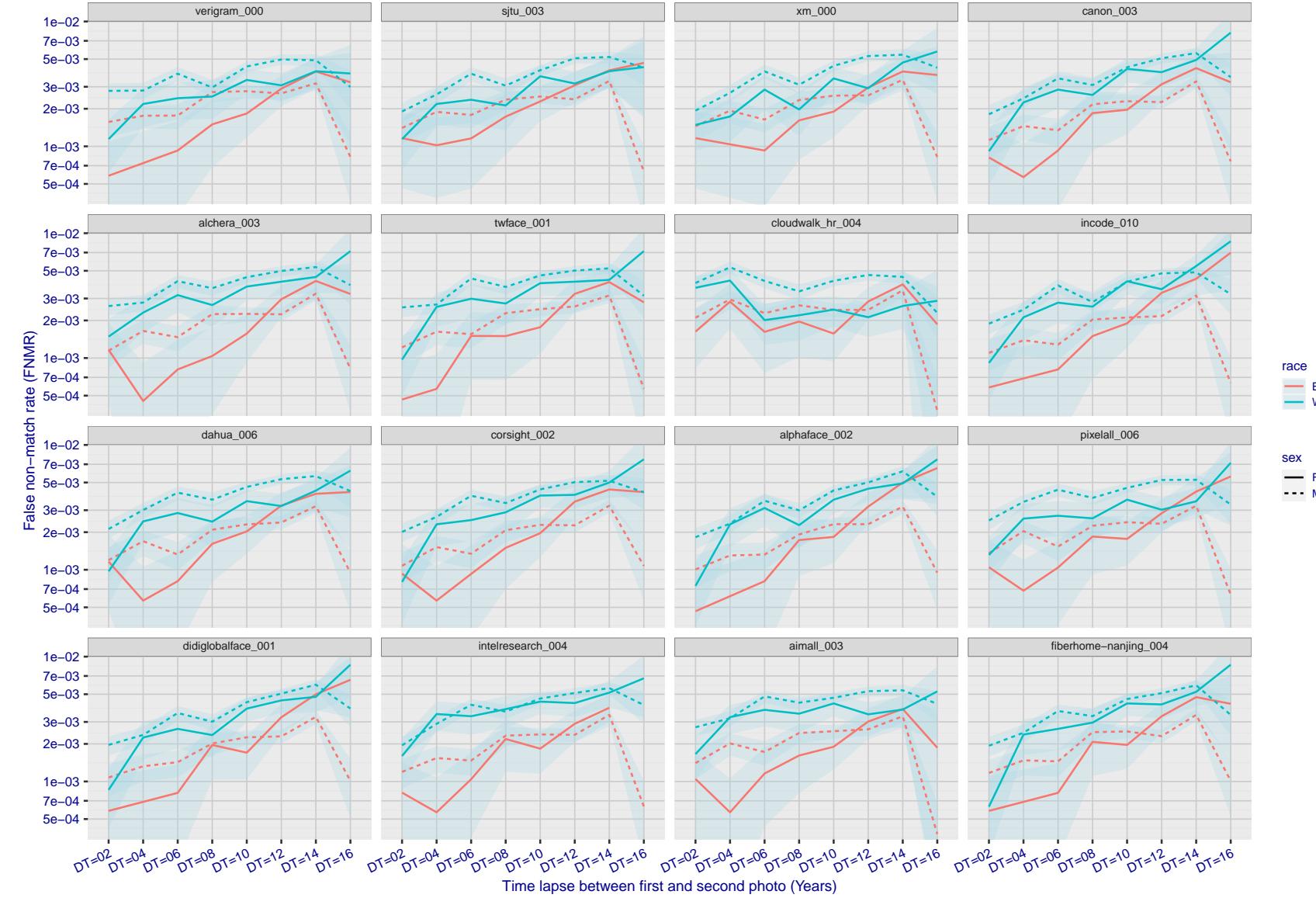


Figure 250: For the mugshot images, FNMR as a function of elapsed time between initial enrollment and second verification images. The panels appear most accurate first, and vertical scale changes on each page. The four traces correspond to images annotated with codes for black female, black male, white female, white male. The threshold is fixed for each algorithm to give $FMR = 0.00001$ over all (10^8) impostor comparisons. For short time-lapses, the most accurate algorithms give very few errors ($FNMR < 0.001$) so that the uncertainty estimates are high.

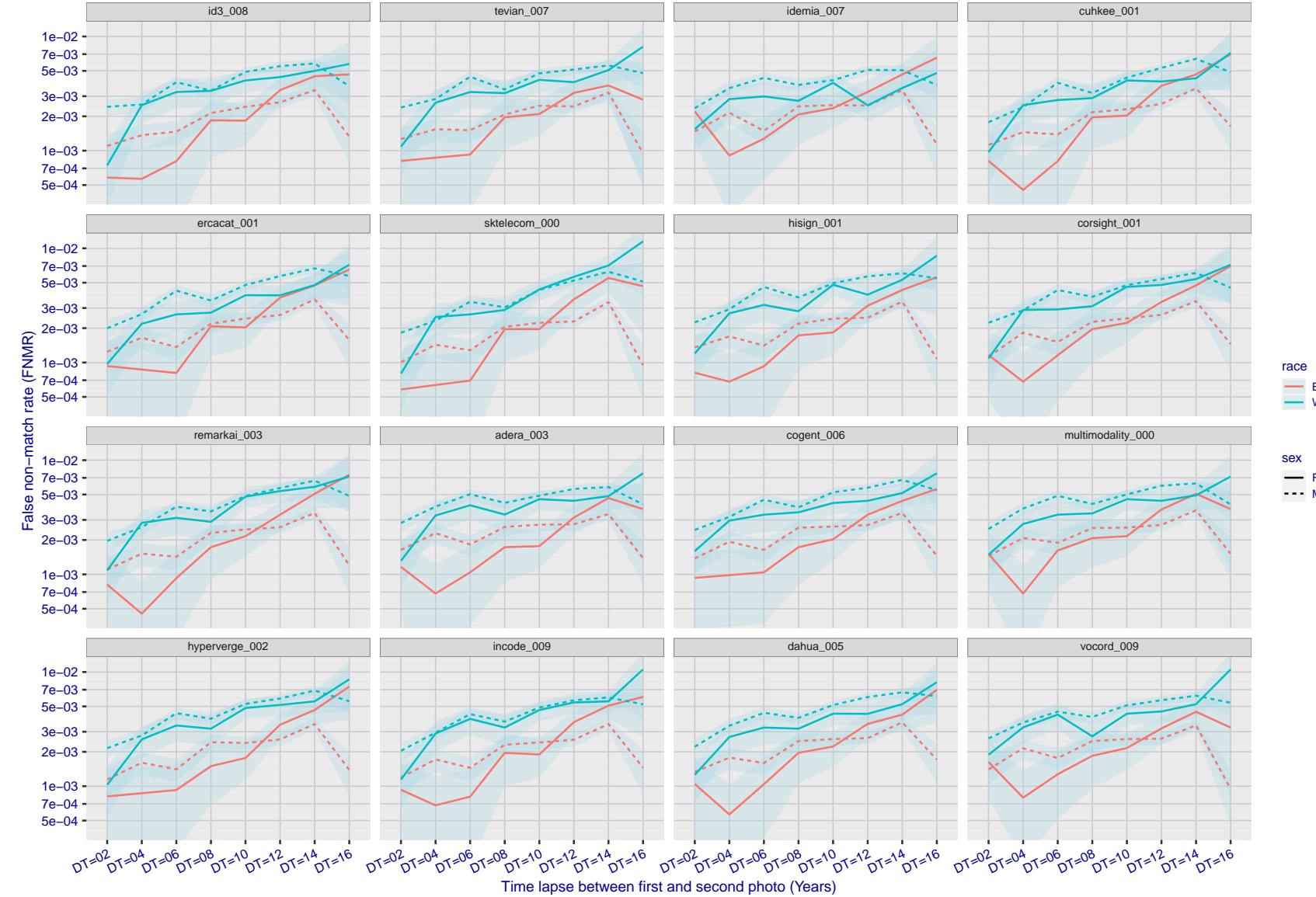


Figure 251: For the mugshot images, FNMR as a function of elapsed time between initial enrollment and second verification images. The panels appear most accurate first, and vertical scale changes on each page. The four traces correspond to images annotated with codes for black female, black male, white female, white male. The threshold is fixed for each algorithm to give FMR = 0.00001 over all (10^8) impostor comparisons. For short time-lapses, the most accurate algorithms give very few errors (FNMR < 0.001) so that the uncertainty estimates are high.

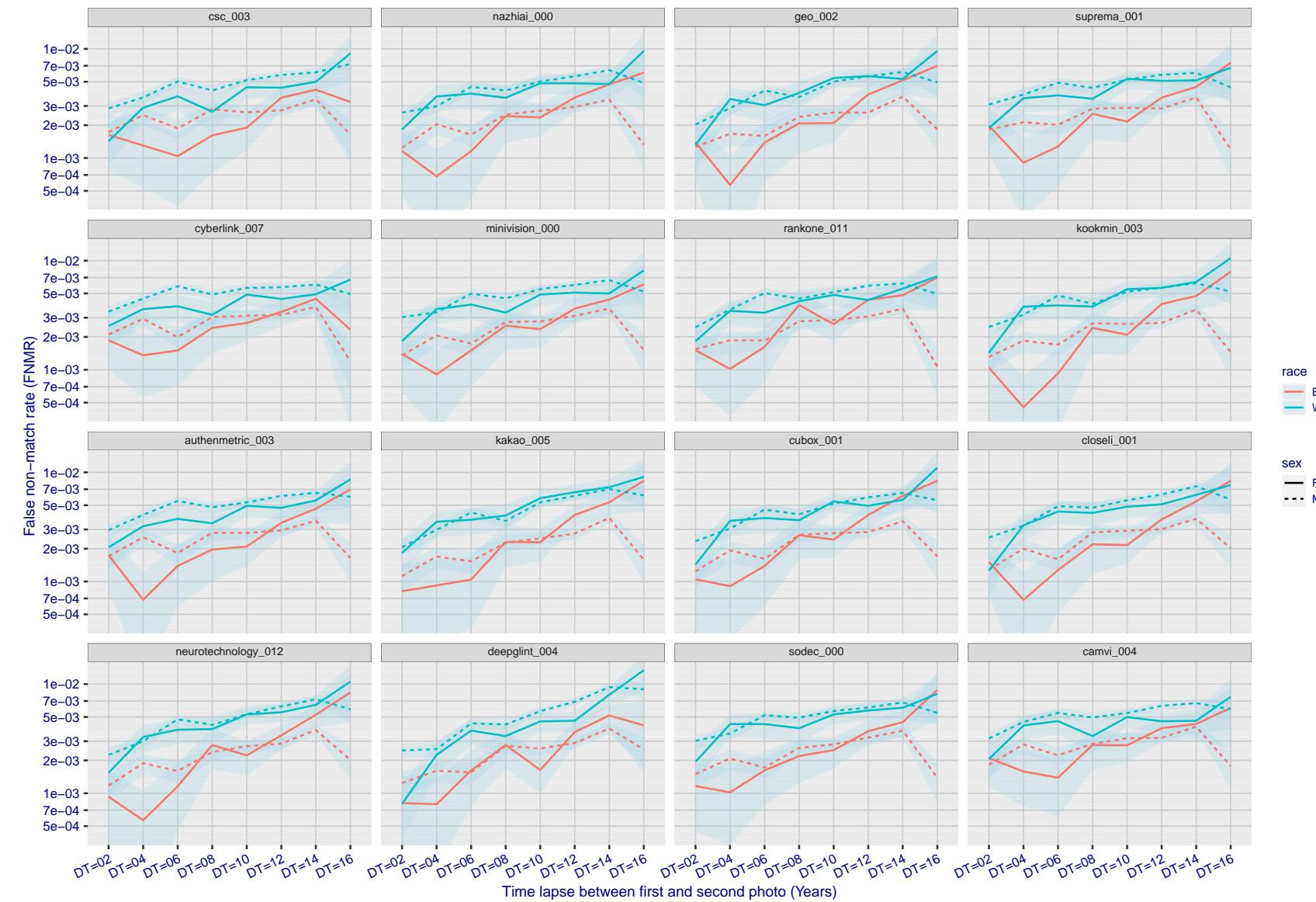


Figure 252: For the mugshot images, FNMR as a function of elapsed time between initial enrollment and second verification images. The panels appear most accurate first, and vertical scale changes on each page. The four traces correspond to images annotated with codes for black female, black male, white female, white male. The threshold is fixed for each algorithm to give $FMR = 0.00001$ over all (10^8) impostor comparisons. For short time-lapses, the most accurate algorithms give very few errors ($FNMR < 0.001$) so that the uncertainty estimates are high.

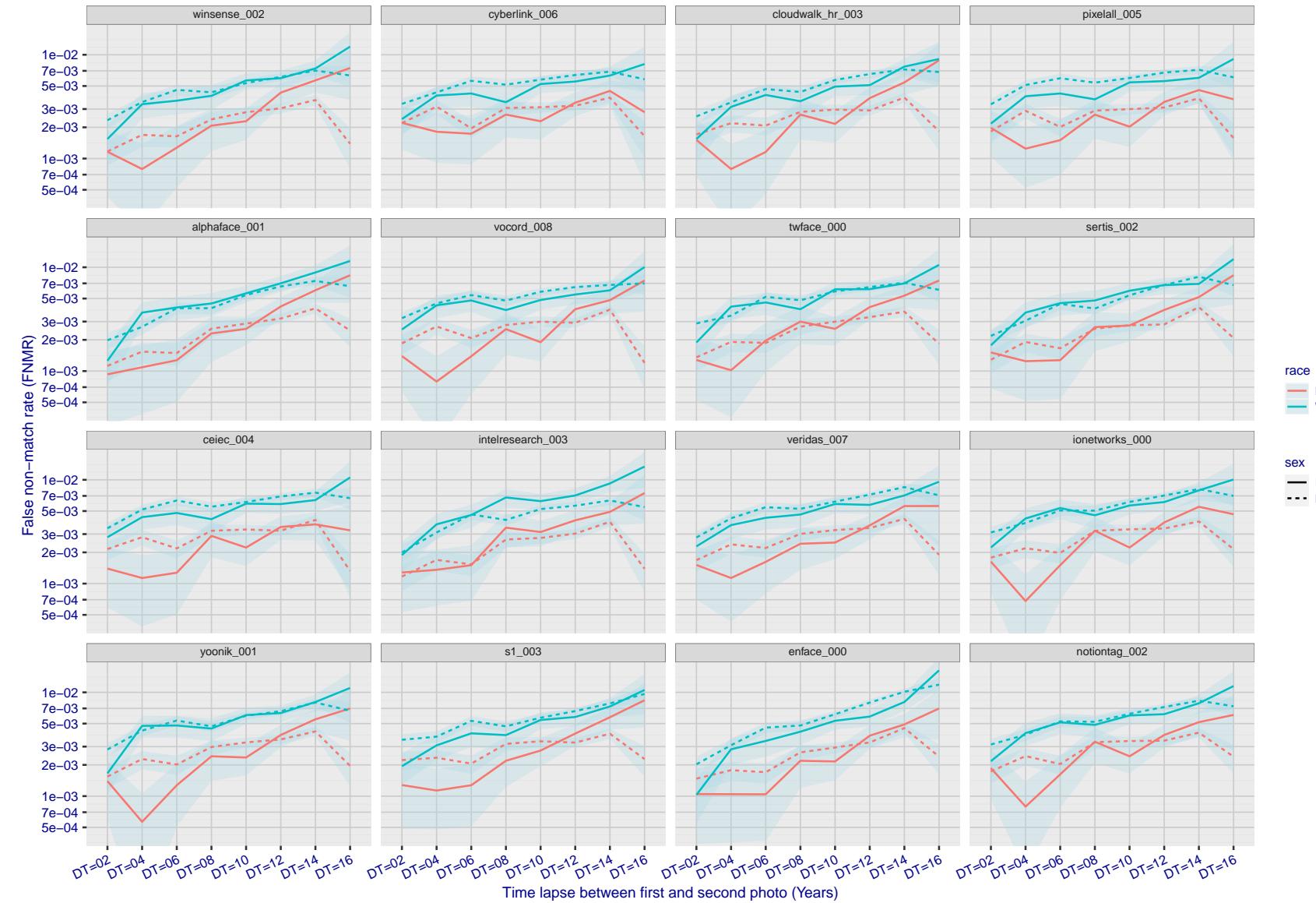


Figure 253: For the mugshot images, FNMR as a function of elapsed time between initial enrollment and second verification images. The panels appear most accurate first, and vertical scale changes on each page. The four traces correspond to images annotated with codes for black female, black male, white female, white male. The threshold is fixed for each algorithm to give $FMR = 0.00001$ over all (10^8) impostor comparisons. For short time-lapses, the most accurate algorithms give very few errors ($FNMR < 0.001$) so that the uncertainty estimates are high.

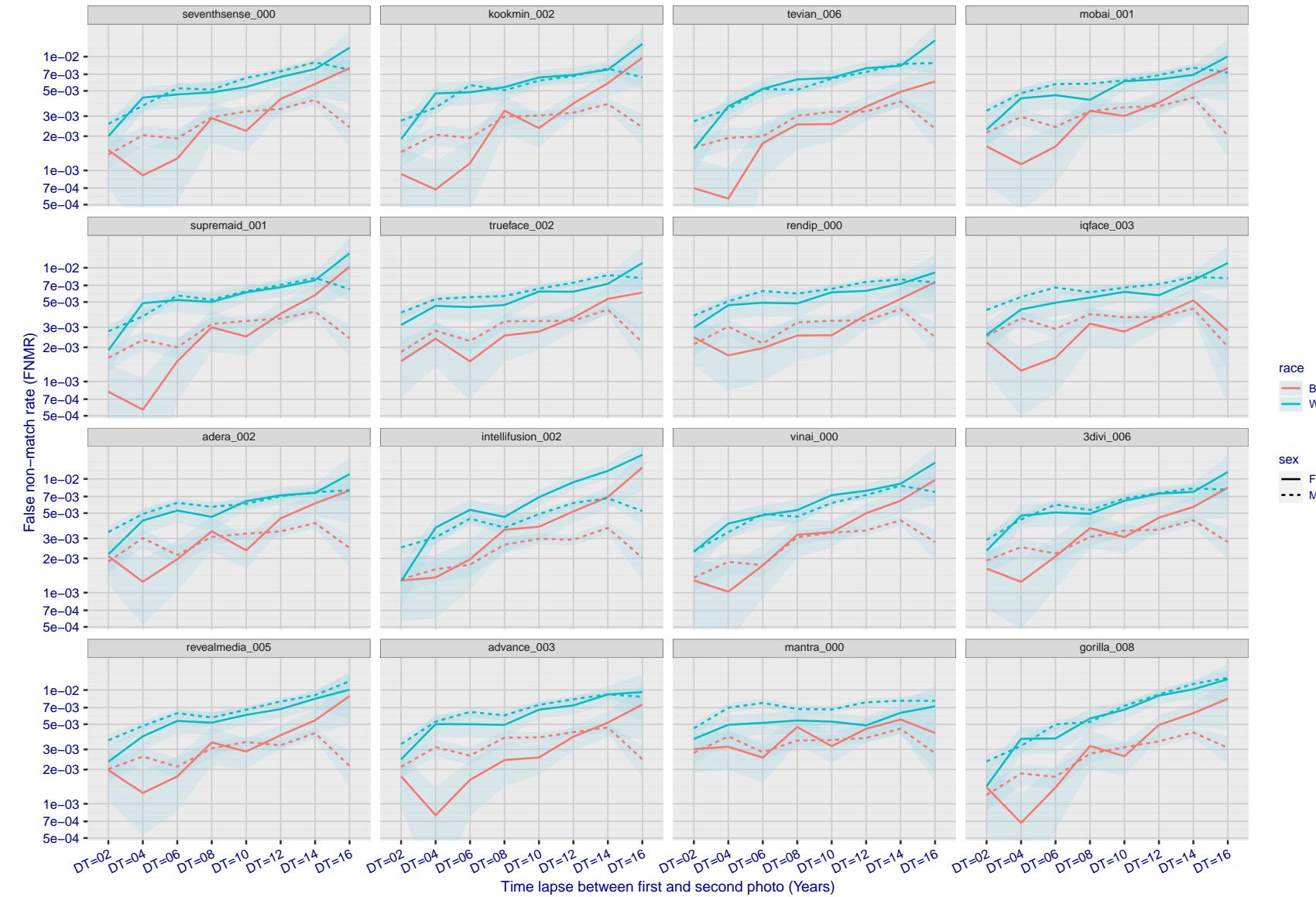


Figure 254: For the mugshot images, FNMR as a function of elapsed time between initial enrollment and second verification images. The panels appear most accurate first, and vertical scale changes on each page. The four traces correspond to images annotated with codes for black female, black male, white female, white male. The threshold is fixed for each algorithm to give $FMR = 0.00001$ over all (10^8) impostor comparisons. For short time-lapses, the most accurate algorithms give very few errors ($FNMR < 0.001$) so that the uncertainty estimates are high.

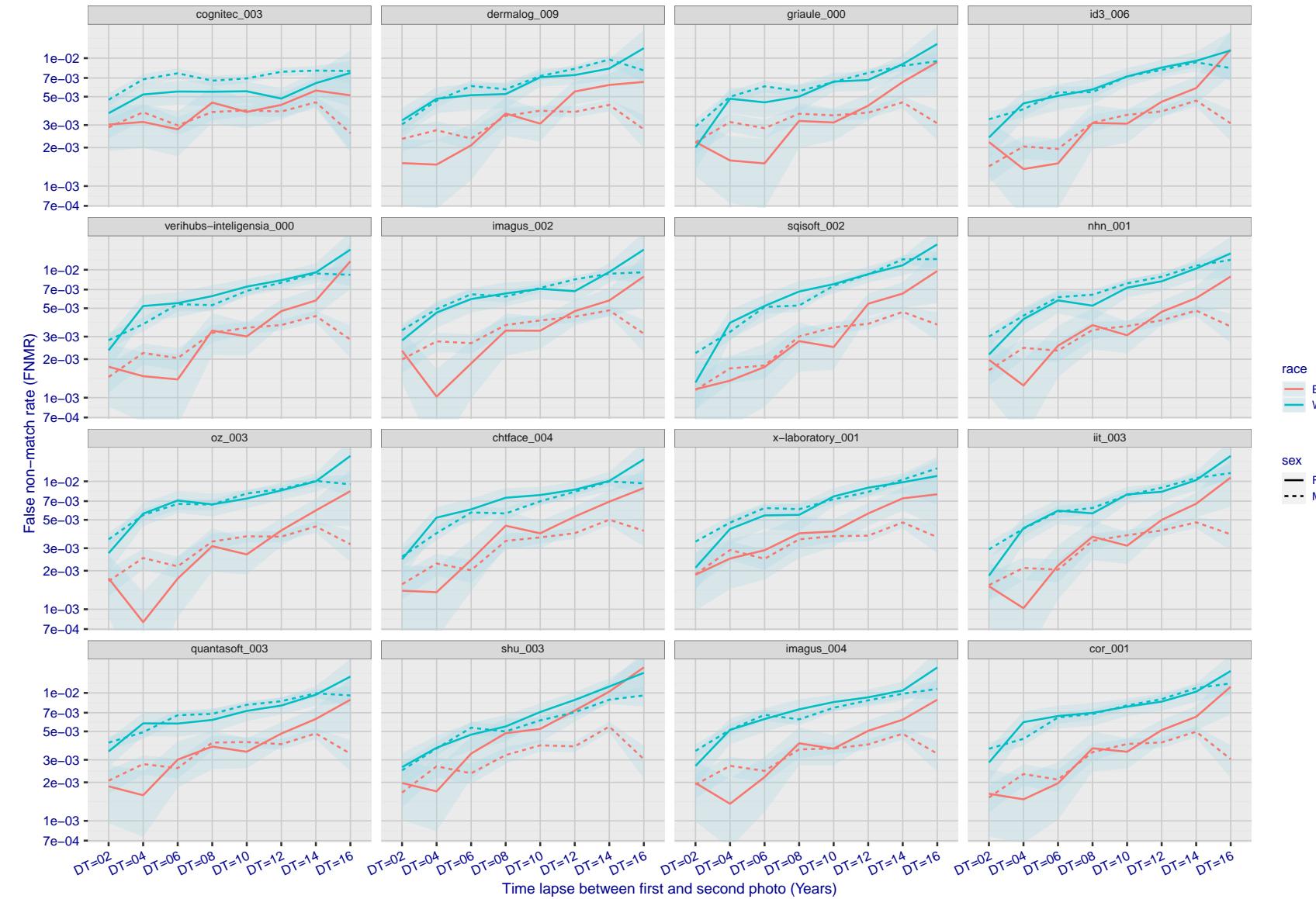


Figure 255: For the mugshot images, FNMR as a function of elapsed time between initial enrollment and second verification images. The panels appear most accurate first, and vertical scale changes on each page. The four traces correspond to images annotated with codes for black female, black male, white female, white male. The threshold is fixed for each algorithm to give $FMR = 0.00001$ over all (10^8) impostor comparisons. For short time-lapses, the most accurate algorithms give very few errors ($FNMR < 0.001$) so that the uncertainty estimates are high.

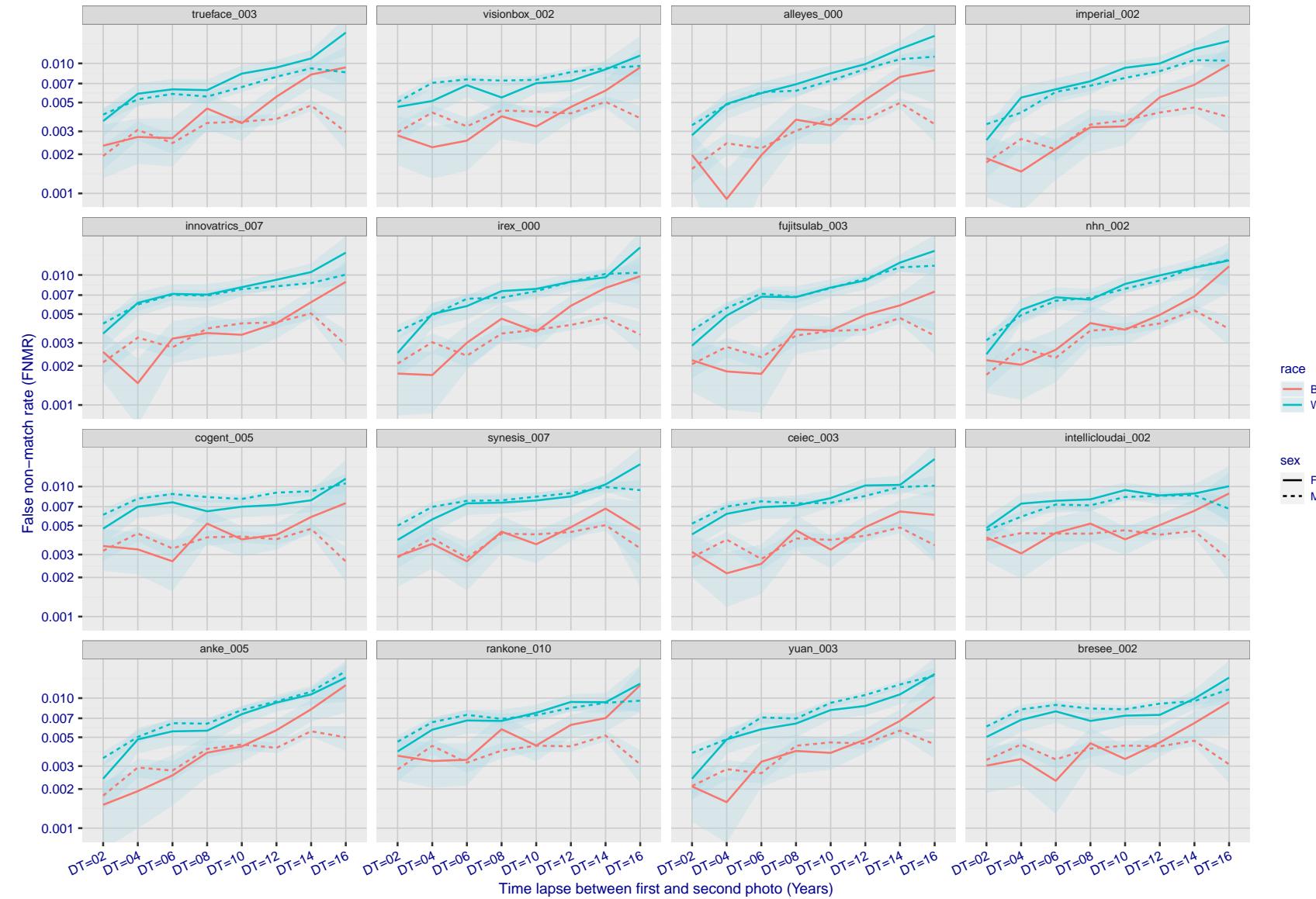


Figure 256: For the mugshot images, FNMR as a function of elapsed time between initial enrollment and second verification images. The panels appear most accurate first, and vertical scale changes on each page. The four traces correspond to images annotated with codes for black female, black male, white female, white male. The threshold is fixed for each algorithm to give $FMR = 0.00001$ over all (10^8) impostor comparisons. For short time-lapses, the most accurate algorithms give very few errors ($FNMR < 0.001$) so that the uncertainty estimates are high.

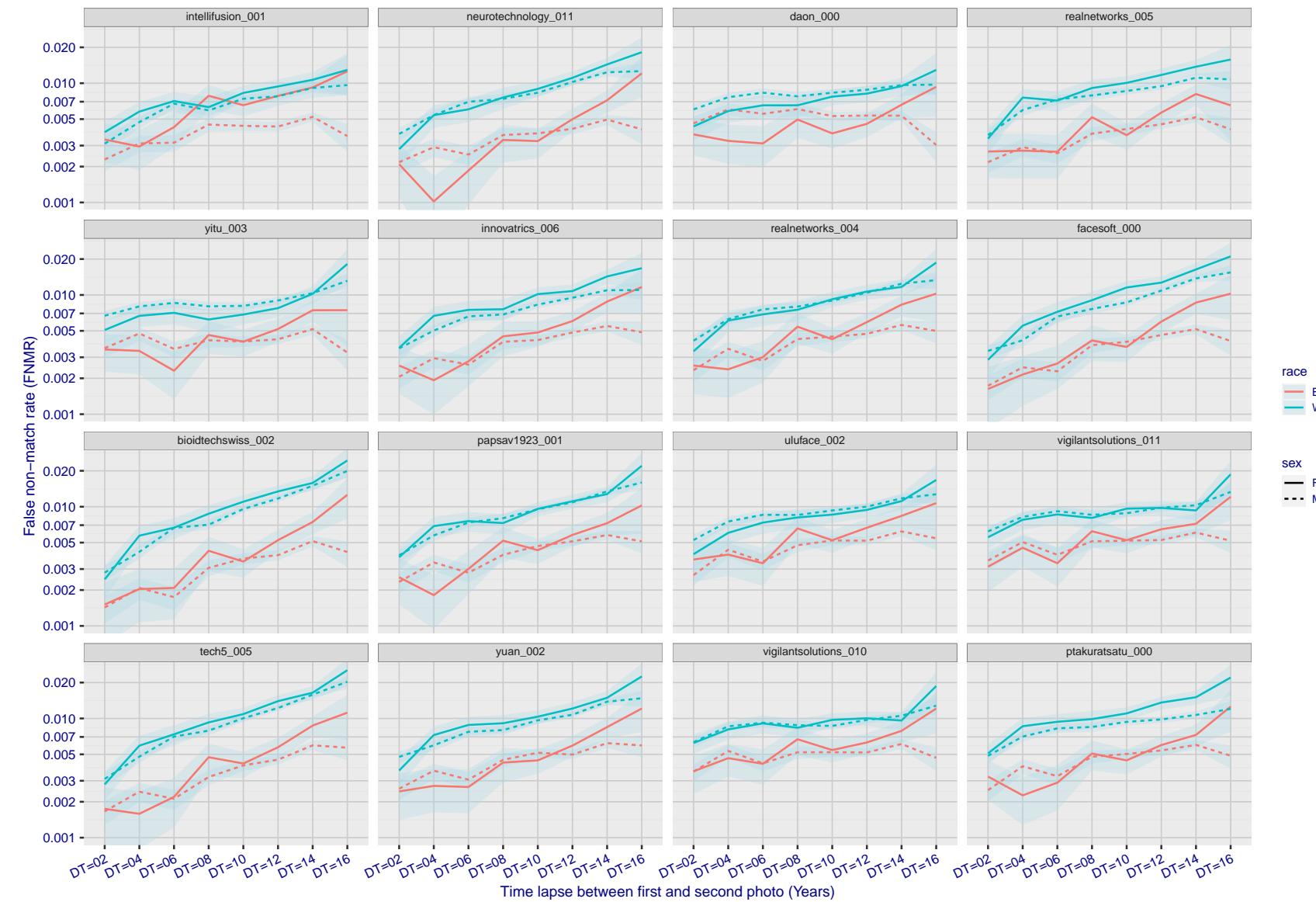


Figure 257: For the mugshot images, FNMR as a function of elapsed time between initial enrollment and second verification images. The panels appear most accurate first, and vertical scale changes on each page. The four traces correspond to images annotated with codes for black female, black male, white female, white male. The threshold is fixed for each algorithm to give FMR = 0.00001 over all (10^8) impostor comparisons. For short time-lapses, the most accurate algorithms give very few errors (FNMR < 0.001) so that the uncertainty estimates are high.

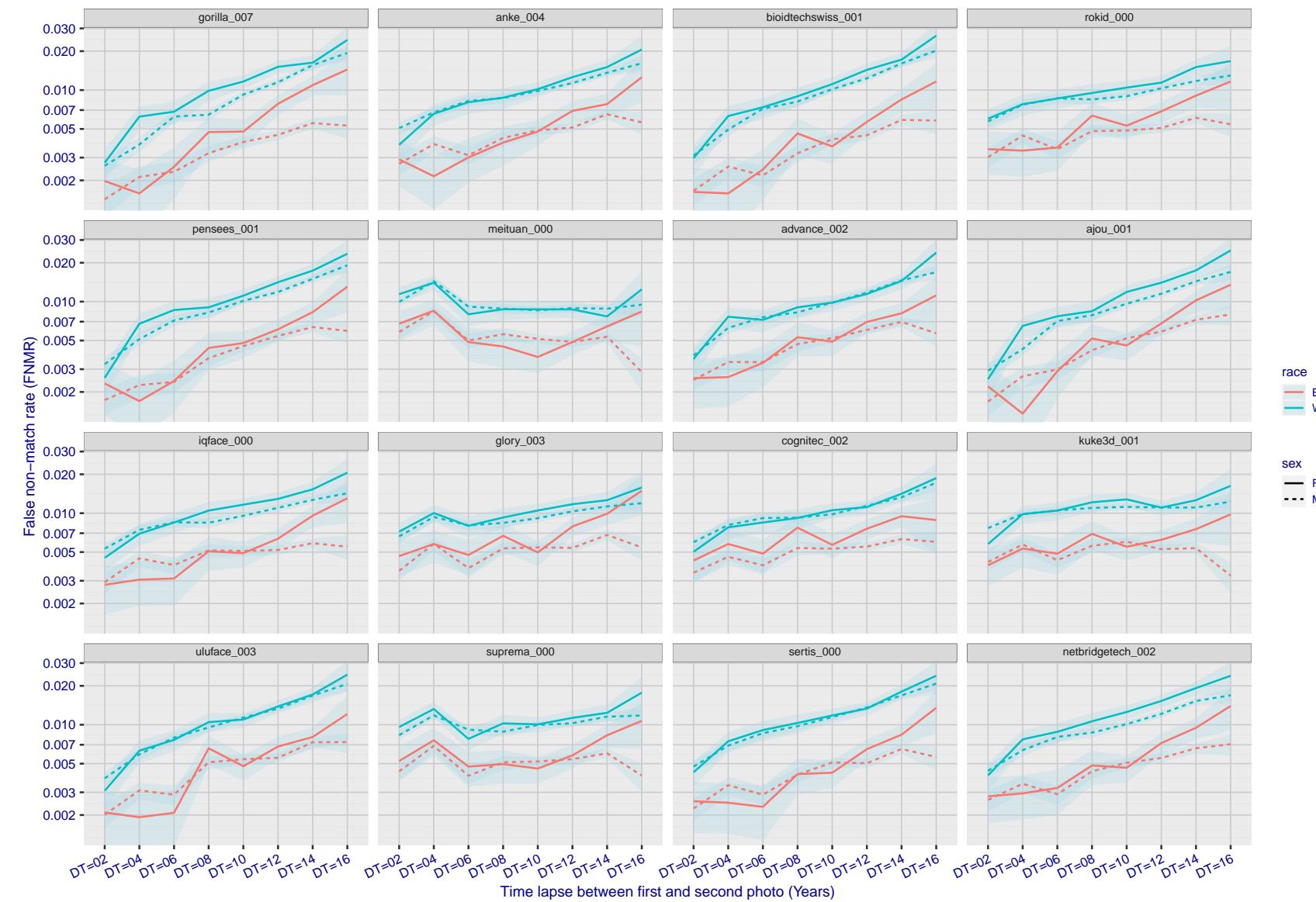


Figure 258: For the mugshot images, FNMR as a function of elapsed time between initial enrollment and second verification images. The panels appear most accurate first, and vertical scale changes on each page. The four traces correspond to images annotated with codes for black female, black male, white female, white male. The threshold is fixed for each algorithm to give $FMR = 0.00001$ over all (10^8) impostor comparisons. For short time-lapses, the most accurate algorithms give very few errors ($FNMR < 0.001$) so that the uncertainty estimates are high.

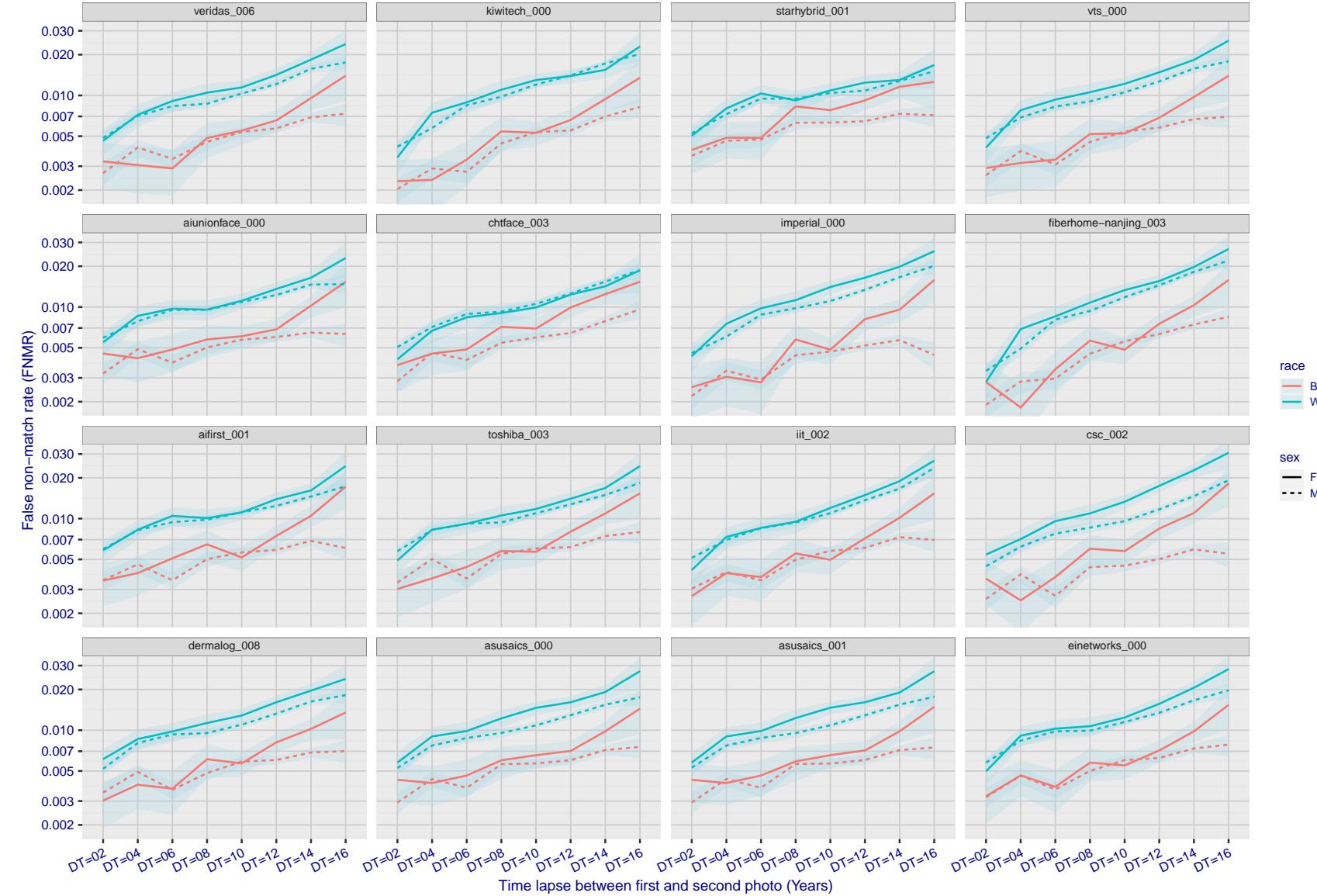


Figure 259: For the mugshot images, FNMR as a function of elapsed time between initial enrollment and second verification images. The panels appear most accurate first, and vertical scale changes on each page. The four traces correspond to images annotated with codes for black female, black male, white female, white male. The threshold is fixed for each algorithm to give FMR = 0.00001 over all (10^8) impostor comparisons. For short time-lapses, the most accurate algorithms give very few errors (FNMR < 0.001) so that the uncertainty estimates are high.

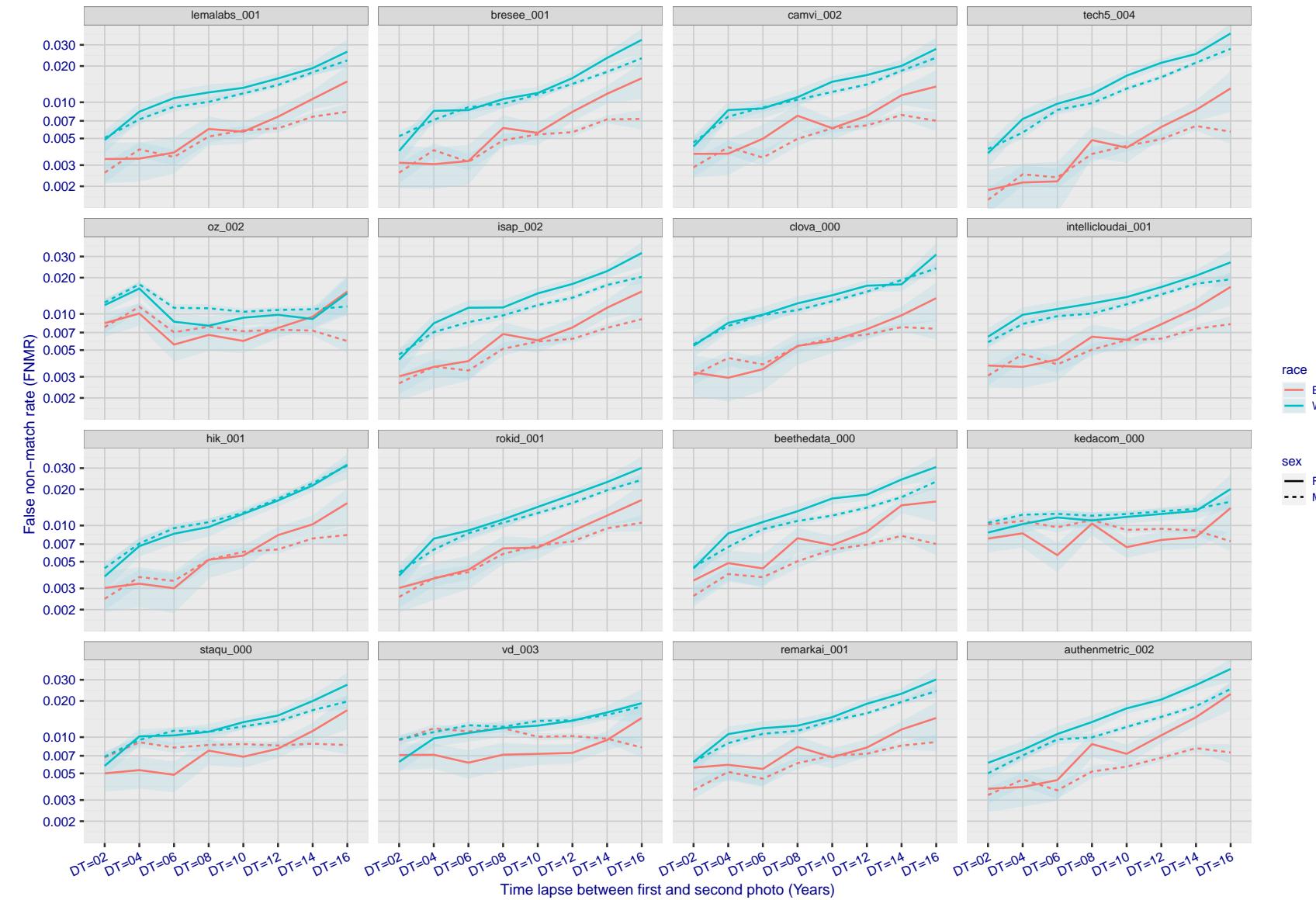


Figure 260: For the mugshot images, FNMR as a function of elapsed time between initial enrollment and second verification images. The panels appear most accurate first, and vertical scale changes on each page. The four traces correspond to images annotated with codes for black female, black male, white female, white male. The threshold is fixed for each algorithm to give $FMR = 0.00001$ over all (10^8) impostor comparisons. For short time-lapses, the most accurate algorithms give very few errors ($FNMR < 0.001$) so that the uncertainty estimates are high.

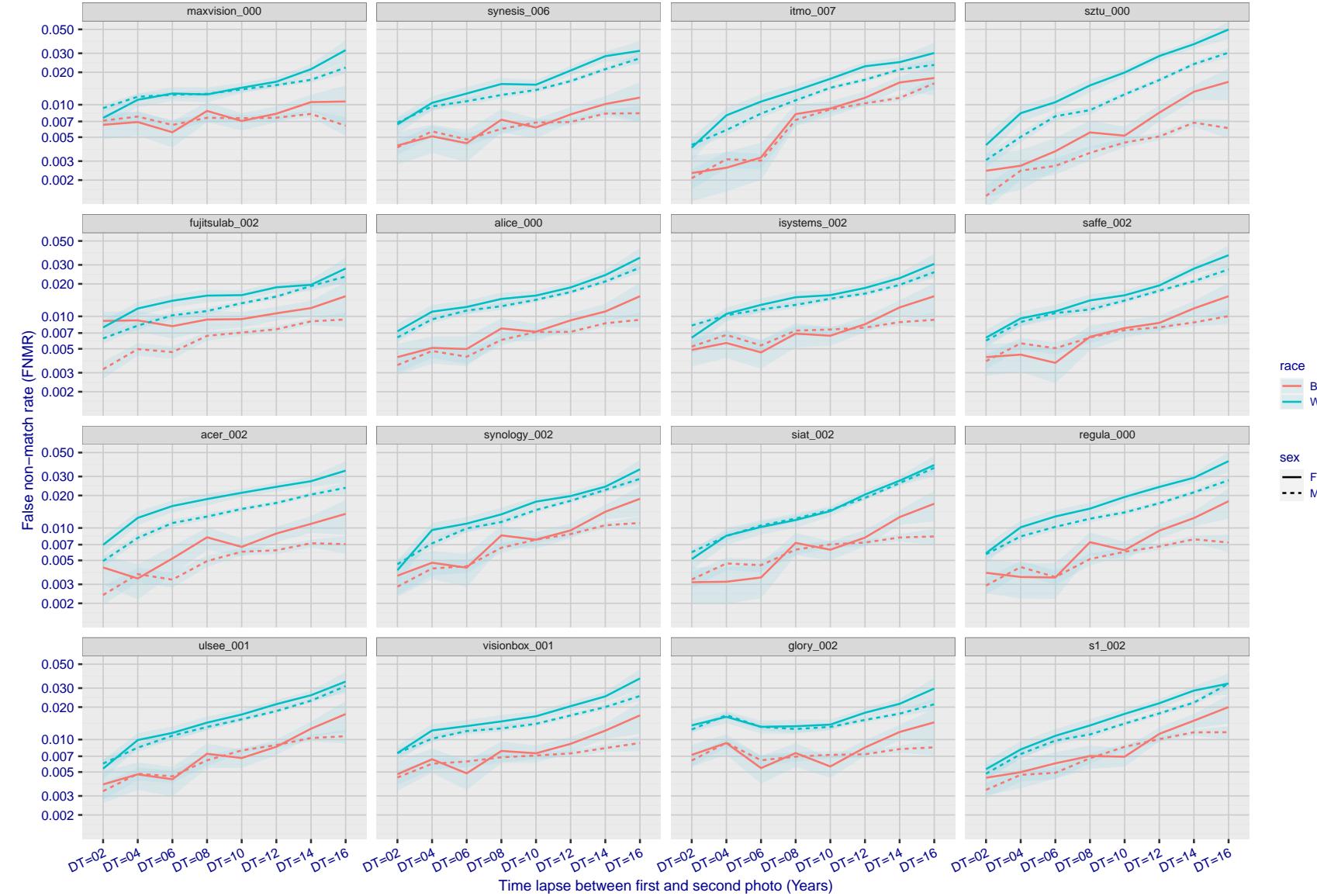


Figure 261: For the mugshot images, FNMR as a function of elapsed time between initial enrollment and second verification images. The panels appear most accurate first, and vertical scale changes on each page. The four traces correspond to images annotated with codes for black female, black male, white female, white male. The threshold is fixed for each algorithm to give FMR = 0.00001 over all (10^8) impostor comparisons. For short time-lapses, the most accurate algorithms give very few errors (FNMR < 0.001) so that the uncertainty estimates are high.

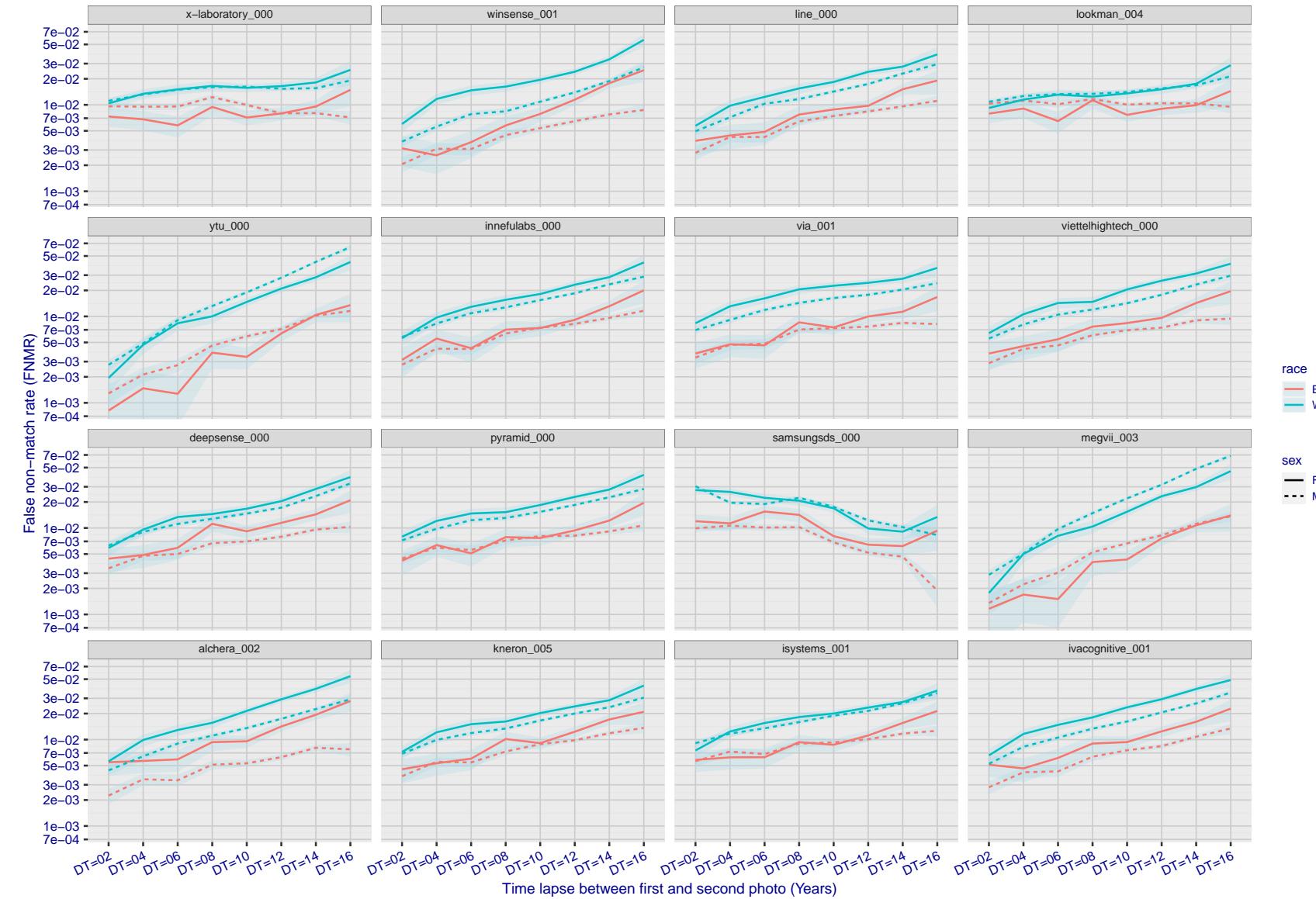


Figure 262: For the mugshot images, FNMR as a function of elapsed time between initial enrollment and second verification images. The panels appear most accurate first, and vertical scale changes on each page. The four traces correspond to images annotated with codes for black female, black male, white female, white male. The threshold is fixed for each algorithm to give FMR = 0.00001 over all (10^8) impostor comparisons. For short time-lapses, the most accurate algorithms give very few errors (FNMR < 0.001) so that the uncertainty estimates are high.

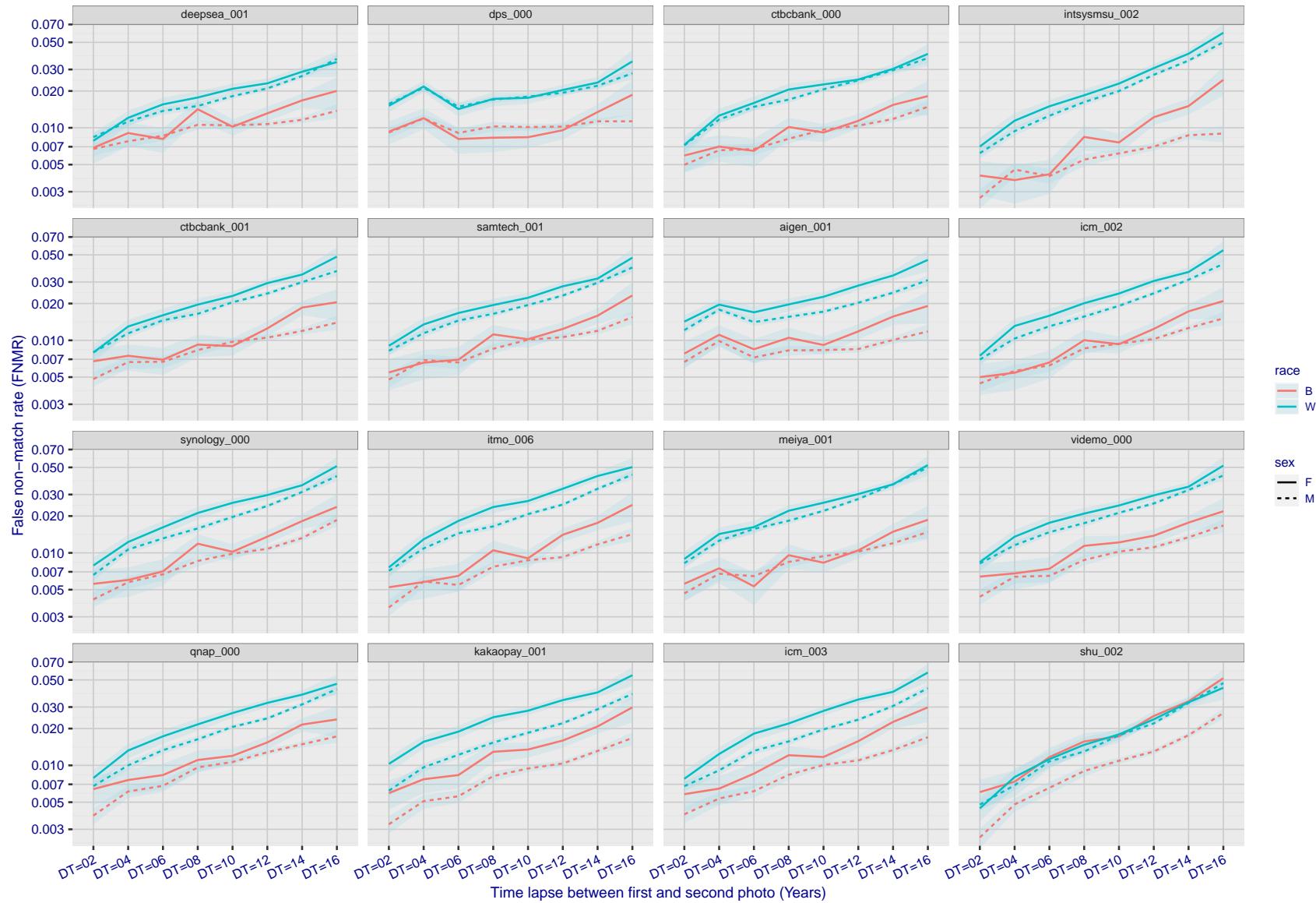


Figure 263: For the mugshot images, FNMR as a function of elapsed time between initial enrollment and second verification images. The panels appear most accurate first, and vertical scale changes on each page. The four traces correspond to images annotated with codes for black female, black male, white female, white male. The threshold is fixed for each algorithm to give FMR = 0.00001 over all (10^8) impostor comparisons. For short time-lapses, the most accurate algorithms give very few errors (FNMR < 0.001) so that the uncertainty estimates are high.

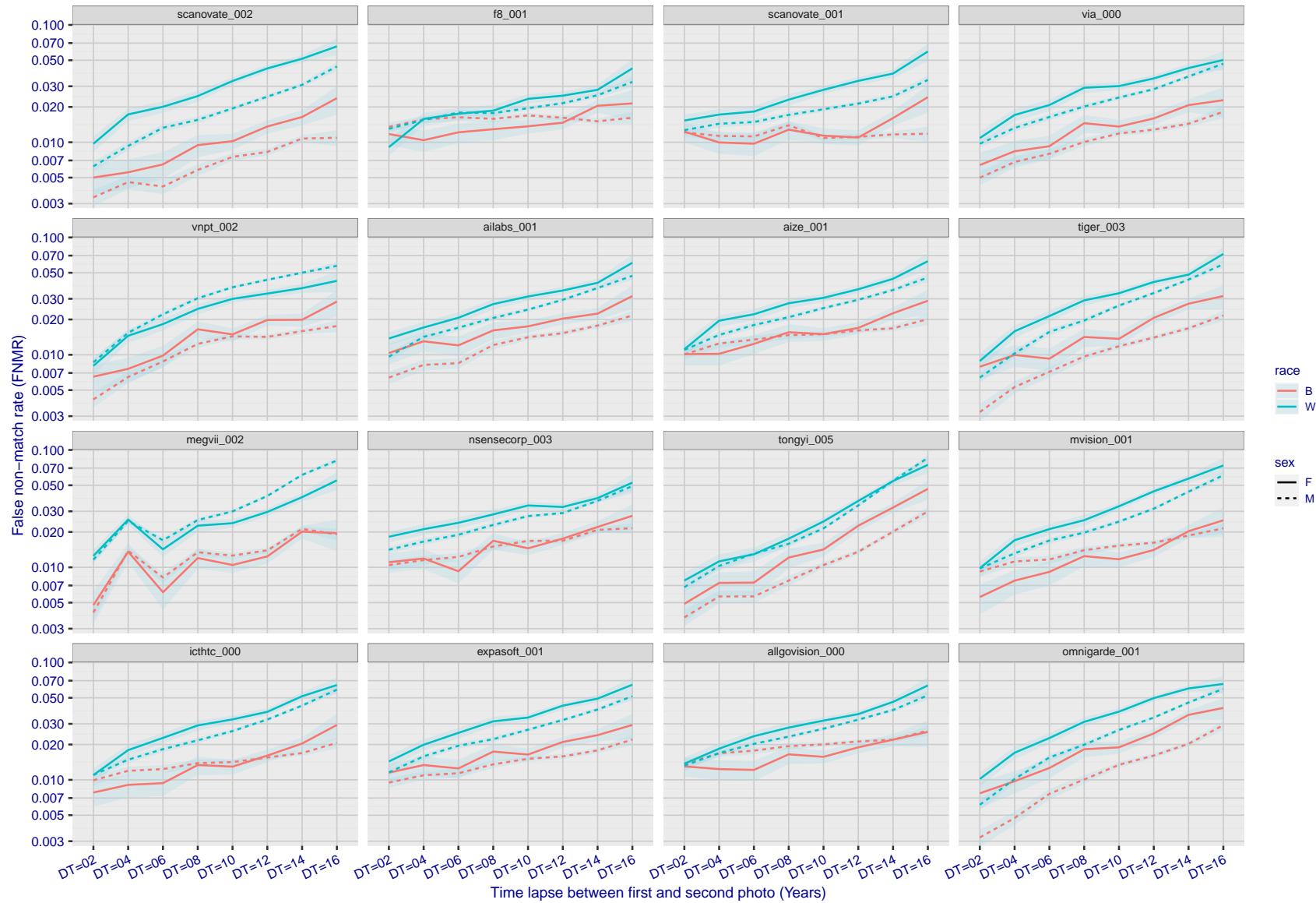


Figure 264: For the mugshot images, FNMR as a function of elapsed time between initial enrollment and second verification images. The panels appear most accurate first, and vertical scale changes on each page. The four traces correspond to images annotated with codes for black female, black male, white female, white male. The threshold is fixed for each algorithm to give FMR = 0.00001 over all (10^8) impostor comparisons. For short time-lapses, the most accurate algorithms give very few errors (FNMR < 0.001) so that the uncertainty estimates are high.

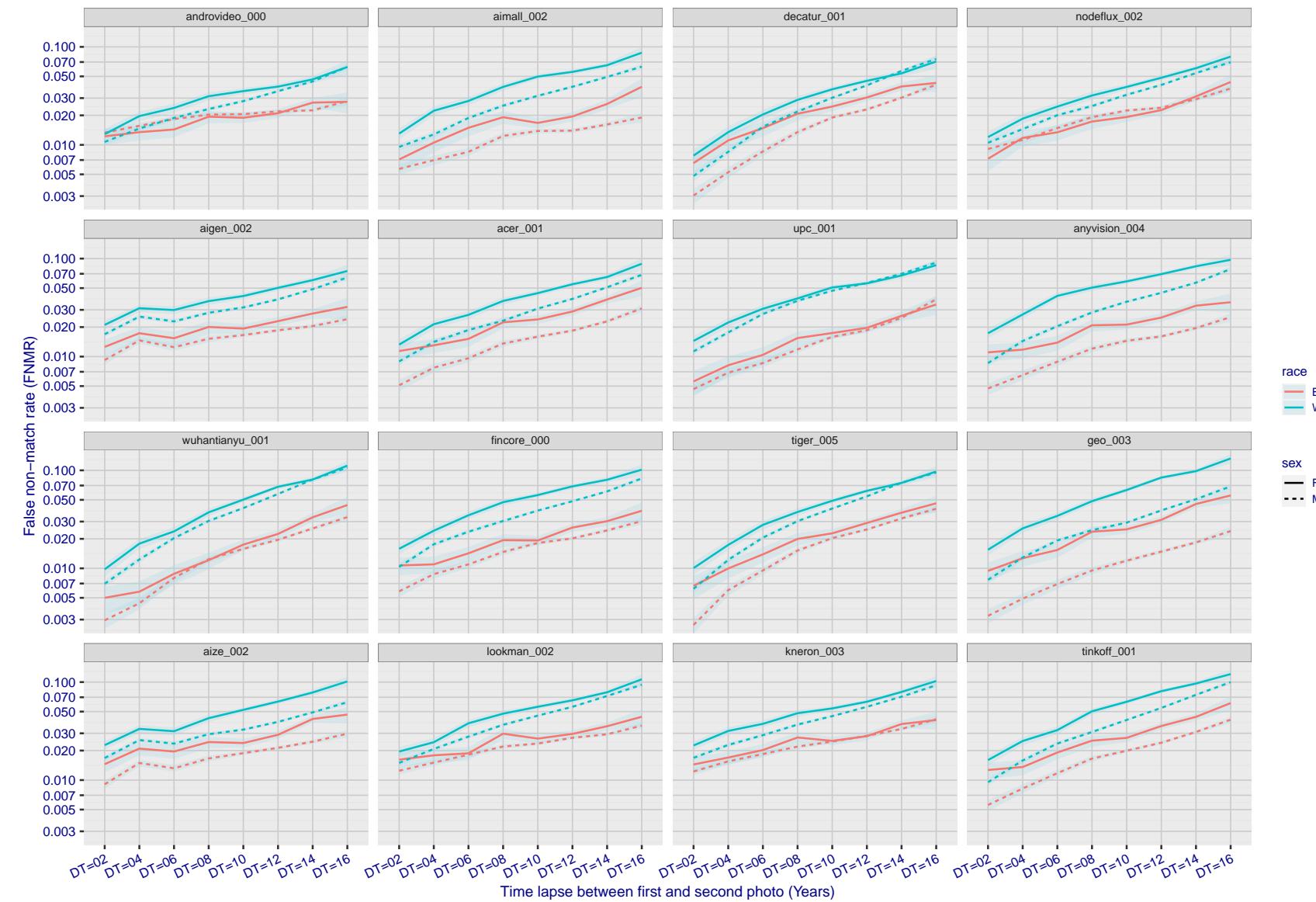


Figure 265: For the mugshot images, FNMR as a function of elapsed time between initial enrollment and second verification images. The panels appear most accurate first, and vertical scale changes on each page. The four traces correspond to images annotated with codes for black female, black male, white female, white male. The threshold is fixed for each algorithm to give FMR = 0.00001 over all (10^8) impostor comparisons. For short time-lapses, the most accurate algorithms give very few errors (FNMR < 0.001) so that the uncertainty estimates are high.

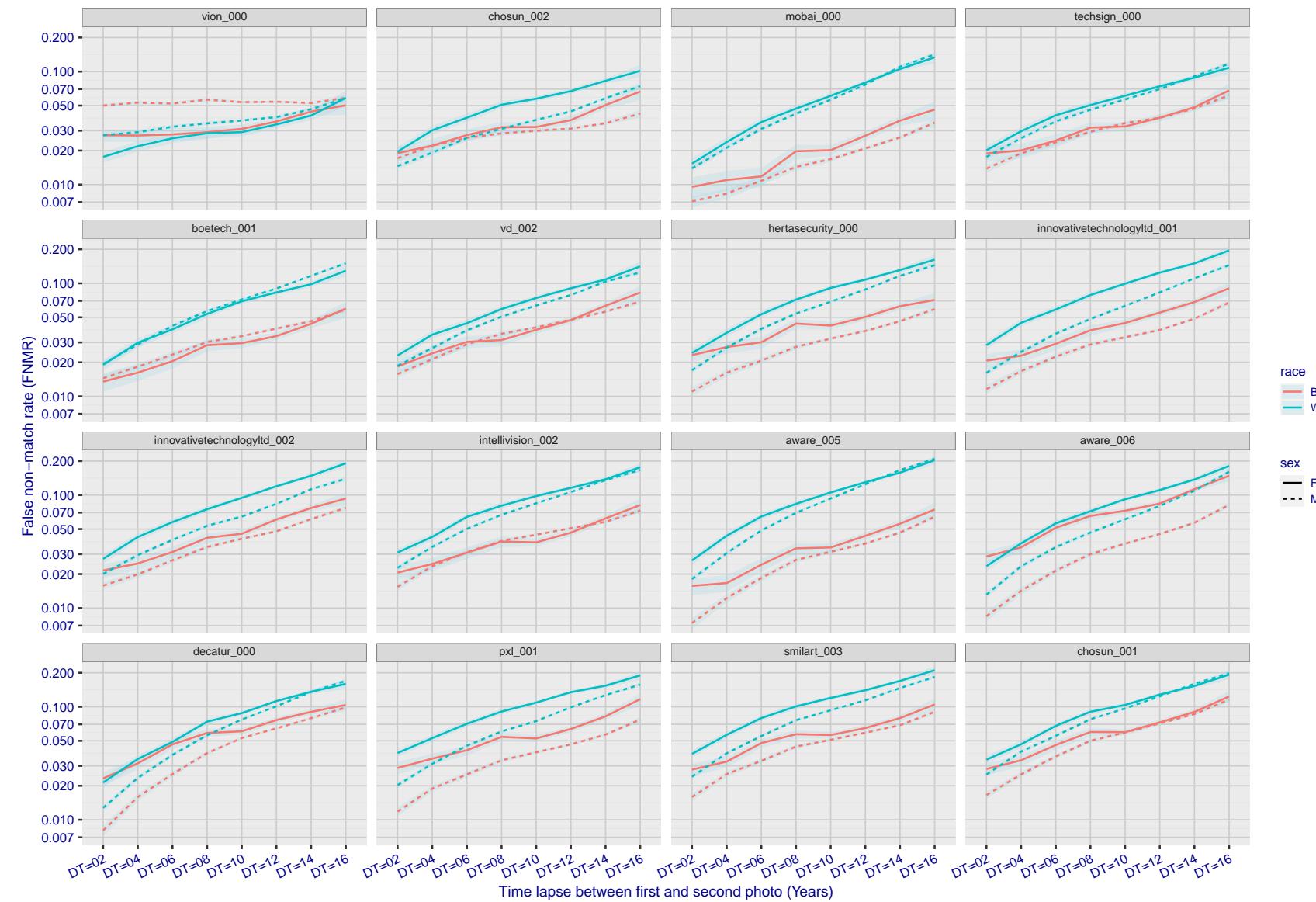


Figure 266: For the mugshot images, FNMR as a function of elapsed time between initial enrollment and second verification images. The panels appear most accurate first, and vertical scale changes on each page. The four traces correspond to images annotated with codes for black female, black male, white female, white male. The threshold is fixed for each algorithm to give FMR = 0.00001 over all (10^8) impostor comparisons. For short time-lapses, the most accurate algorithms give very few errors (FNMR < 0.001) so that the uncertainty estimates are high.

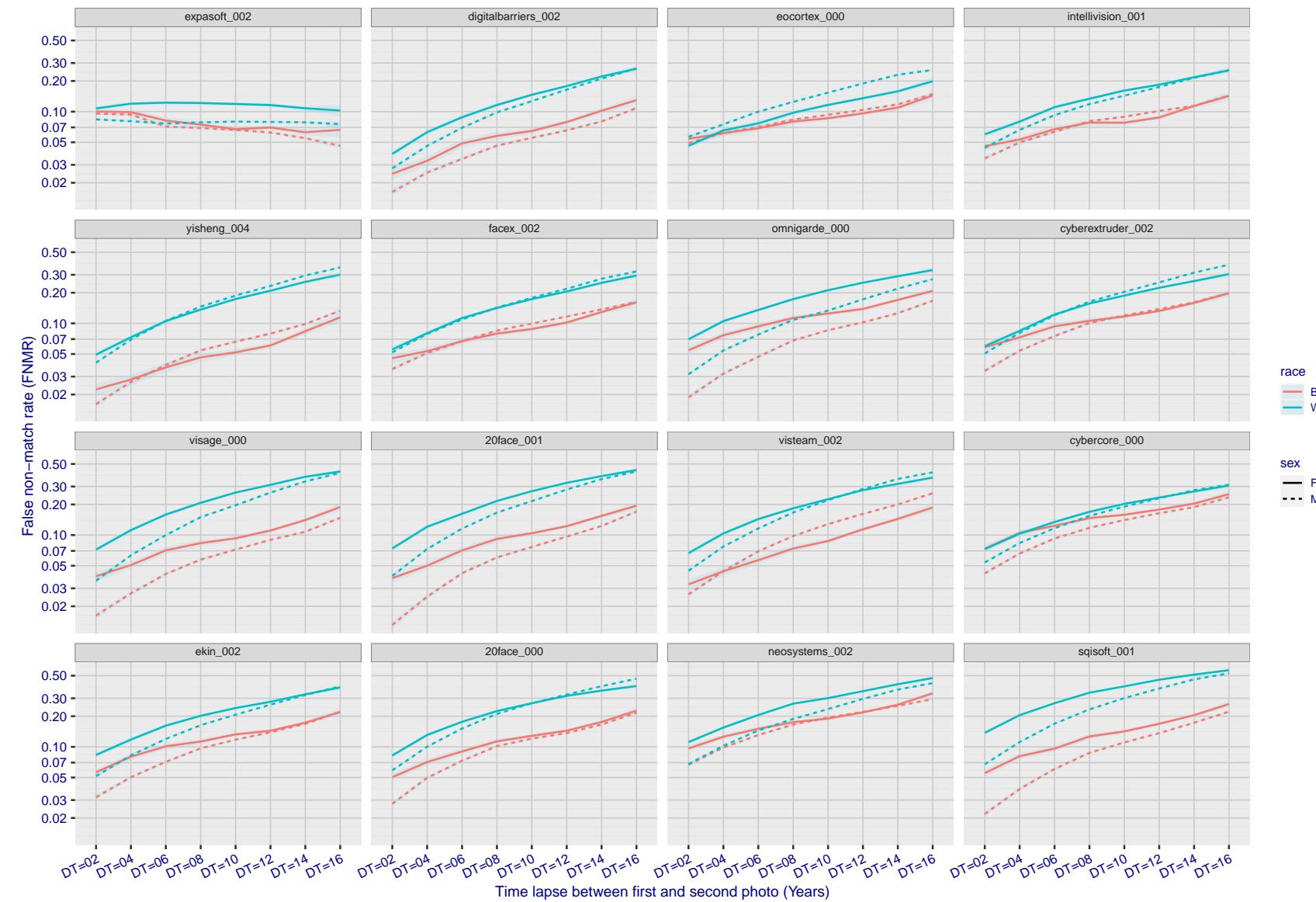


Figure 267: For the mugshot images, FNMR as a function of elapsed time between initial enrollment and second verification images. The panels appear most accurate first, and vertical scale changes on each page. The four traces correspond to images annotated with codes for black female, black male, white female, white male. The threshold is fixed for each algorithm to give FMR = 0.00001 over all (10^8) impostor comparisons. For short time-lapses, the most accurate algorithms give very few errors (FNMR < 0.001) so that the uncertainty estimates are high.

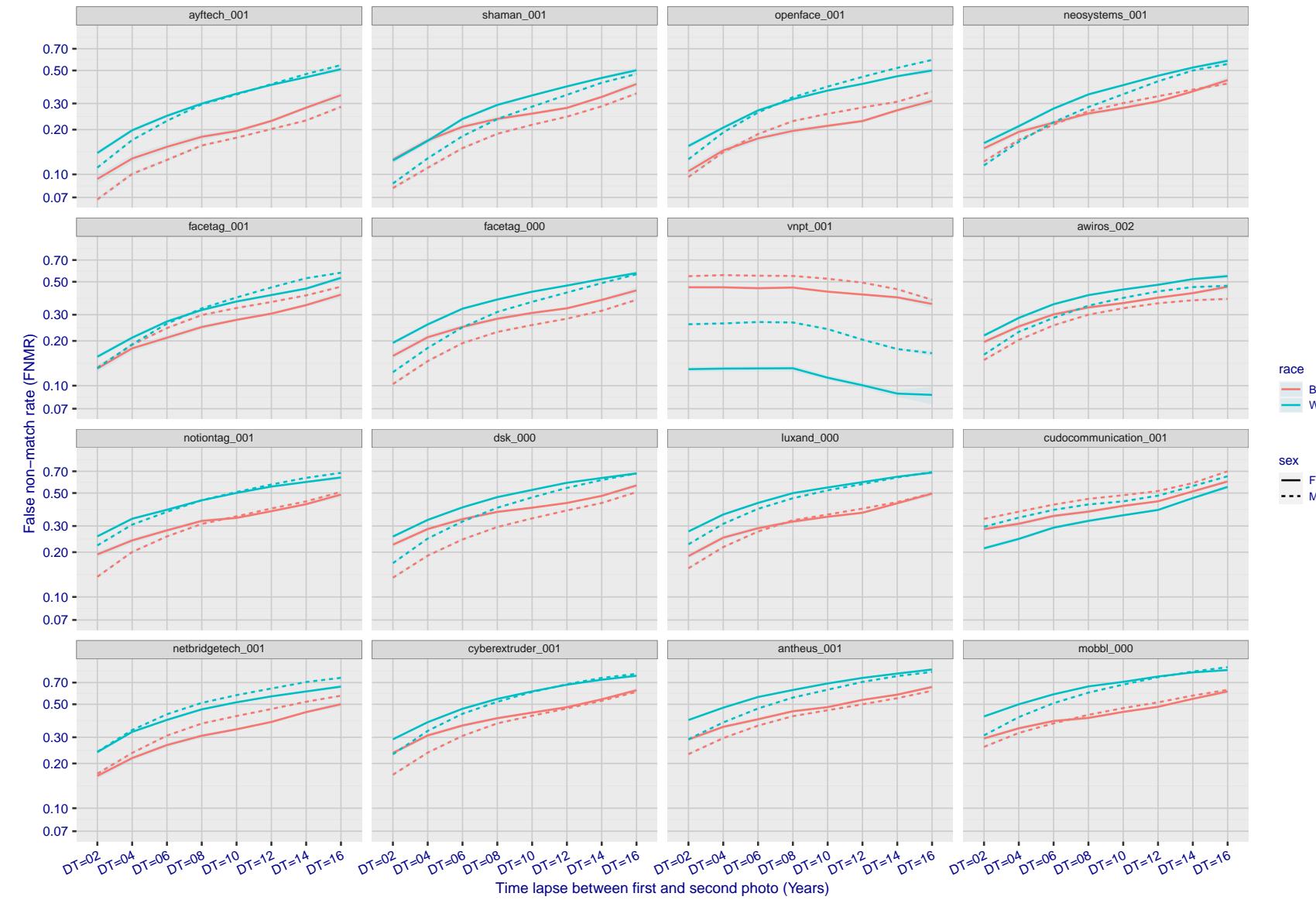


Figure 268: For the mugshot images, FNMR as a function of elapsed time between initial enrollment and second verification images. The panels appear most accurate first, and vertical scale changes on each page. The four traces correspond to images annotated with codes for black female, black male, white female, white male. The threshold is fixed for each algorithm to give $FMR = 0.00001$ over all (10^8) impostor comparisons. For short time-lapses, the most accurate algorithms give very few errors ($FNMR < 0.001$) so that the uncertainty estimates are high.

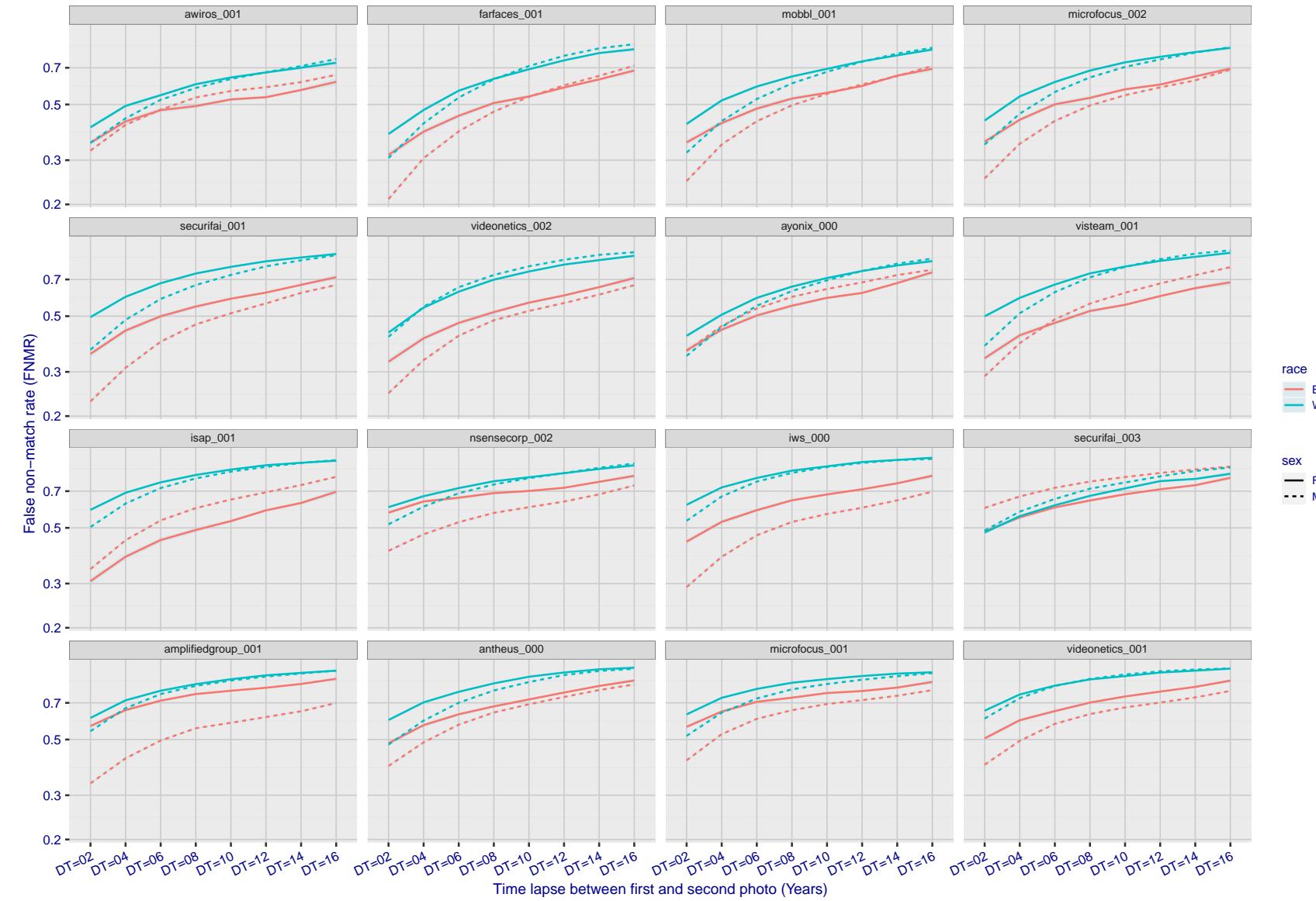


Figure 269: For the mugshot images, FNMR as a function of elapsed time between initial enrollment and second verification images. The panels appear most accurate first, and vertical scale changes on each page. The four traces correspond to images annotated with codes for black female, black male, white female, white male. The threshold is fixed for each algorithm to give FMR = 0.00001 over all (10^8) impostor comparisons. For short time-lapses, the most accurate algorithms give very few errors (FNMR < 0.001) so that the uncertainty estimates are high.

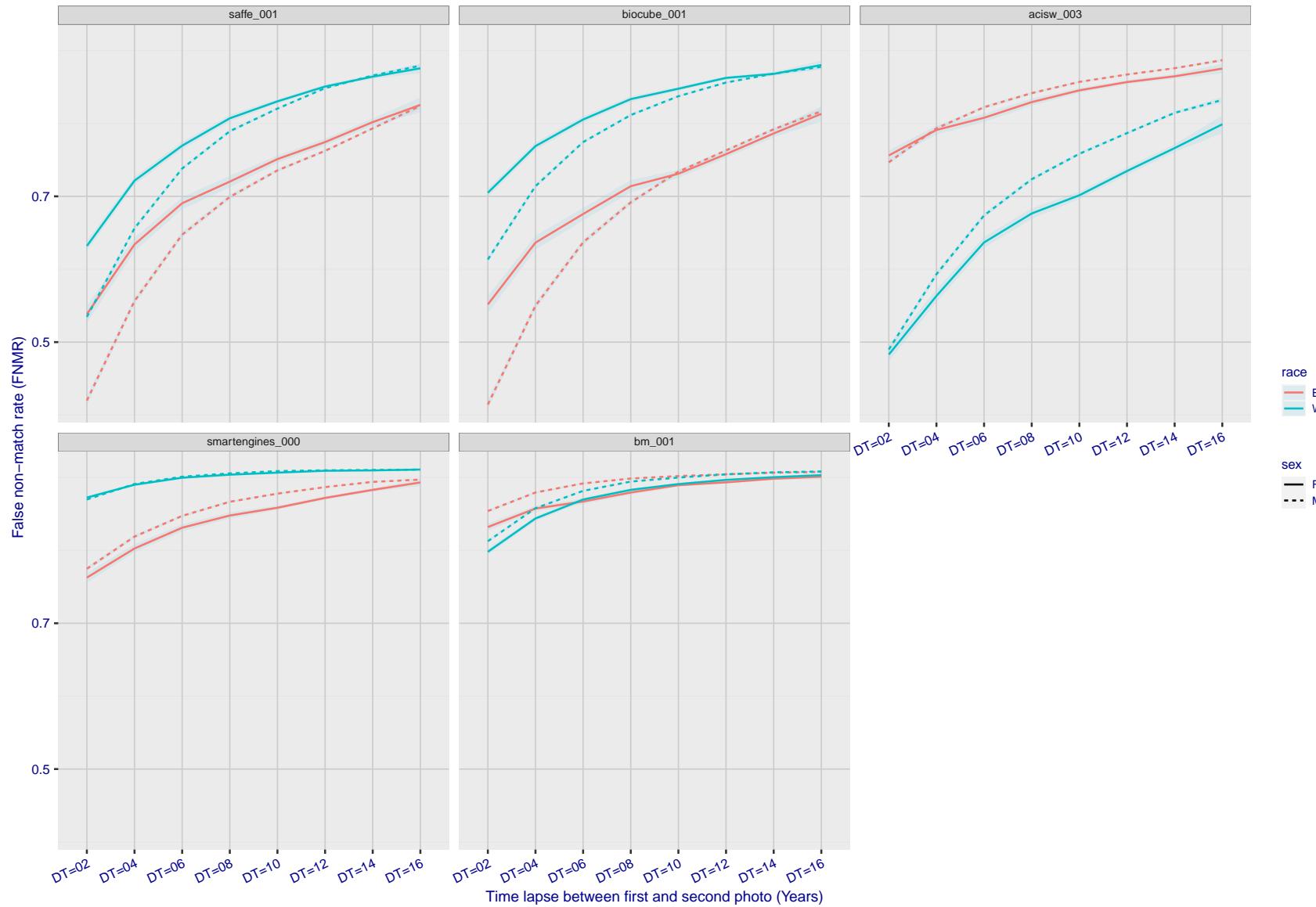


Figure 270: For the mugshot images, FNMR as a function of elapsed time between initial enrollment and second verification images. The panels appear most accurate first, and vertical scale changes on each page. The four traces correspond to images annotated with codes for black female, black male, white female, white male. The threshold is fixed for each algorithm to give FMR = 0.00001 over all (10^8) impostor comparisons. For short time-lapses, the most accurate algorithms give very few errors (FNMR < 0.001) so that the uncertainty estimates are high.

3.5.3 Effect of age on genuine subjects

Background: Faces change appearance throughout life. Face recognition algorithms have previously been reported to give better accuracy on older individuals (See NIST IR 8009).

Goal: To quantify false non-match rates (FNMR) as a function of age, without an ageing component.

Methods: Using the visa images, which span fewer than five years, thresholds are determined that give FMR = 0.001 and 0.0001 over the entire impostor set. Then FNMR is measured over 1000 bootstrap replications of the genuine scores.

Results: For the visa images, Figure 301 shows how false non-match rates for genuine users, as a function of age group. The notable aspects are:

- ▷ Younger subjects give considerably higher FNMR. This is likely due to rapid growth and change in facial appearance.
- ▷ FNMR trends down throughout life. The last bin, AGE > 72, contains fewer than 140 mated pairs, and may be affected by small sample size.



Figure 271: For the visa images, the dots show FNMR by age group for two operating thresholds corresponding to $FMR = \{0.001, 0.0001\}$ computed over all on the order of 10^{10} impostor scores. The FMR in each bin will vary also - see subsequent impostor heatmaps in sec. 3.6.2. Given a pair of face images taken at different times, we assign the comparison to the bin that is the arithmetic average of the subject's ages. This plot shows only the effect of age, not ageing. The number of comparisons in each bin is generally in the thousands, however the first and last bins are computed over 149 and 124 respectively. The error rates in some (adult) cases are zero, and in others the DET is flat so the error rates at the two thresholds are identical. The lines span 1% and 99% of bootstrap replicated FNMR estimates.



Figure 272: For the visa images, the dots show FNMR by age group for two operating thresholds corresponding to $FMR = \{0.001, 0.0001\}$ computed over all on the order of 10^{10} impostor scores. The FMR in each bin will vary also - see subsequent impostor heatmaps in sec. 3.6.2. Given a pair of face images taken at different times, we assign the comparison to the bin that is the arithmetic average of the subject's ages. This plot shows only the effect of age, not ageing. The number of comparisons in each bin is generally in the thousands, however the first and last bins are computed over 149 and 124 respectively. The error rates in some (adult) cases are zero, and in others the DET is flat so the error rates at the two thresholds are identical. The lines span 1% and 99% of bootstrap replicated FNMR estimates.

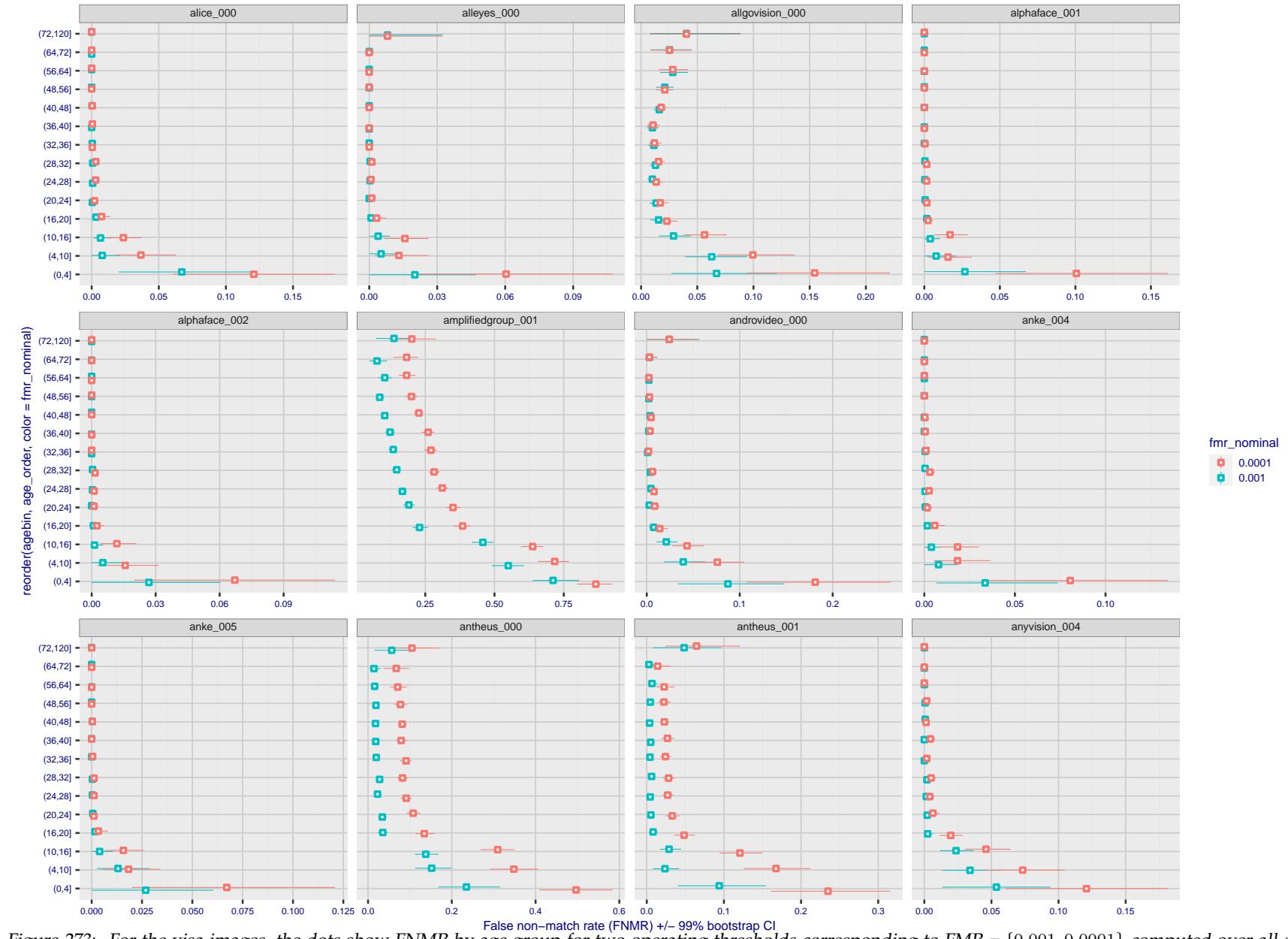


Figure 273: For the visa images, the dots show FNMR by age group for two operating thresholds corresponding to $FMR = \{0.001, 0.0001\}$ computed over all on the order of 10^{10} impostor scores. The FMR in each bin will vary also - see subsequent impostor heatmaps in sec. 3.6.2. Given a pair of face images taken at different times, we assign the comparison to the bin that is the arithmetic average of the subject's ages. This plot shows only the effect of age, not ageing. The number of comparisons in each bin is generally in the thousands, however the first and last bins are computed over 149 and 124 respectively. The error rates in some (adult) cases are zero, and in others the DET is flat so the error rates at the two thresholds are identical. The lines span 1% and 99% of bootstrap replicated FNMR estimates.



Figure 274: For the visa images, the dots show FNMR by age group for two operating thresholds corresponding to $FMR = \{0.001, 0.0001\}$ computed over all on the order of 10^{10} impostor scores. The FMR in each bin will vary also - see subsequent impostor heatmaps in sec. 3.6.2. Given a pair of face images taken at different times, we assign the comparison to the bin that is the arithmetic average of the subject's ages. This plot shows only the effect of age, not ageing. The number of comparisons in each bin is generally in the thousands, however the first and last bins are computed over 149 and 124 respectively. The error rates in some (adult) cases are zero, and in others the DET is flat so the error rates at the two thresholds are identical. The lines span 1% and 99% of bootstrap replicated FNMR estimates.



Figure 275: For the visa images, the dots show FNMR by age group for two operating thresholds corresponding to $FMR = \{0.001, 0.0001\}$ computed over all on the order of 10^{10} impostor scores. The FMR in each bin will vary also - see subsequent impostor heatmaps in sec. 3.6.2. Given a pair of face images taken at different times, we assign the comparison to the bin that is the arithmetic average of the subject's ages. This plot shows only the effect of age, not ageing. The number of comparisons in each bin is generally in the thousands, however the first and last bins are computed over 149 and 124 respectively. The error rates in some (adult) cases are zero, and in others the DET is flat so the error rates at the two thresholds are identical. The lines span 1% and 99% of bootstrap replicated FNMR estimates.



Figure 276: For the visa images, the dots show FNMR by age group for two operating thresholds corresponding to $FMR = \{0.001, 0.0001\}$ computed over all on the order of 10^{10} impostor scores. The FMR in each bin will vary also - see subsequent impostor heatmaps in sec. 3.6.2. Given a pair of face images taken at different times, we assign the comparison to the bin that is the arithmetic average of the subject's ages. This plot shows only the effect of age, not ageing. The number of comparisons in each bin is generally in the thousands, however the first and last bins are computed over 149 and 124 respectively. The error rates in some (adult) cases are zero, and in others the DET is flat so the error rates at the two thresholds are identical. The lines span 1% and 99% of bootstrap replicated FNMR estimates.



Figure 277: For the visa images, the dots show FNMR by age group for two operating thresholds corresponding to $FMR = \{0.001, 0.0001\}$ computed over all on the order of 10^{10} impostor scores. The FMR in each bin will vary also - see subsequent impostor heatmaps in sec. 3.6.2. Given a pair of face images taken at different times, we assign the comparison to the bin that is the arithmetic average of the subject's ages. This plot shows only the effect of age, not ageing. The number of comparisons in each bin is generally in the thousands, however the first and last bins are computed over 149 and 124 respectively. The error rates in some (adult) cases are zero, and in others the DET is flat so the error rates at the two thresholds are identical. The lines span 1% and 99% of bootstrap replicated FNMR estimates.

2021/11/22 14:56:30

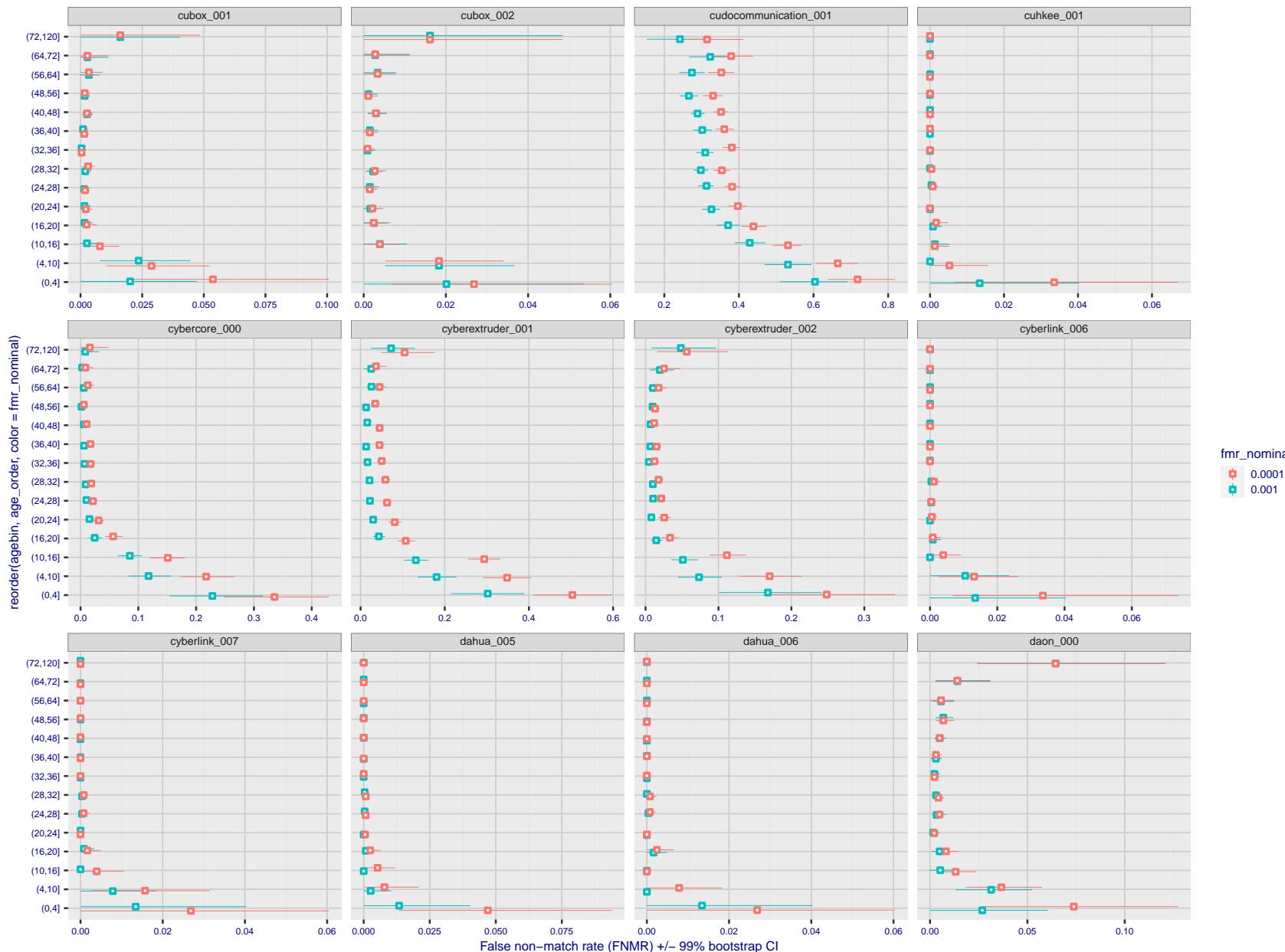


Figure 278: For the visa images, the dots show FNMR by age group for two operating thresholds corresponding to $FMR = \{0.001, 0.0001\}$ computed over all on the order of 10^{10} impostor scores. The FMR in each bin will vary also - see subsequent impostor heatmaps in sec. 3.6.2. Given a pair of face images taken at different times, we assign the comparison to the bin that is the arithmetic average of the subject's ages. This plot shows only the effect of age, not ageing. The number of comparisons in each bin is generally in the thousands, however the first and last bins are computed over 149 and 124 respectively. The error rates in some (adult) cases are zero, and in others the DET is flat so the error rates at the two thresholds are identical. The lines span 1% and 99% of bootstrap replicated FNMR estimates.

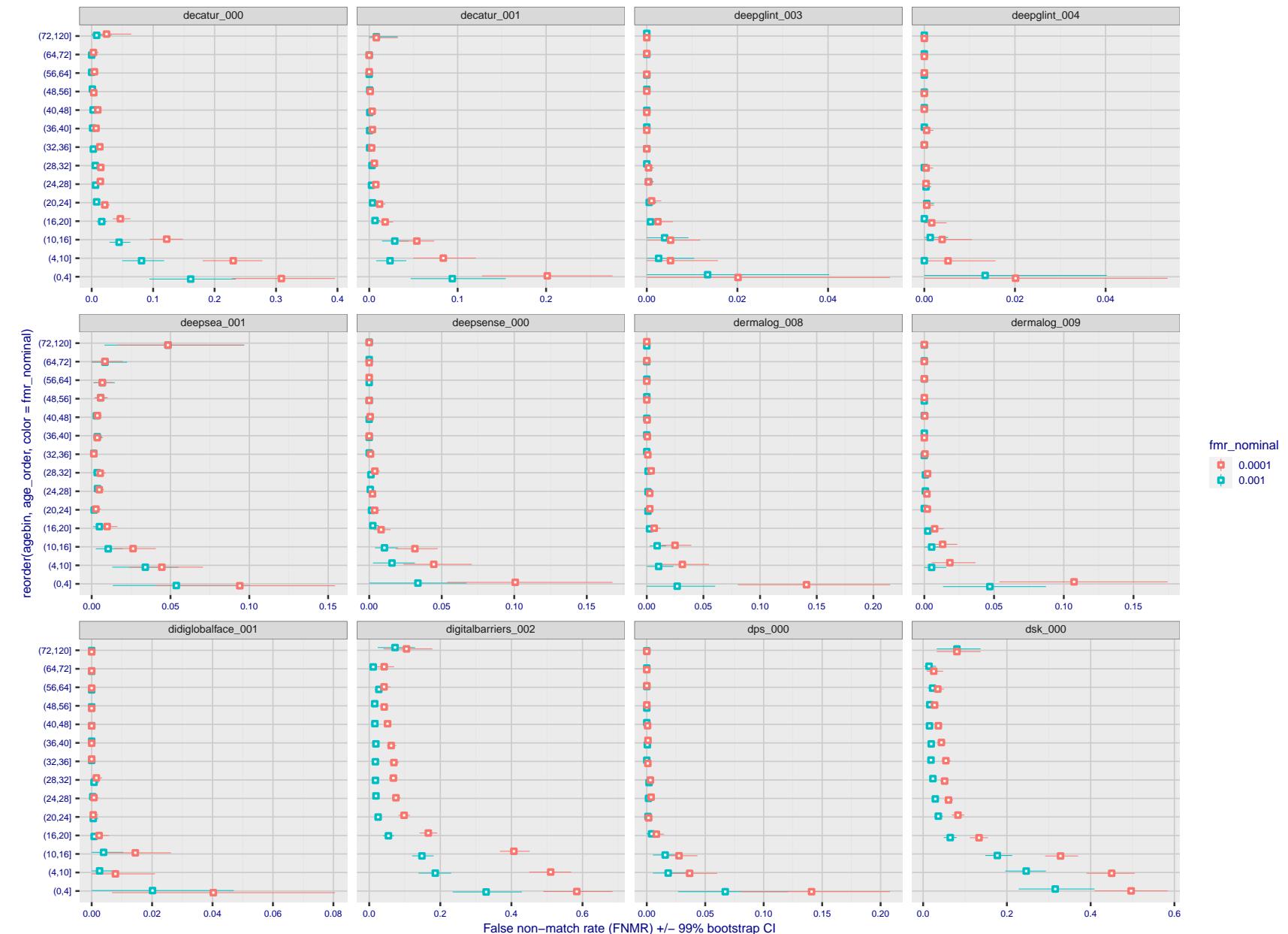


Figure 279: For the visa images, the dots show FNMR by age group for two operating thresholds corresponding to $FMR = \{0.001, 0.0001\}$ computed over all on the order of 10^{10} impostor scores. The FMR in each bin will vary also - see subsequent impostor heatmaps in sec. 3.6.2. Given a pair of face images taken at different times, we assign the comparison to the bin that is the arithmetic average of the subject's ages. This plot shows only the effect of age, not ageing. The number of comparisons in each bin is generally in the thousands, however the first and last bins are computed over 149 and 124 respectively. The error rates in some (adult) cases are zero, and in others the DET is flat so the error rates at the two thresholds are identical. The lines span 1% and 99% of bootstrap replicated FNMR estimates.

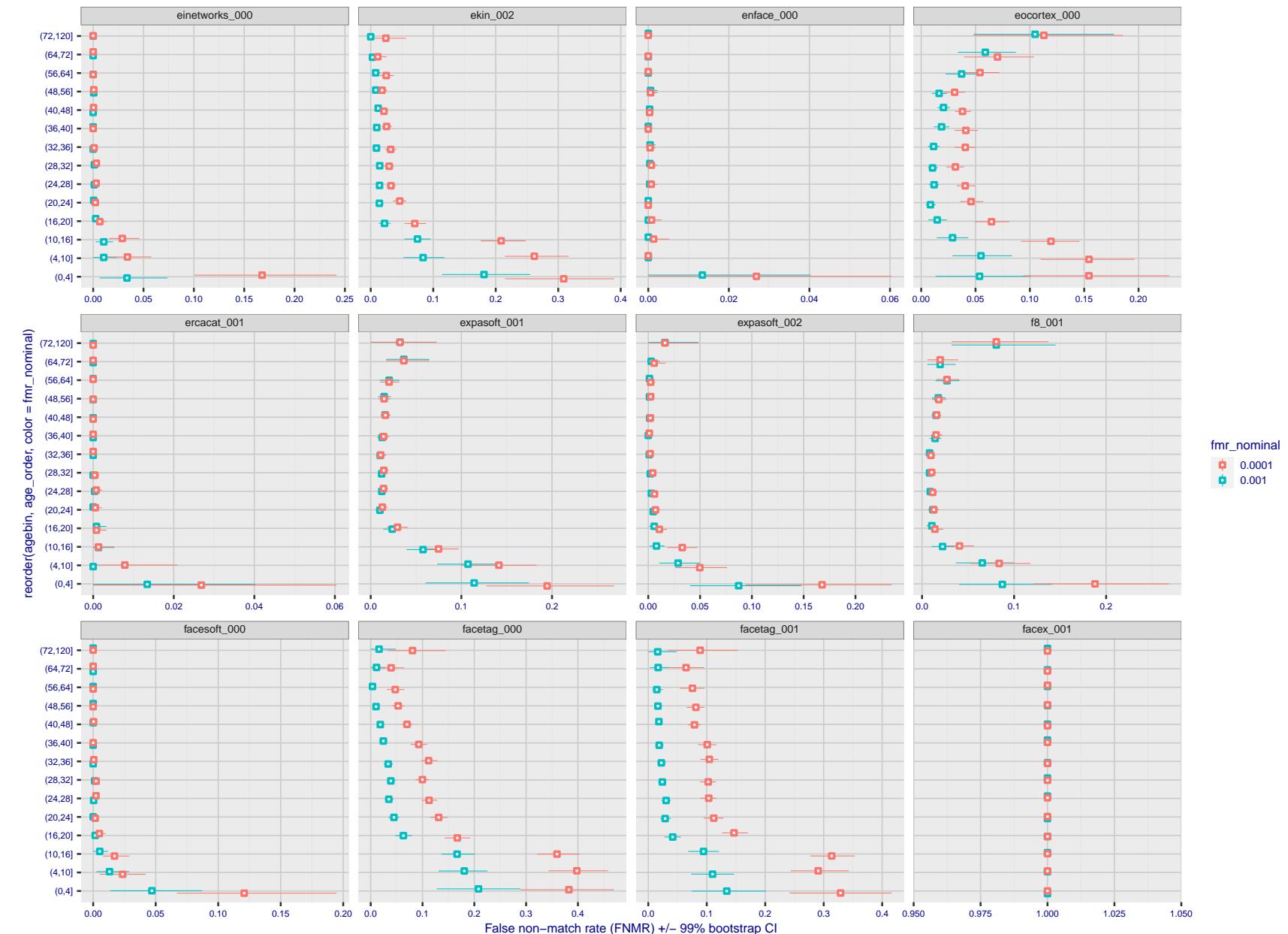


Figure 280: For the visa images, the dots show FNMR by age group for two operating thresholds corresponding to $FMR = \{0.001, 0.0001\}$ computed over all on the order of 10^{10} impostor scores. The FMR in each bin will vary also - see subsequent impostor heatmaps in sec. 3.6.2. Given a pair of face images taken at different times, we assign the comparison to the bin that is the arithmetic average of the subject's ages. This plot shows only the effect of age, not ageing. The number of comparisons in each bin is generally in the thousands, however the first and last bins are computed over 149 and 124 respectively. The error rates in some (adult) cases are zero, and in others the DET is flat so the error rates at the two thresholds are identical. The lines span 1% and 99% of bootstrap replicated FNMR estimates.



Figure 281: For the visa images, the dots show FNMR by age group for two operating thresholds corresponding to $FMR = \{0.001, 0.0001\}$ computed over all on the order of 10^{10} impostor scores. The FMR in each bin will vary also - see subsequent impostor heatmaps in sec. 3.6.2. Given a pair of face images taken at different times, we assign the comparison to the bin that is the arithmetic average of the subject's ages. This plot shows only the effect of age, not ageing. The number of comparisons in each bin is generally in the thousands, however the first and last bins are computed over 149 and 124 respectively. The error rates in some (adult) cases are zero, and in others the DET is flat so the error rates at the two thresholds are identical. The lines span 1% and 99% of bootstrap replicated FNMR estimates.

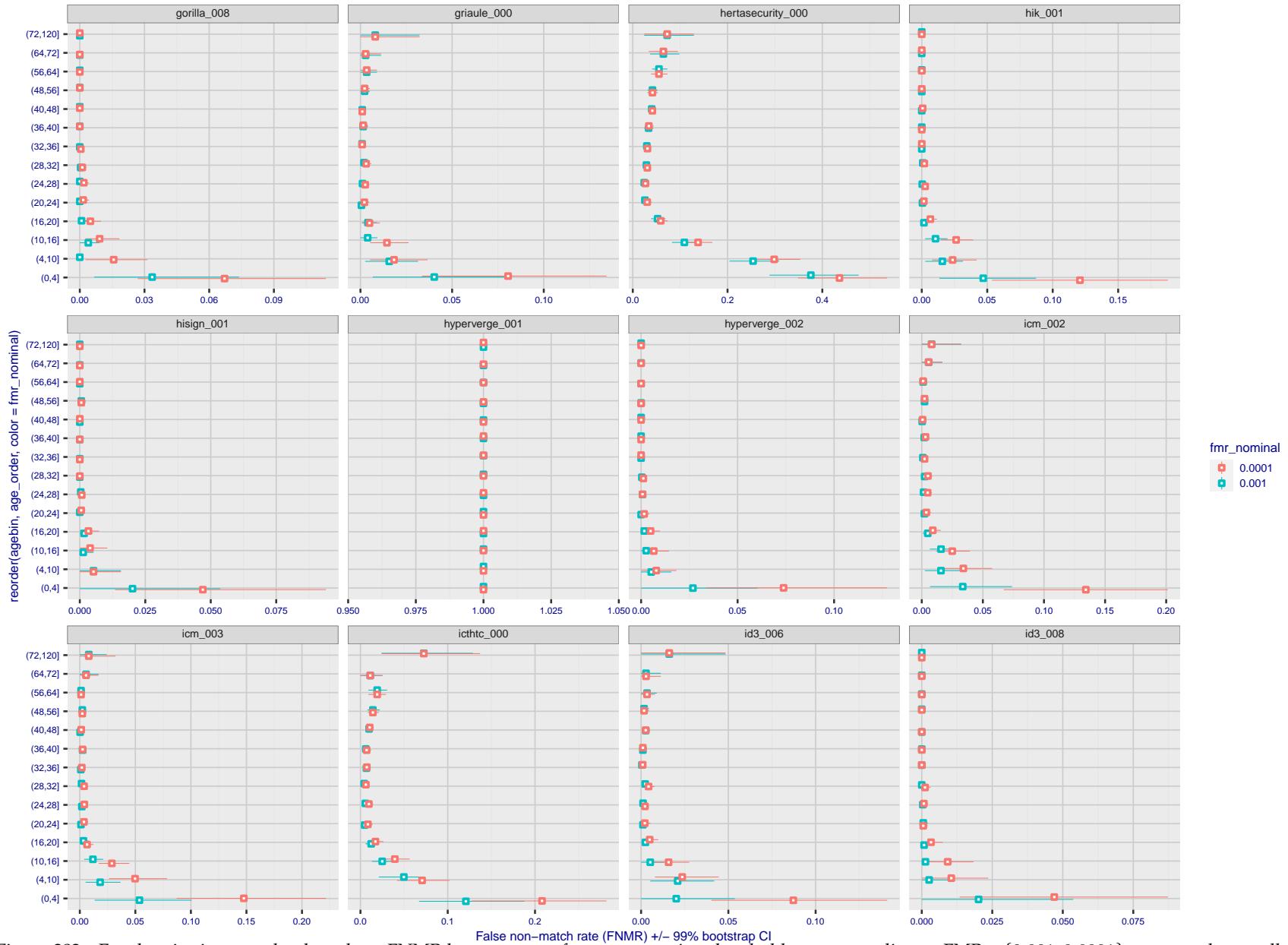


Figure 282: For the visa images, the dots show FNMR by age group for two operating thresholds corresponding to $FMR = \{0.001, 0.0001\}$ computed over all on the order of 10^{10} impostor scores. The FMR in each bin will vary also - see subsequent impostor heatmaps in sec. 3.6.2. Given a pair of face images taken at different times, we assign the comparison to the bin that is the arithmetic average of the subject's ages. This plot shows only the effect of age, not ageing. The number of comparisons in each bin is generally in the thousands, however the first and last bins are computed over 149 and 124 respectively. The error rates in some (adult) cases are zero, and in others the DET is flat so the error rates at the two thresholds are identical. The lines span 1% and 99% of bootstrap replicated FNMR estimates.

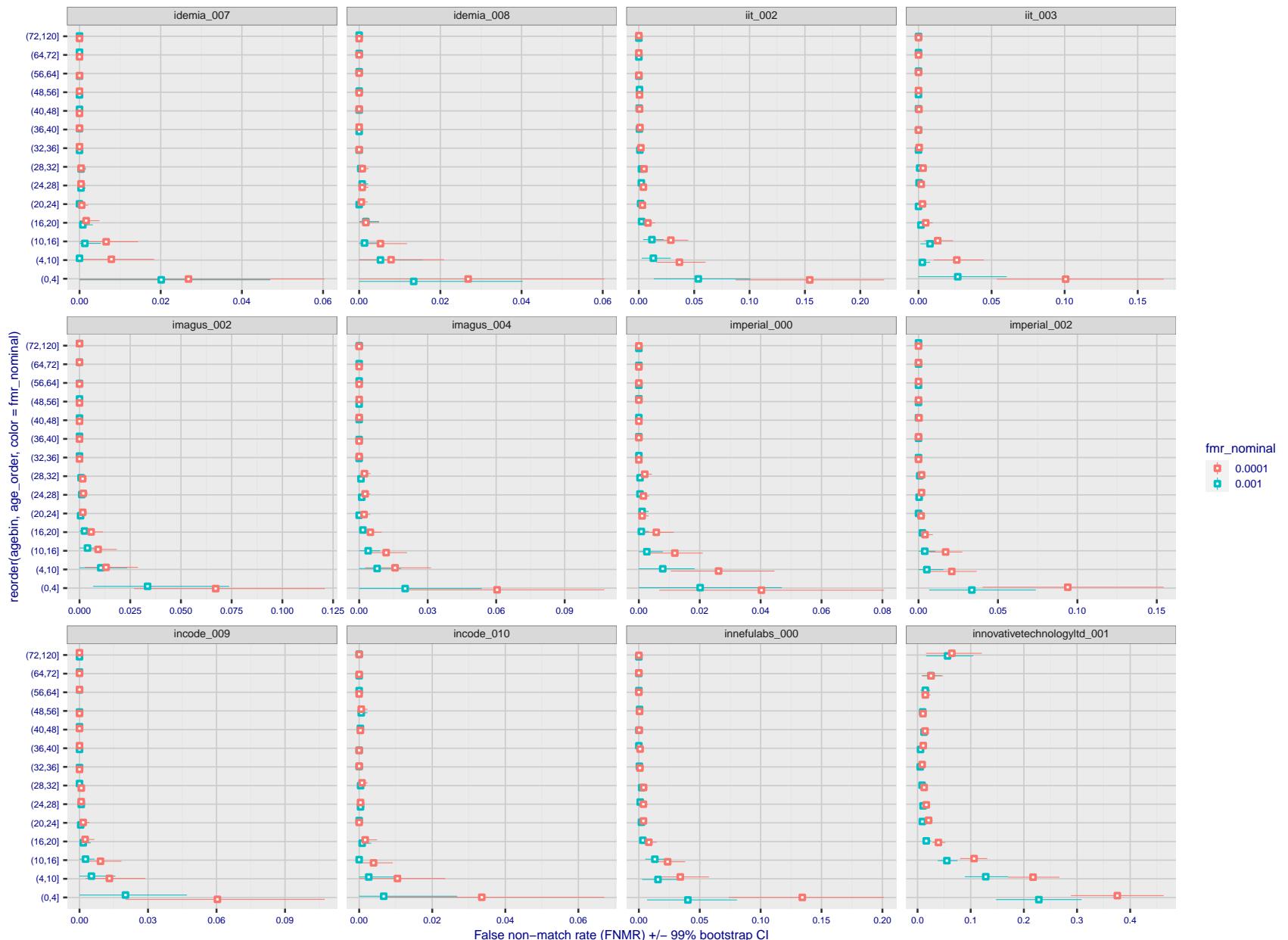


Figure 283: For the visa images, the dots show FNMR by age group for two operating thresholds corresponding to $FMR = \{0.001, 0.0001\}$ computed over all on the order of 10^{10} impostor scores. The FMR in each bin will vary also - see subsequent impostor heatmaps in sec. 3.6.2. Given a pair of face images taken at different times, we assign the comparison to the bin that is the arithmetic average of the subject's ages. This plot shows only the effect of age, not ageing. The number of comparisons in each bin is generally in the thousands, however the first and last bins are computed over 149 and 124 respectively. The error rates in some (adult) cases are zero, and in others the DET is flat so the error rates at the two thresholds are identical. The lines span 1% and 99% of bootstrap replicated FNMR estimates.

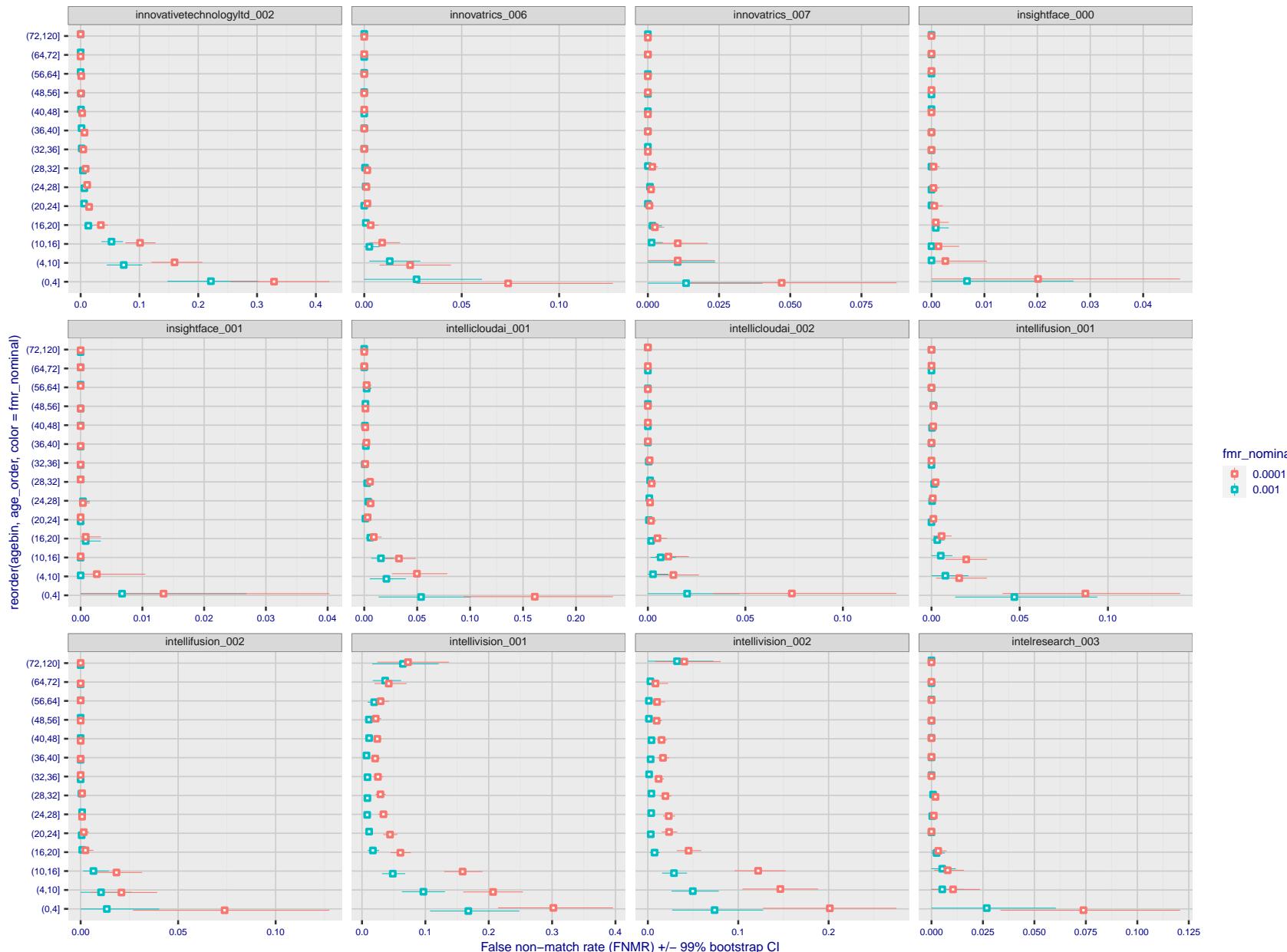


Figure 284: For the visa images, the dots show FNMR by age group for two operating thresholds corresponding to $FMR = \{0.001, 0.0001\}$ computed over all on the order of 10^{10} impostor scores. The FMR in each bin will vary also - see subsequent impostor heatmaps in sec. 3.6.2. Given a pair of face images taken at different times, we assign the comparison to the bin that is the arithmetic average of the subject's ages. This plot shows only the effect of age, not ageing. The number of comparisons in each bin is generally in the thousands, however the first and last bins are computed over 149 and 124 respectively. The error rates in some (adult) cases are zero, and in others the DET is flat so the error rates at the two thresholds are identical. The lines span 1% and 99% of bootstrap replicated FNMR estimates.

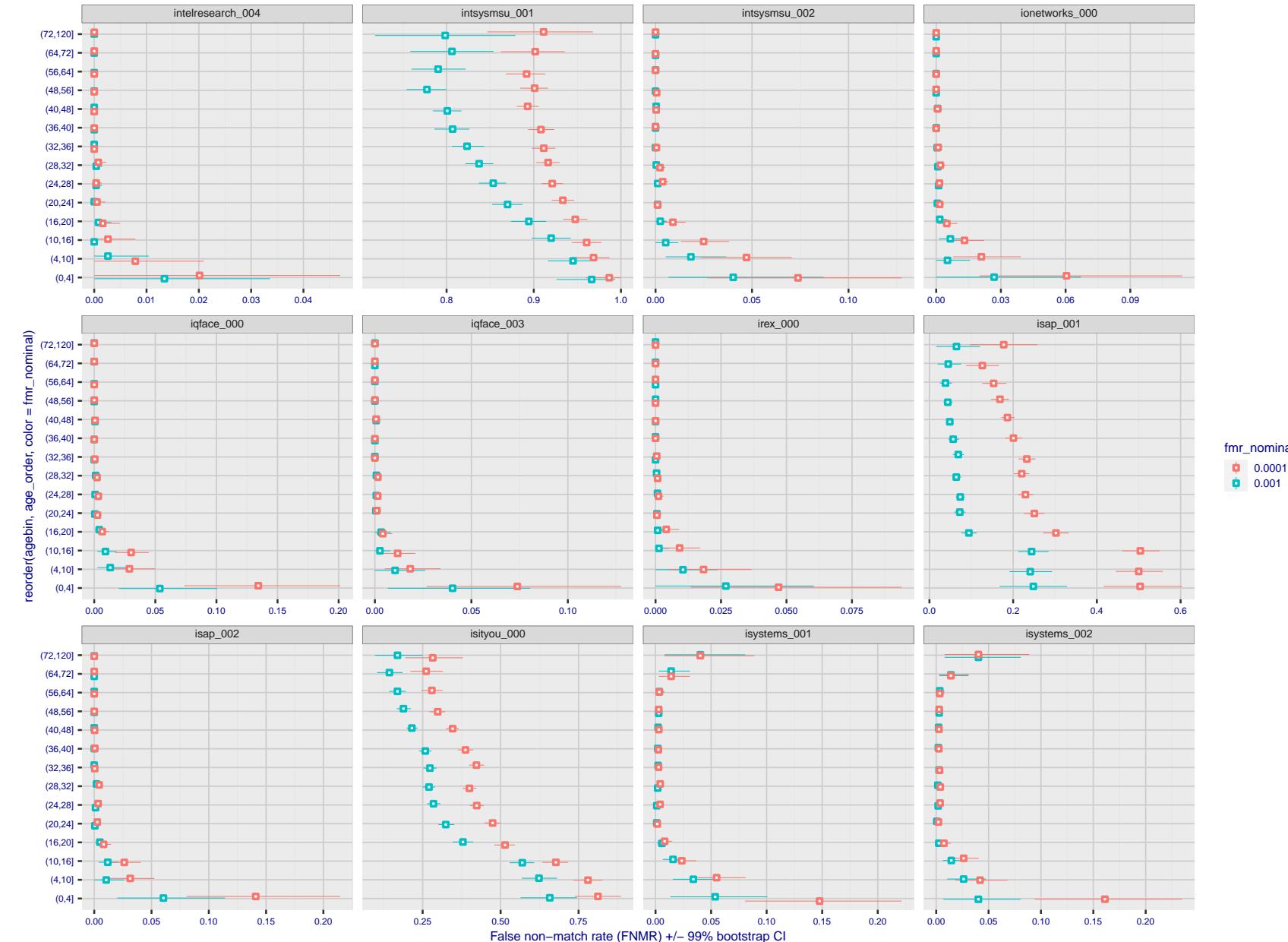
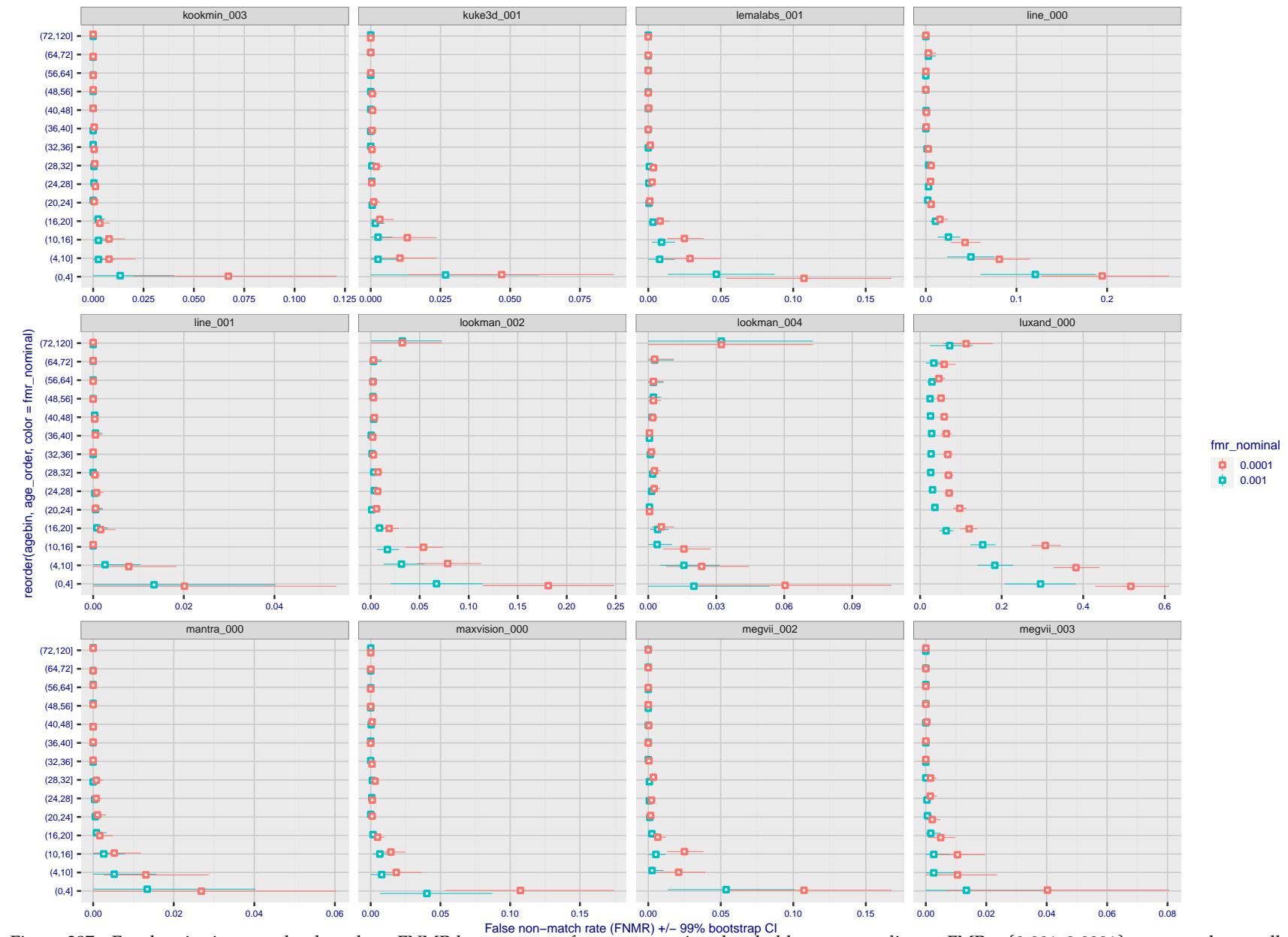


Figure 285: For the visa images, the dots show FNMR by age group for two operating thresholds corresponding to $FMR = \{0.001, 0.0001\}$ computed over all on the order of 10^{10} impostor scores. The FMR in each bin will vary also - see subsequent impostor heatmaps in sec. 3.6.2. Given a pair of face images taken at different times, we assign the comparison to the bin that is the arithmetic average of the subject's ages. This plot shows only the effect of age, not ageing. The number of comparisons in each bin is generally in the thousands, however the first and last bins are computed over 149 and 124 respectively. The error rates in some (adult) cases are zero, and in others the DET is flat so the error rates at the two thresholds are identical. The lines span 1% and 99% of bootstrap replicated FNMR estimates.



Figure 286: For the visa images, the dots show FNMR by age group for two operating thresholds corresponding to $FMR = \{0.001, 0.0001\}$ computed over all on the order of 10^{10} impostor scores. The FMR in each bin will vary also - see subsequent impostor heatmaps in sec. 3.6.2. Given a pair of face images taken at different times, we assign the comparison to the bin that is the arithmetic average of the subject's ages. This plot shows only the effect of age, not ageing. The number of comparisons in each bin is generally in the thousands, however the first and last bins are computed over 149 and 124 respectively. The error rates in some (adult) cases are zero, and in others the DET is flat so the error rates at the two thresholds are identical. The lines span 1% and 99% of bootstrap replicated FNMR estimates.

Figure 287: For the visa images, the dots show FNMR by age group for two operating thresholds corresponding to FMR = {0.001, 0.0001} computed over all on the order of 10^{10} impostor scores.

The FMR in each bin will vary also - see subsequent impostor heatmaps in sec. 3.6.2. Given a pair of face images taken at different times, we assign the comparison to the bin that is the arithmetic average of the subject's ages. This plot shows only the effect of age, not ageing. The number of comparisons in each bin is generally in the thousands, however the first and last bins are computed over 149 and 124 respectively. The error rates in some (adult) cases are zero, and in others the DET is flat so the error rates at the two thresholds are identical. The lines span 1% and 99% of bootstrap replicated FNMR estimates.



Figure 288: For the visa images, the dots show FNMR by age group for two operating thresholds corresponding to $FMR = \{0.001, 0.0001\}$ computed over all on the order of 10^{10} impostor scores. The FMR in each bin will vary also - see subsequent impostor heatmaps in sec. 3.6.2. Given a pair of face images taken at different times, we assign the comparison to the bin that is the arithmetic average of the subject's ages. This plot shows only the effect of age, not ageing. The number of comparisons in each bin is generally in the thousands, however the first and last bins are computed over 149 and 124 respectively. The error rates in some (adult) cases are zero, and in others the DET is flat so the error rates at the two thresholds are identical. The lines span 1% and 99% of bootstrap replicated FNMR estimates.

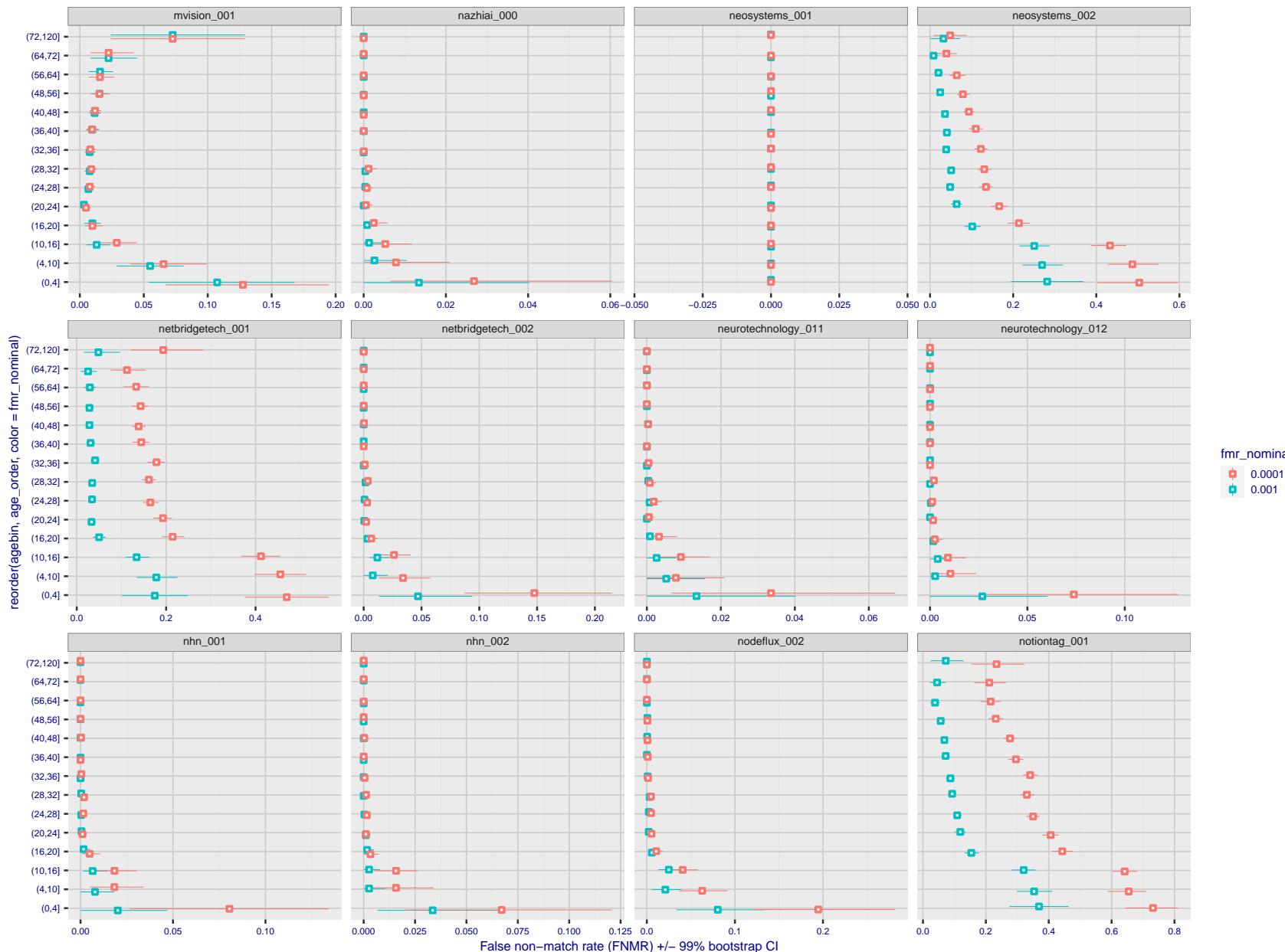


Figure 289: For the visa images, the dots show FNMR by age group for two operating thresholds corresponding to $FMR = \{0.001, 0.0001\}$ computed over all on the order of 10^{10} impostor scores. The FMR in each bin will vary also - see subsequent impostor heatmaps in sec. 3.6.2. Given a pair of face images taken at different times, we assign the comparison to the bin that is the arithmetic average of the subject's ages. This plot shows only the effect of age, not ageing. The number of comparisons in each bin is generally in the thousands, however the first and last bins are computed over 149 and 124 respectively. The error rates in some (adult) cases are zero, and in others the DET is flat so the error rates at the two thresholds are identical. The lines span 1% and 99% of bootstrap replicated FNMR estimates.

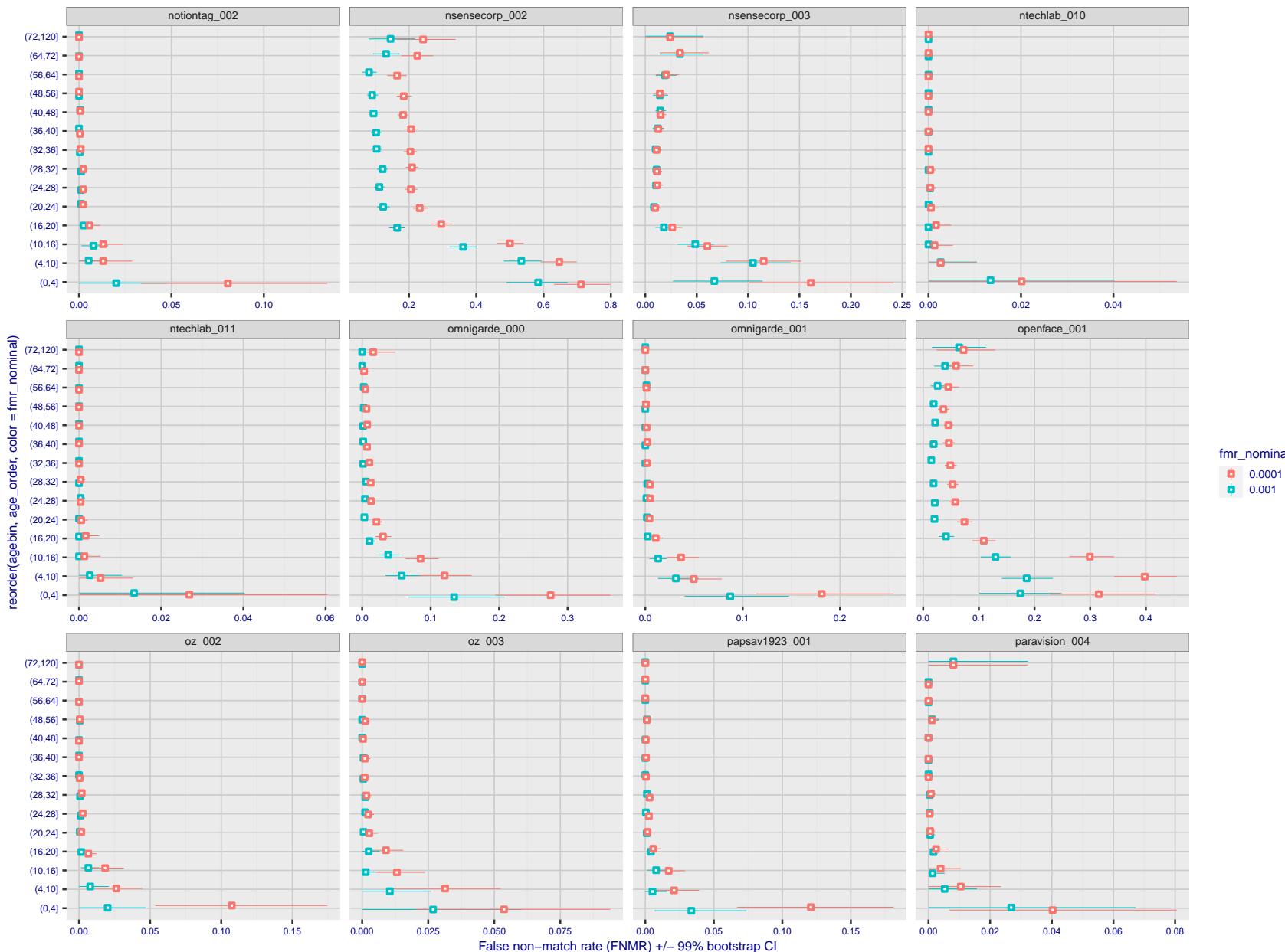


Figure 290: For the visa images, the dots show FNMR by age group for two operating thresholds corresponding to $FMR = \{0.001, 0.0001\}$ computed over all on the order of 10^{10} impostor scores. The FMR in each bin will vary also - see subsequent impostor heatmaps in sec. 3.6.2. Given a pair of face images taken at different times, we assign the comparison to the bin that is the arithmetic average of the subject's ages. This plot shows only the effect of age, not ageing. The number of comparisons in each bin is generally in the thousands, however the first and last bins are computed over 149 and 124 respectively. The error rates in some (adult) cases are zero, and in others the DET is flat so the error rates at the two thresholds are identical. The lines span 1% and 99% of bootstrap replicated FNMR estimates.



Figure 291: For the visa images, the dots show FNMR by age group for two operating thresholds corresponding to $FMR = \{0.001, 0.0001\}$ computed over all on the order of 10^{10} impostor scores. The FMR in each bin will vary also - see subsequent impostor heatmaps in sec. 3.6.2. Given a pair of face images taken at different times, we assign the comparison to the bin that is the arithmetic average of the subject's ages. This plot shows only the effect of age, not ageing. The number of comparisons in each bin is generally in the thousands, however the first and last bins are computed over 149 and 124 respectively. The error rates in some (adult) cases are zero, and in others the DET is flat so the error rates at the two thresholds are identical. The lines span 1% and 99% of bootstrap replicated FNMR estimates.

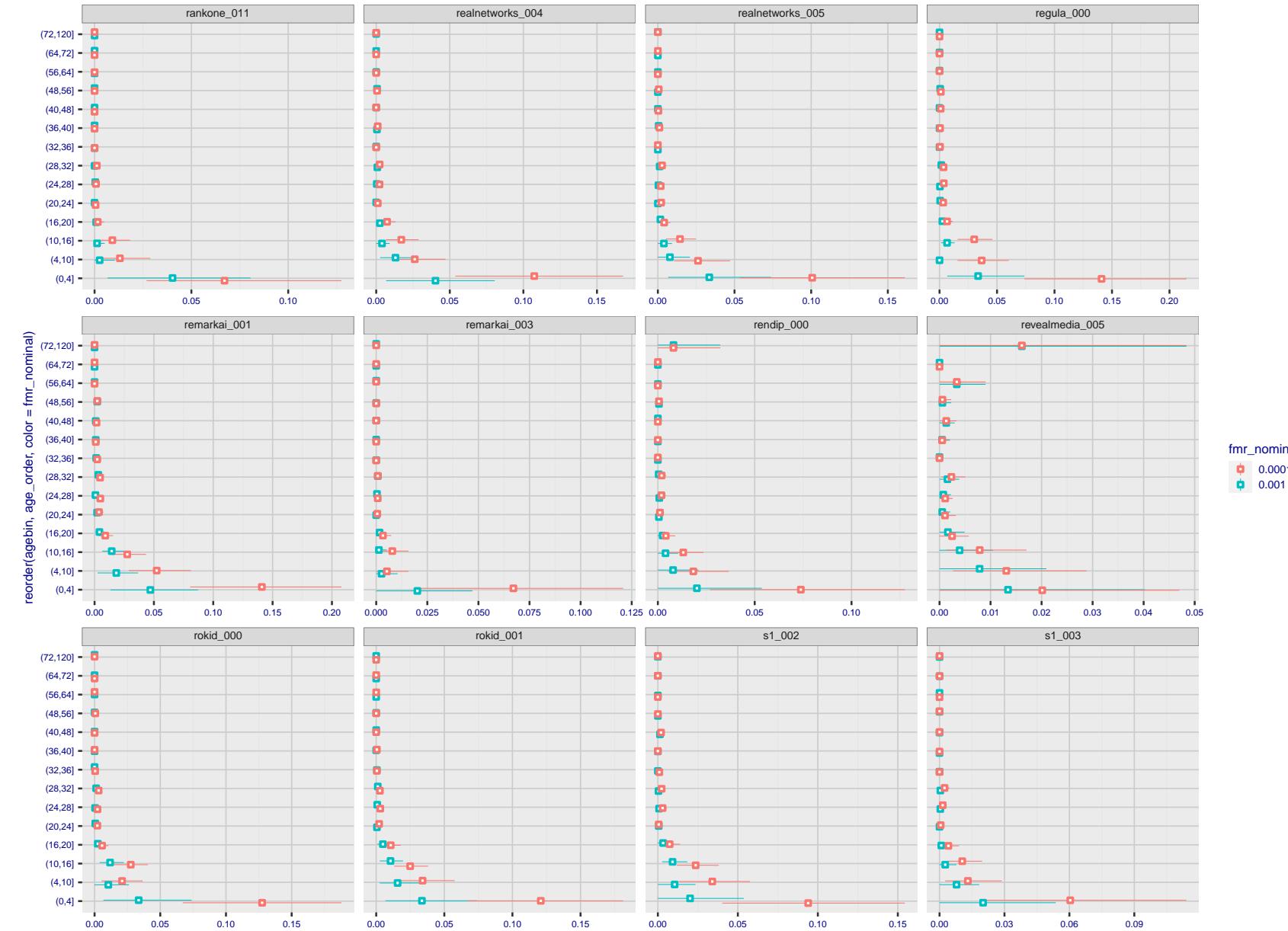


Figure 292: For the visa images, the dots show FNMR by age group for two operating thresholds corresponding to $FMR = \{0.001, 0.0001\}$ computed over all on the order of 10^{10} impostor scores. The FMR in each bin will vary also - see subsequent impostor heatmaps in sec. 3.6.2. Given a pair of face images taken at different times, we assign the comparison to the bin that is the arithmetic average of the subject's ages. This plot shows only the effect of age, not ageing. The number of comparisons in each bin is generally in the thousands, however the first and last bins are computed over 149 and 124 respectively. The error rates in some (adult) cases are zero, and in others the DET is flat so the error rates at the two thresholds are identical. The lines span 1% and 99% of bootstrap replicated FNMR estimates.

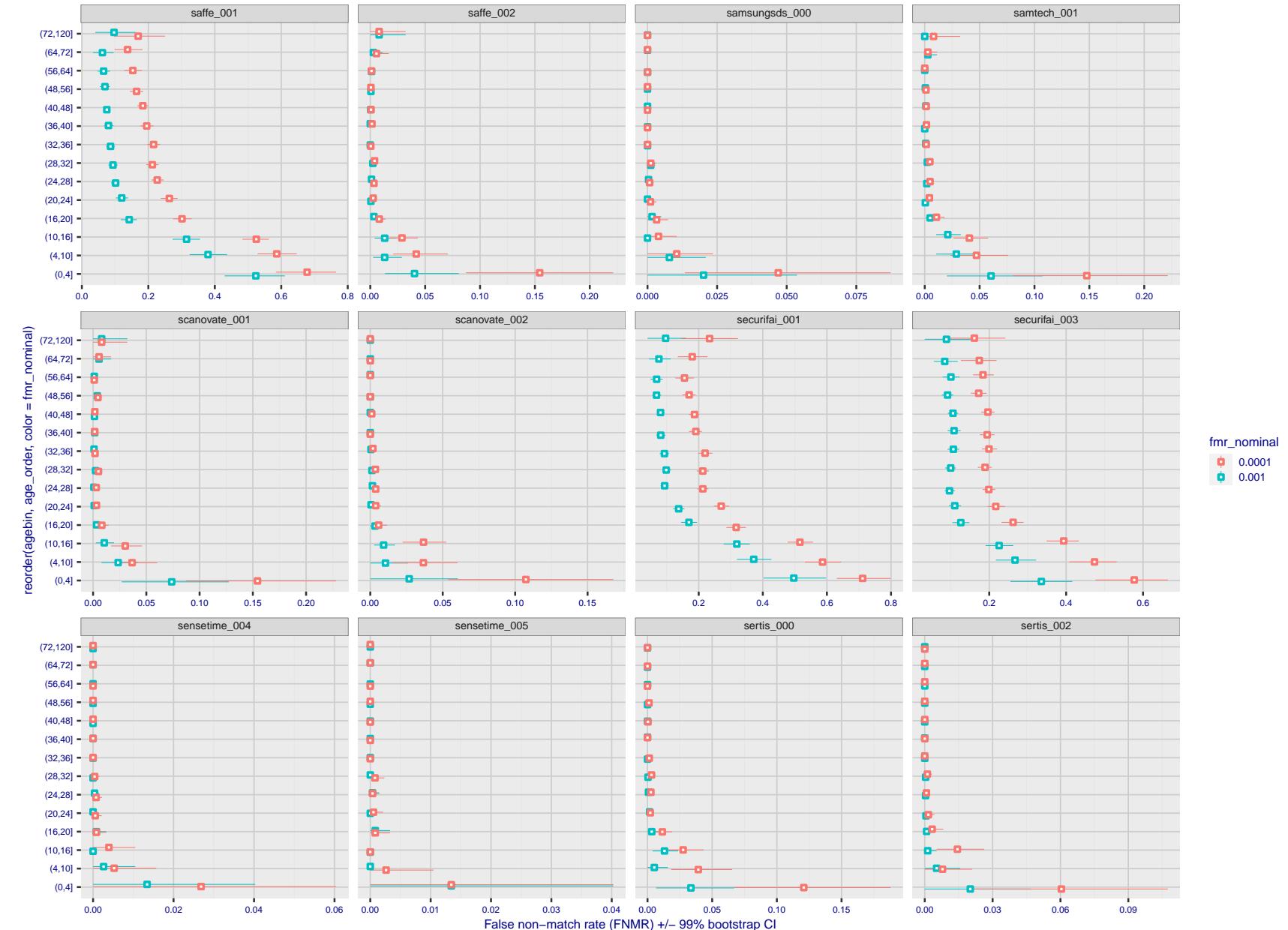


Figure 293: For the visa images, the dots show FNMR by age group for two operating thresholds corresponding to $FMR = \{0.001, 0.0001\}$ computed over all on the order of 10^{10} impostor scores. The FMR in each bin will vary also - see subsequent impostor heatmaps in sec. 3.6.2. Given a pair of face images taken at different times, we assign the comparison to the bin that is the arithmetic average of the subject's ages. This plot shows only the effect of age, not ageing. The number of comparisons in each bin is generally in the thousands, however the first and last bins are computed over 149 and 124 respectively. The error rates in some (adult) cases are zero, and in others the DET is flat so the error rates at the two thresholds are identical. The lines span 1% and 99% of bootstrap replicated FNMR estimates.

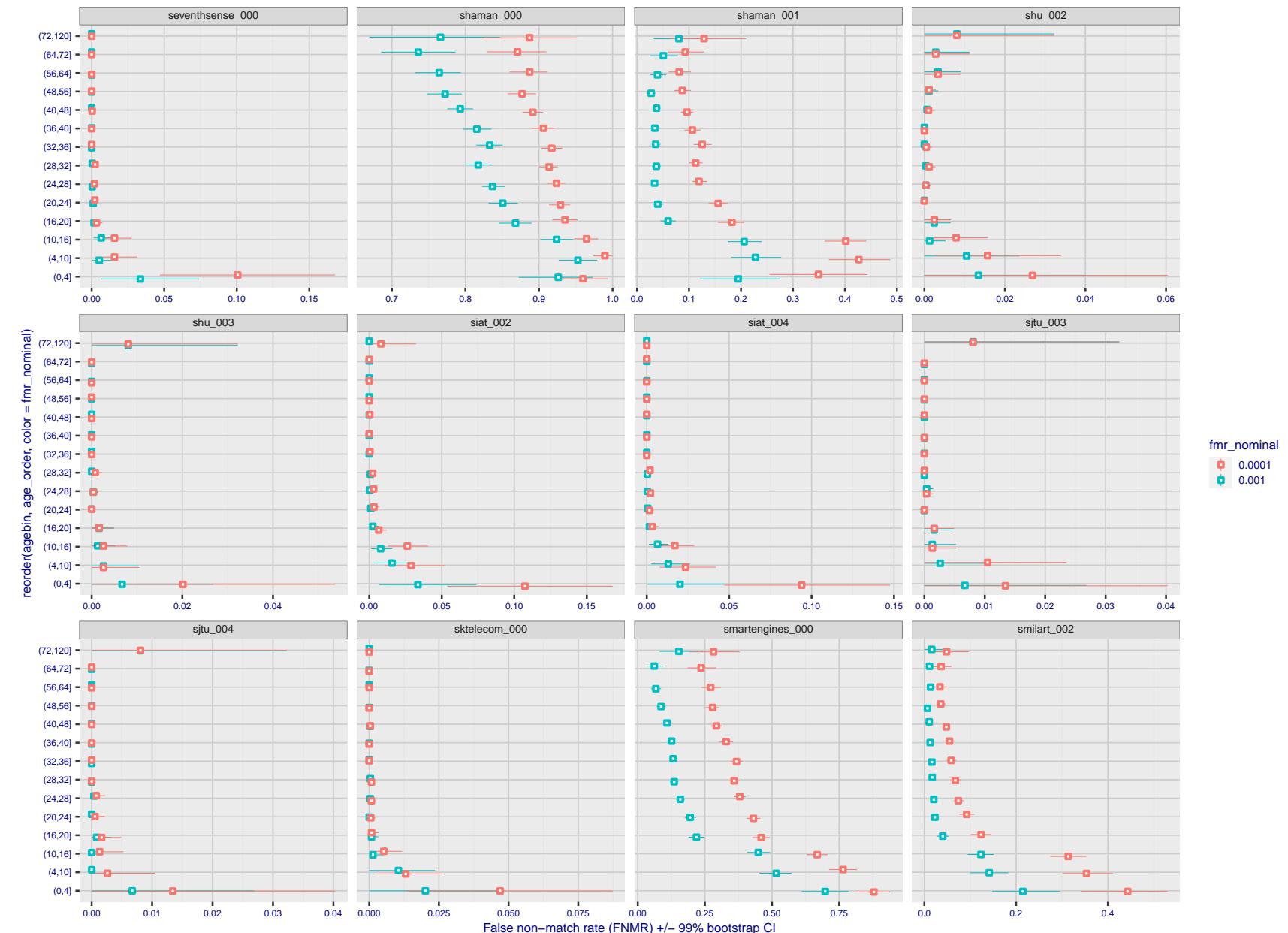


Figure 294: For the visa images, the dots show FNMR by age group for two operating thresholds corresponding to $FMR = \{0.001, 0.0001\}$ computed over all on the order of 10^{10} impostor scores. The FMR in each bin will vary also - see subsequent impostor heatmaps in sec. 3.6.2. Given a pair of face images taken at different times, we assign the comparison to the bin that is the arithmetic average of the subject's ages. This plot shows only the effect of age, not ageing. The number of comparisons in each bin is generally in the thousands, however the first and last bins are computed over 149 and 124 respectively. The error rates in some (adult) cases are zero, and in others the DET is flat so the error rates at the two thresholds are identical. The lines span 1% and 99% of bootstrap replicated FNMR estimates.



Figure 295: For the visa images, the dots show FNMR by age group for two operating thresholds corresponding to $FMR = \{0.001, 0.0001\}$ computed over all on the order of 10^{10} impostor scores. The FMR in each bin will vary also - see subsequent impostor heatmaps in sec. 3.6.2. Given a pair of face images taken at different times, we assign the comparison to the bin that is the arithmetic average of the subject's ages. This plot shows only the effect of age, not ageing. The number of comparisons in each bin is generally in the thousands, however the first and last bins are computed over 149 and 124 respectively. The error rates in some (adult) cases are zero, and in others the DET is flat so the error rates at the two thresholds are identical. The lines span 1% and 99% of bootstrap replicated FNMR estimates.



Figure 296: For the visa images, the dots show FNMR by age group for two operating thresholds corresponding to $FMR = \{0.001, 0.0001\}$ computed over all on the order of 10^{10} impostor scores. The FMR in each bin will vary also - see subsequent impostor heatmaps in sec. 3.6.2. Given a pair of face images taken at different times, we assign the comparison to the bin that is the arithmetic average of the subject's ages. This plot shows only the effect of age, not ageing. The number of comparisons in each bin is generally in the thousands, however the first and last bins are computed over 149 and 124 respectively. The error rates in some (adult) cases are zero, and in others the DET is flat so the error rates at the two thresholds are identical. The lines span 1% and 99% of bootstrap replicated FNMR estimates.



Figure 297: For the visa images, the dots show FNMR by age group for two operating thresholds corresponding to $FMR = \{0.001, 0.0001\}$ computed over all on the order of 10^{10} impostor scores. The FMR in each bin will vary also - see subsequent impostor heatmaps in sec. 3.6.2. Given a pair of face images taken at different times, we assign the comparison to the bin that is the arithmetic average of the subject's ages. This plot shows only the effect of age, not ageing. The number of comparisons in each bin is generally in the thousands, however the first and last bins are computed over 149 and 124 respectively. The error rates in some (adult) cases are zero, and in others the DET is flat so the error rates at the two thresholds are identical. The lines span 1% and 99% of bootstrap replicated FNMR estimates.

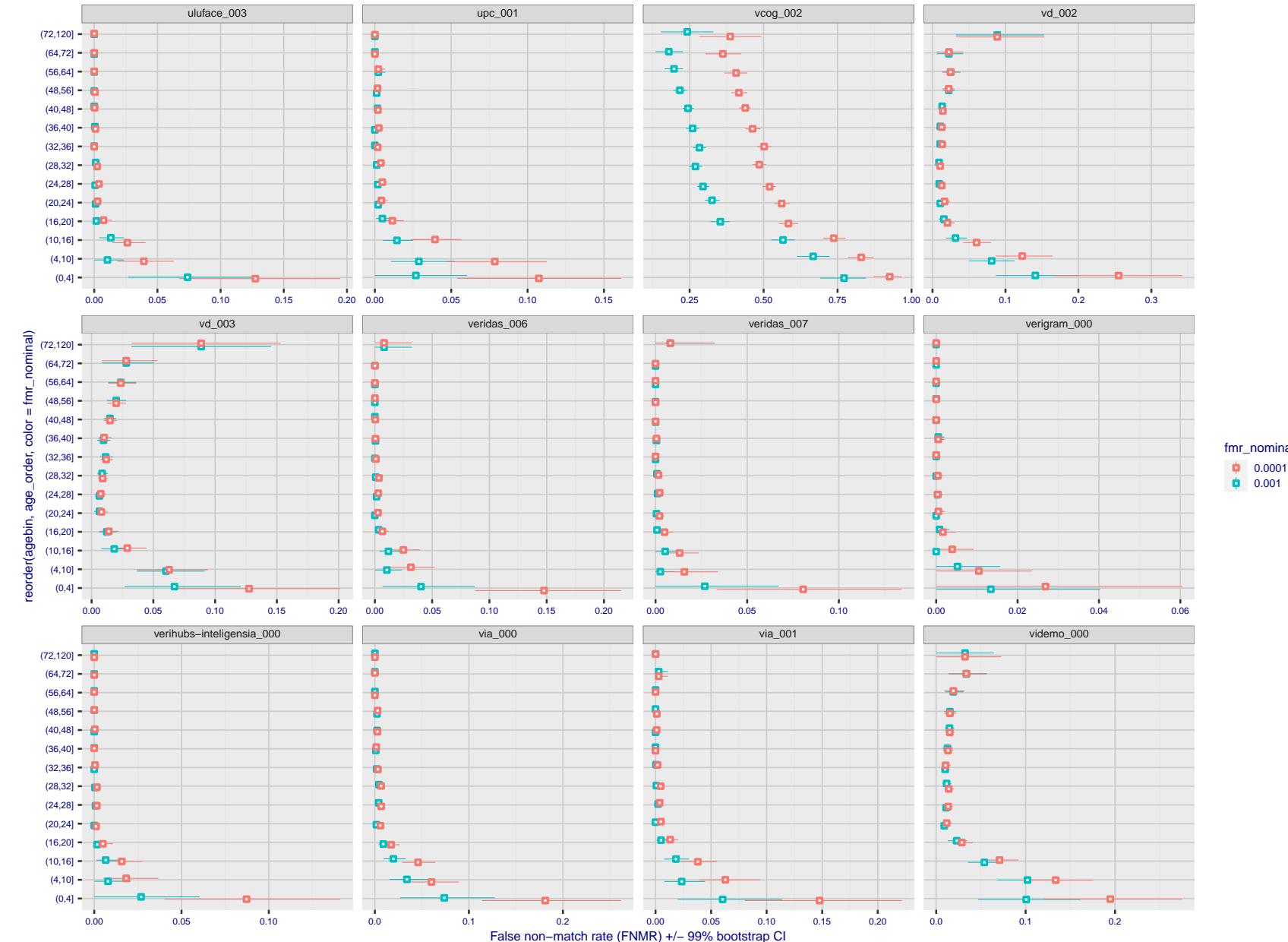


Figure 298: For the visa images, the dots show FNMR by age group for two operating thresholds corresponding to $FMR = \{0.001, 0.0001\}$ computed over all on the order of 10^{10} impostor scores. The FMR in each bin will vary also - see subsequent impostor heatmaps in sec. 3.6.2. Given a pair of face images taken at different times, we assign the comparison to the bin that is the arithmetic average of the subject's ages. This plot shows only the effect of age, not ageing. The number of comparisons in each bin is generally in the thousands, however the first and last bins are computed over 149 and 124 respectively. The error rates in some (adult) cases are zero, and in others the DET is flat so the error rates at the two thresholds are identical. The lines span 1% and 99% of bootstrap replicated FNMR estimates.

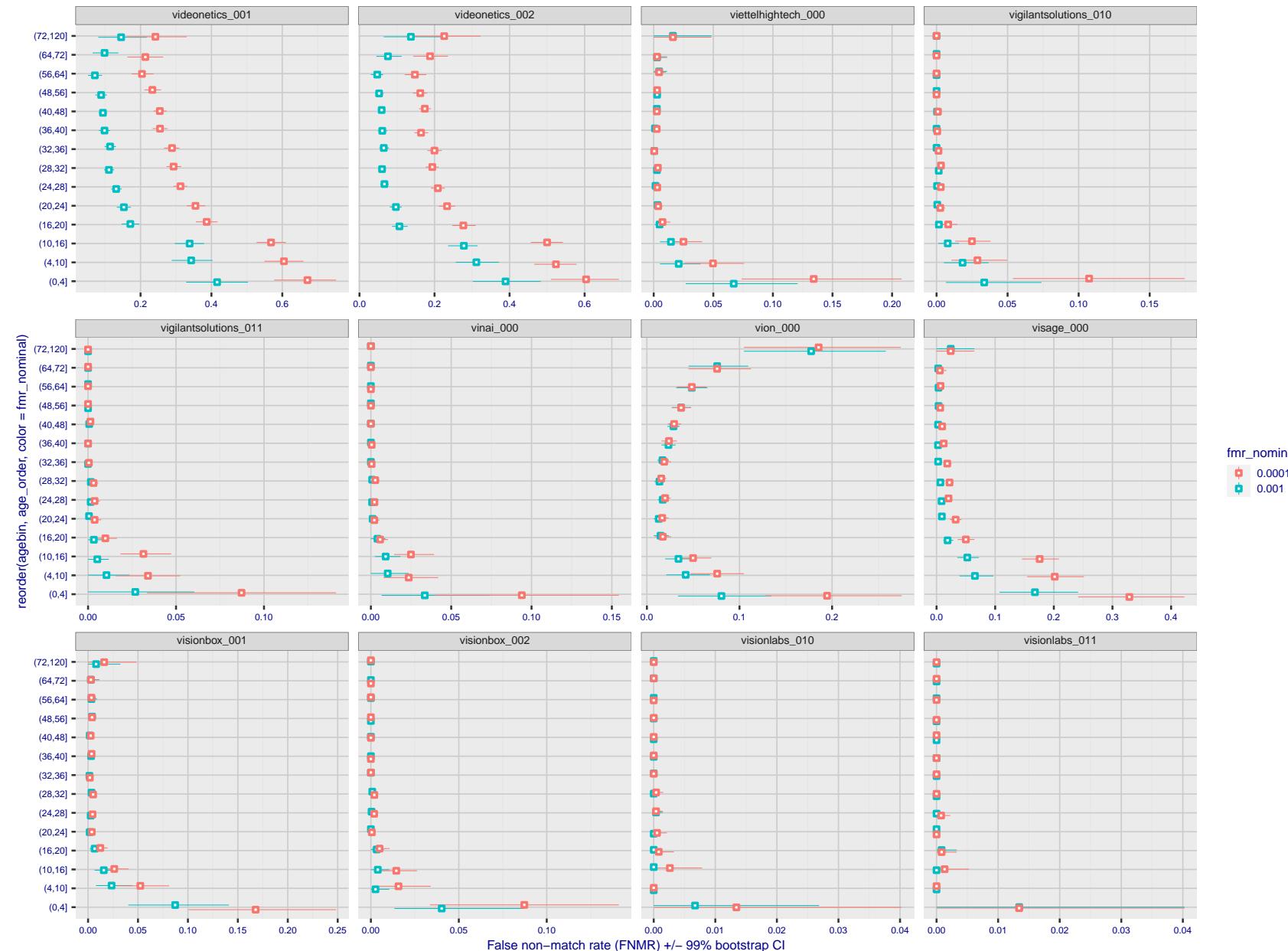


Figure 299: For the visa images, the dots show FNMR by age group for two operating thresholds corresponding to $FMR = \{0.001, 0.0001\}$ computed over all on the order of 10^{10} impostor scores. The FMR in each bin will vary also - see subsequent impostor heatmaps in sec. 3.6.2. Given a pair of face images taken at different times, we assign the comparison to the bin that is the arithmetic average of the subject's ages. This plot shows only the effect of age, not ageing. The number of comparisons in each bin is generally in the thousands, however the first and last bins are computed over 149 and 124 respectively. The error rates in some (adult) cases are zero, and in others the DET is flat so the error rates at the two thresholds are identical. The lines span 1% and 99% of bootstrap replicated FNMR estimates.

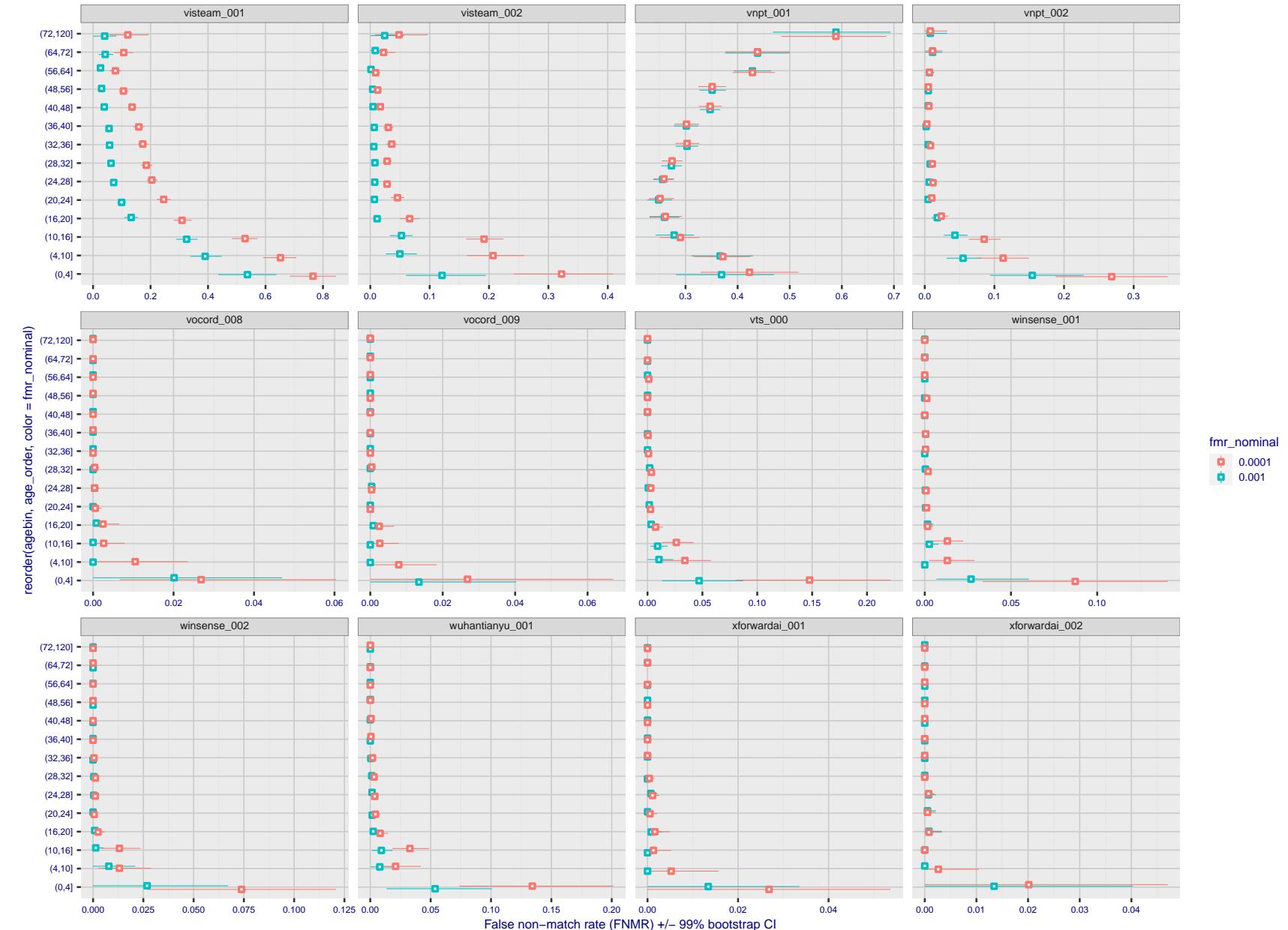


Figure 300: For the visa images, the dots show FNMR by age group for two operating thresholds corresponding to $FMR = \{0.001, 0.0001\}$ computed over all on the order of 10^{10} impostor scores. The FMR in each bin will vary also - see subsequent impostor heatmaps in sec. 3.6.2. Given a pair of face images taken at different times, we assign the comparison to the bin that is the arithmetic average of the subject's ages. This plot shows only the effect of age, not ageing. The number of comparisons in each bin is generally in the thousands, however the first and last bins are computed over 149 and 124 respectively. The error rates in some (adult) cases are zero, and in others the DET is flat so the error rates at the two thresholds are identical. The lines span 1% and 99% of bootstrap replicated FNMR estimates.



Figure 301: For the visa images, the dots show FNMR by age group for two operating thresholds corresponding to $FMR = \{0.001, 0.0001\}$ computed over all on the order of 10^{10} impostor scores. The FMR in each bin will vary also - see subsequent impostor heatmaps in sec. 3.6.2. Given a pair of face images taken at different times, we assign the comparison to the bin that is the arithmetic average of the subject's ages. This plot shows only the effect of age, not ageing. The number of comparisons in each bin is generally in the thousands, however the first and last bins are computed over 149 and 124 respectively. The error rates in some (adult) cases are zero, and in others the DET is flat so the error rates at the two thresholds are identical. The lines span 1% and 99% of bootstrap replicated FNMR estimates.

Caveats: None.

3.6 Impostor distribution stability

3.6.1 Effect of birth place on the impostor distribution

Background: Facial appearance varies geographically, both in terms of skin tone, cranio-facial structure and size. This section addresses whether false match rates vary intra- and inter-regionally.

Goals:

- ▷ To show the effect of birth region of the impostor and enrollee on false match rates.
- ▷ To determine whether some algorithms give better impostor distribution stability.

Methods:

- ▷ For the visa images, NIST defined 10 regions: Sub-Saharan Africa, South Asia, Polynesia, North Africa, Middle East, Europe, East Asia, Central and South America, Central Asia, and the Caribbean.
- ▷ For the visa images, NIST mapped each country of birth to a region. There is some arbitrariness to this. For example, Egypt could reasonably be assigned to the Middle East instead of North Africa. An alternative methodology could, for example, assign the Philippines to *both* Polynesia and East Asia.
- ▷ FMR is computed for cases where all face images of impostors born in region r_2 are compared with enrolled face images of persons born in region r_1 .

$$\text{FMR}(r_1, r_2, T) = \frac{\sum_{i=1}^{N_{r_1, r_2}} H(s_i - T)}{N_{r_1, r_2}} \quad (5)$$

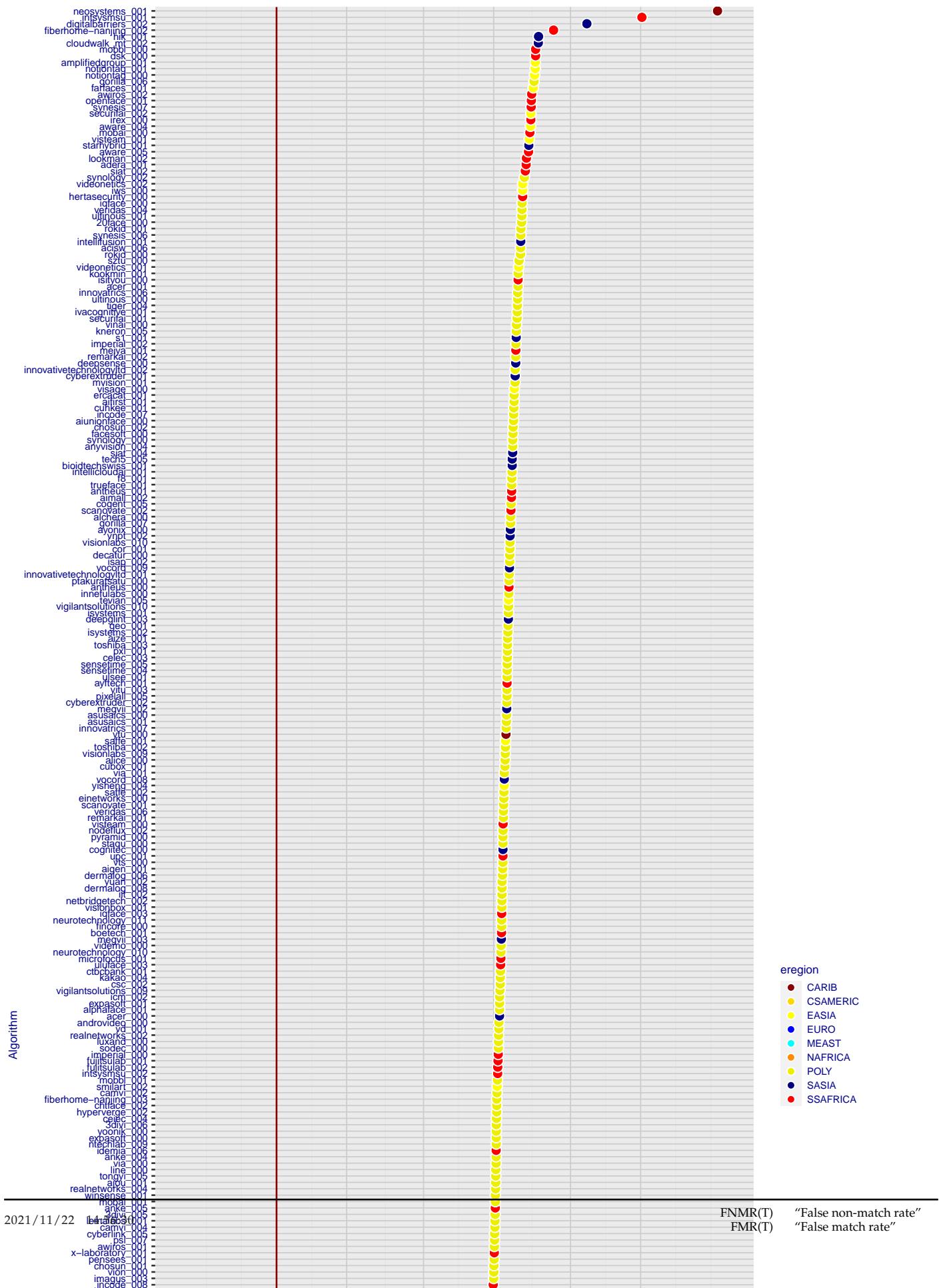
where the same threshold, T , is used in all cells, and H is the unit step function. The threshold is set to give $\text{FMR}(T) = 0.001$ over the entire set of visa image impostor comparisons.

- ▷ This analysis is then repeated by country-pair, but only for those country pairs where both have at least 1000 images available. The countries¹ appear in the axes of graphs that follow.
- ▷ The mean number of impostor scores in any cross-region bin is 33 million. The smallest number of impostor scores in any bin is 135000, for Central Asia - North Africa. While these counts are large enough to support reasonable significance, the number of individual faces is much smaller, on the order of $N^{0.5}$.
- ▷ The numbers of impostor scores in any cross-country bin is shown in Figure ??.

Results: Subsequent figures show heatmaps that use color to represent the base-10 logarithm of the false match rate. Red colors indicate high (bad) false match rates. Dark colors indicate benign false match rates. There are two series of graphs corresponding to aggregated geographical regions, and to countries. The notable observations are:

- ▷ The on-diagonal elements correspond to within-region impostors. FMR is generally above the nominal value of $\text{FMR} = 0.001$. Particularly there is usually higher FMR in, Sub-Saharan Africa, South Asia, and the Caribbean. Europe and Central Asia, on the other hand, usually give FMR closer to the nominal value.
- ▷ The off-diagonal elements correspond to across-region impostors. The highest FMR is produced between the Caribbean and Sub-Saharan Africa.
- ▷ Algorithms vary.

¹These are Argentina, Australia, Brazil, Chile, China, Costa Rica, Cuba, Czech Republic, Dominican Republic, Ecuador, Egypt, El Salvador, Germany, Ghana, Great Britain, Greece, Guatemala, Haiti, Hong Kong, Honduras, Indonesia, India, Israel, Jamaica, Japan, Kenya, Korea, Lebanon, Mexico, Malaysia, Nepal, Nigeria, Peru, Philippines, Pakistan, Poland, Romania, Russia, South Africa, Saudi Arabia, Thailand, Trinidad, Turkey, Taiwan, Ukraine, Venezuela, and Vietnam.



- ▷ We computed the same quantities for a global FMR = 0.0001. The effects are similar.

Caveats:

- ▷ The effects of variable impostor rates on one-to-many identification systems may well differ from what's implied by these one-to-one verification results. Two reasons for this are a) the enrollment galleries are usually imbalanced across countries of birth, age and sex; b) one-to-many identification algorithms often implement techniques aimed at stabilizing the impostor distribution. Further research is necessary.
- ▷ In principle, the effects seen in this subsection could be due to differences in the image capture process. We consider this unlikely since the effects are maintained across geography - e.g. Caribbean vs. Africa, or Japan vs. China.

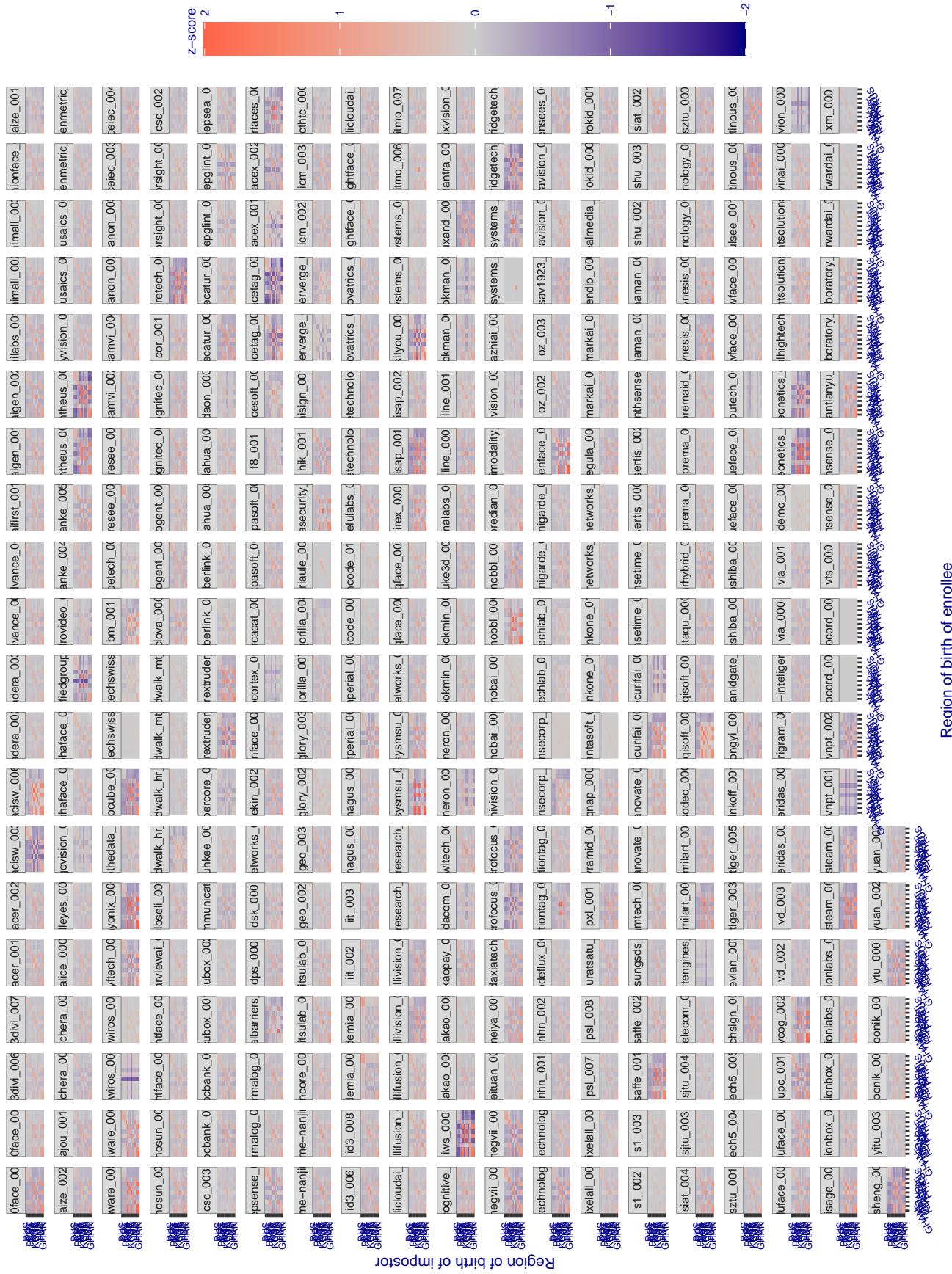


Figure 303: For visa images, the heatmap shows how the mean of the impostor distribution for the country pair (a,b) is shifted relative to the mean of the global impostor distribution, expressed as a number of standard deviations of the global impostor distribution. This statistic is designed to show shifts in the entire impostor distribution, not just tail effects that manifest as the anomalously high (or low) false match rates that appear in the subsequent figures. The countries are chosen to show that skin tone alone does not explain impostor distribution shifts. The reduced shift in Asian populations with the Yitu and TongYiTans algorithms, is accompanied by positive shifts in the European populations. This reversal relative to most other algorithms, may derive from use of nationally weighted training sets. The figure is computed from same-sex and same-age impostor pairs.

3.6.2 Effect of age on impostors

Background: This section shows the effect of age on the impostor distribution. The ideal behaviour is that the age of the enrollee and the impostor would not affect impostor scores. This would support FMR stability over sub-populations.

Goals:

- ▷ To show the effect of relative ages of the impostor and enrollee on false match rates.
- ▷ To determine whether some algorithms have better impostor distribution stability.

Methods:

- ▷ Define 14 age group bins, spanning 0 to over 100 years old.
- ▷ Compute FMR over all impostor comparisons for which the subjects in the enrollee and impostor images have ages in two bins.
- ▷ Compute FMR over all impostor comparisons for which the subjects are additionally of the same sex, and born in the same geographic region.

Results:

The notable aspects are:

- ▷ Diagonal dominance: Impostors are more likely to be matched against their same age group.
- ▷ Same sex and same region impostors are more successful. On the diagonal, an impostor is more likely to succeed by posing as someone of the same sex. If $\Delta \log_{10} \text{FMR} = 0.2$, then same-sex same-region FMR exceeds the all-pairs FMR by factor of $10^{0.2} = 1.6$.
- ▷ Young children impostors give elevated FMR against young children. Older adult impostor give elevated FMR against older adults. These effects are quite large, for example if $\Delta \log_{10} \text{FMR} = 1.0$ larger than a 32 year old, then these groups have higher FMR by a factor of $10^1 = 10$. This would imply an FMR above 0.01 for a nominal (global) FMR = 0.001.
- ▷ Algorithms vary.
- ▷ We computed the same quantities for a global FMR = 0.0001. The effects are similar.

Note the calculations in this section include impostors paired across all countries of birth.

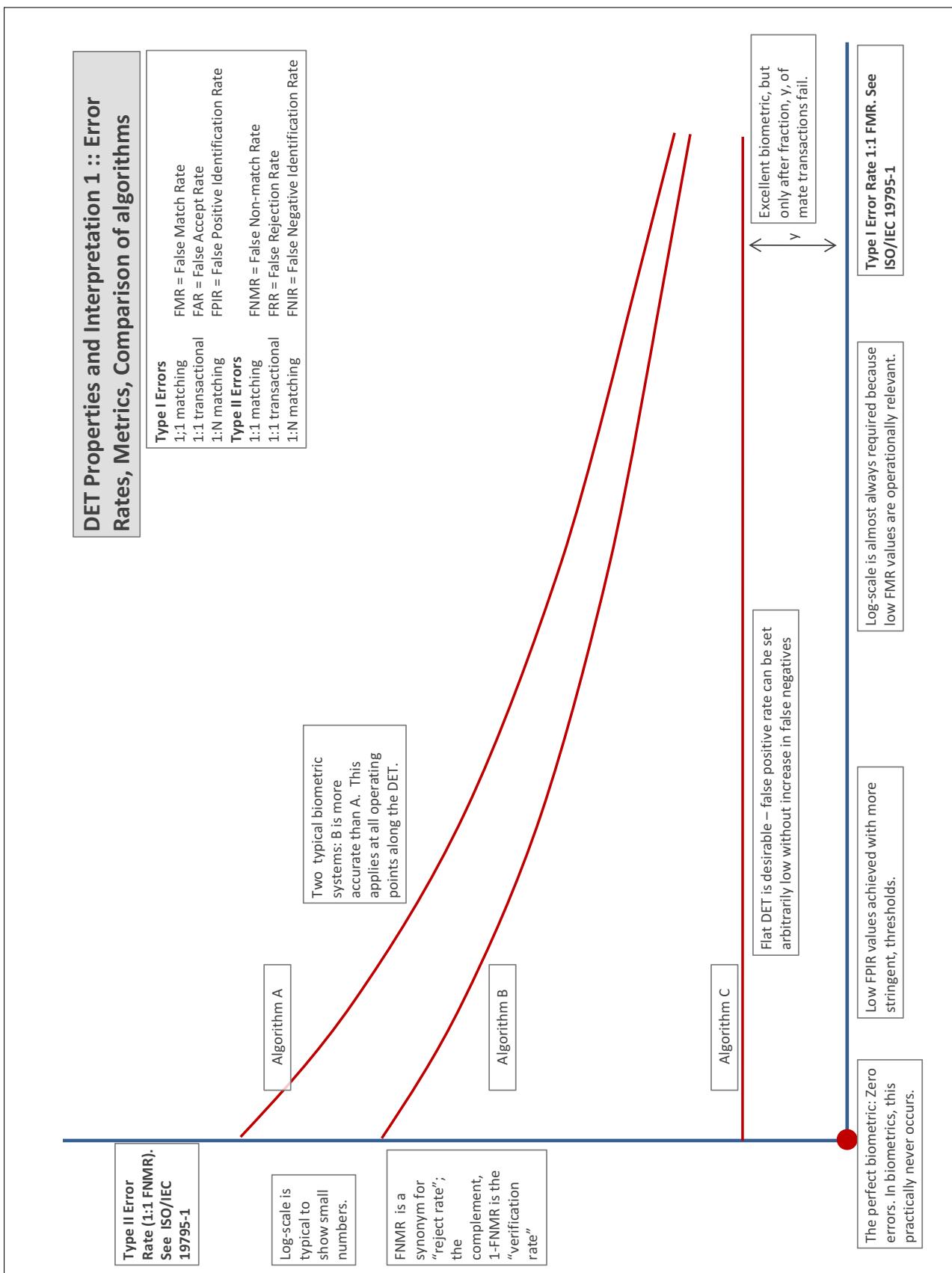
Accuracy Terms + Definitions

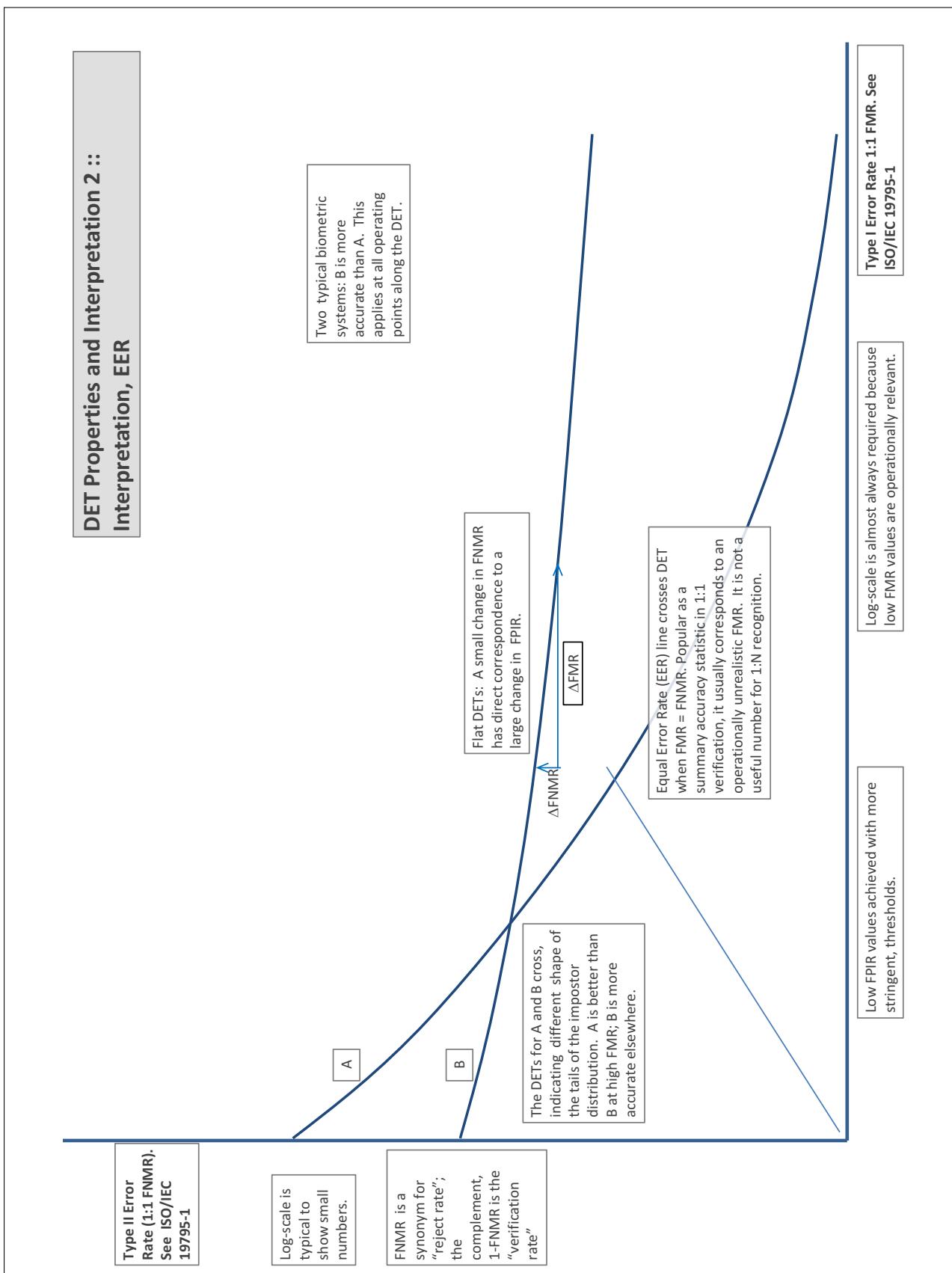
In biometrics, Type II errors occur when two samples of one person do not match – this is called a **false negative**. Correspondingly, Type I errors occur when samples from two persons do match – this is called a **false positive**. Matches are declared by a biometric system when the native comparison score from the recognition algorithm meets some **threshold**. Comparison scores can be either **similarity scores**, in which case higher values indicate that the samples are more likely to come from the same person, or **dissimilarity scores**, in which case higher values indicate different people. Similarity scores are traditionally computed by **fingerprint** and **face** recognition algorithms, while dissimilarities are used in **iris recognition**. In some cases, the dissimilarity score is a distance; this applies only when **metric** properties are obeyed. In any case, scores can be either **mate** scores, coming from a comparison of one person's samples, or **nonmate** scores, coming from comparison of different persons' samples. The words **genuine** or **authentic** are synonyms for mate, and the word **impostor** is used as a synonym for nonmatch. The words mate and nonmatch are traditionally used in identification applications (such as law enforcement search, or background checks) while genuine and impostor are used in verification applications (such as access control).

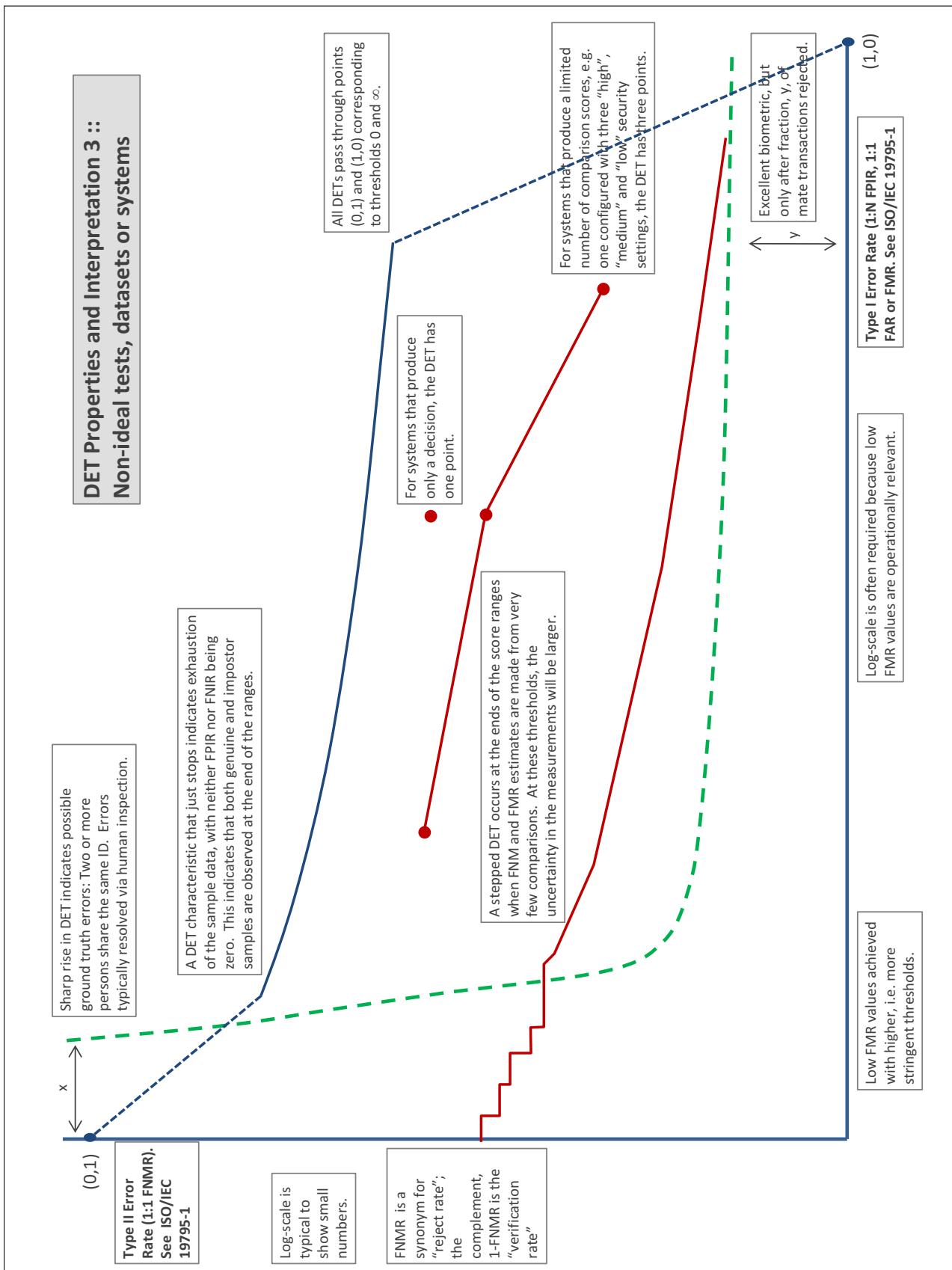
A **error tradeoff** characteristic represents the tradeoff between Type II and Type I classification errors. For verification this plots false non-match rate (FNMR) vs. false match rate (FMR) parametrically with T.

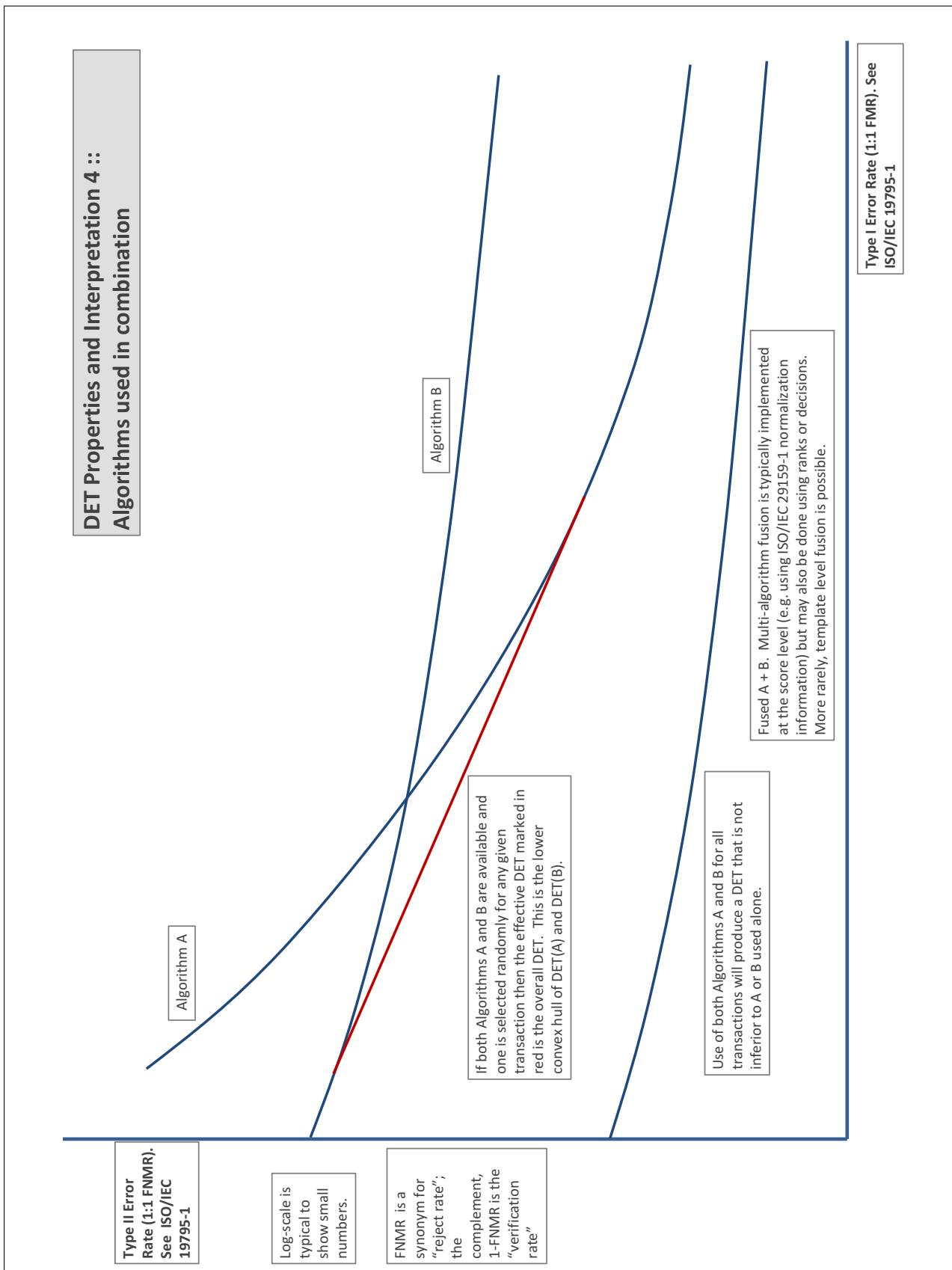
The error tradeoff plots are often called **detection error tradeoff (DET)** characteristics or **receiver operating characteristic (ROC)**. These serve the same function but differ, for example, in plotting the complement of an error rate (e.g., $TMR = 1 - FNMR$) and in transforming the axes most commonly using logarithms, to show multiple decades of FMR. More rarely, the function might be the inverse Gaussian function.

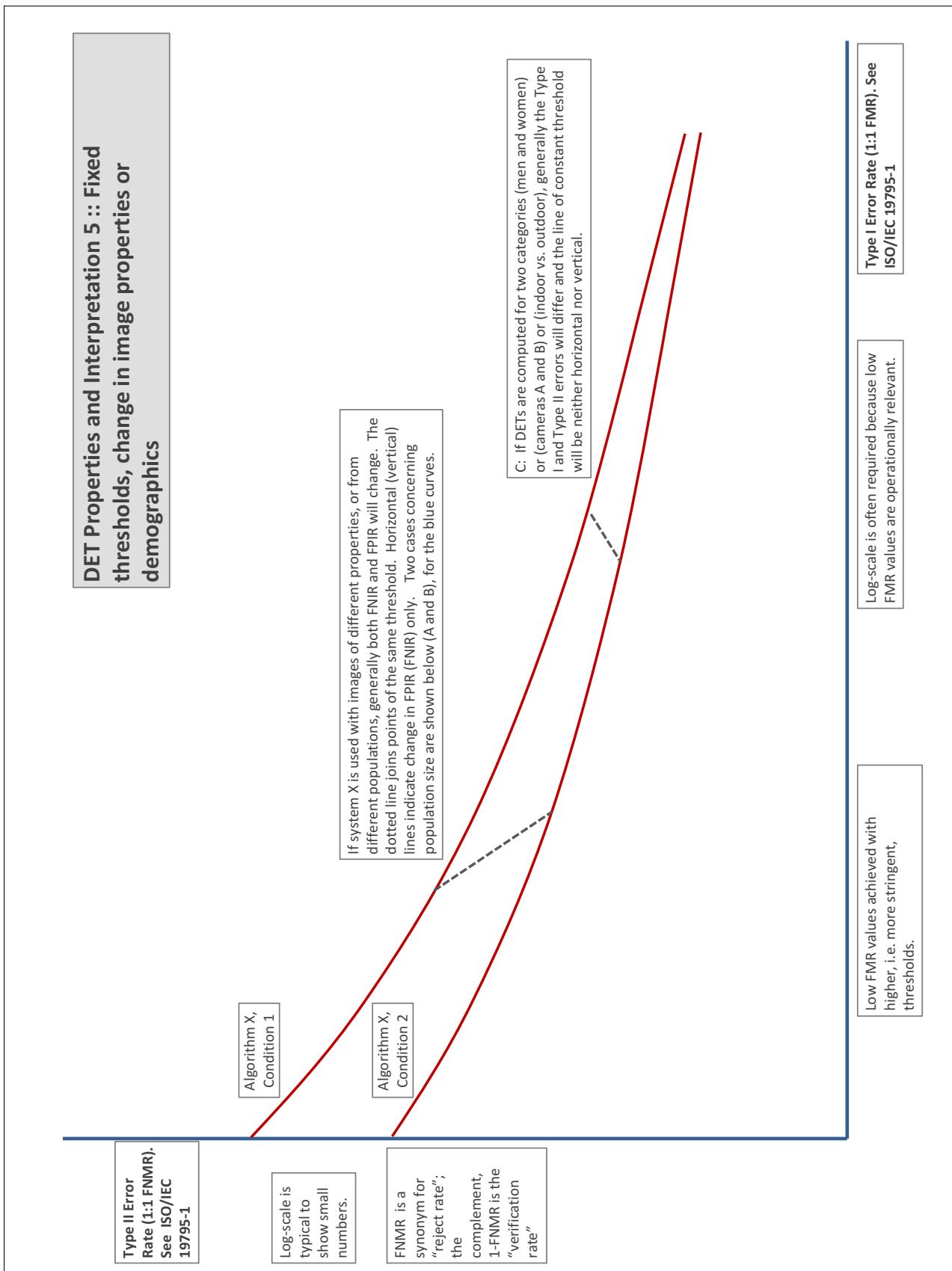
More detail and generality is provided in formal biometrics testing standards, see the various parts of [ISO/IEC 19795 Biometrics Testing and Reporting](#). More terms, including and beyond those to do with accuracy, see [ISO/IEC 2382-37 Information technology -- Vocabulary -- Part 37: Harmonized biometric vocabulary](#)











References

- [1] P. Jonathon Phillips, Amy N. Yates, Ying Hu, Carina A. Hahn, Eilidh Noyes, Kelsey Jackson, Jacqueline G. Cavazos, Géraldine Jeckeln, Rajeev Ranjan, Swami Sankaranarayanan, Jun-Cheng Chen, Carlos D. Castillo, Rama Chellappa, David White, and Alice J. O'Toole. Face recognition accuracy of forensic examiners, superrecognizers, and face recognition algorithms. *Proceedings of the National Academy of Sciences*, 115(24):6171–6176, 2018.